AD-A170 204 BEAM PROPAGATION EXPERIMENTAL STUDY(U) MISSION RESEARCH CORP ALBUQUERQUE NM C A EKDAHL MAR 82 AMRC-R-352 AFOSR-TR-86-0503 F49620-81-C-0016 1/4

UNCLASSIFIED F/G 20/7 NL

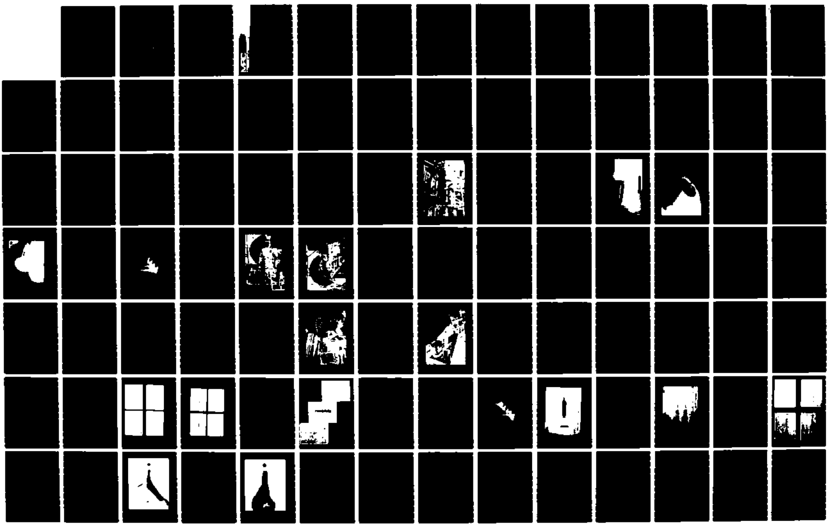

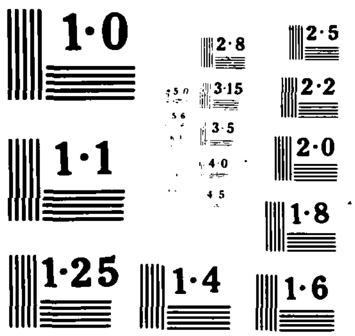
1·0
2·8
2·5
3·15
2·2
3·5
1·1
2·0
4·0
4·5
1·8
1·25
1·4
1·6

(2)

AD-A170 204

Data Entered)

ON PAGE

READ INSTRUCTIONS BEFORE COMPLETING FORM

1. REPORT NUMBER	2. GOVT ACCESSION NO.	3. RECIPIENT'S CATALOG NUMBER
AFOSR-TR- 86-0508		

4. TITLE (and Subtitle) BEAM PROPAGATION EXPERIMENTAL STUDY - ANNUAL REPORT	5. TYPE OF REPORT & PERIOD COVERED Annual Report
	6. PERFORMING ORG. REPORT NUMBER AMRC-R-352
7. AUTHOR(s) C. A. Ekdahl	8. CONTRACT OR GRANT NUMBER(s) F49620-81-C-0016
9. PERFORMING ORGANIZATION NAME AND ADDRESS Air Force Office of Scientific Research Bolling Air Force Base Washington, DC 20332	10. PROGRAM ELEMENT PROJECT, TASK AREA & WORK UNIT NUMBERS 61102F 2301 A7
11. CONTROLLING OFFICE NAME AND ADDRESS Mission Research Corporation 1400 San Mateo Boulevard, S.E. Suite A Albuquerque, New Mexico 87108	12. REPORT DATE March 1982
	13. NUMBER OF PAGES
14. MONITORING AGENCY NAME & ADDRESS (if different from Controlling Office)	15. SECURITY CLASS (of this report) Unclassified
	15a. DECLASSIFICATION DOWNGRADING SCHEDULE

16. DISTRIBUTION STATEMENT (of this Report)

Approved for Public Release, Distribution Unlimited.

17. DISTRIBUTION STATEMENT (of the abstract entered in Block 20, if different from Report)

DTIC ELECTE JUL 25 1986 S D

D

18. SUPPLEMENTARY NOTES

19. KEY WORDS (Continue on reverse side if necessary and identify by block number)

Relativistic electron beam propagation
Relativistic electron beam diagnostics

DTIC FILE COPY

20. ABSTRACT (Continue on reverse side if necessary and identify by block number)

A program of extensively diagnosed experiments to investigate the physics of intense relativistic electron-beam propagation in low-density air is in progress using beam generators at the Air Force Weapons Laboratory. The primary objectives of this research are the rate of erosion of the head of the beam, and to investigate resistive instabilities, such as the hose and hollowing modes, that limit the transport of beam energy over significant distances.

The first year tasks of delineating the pressure range for maximum energy transport and measuring the temporal evolution of the current density profile

DD FORM 1 JAN 73 1473 EDITION OF 1 NOV 65 IS OBSOLETE

SECURITY CLASSIFICATION OF THIS PAGE (When Data Entered)

of the beam producedby the FX-100 have been accomplished. Maximum energy transport (measured calorimetrically) of the FX-100 beam (~ 1.5 MeV, ~ 40 kA, ~ 120 ns) occurred at 0.3-0.5-Torr air pressure. This air-pressure window for maximum energy transport was defined by loss of the tail of the beam at high pressures and by erosion of the beam head at low pressures. Propagation in the window was characterized by a high degree of current neutralization (~ 80% or more), by intense light emission, suggestive of strong avalanche breakdown, and by the onset of a virulent hollowing instability that resulted in as much as 80% of the beam current being carried in a thin annular shell at a radius about twice the Bennett radius characterizing the initially injected current distribution. Space- and time-resolved measurements of the current distribution with a fast-risetime subminiature charge collector array showed that the thin-shell hollowing instability developed late (~ 20 ns or more) into the beam pulse. Sectroscopic measurements of the visible emission suggest that the air near the axis of the beam may have been hotter and more highly ionized in this pressure regime, which may have resulted in a conductivity profile more centrally concentrated than that of the beam.

The appearance of a thin-shell hollwing instability in the pressure regime where avalanching provides an important contribution to the conductivity, which may have a profile more peaked than the beam, and where the current is highly neutralized is in qualitative agreement with existing theory and simulations. The observed delay in onset is not, but may result from imperfect air-chemistry modelling giving an erroneous delay for the buildup of an unstable conductivity profile. Propagation simulations performed in support of our experimental program showed many features consistent with the experimental results, including a high degree of current neutralization, rapid blowoff of the initially-injected beam head followed by a slower erosion, and a lack of instability early in the beam pulse. Linearized simulation suggest instability to thin-shell hollowing in the body of the beam.

The low-pressure air propagation experiments will be continued using the electron beam produced by a new accelerator (VISHNU) being constructed at the Air Force Weapons Laboratory. The VISHNU experiments will incorporate a low-pressure beam preparation cell. The rationale for this is based on our exploratory tests using the FX-25 that demonstrated the stabilization of the hose instability in full-density air by using a low-pressure beam-conditioning cell. VISHNU is design to have electron beam kinetic energy and current (~ 1.5 MeV, ~ 40 kA) close to that of the FX-100 to take advantage of our experience with that beam, but it will have a much shorter pulselength (~ 26 ns). Whether the thin-shell hollowing will be observed in the shorter-pulse experiments remains to be seen.

TR- 86-0503

AMRC-R-352

BEAM PROPAGATION EXPERIMENTAL STUDY - ANNUAL REPORT

C. A. Ekdahl

March 1982

Prepared for: AIR FORCE OFFICE OF SCIENTIFIC RESEARCH
Bolling Air Force Base
Washington, D.C. 20332

Under Contract: F49620-81-C-0016

Prepared by: MISSION RESEARCH CORPORATION
1720 Randolph Road, S.E.
Albuquerque, New Mexico 87106

Research sponsored by the Air Force Office of Scientific Research (AFSC), under contract F49620-81-C-0016. The United States Government is authorized to reproduce and distribute reprints for governmental purposes notwithstanding any copyright notation herein.

DISCLAIMER NOTICE

THIS DOCUMENT IS BEST QUALITY PRACTICABLE. THE COPY FURNISHED TO DTIC CONTAINED A SIGNIFICANT NUMBER OF PAGES WHICH DO NOT REPRODUCE LEGIBLY.

Beam Propagation Experimental Study

Annual Report

C. A. Ekdahl

Mission Research Corporation
1400 San Mateo Blvd. SE
Albuquerque, NM 87108

ABSTRACT

A program of extensively diagnosed experiments to investigate the physics of intense relativistic electron-beam propagation in low-density air is in progress using beam generators at the Air Force Weapons Laboratory. The primary objectives of this research are to measure the rate of erosion of the head of the beam, and to investigate resistive instabilities, such as the hose and hollowing modes, that limit the transport of beam energy over significant distances.

The first year tasks of delineating the pressure range for maximum energy transport and measuring the temporal evolution of the current density profile of the beam produced by the FX-100

have been accomplished. Maximum energy transport (measured calorimetrically) of the FX-100 beam (~1.5 MeV, ~40 kA, ~120 ns) occured at 0.3-0.5-Torr air pressure. This air-pressure window for maximum energy transport was defined by loss of the tail of the beam at high pressures and by erosion of the beam head at low pressures. Propagation in the window was characterized by a high degree of current neutralization (~80% or more), by intense light emission, suggestive of strong avalanche breakdown, and by the onset of a virulent hollowing instability that resulted in as much as 80% of the beam current being carried in a thin annular shell at a radius about twice the Bennett radius characterizing the initially injected current distribution. Space- and time-resolved measurements of the current distribution with a fast-risetime subminiature charge collector array showed that the thin-shell hollowing instability developed late (~20 ns or more) into the beam pulse. Spectroscopic measurements of the visible emission suggest that the air near the axis of the beam may have been hotter and more highly ionized in this pressure regime, which may have resulted in a conductivity profile more centrally concentrated than that of the beam.

The appearance of a thin-shell hollowing instability in the pressure regime where avalanching provides an important contribution to the conductivity, which may have a profile more peaked than the beam, and where the current is highly neutralized is in qualitative agreement with existing theory and simulations.

The observed delay in onset is not, but may result from imperfect air-chemistry modelling giving an erroneous delay for the buildup of an unstable conductivity profile. Propagation simulations performed in support of our experimental program showed many features consistent with the experimental results, including a high degree of current neutralization, rapid blowoff of the initially-injected beam head followed by slower erosion, and a lack of instability early in the beam pulse. Linearized simulations suggest instability to thin-shell hollowing in the body of the beam.

The low-pressure air propagation experiments will be continued using the electron beam produced by a new accelerator (VISHNU) being constructed at the Air Force Weapons Laboratory. The VISHNU experiments will incorporate a low-pressure beam preparation cell. The rational for this is based on our exploratory tests using the FX-25 that demonstrated the stabilization of the hose instability in full-density air by using a low-pressure beam-conditioning cell. VISHNU is designed to have electron beam kinetic energy and current (~1.5 MeV, ~40 kA) close to that of the FX-100 to take advantage of our experience with that beam, but it will have a much shorter pulselength (~26 ns). Whether the thin-shell hollowing will be observed in the shorter-pulse experiments remains to be seen.

CONTENTS

CONTENTS

CONTENTS

I. RESEARCH OBJECTIVES

A. Introduction

Directed energy weapons have the potential to revolutionize modern warfare and greatly affect national defense policies. The application of high-energy particle beams as directed energy weapons is particularly promising because of their ability to penetrate targets. The realization of this concept is dependent on major technical issues in the areas of pulse power, particle accelerators and beam- target interactions.[1] These technical problems can probably be overcome with the expenditure of sufficient technical effort.

However, the physics of beam propagation may prevent delivering sufficient energy over the distances required to make beams practical as weapons. Endoatmospheric propagation remains a key issue that may not yield to a massive research effort. Basic physics questions about the growth rates and nature of instabilities encountered during beam pulse transmission through the atmosphere re. .n unresolved. The complexity of beam propagation physics and air chemistry makes the prediction of beam behavior dificult. Theoretical analysis has used broad assumptions regarding the beam current distribution, evolution and equilibrium in order to make the problem more tractable.[2] Clearly, the issue of propagation will not be fully resolved until full-scale experiments with accelerators having weapons-grade parameters are performed. It is also clear that one cannot wait for the advent of such experiments, because beam propagation will have a significant role in determining the optimal weapon accelerator parameters. It is desirable, therefore, to address the scaling of propagation phenomena with beam parameters by conducting experiments using presently available accelerators.

Realizing the scope and manifold nature of problems arising from beam propagation, we have commenced an experimental investigation initially confined to two crucial topics: the rate of erosion of the beam nose, and the coupling between nose erosion and resistive instabilities, such as the hose and hollowing instabilities. These experiments are being performed using the beam generators available at the Air Force Weapons Laboratory. They are designed to provide both qualitative and quantitative measurements of the rate of nose erosion, effects of the hollowing instability, and the nature of the hose instability.

This study consists of several distinct parts. The pressure window for stable beam propagation must be determined, as well as the evolution of the beam current distribution from injection to an equilibrium profile. The beam erosion rate must be measured in stable- and unstable-propagation pressure regimes. As a result, the absolute or convective nature of the resistive instabilities when coupled to beam-nose erosion will be determined. Finally, analytical and computational studies must be undertaken to support the interpretation of the experimental results.

B. Technical Issues

Suppression of instabilities is a key issue for successful propagation of intense relativistic electron beams over long distances in the atmosphere. Instabilities are, in principle, capable of deflecting a beam from its desired trajectory, fragmenting the beam into filaments, dissipating beam energy, and causing significant emittance growth. All of these effects have been observed experimentally. The instabilities arise from the interaction of negative-energy waves of the electron beam with positive-energy waves of the resistive ionized-gas channel created by the beam. Energy transfer from the negative-energy waves to the positive-energy waves causes both to grow, often with catastrophic result to the beam.

A self-pinched relativistic beam supports two negative energy modes: the space charge wave, and the betatron wave. This research program addresses only the latter. The betatron wave differs from the more familiar cyclotron wave because it occurs as the result of an inhomogeneous azimuthal magnetic field rather than a homogeneous axial field. At long wavelengths the betatron mode gives rise to sausage, kink, and thin-shell hollowing instabilities.[3] The kink, or resistive hose, is thought to be the most dangerous, although recent theoretical results indicate that the sausage, or hollowing, instability may be as serious for beams having a high degree of current neutralization.

Theoretical investigations of the resistive-hose instability have yielded many valuable insights into hose behavior in the body of the beam.[3,4] However, the modeling of beam propagation has proved to be an extremely difficult problem. Derivation of equations and scaling relationships from first principles is not analytically tractable. As a result, the models developed have incorporated a number of assumptions about the beam profile and motion:

1. Beam electron motion is treated in the paraxial approximation with the axial velocity set equal to the speed of light, c. This approximation requires that the transverse components of the electron equations of motion and the

field equations be negligibly small compared with the longitudinal components, and that the ratio of net current to the Alfven limiting current be small.

2. The transverse velocity distribution is taken to be a truncated Bennett distribution.[5]

3. Energetic delta-ray secondaries are ignored, although calculations show that they can constitute a current greater than 10% of the primary current.[6]

4. Beam transverse motion is treated in the rigid beam approximation, with any spread in betatron frequency mocked up by mass spread for the rigid beam disks. This approximation precludes determining the possibly stabilizing effect of orbit precession or the effect of radial variation in betatron frequency.

5. The channel plasma is assumed to be purely resistive, ignoring reactive terms resulting from electron inertia or plasma waves.

6. Realistic plasma conductivity and return current radial profiles are not employed. Usually, the conductivity is taken to be scalar, and the return current profile is taken to be the same as the beam current profile.

7. Only the axial component of the wave vector potential is considered, and it is computed in the long wavelength, diffusion approximation.

The sum total of these assumptions describes a highly idealized state for the beam-plasma system that may not be truly representative of the physics involved. Models using these approximations indicate that the hose growth rate is a maximum at wave frequencies near the average betatron frequency, and that the growth rate can be reduced by a spread in betatron frequencies.[4] This somewhat qualitative picture may not sufficiently accurate for detailed comparison with experiments or for selecting future accelerator designs. Numerical calculations have incorporated many of the same approximations, and therefore their results cannot corroborate the analytic work.

Hose behavior near the nose of the beam is not so well understood, not only because the approximations are less well satisfied, but also because the beam and channel parameters are changing in a scale length short compared with a betatron wavelength. The resistive hose, hollowing, and thin-shell hollowing instabilities are potentially more serious at the nose because, if the nose breaks up or deflects, the beam body is apt to do likewise. At the nose these instabilities need not necessarily grow from noise because slight misalignments between beam and channel can induce lateral oscillations in the beam nose, giving a head start to hose instabilities. Also, near the nose the channel conductivity and beam frequency are more nearly matched, causing larger growth rates, other things being equal. Offsetting these conditions is the great inhomogeneity of the beam and channel near the nose, which reduces growth rate. Also important is the convective nature of the resistive instabilities in the beam frame; perturbations originating in the nose move back in the beam as they grow.[4] On this basis the instability would not be expected to become larger near the beam nose. In fact, the beam nose erodes because of ohmic energy losses and lack of radial force balance. Recently, concern has developed that the erosion rate may match the convection rate so closely that substantial growth may occur in the beam nose.

Analyzing this complicated behavior is very difficult. Beam and channel parameters rapidly change in space and time. Thus, interplay between resistive instabilities and the eroding nose is very complex. Some progress has been achieved in analyzing nose-coupled instabilities, but much remains to be done. Structure of the beam nose is not well understood even in the abscence of instabilities.

It is prudent to compare the analytic predictions with experimental results because of the nature and number of approximations made. One series of experiments appears to confirm the validity of a Bennett radial current profile.[2] However, this may be fortuitous. Even qualitative measurements of nose erosion are scarce. The maximum erosion rate in the low-pressure window for stable propagation has been inferred from measurements of the time delay for the beam arrival at a given axial position.[8] In general, experiments with hose-unstable beams have been qualitative in nature.[2,7,8] Time-integrated (open shutter) photography has been a major diagnostic. The beam current distribution at injection and beam emittance are critical parameters that have never been ascertained in the experiments because of the difficulty of the measurements. This is also true of the time it takes for the beam to evolve to an equilibrium after injection. Nevertheless, these previous experiments have established relationships between hose instability growth rates and certain parameters:

1. At high pressures the hose instability is the limiting factor for beam propagation.

2. High beam impedance increases the hose growth scale length because lower net current implies longer betatron wavelengths.

3. A larger equilibrium radius also increases the hose growth scale length.

4. A high beam temperature (emittance) stabilizes the hose growth, apparently as a result of the betatron frequency spread.

The limitations of the analytical descriptions of beam propagation and the qualitative nature of the measurements made to date underscore the need for our extensively diagnosed program of propagation experiments. Emphasis has been placed on nose erosion, and on erosion-coupled instabilities because of the current lack of understanding of these crucial aspects of propagation physics.

C. Experimental Program

The key to the experimental program is a thorough knowledge of beam parameters at injection and extensive diagnosis of beam evolution in the drift tube. This will enable an unequivocal analysis of beam-nose erosion and the hose instability. It will also address the question of whether the hose instability is absolute or convective as a result of the influence of nose erosion. The required investigations will take two years for completion. The utility of the various diagnostics will be discussed is the context of the individual experiments. It should be realized, however, that these diagnostics and variations on them will be employed in ways in addition to those described here. Also, the use of the different diagnostic devices will be carried over from one series of experiments to another. Finally, the diagnostics described will be supplemented with techniques that we invent and develop during the course of the experiments.

1. First Year Experiments

The program to be carried out using the AFWL beam generators has four distinct phases. First, the range of pressures, or "window", that permits stable beam propagation will be determined. This window has also been measured using different beam machines.[7,8] It has been interpreted as a region between the collisional extinction of the two-stream instability and the onset of the hose instability. The pressure window changes with gas composition, with beam kinetic energy, and with propagation chamber geometry. It can be ascertained from measurements of the beam energy transmitted over the drift tube length at different pressures. Previous experiments have shown that the window can also be determined from measurements of the net current (beam current plus plasma-channel return current). Both of these methods will be used in our experiments. A series of Rogowski coils at different axial positions along the drift tube will measure net current, and a calorimeter at the end of the tube will measure the transmitted beam energy. By plotting the results of these measurements versus pressure the window will be delineated.

The second task of the program is to determine the beam current distribution and its evolution resulting from collisions. This knowledge is crucial for establishing the validity of proposed theoretical models of beam propagation and instability growth. Yet it has never been adequately measured in the laboratory. The beam distribution varies with beam kinetic energy, injected beam current, cathode shape and composition, anode-cathode spacing, and anode foil thickness. A complete parameter search to establish the variation of the beam distribution with these factors would be valuable indeed, but such a study is not within the scope of our research objectives. Instead, the current distribution will be measured for a fixed diode configuration. The foil thickness will be changed once in order to establish the change in the beam profile resulting from scattering.

The beam current distribution will be measured in vacuum and in the stable propagation regime. The vacuum measurement is necessary to separate the effects of foil scattering from gas scattering. The beam will be injected through an anode foil into a large diameter drift tube for these measurements. A Faraday cup array with subnanosecond risetime will be used in order to provide the required spatial resolution. In vacuum the Faraday cup array will be positioned close to the anode foil so that the beam distribution will not be affected by space-charge repulsion among the electrons. This measurement will determine the radial beam current profile at injection. The initial measurement in air (at the propagation-window pressure) also be made close to the anode foil. However, additional measurements will be made at various axial positions. In this way the evolution of the beam distribution to an equilibrium can be observed and the validity of assuming a Bennett profile can be tested.

In addition to these quantitative measurements a large number of diagnostics will be used in order to gain insight into qualitative beam behavior. Among these are radiochromic bleaching foils, which are discolored by electrons with energy of a few electron volts or more. Bleaching foils will be positioned along the drift tube to record the time-integrated beam and channel radial profile. By replacing the bleaching foils with metallic-screen meshes, an X-ray pinhole camera can be used to produce an image of the beam primary electrons. These images can be compared with the bleaching foils to separate the beam and plasma channel radial structures. Another time-integrated diagnostic that will be used is open-shutter photography. The drift tube will have provisions for time-integrated (open-shutter camera) and time-resolved (framing camera) photography of the beam motion. Open shutter photography will produce pictures of axial variation in the plasma channel. Time-resolved observations of the beam and plasma channel will be made with streak and framing cameras.

2. Second Year Experiments

The third task of the proposed experimental program is to measure beam-nose erosion in the stable propagation mode where it will be decoupled from instabilities. It is evident that beam-nose erosion will be occurring at the same time that one is trying to ascertain the evolution of the beam distribution in low-pressure gas (phase two of the program). Consequently, the second and third phases of the experimental program are not disjoint, and the diagnostics described for the first year will be employed in the second year to perform similar, if not identical, tasks.

A magnetic beta spectrometer will be a major diagnostic in the second year. This AFWL instrument, which is based on a Los Alamos Scientific Laboratory spectrometer, magnetically deflects a precollimated sample of the beam, which is detected by an array of Faraday cups located in the 180° focal plane. The detector array will provide a time history of the beam energy distribution because of the energy dependence of the electron trajectories through the spectrometer. Unfolding the output of this device can give an indication of how far into the voltage pulse the nose erosion is occuring. It can also define the amount of beam energy degradation as a function of time into the pulse. By obtaining data at different axial positions the nose erosion as a function of propagation distance can be obtained. Varying parameters such as pressure, kinetic energy, injected current, and beam radial profile will result in important scaling relationships for nose erosion.

Other diagnostics will be developed for this phase of the research program. Faraday cups and scintillators placed near the drift tube wall will be used to observe the passage of the beam front, which expands radially as a result of space-charge repulsion. Placement of these detectors at several axial positions will provide the beam-front velocity and rate of charge loss. X-ray film packets placed on the tube walls can detect the position of the first contact by the beam.

The sum of these diagnostics will produce a wealth of information about beam evolution and nose erosion. The results will produce insights and define initial conditions of the beam that will allow the development of a comprehensive model. The experimental results will not only establish empirical scaling laws, but also create a data base for comparison with theoretical models.

The fourth task of the experimental program is to determine whether nose erosion occurs at a rate that makes the hose instability absolute in the beam-head frame. If this proves to be true, the nose of the pulse will be severely distorted and propagation may be impossible. The same is true if any of the other resistive instabilities (eg., sausage or thin-shell hollowing) are found to be absolute in the frame of the beam head. In order to test this possibility in the case of the hose instability the beam must be injected into air at a pressure above that of the propagation window. This will allow the beam and ionized-gas channel system to be unstable to hose growth. Several methods could be used to insure a growth rate that is slow enough to permit detailed investigation of the possible coupling of erosion to the hose. These include the application of axial magnetic fields, operation at pressures only slightly above the threshold for growth, and the use of small diameter conducting drift tubes. The use of axial magnetic fields is undesirable because it modifies the beam distribution, makes for difficulties in beta spectrometry, and is expensive. A combination of the latter two possibilities appears to be the most promising method for these experiments. By varying tthe diameter of a conducting drift tube the hose growth can be controlled by wall stabilization.[7,8] This stabilization occurs because some of the return current is carried in the conductor rather than in the current channel. The current carried by the return conductor provides an in-phase restoring force on the beam displacement perturbations because of the high conductivity of the drift tube wall.

Using the diagnostic techniques alr ly described, the evolution of the distribution of the hose-unstable beam will be detailed. Measurements will quantify the hose growth as a function of net current, beam kinetic energy, gas pressure, and beam equilibrium radius. Any pressure related changes in coupling of erosion to instability will be observed. Differences in instability growth rates in the head of the beam and in the beam body will be observed. Finally, if the hose instability is indeed convective over the body of the pulse, the convection rate can be measured.

D. Theoretical Support

Using the information obtained from reduction of experimental data an analysis will be made of the beam-nose erosion and hose instability growth. A modification of the linear-stability code GRADR will be used for investigation of the hose instability. GRADR will be used to predict the hose growth and convection rates in the beam body, based on experimentally determined beam parameters and beam current profiles. At first, this interaction between experiment and theory will serve to guide the experiment and subsequently will provide validation of the code in predicting instability behaviour at higher energies.

The nonlinear nature of nose erosion and instability growth at the beam head, on the other hand, necessitates nonlinear analysis. The beam simulation code CCUBE will be used to model these phenomena for comparison with experiment. This two-dimensional, relativistic, electromagnetic, particle-in-cell code is capable of running in any orthogonal coordinate system, and follows all components of particle velocity and electromagnetic fields. Solving the Maxwell equations does not involve inversion of the Poisson equation, a significant advantage in treating the conducting channel. The CCUBE particle transport algorithm is well suited to particle motion in large magnetic fields.

CCUBE will be used to investigate the physics of the nose-coupled hose instability, including the influences of nose blowoff, ohmic energy losses, beam hollowing (if any), conductivity generation, and return currents by direct self-consistant numerical inegration of the Maxwell equations and the single particle relativistic equations of motion. This code will not be used in a parameter search mode, but rather as a tool to provide understanding of the interrelations of factors influencing hose and thin-shell hollowing growth in the beam nose in order to guide formulation of appropriate nose-coupled instability models based on experimental data. CCUBE will be particularly helpful in assessing the causes of unexpected experimental results and suggesting modifications to the experiments when a more detailed diagnosis of parameters is necessary.

Only minor modifications are required for CCUBE to simulate pinched-beam propagation. These include a moving grid option, a conductivity generation routine, and an implicit field solver. A moving grid option permits following the beam nose over longer distances. Thus, it has the effect of a retarded time option, but it is more flexible because the grid velocity can be changed as a function of time. Conductivity can be treated in as simple or as complex a fashion as desired, and several options can be implemented. An implicit field solver is needed because air conductivity varies over many orders of magnitude in the beam nose, from essentially zero ahead of the beam to values well above the characteristic frequencies of the beam several cm into the pulse. Appropriate algorithms have been developed that will allow complete electromagnetic treatment of the beam fields. None of these modifications are particularly difficult to implement.

E. Statement of Work

The following tasks will be performed in the first year of the research in order to resolve critical issues of intense relativistic electron beam propagation.

Task 1. Determine the pressure window for stable beam propagation on the FX-100 machine.

Task 2. Measure the beam distribution at injection and its evolution to an equilibrium profile under the influence of collisions in the stable propagation regime. Develop suitable diagnostic equipment as required.

Task 3. Perform analytical and computational studies necessary for guidance of the experiments and interpretation of experimental results.

The following tasks relating to nose erosion and the hose instability will be carried out in the second year of the research effort.

Task 4. Measure the beam erosion rate in the stable mode of propagation.

Task 5. Measure coupling of beam-nose erosion with hose instability growth for propagation in the unstable pressure region. Determine whether nose erosion renders the hose instability absolute or convective.

Task 6. Perform analytical and computational studies necessary for guidance of the experiments and interpretation of experimental results.

F. References

1. B. D. Guenther, R. Lontz, and J. L. May, in Proceedings of the Particle Beam Research Workshop, U. S. Air Force Academy, 9-11 January 1970

2. E. P. Lee, Phys. Fluids 19, 60(1976)

3. E. P. Lee, Lawrence Livermore National Laboratory Report UCID-16268, 1973

4. E. P. Lee, Phys. Fluids 21, 1327(1978)

5. W. H. Bennett, Phys. Rev. 45, 890(1934)

6. N. Carron, private communication

7. R. B. Miller, Sandia National Laboratory Report SAND 79-2129, January 1980

8. R. Briggs, J. Clark, T. Fessenden, R. E. Hester, and E. Lauer, in Proc. of the 2nd International Conf. on High Power Electron and Ion Beam Research and Technology, Cornell University, Ithaca, New York, 5-7 October 1977

9. E. P. Lee and R. K. Cooper, Part. Accel. 7, 83(1976)

II. STATUS OF THE RESEARCH

A. Introduction

Initial measurements of the hose-stable propagation pressure window and the beam current density distribution have been made using the beam produced by the FX-100 accelerator (1.5 MeV, 40 kA, and 120-ns pulsewidth). Many of the diagnostics for these measurements were developed using the beam from the FX-25 accelerator (1.5 MeV, 23 kA, and 20-ns pulsewidth).

The FX-100 was decommissioned in August 1981, and the propagation experiments will continue using the beam from an accelerator (VISHNU) presently under construction for this purpose. The VISHNU beam is designed to have the same kinetic energy and current as the FX-100 beam (~1,5 MeV and ~40 kA), but with a much shorter pulsewidth (~26 ns). Therefore, the transition to VISHNU should not involve a lengthy delay in the program, because we will be able to establish the propagation pressure window and current distribution evolution based on our experience with the FX-100 beam.

We present here a brief account of the experiments performed and results obtained in the first year of this research. Following this we give the particulars of the FX-100 experiments and results, and the technical specification of the VISHNU accelerator. Details of the FX-25 experiments are to be found in App. A.

1. FX-25 Experiments

In February, 1981 the AFWL FX-25 was made available to us for the development of diagnostics and exploratory propagation experiments. The diagnostic effort focused on the development of arrays of subminiature charge collectors for measurements of the beam spatial distribution. We performed low-pressure experiments to investigate the propagation window using a new diode designed to launch the beam with initial conditions much closer to the expected low-pressure equilibrium than in previous experiments. Finally, experiments were performed to investigate the effect on the hose instability in full-density air of using a low-pressure beam preparation cell.

The low-pressure propagation experiments were performed in a 5-cm diameter, 3-m long conducting drift tube. Most FX-25 propagation experiments in the past have used diodes that generated a hollow, non-equilibrium beam that violently pinched immediately after injection. We used a graphite Rogowski-surface cathode and 25-μm titanium-foil anode that produced a centrally concentrated beam with a 1.7-cm e-folding radius in order to avoid shock excitation of large amplitude waves by injection of a pathological current distribution. At the 1.6-Torr air pressure for maximum energy transport the beam evolved to a Bennett-like beam profile with a Bennett radius a~0.5 cm. Time resolved measurements with the Faraday cup array showed that energy transport was limited by erosion of the beam nose at lower pressures, and by loss of the beam tail at higher pressures.

In order to test the possibility of stabilizing the hose in full density air, the beam was extracted through a 25-μm Kapton foil at the end of the drift tube. The rational for these experiments with a beam conditioning cell is as follows. The resitive hose instability on a self pinched beam is the result of the negative energy mode associated with the betatron wave. Although the betatron wavelength for electrons with different turning radii is different, the growth of the instability can often be associated with a betatron wavelength characteristic of the beam envelope. For a Bennett pinch the characteristic betatron wavelength is $\lambda_\beta \sim 2\pi a(I_A/2I_n)^{1/2}$, where 'a' is the Bennett radius, $I_A = \gamma\beta mc^3/e = 17\gamma\beta$ (kA) is the Alfven limiting current, and I_n is the net current that generates the pinch magnetic fields. Prior to these experiments, all high intensity beams extracted directly into full-density air were observed to become hose unstable within less than ~4 λ_β. In most, if not all, of these prior experiments the injection conditions were not an equilibrium for the full-density air, which resulted in the excitation of a large amplitude betatron wave at injection as the beam rapidly readjusted to a new equilibrium. Using a long conditioning cell can avoid this by establishing, at low pressure, an equilibrium close to that expected in full density air while the beam is wall-stabilized by the drift tube. If the tube is long compared with λ_β, then coherent waves excited at injection into the cell will have a chance to damp by phase mixing before injection into air. If the transition to air is made in a way that does not involve a significant change in λ_β, then it may be possible to avoid excitation of the large amplitude waves and subsequent hose instability. Consideration of the parameters defining the betatron wavelength suggests that another aid in stabilization of resistive instabilities would be to minimize the net current. This might be accomplished by sharpening the beam pulse and relying on the increase in induction fields to rapidly break down the air to increase the conductivity and thereby reduce the return current. This suggests using conditioning-cell pressures below the propagation window, where pulse sharpening by nose erosion is significant.

We performed the experiments using only a minimal set of diagnostics including net current measurements (in the cell and outside) and open-shutter pictures to observe the full-density hose instability. We varied the cell air pressure from above the 1.6 Torr pressure for maximum energy transport to well below this value. A marked stabilization of the hose was observed at drift-tube pressures below 1 Torr. This appeared to be a threshold effect in the sense that there was a very narrow range of pressures (0.7-0.8 Torr) below which the beam was markedly more stable. The full-density propagation was limited to less than ~6 betatron wavelengths by the presence of a shield wall. Whether the stabilization resulted from pulse-sharpening in the drift tube, profile broadening at the lower pressure, or equilibration and betatron phase mixing is unclear at this time. However, the fact that there was no threshold in the pulse sharpening in the drift tube that corresponded to the observed threshold for full-density hose stabilization is suggestive that, although pulse sharpening and the increased return current fraction that results from the enhanced conductivity can be contributory, it is not the major effect. Net current measurements were inconclusive, but they were suggestive that there was no large disparity between internal and external net currents when the beam was stabilized.

2. FX-100 Experiments

Propagation experiments with the FX-100 accelerator commenced in April, 1981 after extensive repairs and modifications. These experiments continued into August, when the FX-100 was decommissioned and removed in order to provide space for the development of the first RADLAC II module. Low-pressure air-propagation experiments were performed to delineate the propagation window and to measure the beam-current distribution in the hose-stable propagation regime.

A graphite Rogowski-surface cathode produced a beam that was injected into the 20-cm diameter conducting drift tube through a 25-μm titanium-foil anode. The injected beam had a 3-cm Bennett radius. As in our FX-25 experiments the propagation window was defined by beam-nose erosion at low pressures and by loss of the beam tail at high pressures, observed now with streak photography so well as with Faraday cups. Maximum energy transport through 5 meters of drift tube occurred at 0.5-Torr pressure. Near this peak in the window we discovered that much of the current was frequently carried in an annular "halo" that apparently developed as the result of a hollowing instability with an onset late in the beam pulse.

Measurements of light emitted by the beam excited and ionized air showed the presence of singly-ionized atomic nitrogen near the axis, at radii much less than the beam Bennett radius, in the pressure range characterized by the hollowing instability. This may be indicative of a hotter, more highly ionized (and, therefore, more conductive) gas near the axis. This condition is theoretically conducive to the development of a hollowing instability.

The appearance of the hollowing instability in the pressure regime where avalanching provides an important contribution to the conductivity, and where the beam was observed to to be highly current neutralized, is in qualitative agreement with theory and simulation. The long delay before onset is not yet fully understood, but may result from the time delay to form a peaked conductivity profile, an imperfect chemistry model in the codes that predict rapid onset, a pathological change in diode characteristics, or some combination of these.

3. Theoretical Support

Throughout the course of the experiments theoretical and computational support in the design of diagnostics and the interpretation of the data was provided by several MRC theorists. The details of these studies are to be found in Appendices E, F, and I in particular. In addition, particle simulations with the MRC codes KMRAD and CPROP provided major insights into the physics of the beam-nose erosion and instabilities observed in the FX-100 experiments.

The beam propagation simulation code CPROP showed large return currents (~80%) when avalanching was included in the conductivity model. In the experiments the return current fraction was 80–90% in the propagation window. At pressures greater than ~0.5 Torr, avalanching causes the conductivity to concentrate on axis, which can drive a beam hollowing instability. The erosion of the beam seen in the simulations was not inconsistent with the observations. The linearized simulation code KMRAD was used to search for m=0 instabilities such as observed experimentally. A short-transverse wavelength instability was instability was observed even with an unpeaked conductivity profile. This mode had a group velocity much less than the beam velocity and may be the source of the fine structure seen experimentally. The details of these studies may be found in Appendix G.

B. Technical Details

1. FX-100 Accelerator

The FX-100 accelerator was a gas-insulated coaxial transmission line that was DC charged with a Van de Graaff belt-charging system, and then was discharged into the field-emission diode with a single output switch. The insulating gas was 10% SF_6 in nitrogen, which was pressurized to ~200 psi in order to provide the required insulation strength. The energy storage transmission line impedance was 43 Ω, and it had a 34 ns one-way electrical transit time. The triggered gas output switch was followed by a 4.2-ns long, 233-Ω stacked-ring envelope and a 3.8-ns long, 160-Ω vacuum transmission line. The last stage of the vacuum line consisted of a short (~1 ns) length with lower impedance (~80-Ω) to reduce shank emission losses. This final section of vacuum coax was terminated with the 55-Ω field-emitting diode consisting of a graphite cathode and titanium foil anode through which the electron beam was injected into the low-pressure propagation chamber (Fig. 1).

The high-impedance envelope and vacuum transmission line of the FX-100 dominated the output impedance regardless of the diode impedance, and produced a diode current waveform with oscillations at a frequency characteristic of the ~70-ns down-and-back time of the charged energy-storage transmission line

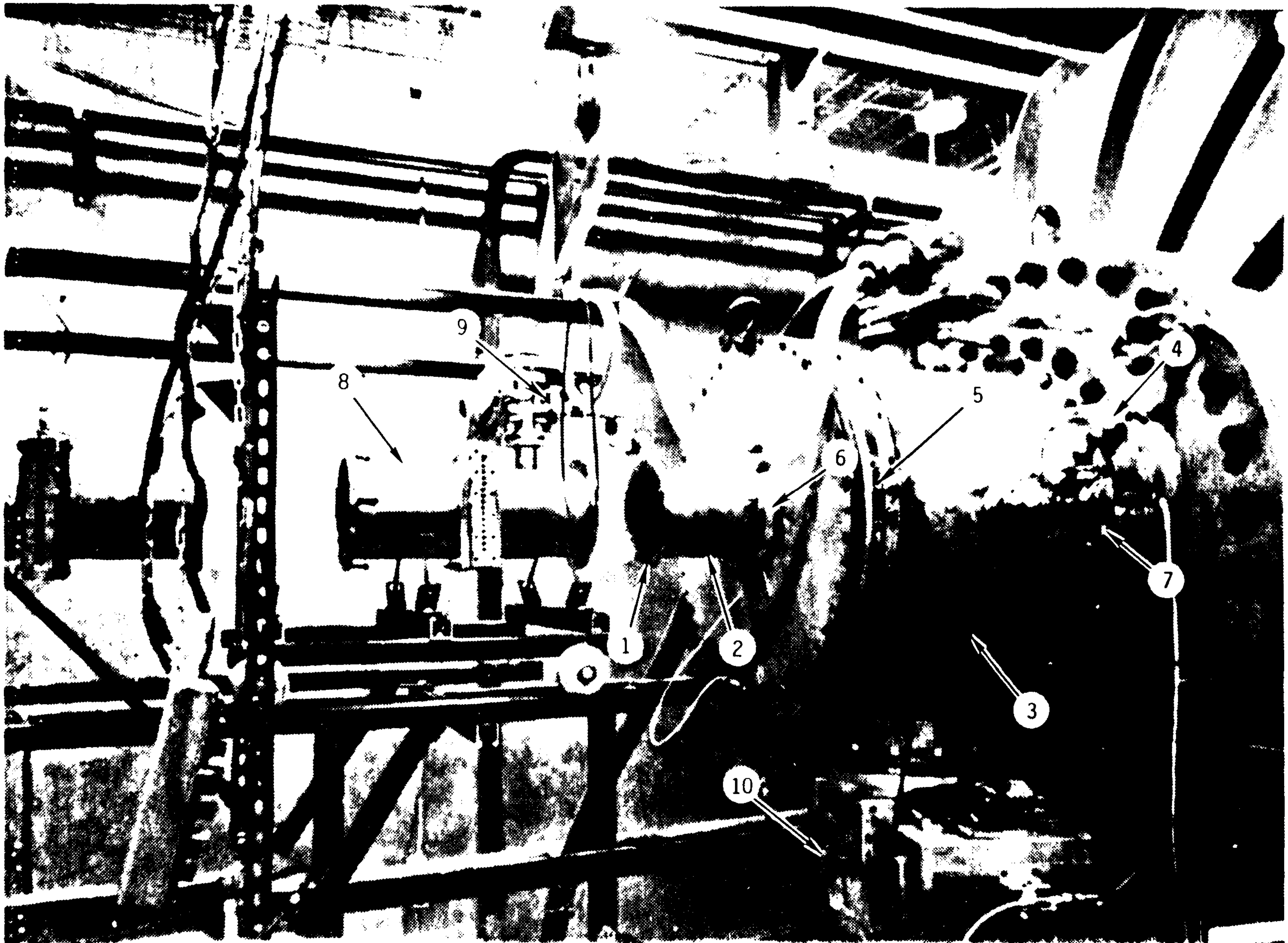

Figure 1. Output section of FX-100 Van de Graaff e-beam generator. (1) Anode foil; (2) Final (80-Ω) vacuum transmission line; (3) 160-Ω vacuum transmission line; (4) Diode vacuum guage; (5) 2-mΩ resistive shunt diode current monitor; (6) Rogowski belt diode current monitor; (7) Capacitive voltage monitor (behind vacuum tee); (8) Two sections of propagation experiment low-pressure drift tube; (9) Propagation experiment gas manifold; (10) Diode vacuum system.

(Fig. 2). The transmission-line stored energy was eventually extracted from the diode in a pulse with ~120 ns width. Although it can be argued that this output pulseshape was not ideal for propagation experiments there was insufficient time to allow for the rather substantial (but straightforward) modifications to the FX-100 that would have resulted in a more closely matched output.

Indeed, a considerable effort was expended to bring the FX-100 up to a performance level suitable for these experiments. A series of high-voltage insulation failures in the Van de Graaff charge-belt insulator stack late in calender 1980 resulted in the incapability of charging the intermediate coax to the required operating voltage. During the lengthy repair of the damage resulting from these failures we implemented a simple modification to the insulator protection spark gaps that prevented a recurrence of this failure mode during the course of the propagation experiments.

An additional technical problem was the output-switch trigger system. It was not sufficiently reliable for the required reproducibility of beam parameters. We corrected the trigger problem by designing and installing a pneumatically operated field-distortion trigger pin. The trigger-pin actuating unit is shown in Fig. 3, and Fig. 4 shows the trigger as installed in the gas-insulated output switch. This trigger pin was designed to be actuated by the pressure differential between two dielectric gas lines run to the exterior of the FX-100 tank. This design avoids a high-voltage discharge through the dielectric lines by maintaining the dry-nitrogen working-gas pressure at greater than the ~200-psi tank pressure. This unit provided reliable

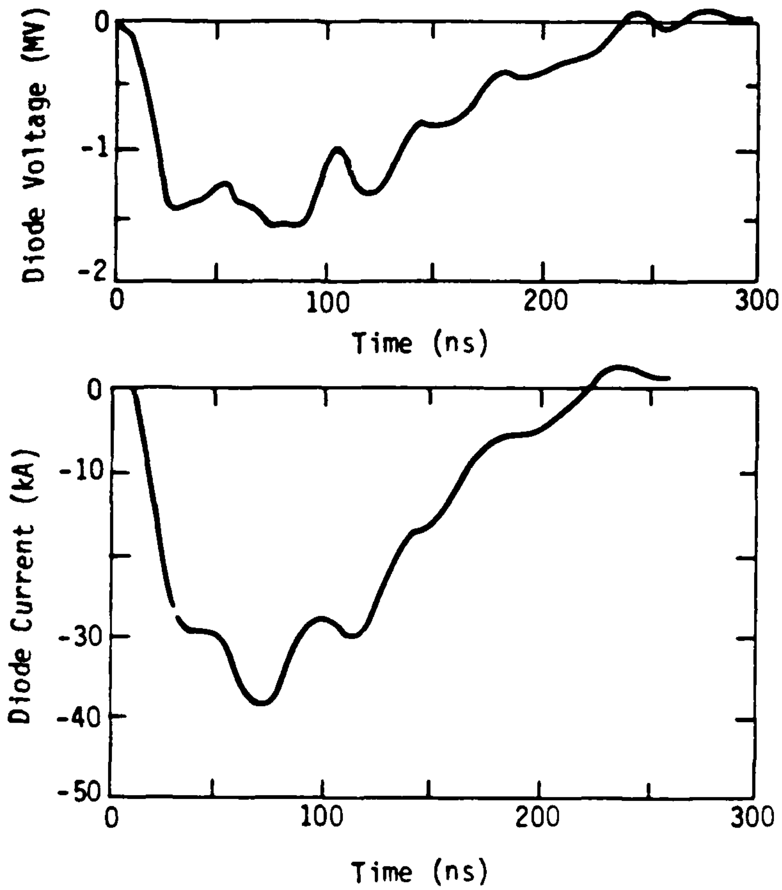

Figure 2. FX-100 diode voltage and current. The gas-insulated coax was charged to 4.2 MV in order to produce this output. This charge voltage remained unchanged during the course of the propagation experiments.

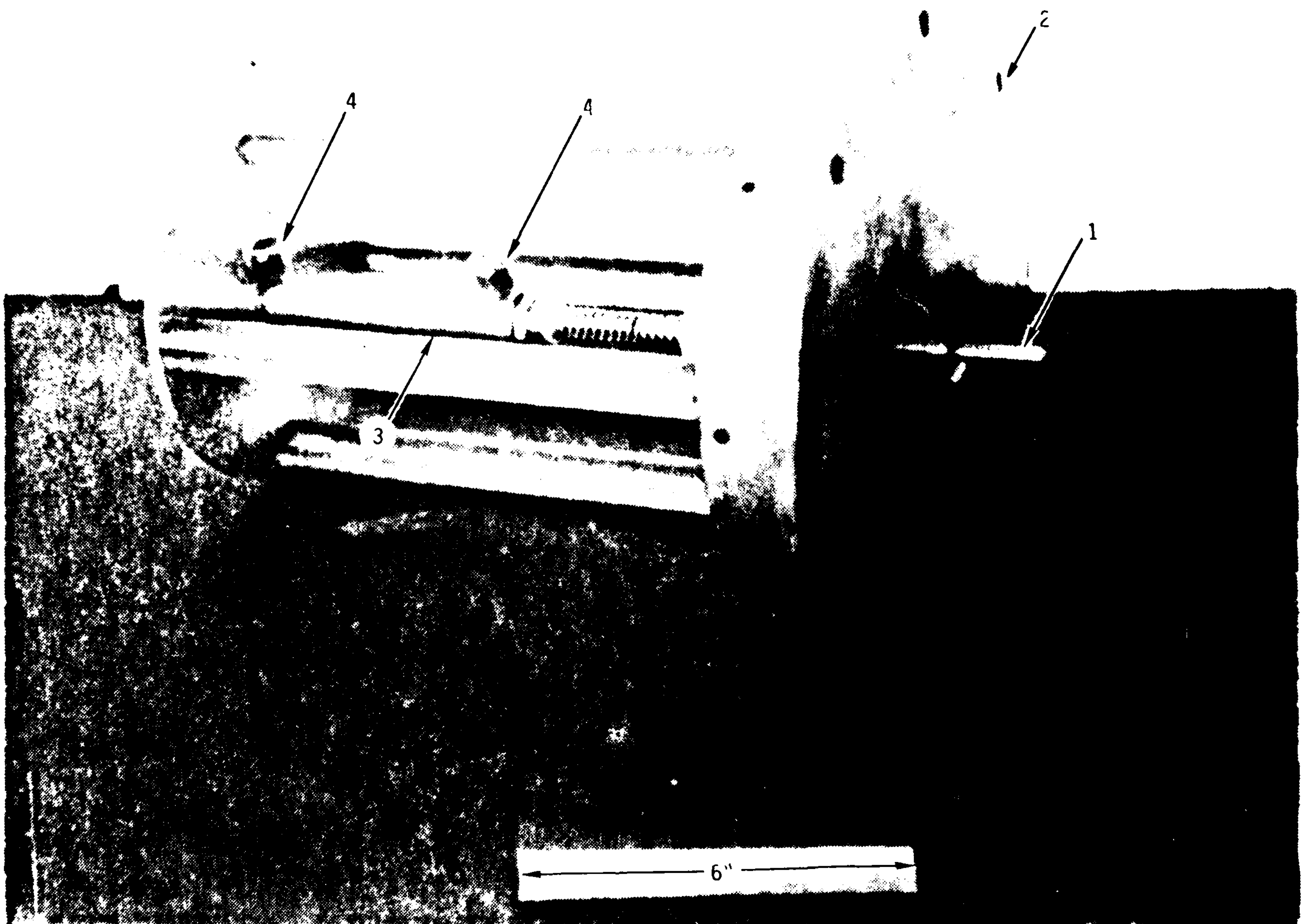

Figure 3. Pneumatic trigger for FX-100 output switch. (1) Field distorting trigger pin (partially extended); (2) Mounting flange; (3) Double-throw pneumatic cylinder; (4) High-pressure nitrogen gas lines. Trigger pin is retracted by maintaining pressure differential on high pressure N_2 lines. Reversing the differential extends the pin, distorts the fields in the gap and initiates the gap spark. Maintaining N_2 pressure in the dielectric lines above the tank pressure prevents breakdown in the lines.

Figure 4. Pneumatic trigger installed on FX-100. (1) Trigger pin (partially extended), (2) Mounting flange; (3) Output switch end of coaxial energy-storage transmission line.

triggering of the output switch and highly reproducible voltage and current pulses for the remainder of the operational lifetime of the FX-100.

The FX-100 was decommissioned in mid-August, 1981 in order to provide space for the development of the RADLAC accelerator. During the ~4-month period that it was available after making the aforementioned repairs and modifications we fired over 500 shots in the execution of the low-pressure air propagation experiments.

2. Field-Emission Diode

We designed the diode used in the FX-100 propagation experiments to produce an electron beam with a radial current distribution close to that expected for a propagating beam equilibrium. That is, the desired current distribution was a Bennett pinch, which would have a current density $j(r)=j(0)[1 + r^2/a^2]^{-2}$, where 'a' is the Bennett radius. In order to achieve a distribution that closely approximated this ideal we used a smoothly-polished graphite cathode that had a surface shape congruent to one of the static vacuum equipotential surfaces of a charged disk. Such a Rogowski surface has little static field enhancement resulting from charge concentration. This electrostatic solution is obviously not self-consistent in the presence of space-charge and magnetic fields of the intense beam produced. However, experience has shown that the field-emission from a smooth Rogowski surface can be readily controlled by selectively roughening small areas in order to provide microscopic field enhancement early in the voltage pulse.

By roughening a small circular region in the center of our FX-100 cathode (shown in Fig. 5) we were able to produce Bennett-like extracted current distributions as illustrated by Fig. 6 and Fig. 7. Figure 6 shows the diode geometry and the current distribution measured 1.3-cm from the titanium foil anode at the time of maximum diode current. From this figure it is clear that the beam-electron scatter resulting from the foil can provide an additional means for increasing the Bennett radius, if so desired. Because we wanted the smallest possible beam radius we used the thinnest foils that survived the beam (25-μm) in all of the propagation experiments. With these anodes the Bennett radius of the extracted beam was ~3 cm (Fig. 6).

From Fig. 7, which shows the temporal and spatial evolution of the beam current profile, it is evident that the beam produced by our diode had a Bennett-like radial distribution during most of the beam pulse. It is also clear that there was very little evidence of shank emission current at large radii, except possibly at very early and very late times.

3. Low-Pressure Propagation Chamber

The low-pressure air propagation experiments were performed with the electron beam injected directly into the 20-cm diameter stainless-steel propagation chamber through the 25-μm titanium-foil anode. This diameter was initially deemed large enough to insure that wall effects would not dominate the 3-cm radius beam propagation, but in retrospect it appears that the chamber should have been larger. The propagation chamber, or "drift tube", consisted of many individual 25-cm long segments bolted together with 'O'-ring sealed

Figure 5. 5-cm diameter polished graphite Rogowski-surface cathode used in FX-100 beam propagation experiments. The central 4-cm diameter area that was roughened to enhance emission is delineated for clarity.

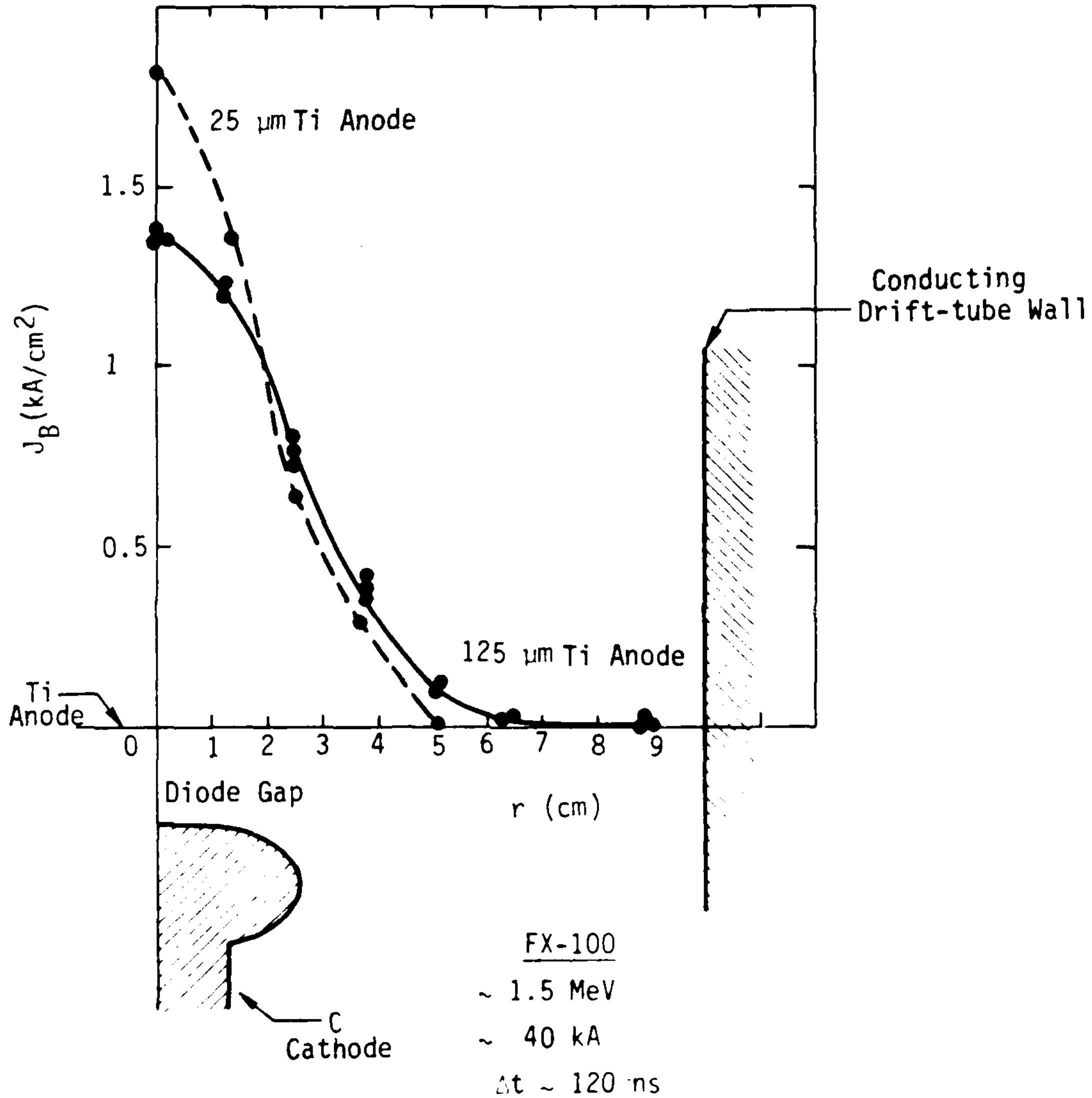

Figure 6. Multiple Faraday collector array measurements of FX-100 beam current density distribution in vacuum 1.3 cm from the anode foil. Distribution for two different foil thicknesses are shown. However, all propagation experiments were performed using 25-μm Ti foil anodes.

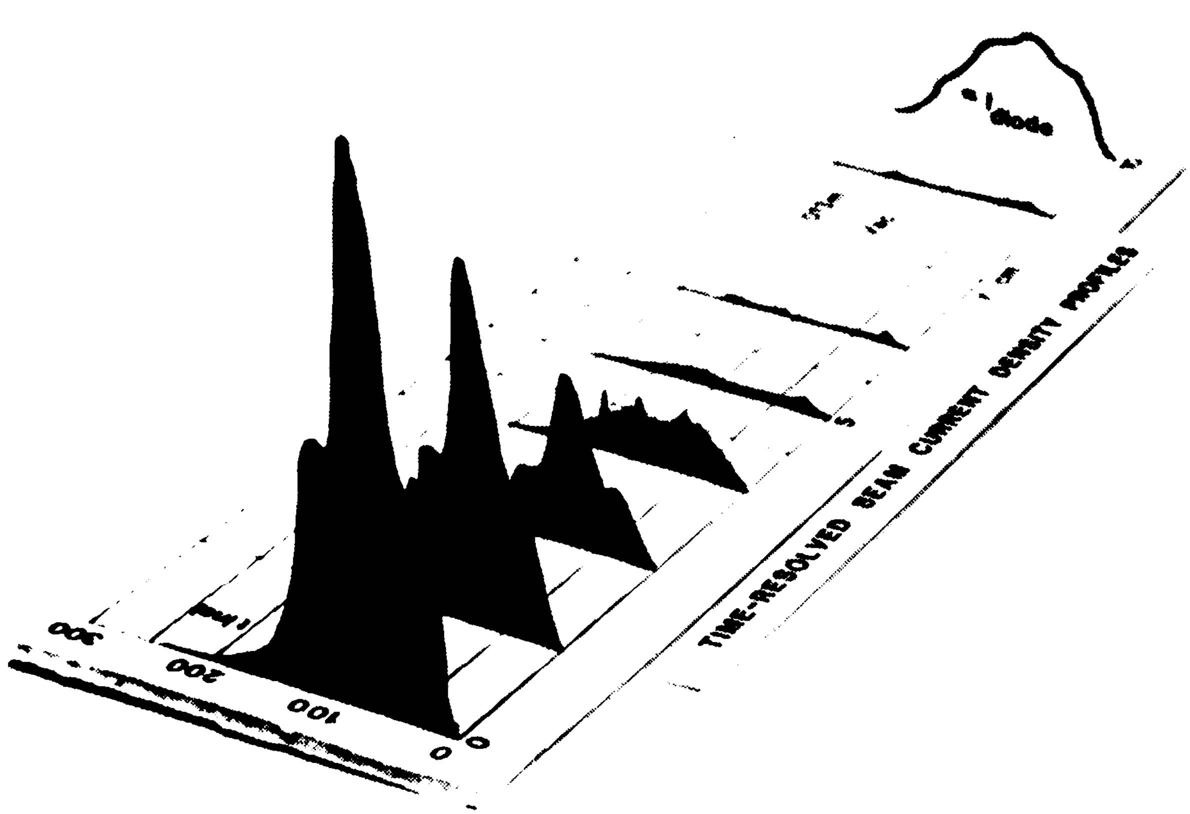

Figure 7. Time-resolved beam current density, profile measured 1.3 cm from 25-μm Ti anode foil in vacuum.

flanges. Several sections of the drift tube are shown in Fig. 1, and the maximum available length of assembled drift tube (> 5 m) is shown in Fig. 8 and Fig. 9. This modular design afforded a great amount of flexibility in the axial location of diagnostics for the propagation experiments.

The air pressure in the propagation chamber was controlled with a pumping manifold and adjustable leak (Fig. 1), and was monitored with a Granville-Philips Pirani guage that was calibrated with an oil manometer. The minimum pressure attainable with this system was ~0.1 Torr, which was low enough to cover the pressure range of interest.

Some of the experiments (eg.,multiple exposure spectroscopy) required high repetition rate firing of the FX-100 (~3-5 minute turn-around per shot). For these experiments the slow leak valve was positioned at the extremity of the drift tube to insure adequate mixing and flushing of possible air-chemistry by-products between the shots. There was no measurable pressure gradient in the tube in this configuration.

For most experiments the turn-around time was sufficiently long that air-chemistry by-products could mix and be evacuated even with the leak valve located near the pumping port. In any event, we detected no effect in our data that could be traced to the accumulation of chemistry by-products.

In order to ascertain the significance of the small amount of water vapour present in the low-humidity ambient air used for most experiments, a limited number of experiments were performed using dried air and pure nitrogen. Except that the red oxygen line emission was not observed in the pure N_2 experiments there was no discernable effects evident in the measurements.

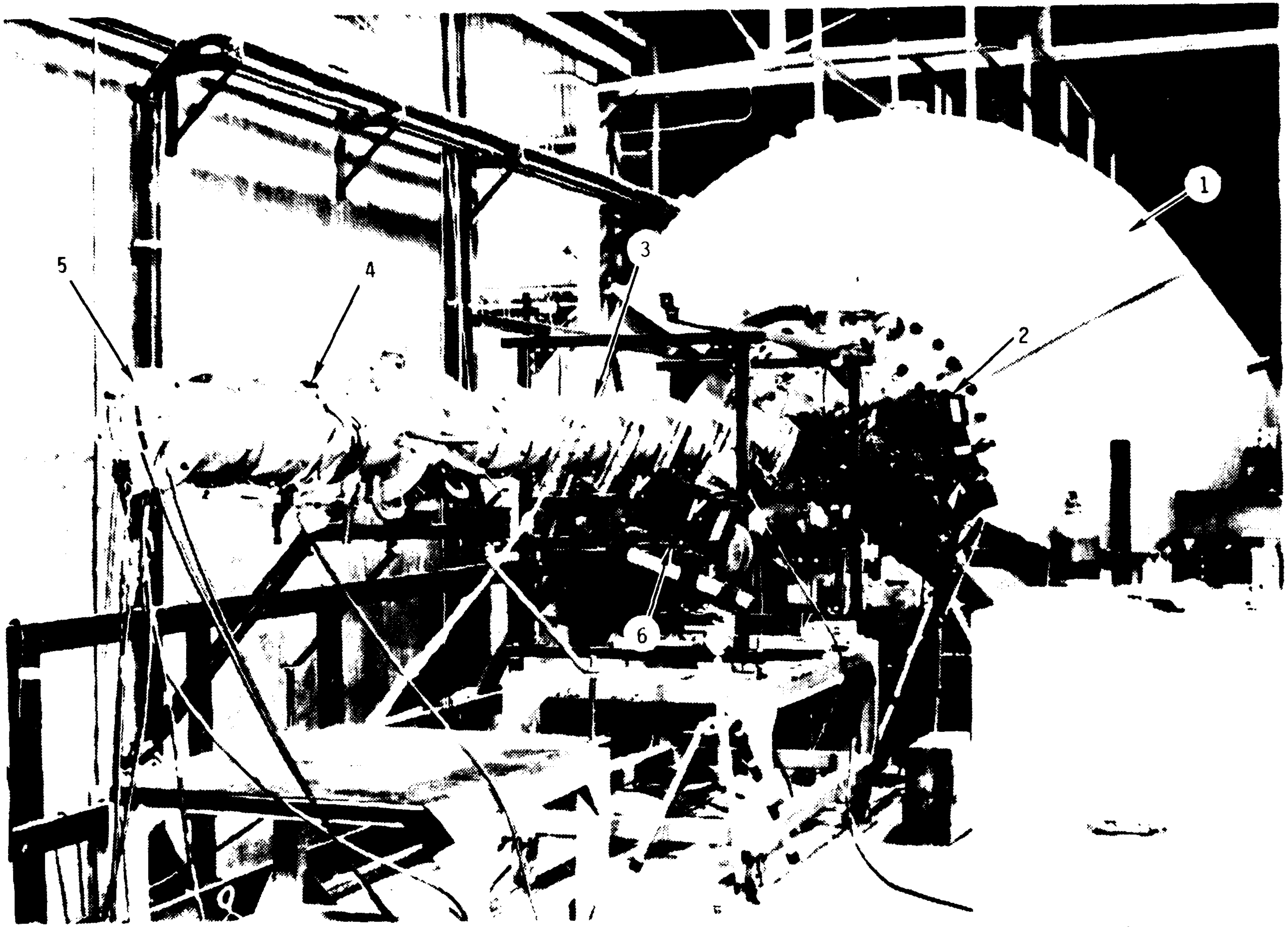

Figure 8. Assembled FX-100 low-pressure air propagation experiment. (Total length > 5 m.) (1) FX-100 tank; (2) Open-shutter camera; (3) 20-cm diameter stainless-steel drift tube; (4) Inductive current monitor; (5) Signal cables for charge collector array and carbon calorimeter; and (6) Open-shutter camera.

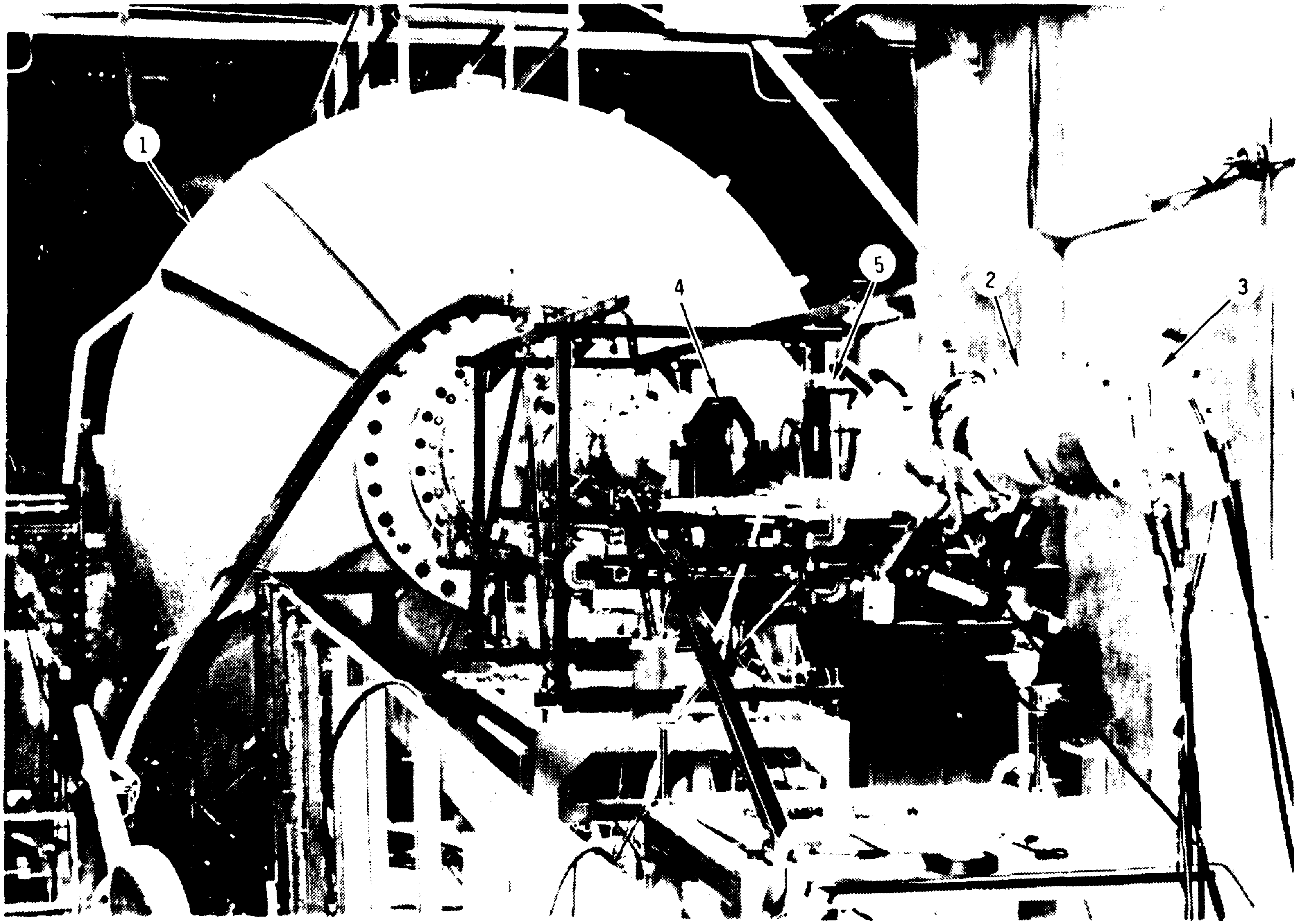

Figure 9. Assembled FX-100 low-pressure air propagation experiment. (Total length > 5 m.) (1) FX-100 tank; (2) Inductive current monitor; (3) Signal cables for array of charge collectors and carbon calorimeter; (4) First turning mirror for streak-camera optical delay path; (5) Viewing window.

4. Data Acquisition

Data acquisition for the propagation experiments was originally limited by the number of signal cables installed between the screen room and the experimental area. During the course of the experiments more cables were installed until eventually it was possible to record 12 channels of time-resolved data, at which point we exhausted the available oscilloscopes. In addition, we recorded time-integrated data, such as calorimetric measurements of the beam energy deposited in a target at the extremity of the drift tube.

All time-resolved data was recorded using Tektronix 7704 oscilloscopes with 7A11 preamplifiers. The bandwidth of this preamp-oscilloscope combination is ~150 MHz, which limited the measurable signal risetimes to ~2.5 ns in the absence of signal-cable dispersion.

The battery of oscilloscopes was triggered with a signal derived from the light emitted by the FX-100 gas output switch. We constructed a simple system consisting of a biased EGG SGD-040A solid state photodiode detector that triggered a PATCO PA-006 avalanche transistor pulse generator. This compact, battery-powered system provided a high-level (~300 V) low-jitter trigger pulse with a fast risetime. Attenuation of this signal in the screen room to a level compatible with the oscilloscopes resulted in a noisefree and reliable trigger. The delay between the onset of light emission from the output switch and the FX-100 electron beam was sufficient to record the entire beam history using 50-ns/division oscilloscope sweep speeds.

The oscilloscope trigger signal was also used to generate a timing fiducial marker in the screen room, which consisted of the differentiated and clipped output of a triggered delay generator. This marker, when added to each data signal at the oscilloscope, provided an accurate means for comparing data obtained on different diagnostic channels after accounting for the different signal cable delays. These cable delays were measured to an accuracy of ~2 ns using time-domain reflectometry techniques.

This data acquisition system allowed a resolution and comparison of photographically recorded oscilloscope traces to within ~2-4 ns, which is comparable to the limitation on the signal risetime from the signal cable dispersion and oscilloscope-preamplifier bandwidths.

5. Diagnostics

Diode Voltage and Current Monitors Interpretation of the experimental data obtained with other diagnostics requires accurate and precise monitoring of the accelerating diode voltage and diode current during the course of the propagation experiments. The diode monitors used for the FX-100 low-pressure propagation experiments are described in this section.

The voltage monitors installed on the FX-100 were found to give irreproducible signals, probably because of electrical noise and electron impact effects. We replaced them with a dielectric protected capacitive detector that gave a signal proportional to the rate of change of the diode voltage (V-dot probe).[1] This probe is a small (~2-cm diameter) copper disk positioned just inside of the outer conductor of the vacuum transmission line.

It is completely encapsulated in epoxy to avoid problems with unwanted signals resulting from low-energy electrons generated by UV irradiation, Compton currents, etc.

The probe capacitively couples to the transmission line voltage and can be represented by the equivalent circuit shown in Fig. 10.

When the load resistance is matched to the signal cable impedance ($R_2 = Z_0$) the output signal, $V_2(t)$, is related to the transmission line voltage waveform, $V_1(t)$, by the differential equation:

$$\frac{dV_2}{dt} + \frac{V_2}{RC} = \frac{R_2C_1}{RC}\frac{dV_1}{dt} \quad , \tag{1}$$

where $R = R_1 + R_2$ and $C = C_1 + C_2$. Clearly there are two possible modes of operation depending on the value of RC. If RC is much less than the fastest rate of change of the signal ($RC \ll \tau$), the second term on the left side of Eq. 1 dominates, and the output signal, V_2, is proportional to the derivative of the transmission line waveform;

$$V_2 = R_2C_1\frac{dV_1}{dt} \quad . \tag{2}$$

This is referred to as the "V-dot" mode of operation, and the signal requires further integration to obtain the input voltage waveform, V_1.

On the other hand, if RC is much greater than the longest time of interest, the first term on the left side of Eq. 1 dominates, and the probe

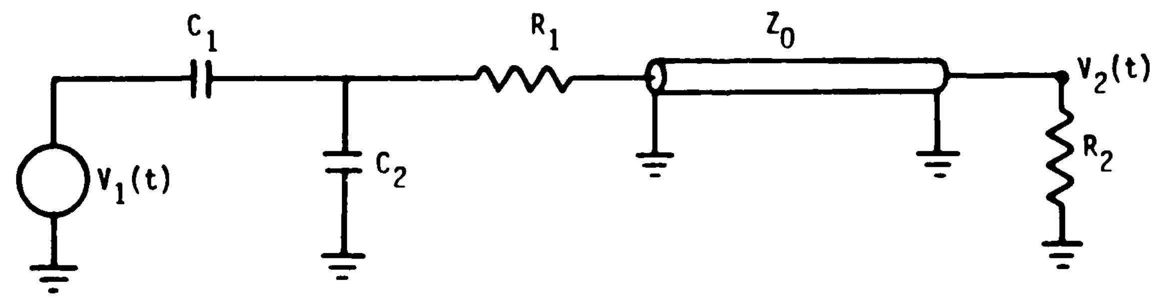

Figure 10. Equivalent circuit of FX-100 diode-voltage capacitive monitor.

acts as a capacitive voltage divider[2,3] with the output signal, V_2, directly proportional to the transmission line voltage, V_1;

$$V_2 = \frac{R_2 C_1}{RC} V_1 \quad . \tag{3}$$

It is clear that a large series resistor, R_1, or additional integrating capacitance, C_2, would be required for the voltage division mode of operation. Because of the high level of electromagnetic noise in the experimental area, the V-dot mode of operation was chosen instead for the FX-100 probes. In this mode, the high signal level was transmitted to the screen room and integrated there with a passive integrator having RC ~ 2 μs with the result that unwanted electromagnetic noise picked up by the signal cables was highly attenuated. In addition to this inherent noise immunity and their compact construction, advantages of V-dot capacitive monitors over resistive dividers for the FX-100 experiments are that they do not distort the fields in the region of measurements, they are immune to surface tracking and breakdown, they do not shunt the load with a lower impedance, and they require no balancing of resistive and capacitive elements or complicated voltage-grading structures.

The V-dot probe was located in the vacuum transmission line within ~0.5 m of the diode anode-cathode gap. It was found that inductive correction for the final short section of transmission line between the monitor and the gap was unnecessary for these experiments. This V-dot probe provided a highly reliable and reproducible monitor of the diode accelerating voltage on each shot.

We monitored the diode current with a Rogowski belt[4,5] supplied by the AFWL. Several of these were made available for the propagation experiments. The Rogowski loop in these current monitors was embedded in an annular groove in a flange that could be inserted at any point in the drift tube. The loop used as a diode-current monitor was positioned on the section of drift tube that we used to form the final vacuum transmission line segment. That is, the current was monitored in the vacuum transmission line within 25-cm of the diode anode-cathode gap (see Fig. 1).

Typical FX-100 diode current and voltage waveforms at the charging voltage used for these experiments are shown in Fig. 2.

<u>Inductive Current Shunts</u> One of our primary research objectives is a study of the beam-head erosion process, which can lead to rapid net-current risetimes in the drift tube. For these measurements we designed and constructed inductive shunt[1] net-current detectors that had substantially faster response times than the available Rogowski loops.

The inductive-shunt current monitors consisted of epoxy-filled annular channels machined in an aluminum flange that was inserted between two sections of the drift tube. As can be seen in Fig. 11, the return current flowing on the drift-tube inner surface was forced to flow around the inside surface of the annular channel. A voltage was thus induced across the insulating gap by the time-varying magnetic field in the annular channel, In the limit of time-scales short compared with the magnetic diffusion time into the aluminum shunt, the voltage appearing around the channel is purely inductive and can be

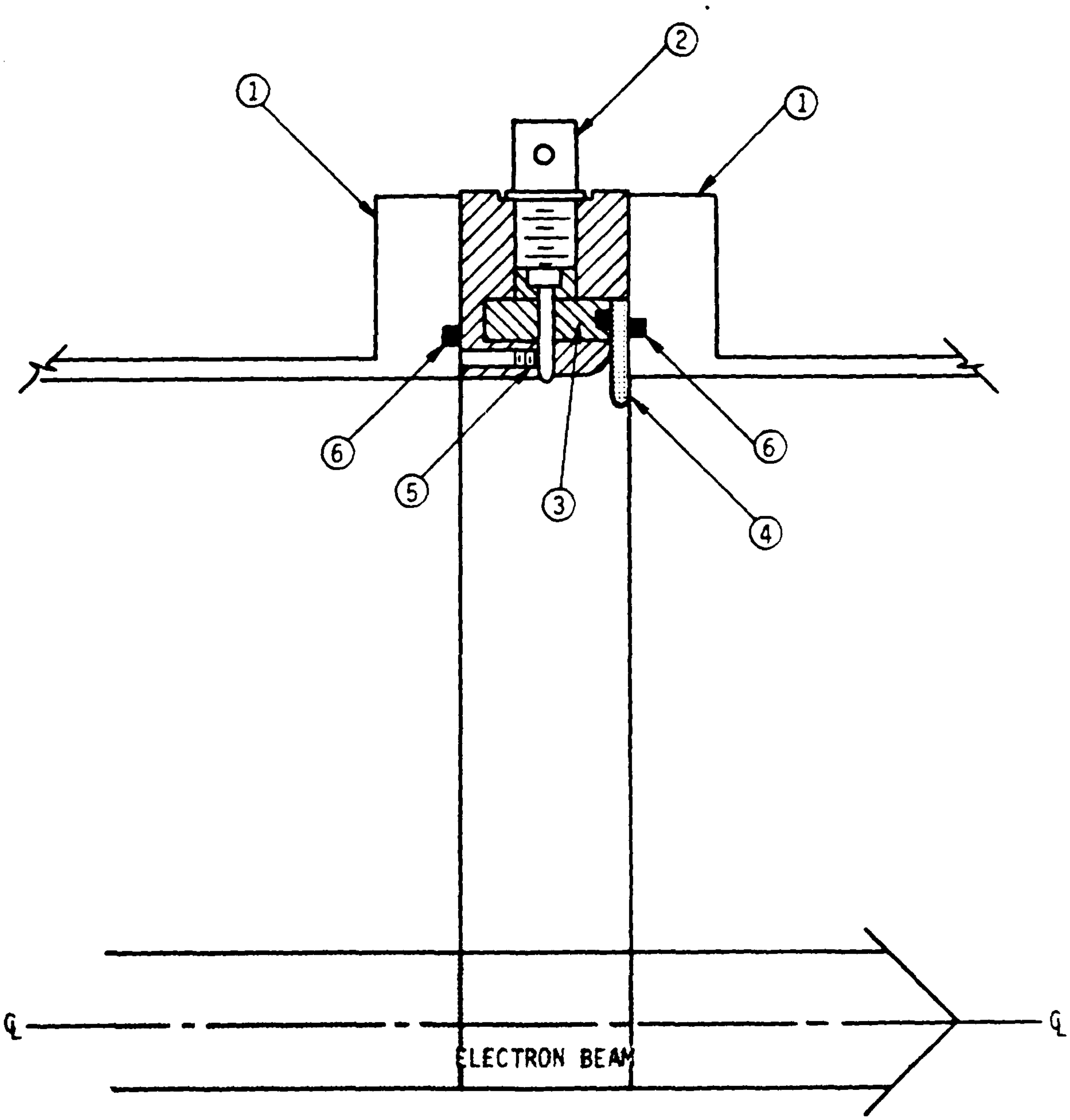

Figure 11. Fast-risetime inductive-shunt current monitor installed between two sections of drift tube (1). (2) is BNC signal-output. (3) is epoxy filled annular channel. (4) is polyethylene insulating gasket. (5) is set screw to provide electrical contact for detector pin. (6) are 'O' ring vacuum seals.

detected by completing a flux loop as shown in Fig. 11. The inductive component of the voltage that appears at the pick-up point is given by;

$$V = -\frac{d\phi}{dt} = -\frac{\mu_o}{2\pi}\frac{dI}{dt}\int\frac{drdz}{r} \quad , \qquad (4)$$

Substituting the inductance, L, for the FX-100 shunt geometry into this equation gives

$$V = -\frac{\mu_o w}{2\pi}\ln\frac{r_o}{r_i}\frac{dI}{dt} \quad , \qquad (5)$$

where r_o is the outer radius of the channel, r_i is the inner radius, and w is the channel depth below the pickup termination.

An advantage of this type of current monitor is that it provides a simple penetration of the conducting drift tube that results in a well-shielded coaxial signal-transmission geometry. In addition, the narrow insulating gap is a wave guide beyond cutoff for low-frequency modes other than the TEM mode that is excited by the time-varying axial current, and thus provides shielding from unwanted electromagnetic noise. Furthermore, although a single voltage pickup is sufficient for an azimuthally symmetric system such as a coaxial transmission line, asymmetric current channels can be accurately measured by summing the signals from several voltage pick-ups separated by equal increments of angle. In this respect, the inductive-shunt monitor can be thought of as the well-shielded limit of a Rogowski belt[4,5] current monitor. Finally, the achievable risetime of an inductive-shunt monitor is substantially faster than for a Rogowski coil because the output signals are summed in parallel rather than in series, thus significantly reducing the inductance and L/R risetime.

For the FX-100 propagation experiments the eight output signals from each shunt were summed in a transformer signal adder that limited the had the capability for summing subnanosecond signals. These net current monitors positioned at various axial positions during the different phases of the program. They provided reliable, low-noise measurements of the net current in the drift tube.

Subminiature Faraday-Cup Array An array of fast-response Faraday charge collectors was developed to measure the time-resolved current distribution. The data from this array provided a picture of the evolution of the radial current profile at a particular axial location without relying on shot-to-shot reproducibility, which is certain to be poor in any experiment involving instabilities. Each detector in the array consisted of a length of Uniform Tubes Co. UT-47 rigid coaxial transmission line that was embedded in a massive graphite block, as shown in Fig. 1, Appendix A. and also Fig. 1, Appendix E. The initial radial spacing of the detectors was chosen to be 1.25 cm. However, our early discovery of significant beam current carried outside of the Bennett radius caused us to modify the array by inceasing the detector density at large radii. The collectors were shielded from the ionized-gas electrons and low-energy secondaries by a thin graphite sheet in the original array developed during the FX-25 experiments. The array that we constructed for the FX-100 propagation experiments used a 125-μm thick titanium foil plasma shield that was insulated from the collectors with 25-μm thick Kapton dielectric foil. Of all dielectric materials that we have experimented with, Kapton (a polyimide) exhibits the most resistance to the intense beam irradiation. Although we replaced the shielding and insulating foils on a regular basis as a precaution, we had few problems with insulator breakdown in this array.

Electron scattering in the array materials results in an energy-sensitive effective collection area. The reason for this is that the more energetic electrons have a higher probability of scattering into the collector because of their greater depth of penetration. We studied this effect by using the Monte Carlo radiation transport code CYLTRAN to obtain the energy sensitivity of the effective collection area. Details of this study are reported in Appendix E. The energy sensitivity appears to be modest over a wide range of energies around the peak energy of the FX-100 beam, but the collection area for these high-energy electrons is significantly (factor of ~2) enhanced over the geometrical area. As a consequence, such a detector cannot be readily adapted to measurements of net current because of the vastly different sensitivities to beam and plasma currents.

The developmental experiments using the FX-25 beam demonstrated that the risetime for these coaxial collectors driving a matched and properly terminated signal cable was limited only by the cable dispersion and oscilloscopes. In those experiments 1-ns risetimes were observed. The combination of the high level signal generated by these collectors and the unbroken coaxially-shielded construction resulted in a high signal-to-noise ratio on the oscillograms. The injected current distribution shown in Fig. 2 was obtained with this array, and many examples of stable and hollowing-mode unstable current profiles are included in the various appendices.

Carbon Calorimetry The graphite block containing the array of Faraday collectors was also used as a beam calorimeter by measuring its temperature rise with a thermistor. Because carbon calorimetry integrates over time, space, and the beam-energy distribution, it is impossible to distinguish beam-electron energy losses from loss of transported charge without simultaneous, precise measurements of beam current. The carbon calorimeter is quite simple to field in this kind of experiment, and it is the traditional diagnostic for definition of the propagation pressure window. Our use of a thermistor sensor simplified the measurements. The thermistor was found to be insensitive to radiation, and when calibrated, it was found to have a linear response over the restricted temperature range of this application.

Incorporation of the charge-collector array into the calorimeter block enabled us to simultaneously determine the beam energy transport and the temporal evolution of the radial current profile at any given axial location. A limited number of measurements were made with the calorimeter in vacuum, and isolated from the ionized-gas channel by a titanium foil. The results of these measurements indicated that the energy deposited on the calorimeter from the plasma was not a significant fraction of the beam energy.

These calorimetric measurements of beam energy transported through the drift tube filled with air at different pressures were used to establish the pressure window for maximum transport shown in Fig. 15.

Radiochromic Foil Dosimetry Blue cellophane is one of the most widely used radiochromic film dosimeters.[6] Blue cellophane exposed to an intense electron beam such as generated by the FX-100 exhibits effects ranging from bleaching of the organic dye through destruction of the film. Although the sandwich structure of the film to some extent discriminates against bleaching resulting from low-energy secondaries and plasma electrons, a sufficiently large low-energy current can produce misleading damage because of the reduced electron range. A means of separating the beam and plasma channel radial structures by comparing bleaching foil records with X-ray pinhole camera pictures of the beam electron bremsstrahlung from a wire mesh was suggested in the proposal for these experiments. We chose instead to employ a more simple method, we shielded the blue cellophane from low-energy electrons with thin metal foils. Typically, we used 25-μm thick titanium-foil shields, which will stop electrons with less than ~180-keV kinetic energy.

Shielded blue-cellophane film dosimeters were used on many of the low-pressure propagation shots to obtain time-integrated records of the beam radial profile at various axial locations in the drift tube. An example of the beam profile record obtained using this technique is shown in Fig. 18, Appendix D.

Thermoluminescent Dosimetry Lithium flouride thermoluminescent dosimeters (TLDs) were on a limited number of shots to verify the beam current profiles measured with the subminiature Faraday cup array. Exposure of an array of dosimeters to the gamma dose produced by the beam striking a thick target provided a more quantitative record of the time-integrated beam profile than that produced by blue-cellophane film dosimetry because the linear response range of the blue-cellophane film was almost always exceeded for the high current density FX-100 beam.

Open Shutter Photography Time-integrated open-shutter photographs of the beam and ionized-channel excited air emission were obtained at viewing ports located at axial positions close to the diode (shown in Fig. 12) and 4.5-m from the diode. The symmetry properties of the drift tube were not disrupted by the ports because a return-current carrying screen was incorporated in each. The exposures with these cameras were recorded with Polaroid Type 58 (ASA 75 speed) color film.

Because of the overexposure resulting from weak, but persistant, light, and the time-integration of motion of the beam or channel or both, open-shutter photography must be thought of as an easily-fielded "early warning" diagnostic to identify effects that require further, more careful, spectral or temporal resolution. A discussion of many of the issues involved in interpretation of the data obtained in this experiment with optical emission diagnostics is contained in Appendix I.

A point not covered in that appendix is the following. As shown in the appendix, the excitation of the upper level of the radiative transitions by the low-energy plasma electrons is $\sim(kT_e)^{1/2}(1 + kT_e/E_o) \exp(-kT_e/E_o)$, where T_e is the temperature of the cold electrons, and E_o is the threshold of the excitation cross-section, $E_o \gg kT_e$. The radiation is, therefore, very sensitive to the population of the high-energy tail of the electron distribution. It is well known that high electric fields can significantly distort the tail of the distribution. For example, a modest E/p of about 100 V/cm/Torr can increase the effective temperature of the tail of the distribution by a factor of 5 or more. As a consequence, the visible emission can be vastly different from regions having the same gas temperature and plasma

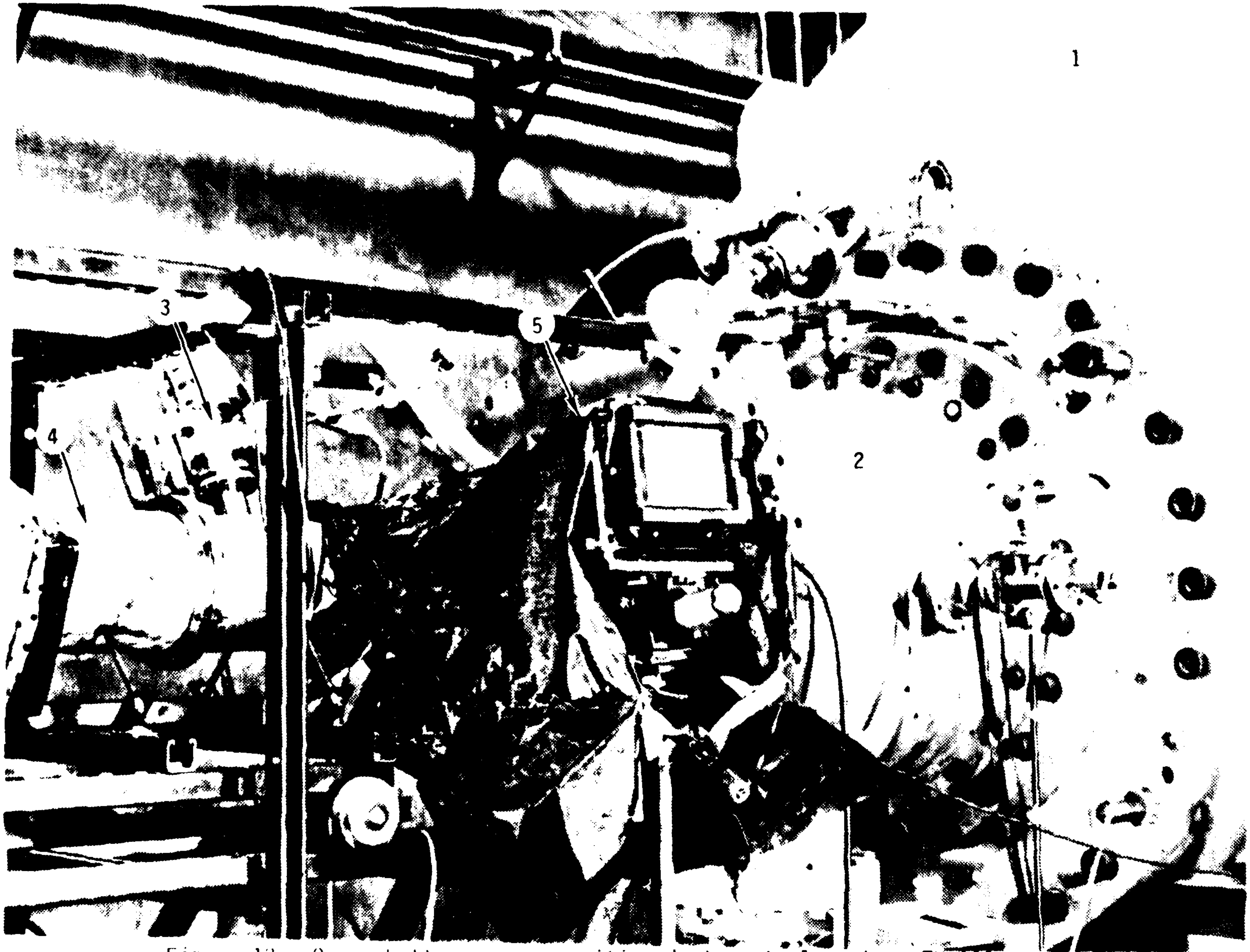

Figure 12. Open-shutter camera positioned at port closest to FX-100 diode. (1) FX-100 tank; (2) Vacuum transmission line; (3) Drift tube pumping manifold; (4) Drift tube; (5) Open-shutter camera.

electron density, but having different widely disparing values of E/p. This may be the cause of some of the more spectacular effects seen in both open-shutter and time-resolved photographs.

Examples of FX-100 open shutter photographs are shown in Fig. 19 and Fig. 24.

Fast Time-Resolved Photography An Imacon 790 image-converter camera on loan from Los Alamos National Laboratory was used to obtain streak and framing photographs of the emission from the beam and plasma channel. These observations were made through the same port at 4.5 m that was used for open-shutter photography on other shots. In order to record the head of the beam it was necessary to delay the light by folding the optical path and locating the Imacon camera next to the FX-100 output switch. The camera trigger was derived directly from the light from the FX-100 switch. This arrangement, shown in Fig. 13, provided sufficient delay of the beam light that the internal triggering delay of camera did not prevent recording the beam head. A 1200-mm Questar collection lens at the camera provided adequate magnification and light intensity that intermediate relay lenses were unnecessary. Streak photographs obtained with this system are shown in Fig. 17 and Fig. 18, and a framing sequence is shown in Fig. 23.

Spectroscopy Time-integrated spectra were obtained at a single pressure (0.35 Torr) using as a dispersing instrument a Jarell-Ash 1/2-m Fastie-Ebert spectrometer supplied by the AFWL. The grating used had 1200 grooves/mm and

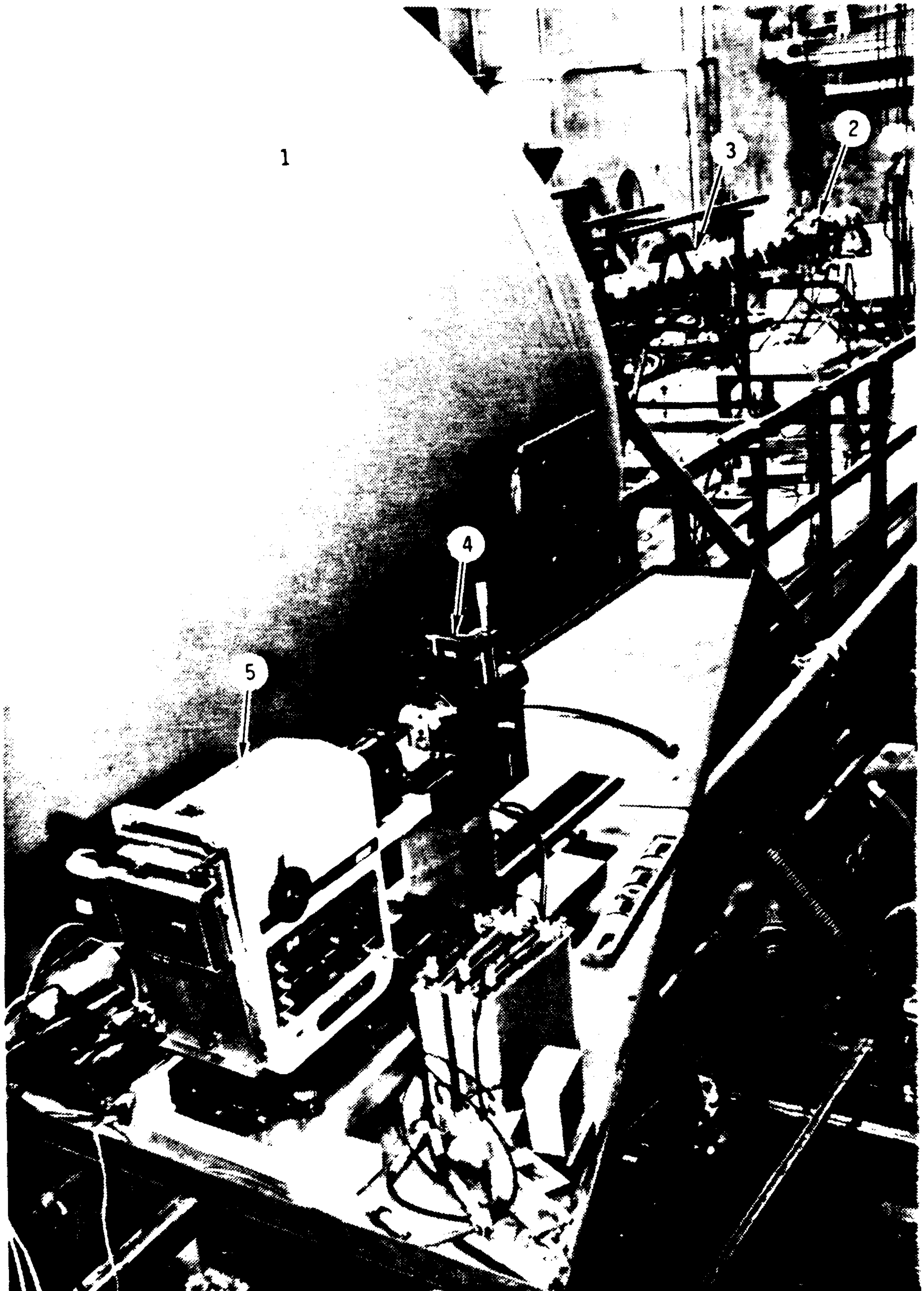

Figure 13. Time-resolved photography experimental arrangement. (1) FX-100 tank; (2) Beam viewing port and first turning mirror (final mirror is out of view); (3) Drift tube; (4) Questar 1200-mm f.l. optics; (5) Imacon 790 image converter camera.

was blazed at 5500 Å. A color-corrected 85-mm camera lens was used to image the beam channel on the input slit in order to provide spatial resolution of the emitted light. All spectra were obtained at the 4.5-m port position. The port material was acrylic, which limited the spectra to the wavelength range above ~3500 Å, although it is doubtful if the Polaroid Type 57 (ASA 3000 speed) film that we used would have had adequate sensitivity below this cutoff. An example of a densitometer scan of a spatially resolved, time-integrated spectrum obtained with this system is shown in Fig. 20.

6. Propagation Experiments

The FX-100 low-pressure air propagation experiments were performed in several different experimental runs, each with the specific diagnostics needed to address a limited set of particular issues. This strategy were necessary because of the limited number of data channels that were available for our use. Furthermore, the impending demise of the FX-100 generator was always foremost in our thinking, and in many cases we hurried though an experimental run more rapidly than we would have liked, in order that we could complete all the baseline measurements before the accelerator was decomissioned.

Our first set of experimental runs was designed to delineate the stable-propagation pressure window with carbon calorimetry, while at the same time accumulating measurements of the spatial current distribution with the charge-collector array. Other diagnostics fielded to provide corroboration of the current distribution included radiochromic-film dosimetry, TLD arrays, and openshutter photography. Because of our discovery of the unexpected "halo" of current surrounding the central beam, we devoted a number of shots to extensive investigations into its cause. These included the use of a series of carbon collimators at the anode foil in order to eliminate the possibility that shank emission in the diode was causing the halo current. It was not.

Because the propagation pressure window is also delineated by a minimum in the net current,[7] we devoted a limited number of shots to measurements of net and beam currents at various axial positions. The importance of the channel conductivity and the possibility of using visible light emitted to obtain information about this parameter led us to design an extensive series of runs devoted to optical diagnostics, for example, spectroscopy and time-resolved streak and framing photography. Finally, a limited test of a compact magnetic beta-spectrometer designed and constructed at Los Alamos Scientific Laboratory was made in order to test the feasibility of using this design in the second year low-pressure propagation experiments.

The diagnostics used and pressures surveyed in these experiments is tabulated in Appendix H. These experiments produced a large bank of data, all of which has not been fully analyzed. The analysis of these data continues as an ongoing project.

7. Simulations

Under a separate contract a linearized, three-dimensional, fully electromagnetic particle-in-cell code (KMRAD) was written to investigate resistive instabilities. KMRAD was used to predict instability growth and convention rates in the beam body for the parameters of the FX-100 experiments. Under yet another contract MRC developed a propagation code, CPROP, based on the two-dimensional, relativistic, electromagnetic, particle-in-cell beam simulation code CCUBE. CPROP is being used to investigate the physics of the nose-coupled hollowing instability, including the effects of nose blowoff at injection, ohmic energy losses, conductivity generation, and return current formation. This code treats blowoff, ohmic losses, beam hollowing, and return currents by direct self-consistent numerical integration of the Maxwell equations and the single particle relativistic equations of motion. Conductivity has been based on models developed at Lawrence Livermore National Laboratory. Improved models more appropriate for the low-pressure experiments at AFWL are now being developed at MRC for DARPA and will be added to CPROP in due course. Details of the comparisons between KMRAD and CPROP simulations and the experiments are to be found in Appendix G.

C. Experimental Results and Discussion

In both the FX-25 and FX-100 experiments the energy deposited in a calorimeter at the end of the drift tube was used to define the propagation window in pressure. This measurement integrates over both particle energy and current and is not necessarily indicative of electron kinetic energy loss. For example, we found in our experiments that the low and high pressure limits of the propagation window were largely determined by loss of particles from the beam, rather than by beam-electron kinetic energy loss. In Fig. 14 is shown the beam-current density measured on axis at the end of the FX-25 drift tube at different pressures. Here one can clearly see the definition of the propagation window at high pressures through the loss of the beam tail, and at low pressures through the erosion of the beam head. The current history measured at the diode can be overlaid on these data as an envelope, but has been omitted for clarity. It is also evident that there is a regime of pressure in which both nose-erosion and tail-loss are simultaneously limiting the beam charge transport through the 3-m drift tube. The propagation window for the FX-100 is shown in Fig. 15. Two measurements of net current for pressures on either side of the window "center" for the FX-100 beam are shown in Fig. 16. It appears that nose-erosion was not so significant for this beam as for the FX-25, however, it must be remembered that the FX-100 pulsewidth was ~6 times that of the FX-25 to begin with, and, therefore, the loss of calorimetrically measured transported energy resulting from equivalent erosion of transported charge would not be so large a fraction of the total in the FX-100 experiments as in the FX-25 experiments. The fact that erosion of the FX-100 beam did not play so large a role as for the FX-25 beam resulted in the

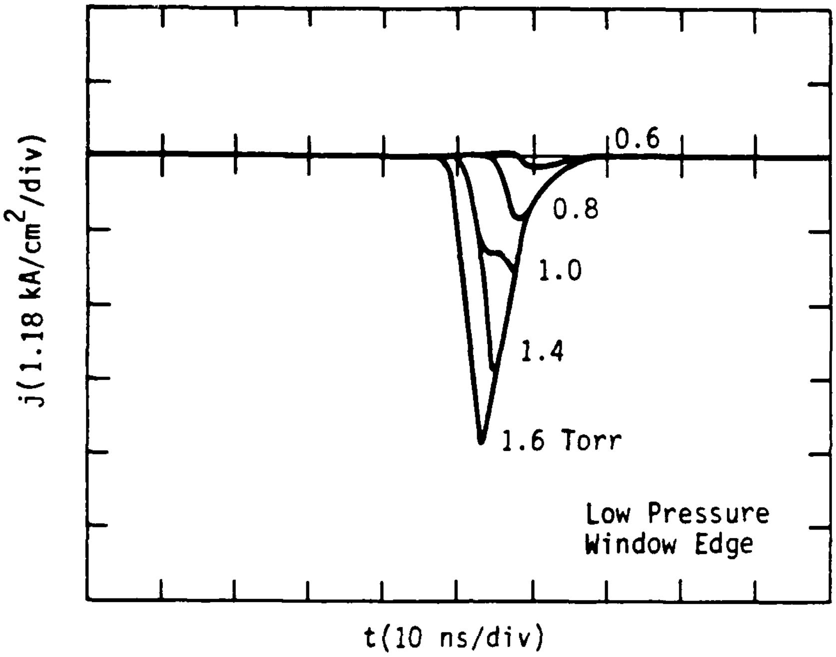

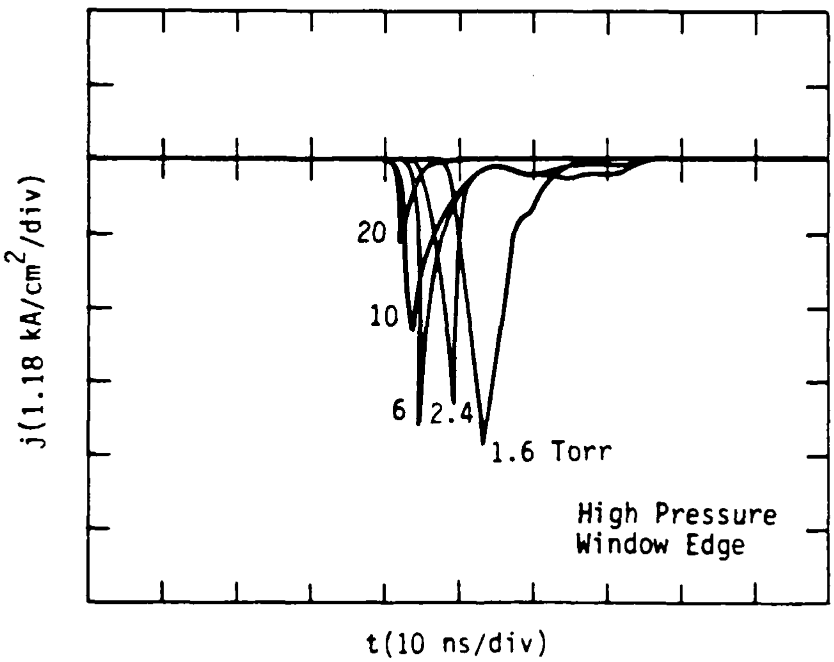

Figure 14. FX-25 beam current density on axis for different pressures. Maximum energy transport was at 1.6 Torr. The current density near the diode had a waveform that approximated the envelope of these signals. The erosion of the beam nose is clearly evident at pressures below 1.6 Torr (upper). At higher pressures both nose erosion and tail loss resulting from hosing are evident (lower).

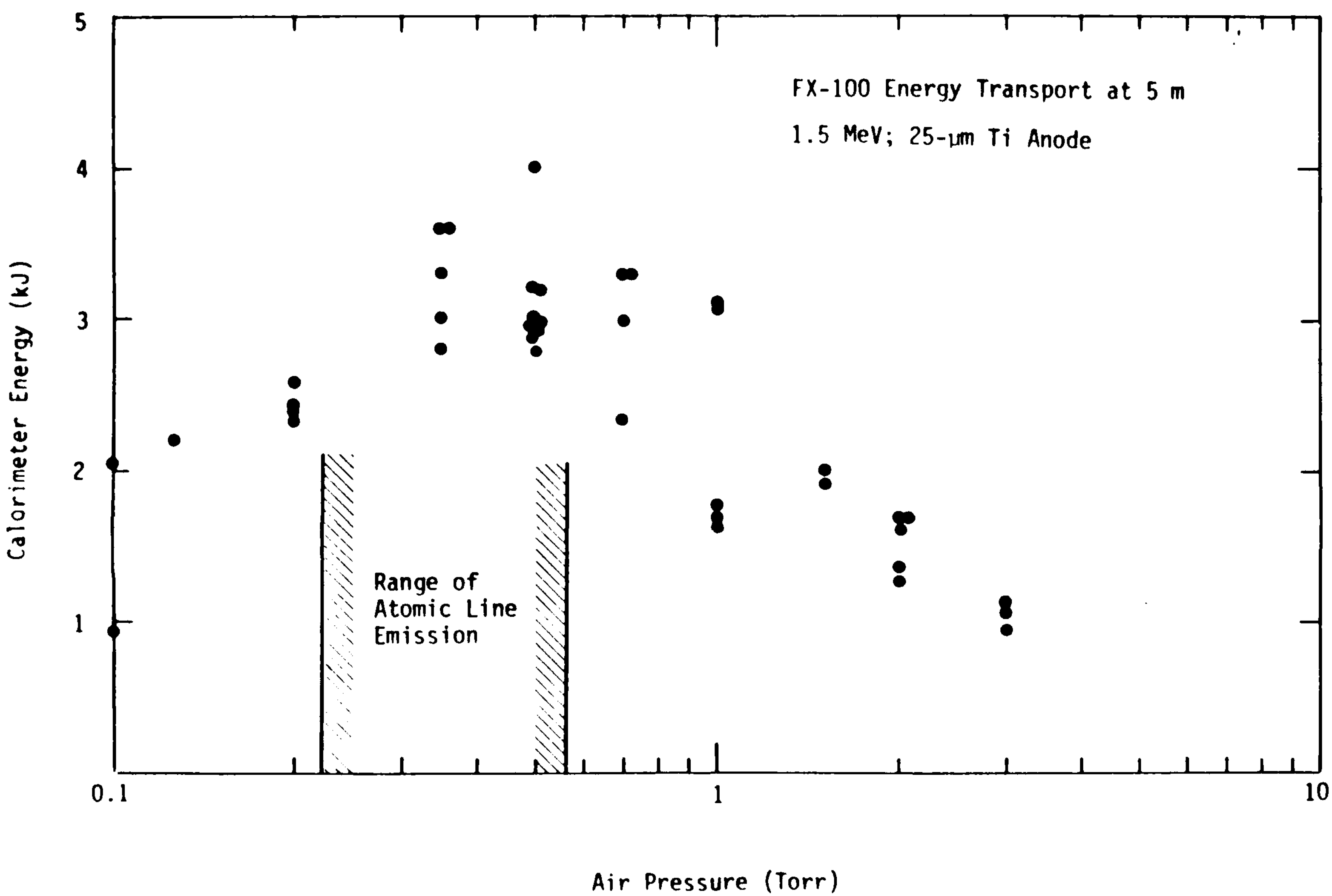

Figure 15. FX-100 propagation window in air for 5-m propagation length. In the range indicated there was intense emission of atomic line radiation as well as the characteristic molecular band emission.

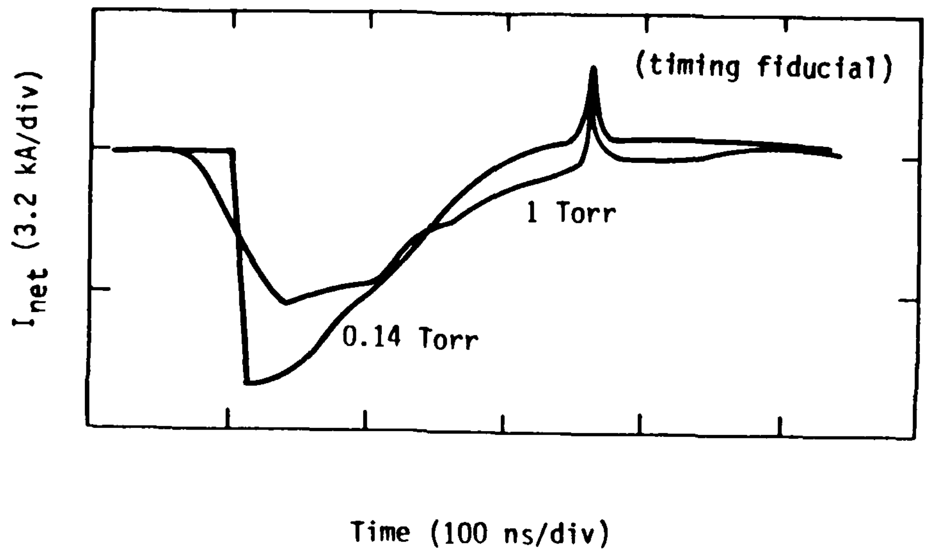

Figure 16. Net current measured in FX-100 propagation experiments at high and low air pressures in the propagation window. The pulse sharpening seen at pressures lower than that for maximum energy transport (~ 0.5 Torr) is thought to result from rapid loss of the beam front and subsequent slow erosion.

comparatively gentle decrease on the low-energy side of the window. The erosion of the beam head can be seen in streak photographs taken at pressures lower than the window center. These are shown in Fig. 17. In Fig. 18 we show streak photographs taken at pressures on the high side of the window, and here it is clearly seen that the loss of the beam tail is the result of hosing of the beam into the wall prior to its reaching the observation port at 4.5 m. Note especially that the hose in Fig. 18 (b) appears to be convective, and that in Fig. 18 (c) a piece of the beam has been detached from the head by the extreme motion of the hose. We should emphasize that we always detected a small piece of the beam head transported to the end of the tube even in the presence of the most violent hosing at pressures in excess of 20 Torr. A small piece of the beam head propagating significant distances on axis has apparently been observed in full-density air-propagation experiments[8,9] on large accelerators, and there was some circumstantial evidence for this in our full-density FX-25 experiments. This was true for both FX experiments, and may be an initial indication of the lack of nose-hose coupling at these experimental parameters. It should be mentioned that this effect has been observed in many prior propagation experiments.[7,8,9]

In the FX-100 experiments the pressure window for propagation was also delineated by vivid displays of visible emission as is illustrated by the open-shutter photographs in Fig. 19. Spatially resolved spectral measurements of the light emitted showed that in a concentrated region near the axis much of the emission was from dissociated and ionized nitrogen (Fig. 20). Because it requires ~24 eV to form this species, we infer a high energy density for the ionized gas on axis. The radial extent of the high energy region is much less

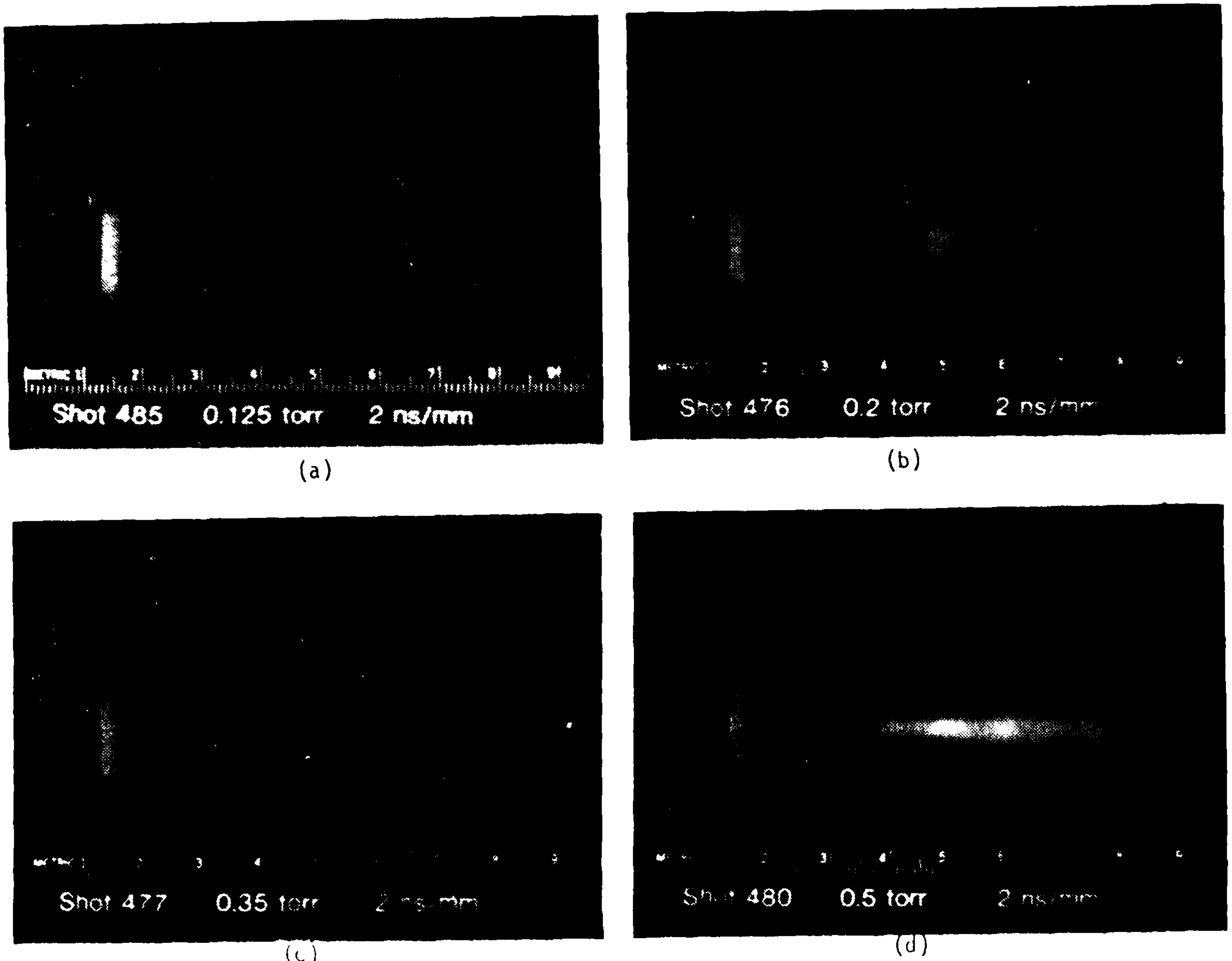

Figure 17. Streak-camera photographs of the beam-excited air emission at Z = 4.5-m as pressure is increased from below the propagation pressure window (a) to the center of the window (d). (Ignore the image converter-tube blemish in the far left of each photograph.) The beam head is at the left of each streak (taken through a vertical slit. The delay in start of emission in (a) as compared with (d) is presumably the result of erosion at lower pressures.

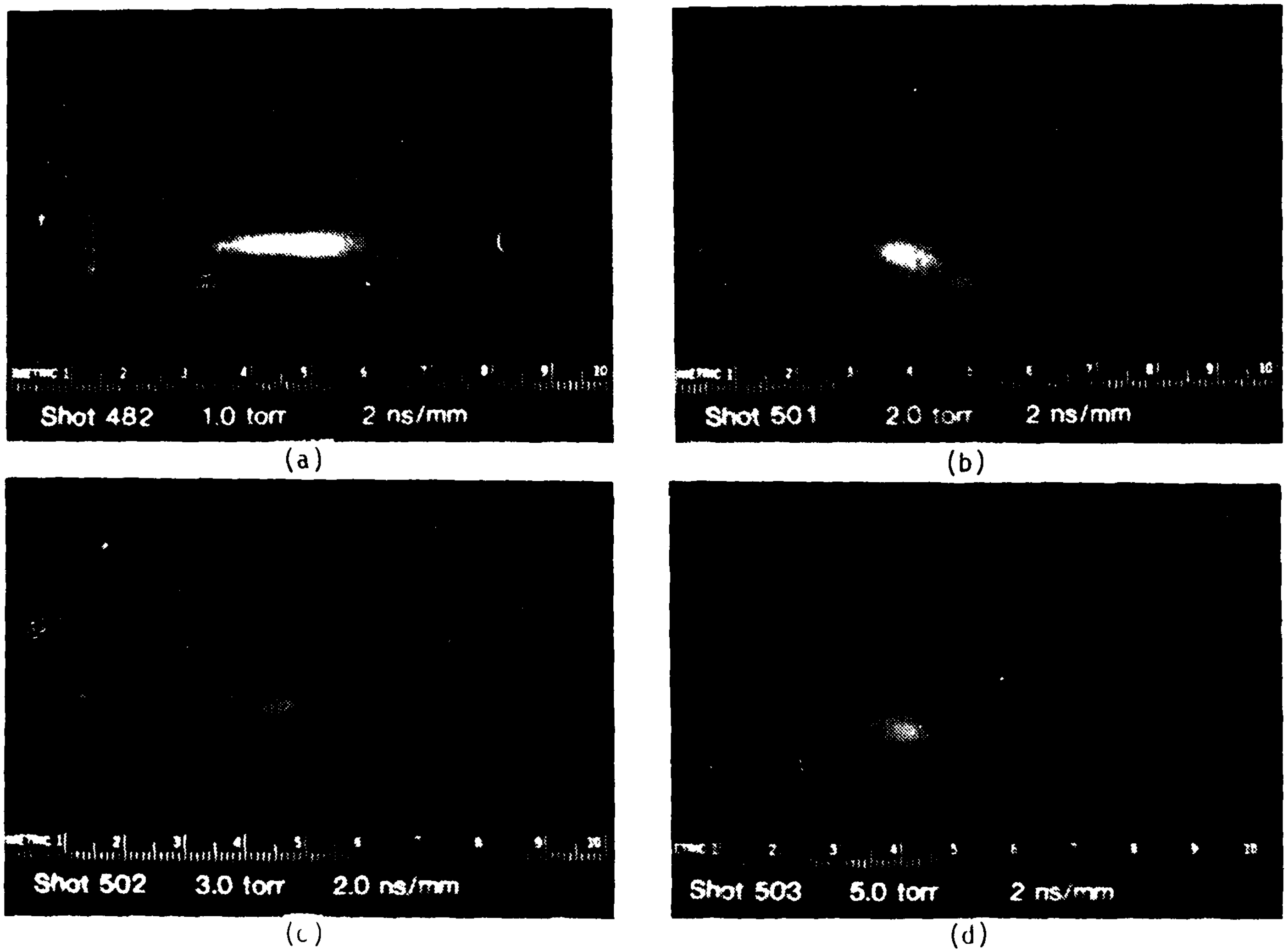

Figure 18. Streak-camera photographs of the FX-100 beam at 4.5-m as air pressure is increased above the propagation window showing loss of the tail of the beam. Figures (b) and (c) show especially clear evidence of hosing in the tail.

Figure 19. FX-100 open-shutter photographs at Z = 4.5 m and pressures spanning the propagation window showing the molecular band emission at high and low pressures and atomic (O) line emission at intermediate pressures. (Beam propagating left to right, circular aperture 17.5 cm diameter). Note the apparent annular halo of emission surrounding the beam.

0.7 Torr

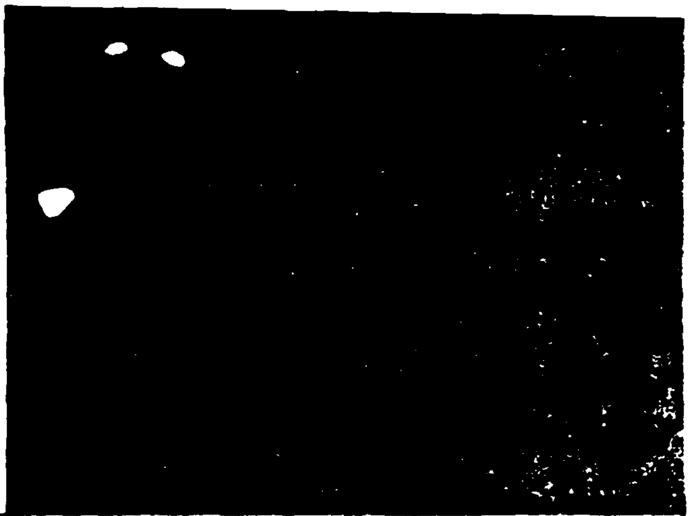

0.25 Torr

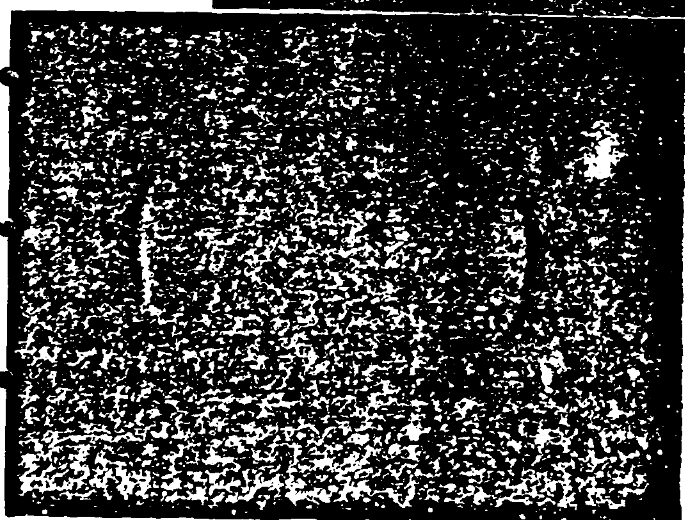

0.13 Torr

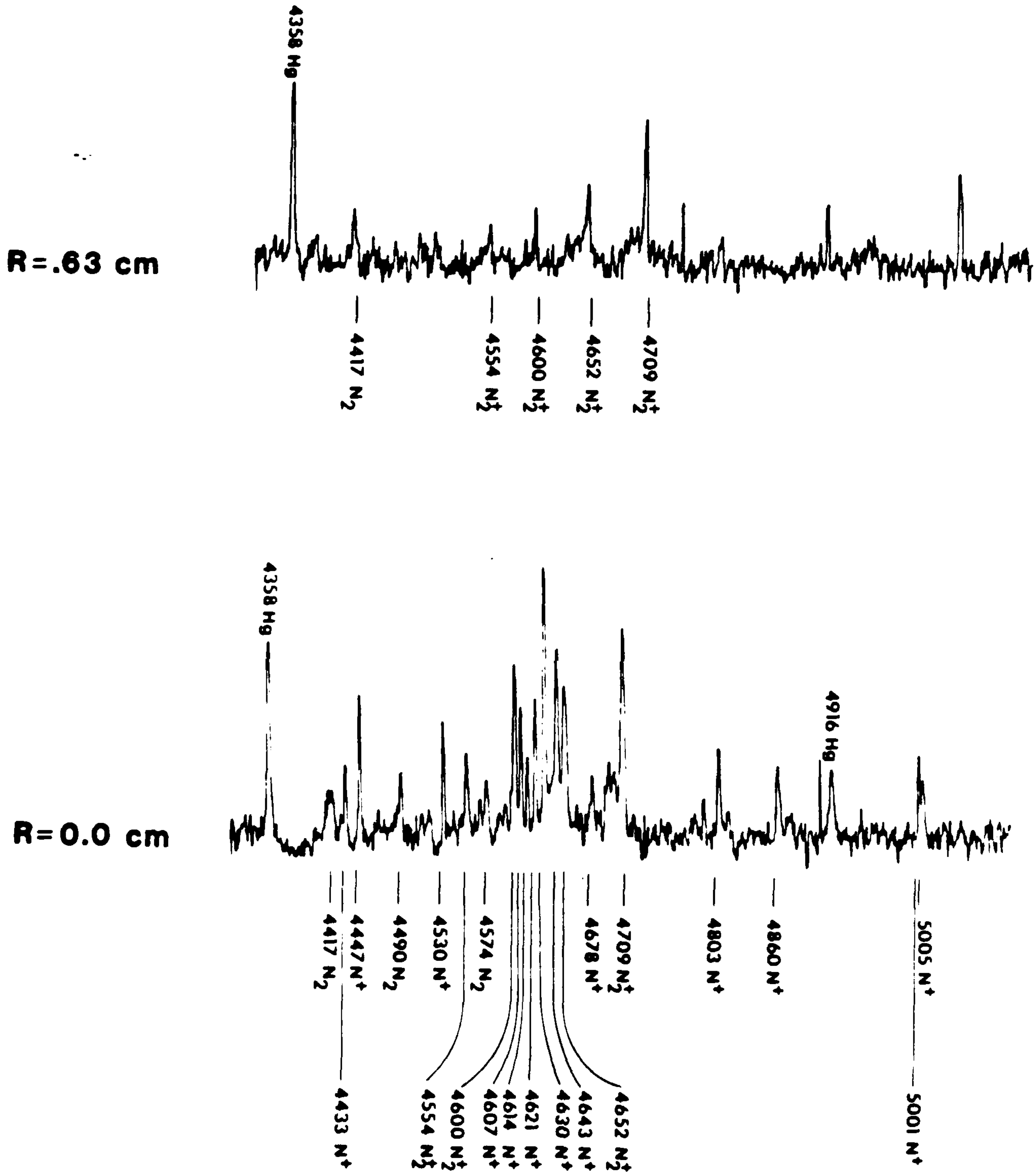

Figure 20. Atomic emission observed in the propagation window (p = 0.35 Torr) is confined to region near the beam axis well inside of the beam Bennett radius (a ~ 3 cm).

than the radius characteristic of the Bennett-like beam current profile (a~3 cm). Although these spectra do not constitute a direct measurement of the channel conductivity, they are suggestive of a hotter and hence more highly-ionized and conductive gas on the axis.

The propagation window was also characterized by the appearance of a virulent azimuthally symmetric instability that caused a large fraction of the beam current to be expelled from the central channel into an annular "halo" region . This thin shell of current then propagated with the residue of the central core to the end of the drift tube. This phenomenon was observed with radiochromic foils, open-shutter photography, streak photography, and our array of fast-risetime subminiature charge collectors. The radiochromic (blue cellophane) film measurements were made with 125-μm titanium foils shielding the film from exposure to any electrons with kinetic energy below ~180 keV. The same titanium foil thickness was used to shield the array of charge collectors. A time and space resolved plot of the current density at a distance less than 1 m from the diode is shown in Fig. 21. The data plotted in this figure clearly show the evolution of the annular shell at a time late in the beam pulse. An example of a radiochromic film exposure can be seen in Fig. 18 Appendix D. Many other examples of the time history of the spatial distribution of current associated with this thin-shell hollowing instability can be found throughout the appendices. The hollow current carrying shell is also evident in both time-integrated and time-resolved photographs. It is seen in the open-shutter photograph in Fig. 19 that was taken at 0.25 Torr and in the photograph taken at 0.7 Torr. Figure 22 is a streak photograph showing a well developed shell of current. The open shutter photographs show other

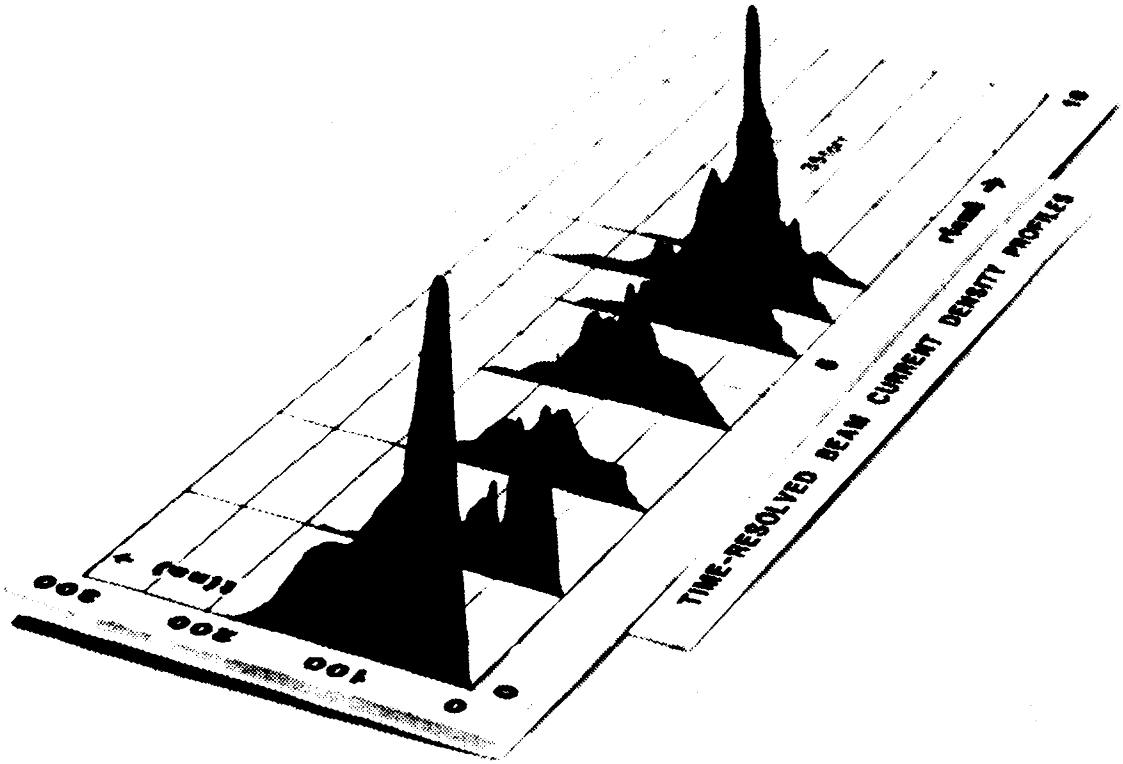

Figure 21. Time-resolved beam current density profile at Z = 0.81-m. p_0 = 0.35 Torr. Note development of "halo" current of high energy (≳ 150 keV) electrons at late time in beam pulse.

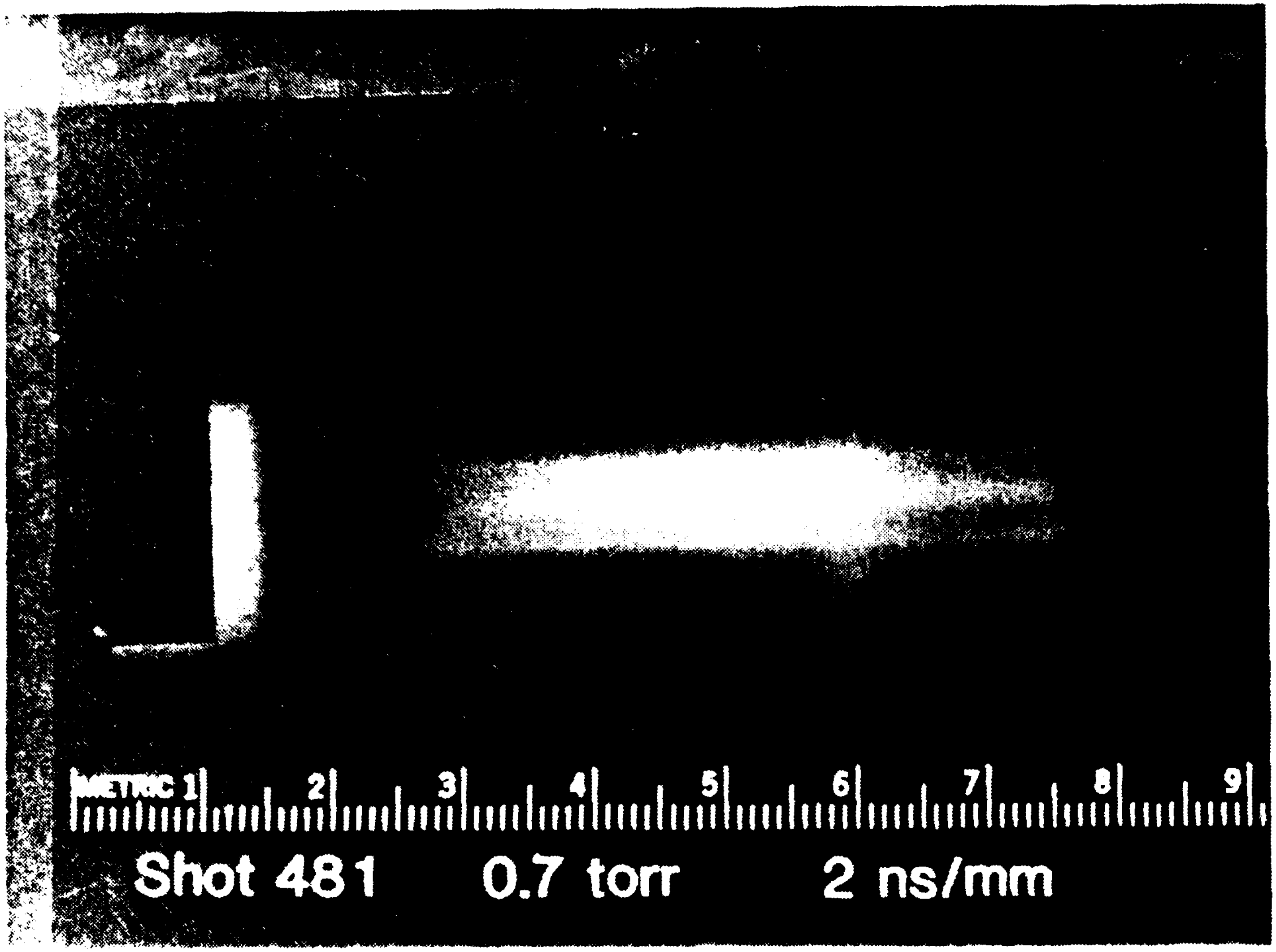

Figure 22. Imacon streak-camera picture taken through a vertical slit at 4.5 m showing emission from fully developed annular halo.

rather spectacular effects in addition to the hollowing. It is of interest to resolve these in time to try to understand their causes. In particular, the intense atomic emission concentrated near the axis persists for very long times after the passage of the beam, as seen from the framing camera sequence in Fig. 23. The time integration of this afterglow radiation accounts for the "hot spots" seen in the open shutter pictures. The most likely explanation for the persistance of this afterglow radiation is the extremely slow deionization rates for the ionized atomic nitrogen in the central core. Also evident in Fig. 23 is the apparent formation of the "streamers" during the latter part of the beam pulse. Additional observations about the streamers are that they always open in the direction of beam propagation, as if they were ejected from the channel by primaries, and the opening angle is more acute near the diode. These might be particle tracks "exposed" by the high E/p environment, they could be instabilities in the beam, or they could be low-energy electron exposures of electromagnetic-field effects. Which of these, or other, causes is responsible for the vivid streamer displays is highly speculative at this juncture. The streamers may be masked at earlier times by direct beam excited emission, but on the basis of these photographs one cannot be certain that they are not formed during the switching off of the space-charge neutralized beam current, which may lead to pinching of the remaining unbalanced charge channel.

The appearance of a thin-shell hollowing instability in the pressure regime where avalanching provides an important contribution to the conductivity, which may have a profile more peaked than the beam, and where the current is highly neutralized is in qualitative agreement with existing theory and simulations. However, the >20-ns delay into the beam pulse before the

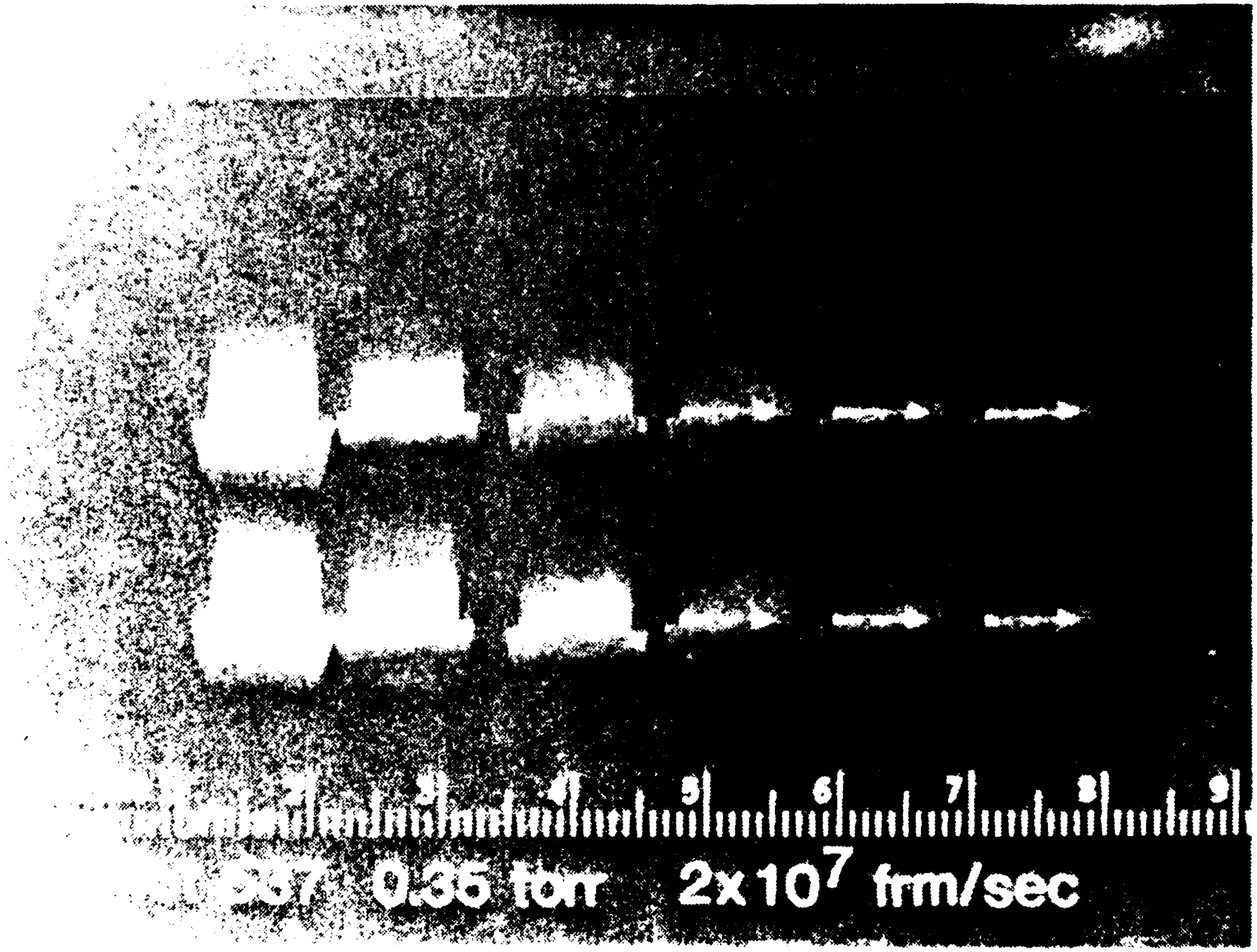

Figure 23. Framing-camera photograph of FX-100 beam at Z = 4.5-m. The exposure time for each frame is 10 ns. This shows the apparent development of a hollowing instability late in the beam pulse, and the persistence of the emission on axis, compared with the rapidly quenched emission from the beam body.

Figure 24. Open-shutter photographs at Z ~ 10-cm from the diode at air pressures near the peak of the propagation window. This clearly shows the initial ejection of current from the main channel to form the current halo. (Beam propagating right to left, clear aperture length ~ 24-cm, air pressures in Torr indicated on pictures.)

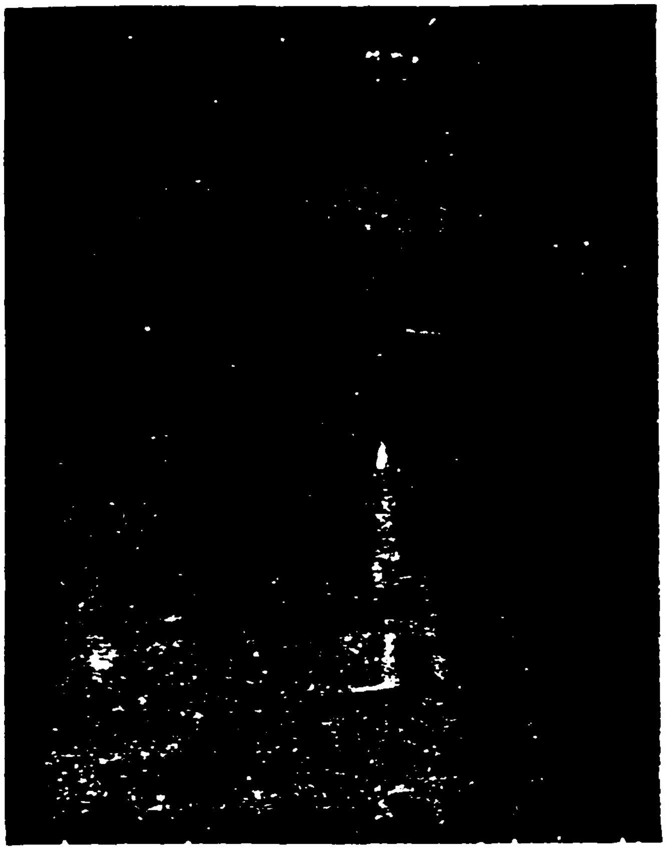
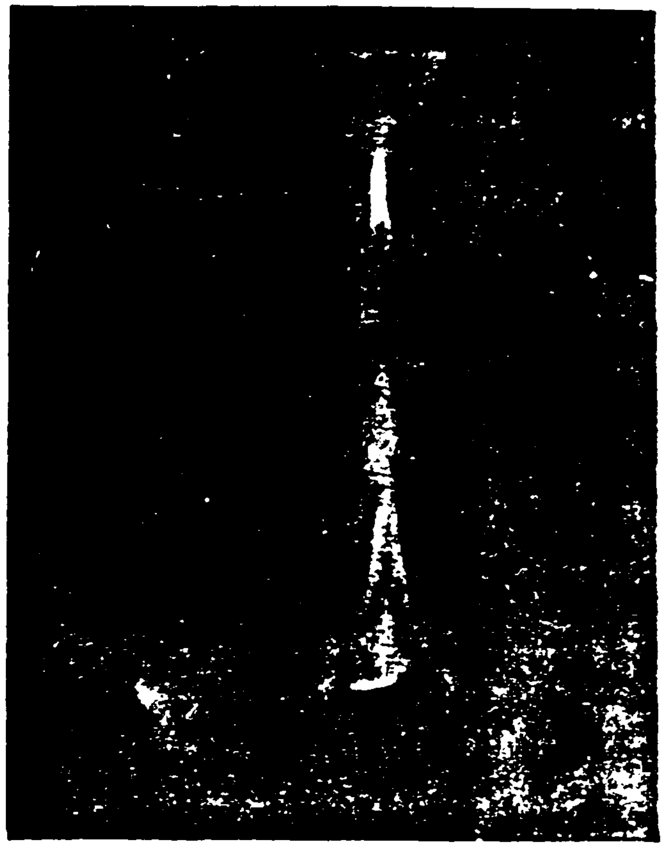

.5

.35

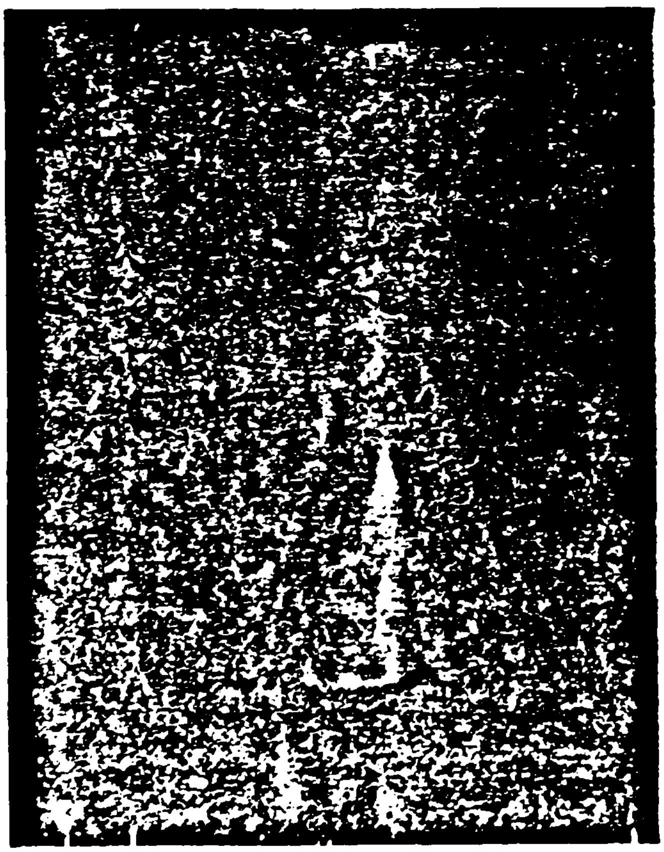
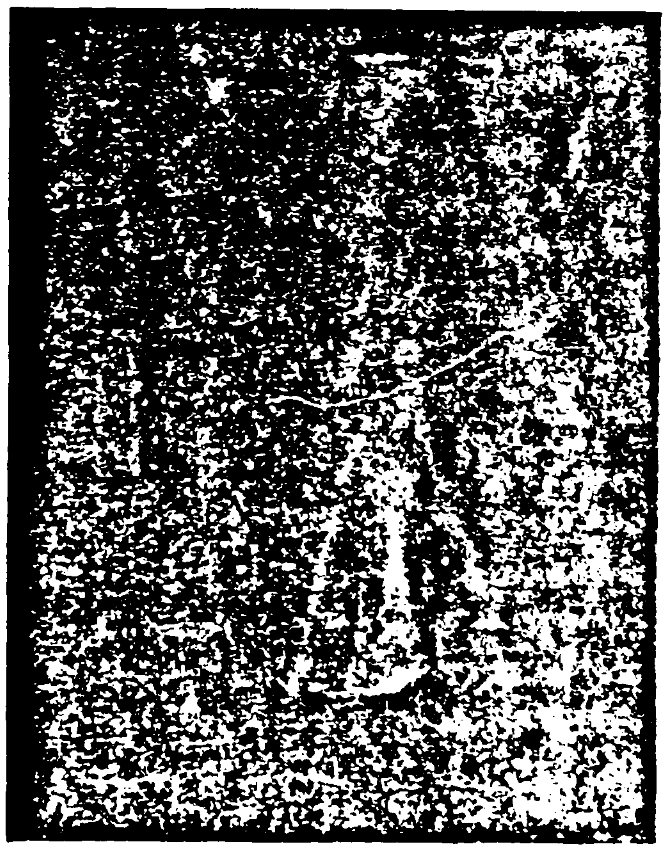

instability onset is not clear. It may be that this is simply the delay for the conductivity to form the required profile for instability, or the result of a pathological change in the diode characteristics late in the pulse.

Finally, a word about our FX-25 beam extraction experiments is in order. A marked threshold for the stabilization of the full-density-air hose instability was observed when the preparation cell pressure was reduced below 1 Torr. Because there appeared to be no associated threshold in the erosion-caused pulse sharpening in the drift tube, it is unlikely that this was the dominant mechanism for stabilization, although it may be a necessary ingredient. The same may be said for phase-mixed damping of initial oscillations that are shock-excited at the diode. The probable reason for the threshold is the matching of λ_β inside the cell and just outside of the extraction foil in full-density air. This implies matching both the beam radius and net current. Our diagnostics were insufficient to provide conclusive evidence for matching at the stabilization threshold in this limited set of exploratory tests of the use of a beam conditioning cell. The effect is shown in the open shutter photographs in Fig. 25 (3-Torr in preparation cell), and Fig. 26 (0.6-Torr in preparation cell). Note that even when violently unstable in Fig. 25, there is evidence for a part of the beam transporting straight to the wall (as indicated by the fluorescence of the wall on axis). In Fig. 26 the stable propagation length is limited by the wall to about 5 or 6 betatron wavelengths. These experiments show that there is great promise for the use of the preparation cell technique for providing greater control of the beam stability properties.

Figure 25. Open-shutter photograph of the FX-25 beam extracted into full-density air (630 Torr) through a 25 m Kapton foil after drifting through 3-m of 3-Torr air.

3 Torr air pressure in 3-m drift tube

Figure 26. Open-shutter photograph of the FX-25 beam extracted into full density air after drifting through 3-m of 0.6-Torr air.

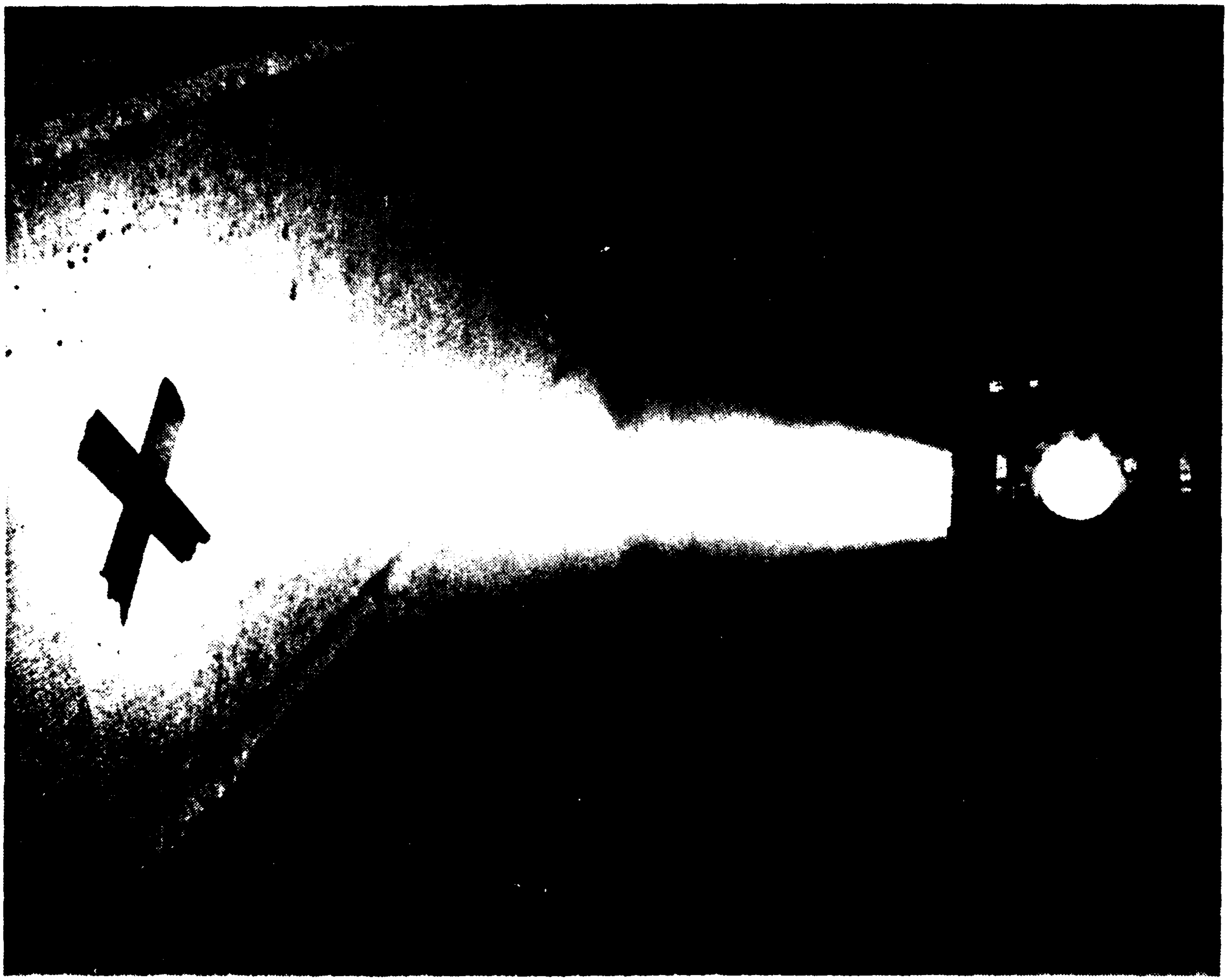

0.6 Torr air pressure in 3-m drift tube

D. Plans for Future Experiments

The FX-100 and FX-25 accelerators, on which the first year experiments were performed, have been decommissioned. In order to continue the propagation experiments a new laboratory facility has been organized at the AFWL. The heart of this new laboratory is the VISHNU accelerator described in the following few paragraphs. Once VISHNU is fully operational, a minimal number of measurements to establish the low-pressure propagation window and current distribution will be made. These should proceed rapidly because of our accumulated experience with the FX-100 and FX-25 beams. Once this has been completed, we will proceed to the second year research objectives outlined in Sec. I of this report.

1. VISHNU Accelerator

VISHNU is an intense relativistic electron beam generator that is under construction at the AFWL from the components of a decommissioned Pulse Rad 4-15 generator. In its initial incarnation VISHNU has a 16 stage Marx generator that could store a maximum of 8 kJ if each stage were charged to the maximum rating of 100 kV. In practice, we will only charge to ~80% of this maximum rating in order to extend the lifetime of the components (eg., the number of capacitor discharge cycles prior to failure is roughly proportional to the seventh power of the charging voltage). When erected, the VISHNU Marx generator pulse charges a 10-Ω oil-insulated coaxial transmission line, which has a (one-way) electrical length of ~13 ns, and a capacitance small compared with the Marx generator. The calculated ringing gain for this line is ~1.7, and it would be charged to ~2.7 MV with the maximum voltage on the Marx. The oil insulation would be severely overstressed at this voltage, however, and consequently we intend to set the untriggered single-channel oil output switch to self break when the voltage reaches 90% of the ring-up for an 80% Marx charge. This gives the oil line a 1.9 MV charge, which will produce a 0.9-MV, 90-kA, 26-ns pulse into a matched load. A field-emitting diode with these parameters would produce a highly pinched beam, and, furthermore, we wish to perform our propagation experiments with a higher kinetic energy beam having parameters close to those of our past experiments on the FX machines. Therefore, we will attempt to mismatch the diode to obtain a 1.5-MeV, 40-kA, 26-ns electron beam output.

The VISHNU diode could, of course, be designed to provide other beam parameters within the constraints of the 10-Ω generator load-line and diode pinching. The region of beam kinetic energy and current accessible by VISHNU is shown in Fig. 27 for comparison with other accelerators that are being used or planned for intense electron-beam air-propagation experiments.

At the time that MRC became involved in the VISHNU project, a number of modifications were required to make VISHNU into an operating machine. The principal task that we undertook was the design of a new oil-vacuum interface/high-voltage insulator (or diode envelope). Other tasks included the design of an adapter plate between the Marx generator tank and the pulse-line, the design of new supports for the pulse-line inner conductor, and guidance in the design of the field emitting cathode.

Design of the envelope was complicated by the temporary loss of the switch housing from the old Pulse Rad 4-15. The envelope is a conventional insulator stack with 14 angled and graded plastic rings. The metal grading rings were

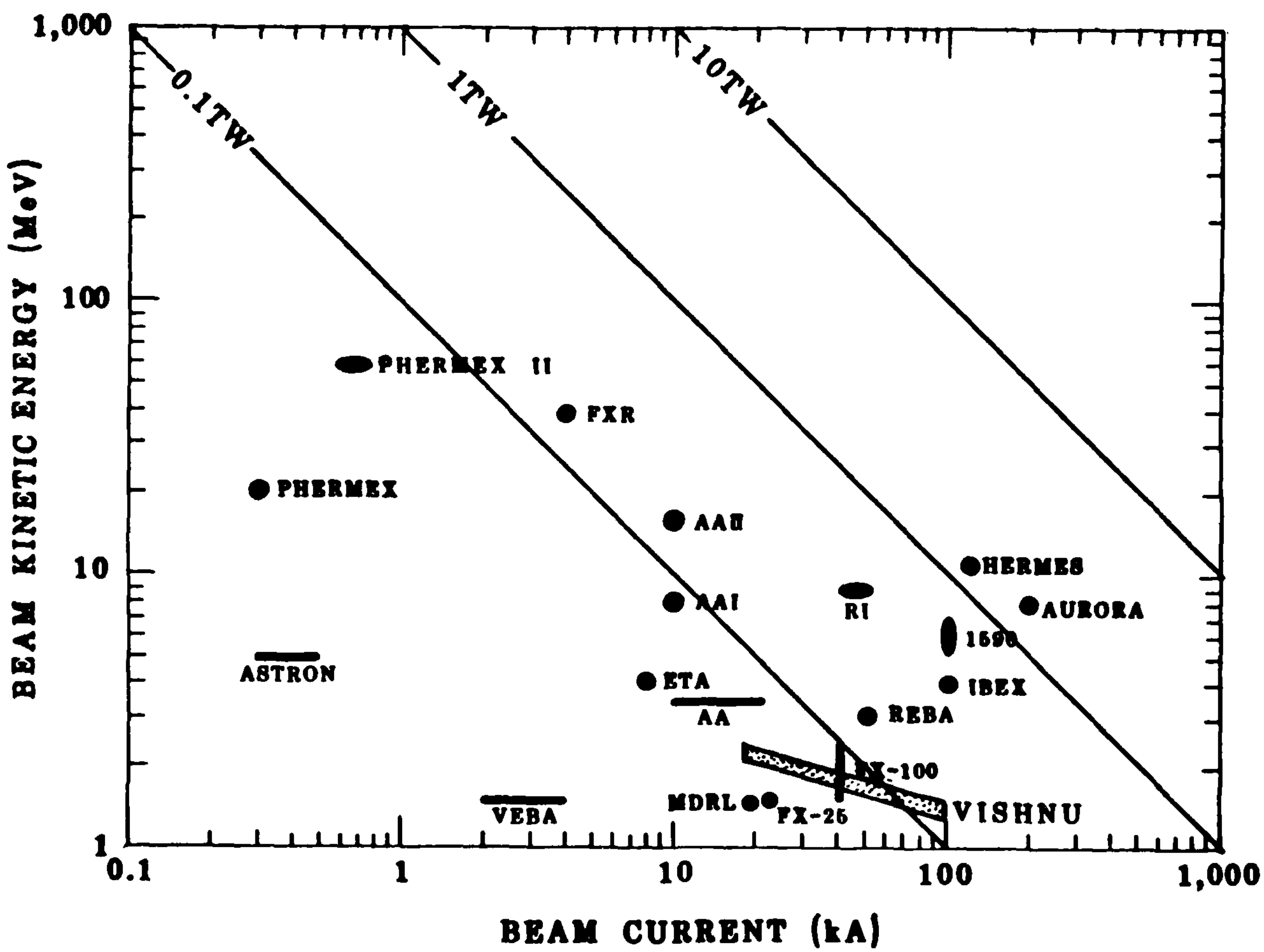

Figure 27. Intense electron beam accelerators available for air propagation experiments. Also shown are several upgrades and accelerators under development. The entire available range of current and voltage of the AFWL VISHNU accelerator is shown.

spares originally fabricated for the RADLAC accelerator, and their availability dictated the envelope diameter. Similar structures are rated at ~125 kV/cm, and in principle, the VISHNU envelope could be used for an output as high as ~4.5 MV. However, in practice non-uniform fields limit the usable gradient. The voltage standoff capability will be further limited by electron bombardment of the insulators, which may lead to flashover. Experimental data from the RADLAC accelerator program indicates that in the presence of currents, insulator breakdown is time dependent, and the VISHNU envelope may break down at ~2.5 MV.

A major problem with the present design is that the limited space available for the output oil switch increased the capacitive coupling between the pulseline and the diode. This capacitance is ~25 pF and that of the envelope transmission line is between 25 pF and 38 pF. For the 1.9 MV pulseline charging voltage the resulting capacitive coupling can be expected to give a prepulse of 0.7-1.0 MV. This rather large value would certainly cause the graphite cathode to emit, consequently an effort has been made to suppress the prepulse through the use of a dielectric-flashover switch in the vacuum transmission-line center conductor. This should lower the prepulse at the cathode to less than ~50 kV. Furthermore, a comparatively small prepulse leakage current of ~500 A would reduce the prepulse by a factor of ~8. If it turns out that the prepulse is unacceptably large, a 2-kΩ shunt resistor m y solve the problem. Other solutions include the use of a groundplane shield in the oil switch.

Another problem we may face is that the single-channel oil switch and high-impedance vacuum transmission line output can be expected to result in a risetime longer than ~10 ns. If this causes a serious degradation of the short, ~25-ns, pulse produced by the oil insulated coax we may need to resort to a lower impedance switch or output.

The diode envelope is supported by tie rods fabricated from "Superstud CR", a new high-strength glass-fibre reinforced polyester manufactured by Permali Corp. Other features of the design include an adjustable cathode shank, and a switch gap that is adjustable from the vacuum side of the envelope. Finally, access ports have been provided for the placement of capacitive V-dot voltage monitors on the oil side of the envelope, and for B-dot current monitors on the output transmission line.

When fully operational, VISHNU will be a versatile and reliable accelerator for the production of the electron beams required for the completion of our second year propagation experiments.

2. Beam Conditioning Cell

It seems clear from the results of the FX-100 experiments that any diode-generated beam will not be in equilibrium when injected into the air-propagation experimental chamber. This makes for poor reproducibility and lack of control of the beam behavior through the variation of external parameters (ie., air pressure, return-conductor radius, etc.). Because our second year research objectives require a much more precise control of the beam characteristics than we feel is obtainable with direct diode injection into the chamber, we will attempt to precondition the beam by equilibrating it in a short conditioning cell. This is based in part on our FX-25 experiments with the stabilization of the full-density-air hose instability by the use of a conditioning cell. We intend to use helium gas in this cell because of its reduced scattering and simpler chemistry.

3. Propagation Chamber

Several large-diameter chambers have been located at the AFWL, and we have set these aside for use as a large diameter ($r > 60$ cm) propagation chamber in order to avoid unwanted wall effects. These have large viewing ports that will allow us to observe a significant beam propagation length without impediment. It will be a simple matter to use conducting-screen tubes with varying diameters in this chamber to investigate wall effects on hose growth, nose erosion, and coupling. We will also be able to explore the thin-shell hollowing instability in the absence of return conductors, if indeed this mode is observed in experiments with the shorter-pulse VISHNU beam.

E. Summary

In summary, we have accomplished our first year objectives of delineating the pressure window for propagation of the FX-100 beam, of measuring the temporal evolution of the spatially resolved beam current distribution, and of providing insight into the experimental results through strong theoretical support.

We utilized available experimental time on the FX-25 to develop the subminiature charge collector diagnostic that was to prove invaluable in the following FX-100 experiments. We also used the FX-25 to perform experiments on the stabilization of the full-density-air hose through the use of a low-pressure beam-preparation cell. The encouraging results of this exploratory use of a preparation cell will enable us to exercise greater control over the beam in future experiments.

Maximum energy transport of the FX-100 beam occured at 0.3-0.5-Torr air pressure. The window for maximum energy transport was defined by loss of the tail of the beam at high pressures and by erosion of the beam head at low pressures in both the FX-25 and FX-100 experiments. Propagation in the window was characterized by a high degree of current neutralization (~80% or more). In the propagation pressure window we observed a strong hollowing instability. The hollowing caused as much as 80% of the beam current to be carried in a thin annular shell at a radius about twice the Bennett radius that characterized the injected current distribution. Space- and time-resolved measurements of the current distribution with a fast-risetime subminiature charge collector array showed that the thin-shell hollowing instability developed late (~20 ns or more) into the beam pulse. Spectroscopic measurements of the visible emission suggest that the air near the axis of the beam may have been hotter and more highly ionized in this pressure regime, which may have resulted in a conductivity profile more centrally concentrated than that of the beam.

The appearance of a thin-shell hollowing instability in the pressure regime where avalanching provides an important contribution to the conductivity, which may have a profile more peaked than the beam, and where the current is highly neutralized is in qualitative agreement with existing theory and simulations. The observed delay in onset is not, The source of the disagreement may lie in imperfect air-chemistry modelling giving an erroneous delay for the buildup of an unstable conductivity profile. Simulations with CPROP showed many features consistent with the experimental results, including a high degree of current neutralization, rapid blowoff of the beam head after injection followed by slower erosion, and a lack of instability early in the beam pulse. Simulations with KMRAD showed instability to thin-shell hollowing in the body of the beam.

The experimental low-pressure air propagation experiments will be continued using the electron beam produced by a new accelerator (VISHNU) being constructed at the Air Force Weapons Laboratory. VISHNU is designed to have electron beam parameters close to those of the FX accelerators in order to take advantage of our experience with those beams. It will, however, have a shorter pulsewidth than the FX-100, which may have an effect on the onset of the hollowing instability.

F. References

1. C. A. Ekdahl, Rev. Sci. Instrum. 51, 1645(1980) and references therin.

2. G. E. Leavit, J. D. Shipman, Jr., and L. M. Vitkovitsky, Rev. Sci. Instrum. 36, 1371 (1965).

3. N. W. Harris, Rev. Sci. Instr. 45, 961 (1974).

4. W. Rogowski and W. Steinhaus, Arch. Elektrotech. 1, 141(1912).

5. D. Honea and S. S. Medley, J. Phys. E. 7, 537(1974).

6. P. Gehringer, E. Proksch, and H. Eschweiler, Int. J. Appl. Radiat. Isot. 33, 27(1982) and references therein.

7. T. J. Fessenden, R. J. Briggs, J. C. Clark, E. J. Lauer, and D. O. Trimble, Lawrence Livermore Laboratory Report UCID-17840, 1978.

8. R. B. Miller, private communication.

9. M. C. Clark, private communication.

AD-A170 204 BEAM PROPAGATION EXPERIMENTAL STUDY(U) MISSION RESEARCH CORP ALBUQUERQUE NM C A EKDAHL MAR 82 AMRC-R-352 AFOSR-TR-86-0503 F49620-81-C-0016 2/4

UNCLASSIFIED F/G 20/7 NL

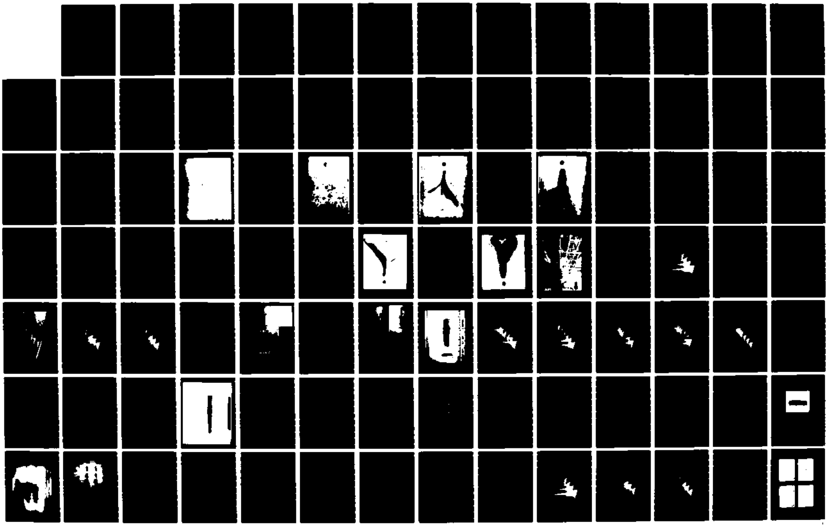

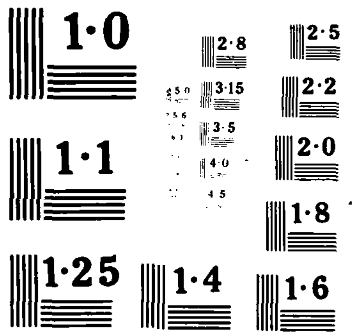
1·0
2·8
2·5
3·15
2·2
3·5
1·1
2·0
4·0
4·5
1·8
1·25
1·4
1·6

III. PUBLICATIONS

A. Mission Research Corporation Reports

"Interim Report - Beam Propagation Experimental Study," C. A. Ekdahl, Mission Research Corporation Report AMRC-N-167, April 1981

"Intense Relativistic Electron Beam Propagation Experiments," C. A. Ekdahl and W. H. Bostick, Mission Research Corporation Report AMRC-N-182, January 1982

"Spectral Measurements of Relativistic Electron Beam Generated Emission in Air," L. A. Wright and C. A. Ekdahl, Mission Research Corporation Report AMRC-N-183, December 1981

"FX-100 Propagation Experiments - DARPA/Services Experimental Coordination Meeting," C. A. Ekdahl, Mission Research Corporation Report AMRC-N-184, October 1981

"Electron Beam Transport in a Small Aperture Faraday Cup," D. J. Sullivan and C. Ekdahl, Mission Research Corporation Report AMRC-N-185, January 1982

"Monte Carlo Electron Beam Transport in Air," D. J. Sullivan and C. A. Ekdahl, Mission Research Corporation Report AMRC-N-186, January 1982

"Particle Simulation of FX-100 Beam Propagation and Comparison with Experiment," T. P. Hughes, C. Ekdahl, and B. Godfrey, Mission Research Corporation Report AMRC-N-187, January 1982

"FX-100 Propagation Experiments- RADLAC Review Meeting," C. A. Ekdahl, Mission Research Corporation Report AMRC-N-189, January 1982

"Optical Emission from Intense Relativistic Electron Beam Excited Air," L. A. Wright, C. A. Ekdahl, R. F. Benjamin, and T. P. Starke, Mission Research Corporation Report AMRC-R-326, November 1981

B. Journal Publications

"Optical Emission from Intense Relativistic Electron Beam Excited Air," L. A. Wright, C. A. Ekdahl, R. F. Benjamin, and T. P. Starke, In preparation for J. Appl. Phys.

"Nanosecond Risetime Subminiature "Nanosecond Risetime Subminiature Charge Collectors for Electron Beam Current Density Distribution Measurements," C. A. Ekdahl and W. H. Bostick, In Preparation for Rev. Sci. Instrum.

"Observation of a Hollowing Instability in an Electron Beam Propagating in Low-Pressure Air," In preparation for Appl. Phys. Lett.

IV. PROFESSIONAL PERSONNEL ASSOCIATED WITH THE RESEARCH

Dr. C. A. Ekdahl, Mission Research Corporation, Principal Investigator

Dr. B. B. Godfrey, Mission Research Corporation, Particle Beam Applications Group Leader

Dr. T. P. Hughes, Mission Research Corporation

Mr. D. J. Sullivan, Mission Research Corporation

Dr. L. A. Wright, Mission Research Corporation

Prof. W. Bostick, AFOSR University Resident at the Air Force Weapons Laboratory

We are also indebted to the following members of the Dynamic Testing (M) Division at the Los Alamos National Laboratory for providing the time-resolved photography of the FX-100 propagation experiments:

Dr. R. F. Benjamin (M-6)

Dr. S. Schmidt (M-6)

Dr. D. Moir (M-2)

Dr. T. P. Starke (M-2)

V. INTERACTIONS

Results of the FX-100 propagation experiments were reported at the 23rd Annual Meeting of the Division of Plasma Physics of the American Physical Society, New York, New York, 12-16 October, 1981:

"Intense Relativistic Electron Beam Propagation Experiments," C. A. Ekdahl and W. H. Bostick, Bull. Am. Phys. Soc. 26, 853(1981) and Mission Research Corporation Report AMRC-N-182, January 1982

"Spectral Measurements of Relativistic Electron Beam Generated Emission in Air," L. A. Wright and C. A. Ekdahl, Bull. Am. Phys. Soc. 26, 853(1981) and Mission Research Corporation Report AMRC-N-183, December 1981

In addition, results of the propagation experiments were reported in substantial detail in oral presentations at the following meetings:

DARPA/Services Propagation Meeting, Lawrence Livermore National Laboratory, 15-18 June, 1981

"DARPA/Services Propagation Review Meeting Presentations," C. Ekdahl, B. Godfrey, and T. Hughes, Mission Research Corporation Report AMRC-N-172, June 1981

Dynamic Testing Division Seminar, Los Alamos National Laboratory, 5 October 1981

"Atmospheric Propagation of Relativistic Electron Beams," B. Godfrey and C. Ekdahl, Mission Research Corporation Report AMRC 81-1254

DARPA/Services Experimental Coordination Meeting, Lawrence Livermore National Laboratory, 27-28 October, 1981

"FX-100 Propagation Experiments - DARPA/Services Experimental Coordination Meeting," C. A. Ekdahl, Mission Research Corporation Report AMRC-N-184, October 1981

RADLAC Annual Review Meeting, Air Force Weapons Laboratory, 14 January 1982

"FX-100 Propagation Experiments- RADLAC Review Meeting," C. A. Ekdahl, Mission Research Corporation Report AMRC-N-189, January 1982

VI. ACKNOWLEDGEMENTS

This reseach was sponsored by the Air Force Office of Scientific Research (AFSC) under contract F49620-81-C-0016. The author gratefuly acknowledges the able, and always enthusiastic, assistance of Winston Bostick in performing these experiments. Professor Bostic was a senior research physicist in the University Residency Program at the Air Force Weapons Laboratory sponsored by the Air Force Office of Scientific Research under IPA-905-79-01016C. The author is also indebted to the entire staff of the particle beam group at the Air Force Weapons Laboratory, in particular Dr. M. C. Clark and Dr. D. Straw, for their cooperation and assistance in this research. Finally, the author is indebted to the following members of the Dynamic Testing Division at Los Alamos National Laboratory for the time-resolved framing and streak camera photography of the FX-100 propagation experiments: Dr. R. Benjamin, L. Builta, Dr. D. Moir, Dr. S. Schmidt, and Dr. T. Starke.

VII. APPENDICES

APPENDIX A

INTERIM REPORT - BEAM PROPAGATION EXPERIMENTAL STUDY

SECURITY CLASSIFICATION OF THIS PAGE (When Data Entered)

REPORT DOCUMENTATION PAGE

READ INSTRUCTIONS BEFORE COMPLETING FORM

Field	Entry
1. REPORT NUMBER	
2. GOVT ACCESSION NO.	
3. RECIPIENT'S CATALOG NUMBER	
4. TITLE (and Subtitle)	BEAM PROPAGATION EXPERIMENTAL STUDY
5. TYPE OF REPORT & PERIOD COVERED	Interim Report
6. PERFORMING ORG. REPORT NUMBER	AMRC-N-167
7. AUTHOR(s)	Carl Ekdahl
8. CONTRACT OR GRANT NUMBER(s)	F49620-81-C-0016
9. PERFORMING ORGANIZATION NAME AND ADDRESS	MISSION RESEARCH CORPORATION 1400 San Mateo Boulevard, S.E., Suite A Albuquerque, New Mexico 87108
10. PROGRAM ELEMENT, PROJECT, TASK AREA & WORK UNIT NUMBERS	
11. CONTROLLING OFFICE NAME AND ADDRESS	AIR FORCE OFFICE OF SCIENTIFIC RESEARCH Building 410 Bolling AFB, D.C. 20332
12. REPORT DATE	08 April 1981
13. NUMBER OF PAGES	
14. MONITORING AGENCY NAME & ADDRESS (if different from Controlling Office)	
15. SECURITY CLASS. (of this report)	Unclassified
15a. DECLASSIFICATION DOWNGRADING SCHEDULE	
16. DISTRIBUTION STATEMENT (of this Report)	
17. DISTRIBUTION STATEMENT (of the abstract entered in Block 20, if different from Report)	
18. SUPPLEMENTARY NOTES	
19. KEY WORDS (Continue on reverse side if necessary and identify by block number)	Relativistic electron beam propagation Relativistic electron beam diagnostics

20. ABSTRACT (Continue on reverse side if necessary and identify by block number)

The pressure regime for stable propagation of an internal relativistic electron beam ($I > 20$ kA, W · 1.5 MeV, $t > 20$ ns) was determined and the beam-current density distribution was measured using an array of fast-response, subminiature Faraday cups. Experiments were performed on the stabilization of this pre-equilibrated beam when it was extracted into full-density air.

DD FORM 1 JAN 73 1473 EDITION OF 1 NOV 65 IS OBSOLETE

SECURITY CLASSIFICATION OF THIS PAGE (When Data Entered)

INTRODUCTION

During February, 1981 the FX-25 accelerator was made available for development of diagnostics and exploratory propagation experiments. The diagnostic effort focused on the development of an array of subminiature Faraday cups for the determination of the beam spatial distribution. Experiments were also performed with a new technique for the measurement of the divergence of high energy density beams. In the propagation experiments the previously established range of pressures for stable propagation was confirmed for the particular geometry used; the beam spatial distribution was measured; and data was obtained on beam emittance. These measurements were made over a range of pressures that extended above and below the window for stable propagation. Finally, the beam was extracted into full density air after having propagated through the low pressure drift tube in order to investigate the effect on the hose instability of pulse sharpening, profile broadening, and phase mixing.

I. DIAGNOSTIC DEVELOPMENT

A. Subminiature Faraday-Cup Array

An array of fast-response Faraday-cup charge collecters was developed to measure the time-resolved current density spatial distribution. The use of this array allows the determination of the evolution of the radial beam profile on a single shot. The array used for the measurements reported here consisted of several coaxial Faraday collectors embedded in a carbon beam stop and shielded from the plasma electrons with a thin carbon sheet. The use of subminiature charge collectors eliminates the noise and response time problems associated with the detection of high currents. Furthermore, using a coaxial collector driving a matched and terminated signal cable provides the fastest possible response time. The response time of the signals observed in this experiment was limited by the bandwidth of the oscilloscopes to ~1 ns. The high signal level and unbroken coaxially-shielded construction gave essentially noise-free oscillograms.

Graphite was used throughout the design because of its superior resistance to damage by the high energy density beam. In a further development of this design, which had equivalent performance, the insulating gap, t_g, was replaced with a thin sheet (25 μm) of Kapton, which also had a high resistance to damage in this intense beam. A large version of this array has been constructed for use in the FX-100 experiments.

Electron scattering in the probe materials make it difficult to accurately predict the effective area of the coaxial charge collecter. Existing Monte Carlo electron-transport codes are being investigated as a means for establishing the sensitivity of the probes. This calibration was established experimentally for the FX-25 array by normalizing current density distributions measured close to the diode (Fig. 2) to the total diode current (measured with a resistive shunt). The same procedure will be used to experimentally calibrate the FX-100 array.

B. Faraday Cup Beam-Emittance Measurements

A new technique for making a time resolved measurement of the beam emittance was experimented with on the FX-25. Consider the geometry of Figure 1 with the thin carbon sheet (t_c) removed and the UT-47 solid coax retracted into the hole in the carbon block to a depth, δ, from the front surface. If the carbon were a perfect absorber then the only electrons that would be collected would be those with angles of incidence less than $\tan^{-1} D/2\delta$. A set of such probes retracted to different depths would thus provide a quantitative time-resolved measurement of the angular distribution of the incident beam. In fact, scattering in the carbon complicates the interpretation of the data obtained with this geometry and without elaborate Monte Carlo calculations, the results of the measurements made on the FX-25 can be only considered crude estimates, at best. Even using the scattering by known foil thicknesses as a means of establishing an empirical calibration does little to reduce the difficulty in interpreting data collected with this geometry. These preliminary experiments did, however, result in an improved design that should give easily interpreted data, and has been constructed for the FX-100 experiments. In this apparatus the coax charge collectors are set at the bottom of conical (rather than cylindrical) holes with varying cone angles. The depth of each hole is the same and is greater than one practical range in carbon for the FX-100 electron energy. This should sharpen the angular discrimination lacking in the previous design. Multiply-scattered electrons, secondaries, and plasma electrons will be discriminated against by use of a Kapton insulated tantalum sheet over the end of the coax detecter. An experimental calibration will be effected by exposing the array to the FX-100 beam scattered in anode foils of known thickness. This will be backed up with Monte Carlo scattering calculations.

II. PROPAGATION EXPERIMENTS

The propagation experiments reported here were performed in reduced pressure air in a 5-cm inner diameter, 307-cm long conducting drift tube. A graphite Rogowski surface cathode was used with a 25-μm Ti foil anode to produce a ~20 μs, 20 - 25 kA, 1.5 - 2.0 MeV beam from the FX-25 accelerator (Fig. 2). It has been previously established that the pressure window for stable propagation for this accelerator is 1 - 2 Torr. This was confirmed for this particular geometry by measurements of the beam energy deposited in a graphite calorimeter especially constructed for these experiments. The maximum energy was deposited in the calorimeter when the drift tube pressure was 1.6 Torr. This was only about 15 - 20% of the initial beam energy. The reason for this inefficient transport became clear when time-resolved measurements of the current density at 3 m were made. As seen in the data for the on-axis probe (Fig. 2) there was no pressure for which the full ~20 ns diode-current pulse width was propagated to the end of this drift tube. At the lower pressures, erosion of the beam head shortened the pulse from the maximum width of ~12 - 15 ns observed at ~1.6 Torr, while at higher pressure the hose instability eroded the tail of the beam as well. This overlap of the pressure regimes for severe nose erosion and hose instability was not observed on earlier FX-25 experiments with larger-diameter drift tubes, and is probably a result of the small-diameter tube used for these experiments.

The beam distribution at peak current evolved into a Bennett-like profile at the end of the drift tube as shown in Figure 4. The Bennett radius for the beam propagated in 1.6 Torr air inferred from these data is ~0.5 cm, and corresponds closely to the radius inferred from damage to dielectric foils (Fig. 4). However, the radius inferred from open shutter photographs of N_2^+ fluorescence at 3914 Å is about a factor of two greater, probably as a result of excitation by lower energy secondaries and plasma electrons.

As the pressure was reduced below 1.6 Torr into the regime of severe erosion of the beam, the profile broadened (Fig. 5), and an increase of current transported in the wings was observed. The inferred Bennett radius increased with reduced pressure until it was approximately equal to the tube radius at a pressure of ~0.8 Torr.

The total beam current inferred from the distribution profiles and maximum current rate of change are shown in Figure 6. It is seen here that although the current may be sharpened by erosion at lower pressures, the reduction in current results in an overall reduction in the rate of change.

III. BEAM EXTRACTION EXPERIMENTS

To date, all high intensity beams extracted directly from the diode into full density air have been observed to become hose unstable within a few (1 - 4) betatron wavelengths. The betatron wavelength is $\lambda_\beta \sim 2\pi a (I_A/2I_{net})^{\frac{1}{2}}$, where I_{net} is the net (beam plus plasma) current, "a" is the Bennett equilibrium radius, and $I_A = \gamma\beta mc^3/e$ is the Alfven current. Therefore, effects that increase the equilibrium radius (such as increased beam emittance from foil scattering) have been observed to increase the hose-free propagation distance in previous experiments. Thick foil scattering also appears to have increased the number of betatron wavelengths before hose disruption, perhaps because of a reduction in growth rate resulting from more rapid phase mixing of the betatron motions. Finally, it is noted that a reduction of I_{net} will also increase λ_β and thus the hose-free propagation distance.

Extraction of the FX-25 beam into full-density air after it propagates through the 3-m low-pressure drift cell could be expected to produce a more stable beam by some combination of the aforementioned effects. The beam was observed to have a higher emittance at the end of the drift tube than at the diode. Furthermore, at the lower pressures the observed larger Bennett equilibrium radius would favor a larger hose-free propagation path. Finally, erosion-sharpened beam fronts could produce higher conductivity (as a result of avalanching in the high induction field) that in turn would result in reduced net currents and the associated increased λ_β.

To test the possibility of stabilizing the hose by pre-equilibration in a low-pressure propagation cell, the FX-25 beam was extracted through a 25-μm Kapton foil at the end of the 3-m drift tube. As the propagation-cell air pressure was reduced from slightly above the propagation window to slightly below, a marked stabilization of the hose was observed (Fig. 7 - 10) at pressures ≲1 Torr. Hose-free propagation was observed below this threshold until the beam struck the shield-block wall ~1 m from the exit point. (Presumably, if the available space for propagation were greater, then the extracted beam would eventually destabilize.) Hose stabilization in these experiments apparently resulted from increased emittance and Bennett-equilibrium radius at the reduced pressures. Enhanced conductivity was probably not contributory, because, as shown in Figure 6, the rate-of-change of beam current did not increase significantly as the cell pressure was dropped.

In conclusion, the availability of time on the FX-25 made it possible to develop two of the more important diagnostics required for the forthcoming FX-100 propagation experiments. A limited set of propagation experiments in a 3-m drift tube was performed that indicated an increased Bennett equilibrium radius at pressures below the pressure for maximum beam energy transport. This effect was used to stabilize the beam extracted into full-density air.

The author wishes to acknowledge the assistance of Winston Bostick in performing these experiments; especially in the development stages of the subminiature Faraday collectors.

This research was sponsored by the Air Force Office of Scientific Research (AFSC) under contract F49620-81-C-0016. Professor Bostick is a senior research physicist in the University Residency Research Program sponsored by the Air Force Office of Scientific Research under IPA-905-79-01016C.

Figure 1. Subminiature Faraday collector for beam current density measurements. The graphite shield thickness (t_c = 1.8 mm) is sufficient to stop electrons with energies less than 700 keV. An insulating gap (t_g = 1.7 mm) is provided between the shield and the graphite beam stop, which houses the array of rigid coaxial cable (UT-47) detectors. These have solid copper outer (D = 1.2 mm) and inner (d = 0.29 mm) conductors, and Teflon insulation.

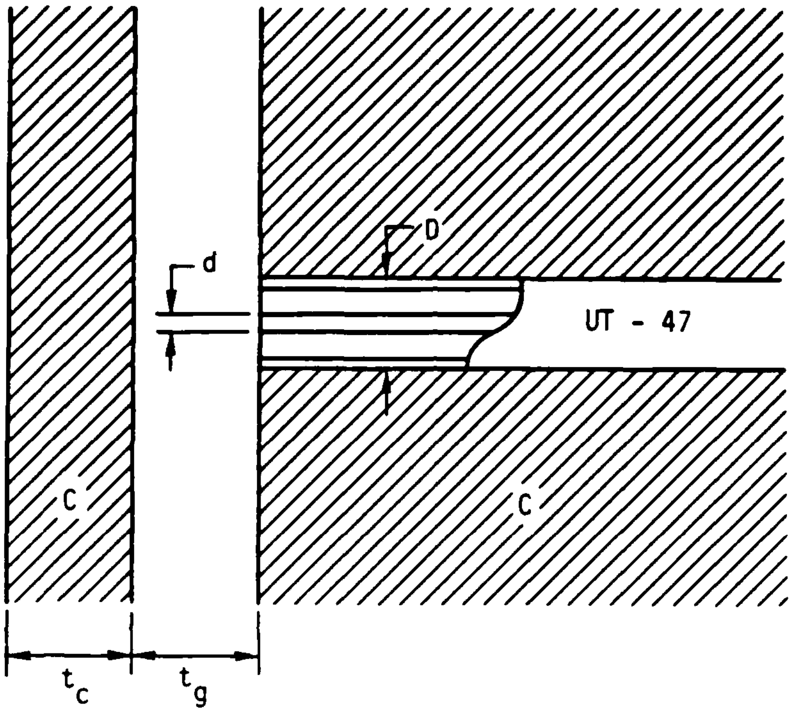
D
d
UT - 47
C
C
t_c
t_g

Figure 2. FX-25 diode geometry and beam current density profile measured in vacuum 0.5 cm from the titanium anode foil. The 51-μm anode foil induces a mean scattering angle of 16-20°. The current density profile shown was obtained at the time of peak current (I_{max} = 22 kA). The FX-25 produced beams having nominal values for parameters shown.

MRC

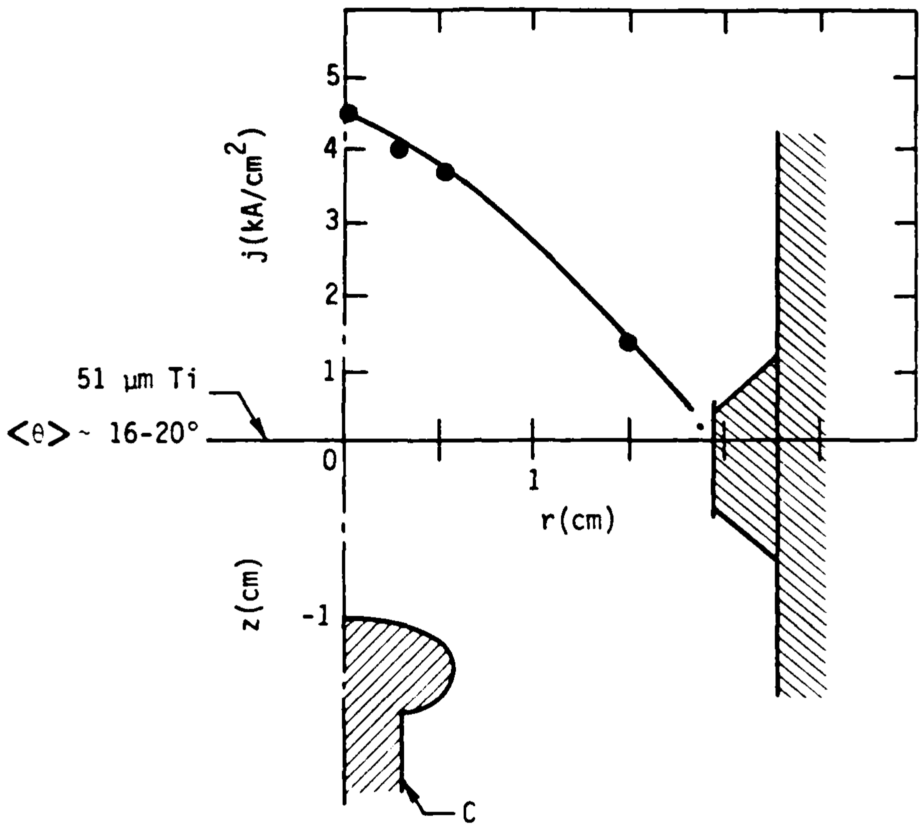

<u>FX-25</u>

1.5-2.0 MeV

20-25 kA

Δt ~ 20 ns

t_r ~ 5 ns

Figure 3. Beam current density on axis for different pressures near the propagation window. The current density near the diode had a waveform that approximated the envelope of these signals. The erosion of the beam nose is clearly evident at pressures below 1.6 Torr (upper). At higher pressures both nose erosion and tail loss resulting from hosing are evident (lower). (lower).

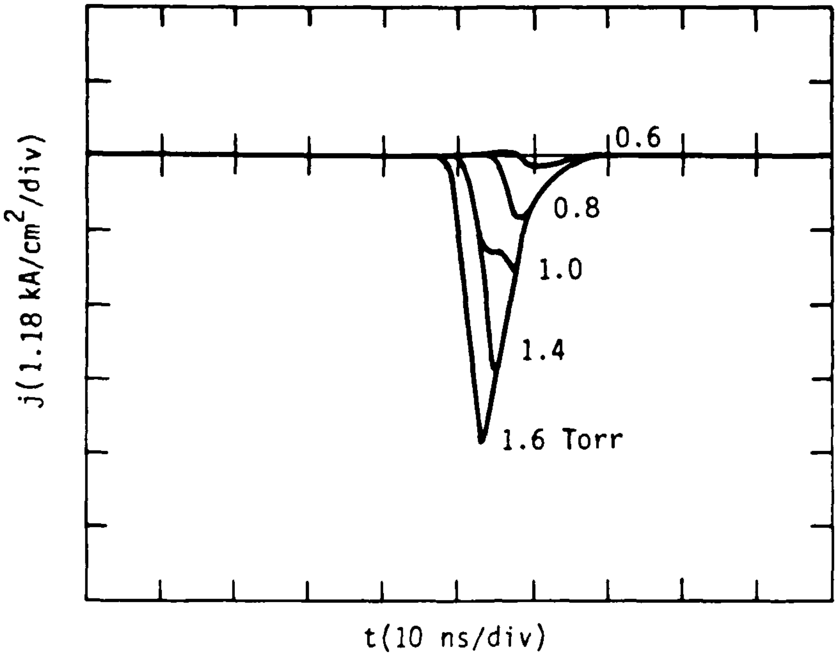
0.6
0.8
1.0
1.4
1.6 Torr
j(1.18 kA/cm²/div)
t(10 ns/div)

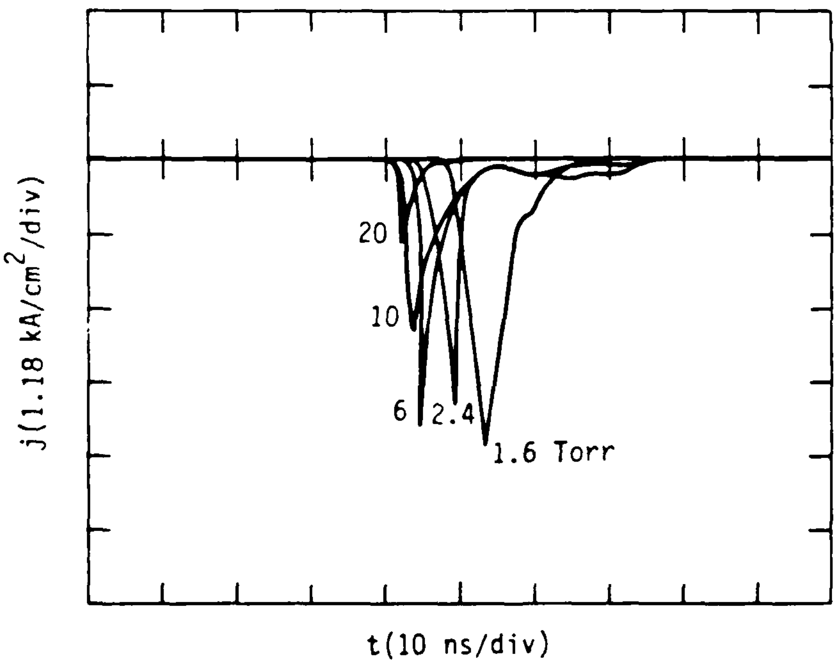
20
10
6
2.4
1.6 Torr
j(1.18 kA/cm²/div)
t(10 ns/div)

Figure 4. Evaluation of the beam current distribution near the diode (upper figure) into a Bennett-like profile (lower figure) after propagating 3-m in 1.6-Torr air (the pressure for maximum energy transport). Also shown are the range of radii determined from damage to dielectric foils (centered at r ~ 0.5 cm), and determined from extent of 3914 Å (N_2^+) emission (centered at r ~ 1 cm).

MRC

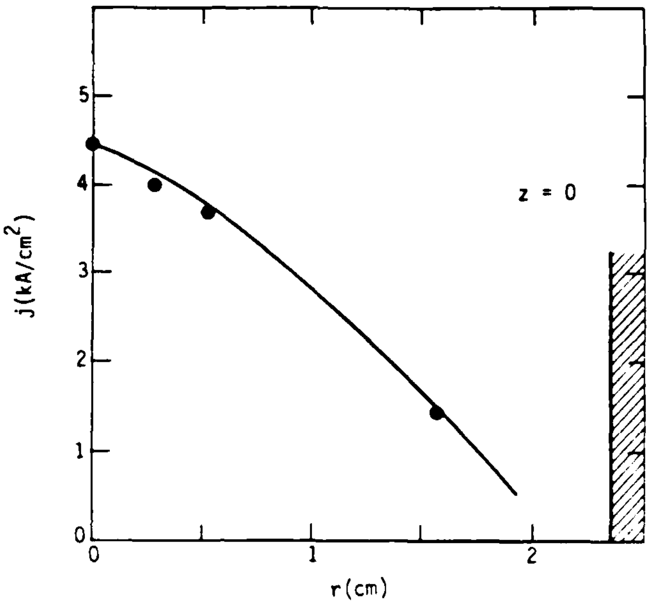

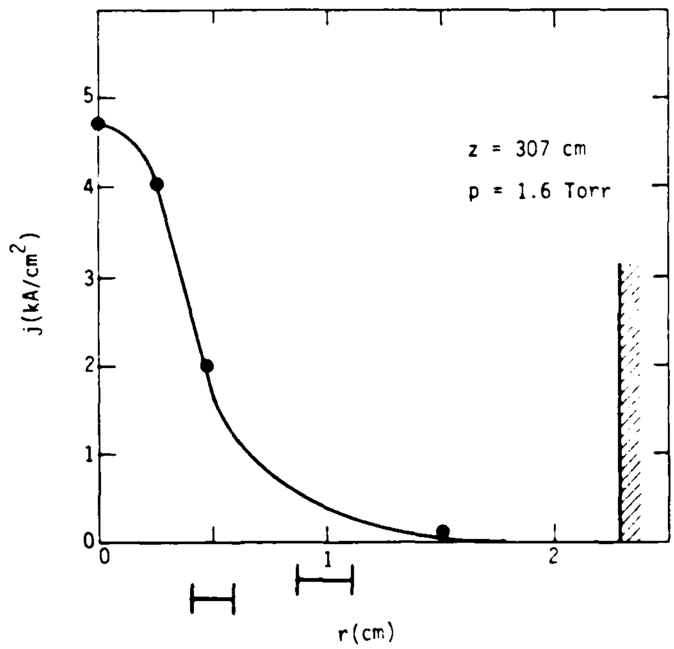

Figure 5. Beam current distributions at 3 m for several air pressures. Maximum energy transport was observed at 1.6 Torr. The increased current density in the wings of the profiles at lower pressures was an effect noted on all of the shots at these pressures.

MRC

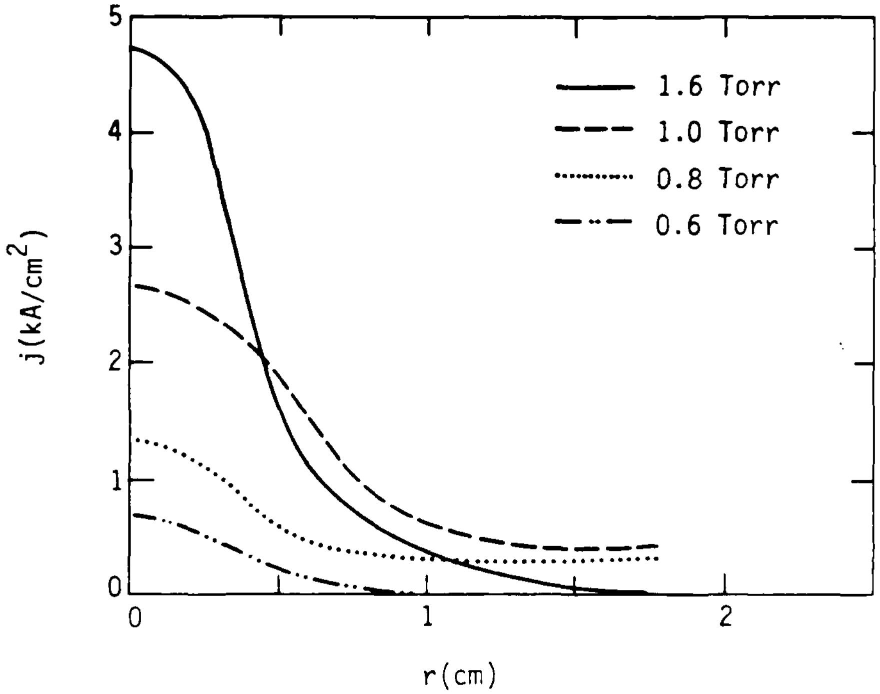

Figure 6. (Upper figure) Total beam current at the end of 3 m. These data were obtained by integrating the current distributions measured with the array of miniature Faraday cups. (Lower figure) Maximum time rate-of-change of the beam current at the end of the three meter drift tube.

MRC

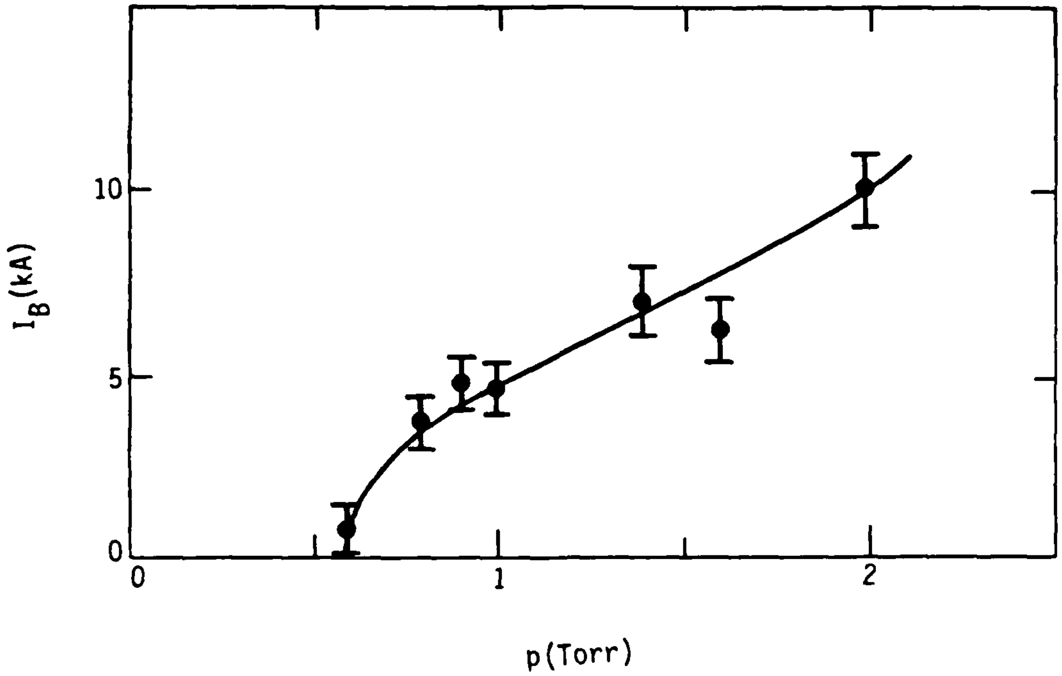

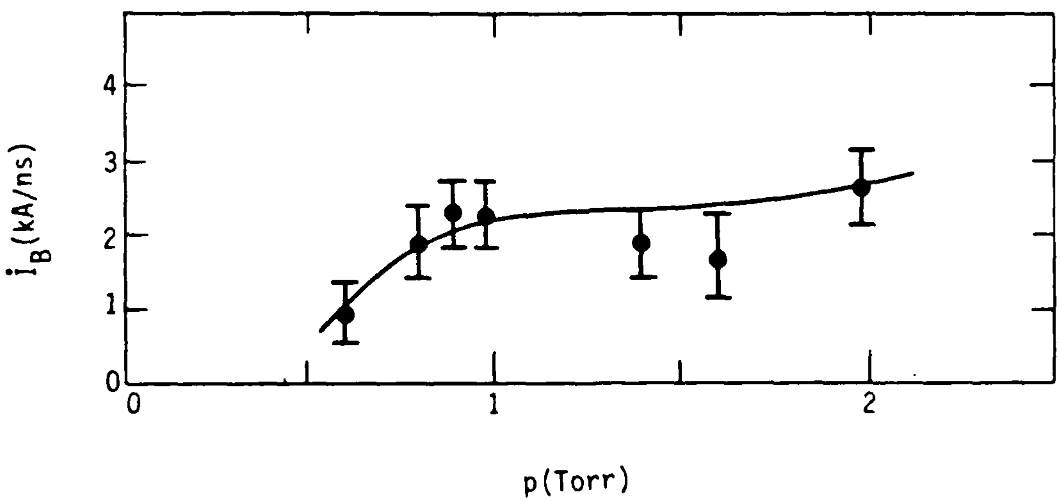

Figure 7. Open shutter (time integrated) photograph of FX-25 beam extracted into full-density air (630 Torr) through a 25-μm Kapton foil after propagating 3-m in a 5-cm diameter conducting drift tube. The air pressure in the drift tube was 1.6 Torr, the pressure for maximum beam energy transport. The beam in the drift tube is visible through the round port on the drift tube.

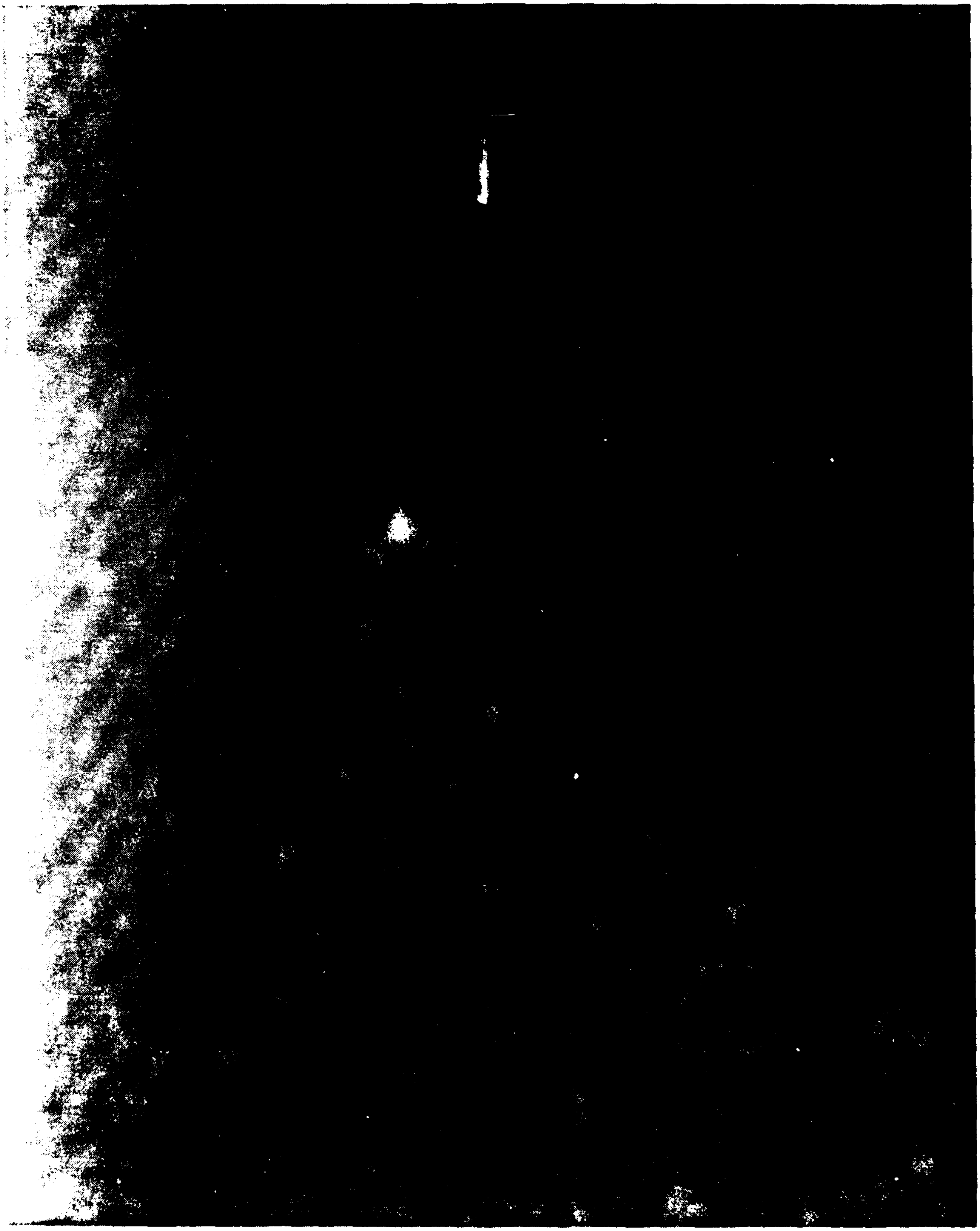

Figure 8. Open shutter photograph of the FX-25 beam extracted into full-density air after drifting through 3-m of 0.8 Torr air.

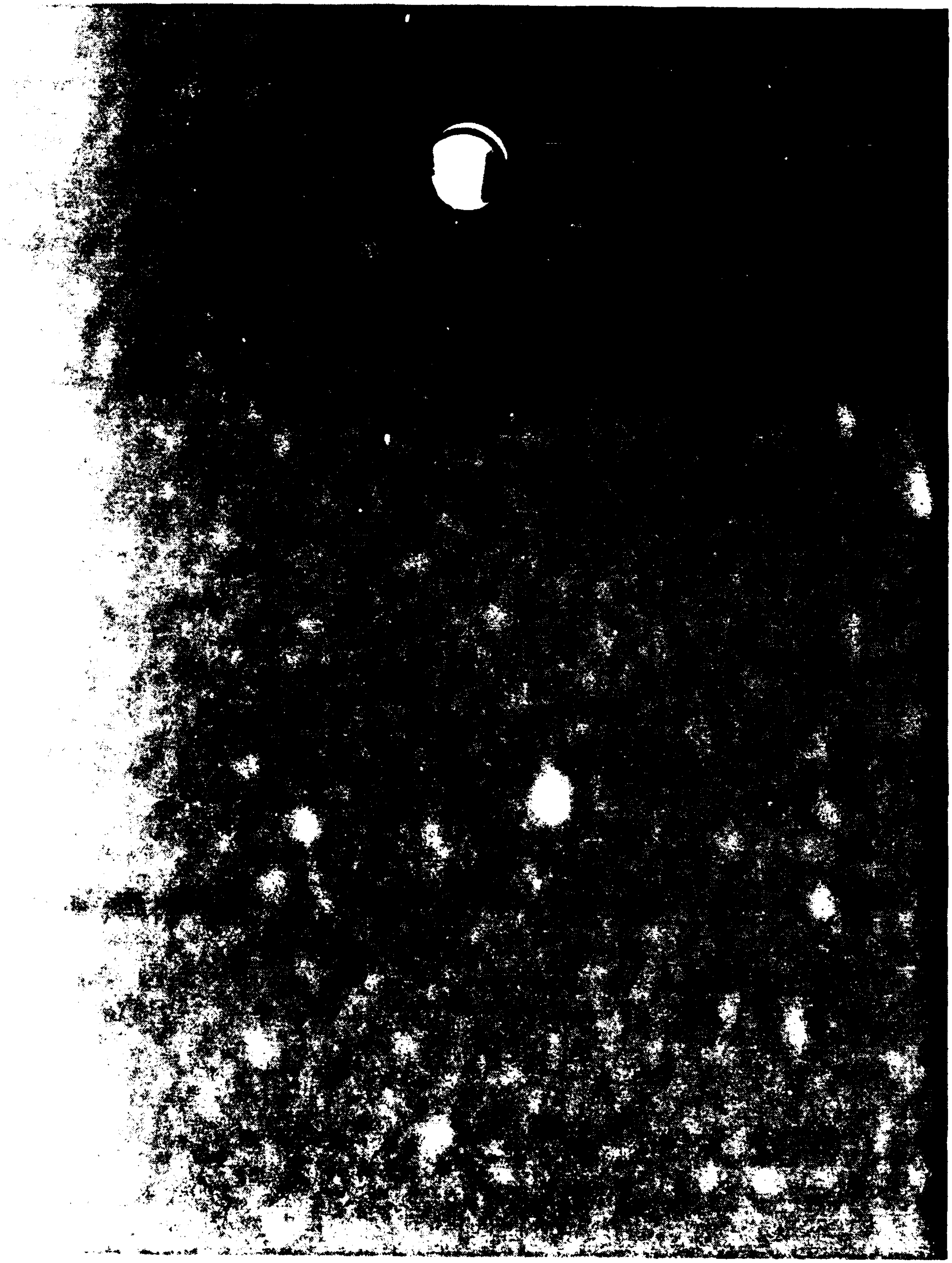

Figure 9. Open shutter photograph of the FX-25 beam extracted into full-density air after drifting thorough 3-m of 3-Torr air.

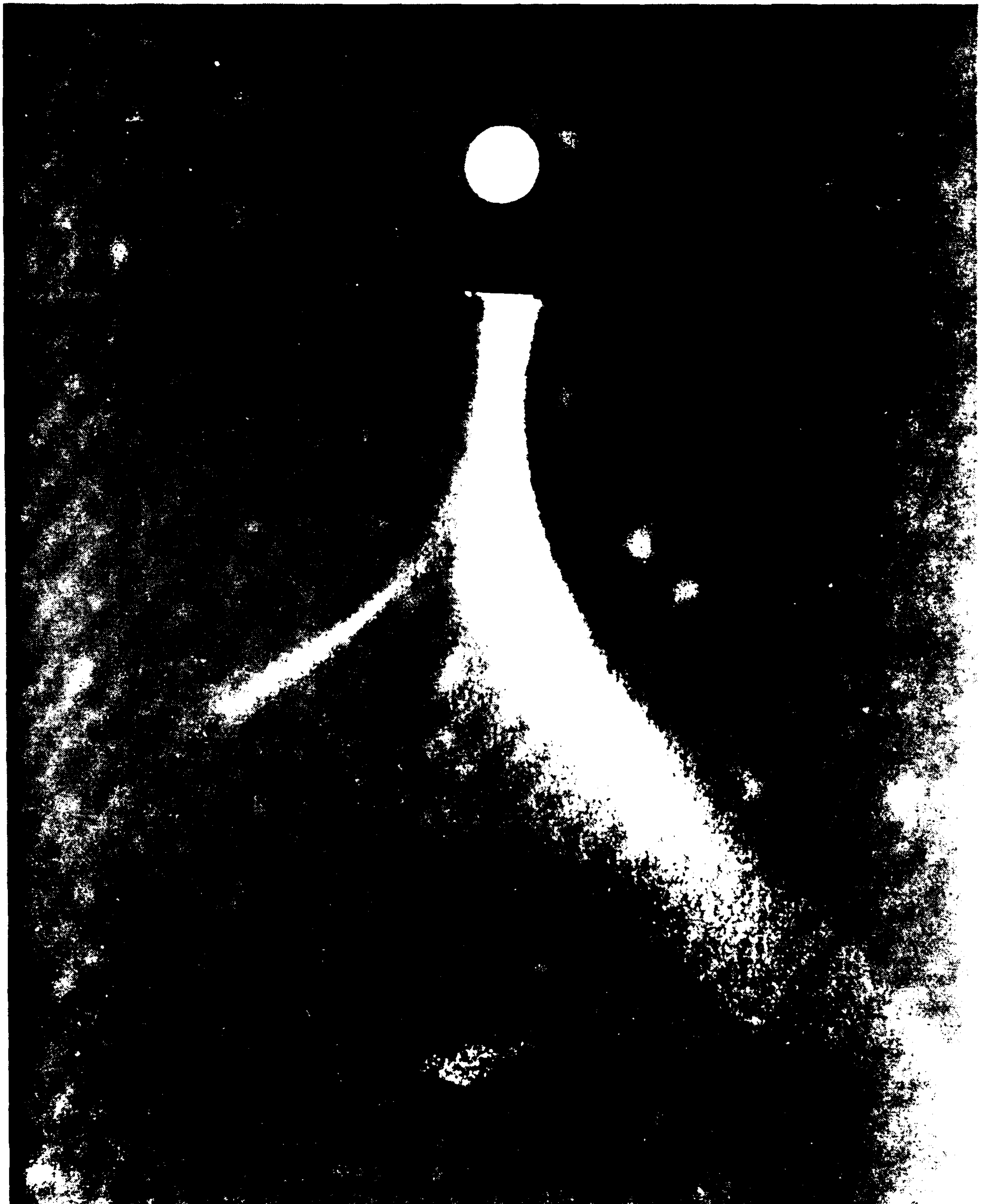

Figure 10. Open shutter photograph of the FX-25 beam extracted into full density air after drifting through 3-m of 0.6-Torr air.

APPENDIX B

INTENSE RELATIVISTIC ELECTRON BEAM PROPAGATION EXPERIMENTS

SECURITY CLASSIFICATION OF THIS PAGE (When Data Entered)

REPORT DOCUMENTATION PAGE		READ INSTRUCTIONS BEFORE COMPLETING FORM
1. REPORT NUMBER	2. GOVT ACCESSION NO.	3. RECIPIENT'S CATALOG NUMBER
4. TITLE (and Subtitle) Intense Relativistic Electron Beam Propagation Experiments		5. TYPE OF REPORT & PERIOD COVERED Interim Report
		6. PERFORMING ORG. REPORT NUMBER AMRC-N-182
7. AUTHOR(s) Carl Ekdahl, Winston Bostick		8. CONTRACT OR GRANT NUMBER(s) F49620-81-C-0016
9. PERFORMING ORGANIZATION NAME AND ADDRESS Mission Research Corporation, 1400 San Mateo Blvd., S.E., Suite A, Albuquerque, New Mexico 87108		10. PROGRAM ELEMENT, PROJECT, TASK AREA & WORK UNIT NUMBERS
11. CONTROLLING OFFICE NAME AND ADDRESS Air Force Office of Scientific Research, Building 410, Bolling Air Force Base, Washington, DC 20332		12. REPORT DATE January 1982
		13. NUMBER OF PAGES 31
14. MONITORING AGENCY NAME & ADDRESS (if different from Controlling Office)		15. SECURITY CLASS. (of this report) Unclassified
		15a. DECLASSIFICATION DOWNGRADING SCHEDULE

16. DISTRIBUTION STATEMENT (of this Report)

Approved for Public Release; Distribution Unlimited

17. DISTRIBUTION STATEMENT (of the abstract entered in Block 20, if different from Report)

18. SUPPLEMENTARY NOTES

19. KEY WORDS (Continue on reverse side if necessary and identify by block number)

Relativistic electron beam propagation
Relativistic electron beam diagnostics

20. ABSTRACT (Continue on reverse side if necessary and identify by block number)

The propagation of intense relativistic electron beams generated by the AFWL FX-25 (1.5 MV, 23 kA, 20 ns) and FX-100 (1.5 MV, 40 kA, 120 ns) accelerators was studied with a variety of diagnostics. The maximum energy transport in low density air (measured calorimetrically) occurred at 1.5 Torr (FX-25) and 0.5 Torr (FX-100). The evolution of the beam current density to a Bennett profile was measured using arrays of subminiature Faraday collectors. Net current measurements with fast response monitors showed significant sharpening of the leading edge of the FX-100 beam at pressures lower than that for maximum energy

DD FORM 1 JAN 73 1473

SECURITY CLASSIFICATION OF THIS PAGE (When Data Entered)

THE PROPAGATION OF INTENSE RELATIVISTIC ELECTRON BEAMS GENERATED BY THE AFWL FX-25 (1.5 MV, 23 KA, 20 NS) AND FX-100 (1.5 MV, 40 KA, 120 NS) ACCELERATORS WAS STUDIED WITH A VARIETY OF DIAGNOSTICS. THE MAXIMUM ENERGY TRANSPORT IN LOW DENSITY AIR (MEASURED CALORIMETRICALLY) OCCURRED AT 1.5 TORR (FX-25) AND 0.5 TORR (FX-100). THE EVOLUTION OF THE BEAM CURRENT DENSITY TO A BENNETT PROFILE WAS MEASURED USING ARRAYS OF SUBMINIATURE FARADAY COLLECTORS. NET CURRENT MEASUREMENTS WITH FAST RESPONSE MONITORS SHOWED SIGNIFICANT SHARPENING OF THE LEADING EDGE OF THE FX-100 BEAM AT PRESSURES LOWER THAN THAT FOR MAXIMUM ENERGY TRANSPORT. PHOTOGRAPHY AND RADIOCHROMIC FILM DOSIMETRY PROVIDE EVIDENCE FOR A HALO OF HIGH ENERGY ELECTRONS THAT ACCOMPANIED THE MAIN BODY OF THE BEAM. EXPERIMENTS WITH EXTRACTION OF THESE PRE-EQUILIBRATED BEAMS INTO FULL DENSITY AIR WILL BE DISCUSSED.

*THIS RESEARCH WAS SUPPORTED BY THE AIR FORCE OFFICE OF SCIENTIFIC RESEARCH (AFSC) UNDER CONTRACTS F49620-81-C-0016 AND IPA-905-79-01016C.

†ON LEAVE FROM STEVENS INSTITUTE OF TECHNOLOGY.

COMPARISON OF EXPERIMENTS

FX-25	FX-100
~1.5 MEV	~1.5 MEV
20-25 KA	35-45 KA
~20 NS	~120 NS
3 M DRIFT TUBE	5 M DRIFT TUBE
5 CM DIAMETER	20 CM DIAMETER

Figure 1. Comparison of experimental parameters for FX-25 and FX-100 propagation experiments.

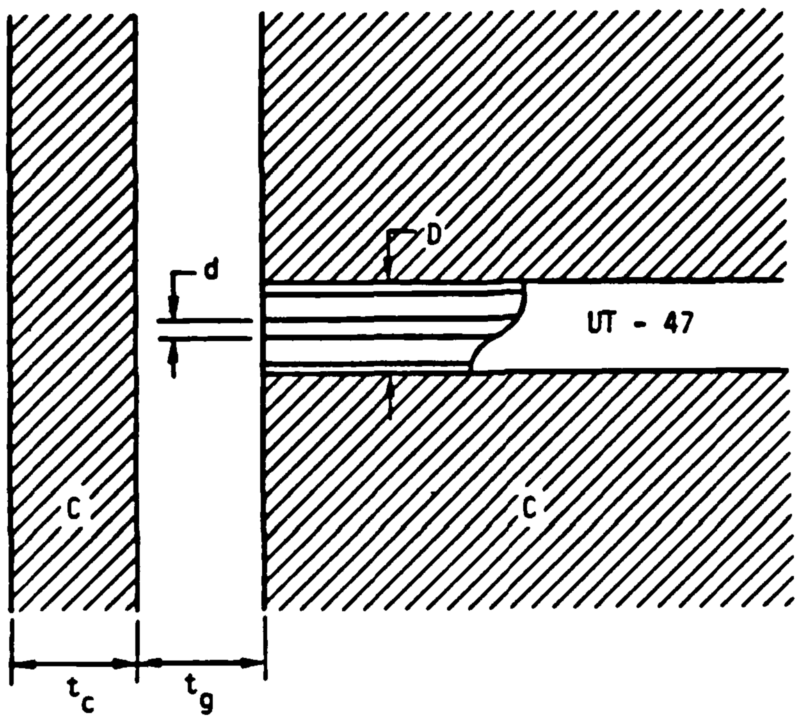

Figure 2. Subminiature Faraday collector for FX-25 beam current density measurements. The graphite shield thickness (t_c = 1.8 mm) is sufficient to stop electrons with energies less than 700 keV. An insulating gap (t_g = 1.7 mm) is provided between the shield and the graphite beam stop, which houses the array of rigid coaxial cable (UT-47) detectors. These have solid copper outer (D = 1.2 mm) and inner (d = 0.29 mm) conductors, and Teflon insulation. FX-100 array similar, except shield was 125 μm Ti and gap was insulated with 25 μm of Kapton.

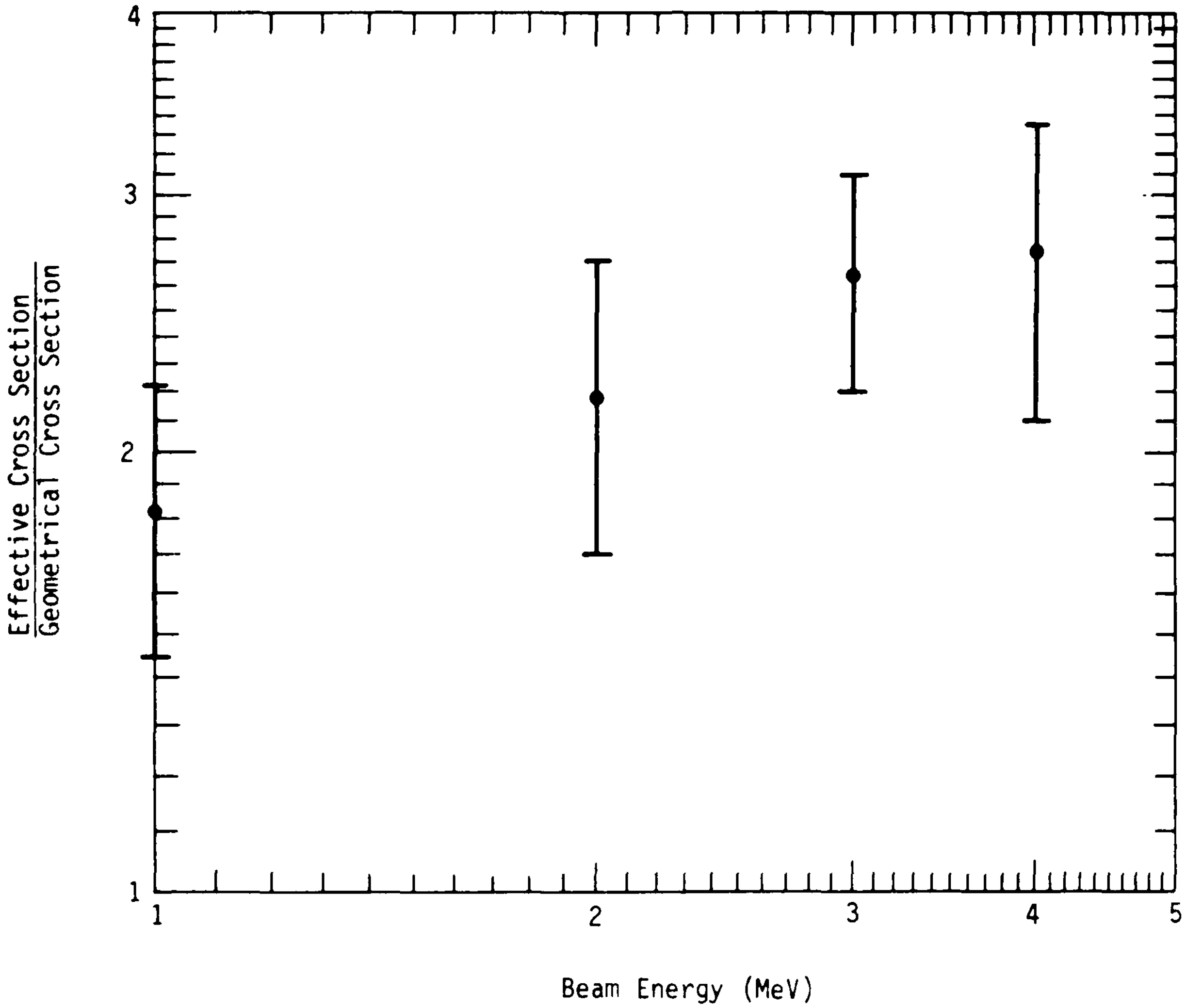

Figure 3. Energy dependence of effective collection area of FX-25 subminiature charge collectors. This dependence is the result of electron scattering in surrounding materials.

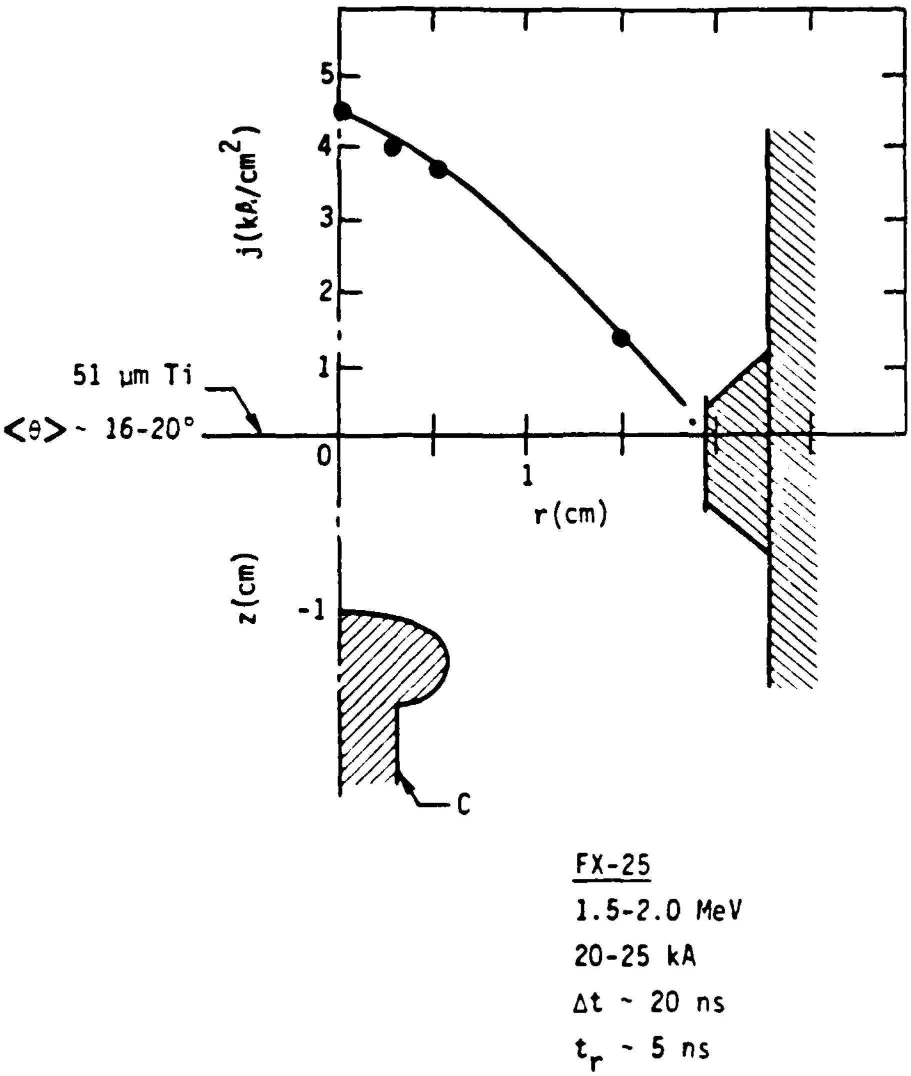

Figure 4. FX-25 diode geometry and beam current density profile measured in vacuum 0.5 cm from the titanium anode foil. The 51-μm anode foil induces a mean scattering angle of 16-20°. The current density profile shown was obtained at the time of peak current (I_{max} = 22 kA). The FX-25 produced beams having nominal values for parameters shown.

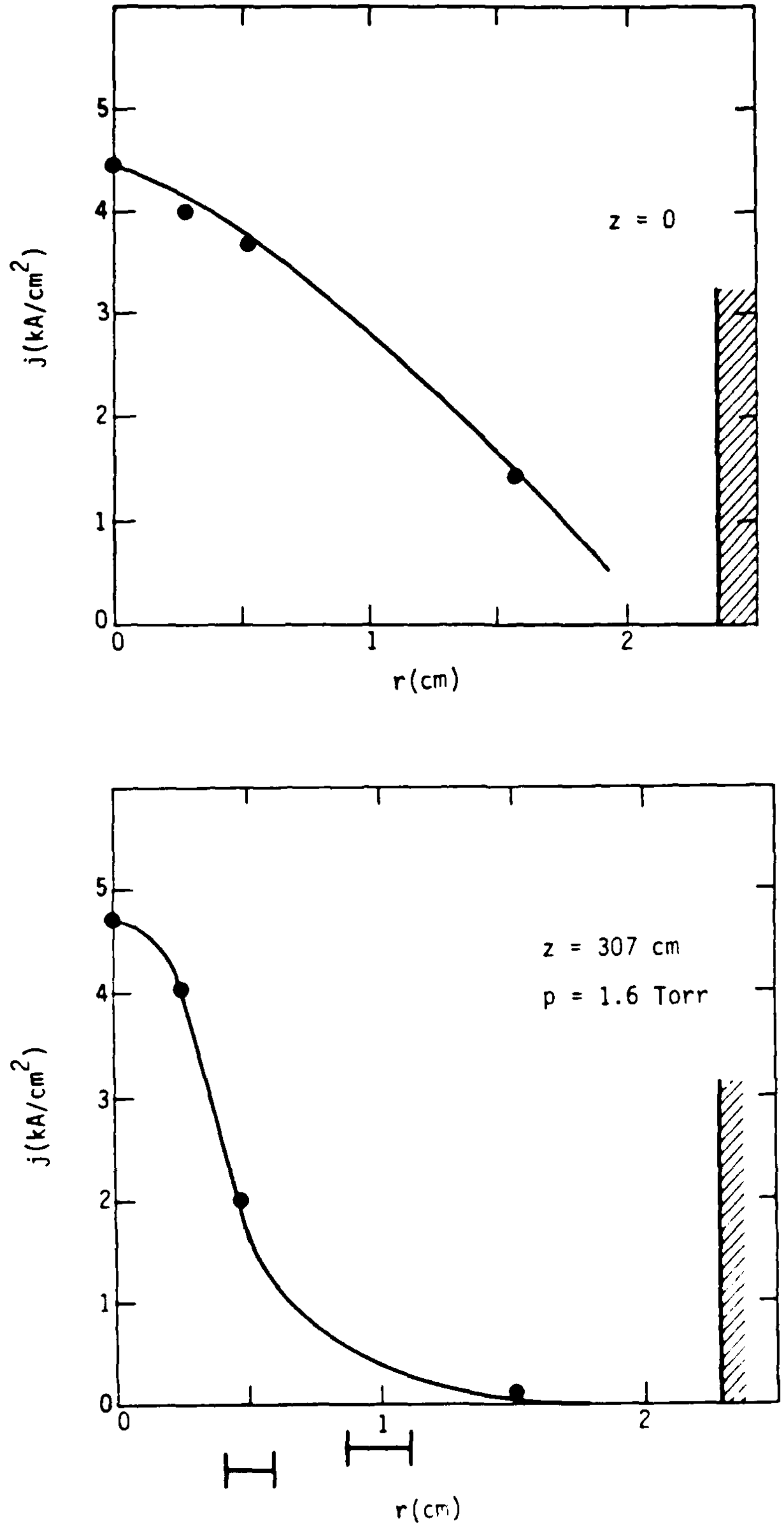

Figure 5. Evolution of the FX-25 beam current distribution near the diode (upper figure) into a Bennett-like profile (lower figure) after propagating 3-m in 1.6-Torr air (the pressure for maximum energy transport). Also shown are the range of radii determined from damage to dielectric foils (centered at r 0.5 cm), and determined from extent of 3914 Å (N_2^+) emission (centered at r 1 cm).

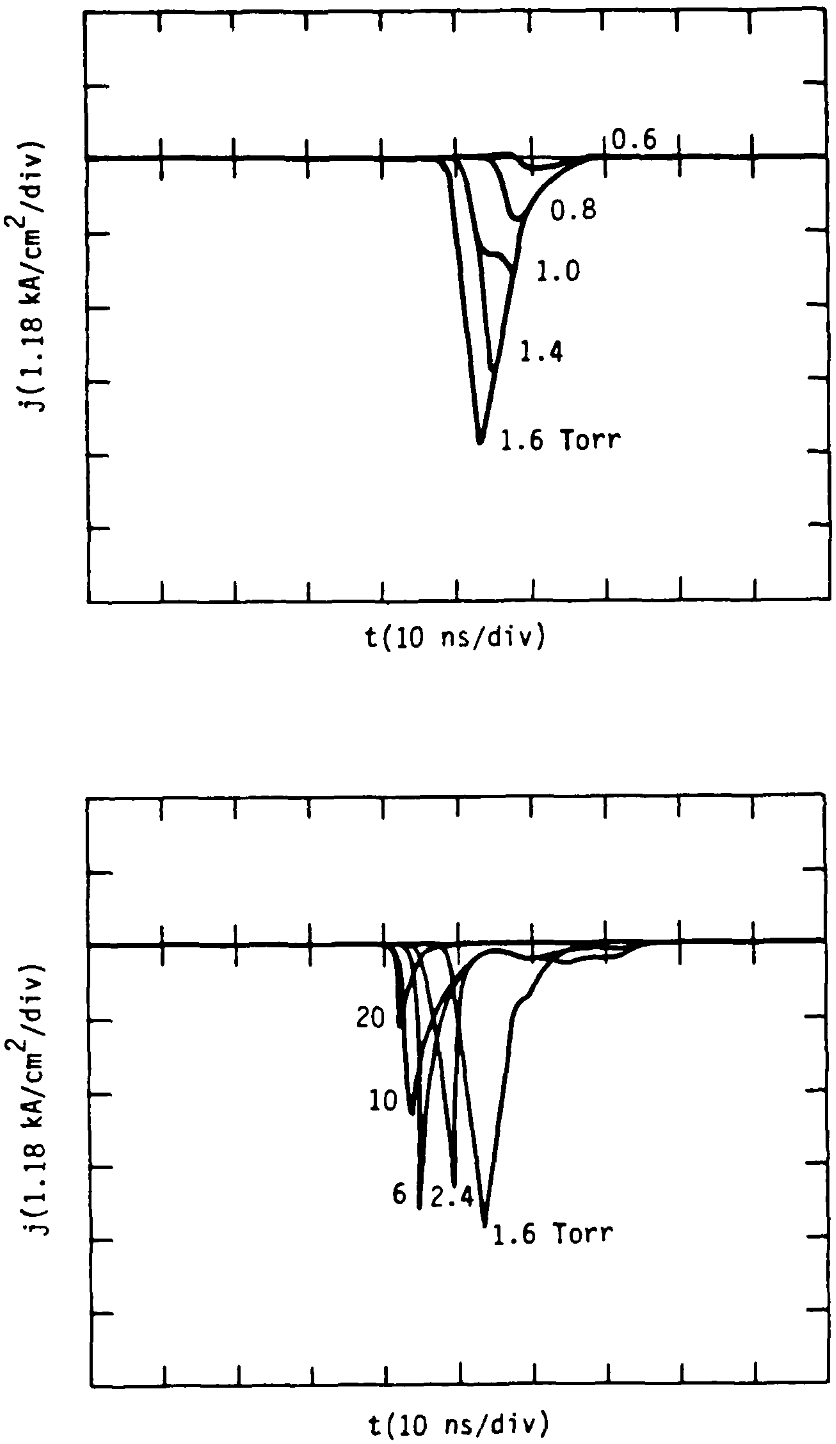

Figure 6. Beam current density on axis at Z = 3 m for different pressures near the propagation window. The current density near the diode had a waveform that approximated the envelope of these signals. The erosion of the beam nose is clearly evident at pressures below 1.6 Torr (upper). At higher pressures both nose erosion and tail loss resulting from hosing are evident (lower).

Figure 7. Open shutter (time integrated) photograph of FX-25 beam extracted into full-density air (630 Torr) through a 25-μm Kapton foil after propagating 3-m in a 5-cm diameter conducting drift tube. The air pressure in the drift tube was 1.6 Torr, the pressure for maximum beam energy transport. The beam in the drift tube is visible through the round port on the drift tube. The apparent flaring of the beam in full density air is interpreted as the time integration of the beam motion resulting from the hose instability.

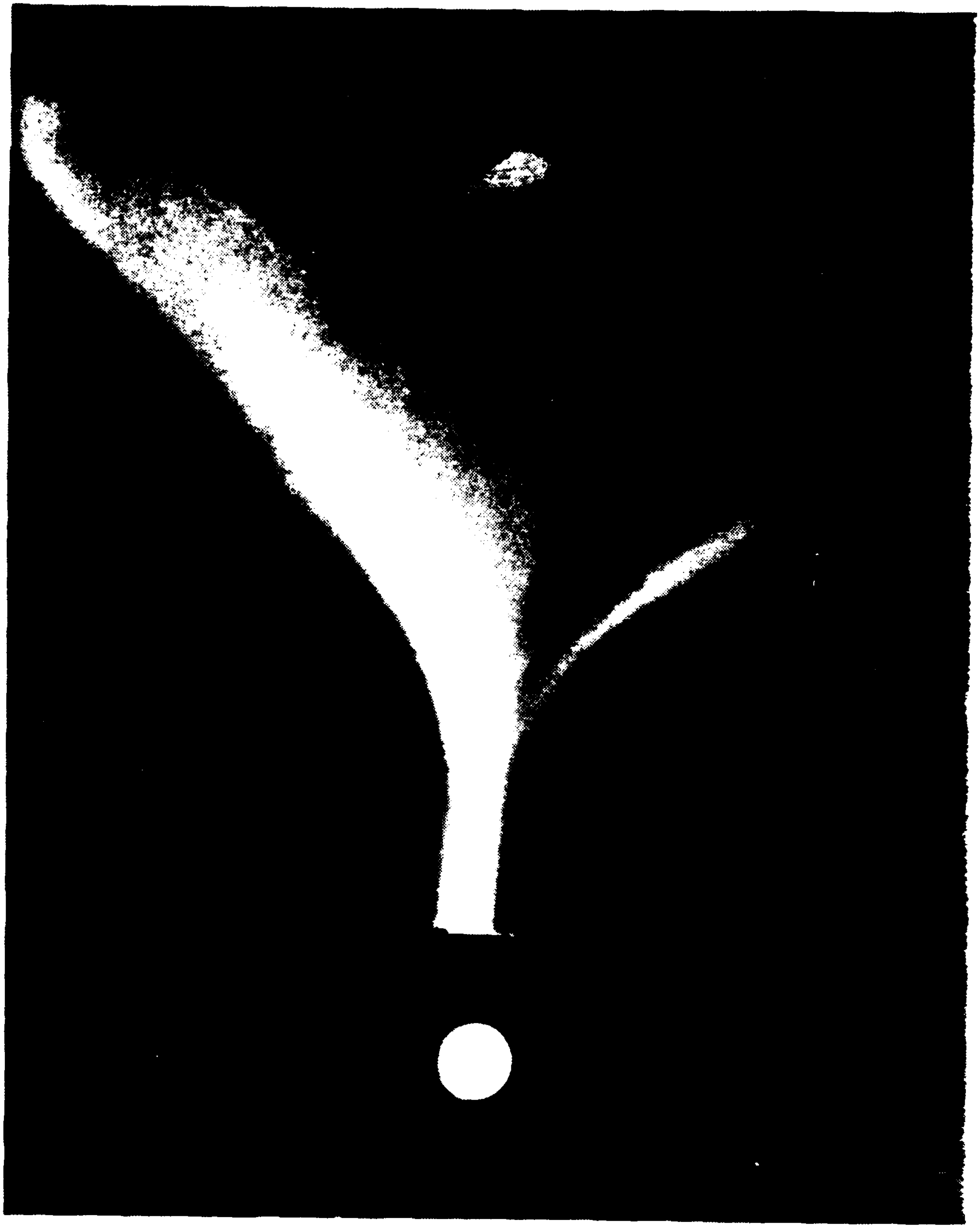

Figure 8. Open shutter photograph of the FX-25 beam extracted into full-density air after drifting through 3-m of 0.8 Torr air. The preparation of the beam by drifting through this lower-density gas cell has stabilized the hose instability in full density air.

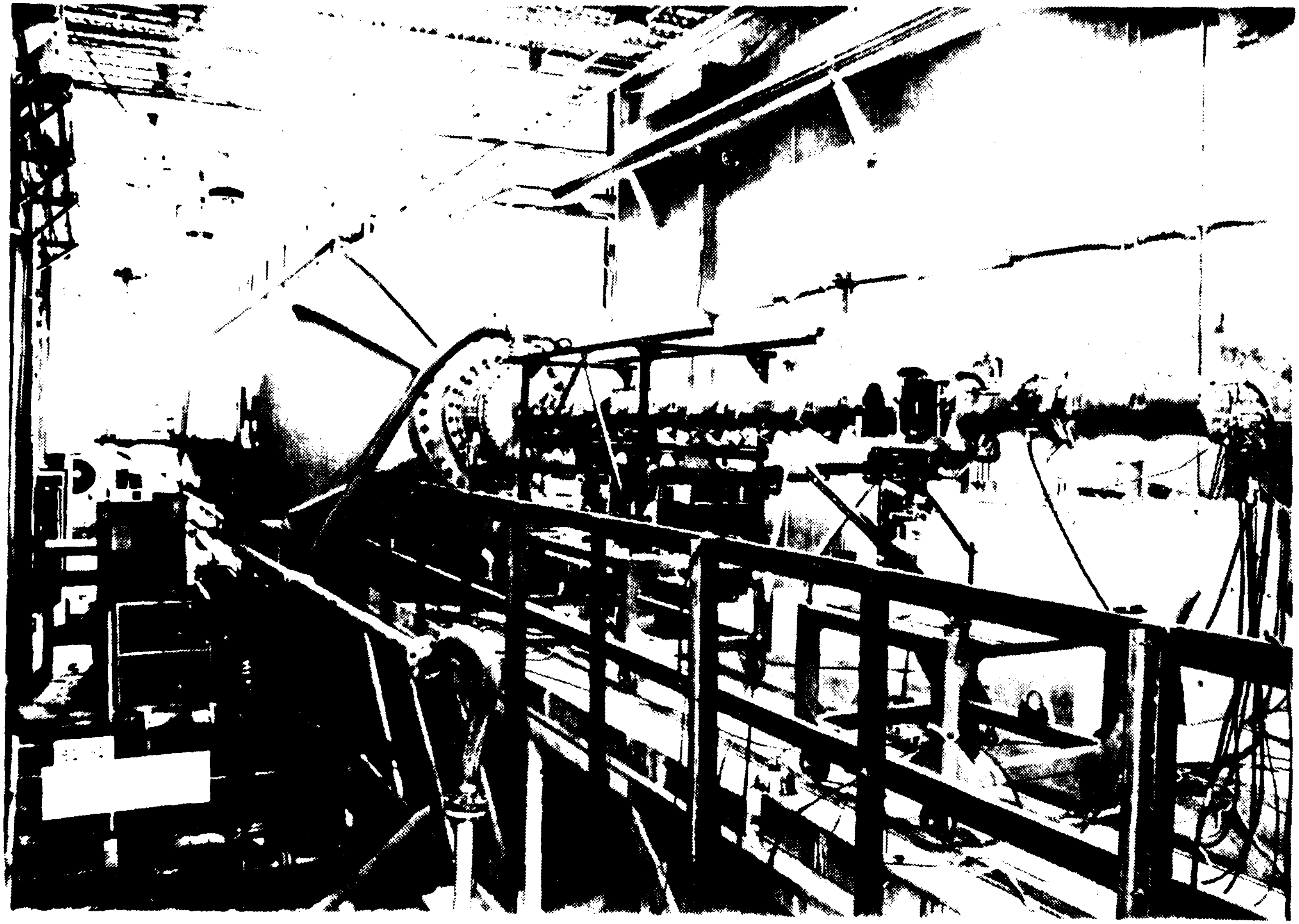

Figure 9. FX-100 Van de Graaff e-beam generator with 5.5-m low-pressure drift tube for propagation experiments.

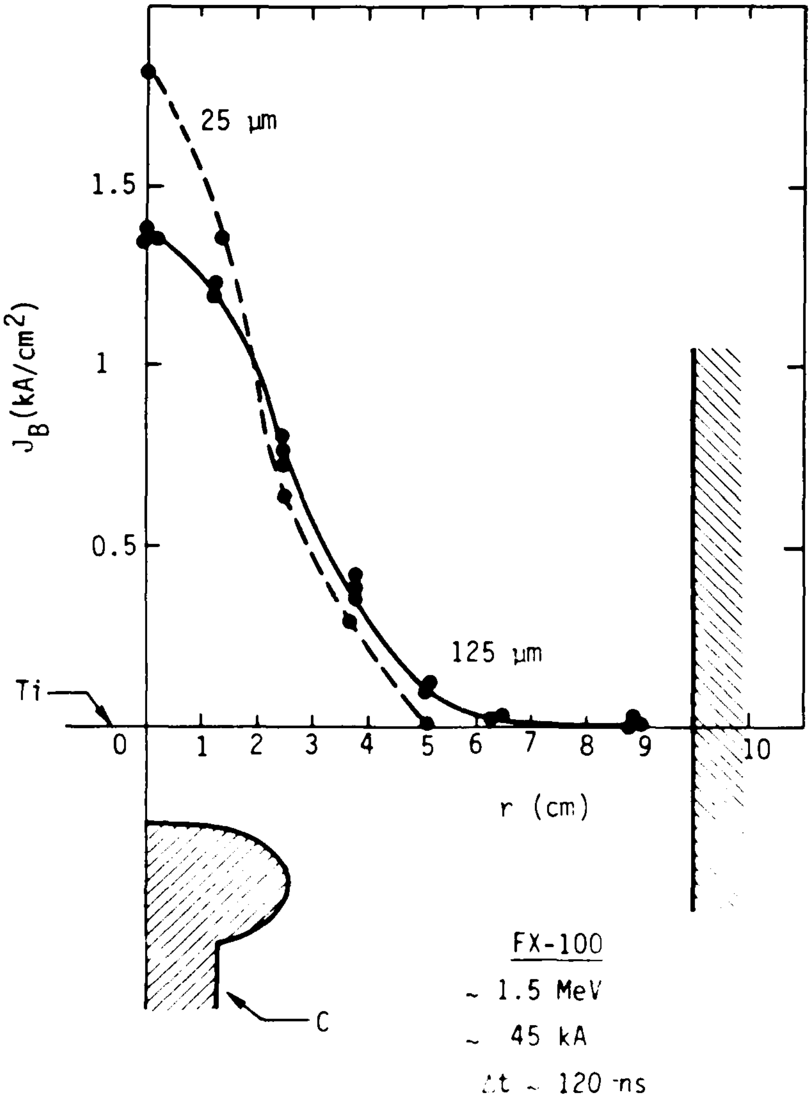

Figure 10. Multiple Faraday collector array measurements of FX-100 beam current density distribution in vacuum 1.3 cm from the anode foil. Distribution for two different foil thicknesses are shown. However, all propagation experiments were performed using 25-μm Ti foil anodes.

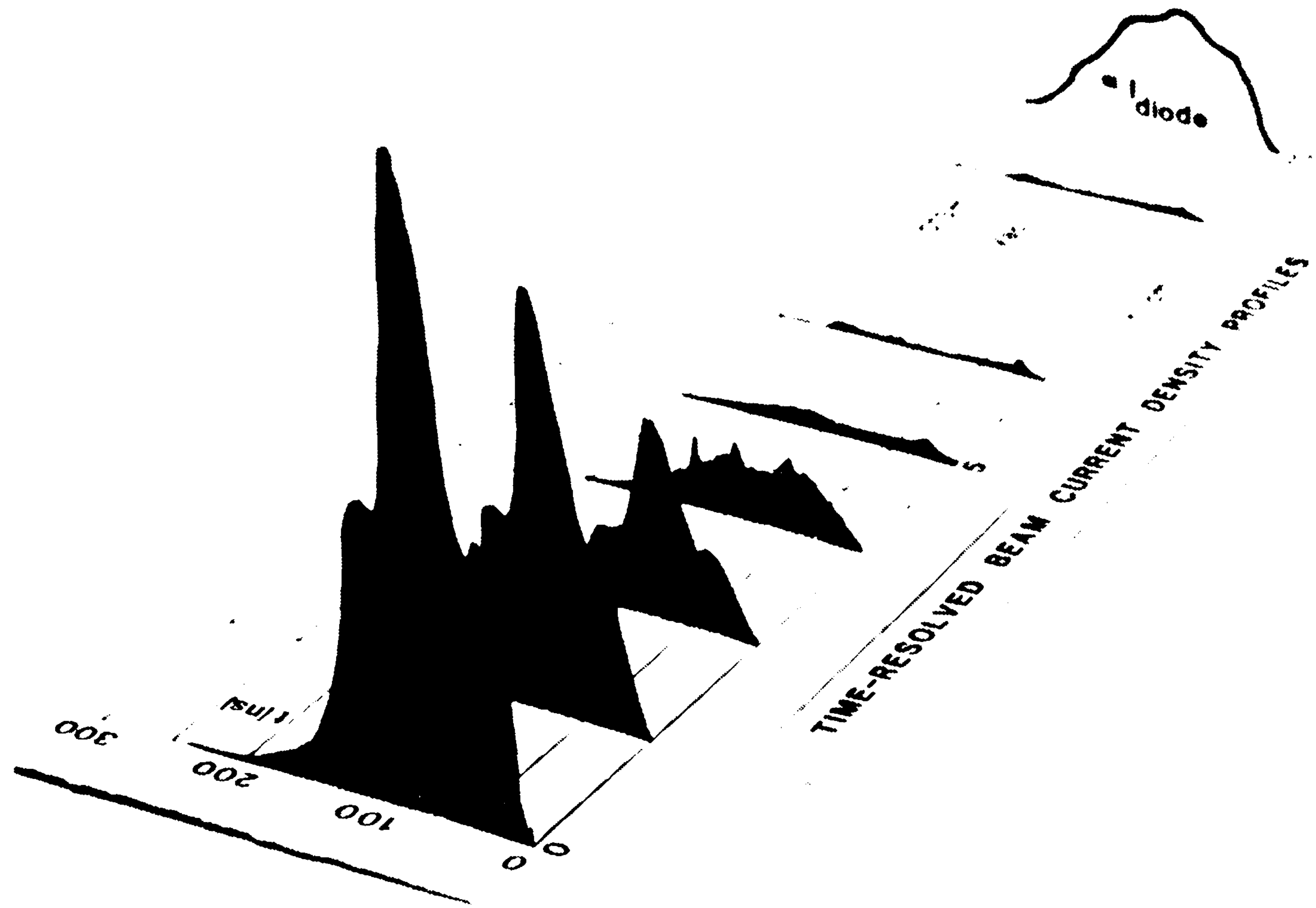

Figure 11. Time resolved beam current density, profile measured 1.3 cm from 25 μm Ti anode foil in vacuum.

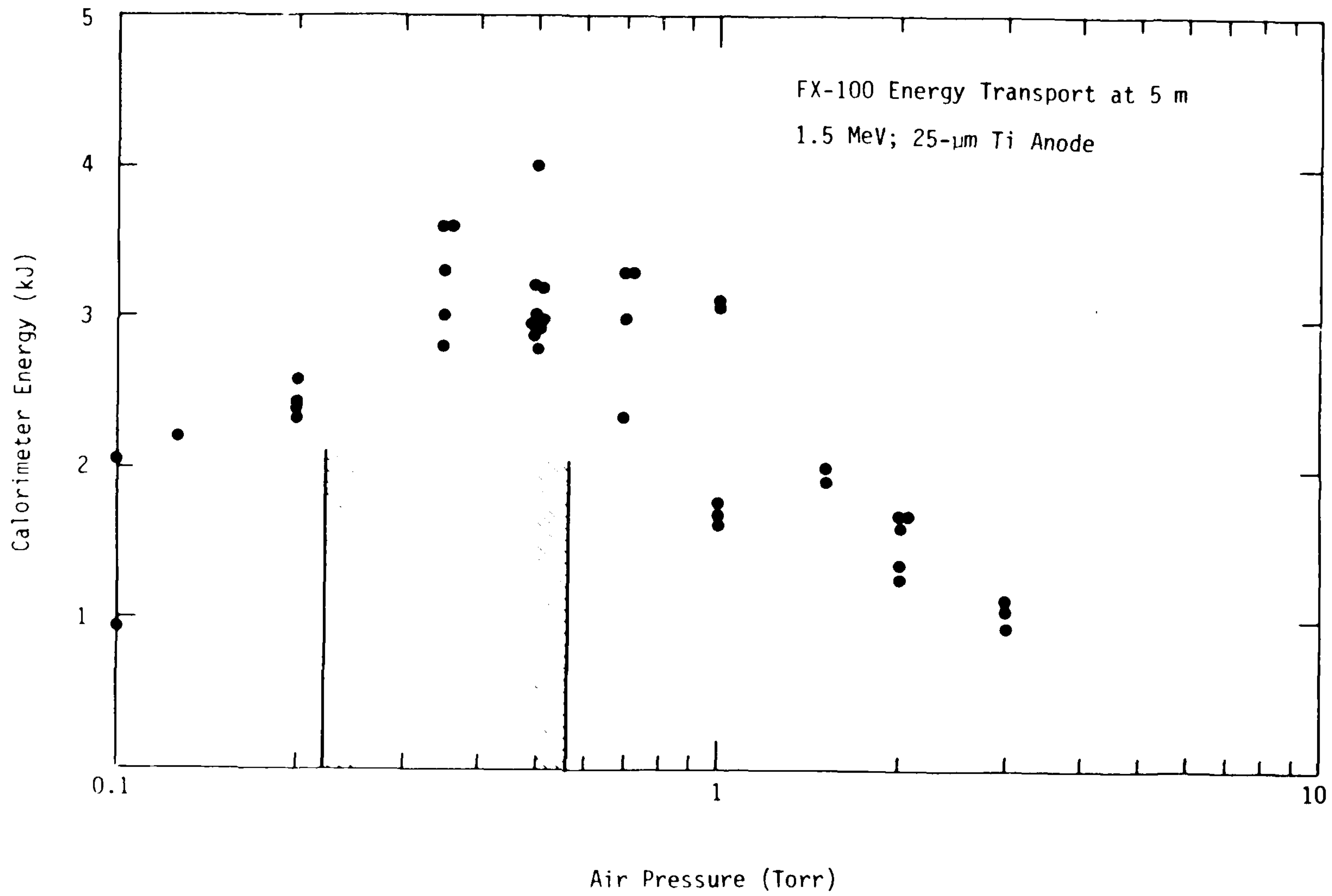

Figure 12. FX-100 beam energy deposition in C calorimeter at end of 5-m drift tube filled with air at pressure shown.

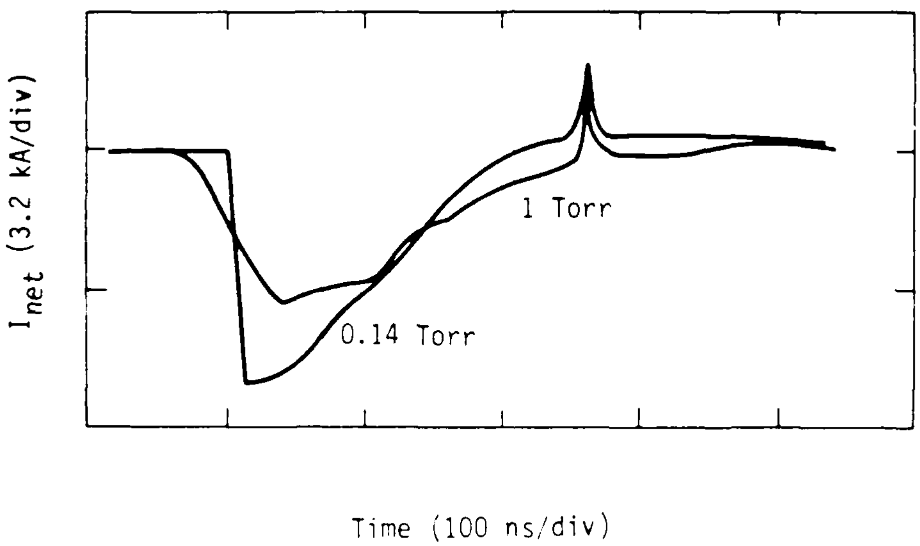

Figure 13. Measurements of net current in FX-100 propagation experiments at pressures slightly less and greater than the pressure for maximum energy transport (0.5 Torr). This shows the pulse sharpening effect at low pressures.

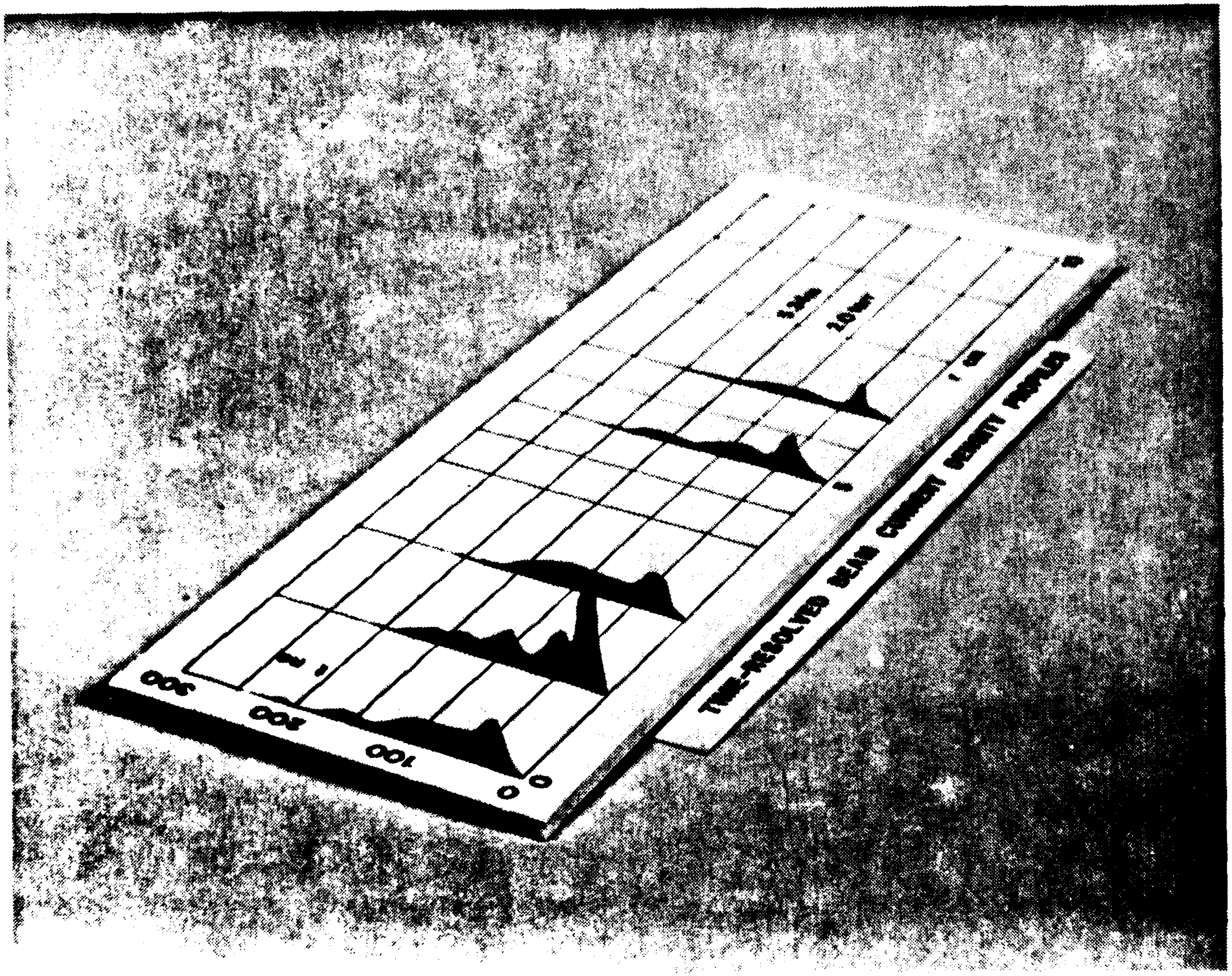

Figure 14. Time resolved beam current density profile at Z = 5.34 m.
p_o = 2.0 Torr.

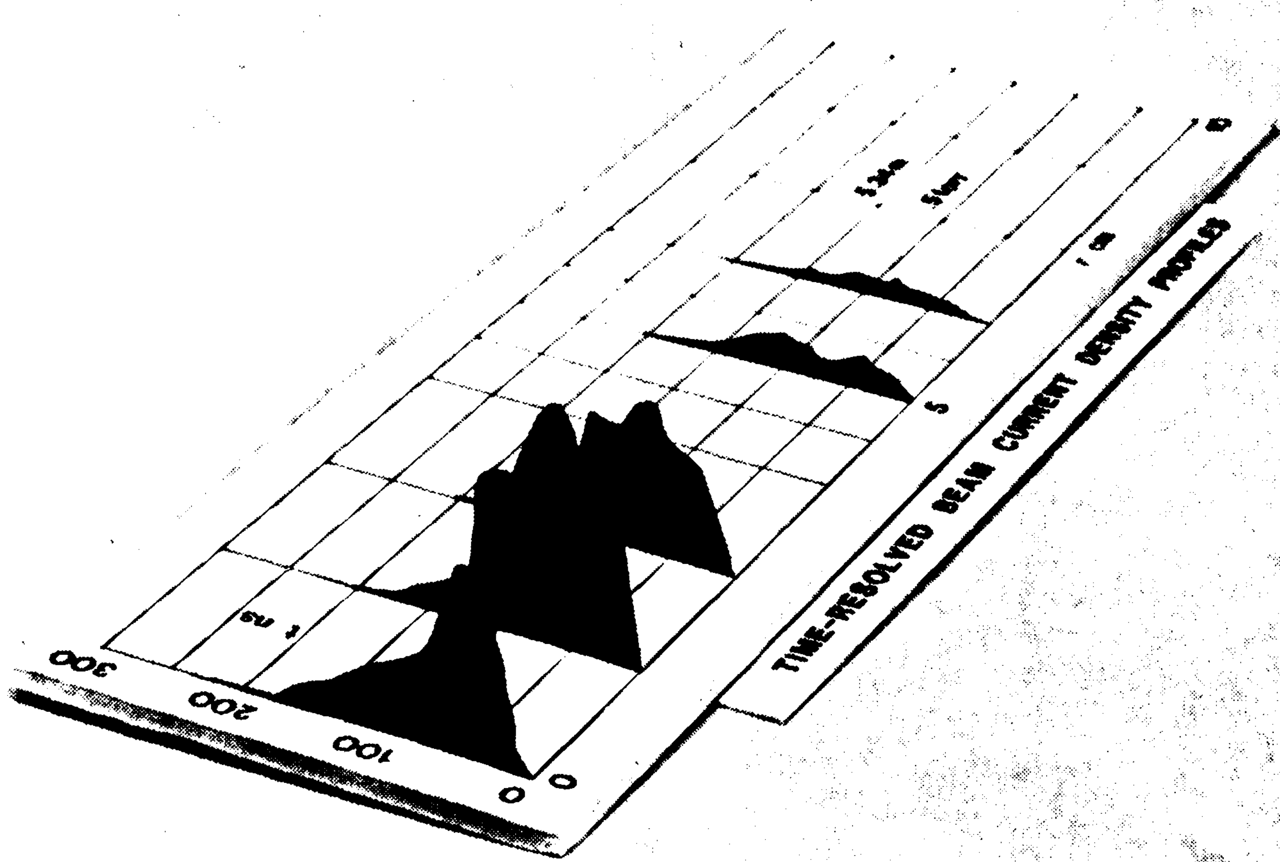

Figure 15. Time resolved beam current density profile at Z = 5.34 m. p_0 = 0.5 Torr.

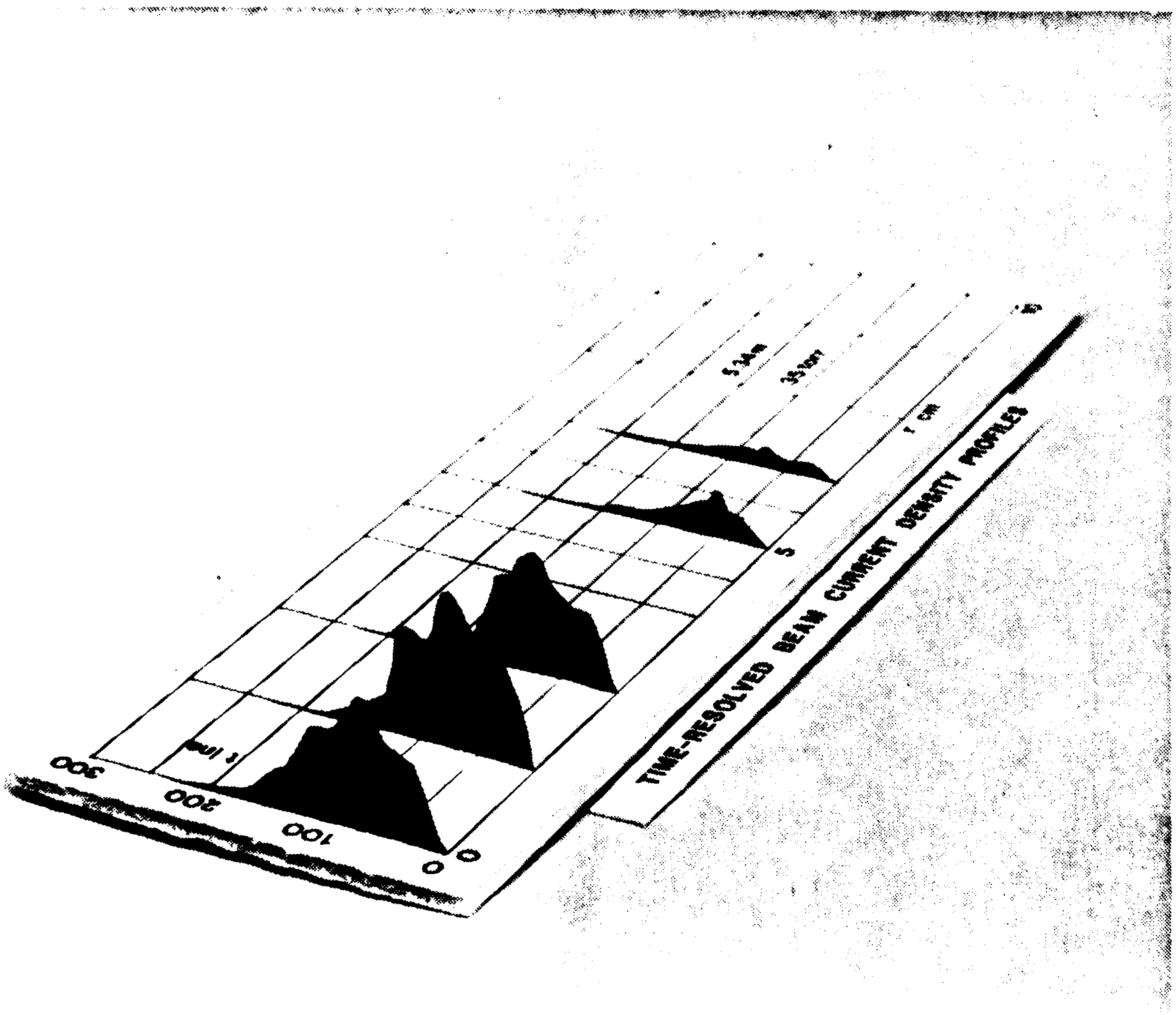

Figure 16. Time-resolved beam current density profile at Z = 5.34 m. p_0 = 0.35 Torr.

Figure 17. FX-100 open shutter photographs at Z = 4.5 m and pressures spanning the propagation window showing the molecular band emission at high and low pressures and atomic (O) line emission at intermediate pressures. (Beam propagating left to right, circular aperture ~17.5 cm diameter). Note the apparent annular halo of emission surrounding the beam.

[illegible] Torr

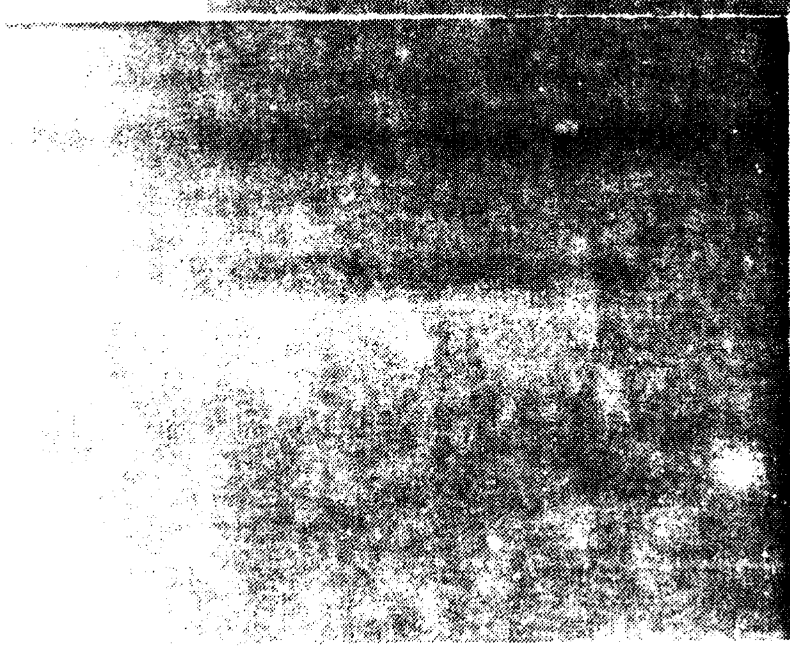

Figure 18. Open shutter photographs at Z ~10 cm at air pressures near the peak of the propagation window. (Beam propagating right to left, axial clear aperature ~24 cm.) Note the apparent development of an annular "halo". The air pressure in Torr for these photographs is indicated between each pair (obtained at the same pressures).

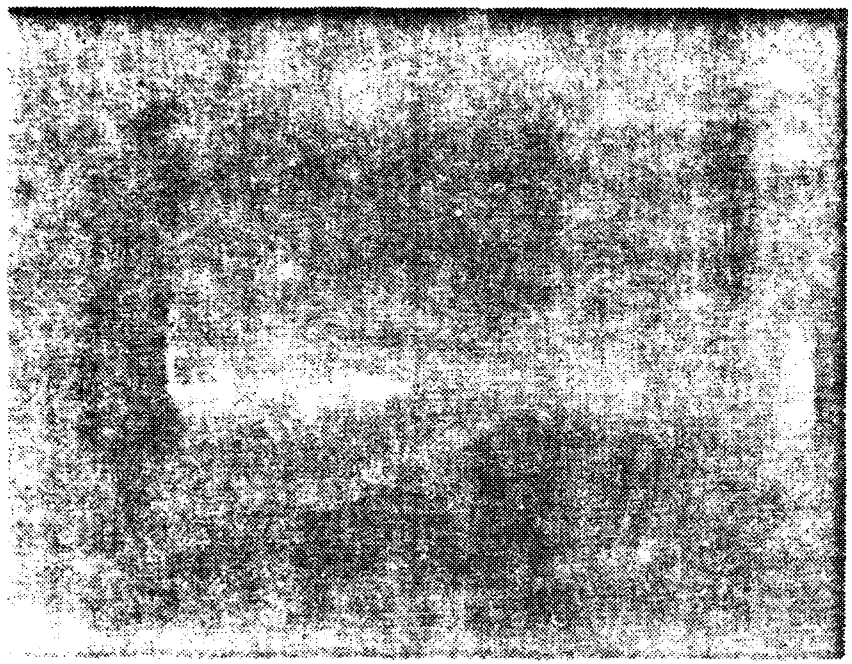

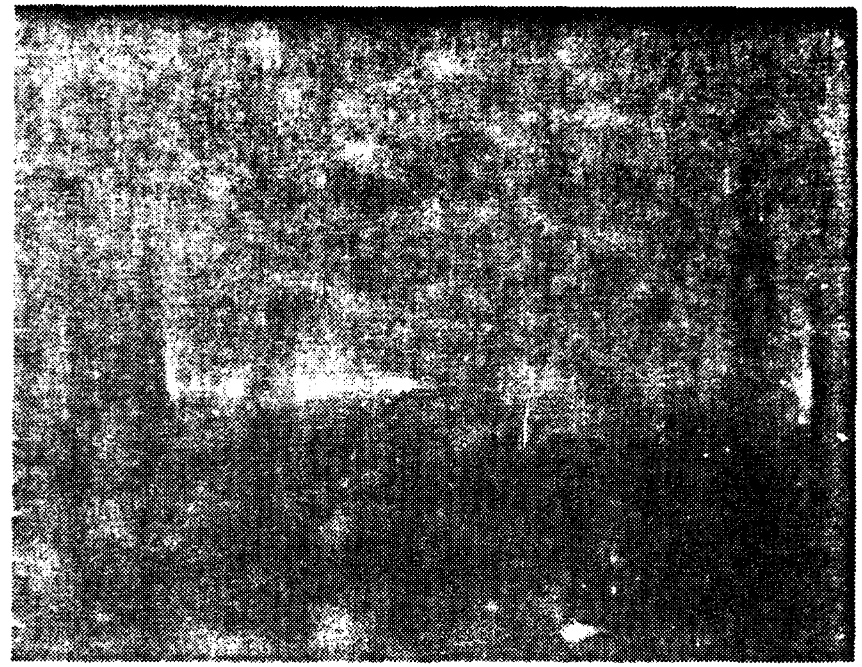

.5

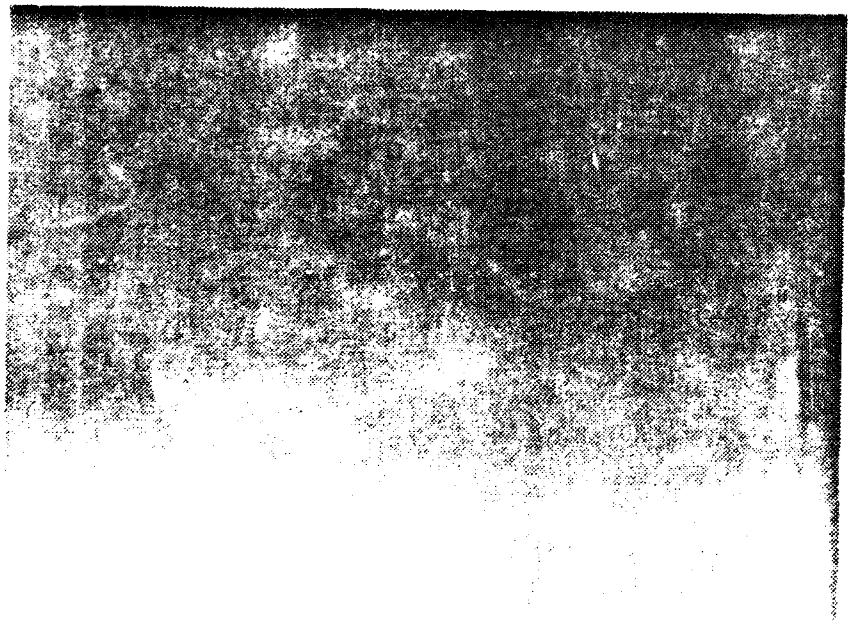

.35

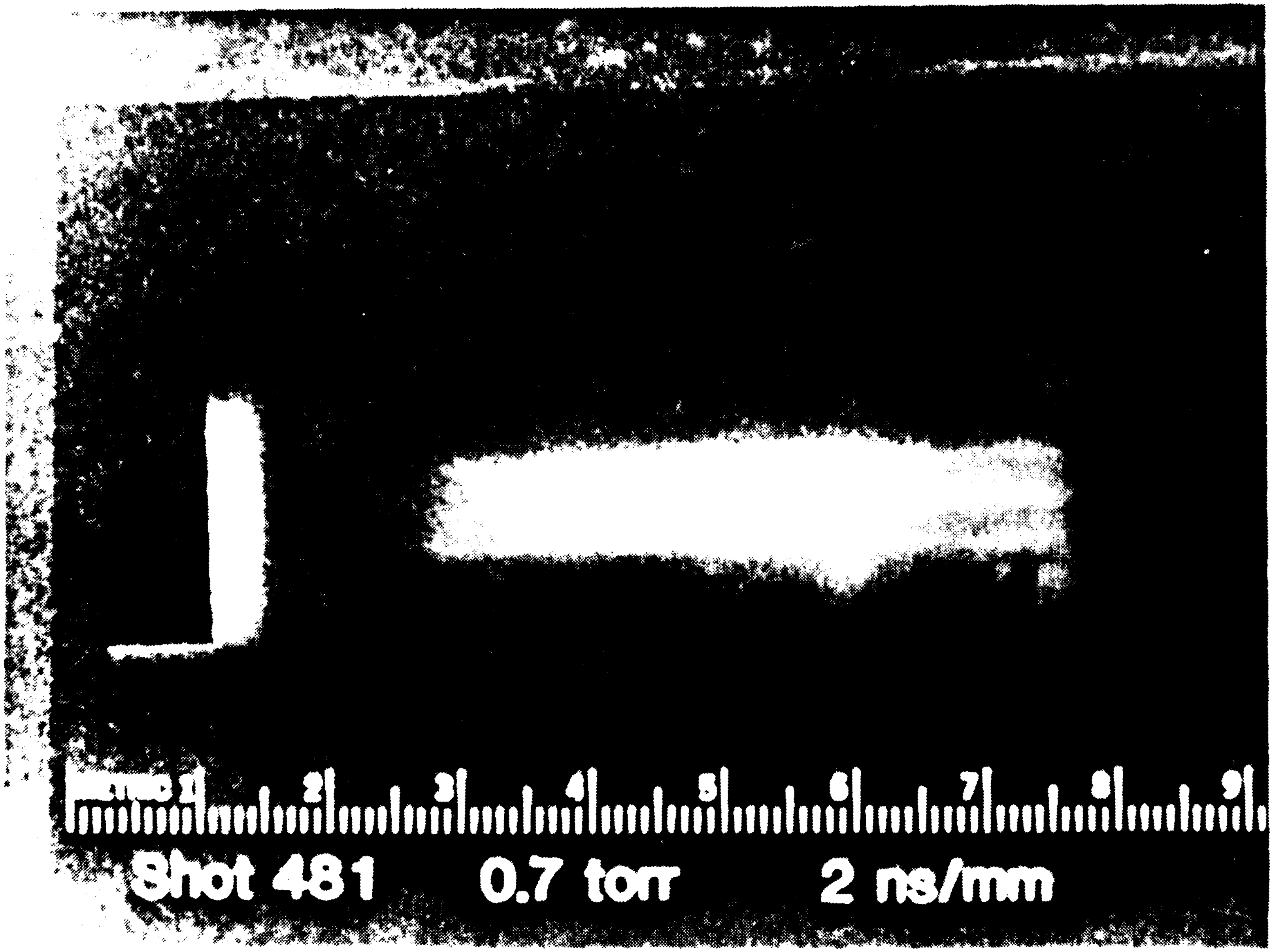

Figure 19. Imacon streak comera picture taken through a vertical slit at 4.5 m showing development of annular halo emission.

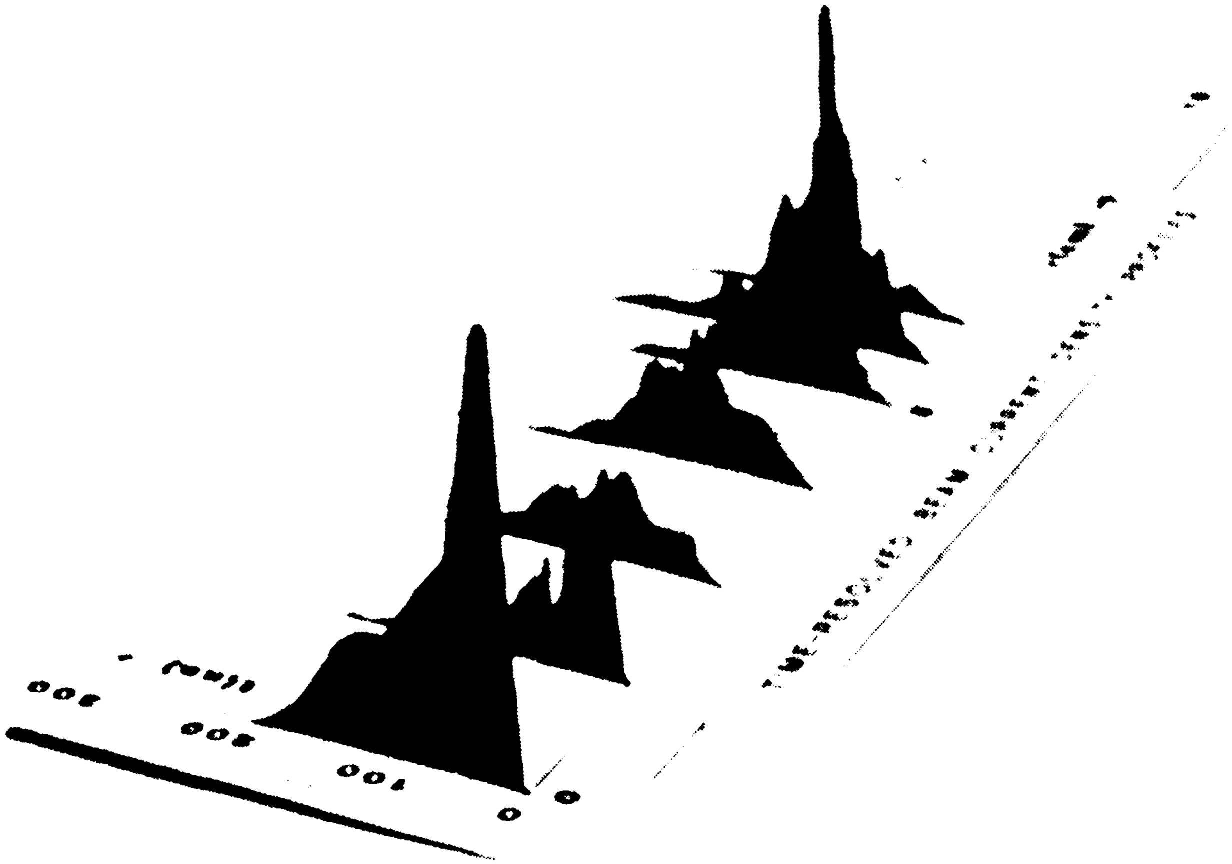

Figure 20. Time resolved beam current density profile at Z = 0.81 m. p_0 = 0.35 Torr. Note development of "halo" current of high energy (≳150 keV) electrons.

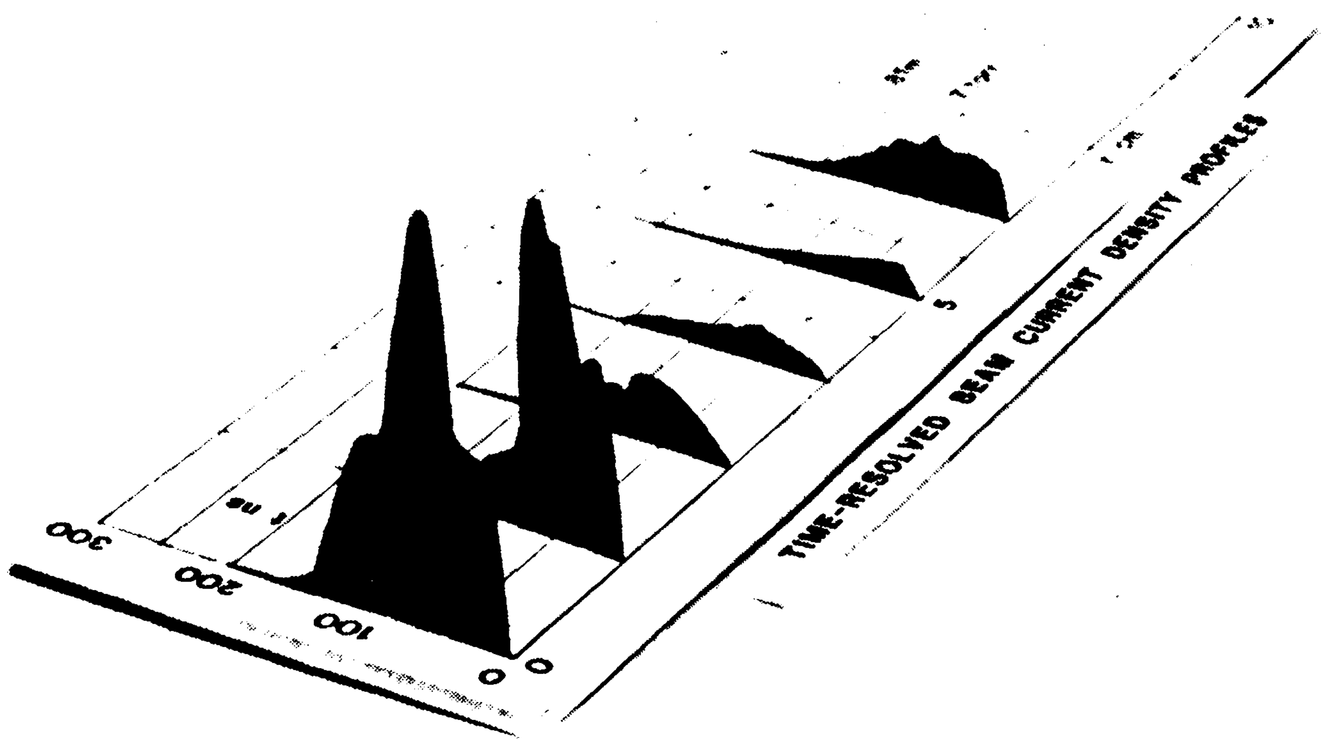

Figure 21. Time resolved beam current density profile at Z = 0.81 m. p_o = 0.7 Torr.

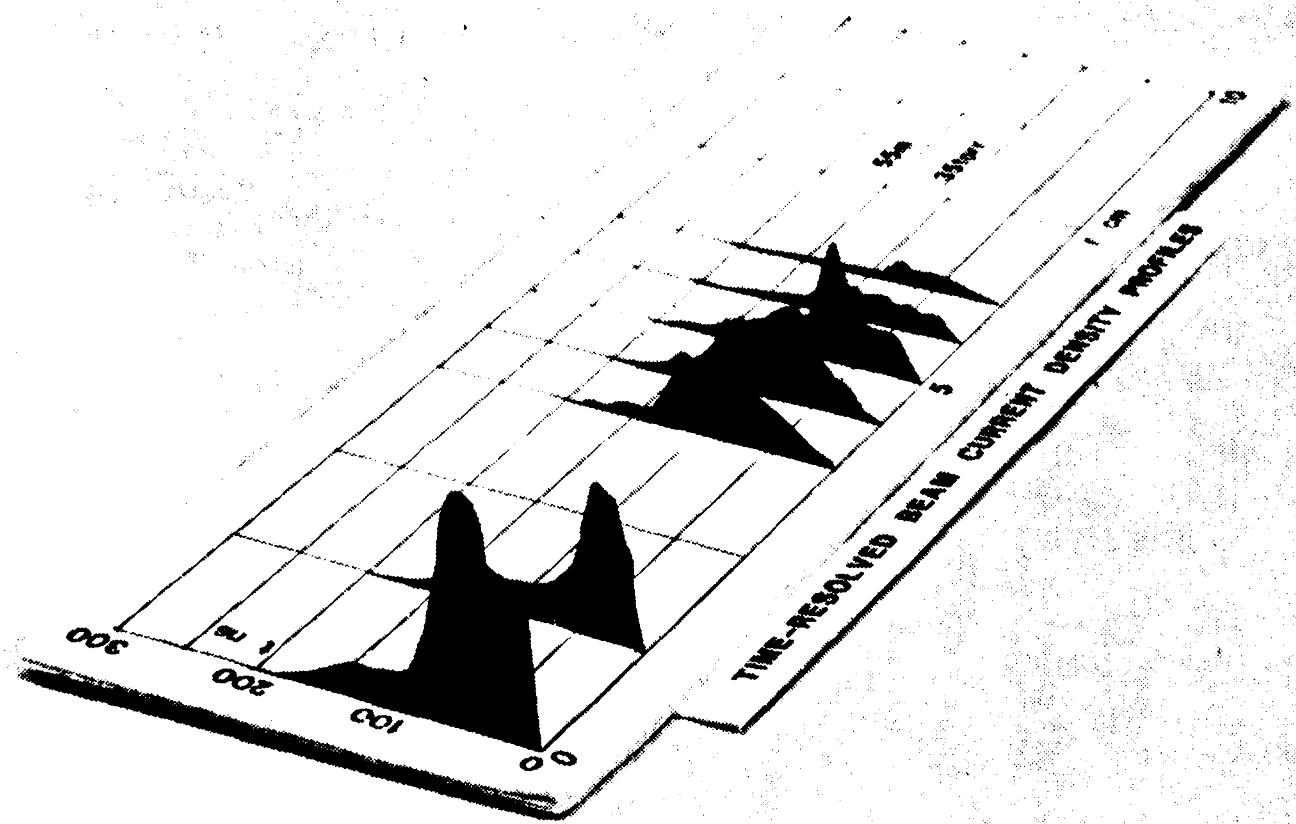

Figure 22. Time resolved beam current density profile at Z = 0.55 m. p_o = 0.35 Torr.

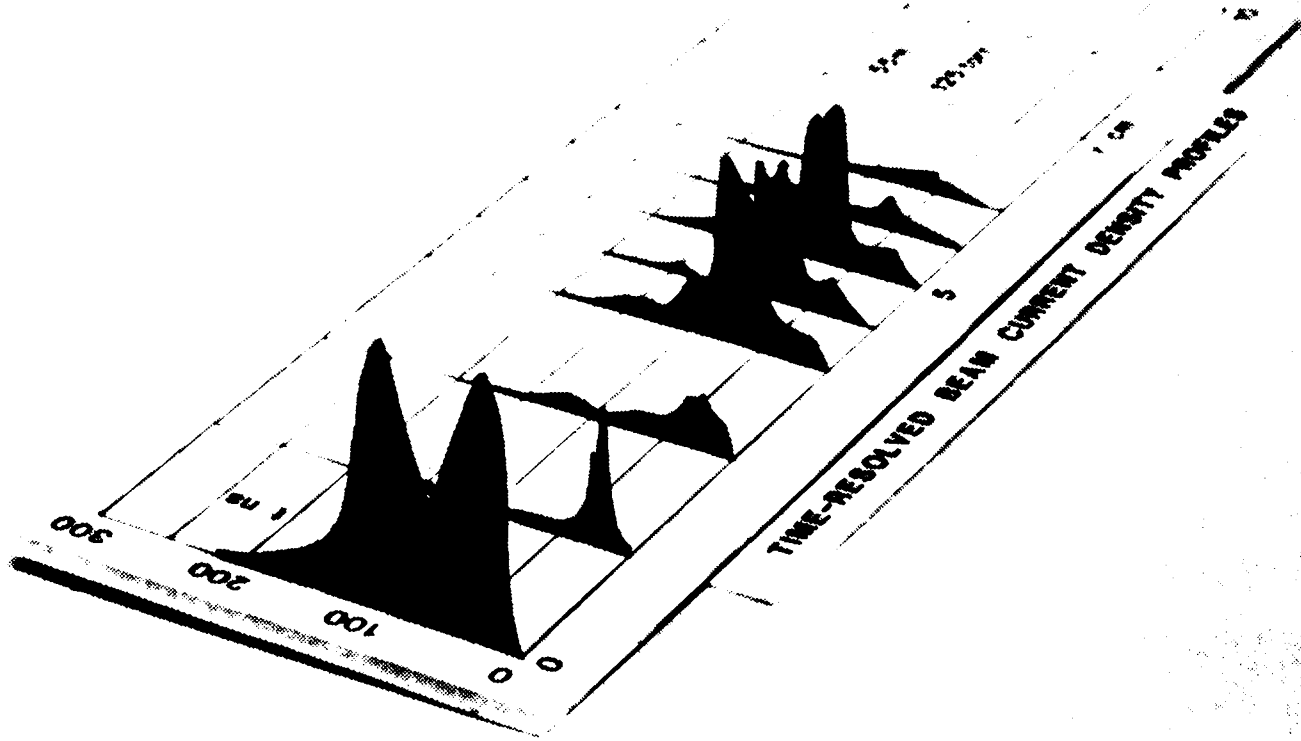

Figure 23. Time resolved beam current density profile at Z - 0.55 m. p_o = 0.125 Torr.

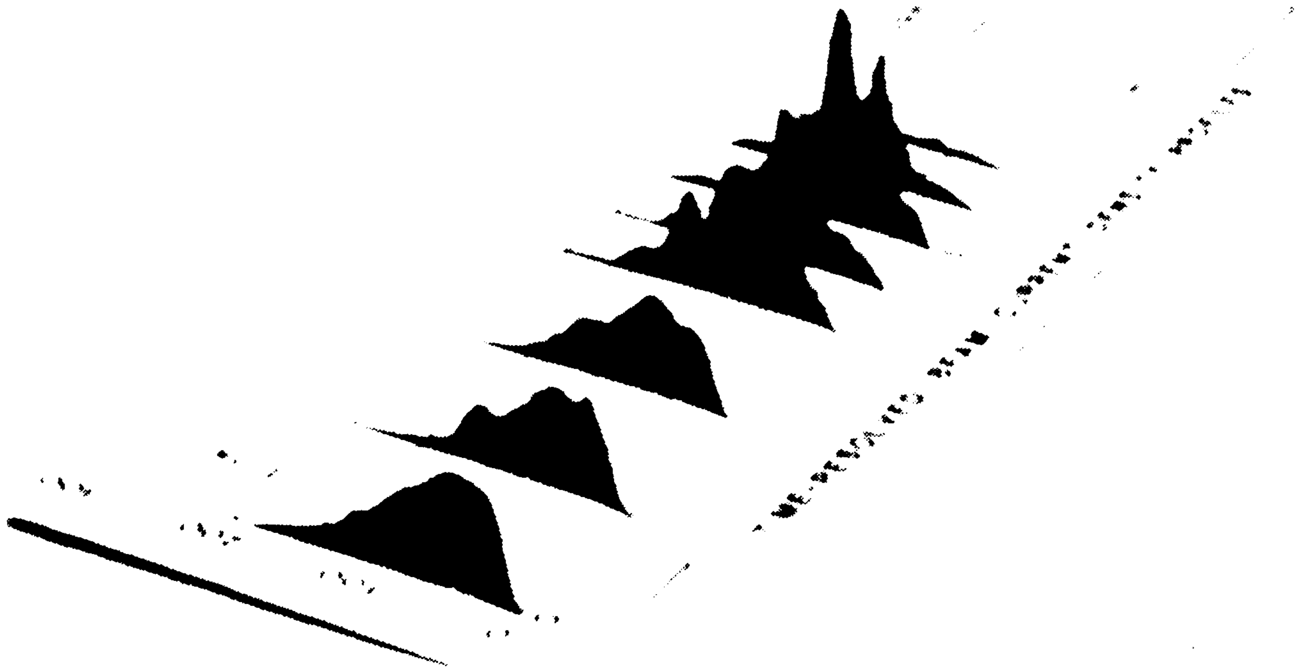

Figure 24. Time-resolved beam current density profile at Z = 0.29 m. p_o = 0.7 Torr.

The authors are indebted to the following members of the Dynamic Testing Division at LANL for the time resolved photography of the FX-100 propagation experiments: Bob Benjamin (M-6), Steve Schmidt (M-6), Tom Starke (M-2), Dave Moir (M-2), and Lee Builta (M-2).

APPENDIX C

SPECTRAL MEASUREMENTS OF RELATIVISTIC ELECTRON BEAM GENERATED EMISSION IN AIR

SECURITY CLASSIFICATION OF THIS PAGE (When Data Entered)

REPORT DOCUMENTATION PAGE		READ INSTRUCTIONS BEFORE COMPLETING FORM
1. REPORT NUMBER	2. GOVT ACCESSION NO.	3. RECIPIENT'S CATALOG NUMBER
4. TITLE (and Subtitle) Spectral Measurements of Relativistic Electron Beam Generated Emissions in Air		5. TYPE OF REPORT & PERIOD COVERED Interim Report
		6. PERFORMING ORG. REPORT NUMBER AMRC-N-183
7. AUTHOR(s) L. A. Wright, C. A. Ekdahl		8. CONTRACT OR GRANT NUMBER(s) F49620-81-C-0016
9. PERFORMING ORGANIZATION NAME AND ADDRESS Mission Research Corporation, 1400 San Mateo Blvd., S.E., Suite A, Albuquerque, New Mexico 87108		10. PROGRAM ELEMENT PROJECT, TASK AREA & WORK UNIT NUMBERS
11. CONTROLLING OFFICE NAME AND ADDRESS Air Force Office of Scientific Research, Bolling AFB, Washington DC 20332		12. REPORT DATE January 1982
		13. NUMBER OF PAGES 15
14. MONITORING AGENCY NAME & ADDRESS (if different from Controlling Office)		15. SECURITY CLASS (of this report) Unclassified
		15a. DECLASSIFICATION DOWNGRADING SCHEDULE

16. DISTRIBUTION STATEMENT (of this Report)

Approved for public release; distribution unlimited.

17. DISTRIBUTION STATEMENT (of the abstract entered in Block 20, if different from Report)

18. SUPPLEMENTARY NOTES

19. KEY WORDS (Continue on reverse side if necessary and identify by block number)

Spectra
Intense Relativistic Electron Beams
Molecular Nitrogen
Molecular Nitrogen Ions
Atomic Oxygen
Electron Beam Diagnostics

20. ABSTRACT (Continue on reverse side if necessary and identify by block number)

Spectral data in the visible region has been taken during recent FX100 relativistic e-beam propagation experiments. At the pressure of the experiments (.35 Torr), the typical N_2 second positive and N_2^+ first negative band systems were observed as well as the characteristic red emission. The latter has been tentatively identified as the $4d^5D - 3p^5P$ transition (6157A) in atomic oxygen, the result of $O^+ + e$ recombination.

DD FORM 1 JAN 73 1473 EDITION OF 1 NOV 65 IS OBSOLETE

SECURITY CLASSIFICATION OF THIS PAGE (When Data Entered)

SPECTRAL DATA IN THE VISIBLE REGION HAS BEEN TAKEN DURING RECENT FX100 RELATIVISTIC E-BEAM PROPAGATION EXPERIMENTS. AT THE PRESSURE OF THE EXPERIMENTS (.35 TORR), THE TYPICAL N_2 SECOND POSITIVE AND N_2^+ FIRST NEGATIVE BAND SYSTEMS WERE OBSERVED AS WELL AS THE CHARACTERISTIC RED EMISSION. THE LATTER HAS BEEN TENTATIVELY IDENTIFIED AS THE $4D^5D$ - $3P^5P$ TRANSITION (6157A) IN ATOMIC OXYGEN, THE RESULT OF O^+ + E RECOMBINATION.

* THIS WORK SPONSORED BY THE AIR FORCE OFFICE OF SCIENTIFIC RESEARCH (AFSC), UNDER CONTRACT F49620-81-C-0016.

THE AUTHORS ARE INDEBTED TO THE FOLLOWING MEMBERS OF THE DYNAMIC TESTING DIVISION AT LANL FOR THE TIME RESOLVED PHOTOGRAPHY OF THE FX-100 PROPAGATION EXPERIMENTS: BOB BENJAMIN (M-6), STEVE SCHMIDT (M-6), TOM STARKE (M-2), DAVE MOIR (M-2), AND LEE BUILTA (M-2).

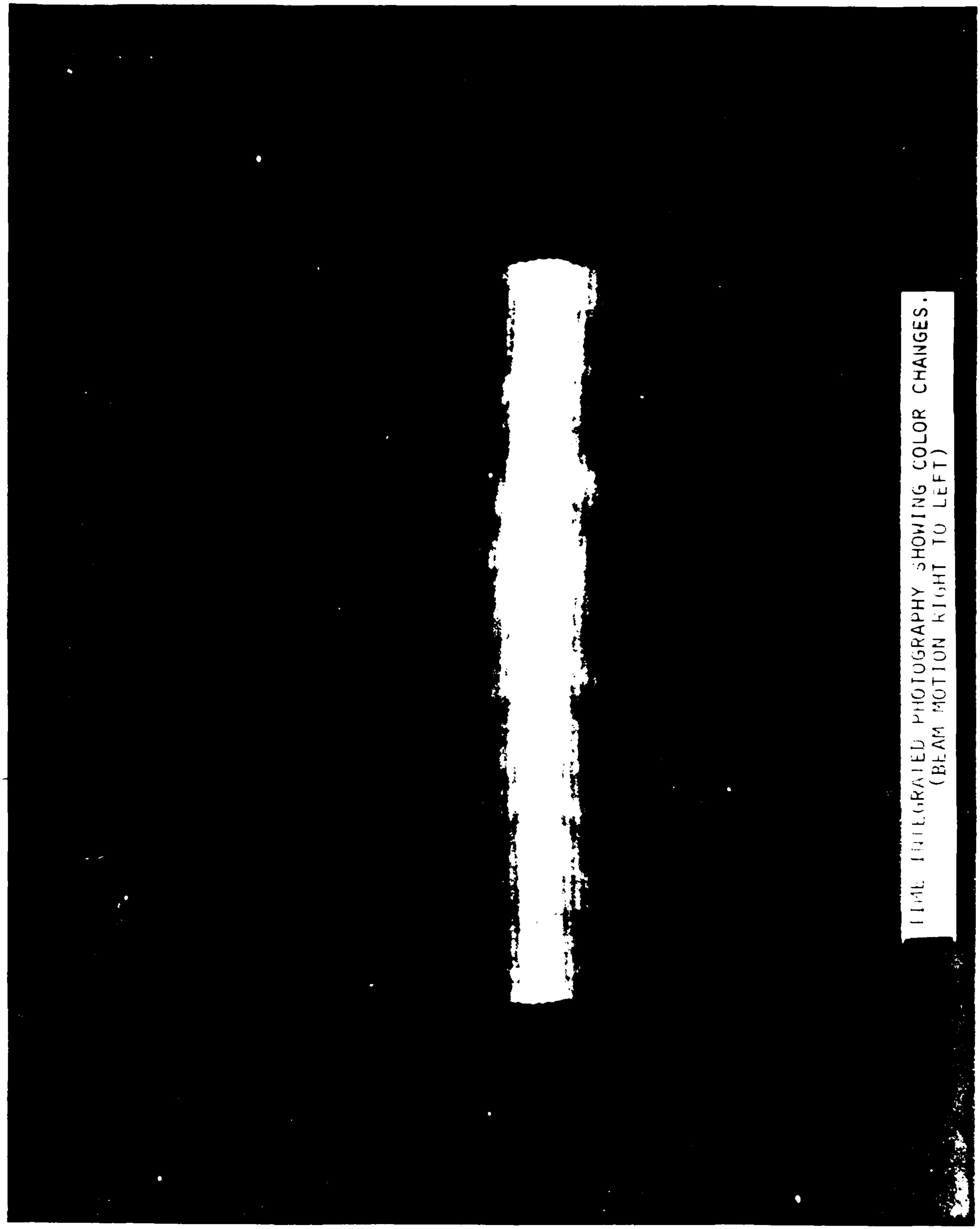

TIME INTEGRATED PHOTOGRAPHY SHOWING COLOR CHANGES.
(BEAM MOTION RIGHT TO LEFT)

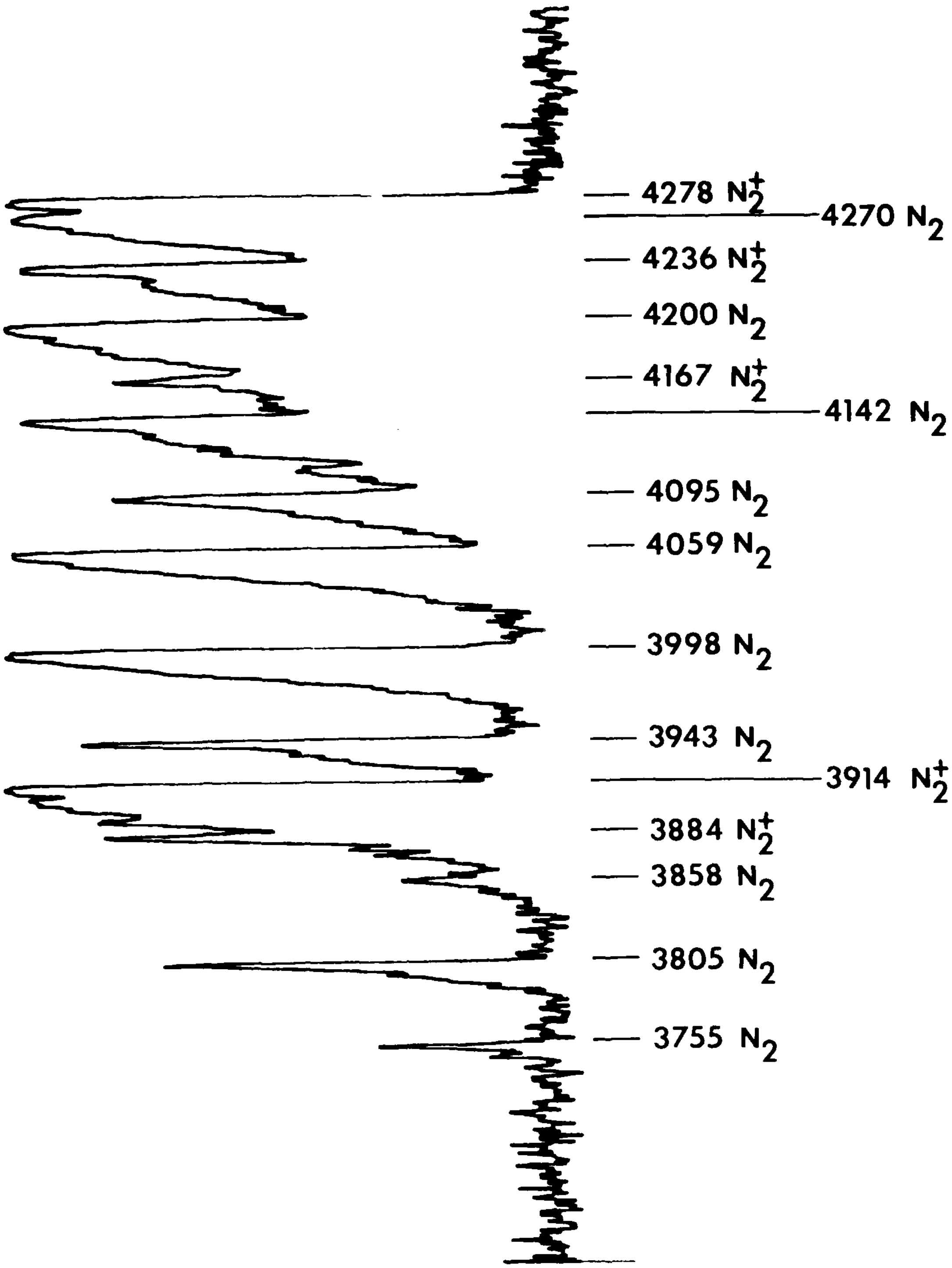

ELECTRON BEAM GENERATED SPECTRA IN AIR

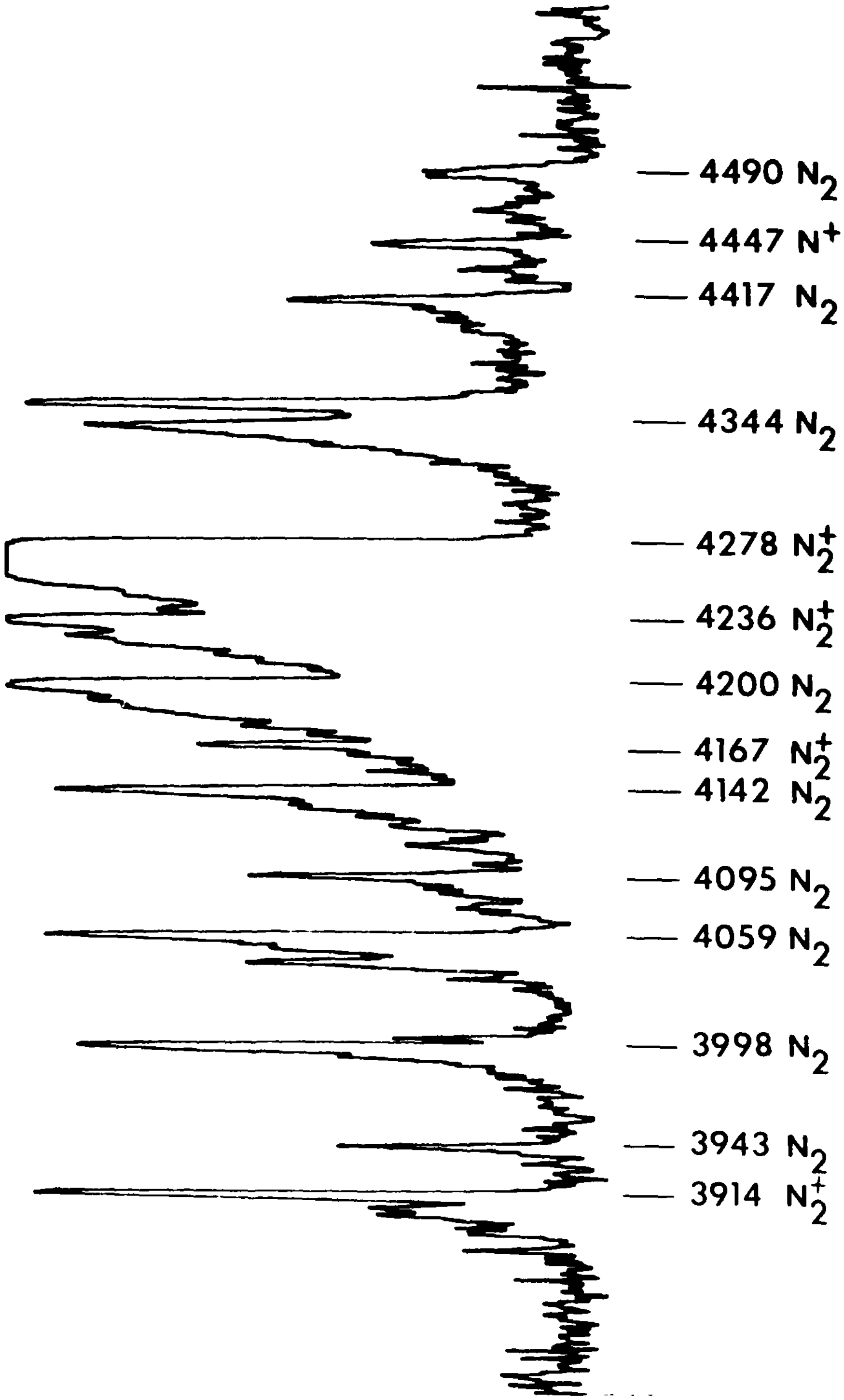

ELECTRON BEAM GENERATED SPECTRA IN AIR

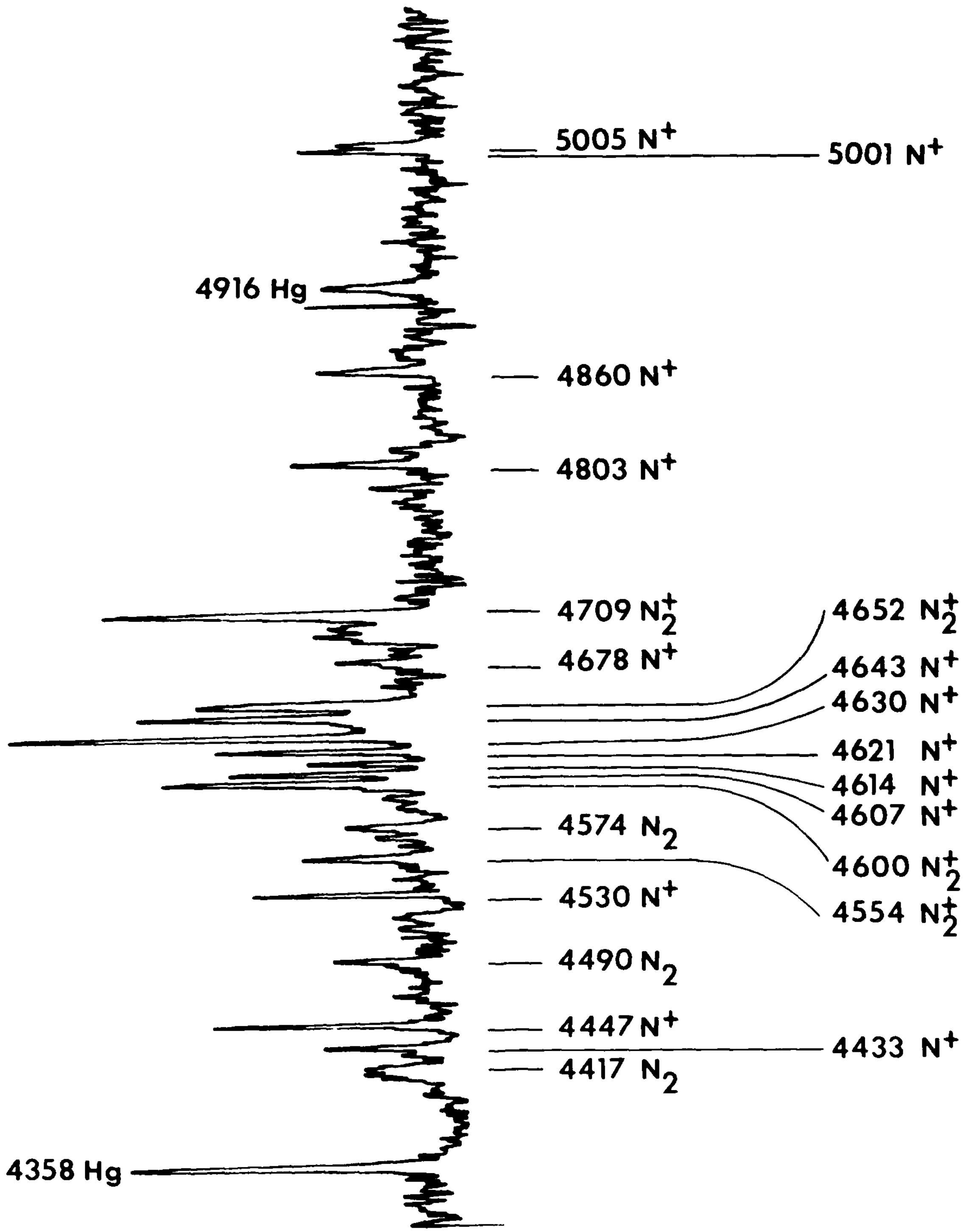

ELECTRON BEAM GENERATED SPECTRA IN AIR (RIGHT) AND CALIBRATION LINES (LEFT)

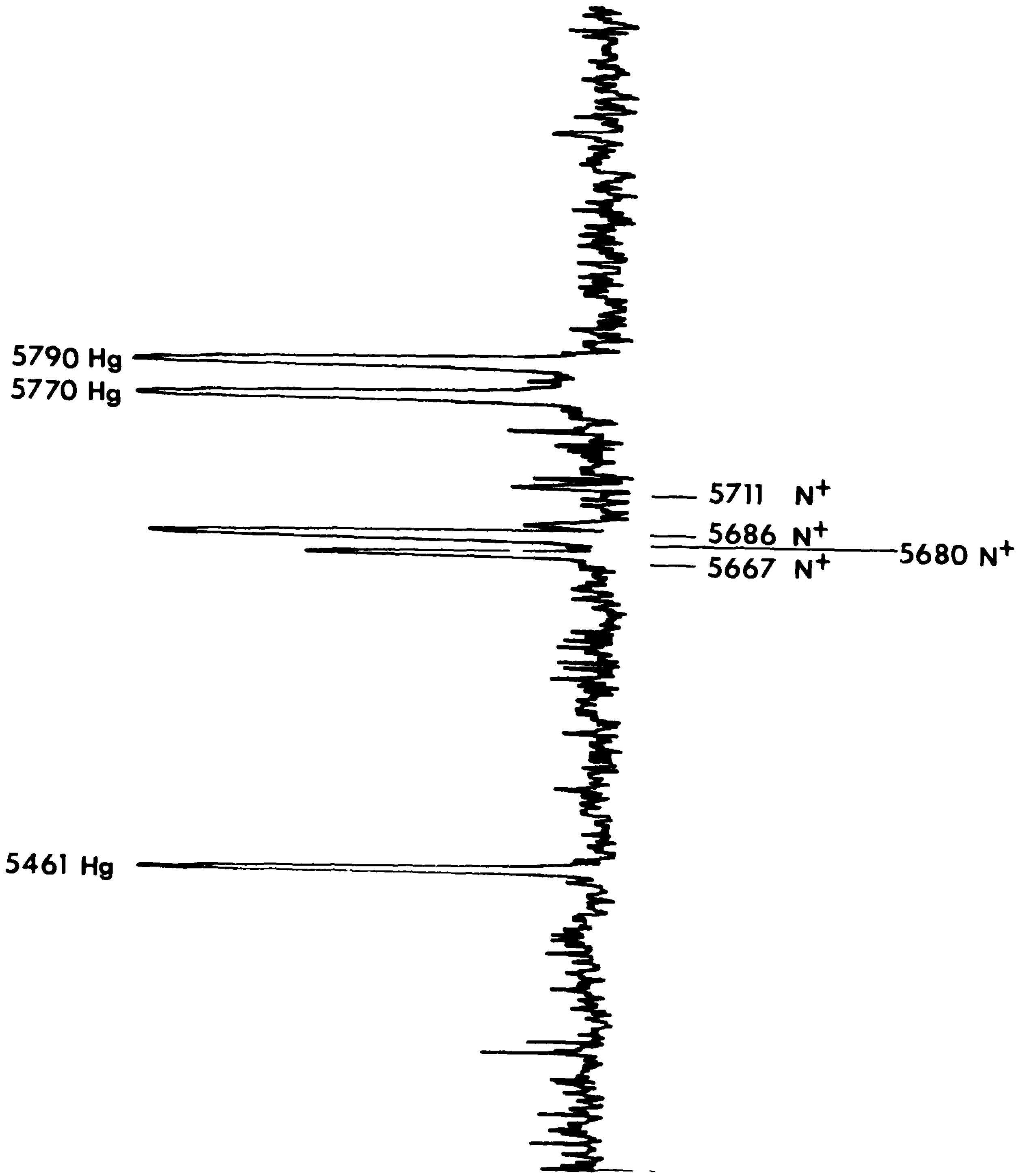

ELECTRON BEAM GENERATED SPECTRA IN AIR (RIGHT) AND CALIBRATION LINES (LEFT)

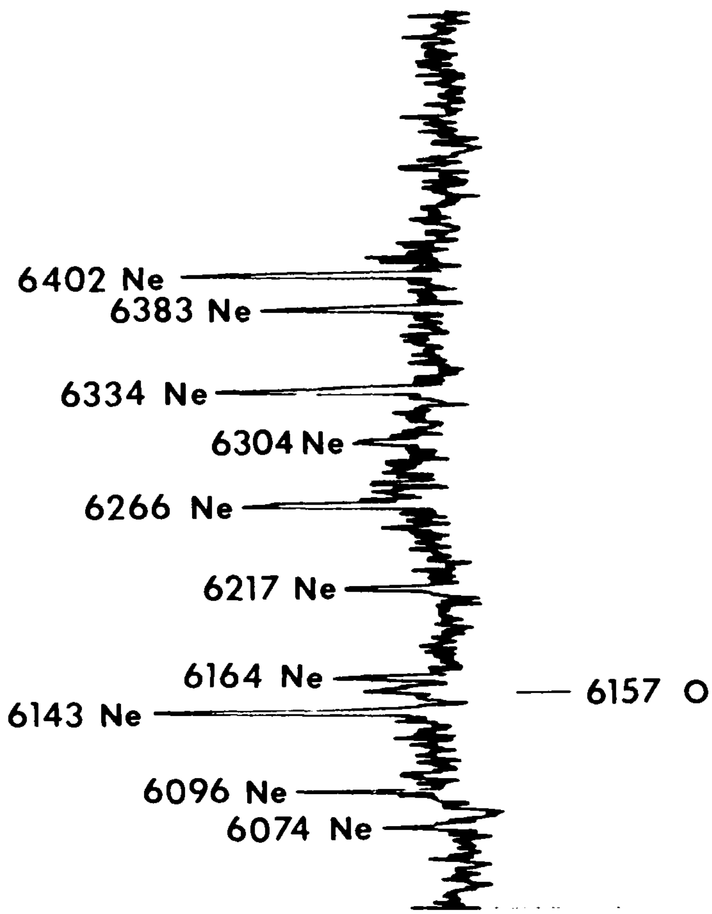

ELECTRON BEAM GENERATED SPECTRA IN AIR (RIGHT) AND CALIBRATION LINES (LEFT)

WAVELENGTH Å	ATOM/MOLECULE	TRANSITION (band)	(v', v")
3755	N_2	(2+)	(1,3)
3805	N_2	(2+)	(0,2)
3858	N_2	(2+)	(4,7)
3884	$N_2{+}$	(1-)	(1,1)
3914	$N_2{+}$	(1-)	(0,0)
3943	N_2	(2+)	(2,5)
3998	N_2	(2+)	(1,4)
4059	N_2	(2+)	(0,3)
4095	N_2	(2+)	(4,8)
4142	N_2	(2+)	(3,7)
4167	$N_2{+}$	(1-)	(3,4)
4200	N_2	(2+)	(2,6)
4236	$N_2{+}$	(1-)	(1,2)
4270	N_2	(2+)	(1,5)
4278	$N_2{+}$	(1-)	(0,1)
4344	N_2	(2+)	(0,4)
4417	N_2	(2+)	(3,8)
4433	N+	3d $^3P^o$-4f D(5/2)	
4447	N+	3p ^3D - 3d $^3D^o$	
4490	N_2	(2+)	(2,7)
4530	N+	3d ^1F - 4f G(9/2)	
4554	$N_2{+}$	(1-)	(3,5)
4574	N_2	(2+)	(1,6)
4600	$N_2{+}$	(1-)	(2,4)
4607	N+	3s $^3P^o$ - 3p ^3P	
4614	N+	3s $^3P^o$ - 3p ^3P	
4621	N+	3s $^3P^o$ - 3p ^3P	
4630	N+	3s $^3P^o$ - 3p ^3P	
4643	N+	3s $^3P^o$ - 3p ^3P	
4652	$N_2{+}$	(1-)	(1,3)
4678	N+	3d $^1P^o$ - 4f D(3/2)	
4709	$N_2{+}$	(1-)	(0,2)
4803	N+	3p ^3D - 3d $^3D^o$	
4860	N+	3p ^3D - 3d $^3D^o$	
5001	N+	3p ^3D - 3d $^3F^o$	
5005	N+	3s ^5P - 3p $^5P^o$ 3p ^3D - 3d $^3F^o$	
5667	N+	3s ^3P - 3p ^3D	
5680	N+	3s ^3P - 3p ^3D	
5686	N+	3s ^3P - 3p ^3D	
5711	N+	3s ^3P - 3p ^3D	
6157	O	3p ^5P - 4d $^5D^o$	

IDENTIFICATION OF OBSERVED LINES

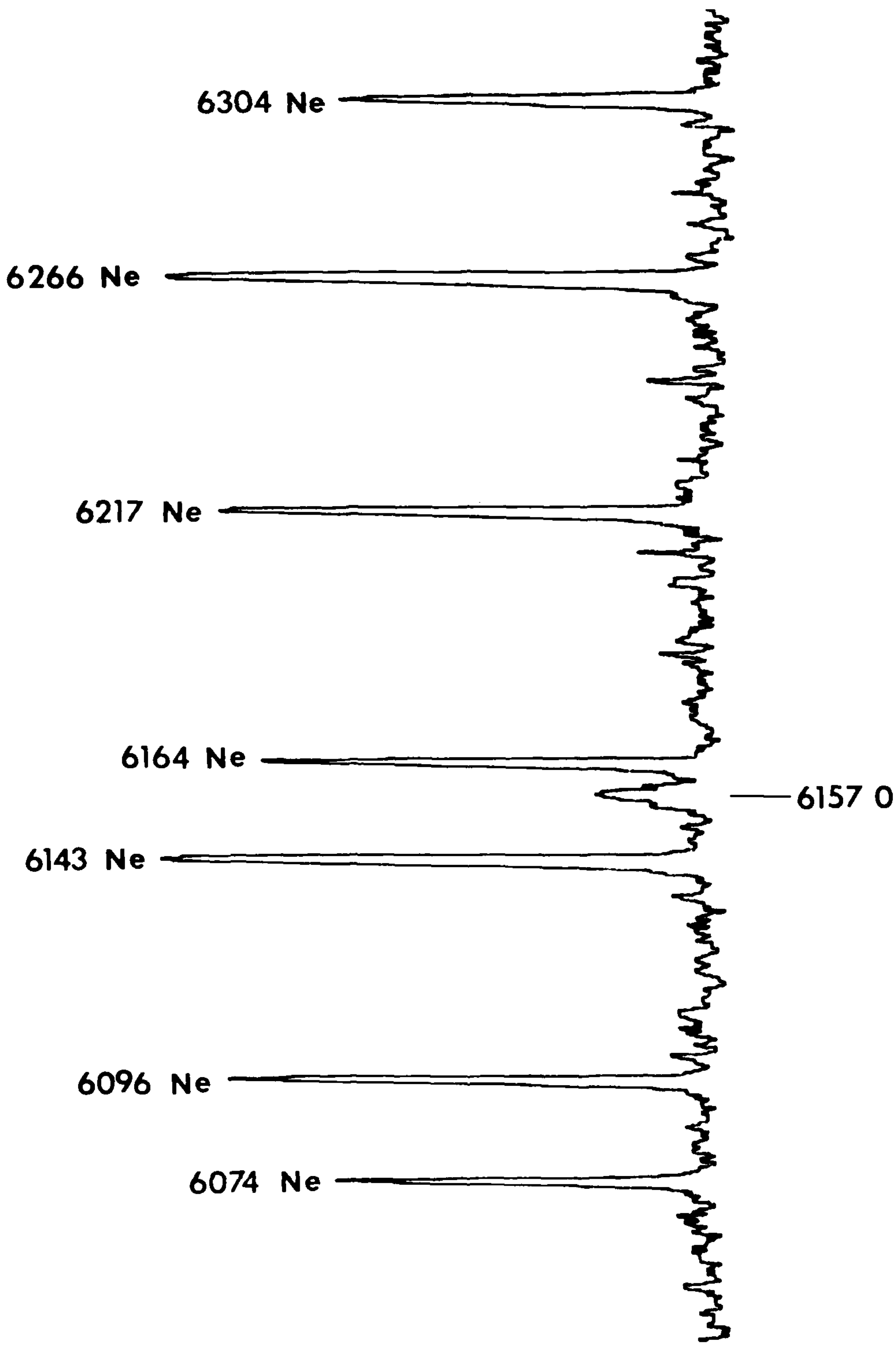

DETAILED SCAN OF THE OXYGEN LINE (RIGHT)
(CALIBRATION LINES IDENTIFIED ON LEFT)

	OBSERVED	AURORAL
WAVELENGTH:	6157 A	6300 A
DESIGNATION:	$4d\ ^5D-3p\ ^5P$	$2p^4\ ^1D-2p^4\ ^3P$
ASSOCIATED LINES:	NONE WITH SAME INTENSITY	$^1D-^3P$ 6364 A $^1S-^1D$ 5577 A (NOT OBSERVED)
EXCITATION:	PROBABLY RECOMBINATION $O^+ + e + M \rightarrow O^* + M$ OR $O^+ + e + e \rightarrow O^* + e$	LARGELY PHOTODETACHMENT
QUENCHING:	-	HIGHLY QUENCHED BY ELECTRONS

MISCELLANEOUS: NO FORBIDDEN TRANSITIONS ARE OBSERVED
TOO MUCH IS HAPPENING AROUND THE BEAM

THE OBSERVED RED EMISSION IS NOT THE AURORAL OXYGEN LINE

MRC

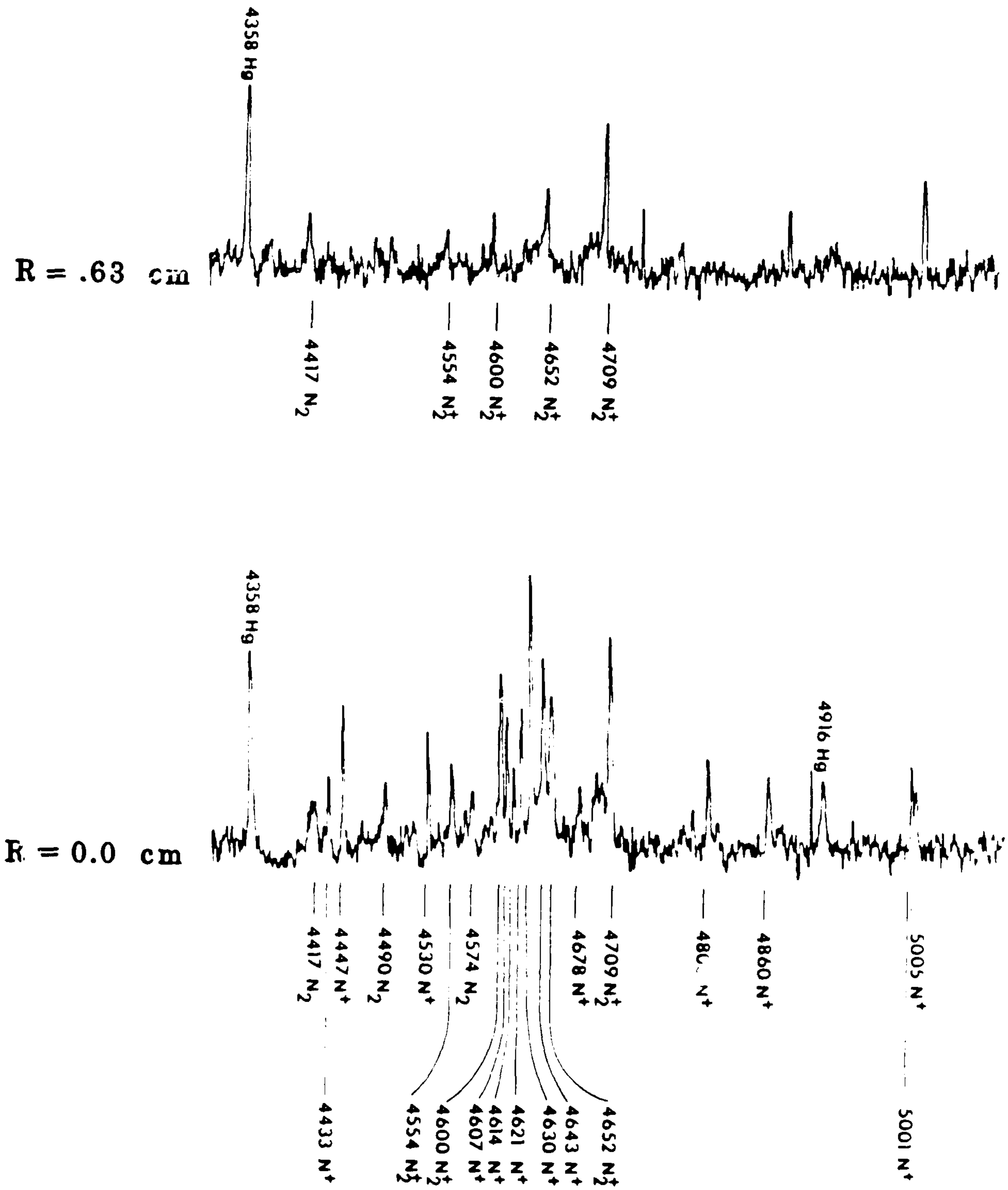

ATOMIC AND MOLECULAR LINES HAVE DIFFERENT SPATIAL DEPENDENCE

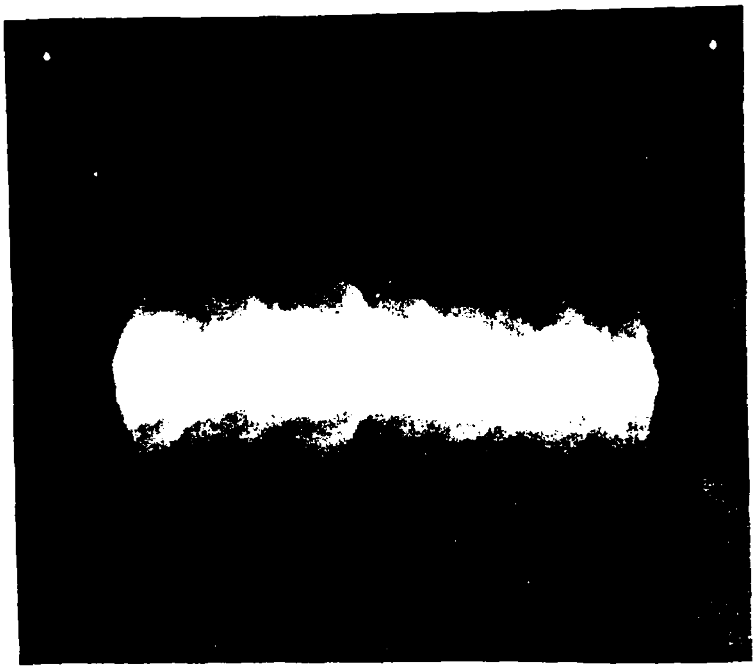

TIME INTEGRATED PHOTOGRAPH
SHOWING STRUCTURE.
(BEAM MOTION RIGHT TO LEFT)

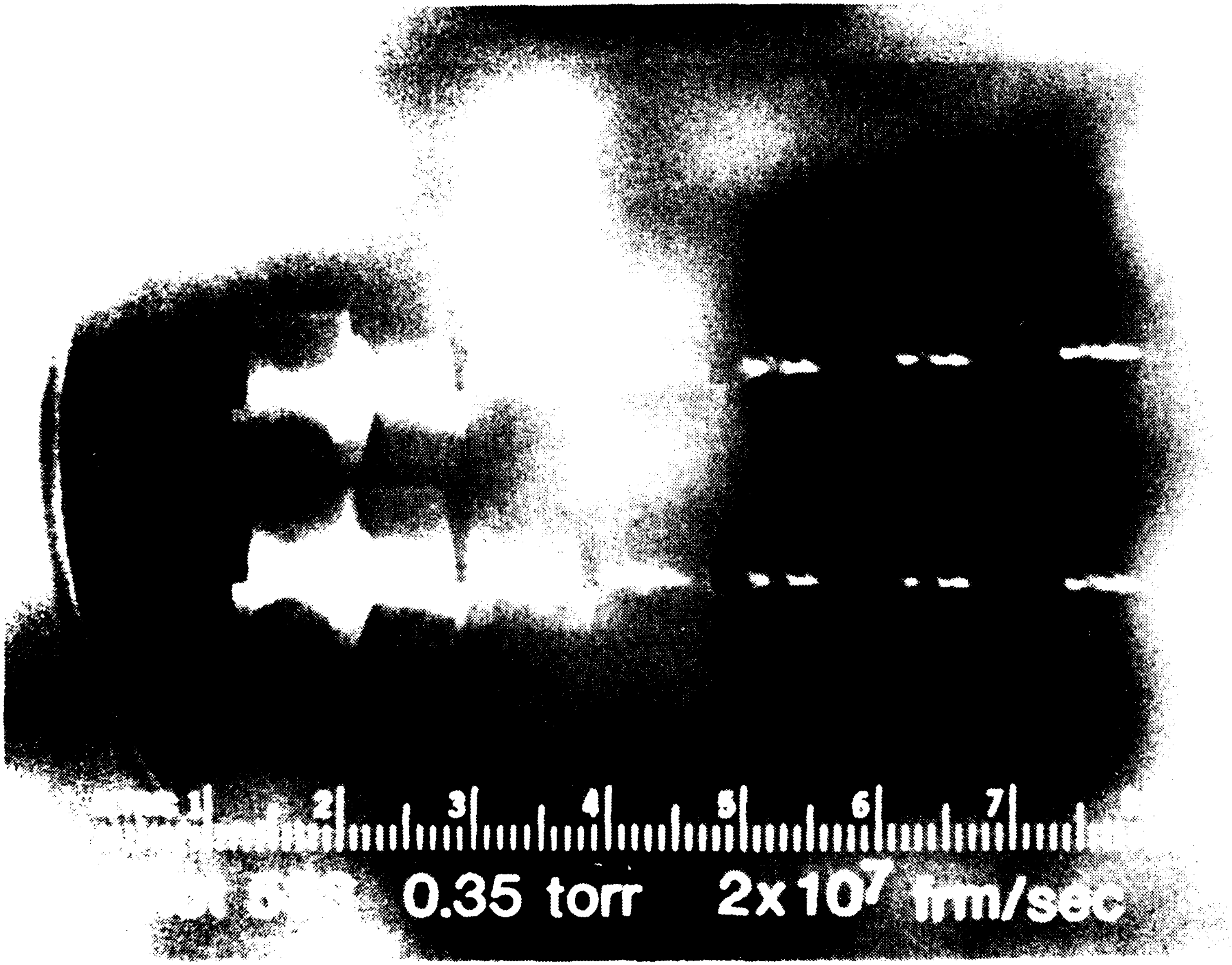

FAST FRAMING PHOTOGRAPH (WITH M-2 AND M-6 LANL)

(BEAM MOTION RIGHT TO LEFT)

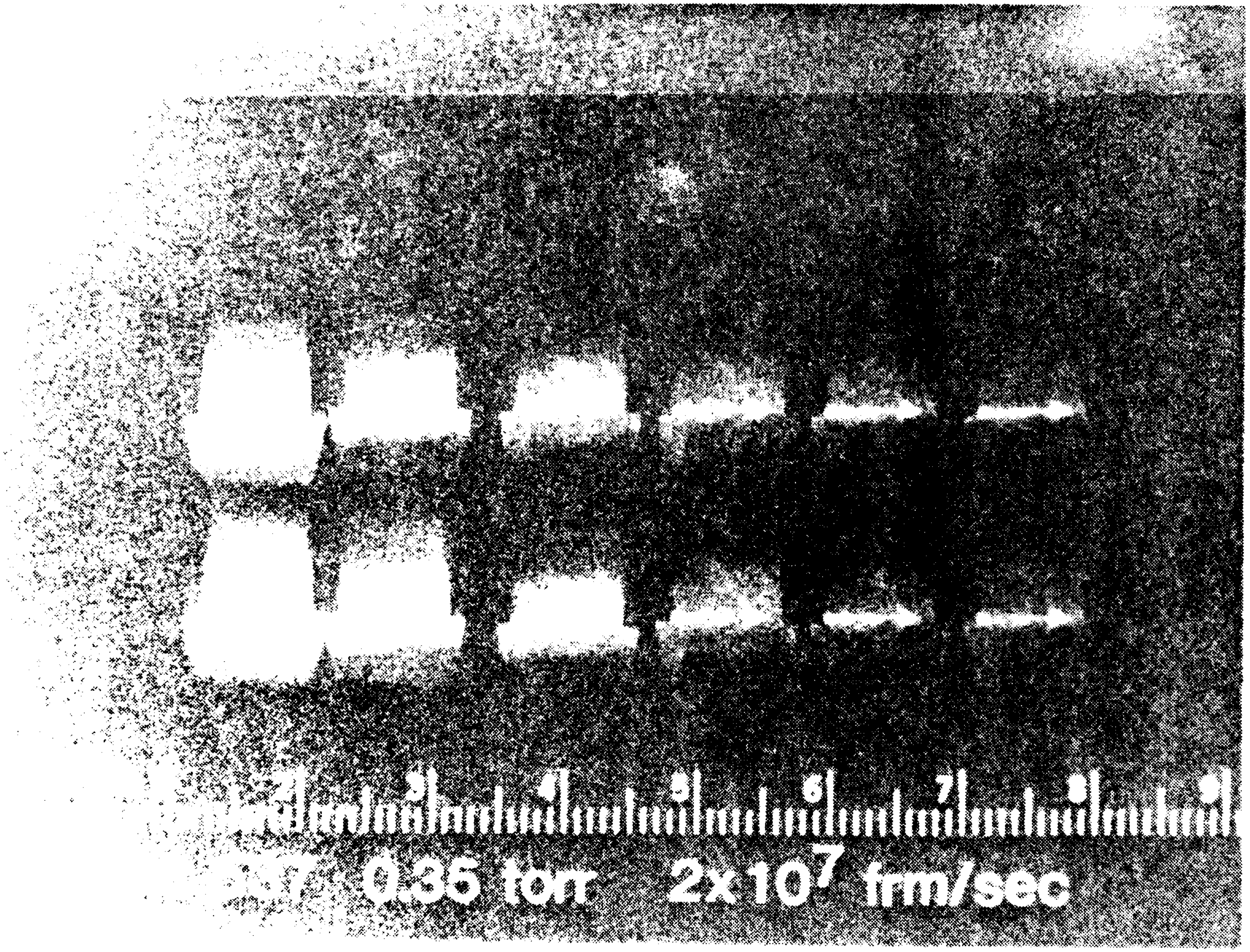

FAST FRAMING PHOTOGRAPH (WITH M-2 AND M-6 LANL)

(BEAM MOTION RIGHT TO LEFT)

APPENDIX D

FX-100 PROPAGATION EXPERIMENTS - DARPA/SERVICES
EXPERIMENTAL COORDINATION MEETING

SECURITY CLASSIFICATION OF THIS PAGE (When Data Entered)

REPORT DOCUMENTATION PAGE		READ INSTRUCTIONS BEFORE COMPLETING FORM
1. REPORT NUMBER	2. GOVT ACCESSION NO.	3. RECIPIENT'S CATALOG NUMBER
4. TITLE (and Subtitle) FX-100 Experiments - DARPA/Services Experimental Coordination Meeting		5. TYPE OF REPORT & PERIOD COVERED Interim Report
		6. PERFORMING ORG. REPORT NUMBER AMRC-N-184
7. AUTHOR(s) Carl Ekdahl		8. CONTRACT OR GRANT NUMBER(s) F49620-81-C-0016
9. PERFORMING ORGANIZATION NAME AND ADDRESS Mission Research Corporation, 1400 San Mateo Boulevard, S. E., Suite A, Albuquerque, New Mexico 87108		10. PROGRAM ELEMENT PROJECT, TASK AREA & WORK UNIT NUMBERS
11. CONTROLLING OFFICE NAME AND ADDRESS Air Force Office of Scientific Research, Building 410, Bolling Air Force Base, Washington, D. C. 20332		12. REPORT DATE October 1981
		13. NUMBER OF PAGES 24
14. MONITORING AGENCY NAME & ADDRESS (if different from Controlling Office)		15. SECURITY CLASS (of this report) unclassified
		15a. DECLASSIFICATION DOWNGRADING SCHEDULE

16. DISTRIBUTION STATEMENT (of this Report)

Approved for public release; distribution unlimited

17. DISTRIBUTION STATEMENT (of the abstract entered in Block 20, if different from Report)

18. SUPPLEMENTARY NOTES

19. KEY WORDS (Continue on reverse side if necessary and identify by block number)

Relativistic Electron Beam Propagation
Relativistic Electron Beam Diagnostics

20. ABSTRACT (Continue on reverse side if necessary and identify by block number)

The air pressure regime for maximum energy transport by the FX-100 relativistic electron beam (I~40 kA, W 1.5 MeV, t~120 ns) was observed to occur at lower pressures (0.3-0.7 Torr) than experiments with the short pulse (~20 ns) AFWL F -25 beam (I~ 20 kA, W 1.5 MeV). Time integrated open shutter photography and radiochromic-foil beam profile measurements showed evidence for the propagation of an annulus of high-energy electrons (>150 keV) accompanying the central core of the beam. Subsequent time-resolved beam profile

DD FORM 1 JAN 73 1473 EDITION OF 1 NOV 65 IS OBSOLETE

SECURITY CLASSIFICATION OF THIS PAGE (When Data Entered)

20. (Continued)

measurements obtained with an array of subminiature Faraday collectors and time-resolved (streak) photographs showed that the annulus was the result of a hollowing instability that developed late (~20 μs) into the beam pulse. This instability was most evident at the air pressures corresponding to maximum energy transport. Spectroscopic measurements of the light emitted during these experiments showed the presence of singly ionized atomic nitrogen (N^+) and atomic oxygen (O) near the axis of the beam that persisted long after the beam pulse (≥500 us, determined with streak and framing photography).

MRC

BEAM PROPAGATION EXPERIMENTS USING AFWL FX-25 AND FX-100

CARL EKDAHL (MRC)

WINSTON BOSTICK (UNIVERSITY RESIDENT AT AFWL)

SPONSORED BY THE AIR FORCE OFFICE OF SCIENTIFIC RESEARCH UNDER CONTRACT F49620-81-C-0016 AND IPA-905-79-01016C.

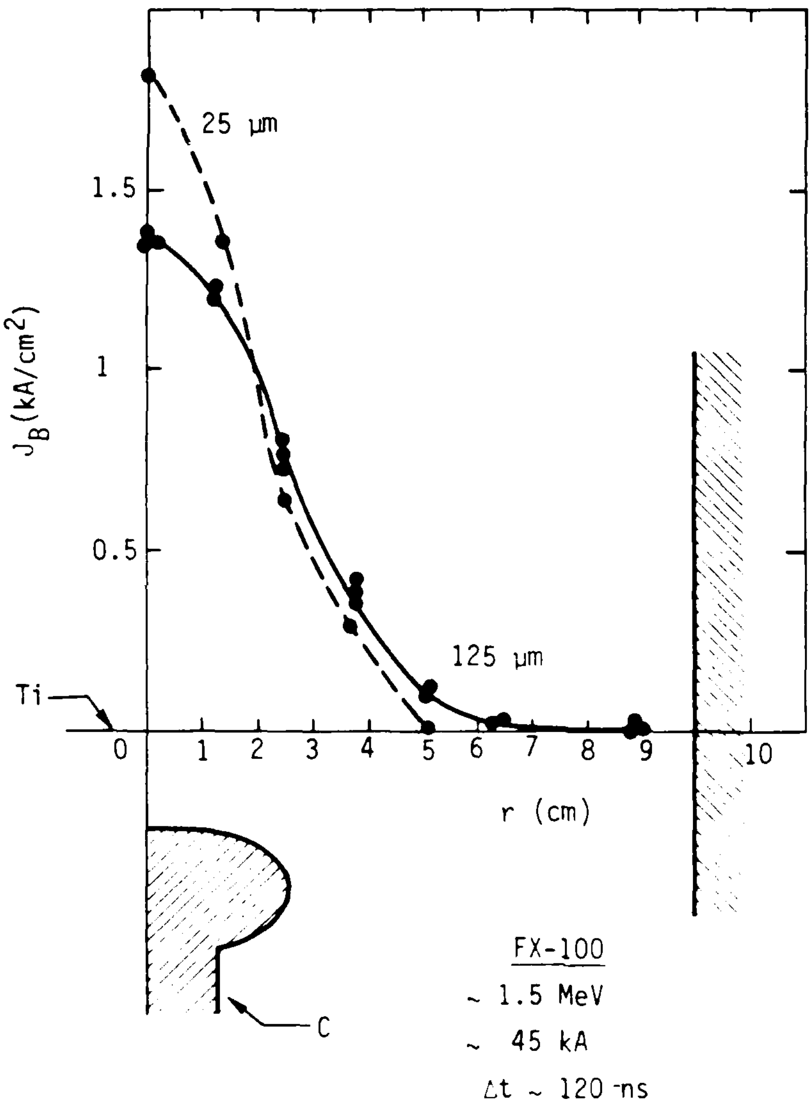

Figure 1. Beam profile at peak current at injection into drift tube. Also shown is the geometry of the Rogowski surface cathode used to obtain quasi-Bennett beam profiles. Data is shown for two anode-foil thicknesses, however, only 25-µm foils were used for the progagation experiments.

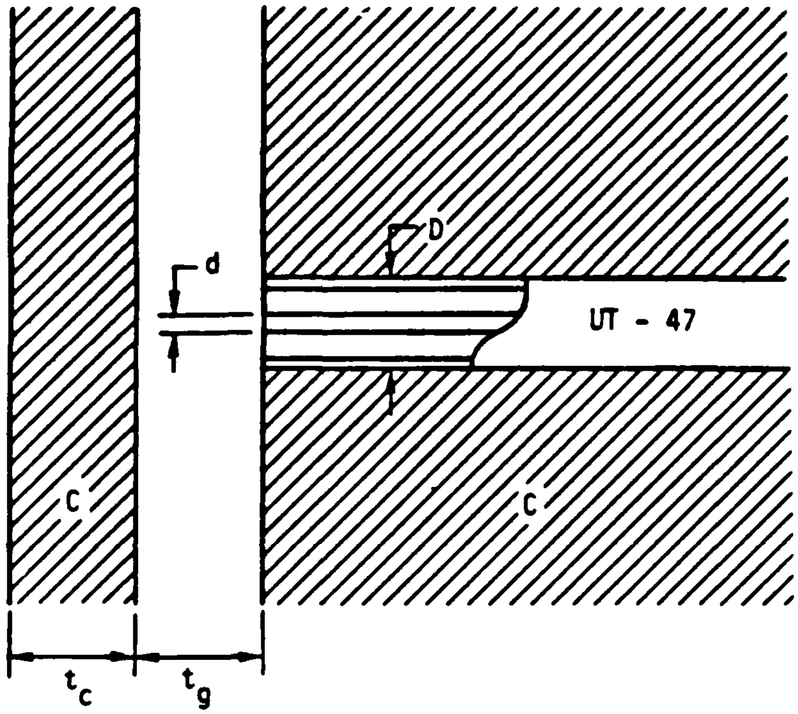

Figure 2. Geometry of subminiature Faraday collector. For FX-25 array the C plasma shield was t_c = 1.8 mm thick and was insulated by a t_g = 1.7 mm vacuum gap. The FX-100 array used a t_c = 0.125 mm thick Ti shield and t_g = 0.025 mm Kapton foil insulator. Both arrays used UT-47 rigid-coax collectors with d = 0.29 mm diameter inner conductors and D = 1.2 mm diameter outer conductors with Teflon insulation.

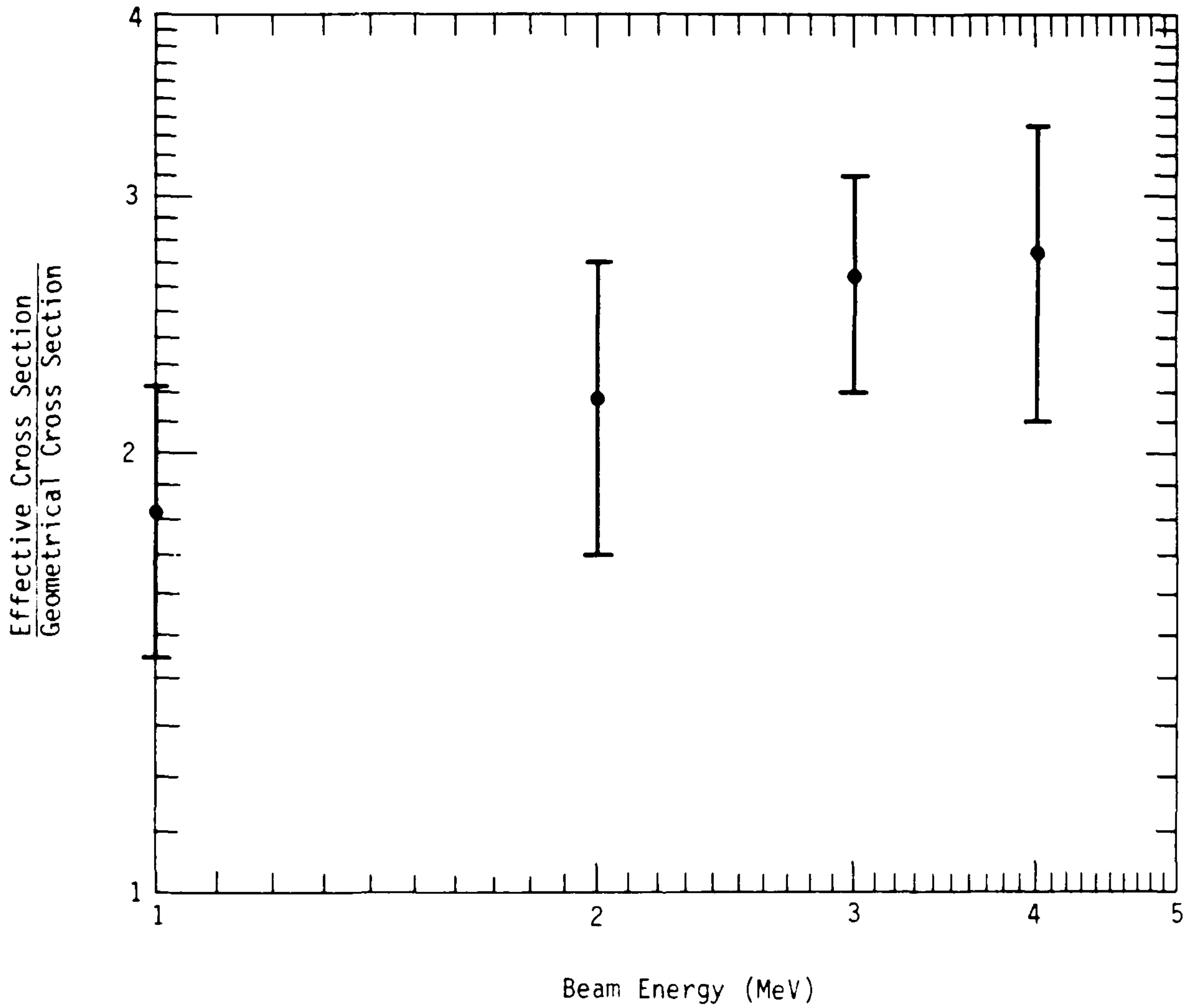

Figure 3. Energy sensitivity of the effective collection area for the subminiature Faraday cup array. The Monte Carlo transport code, CYLTRAN, was used to calculate this sensitivity, which results from scattering of electrons into the collector from the surrounding materials.

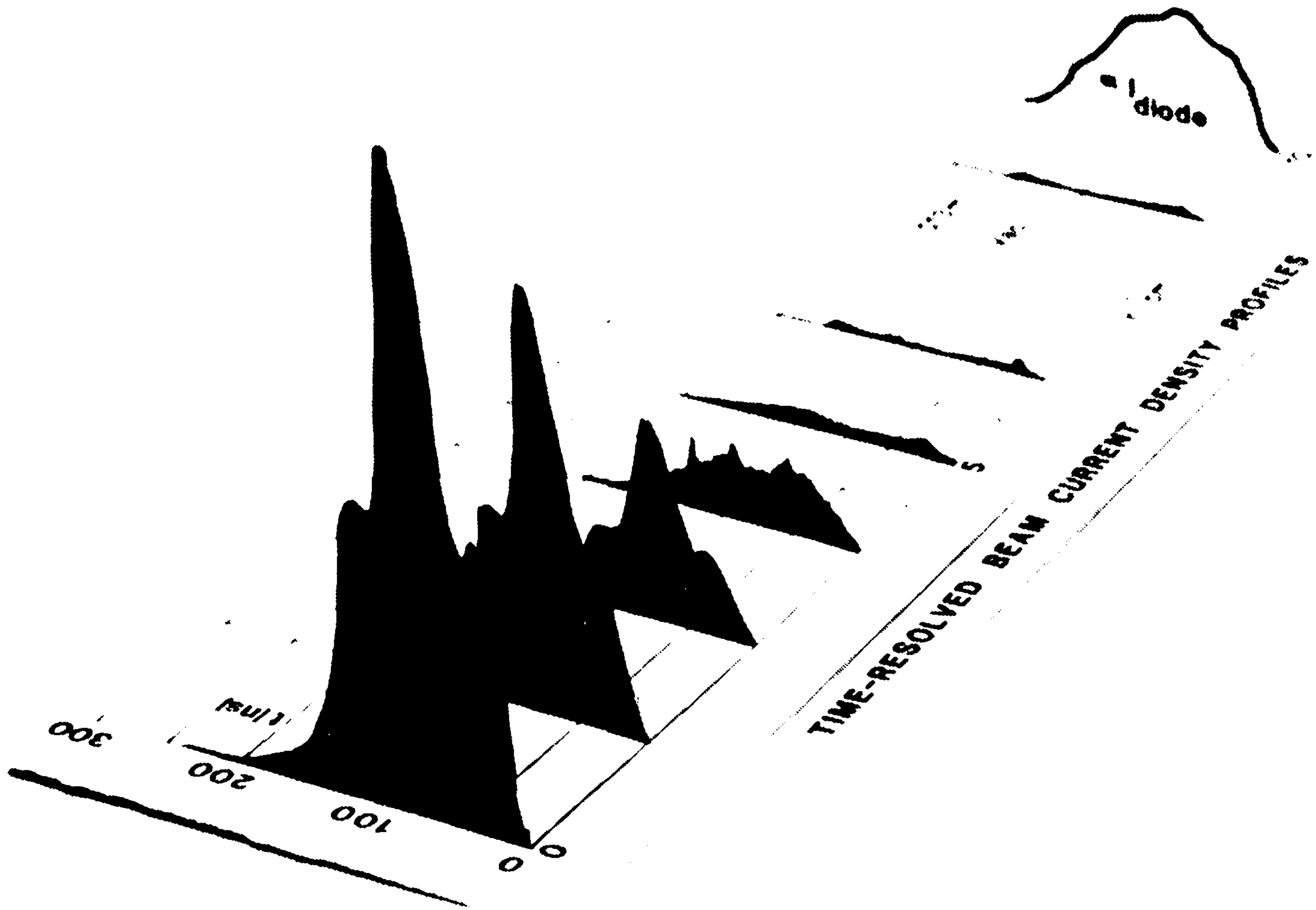

Figure 4. Time-resolved FX-100 beam current density profile at injection obtained with the subminiature Faraday collector array. This shows very little diode shark emission (at large radii).

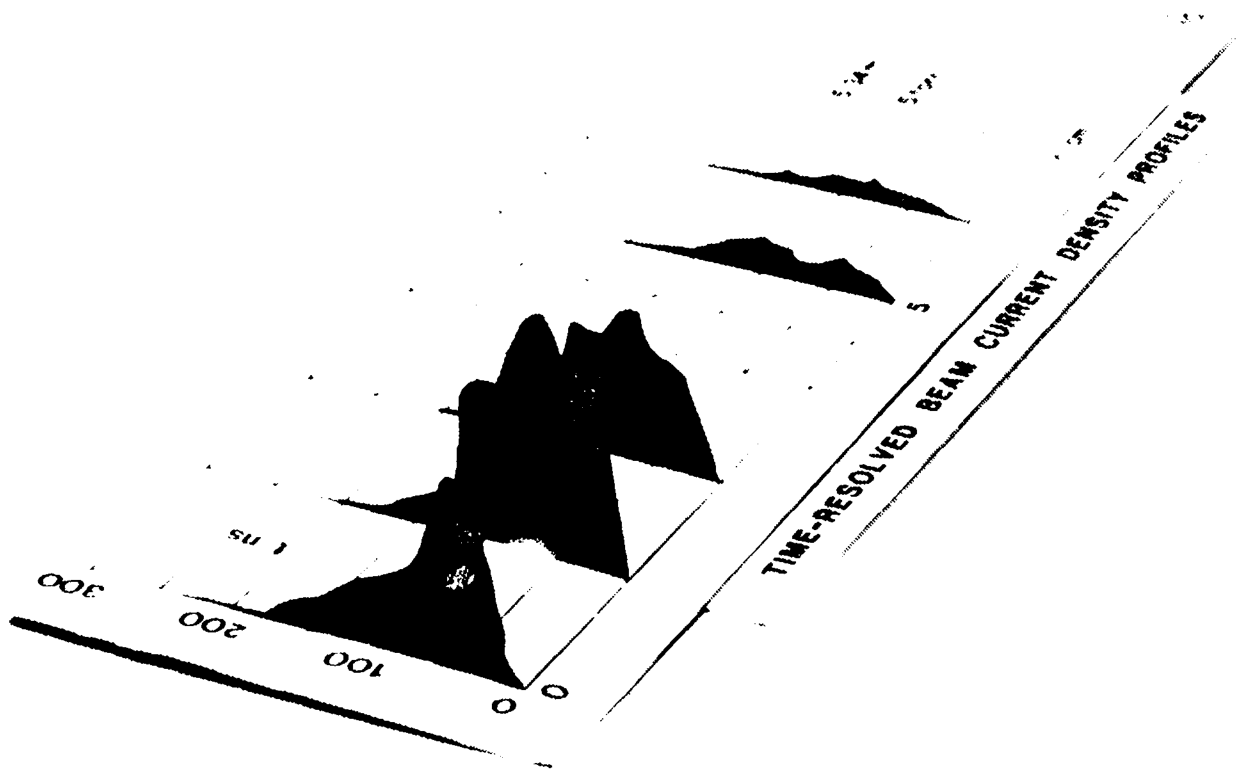

Figure 5. FX-100 beam current density profile after propagating 5.34 m through air at a pressure of 0.5 Torr. In this shot the beam was slightly off axis.

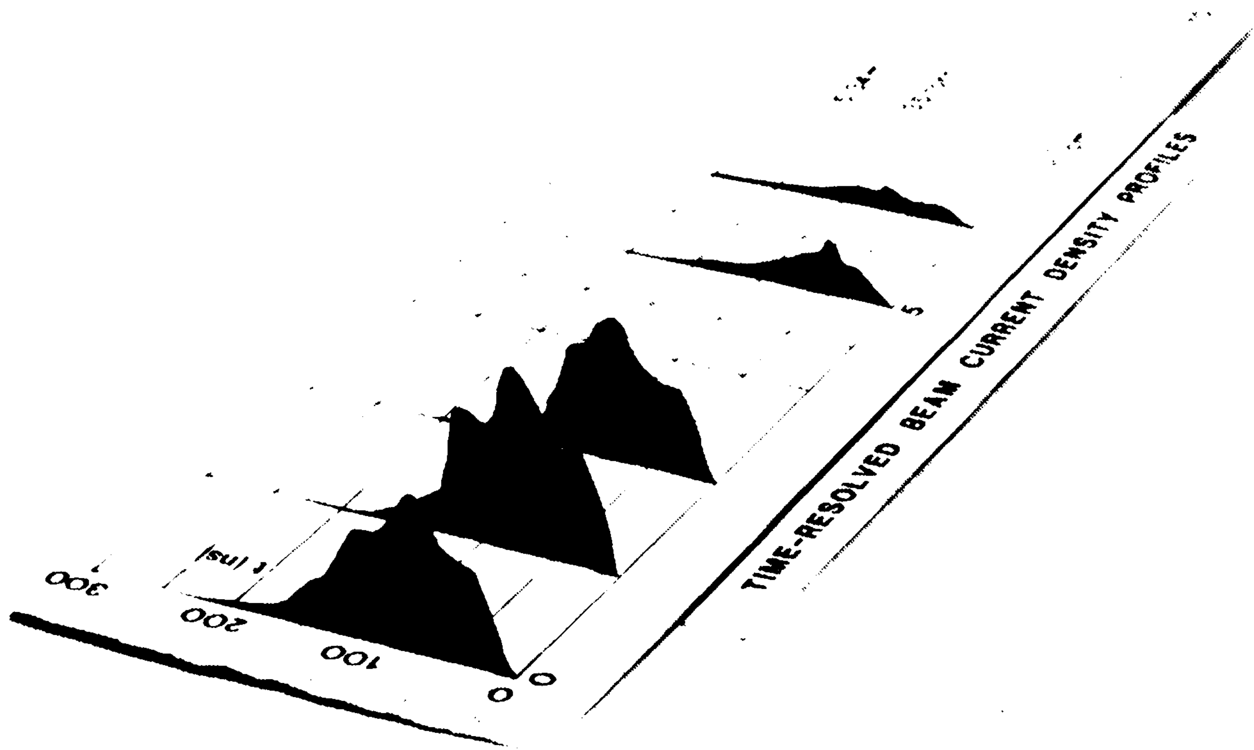

Figure 6. Time-resolved beam current density profile after propagating 5.34 m in 0.35-Torr air. This shot shows the development of an annular region of current transport (at r~5 cm).

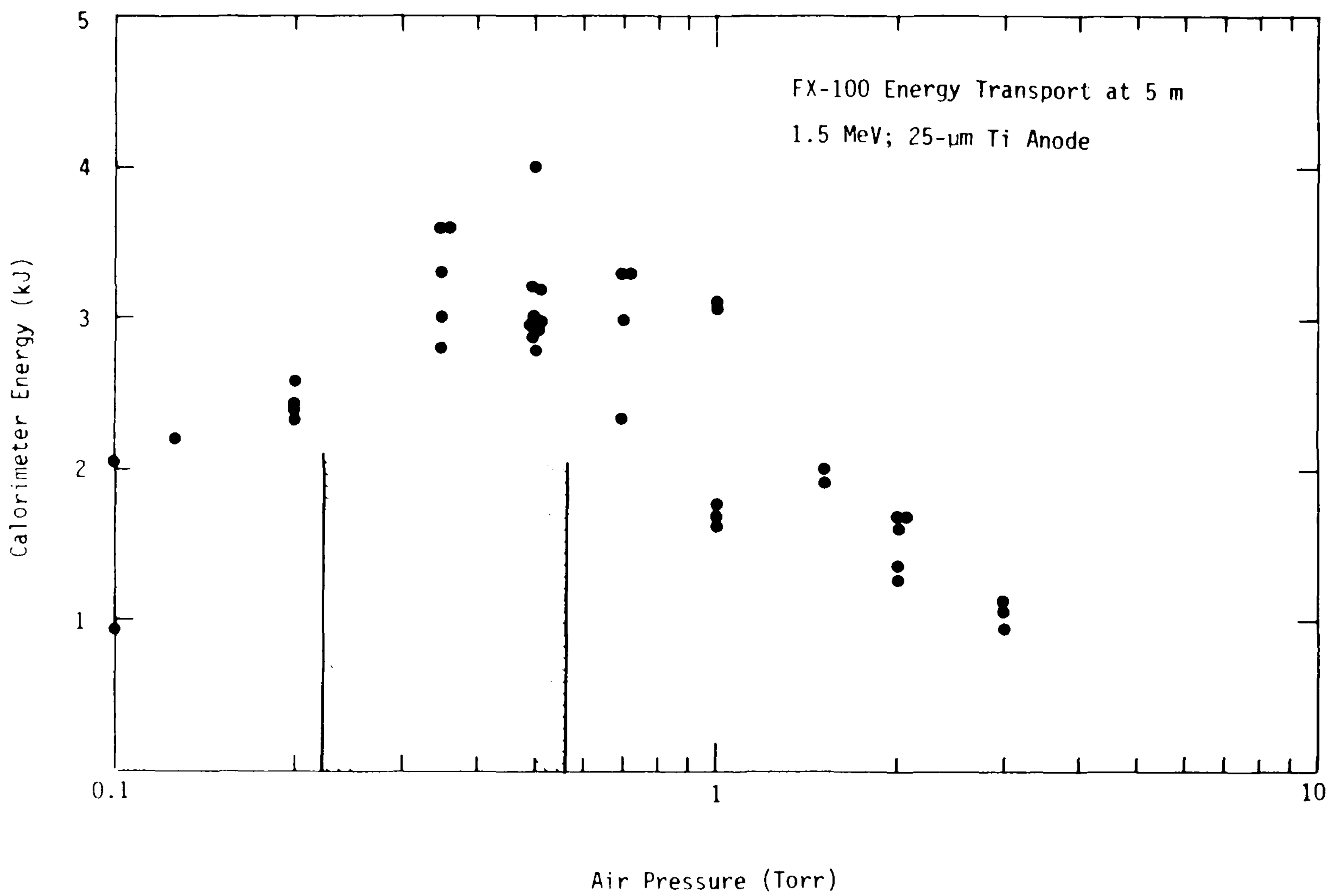

Figure 7. Energy deposition by FX-100 beam in a carbon calorimeter at the end of the 5.3 m drift tube. The shaded region indicates the pressure window in which spectra showed evidence for atomic line emission near the beam axis.

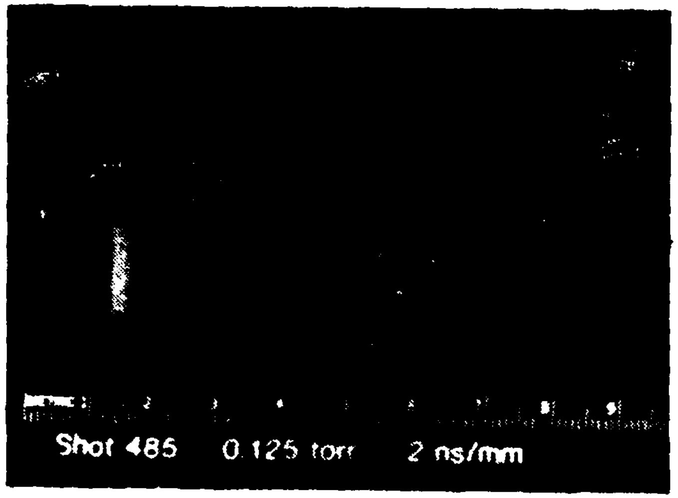

(a)

(b)

(c)

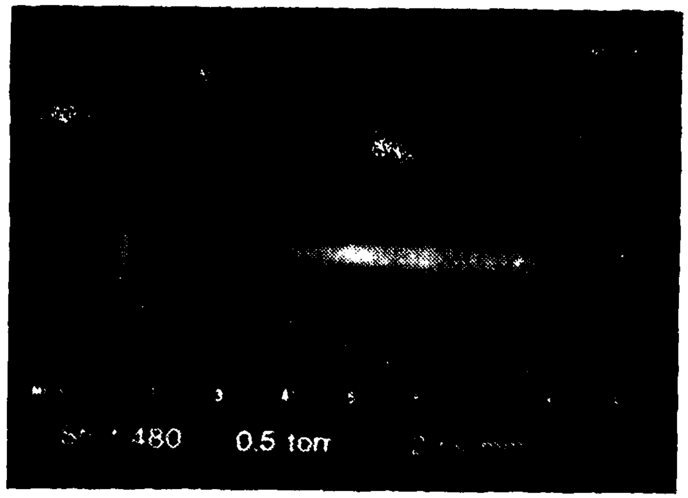

(d)

Figure 8. Streak-camera photographs of the beam-excited air emission at Z = 4.5 m as pressure is *increased from below the propagation pressure window* (a) to the center of the window (d). (Ignore the image conver r-tube blemish in the far left of each photograph.) The beam head is at the left of each streak (taken through a vertical slit). The delay in start of emission in (a) as compared with (d) is presumably the result of erosion at lower pressures.

AD-A170 204 BEAM PROPAGATION EXPERIMENTAL STUDY(U) MISSION RESEARCH 3/4
CORP ALBUQUERQUE NM C A EKDAHL MAR 82 AMRC-R-352
AFOSR-TR-86-0503 F49620-81-C-0016

UNCLASSIFIED F/G 20/7 NL

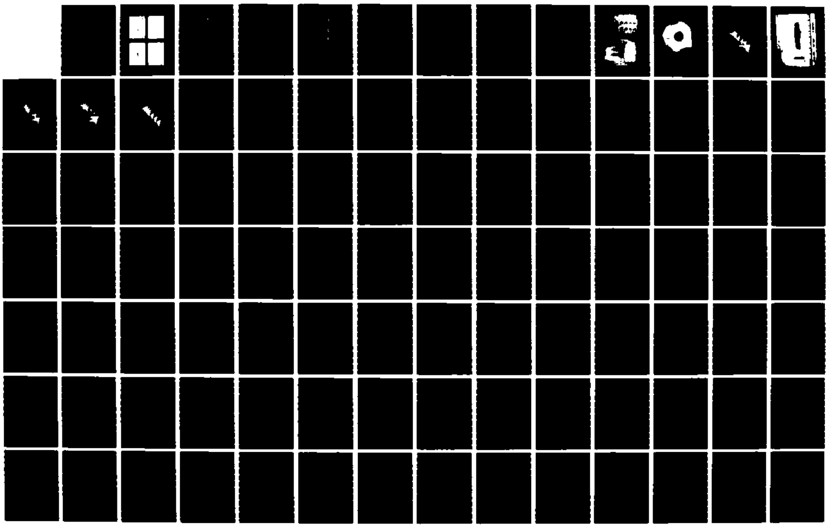

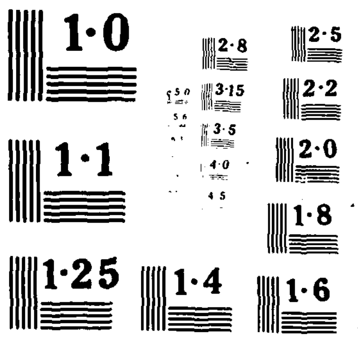
1·0
2·8
2·5
3·15
2·2
3·5
1·1
4·0
2·0
4·5
1·8
1·25
1·4
1·6

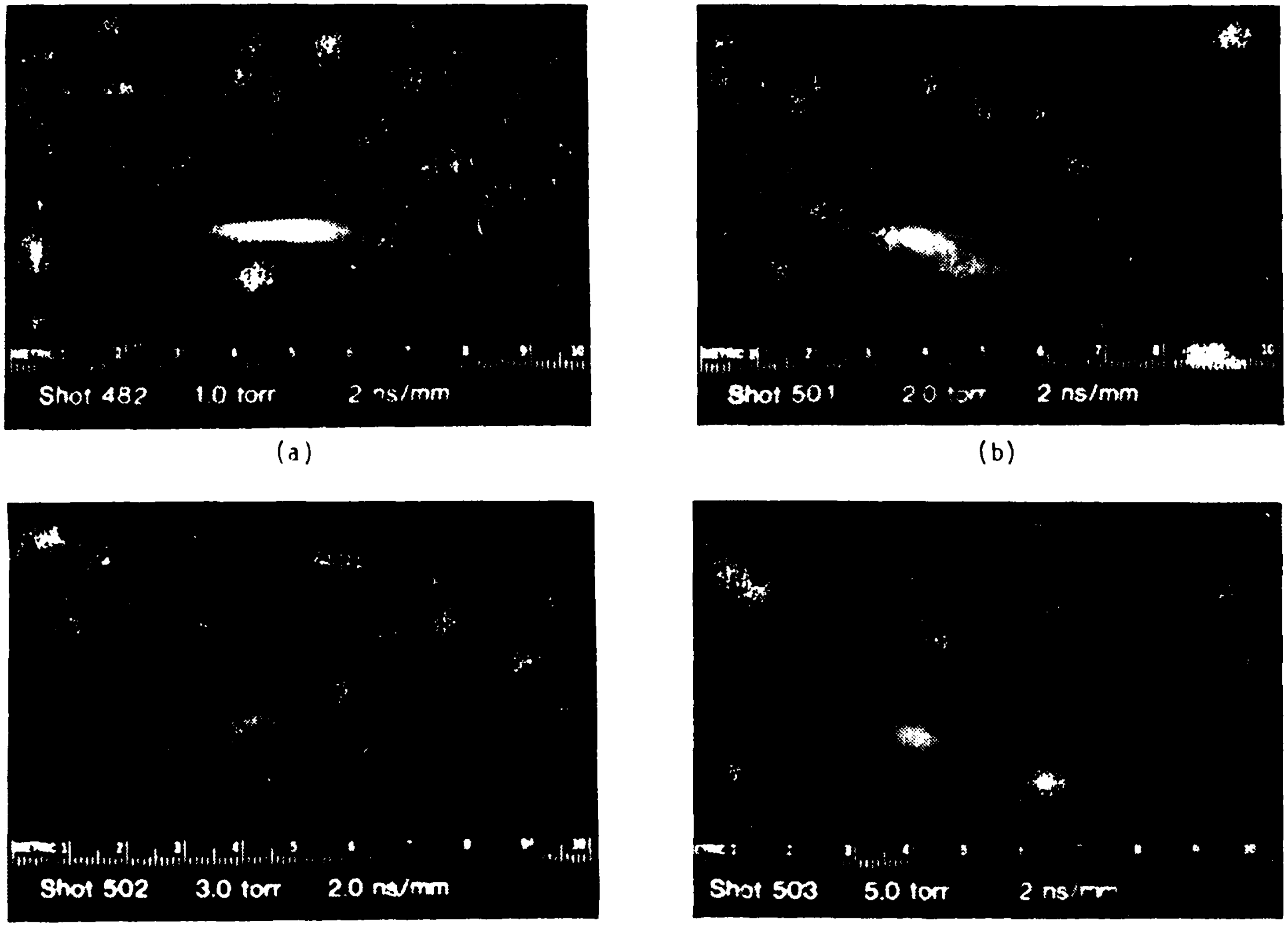

(a) (b)

(c) (d)

Figure 9. Streak-camera photographs of the FX-100 beam at 4.5 m as air pressure is increased above the propagation window showing loss the the tail of the beam. Figures (b) and (c) show especially clear evidence of hosing in the tail.

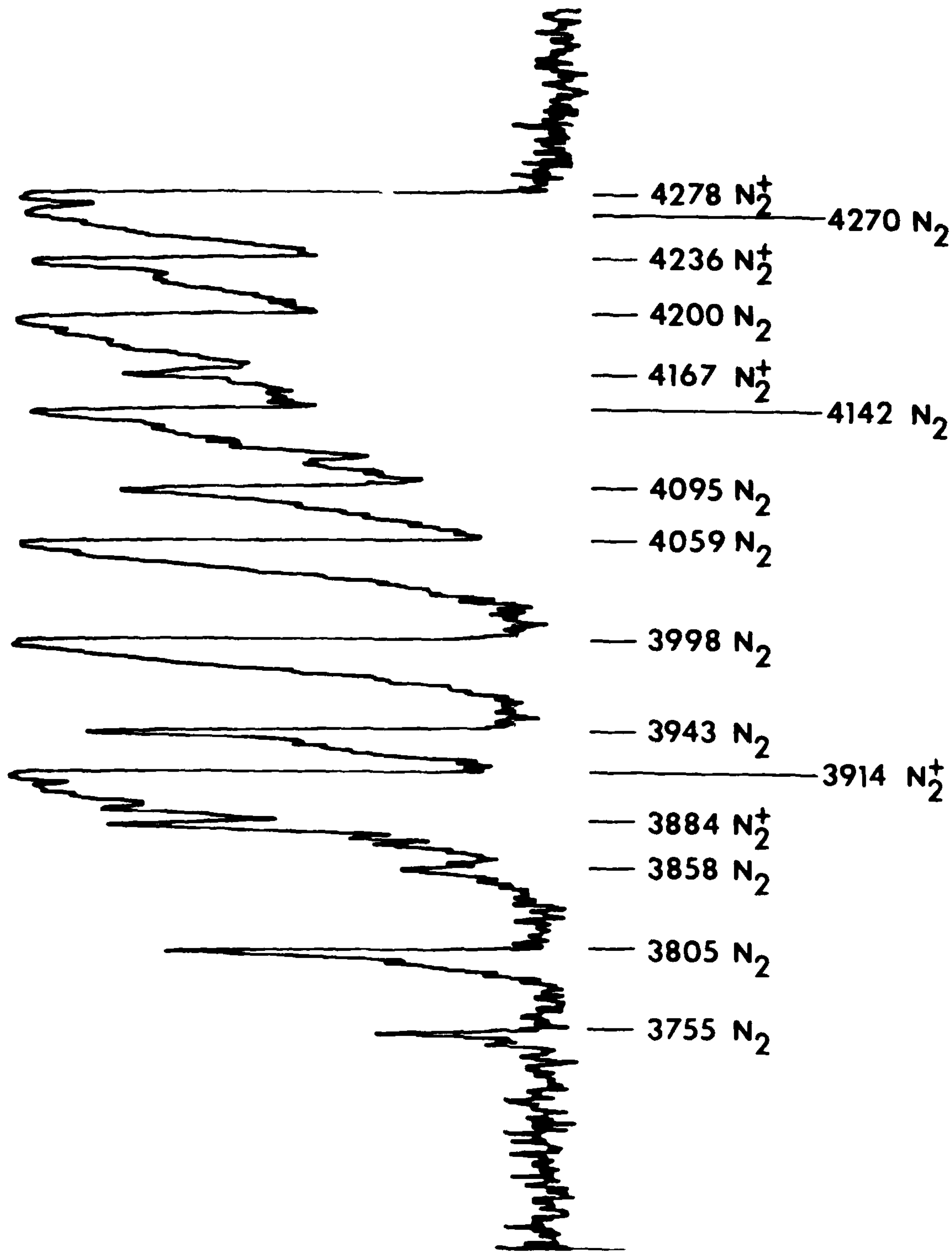

Figure 10. Microdensitometer scan of time-integrated spectrometer photograph of the emission from FX-100 beam-excited air at 0.35-Torr pressure. This scan shows the characteristic molecular nitrogen band emission that gives rise to the blue color in beam excited air.

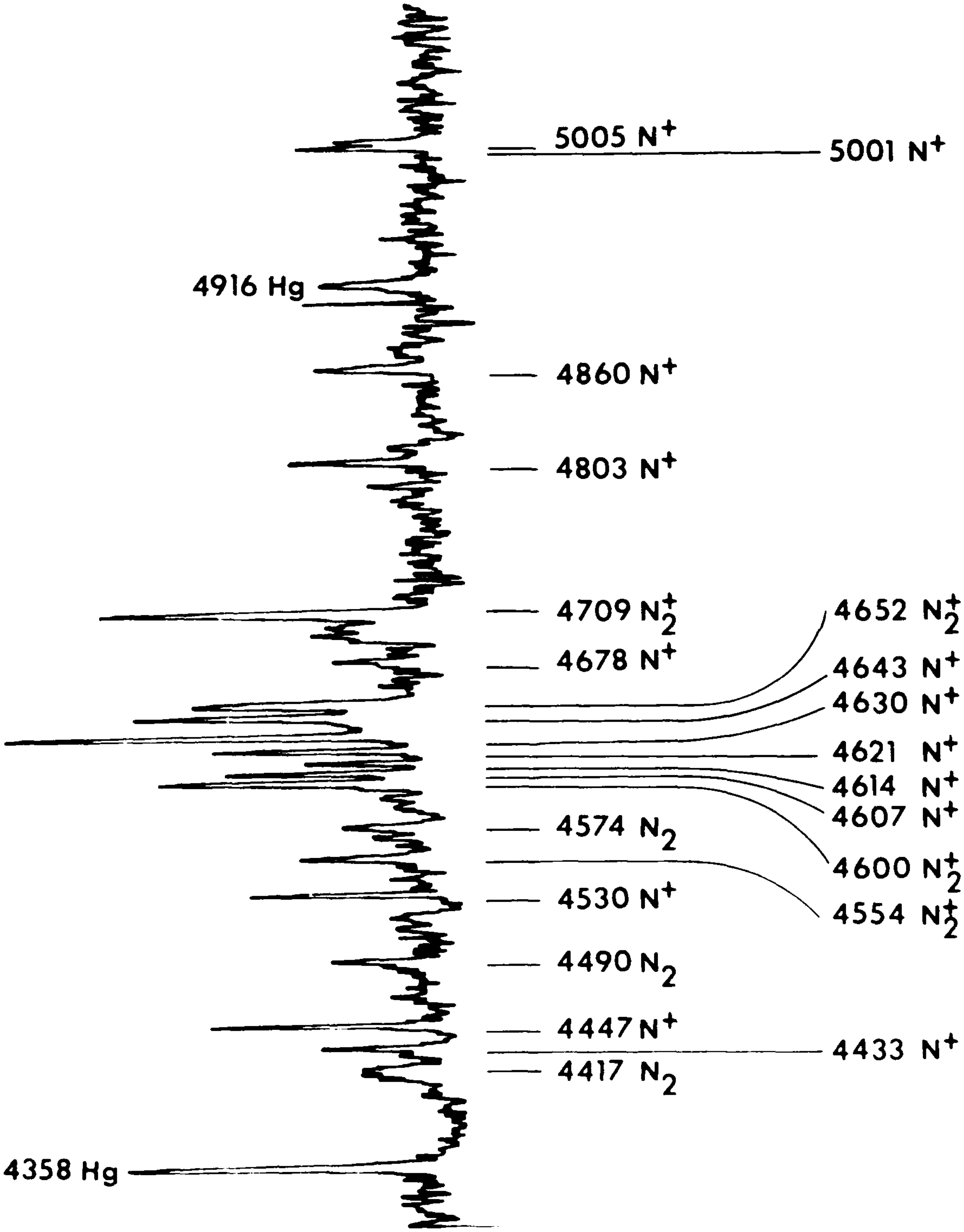

Figure 11. FX-100 beam-excited air spectrum in blue-green region. (Hg lines from calibration source.) This shows the appearance of singly ionized nitrogen lines (N+) in 0.35-Torr air experiments, which is indicative of high plasma electron temperatures.

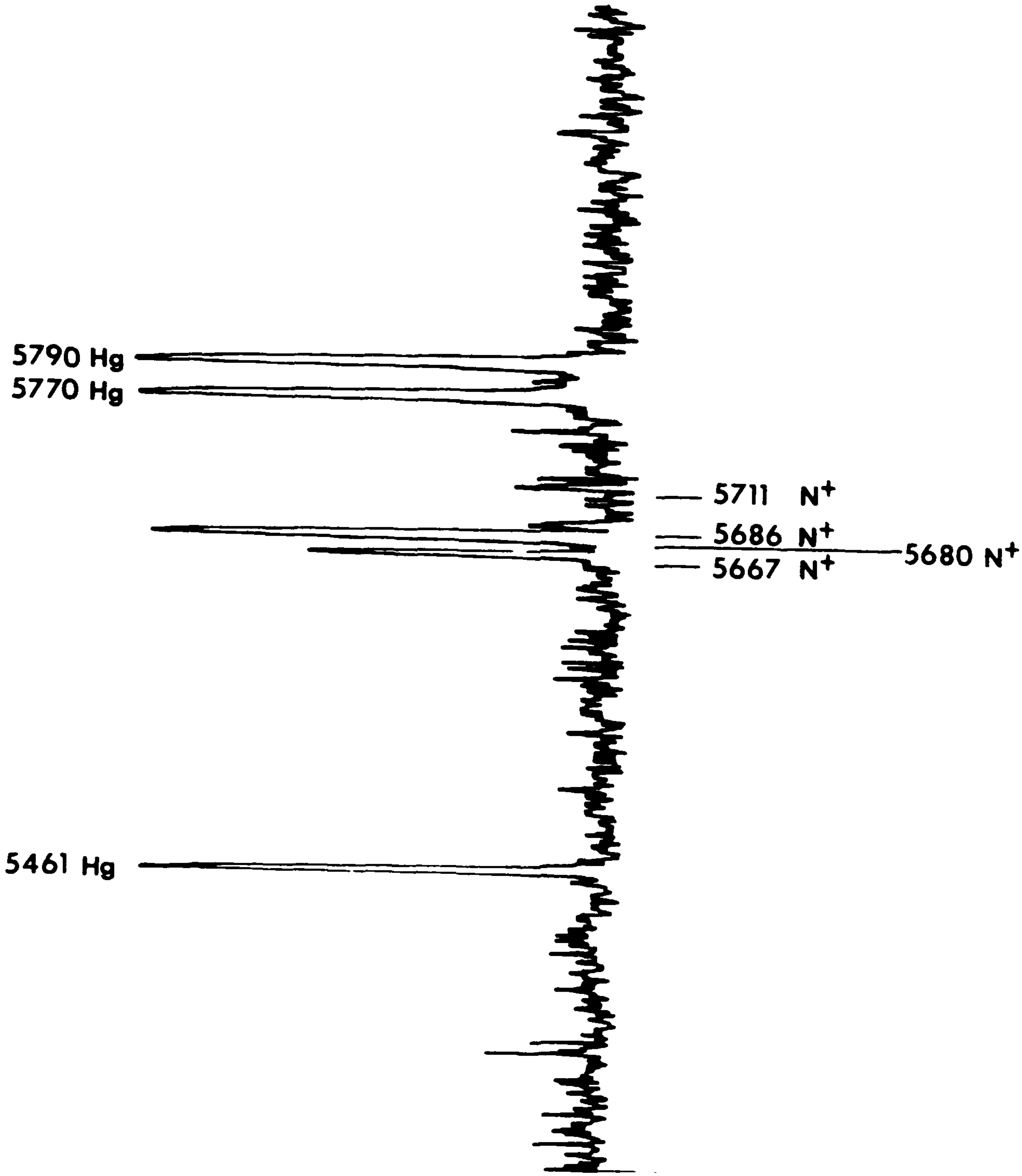

Figure 12. FX-100 beam-excited 0.35-Torr air spectrum in the yellow region showing further N+ line emission. Note that ~24 eV is required to dissociate and ionize nitrogen.

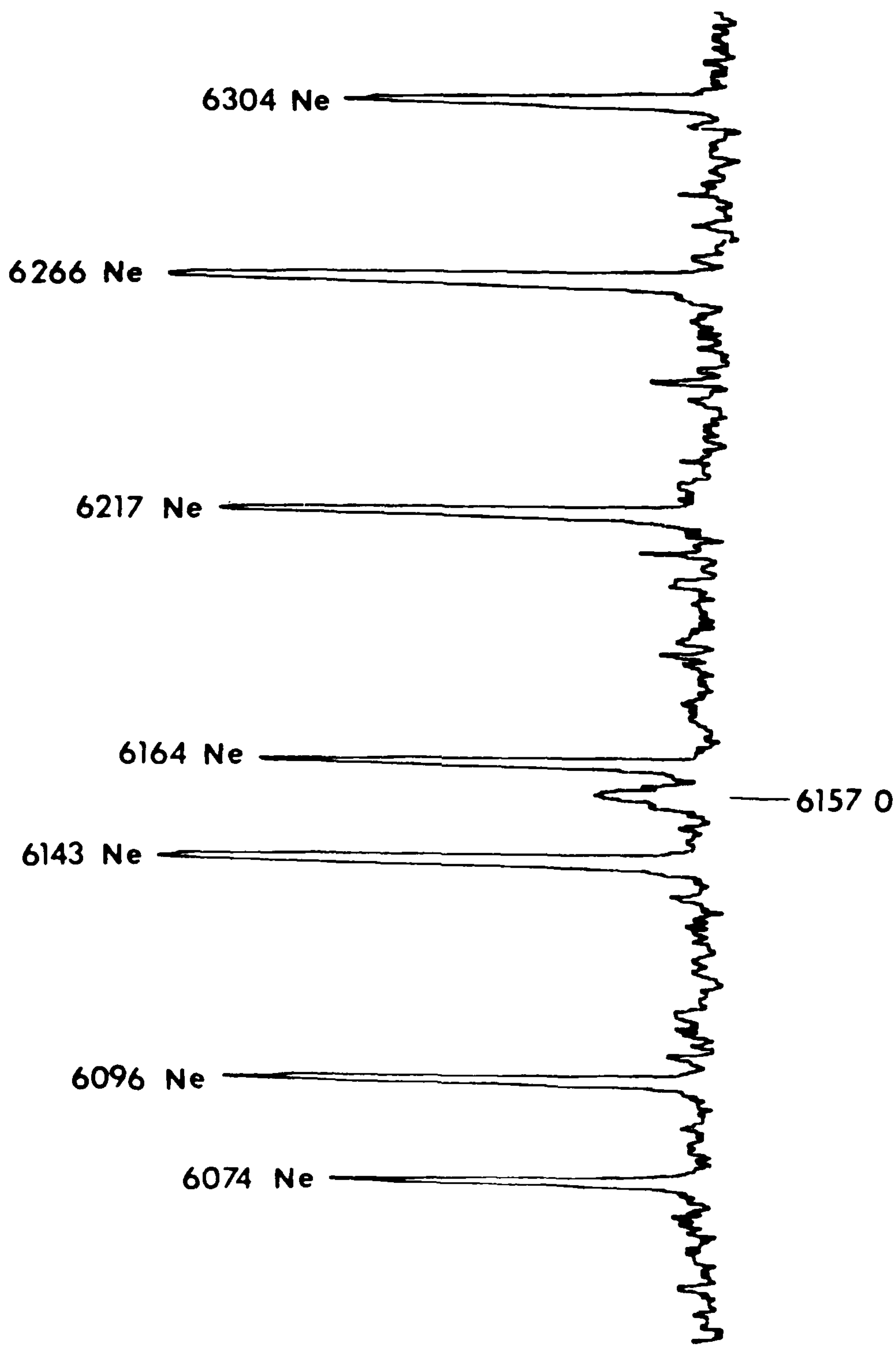

Figure 13. FX-100 beam excited 0.35-Torr air spectrum in the red region showing the atomic oxygen line responsible for the vivid red that appears in open shutter photographs taken in this pressure regime.

WAVELENGTH Å	ATOM/MOLECULE	TRANSITION (band) (v', v")
3755	N_2	(2+) (1,3)
3805	N_2	(2+) (0,2)
3858	N_2	(2+) (4,7)
3884	N_2^+	(1-) (1,1)
3914	N_2^+	(1-) (0,0)
3943	N_2	(2+) (2,5)
3998	N_2	(2+) (1,4)
4059	N_2	(2+) (0,3)
4095	N_2	(2+) (4,8)
4142	N_2	(2+) (3,7)
4167	N_2^+	(1-) (3,4)
4200	N_2	(2+) (2,6)
4236	N_2^+	(1-) (1,2)
4270	N_2	(2+) (1,5)
4278	N_2^+	(1-) (0,1)
4344	N_2	(2+) (0,4)
4417	N_2	(2+) (3,8)
4433	N^+	3d $^3P^o$-4f D(5/2)
4447	N^+	3p ^3D - 3d $^3D^o$
4490	N_2	(2+) (2,7)
4530	N^+	3d ^1F - 4f G(9/2)
4554	N_2^+	(1-) (3,5)
4574	N_2	(2+) (1,6)
4600	N_2^+	(1-) (2,4)
4607	N^+	3s $^3P^o$ - 3p ^3P
4614	N^+	3s $^3P^o$ - 3p ^3P
4621	N^+	3s $^3P^o$ - 3p ^3P
4630	N^+	3s $^3P^o$ - 3p ^3P
4643	N^+	3s $^3P^o$ - 3p ^3P
4652	N_2^+	(1-) (1,3)
4678	N^+	3d $^1P^o$ - 4f D(3/2)
4709	N_2^+	(1-) (0,2)
4803	N^+	3p ^3D - 3d $^3D^o$
4860	N^+	3p ^3D - 3d $^3D^o$
5001	N^+	3p ^3D - 3d $^3F^o$
5005	N^+	3s ^5P - 3p $^5P^o$ 3p ^3D - 3d $^3F^o$
5667	N^+	3s ^3P - 3p ^3D
5680	N^+	3s ^3P - 3p ^3D
5686	N^+	3s ^3P - 3p ^3D
5711	N^+	3s ^3P - 3p ^3D
6157	O	3p ^5P - 4d $^5D^o$

Figure 14. Identification of the spectral lines and bands observed from 0.35-Torr air emission.

	OBSERVED	AURORAL
WAVELENGTH:	6157 A	6300 A
DESIGNATION:	$4d\,^5D-3p\,^5P$	$2p^4\,^1D-2p^4\,^3P$
ASSOCIATED LINES:	NONE WITH SAME INTENSITY	$^1D-^3P$ 6364 A $^1S-^1D$ 5577 A (NOT OBSERVED)
EXCITATION:	PROBABLY RECOMBINATION $O^+ + e + M \rightarrow O^* + M$ OR $O^+ + e + e \rightarrow O^* + e$	LARGELY PHOTODETACHMENT
QUENCHING:	-	HIGHLY QUENCHED BY ELECTRONS
MISCELLANEOUS:	NO FORBIDDEN TRANSITIONS ARE OBSERVED TOO MUCH IS HAPPENING AROUND THE BEAM	

Figure 15. The observed red emission, although an atomic oxygen line, was not the 6300 Å auroral line as was initially speculated after first seeing the vivid red in open shutter photographs.

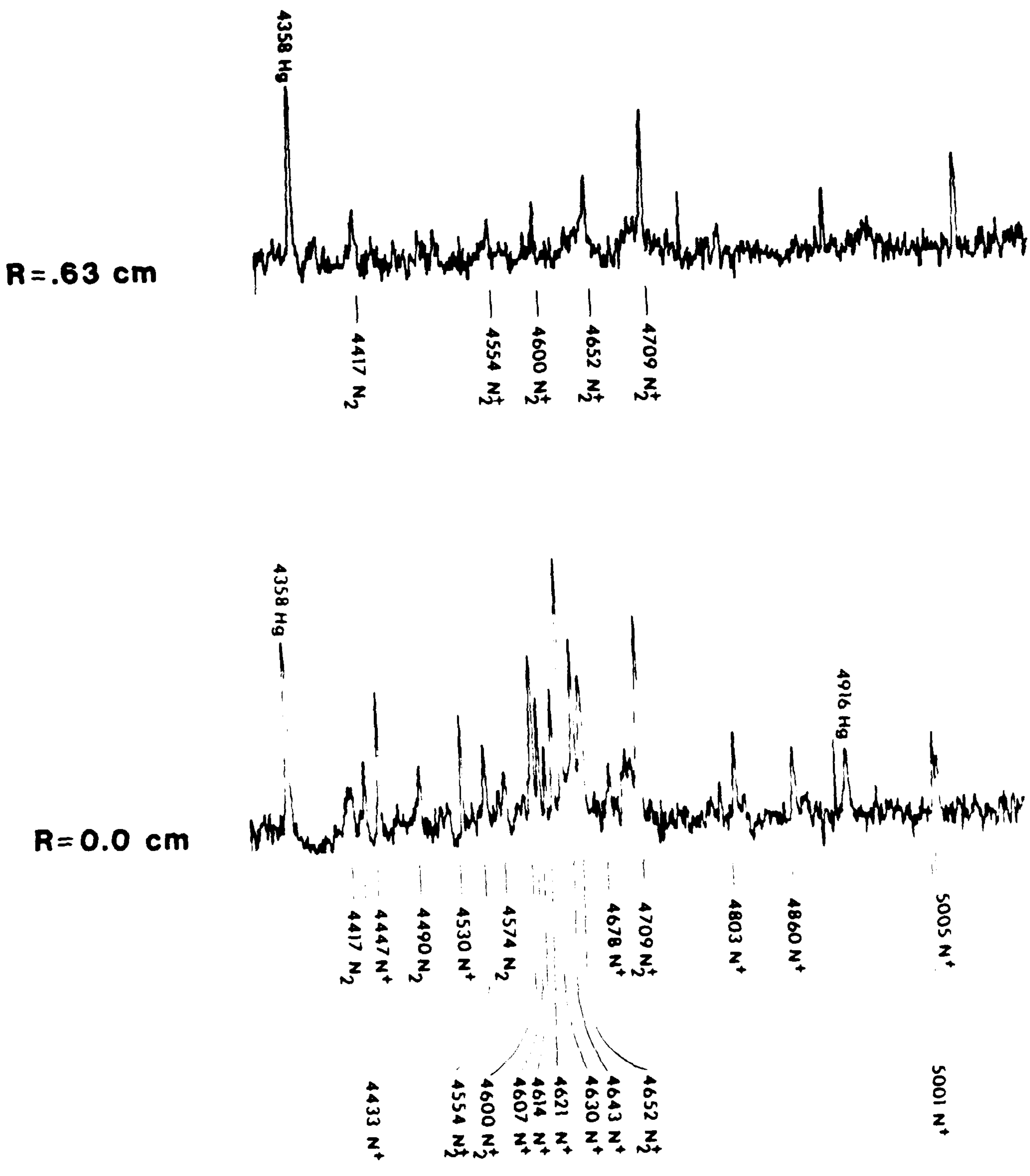

Figure 16. The atomic line emission appears only near the axis of the beam indicative of the high plasma electron temperature on axis.

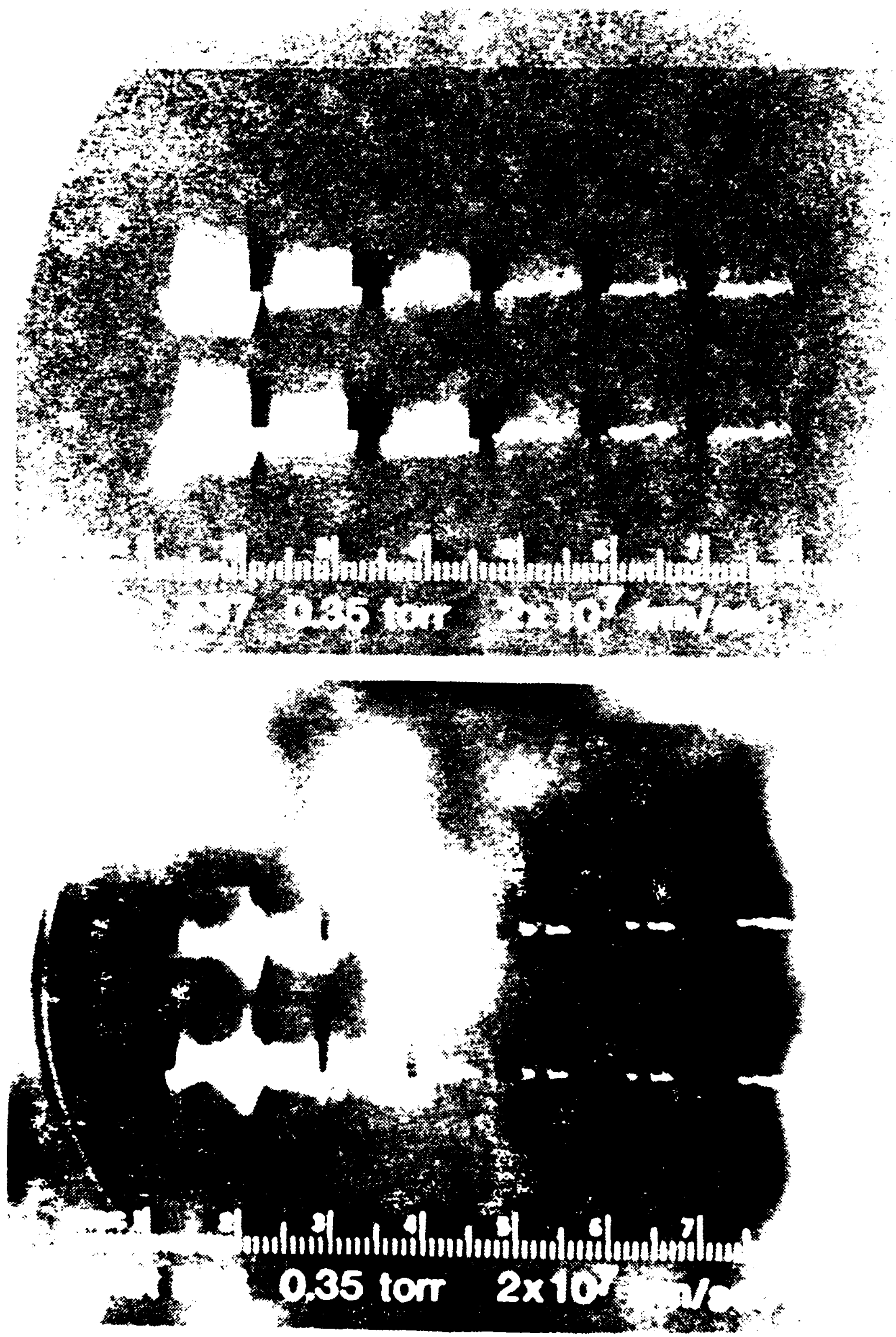

Figure 17. Framing-camera photographs (10-ns exposure) of beam excited 0.35-Torr air showing persistance of radiation from ionized gas near the beam axis after the passage of the 12[illegible]-ns beam. This is probably the result of the slow deionization of [illegible] at this pressure.

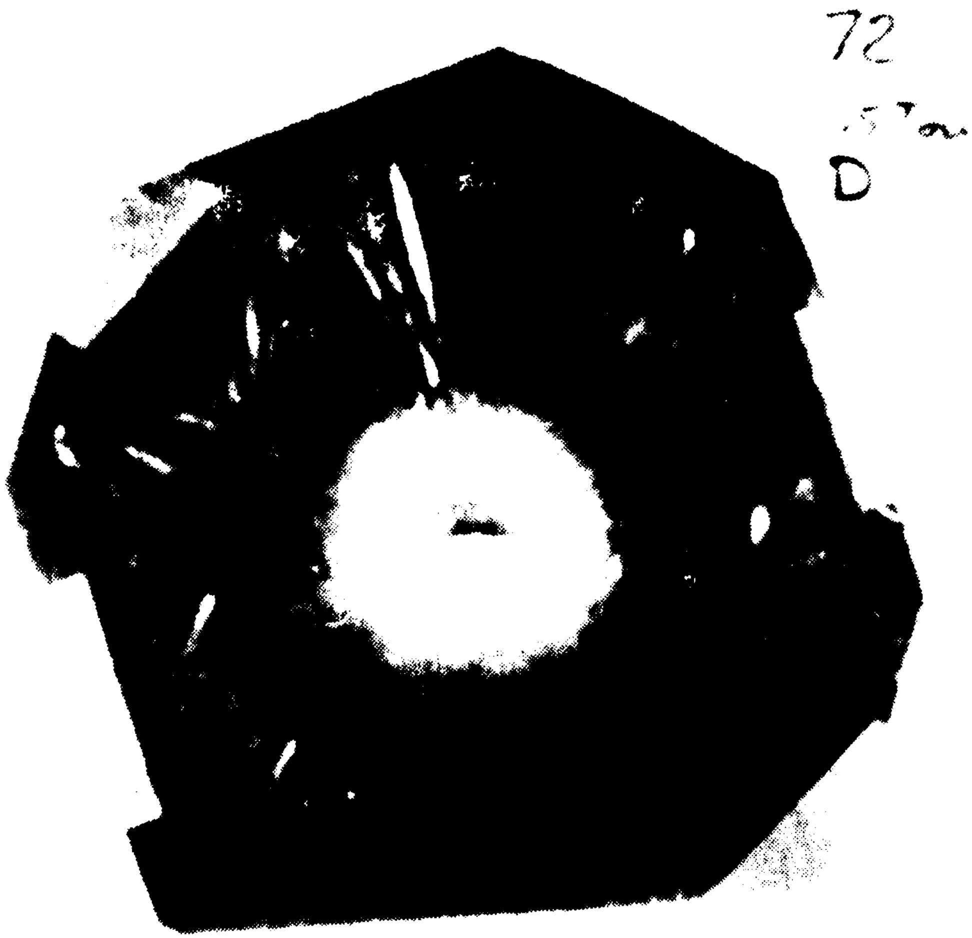

Figure 18. Radiochronic (blue cellophane) foil exposed to FX-100 beam after propagating 5 m in 0.5-Torr air. Note the bleaching at large radii resulting from annular "halo" of electrons.

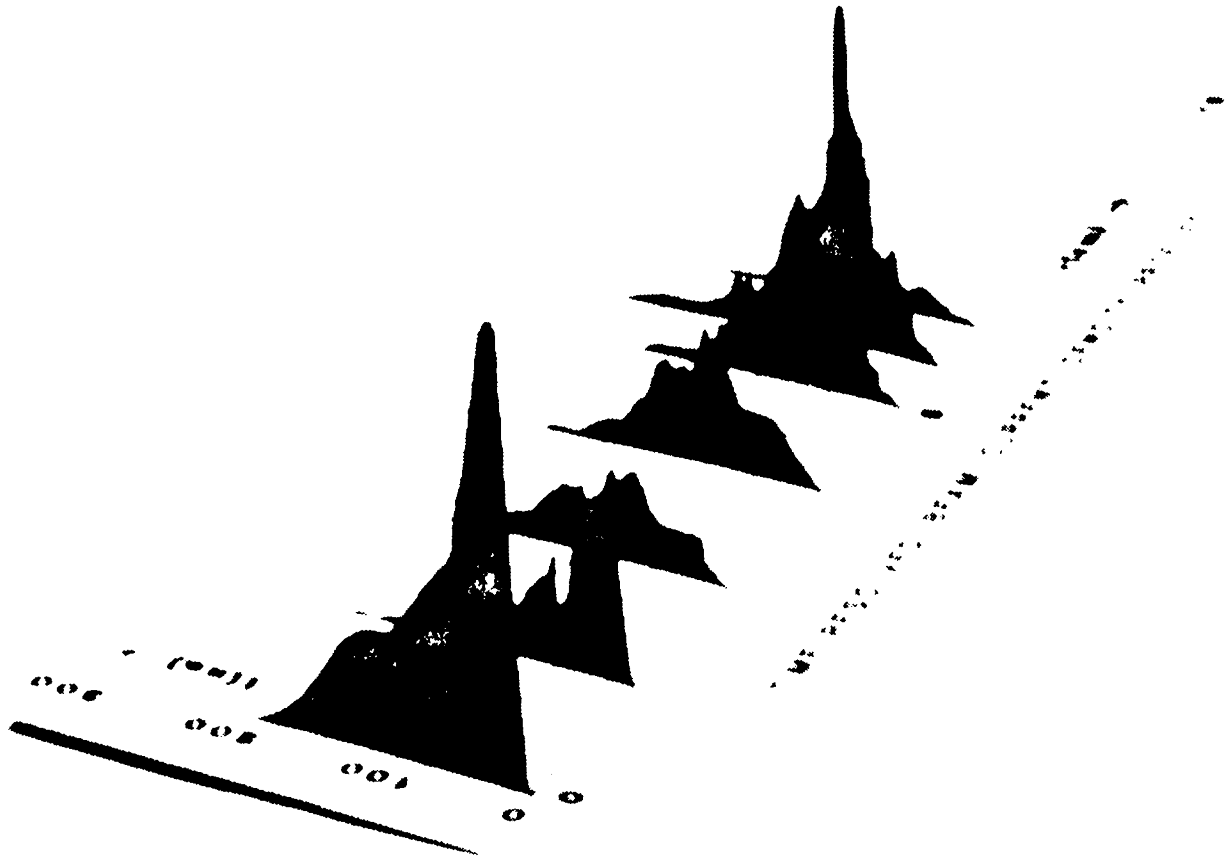

Figure 19. Time-resolved FX-100 beam current density profile at $Z = 0.81$ m showing the expulsion of current from the central channel to form the halo at large radii.

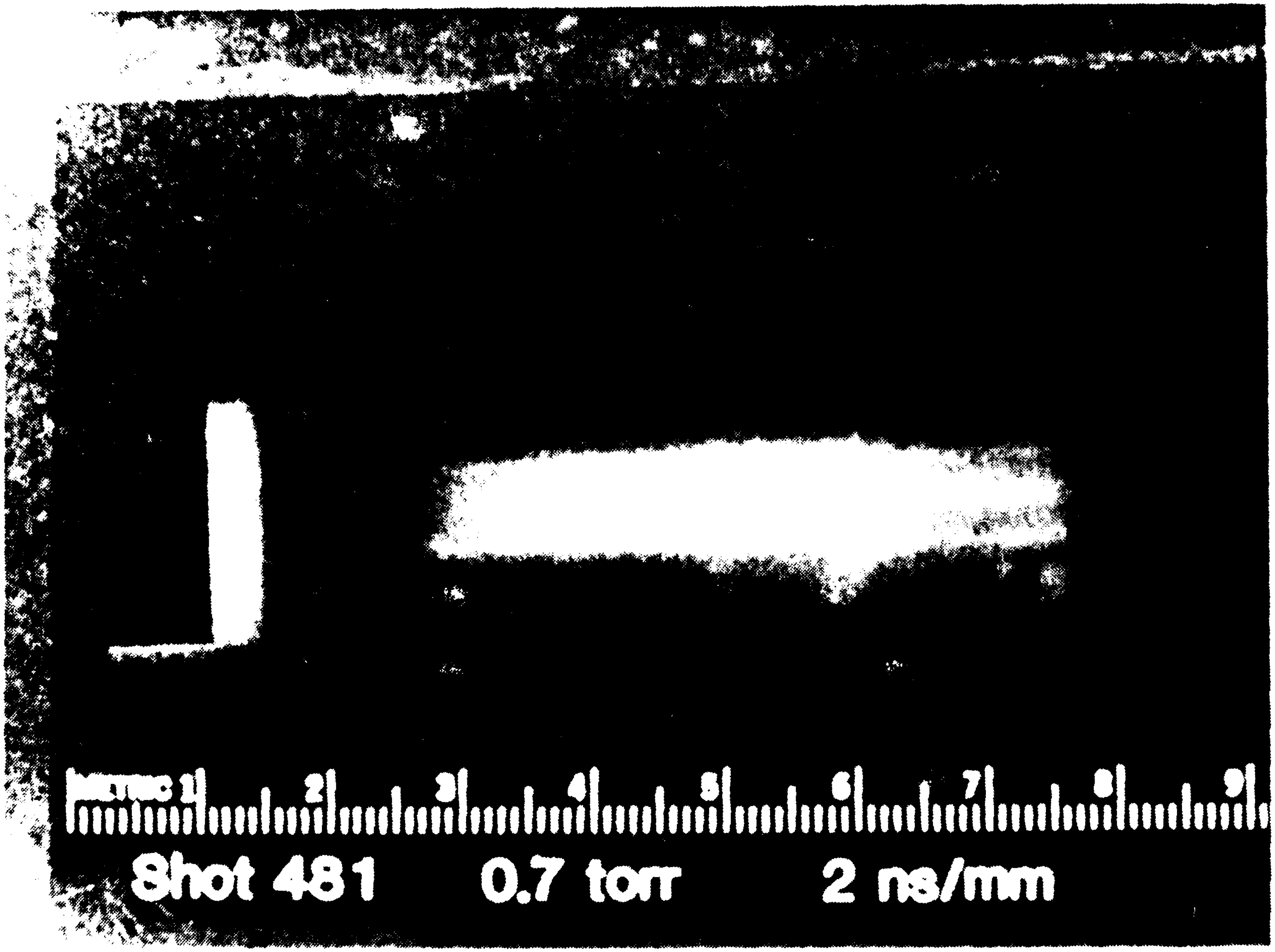

Figure 20. Streak photograph at Z = 4.5 m showing a fully developed halo of current surrounding the main beam current.

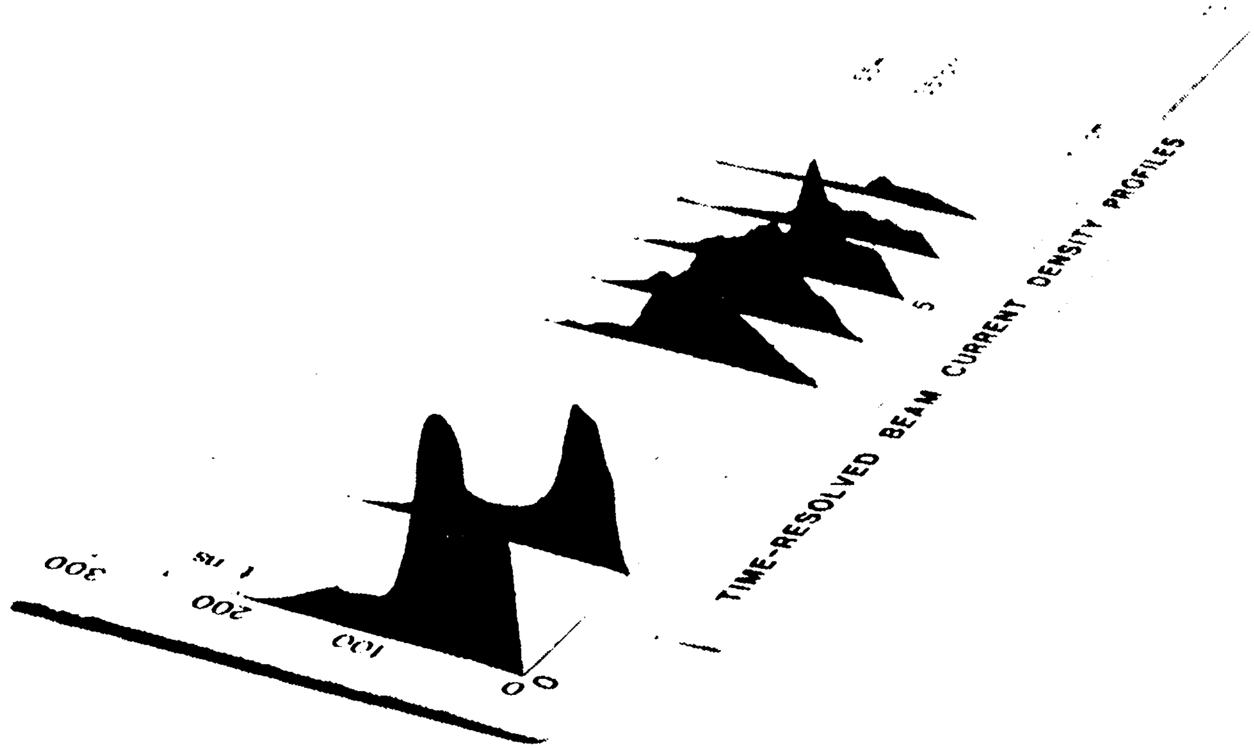

Figure 21. Time-resolved current density profile showing development of halo at Z = 0.55 m in 0.35-Torr air.

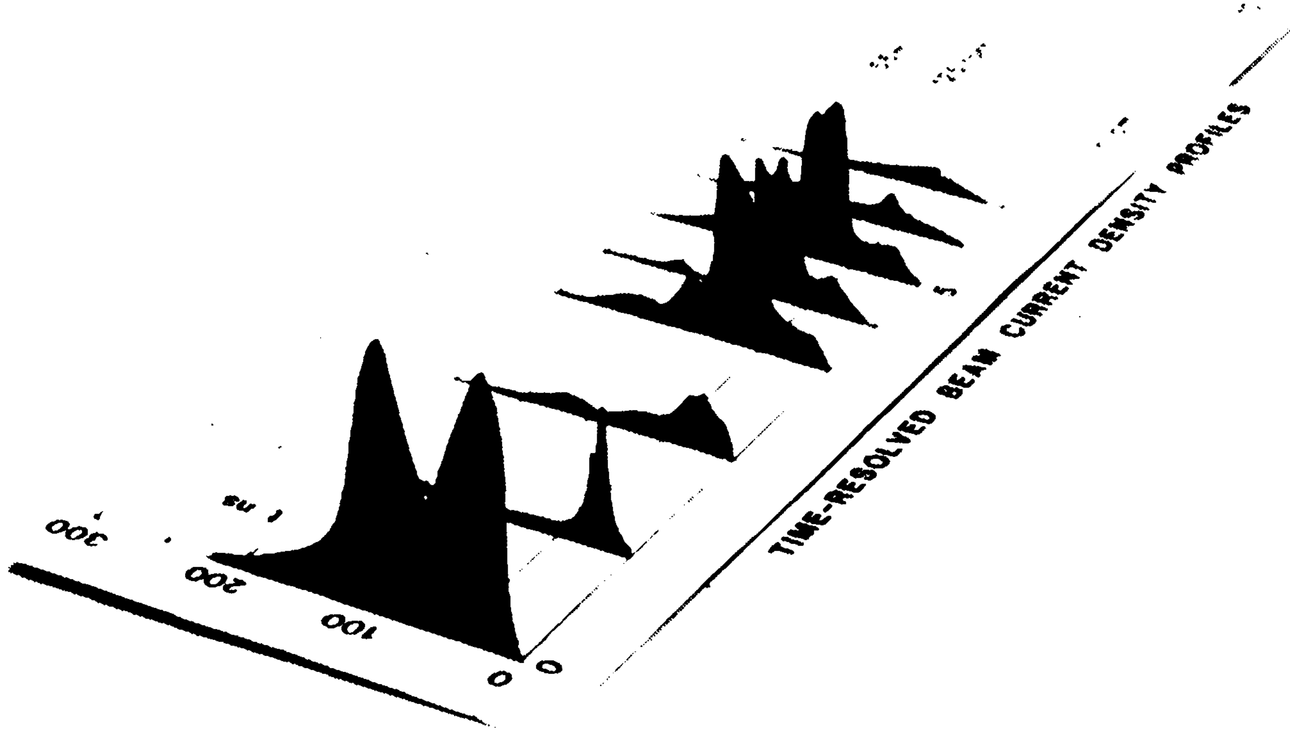

Figure 22. Time-resolved current density profile showing halo development at 0.55 m at lowest pressures (0.125 Torr).

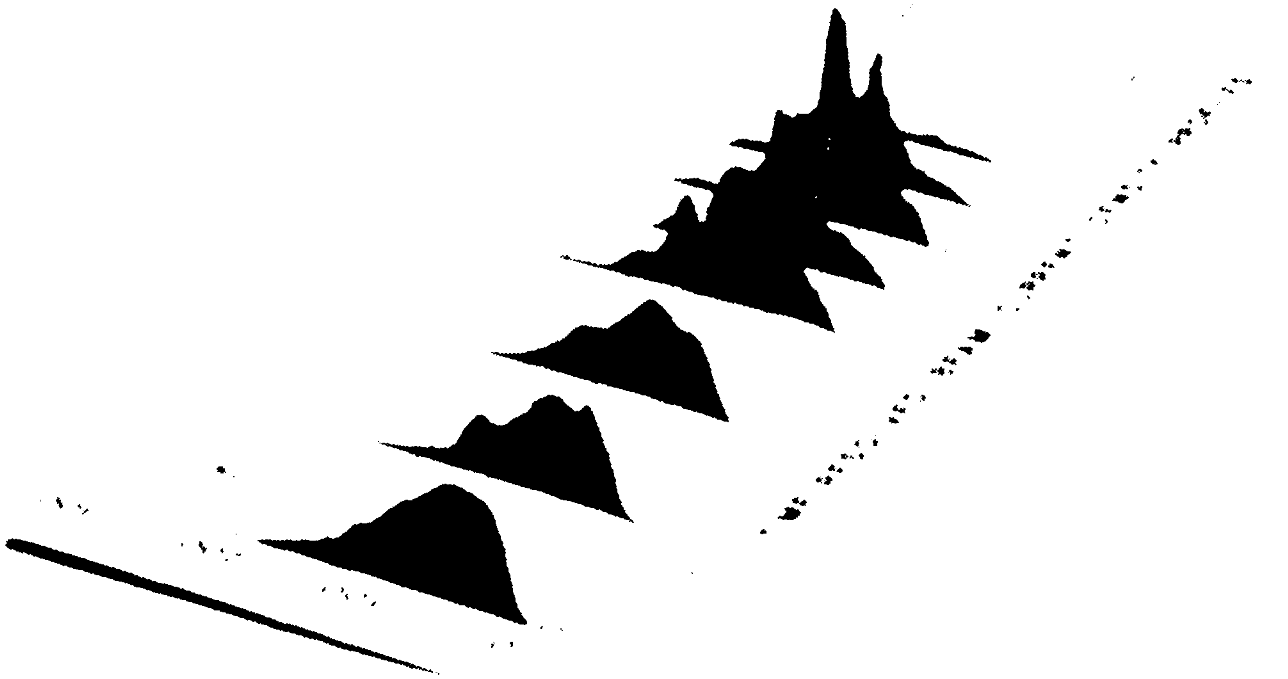

Figure 23. Time-resolved current density profile showing halo development at slightly higher pressure (0.7-Torr).

APPENDIX E

ELECTRON BEAM TRANSPORT IN A SMALL APERTURE FARADAY CUP

SECURITY CLASSIFICATION OF THIS PAGE (When Data Entered)

REPORT DOCUMENTATION PAGE		READ INSTRUCTIONS BEFORE COMPLETING FORM
1. REPORT NUMBER	2. GOVT ACCESSION NO.	3. RECIPIENT'S CATALOG NUMBER
4. TITLE (and Subtitle) ELECTRON BEAM TRANSPORT IN A SMALL APERTURE FARADAY CUP		5. TYPE OF REPORT & PERIOD COVERED Interim Report
		6. PERFORMING ORG. REPORT NUMBER AMRC-N-185
7. AUTHOR(s) D. J. Sullivan, C. A. Ekdahl		8. CONTRACT OR GRANT NUMBER(s) F49620-81-C-0016
9. PERFORMING ORGANIZATION NAME AND ADDRESS MISSION RESEARCH CORPORATION, 1400 San Mateo Blvd. S. E., Suite A, Albuquerque, New Mexico 87108		10. PROGRAM ELEMENT, PROJECT, TASK AREA & WORK UNIT NUMBERS
11. CONTROLLING OFFICE NAME AND ADDRESS Air Force Office of Scientific Research, Bolling Air Force Base, Washington, D. C. 20332		12. REPORT DATE January 1982
		13. NUMBER OF PAGES 65
14. MONITORING AGENCY NAME & ADDRESS (if different from Controlling Office)		15. SECURITY CLASS (of this report) Unclassified
		15a. DECLASSIFICATION DOWNGRADING SCHEDULE

16. DISTRIBUTION STATEMENT (of this Report)

Approved for public release; distribution unlimited.

17. DISTRIBUTION STATEMENT (of the abstract entered in Block 20, if different from Report)

18. SUPPLEMENTARY NOTES

19. KEY WORDS (Continue on reverse side if necessary and identify by block number)

Electron Beam Diagnostics
Electron Monte-Carlo Transport Calculations
Faraday Cup

20. ABSTRACT (Continue on reverse side if necessary and identify by block number)

The Monte Carlo transport code CYCLTRAN is used to study electron transport and scattering in a Faraday cup consisting of a small cross section coaxial cable surrounded concentrically by a massive carbon block. Electrons impinging on the center wire of the coax generate a signal proportional to the electron beam current. As expected, it is found that the effective cross section of the wire is greater than its geometrical cross section due to scattering of primaries into it. The cross section is only slightly modified by production

DD FORM 1 JAN 73 1473 EDITION OF 1 NOV 65 IS OBSOLETE

SECURITY CLASSIFICATION OF THIS PAGE (When Data Entered)

20. and deposition of secondary electrons in the form of knockons. These effects are dependent on electron beam energy.

TABLE OF CONTENTS

ABSTRACT

The Monte Carlo transport code CYLTRAN is used to study electron transport and scattering in a Faraday cup consisting of a small cross section coaxial cable surrounded concentrically by a massive carbon block. Electrons impinging on the center wire of the coax generate a signal proportional to the electron beam current. As expected, it is found that the effective cross section of the wire is greater than its geometrical cross section due to scattering of primaries into it. The cross section is only slightly modified by production and deposition of secondary electrons in the form of knockons. These effects are dependent on electron beam energy.

PROBLEM CONFIGURATION

The design of a small aperture Faraday cup to measure electron beam current is given in Figure 1. It consists of a UT-47 coaxial cable embedded in a cylindrically shaped massive carbon block. In experiments, the block is sufficiently large in axial and radial extent to stop all primary and secondary electrons. Figure 1 depicts the accurate coaxial cable dimensions. However, the carbon block shown was utilized in code runs to minimize necessary computer time. The length is sufficient to effectively stop all electrons up to 4 MeV - the maximum energy tested. Because we were not interested in electrons scattered outward, the block radius was set equal to the beam radius.

CODE RESULTS

The Monte Carlo transport code CYLTRAN was used in this study. It is particularly suitable, because it can calculate both electron and photon transport in cylindrical geometry. The problem may involve up to five materials each consisting of a maximum of ten elements without code modification. The problem cylinder may be zoned axially and radially into 100 compartments, if necessary. CYLTRAN is detailed in Reference 1.

Data on materials used in the Faraday cup pertaining to beam stopping power, range and radiation yield up to a maximum beam energy of 4 MeV is compiled in Appendix A. It is generated based on material density, composition, and tabulated cross sections for the various elements.

The largest obstacle in producing statistically significant results from this problem was the exceedingly small ratio of the area of the central wire, which generates the signal, to the beam area. That ratio is $.367 \times 10^{-3}$. The beam is assumed to have a uniform current density and is monoenergetic. Increasing the particle substep size in zones comprising

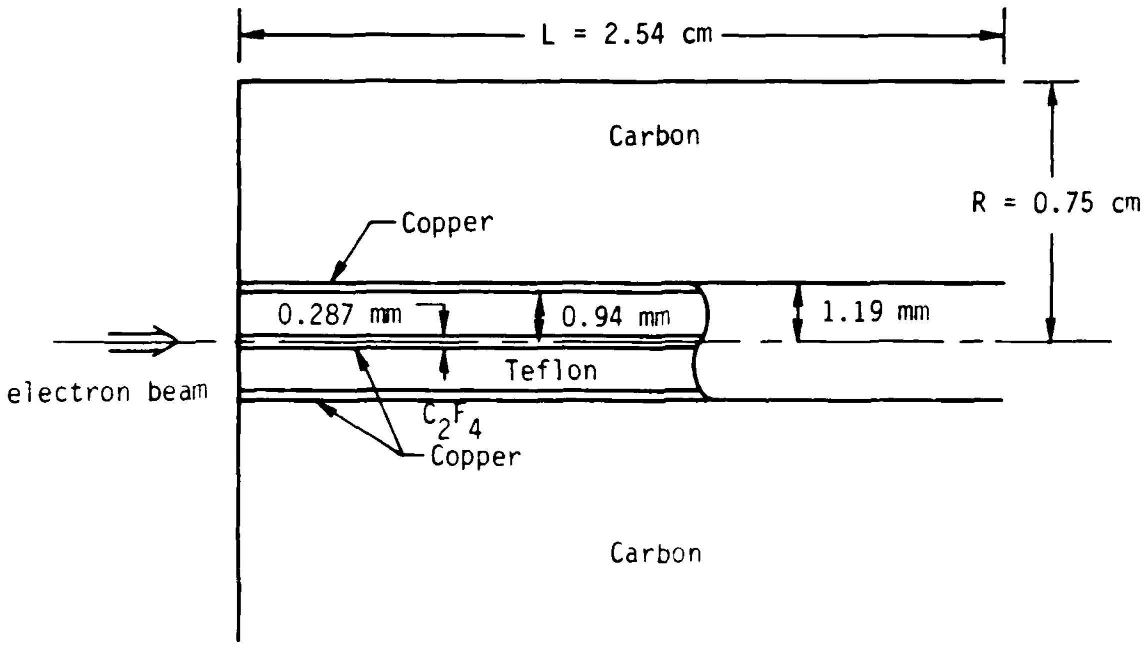

Figure 1. Physical dimensions and material composition of a small aperture Faraday cup. The electron beam in uniformly distributed over the entire cross sectional area.

the coaxial cable improved the statistics only marginally. Eventually, ten batches of 3000 particles were utilitzed. Further statistical improvement could be obtained by increasing the number of primaries. However, the increased accuracy was not deemed necessary for the present application.

The main purpose of this study was to determine the amount of charge deposited in the central wire due to scattering and secondary electron producton versus that predicted from its cross section area. Electrons with energies greater than approximately 10 keV were followed. It was found that the number of electrons deposited was several times larger than could be explained by purely geometric considerations. This is the result of the higher density of copper in relation to the other materials present in the problem. The higher density results in a shorter range and larger stopping power for electrons in the wire than in carbon or Teflon. This effect was observed over the range of energies studied from 1 to 4 MeV. Results are presented in Figure 2. The error bars are too large to derive an exact energy dependence for the ratio of effective to geometric cross sections. However, it appears to be logarithmic in energy. Finally, it is noteworthy that although, depending on beam energy, five to ten secondary electrons are created for each primary electron, they insignificantly modify the charge distribution in the various zones. This indicates that on average the number of knockons created in a zone is equal to the number whose histories are terminated in that zone by dropping below the minimum energy level of 10 keV.

ACKNOWLEDGEMENT

The author is pleased to acknowledge helpful discussions with J. Mack of Los Alamos National Laboratory and J. A. Halbleib of Sandia National Laboratory on the use of the CYLTRAN code.

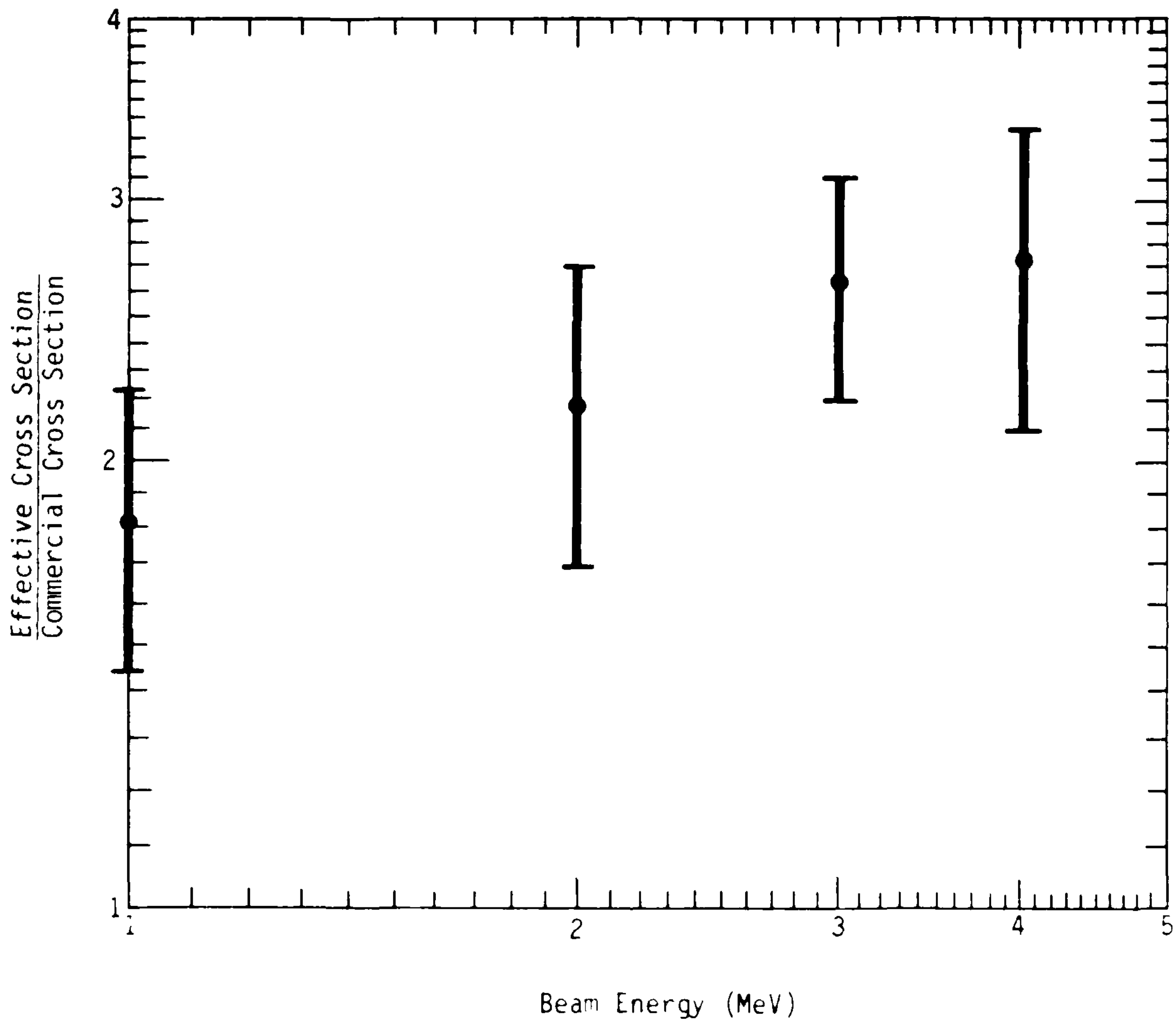

Figure 2. Ratio of effective to geometrical cross section versus electron beam energy.

REFERENCES

1. J. A. Halbleib Sr. and W. H. Vandevender, CYLTRAN: A Cylindrical-Geometry Multimaterial Electron/Photon Monte Carlo Transport Code, SAND 74-0030, Sandia National Laboratories, (1975), unpublished.

APPENDIX A

FARADAY CUP MATERIAL DATA

COPPER

```
   324 mev electron beam into bare fx-100 faraday cup**
0
0 nmat  itre  isip  iagn  isub  inel  icyc  ncyc  nmax        emax
    1     5     0     1    50     1     1     8    64     .40000e+01
0input data tape identification
 datatape-2 (roster-aiginger ph-rad corr), 54 sternheimer sets. 30 jan 6
0detour          density
   .53000e+00    .89600e+01
0
0range table
0      emax         ncyc        efac        nmax    t(nmax+1)    ncal     t(ncal)
    .40000e+01        8     .91700e+00     64    .15625e-01     97    .97656e-03
0 jmax   lmax
    1      1
0       z            a            w
    29.00000     63.54006     1.00000
0       pi          pid
   314.05142   314.05142
0  ---------------------parameters for density effect---------------------
        pi            c             b            dm            x1           x0

   314.05142     -4.37108       .15716       3.00000       3.00000       .20000
   314.05142     -4.37108       .15716       3.00000       3.00000       .20000
   .1372e+00   -.1410e+02     .7010e-01
1                                                    electron results
0     effective z/a =  .45640     effective mean ionization potential =  314.05 ev     critical energy =   0.000 mev
```

n	energy (mev)	stopping power collision (mev cm2/g)	stopping power radiation (mev cm2/g)	stopping power total (mev cm2/g)	range (g/cm2)	radiation yield	beta**2	density corr (mev cm2/g)	rad/col	drange (g/cm2)	dyield
97	.9766e-03	.473e+02	.180e-01	.473e+02	.103e-04	0.	.381e-02	0.	.380e-03	0.	0.
96	.1065e-02	.463e+02	.180e-01	.463e+02	.122e-04	.318e-04	.416e-02	0.	.388e-03	.189e-05	.339e-07
95	.1161e-02	.452e+02	.180e-01	.452e+02	.143e-04	.617e-04	.453e-02	0.	.397e-03	.211e-05	.378e-07
94	.1266e-02	.439e+02	.179e-01	.439e+02	.167e-04	.901e-04	.494e-02	0.	.409e-03	.236e-05	.424e-07
93	.1381e-02	.425e+02	.179e-01	.425e+02	.193e-04	.117e-03	.538e-02	0.	.422e-03	.265e-05	.476e-07
92	.1506e-02	.411e+02	.179e-01	.411e+02	.223e-04	.143e-03	.587e-02	0.	.437e-03	.299e-05	.536e-07
91	.1642e-02	.396e+02	.179e-01	.396e+02	.257e-04	.168e-03	.640e-02	0.	.453e-03	.338e-05	.606e-07
90	.1791e-02	.380e+02	.179e-01	.381e+02	.295e-04	.192e-03	.697e-02	0.	.471e-03	.383e-05	.686e-07
89	.1953e-02	.365e+02	.179e-01	.365e+02	.339e-04	.216e-03	.760e-02	0.	.490e-03	.435e-05	.779e-07
88	.2130e-02	.349e+02	.179e-01	.350e+02	.388e-04	.240e-03	.828e-02	0.	.512e-03	.495e-05	.886e-07
87	.2323e-02	.334e+02	.179e-01	.334e+02	.445e-04	.263e-03	.903e-02	0.	.535e-03	.564e-05	.101e-06
86	.2533e-02	.319e+02	.179e-01	.319e+02	.509e-04	.287e-03	.984e-02	0.	.560e-03	.644e-05	.115e-06
85	.2762e-02	.304e+02	.179e-01	.304e+02	.583e-04	.311e-03	.107e-01	0.	.588e-03	.737e-05	.132e-06
84	.3012e-02	.289e+02	.178e-01	.289e+02	.667e-04	.335e-03	.117e-01	0.	.617e-03	.843e-05	.151e-06
83	.3285e-02	.275e+02	.178e-01	.275e+02	.764e-04	.360e-03	.127e-01	0.	.649e-03	.967e-05	.172e-06
82	.3582e-02	.261e+02	.178e-01	.261e+02	.875e-04	.385e-03	.139e-01	0.	.683e-03	.111e-04	.198e-06
81	.3906e-02	.248e+02	.178e-01	.248e+02	.100e-03	.411e-03	.151e-01	0.	.719e-03	.128e-04	.227e-06
80	.4260e-02	.235e+02	.178e-01	.235e+02	.115e-03	.438e-03	.165e-01	0.	.759e-03	.147e-04	.261e-06
79	.4645e-02	.222e+02	.178e-01	.222e+02	.132e-03	.467e-03	.179e-01	0.	.801e-03	.169e-04	.300e-06
78	.5066e-02	.210e+02	.178e-01	.210e+02	.151e-03	.496e-03	.195e-01	0.	.846e-03	.195e-04	.346e-06
77	.5524e-02	.199e+02	.178e-01	.199e+02	.174e-03	.527e-03	.213e-01	0.	.894e-03	.224e-04	.399e-06
76	.6024e-02	.188e+02	.177e-01	.188e+02	.200e-03	.560e-03	.232e-01	0.	.946e-03	.259e-04	.460e-06
75	.6570e-02	.177e+02	.177e-01	.177e+02	.230e-03	.594e-03	.252e-01	0.	.100e-02	.299e-04	.530e-06
74	.7164e-02	.167e+02	.177e-01	.167e+02	.264e-03	.630e-03	.275e-01	0.	.106e-02	.346e-04	.612e-06
73	.7812e-02	.157e+02	.177e-01	.158e+02	.304e-03	.668e-03	.299e-01	0.	.112e-02	.400e-04	.708e-06
72	.8520e-02	.148e+02	.177e-01	.149e+02	.350e-03	.709e-03	.325e-01	0.	.119e-02	.462e-04	.818e-06
71	.9291e-02	.140e+02	.177e-01	.140e+02	.404e-03	.752e-03	.354e-01	0.	.126e-02	.535e-04	.946e-06
70	.1013e-01	.132e+02	.177e-01	.132e+02	.466e-03	.798e-03	.386e-01	0.	.134e-02	.620e-04	.109e-05
69	.1105e-01	.124e+02	.176e-01	.124e+02	.538e-03	.846e-03	.419e-01	0.	.142e-02	.718e-04	.127e-05
68	.1205e-01	.116e+02	.176e-01	.117e+02	.621e-03	.898e-03	.456e-01	0.	.151e-02	.832e-04	.147e-05

61	67	.1314e-01	.110e+02	.176e-01	.110e+02	.717e-03	.952e-03	.495e-01	0.	.161e-02	.904e-04	.170e-06
62	66	.1433e-01	.103e+02	.176e-01	.103e+02	.829e-03	.101e-02	.538e-01	0.	.171e-02	.112e-03	.197e-06
63	65	.1562e-01	.969e+01	.176e-01	.970e+01	.959e-03	.107e-02	.585e-01	0.	.182e-02	.130e-03	.228e-06
64	64	.1704e-01	.911e+01	.176e-01	.912e+01	.111e-02	.114e-02	.635e-01	0.	.193e-02	.150e-03	.264e-06
65	63	.1858e-01	.856e+01	.176e-01	.858e+01	.128e-02	.121e-02	.689e-01	0.	.205e-02	.174e-03	.306e-06
66	62	.2026e-01	.804e+01	.175e-01	.806e+01	.149e-02	.128e-02	.748e-01	0.	.218e-02	.202e-03	.356e-05
67	61	.2210e-01	.756e+01	.175e-01	.758e+01	.172e-02	.136e-02	.812e-01	0.	.232e-02	.235e-03	.412e-05
68	60	.2410e-01	.711e+01	.175e-01	.712e+01	.199e-02	.145e-02	.880e-01	0.	.247e-02	.272e-03	.477e-05
69	59	.2628e-01	.668e+01	.175e-01	.670e+01	.231e-02	.154e-02	.954e-01	0.	.262e-02	.316e-03	.553e-05
70	58	.2866e-01	.628e+01	.175e-01	.630e+01	.268e-02	.164e-02	.103e+00	0.	.279e-02	.367e-03	.641e-05
71	57	.3125e-01	.590e+01	.175e-01	.592e+01	.310e-02	.174e-02	.112e+00	0.	.296e-02	.425e-03	.743e-05
72	56	.3408e-01	.555e+01	.175e-01	.557e+01	.359e-02	.185e-02	.121e+00	0.	.315e-02	.493e-03	.862e-05
73	55	.3716e-01	.522e+01	.175e-01	.524e+01	.416e-02	.196e-02	.131e+00	0.	.335e-02	.571e-03	.998e-05
74	54	.4053e-01	.492e+01	.175e-01	.493e+01	.483e-02	.208e-02	.142e+00	0.	.356e-02	.662e-03	.116e-04
75	53	.4419e-01	.463e+01	.175e-01	.465e+01	.559e-02	.221e-02	.153e+00	0.	.378e-02	.767e-03	.134e-04
76	52	.4819e-01	.436e+01	.175e-01	.438e+01	.648e-02	.235e-02	.165e+00	0.	.401e-02	.887e-03	.155e-04
77	51	.5256e-01	.411e+01	.175e-01	.413e+01	.751e-02	.250e-02	.178e+00	0.	.426e-02	.103e-02	.180e-04
78	50	.5731e-01	.388e+01	.176e-01	.389e+01	.869e-02	.266e-02	.192e+00	0.	.453e-02	.119e-02	.208e-04
79	49	.6250e-01	.366e+01	.176e-01	.368e+01	.101e-01	.282e-02	.206e+00	0.	.481e-02	.137e-02	.241e-04
80	48	.6816e-01	.346e+01	.176e-01	.347e+01	.117e-01	.300e-02	.222e+00	0.	.510e-02	.158e-02	.279e-04
81	47	.7433e-01	.327e+01	.177e-01	.328e+01	.135e-01	.318e-02	.238e+00	0.	.542e-02	.183e-02	.323e-04
82	46	.8105e-01	.309e+01	.178e-01	.311e+01	.156e-01	.338e-02	.255e+00	0.	.575e-02	.211e-02	.373e-04
83	45	.8839e-01	.293e+01	.179e-01	.295e+01	.180e-01	.359e-02	.273e+00	0.	.610e-02	.242e-02	.432e-04
84	44	.9639e-01	.278e+01	.179e-01	.280e+01	.208e-01	.381e-02	.292e+00	0.	.646e-02	.279e-02	.499e-04
85	43	.1051e+00	.264e+01	.181e-01	.266e+01	.240e-01	.404e-02	.312e+00	0.	.685e-02	.320e-02	.577e-04
86	42	.1146e+00	.251e+01	.182e-01	.253e+01	.277e-01	.429e-02	.333e+00	0.	.726e-02	.368e-02	.667e-04
87	41	.1250e+00	.239e+01	.184e-01	.241e+01	.319e-01	.455e-02	.354e+00	0.	.769e-02	.421e-02	.770e-04
88	40	.1363e+00	.228e+01	.186e-01	.230e+01	.367e-01	.482e-02	.377e+00	0.	.815e-02	.482e-02	.889e-04
89	39	.1487e+00	.217e+01	.188e-01	.219e+01	.422e-01	.511e-02	.400e+00	0.	.863e-02	.550e-02	.103e-03
90	38	.1621e+00	.208e+01	.190e-01	.210e+01	.485e-01	.542e-02	.424e+00	0.	.915e-02	.627e-02	.119e-03
91	37	.1768e+00	.199e+01	.193e-01	.201e+01	.556e-01	.574e-02	.448e+00	0.	.969e-02	.714e-02	.137e-03
92	36	.1928e+00	.191e+01	.196e-01	.193e+01	.637e-01	.609e-02	.473e+00	0.	.103e-01	.812e-02	.158e-03
93	35	.2102e+00	.184e+01	.200e-01	.186e+01	.729e-01	.645e-02	.498e+00	0.	.109e-01	.920e-02	.183e-03
94	34	.2293e+00	.177e+01	.205e-01	.179e+01	.834e-01	.684e-02	.523e+00	0.	.115e-01	.104e-01	.211e-03
95	33	.2500e+00	.171e+01	.210e-01	.173e+01	.951e-01	.724e-02	.549e+00	0.	.122e-01	.118e-01	.244e-03
96	32	.2726e+00	.166e+01	.215e-01	.168e+01	.108e+00	.767e-02	.575e+00	0.	.130e-01	.133e-01	.282e-03
97	31	.2973e+00	.161e+01	.222e-01	.163e+01	.123e+00	.813e-02	.600e+00	0.	.138e-01	.149e-01	.326e-03
98	30	.3242e+00	.156e+01	.229e-01	.159e+01	.140e+00	.862e-02	.626e+00	0.	.146e-01	.167e-01	.377e-03
99	29	.3536e+00	.152e+01	.237e-01	.156e+01	.159e+00	.914e-02	.651e+00	0.	.156e-01	.187e-01	.436e-03
100	28	.3856e+00	.149e+01	.246e-01	.151e+01	.180e+00	.969e-02	.675e+00	0.	.166e-01	.209e-01	.506e-03
101	27	.4204e+00	.146e+01	.256e-01	.148e+01	.203e+00	.103e-01	.699e+00	0.	.176e-01	.233e-01	.586e-03
102	26	.4585e+00	.143e+01	.268e-01	.145e+01	.229e+00	.109e-01	.722e+00	.667e-03	.188e-01	.259e-01	.680e-03
103	25	.5000e+00	.140e+01	.281e-01	.143e+01	.258e+00	.116e-01	.745e+00	.289e-02	.200e-01	.288e-01	.790e-03
104	24	.5453e+00	.138e+01	.296e-01	.141e+01	.290e+00	.123e-01	.766e+00	.518e-02	.214e-01	.319e-01	.919e-03
105	23	.5946e+00	.136e+01	.311e-01	.139e+01	.325e+00	.131e-01	.786e+00	.753e-02	.230e-01	.353e-01	.107e-02
106	22	.6484e+00	.134e+01	.330e-01	.137e+01	.364e+00	.139e-01	.806e+00	.997e-02	.246e-01	.390e-01	.125e-02
107	21	.7071e+00	.133e+01	.350e-01	.136e+01	.407e+00	.148e-01	.824e+00	.125e-01	.264e-01	.430e-01	.146e-02
108	20	.7711e+00	.131e+01	.373e-01	.135e+01	.454e+00	.158e-01	.841e+00	.151e-01	.284e-01	.472e-01	.171e-02
109	19	.8409e+00	.130e+01	.398e-01	.134e+01	.506e+00	.169e-01	.857e+00	.178e-01	.305e-01	.518e-01	.200e-02
110	18	.9170e+00	.130e+01	.425e-01	.134e+01	.563e+00	.180e-01	.872e+00	.207e-01	.328e-01	.568e-01	.234e-02
111	17	.1000e+01	.129e+01	.456e-01	.134e+01	.625e+00	.193e-01	.886e+00	.237e-01	.353e-01	.621e-01	.274e-02
112	16	.1091e+01	.129e+01	.491e-01	.133e+01	.693e+00	.206e-01	.898e+00	.268e-01	.382e-01	.678e-01	.321e-02
113	15	.1189e+01	.128e+01	.530e-01	.134e+01	.767e+00	.221e-01	.910e+00	.301e-01	.413e-01	.739e-01	.377e-02
114	14	.1297e+01	.128e+01	.574e-01	.134e+01	.847e+00	.237e-01	.920e+00	.335e-01	.448e-01	.804e-01	.444e-02
115	13	.1414e+01	.128e+01	.623e-01	.135e+01	.934e+00	.254e-01	.930e+00	.371e-01	.485e-01	.874e-01	.523e-02
116	12	.1542e+01	.129e+01	.677e-01	.136e+01	.103e+01	.273e-01	.938e+00	.408e-01	.527e-01	.949e-01	.617e-02
117	11	.1682e+01	.129e+01	.738e-01	.136e+01	.113e+01	.293e-01	.946e+00	.448e-01	.573e-01	.103e+00	.727e-02
118	10	.1834e+01	.129e+01	.806e-01	.137e+01	.124e+01	.316e-01	.953e+00	.489e-01	.623e-01	.111e+00	.858e-02
119	9	.2000e+01	.130e+01	.881e-01	.139e+01	.136e+01	.340e-01	.959e+00	.532e-01	.679e-01	.120e+00	.101e-01
120	8	.2181e+01	.130e+01	.965e-01	.140e+01	.149e+01	.367e-01	.964e+00	.578e-01	.740e-01	.130e+00	.120e-01

TEFLON

```
     7  .2378e+01  .131e+01  .106e+00  .142e+01  .163e+01  .396e-01   .969e+00  .625e-01  .809e-01  .140e+00  .142e-01
     6  .2594e+01  .132e+01  .116e+00  .143e+01  .179e+01  .428e-01   .973e+00  .674e-01  .886e-01  .151e+00  .168e-01
     5  .2828e+01  .132e+01  .128e+00  .145e+01  .196e+01  .463e-01   .977e+00  .726e-01  .968e-01  .163e+00  .199e-01
     4  .3084e+01  .133e+01  .141e+00  .147e+01  .212e+01  .501e-01   .980e+00  .779e-01  .106e+00  .176e+00  .236e-01
     3  .3364e+01  .134e+01  .156e+00  .150e+01  .231e+01  .543e-01   .983e+00  .834e-01  .116e+00  .188e+00  .279e-01
     2  .3668e+01  .135e+01  .172e+00  .152e+01  .251e+01  .588e-01   .985e+00  .892e-01  .128e+00  .202e+00  .331e-01
     1  .4000e+01  .136e+01  .190e+00  .155e+01  .273e+01  .637e-01   .987e+00  .952e-01  .140e+00  .216e+00  .392e-01
0
0 nset  itrm  isip  iegn  isub  inel  icyc  ncyc  nmax       emax
     2     5     0     1    14     1     1     8    64     .40000e+01
0input data tape identification
 datatape-2 (rester-aiginger ph-rad corr), 54 sternheimer sets. 30 jan 6
0detour        density
   .81500e+00   .23000e+01
0
0range table
0      emax       ncyc       efac       nmax    t(nmax+1)   ncal      t(ncal)
    .40000e+01      8     .91700e+00    64     .15625e-01    97     .97656e-03
0 jmax  lmax
    2     1
0        z          a          w
     6.00000    12.01115     .24000
     9.00000    18.99840     .76000
0       pi         pid
     88.28321   88.28321
0 -----------------parameters for density effect--------------------
        pi           c           b           dm          x1          x0

     88.28321    -3.14158     .38072     3.00000     2.00000      .20000
     88.28321    -3.14158     .38072     3.00000     2.00000      .20000
     .1443e+00  -.1663e+02   .7371e-01
1                                                 electron results
0     effective z/a =  .47992     effective mean ionization potential =   88.28 ev     critical energy =   0.000 mev
0        energy               stopping power             range   radiation    beta222   density   rad/col   drange    dyield
   n                  collision radiation   total                  yield                  corr
             mev       mev cm2/g mev cm2/g mev cm2/g   g/cm2                             mev cm2/g             g/cm2

    97   .9766e-03   .988e+02  .582e-02  .988e+02  .494e-05 0.           .381e-02 0.          .589e-04 0.         0.
    96   .1065e-02   .937e+02  .581e-02  .937e+02  .586e-05  .502e-05    .416e-02 0.          .620e-04  .919e-06  .534e-08
    95   .1161e-02   .888e+02  .581e-02  .888e+02  .692e-05  .989e-05    .453e-02 0.          .654e-04  .106e-05  .614e-08
    94   .1266e-02   .840e+02  .580e-02  .840e+02  .813e-05  .146e-04    .494e-02 0.          .690e-04  .122e-05  .707e-08
    93   .1381e-02   .794e+02  .579e-02  .795e+02  .954e-05  .193e-04    .538e-02 0.          .729e-04  .140e-05  .814e-08
    92   .1506e-02   .751e+02  .579e-02  .751e+02  .112e-04  .239e-04    .587e-02 0.          .771e-04  .162e-05  .938e-08
    91   .1642e-02   .708e+02  .578e-02  .708e+02  .130e-04  .285e-04    .640e-02 0.          .815e-04  .187e-05  .108e-07
    90   .1791e-02   .668e+02  .577e-02  .668e+02  .152e-04  .331e-04    .697e-02 0.          .863e-04  .216e-05  .125e-07
    89   .1953e-02   .630e+02  .576e-02  .630e+02  .177e-04  .378e-04    .760e-02 0.          .914e-04  .250e-05  .144e-07
    88   .2130e-02   .593e+02  .575e-02  .593e+02  .206e-04  .424e-04    .828e-02 0.          .969e-04  .289e-05  .166e-07
    87   .2323e-02   .558e+02  .573e-02  .558e+02  .239e-04  .472e-04    .903e-02 0.          .103e-03  .335e-05  .192e-07
    86   .2533e-02   .525e+02  .572e-02  .525e+02  .278e-04  .521e-04    .984e-02 0.          .109e-03  .388e-05  .222e-07
    85   .2762e-02   .494e+02  .571e-02  .494e+02  .323e-04  .571e-04    .107e-01 0.          .116e-03  .450e-05  .257e-07
    84   .3012e-02   .464e+02  .569e-02  .464e+02  .375e-04  .622e-04    .117e-01 0.          .123e-03  .522e-05  .298e-07
    83   .3285e-02   .436e+02  .567e-02  .436e+02  .436e-04  .675e-04    .127e-01 0.          .130e-03  .606e-05  .344e-07
    82   .3582e-02   .409e+02  .565e-02  .409e+02  .506e-04  .731e-04    .139e-01 0.          .138e-03  .704e-05  .399e-07
    81   .3906e-02   .384e+02  .564e-02  .384e+02  .588e-04  .788e-04    .151e-01 0.          .147e-03  .818e-05  .462e-07
    80   .4260e-02   .360e+02  .561e-02  .360e+02  .683e-04  .848e-04    .165e-01 0.          .156e-03  .951e-05  .536e-07
    79   .4645e-02   .338e+02  .559e-02  .338e+02  .794e-04  .911e-04    .179e-01 0.          .166e-03  .111e-04  .620e-07
    78   .5066e-02   .317e+02  .557e-02  .317e+02  .923e-04  .977e-04    .195e-01 0.          .176e-03  .129e-04  .718e-07
    77   .5524e-02   .297e+02  .555e-02  .297e+02  .107e-03  .105e-03    .213e-01 0.          .187e-03  .150e-04  .832e-07
    76   .6024e-02   .278e+02  .552e-02  .278e+02  .125e-03  .112e-03    .232e-01 0.          .199e-03  .174e-04  .964e-07
    75   .6570e-02   .260e+02  .550e-02  .260e+02  .145e-03  .120e-03    .252e-01 0.          .211e-03  .203e-04  .112e-06
```

181	74	.7164e-02	.244e+02	.547e-02	.244e+02	.169e-03	.128e-03	.275e-01	0.	.225e-03	.236e-04	.130e-06
182	73	.7812e-02	.228e+02	.546e-02	.228e+02	.196e-03	.136e-03	.299e-01	0.	.239e-03	.275e-04	.150e-06
183	72	.8520e-02	.213e+02	.542e-02	.214e+02	.228e-03	.146e-03	.325e-01	0.	.254e-03	.321e-04	.174e-06
184	71	.9291e-02	.200e+02	.540e-02	.200e+02	.265e-03	.155e-03	.354e-01	0.	.270e-03	.374e-04	.202e-06
185	70	.1013e-01	.187e+02	.537e-02	.187e+02	.309e-03	.166e-03	.385e-01	0.	.287e-03	.435e-04	.234e-06
186	69	.1105e-01	.175e+02	.534e-02	.175e+02	.360e-03	.176e-03	.419e-01	0.	.306e-03	.507e-04	.272e-06
187	68	.1205e-01	.164e+02	.532e-02	.164e+02	.419e-03	.188e-03	.465e-01	0.	.325e-03	.592e-04	.315e-06
188	67	.1314e-01	.153e+02	.529e-02	.153e+02	.488e-03	.200e-03	.495e-01	0.	.346e-03	.690e-04	.366e-06
189	66	.1433e-01	.143e+02	.526e-02	.143e+02	.568e-03	.213e-03	.538e-01	0.	.368e-03	.804e-04	.424e-06
190	65	.1562e-01	.134e+02	.524e-02	.134e+02	.662e-03	.227e-03	.585e-01	0.	.391e-03	.937e-04	.492e-06
191	64	.1704e-01	.125e+02	.521e-02	.125e+02	.771e-03	.242e-03	.635e-01	0.	.417e-03	.109e-03	.571e-06
192	63	.1858e-01	.117e+02	.519e-02	.117e+02	.899e-03	.257e-03	.689e-01	0.	.443e-03	.127e-03	.663e-06
193	62	.2026e-01	.110e+02	.517e-02	.110e+02	.105e-02	.274e-03	.748e-01	0.	.472e-03	.148e-03	.769e-06
194	61	.2210e-01	.103e+02	.515e-02	.103e+02	.122e-02	.292e-03	.812e-01	0.	.502e-03	.173e-03	.892e-06
195	60	.2410e-01	.960e+01	.513e-02	.960e+01	.142e-02	.310e-03	.880e-01	0.	.534e-03	.202e-03	.104e-05
196	59	.2628e-01	.898e+01	.511e-02	.899e+01	.166e-02	.330e-03	.954e-01	0.	.568e-03	.235e-03	.120e-05
197	58	.2866e-01	.841e+01	.509e-02	.842e+01	.193e-02	.352e-03	.103e+00	0.	.605e-03	.274e-03	.139e-05
198	57	.3125e-01	.788e+01	.507e-02	.788e+01	.225e-02	.374e-03	.112e+00	0.	.644e-03	.319e-03	.162e-05
199	56	.3408e-01	.738e+01	.506e-02	.739e+01	.262e-02	.398e-03	.121e+00	0.	.685e-03	.371e-03	.188e-05
200	55	.3716e-01	.692e+01	.505e-02	.693e+01	.305e-02	.424e-03	.131e+00	0.	.729e-03	.431e-03	.218e-05
201	54	.4053e-01	.649e+01	.504e-02	.650e+01	.355e-02	.451e-03	.142e+00	0.	.776e-03	.502e-03	.253e-05
202	53	.4419e-01	.609e+01	.503e-02	.610e+01	.414e-02	.480e-03	.153e+00	0.	.826e-03	.583e-03	.294e-05
203	52	.4819e-01	.572e+01	.503e-02	.572e+01	.481e-02	.511e-03	.165e+00	0.	.879e-03	.678e-03	.341e-05
204	51	.5256e-01	.537e+01	.503e-02	.538e+01	.560e-02	.544e-03	.178e+00	0.	.935e-03	.787e-03	.395e-05
205	50	.5731e-01	.505e+01	.503e-02	.506e+01	.651e-02	.579e-03	.192e+00	0.	.995e-03	.913e-03	.459e-05
206	49	.6250e-01	.475e+01	.504e-02	.476e+01	.757e-02	.616e-03	.206e+00	0.	.106e-02	.106e-02	.532e-05
207	48	.6816e-01	.448e+01	.505e-02	.448e+01	.880e-02	.655e-03	.222e+00	0.	.113e-02	.123e-02	.618e-05
208	47	.7433e-01	.422e+01	.506e-02	.423e+01	.102e-01	.697e-03	.238e+00	0.	.120e-02	.142e-02	.716e-05
209	46	.8105e-01	.398e+01	.508e-02	.399e+01	.119e-01	.742e-03	.255e+00	0.	.127e-02	.164e-02	.831e-05
210	45	.8839e-01	.376e+01	.510e-02	.377e+01	.137e-01	.789e-03	.273e+00	0.	.136e-02	.189e-02	.964e-05
211	44	.9639e-01	.356e+01	.513e-02	.357e+01	.159e-01	.840e-03	.292e+00	0.	.144e-02	.218e-02	.112e-04
212	43	.1051e+00	.337e+01	.517e-02	.338e+01	.184e-01	.893e-03	.312e+00	0.	.153e-02	.252e-02	.130e-04
213	42	.1146e+00	.320e+01	.521e-02	.320e+01	.213e-01	.950e-03	.333e+00	0.	.163e-02	.289e-02	.150e-04
214	41	.1250e+00	.304e+01	.526e-02	.304e+01	.247e-01	.101e-02	.354e+00	0.	.173e-02	.332e-02	.174e-04
215	40	.1363e+00	.289e+01	.532e-02	.290e+01	.285e-01	.107e-02	.377e+00	0.	.184e-02	.381e-02	.202e-04
216	39	.1487e+00	.275e+01	.539e-02	.276e+01	.328e-01	.114e-02	.400e+00	0.	.196e-02	.437e-02	.234e-04
217	38	.1621e+00	.263e+01	.547e-02	.263e+01	.378e-01	.122e-02	.424e+00	0.	.208e-02	.499e-02	.271e-04
218	37	.1768e+00	.251e+01	.556e-02	.252e+01	.435e-01	.129e-02	.448e+00	0.	.221e-02	.570e-02	.315e-04
219	36	.1928e+00	.241e+01	.567e-02	.241e+01	.500e-01	.137e-02	.473e+00	0.	.235e-02	.649e-02	.365e-04
220	35	.2102e+00	.231e+01	.579e-02	.232e+01	.574e-01	.146e-02	.498e+00	0.	.251e-02	.738e-02	.423e-04
221	34	.2293e+00	.222e+01	.593e-02	.223e+01	.658e-01	.155e-02	.523e+00	0.	.267e-02	.838e-02	.491e-04
222	33	.2500e+00	.214e+01	.608e-02	.215e+01	.753e-01	.165e-02	.549e+00	0.	.284e-02	.949e-02	.570e-04
223	32	.2726e+00	.207e+01	.626e-02	.208e+01	.860e-01	.176e-02	.575e+00	0.	.302e-02	.107e-01	.661e-04
224	31	.2973e+00	.200e+01	.646e-02	.201e+01	.981e-01	.187e-02	.600e+00	0.	.322e-02	.121e-01	.768e-04
225	30	.3242e+00	.194e+01	.668e-02	.195e+01	.112e+00	.199e-02	.626e+00	0.	.344e-02	.136e-01	.893e-04
226	29	.3536e+00	.189e+01	.694e-02	.190e+01	.127e+00	.212e-02	.651e+00	0.	.367e-02	.153e-01	.104e-03
227	28	.3856e+00	.184e+01	.723e-02	.185e+01	.144e+00	.226e-02	.675e+00	0.	.392e-02	.171e-01	.121e-03
228	27	.4204e+00	.180e+01	.755e-02	.181e+01	.163e+00	.241e-02	.699e+00	0.	.420e-02	.191e-01	.141e-03
229	26	.4585e+00	.176e+01	.792e-02	.177e+01	.184e+00	.257e-02	.722e+00	.702e-03	.450e-02	.213e-01	.165e-03
230	25	.5000e+00	.172e+01	.834e-02	.173e+01	.208e+00	.274e-02	.745e+00	.310e-02	.484e-02	.237e-01	.193e-03
231	24	.5453e+00	.169e+01	.880e-02	.170e+01	.235e+00	.293e-02	.766e+00	.565e-02	.520e-02	.264e-01	.226e-03
232	23	.5946e+00	.166e+01	.933e-02	.167e+01	.264e+00	.313e-02	.786e+00	.835e-02	.561e-02	.293e-01	.265e-03
233	22	.6484e+00	.164e+01	.992e-02	.165e+01	.296e+00	.335e-02	.806e+00	.112e-01	.605e-02	.324e-01	.312e-03
234	21	.7071e+00	.162e+01	.106e-01	.163e+01	.332e+00	.359e-02	.824e+00	.142e-01	.654e-02	.358e-01	.367e-03
235	20	.7711e+00	.160e+01	.113e-01	.161e+01	.371e+00	.385e-02	.841e+00	.174e-01	.708e-02	.395e-01	.433e-03
236	19	.8409e+00	.159e+01	.122e-01	.160e+01	.415e+00	.414e-02	.857e+00	.208e-01	.768e-02	.435e-01	.511e-03
237	18	.9170e+00	.157e+01	.131e-01	.159e+01	.463e+00	.446e-02	.872e+00	.244e-01	.834e-02	.478e-01	.605e-03
238	17	.1000e+01	.156e+01	.142e-01	.158e+01	.515e+00	.481e-02	.886e+00	.282e-01	.908e-02	.524e-01	.717e-03
239	16	.1091e+01	.156e+01	.154e-01	.157e+01	.573e+00	.519e-02	.898e+00	.322e-01	.989e-02	.575e-01	.850e-03
240	15	.1189e+01	.156e+01	.167e-01	.157e+01	.636e+00	.560e-02	.910e+00	.364e-01	.108e-01	.629e-01	.101e-02

```
   14   .1287e+01   .155e+01  .182e-01  .156e+01  .704e+00  .607e-02   .920e+00  .409e-01  .118e-01  .687e-01  .120e-02
   13   .1414e+01   .154e+01  .199e-01  .156e+01  .779e+00  .657e-02   .930e+00  .456e-01  .129e-01  .760e-01  .143e-02
   12   .1542e+01   .154e+01  .218e-01  .157e+01  .861e+00  .714e-02   .938e+00  .506e-01  .141e-01  .818e-01  .171e-02
   11   .1682e+01   .154e+01  .239e-01  .157e+01  .950e+00  .775e-02   .946e+00  .558e-01  .155e-01  .891e-01  .204e-02
   10   .1834e+01   .155e+01  .263e-01  .157e+01  .105e+01  .844e-02   .953e+00  .613e-01  .170e-01  .970e-01  .243e-02
    9   .2000e+01   .156e+01  .289e-01  .158e+01  .115e+01  .919e-02   .959e+00  .671e-01  .187e-01  .105e+00  .291e-02
    8   .2181e+01   .155e+01  .318e-01  .158e+01  .127e+01  .100e-01   .964e+00  .731e-01  .205e-01  .115e+00  .348e-02
    7   .2378e+01   .156e+01  .351e-01  .159e+01  .139e+01  .109e-01   .969e+00  .794e-01  .225e-01  .124e+00  .416e-02
    6   .2594e+01   .156e+01  .387e-01  .160e+01  .153e+01  .119e-01   .973e+00  .860e-01  .248e-01  .135e+00  .498e-02
    5   .2828e+01   .157e+01  .428e-01  .161e+01  .167e+01  .131e-01   .977e+00  .929e-01  .273e-01  .146e+00  .596e-02
    4   .3084e+01   .157e+01  .473e-01  .162e+01  .183e+01  .143e-01   .980e+00  .100e+00  .301e-01  .158e+00  .714e-02
    3   .3364e+01   .158e+01  .524e-01  .163e+01  .200e+01  .157e-01   .983e+00  .108e+00  .331e-01  .172e+00  .856e-02
    2   .3668e+01   .159e+01  .579e-01  .164e+01  .219e+01  .171e-01   .985e+00  .115e+00  .365e-01  .186e+00  .102e-01
    1   .4000e+01   .159e+01  .642e-01  .166e+01  .239e+01  .188e-01   .987e+00  .123e+00  .403e-01  .201e+00  .123e-01
0
0 nset  itre  izip  iegn  isub  inel  icyc  ncyc  nmax          emax
     3     5     0     1     3     1     1     8    64      .40000e+01
0input data tape identification
 datatape-2 (rester-aiginger ph-rad corr), 54 sternheimer sets. 30 jan 6
0dstour          density
   .87000e+00   .19000e+01
0
0range table
0       emax         ncyc       efac        nmax    t(nmax+1)   ncal      t(ncal)
   .40000e+01          8    .91700e+00      64    .15625e-01     97    .97656e-03
0 jmax  lmax
    1     1
0        z              a              w
     6.00000       12.01115       1.00000
0       pi             pid
    78.00000       78.00000
0 ---------------------parameters for density effect---------------------------
         pi              c               b              dm             x1             x0

    78.00000       -3.04489          .36414        3.00000        2.00000         .20000
    78.00000       -3.04489          .36414        3.00000        2.00000         .20000
   .1502e+00    -.1682e+02       .7672e-01
1                                                               electron results
0      effective z/a =  .49954     effective mean ionization potential =   78.00 ev     critical energy =   0.000 mev
0        energy              stopping power              range     radiation    beta**2    density    rad/col    drange     dyield
     n                 collision radiation   total                  yield                  corr
            mev        mev cm2/g mev cm2/g mev cm2/g   g/cm2                              mev cm2/g              g/cm2

    97   .9766e-03   .108e+03  .456e-02  .108e+03  .453e-05 0.          .381e-02 0.          .423e-04 0.         0.
    96   .1065e-02   .102e+03  .455e-02  .102e+03  .537e-05  .360e-05   .416e-02 0.          .446e-04  .842e-06  .384e-08
    95   .1161e-02   .966e+02  .454e-02  .966e+02  .634e-05  .710e-05   .453e-02 0.          .470e-04  .971e-06  .441e-08
    94   .1266e-02   .913e+02  .453e-02  .913e+02  .746e-05  .105e-04   .494e-02 0.          .496e-04  .112e-05  .508e-08
    93   .1381e-02   .862e+02  .452e-02  .862e+02  .876e-05  .139e-04   .538e-02 0.          .524e-04  .129e-05  .585e-08
    92   .1506e-02   .814e+02  .451e-02  .814e+02  .102e-04  .172e-04   .587e-02 0.          .554e-04  .149e-05  .674e-08
    91   .1642e-02   .767e+02  .450e-02  .767e+02  .120e-04  .205e-04   .640e-02 0.          .586e-04  .173e-05  .777e-08
    90   .1791e-02   .723e+02  .448e-02  .723e+02  .140e-04  .238e-04   .697e-02 0.          .620e-04  .200e-05  .897e-08
    89   .1953e-02   .681e+02  .447e-02  .681e+02  .163e-04  .271e-04   .760e-02 0.          .656e-04  .231e-05  .103e-07
    88   .2130e-02   .640e+02  .445e-02  .640e+02  .190e-04  .305e-04   .828e-02 0.          .695e-04  .268e-05  .119e-07
    87   .2323e-02   .602e+02  .443e-02  .602e+02  .221e-04  .339e-04   .903e-02 0.          .736e-04  .311e-05  .138e-07
    86   .2533e-02   .566e+02  .442e-02  .566e+02  .257e-04  .374e-04   .984e-02 0.          .780e-04  .360e-05  .159e-07
    85   .2762e-02   .532e+02  .440e-02  .532e+02  .298e-04  .409e-04   .107e-01 0.          .827e-04  .418e-05  .184e-07
    84   .3012e-02   .499e+02  .438e-02  .499e+02  .347e-04  .446e-04   .117e-01 0.          .877e-04  .485e-05  .213e-07
    83   .3285e-02   .469e+02  .436e-02  .469e+02  .403e-04  .484e-04   .127e-01 0.          .930e-04  .564e-05  .246e-07
    82   .3583e-02   .440e+02  .434e-02  .440e+02  .469e-04  .524e-04   .139e-01 0.          .987e-04  .655e-05  .285e-07
    81   .3906e-02   .412e+02  .432e-02  .412e+02  .545e-04  .564e-04   .151e-01 0.          .105e-03  .762e-05  .330e-07
```

CARBON

301	80	.4860e-02	.386e+02	.429e-02	.387e+02	.634e-04	.607e-04	.165e-01	0.	.111e-03	.886e-05	.381e-07
302	79	.4645e-02	.362e+02	.427e-02	.362e+02	.737e-04	.652e-04	.179e-01	0.	.118e-03	.103e-04	.442e-07
303	78	.5066e-02	.339e+02	.425e-02	.339e+02	.857e-04	.699e-04	.196e-01	0.	.125e-03	.120e-04	.511e-07
304	77	.5524e-02	.318e+02	.423e-02	.318e+02	.997e-04	.748e-04	.213e-01	0.	.133e-03	.140e-04	.592e-07
305	76	.6024e-02	.297e+02	.420e-02	.298e+02	.116e-03	.800e-04	.232e-01	0.	.141e-03	.163e-04	.686e-07
306	75	.6570e-02	.278e+02	.418e-02	.278e+02	.135e-03	.854e-04	.252e-01	0.	.150e-03	.190e-04	.794e-07
307	74	.7164e-02	.261e+02	.416e-02	.261e+02	.157e-03	.912e-04	.275e-01	0.	.159e-03	.221e-04	.920e-07
308	73	.7812e-02	.244e+02	.413e-02	.244e+02	.183e-03	.972e-04	.299e-01	0.	.170e-03	.257e-04	.107e-06
309	72	.8520e-02	.228e+02	.411e-02	.228e+02	.213e-03	.104e-03	.325e-01	0.	.180e-03	.300e-04	.124e-06
310	71	.9291e-02	.213e+02	.409e-02	.213e+02	.248e-03	.111e-03	.354e-01	0.	.192e-03	.350e-04	.143e-06
311	70	.1013e-01	.199e+02	.407e-02	.200e+02	.288e-03	.118e-03	.385e-01	0.	.204e-03	.408e-04	.166e-06
312	69	.1106e-01	.187e+02	.404e-02	.187e+02	.336e-03	.125e-03	.419e-01	0.	.217e-03	.476e-04	.193e-06
313	68	.1205e-01	.174e+02	.402e-02	.174e+02	.391e-03	.134e-03	.455e-01	0.	.231e-03	.555e-04	.224e-06
314	67	.1314e-01	.163e+02	.400e-02	.163e+02	.456e-03	.142e-03	.495e-01	0.	.245e-03	.647e-04	.260e-06
315	66	.1433e-01	.152e+02	.398e-02	.153e+02	.532e-03	.151e-03	.538e-01	0.	.261e-03	.754e-04	.301e-06
316	65	.1562e-01	.143e+02	.396e-02	.143e+02	.620e-03	.161e-03	.585e-01	0.	.278e-03	.880e-04	.350e-06
317	64	.1704e-01	.133e+02	.395e-02	.133e+02	.722e-03	.172e-03	.635e-01	0.	.296e-03	.103e-03	.406e-06
318	63	.1858e-01	.125e+02	.393e-02	.125e+02	.842e-03	.183e-03	.689e-01	0.	.315e-03	.120e-03	.471e-06
319	62	.2026e-01	.117e+02	.391e-02	.117e+02	.981e-03	.195e-03	.748e-01	0.	.336e-03	.140e-03	.547e-06
320	61	.2210e-01	.109e+02	.390e-02	.109e+02	.114e-02	.207e-03	.812e-01	0.	.357e-03	.163e-03	.635e-06
321	60	.2410e-01	.102e+02	.389e-02	.102e+02	.133e-02	.221e-03	.880e-01	0.	.381e-03	.190e-03	.738e-06
322	59	.2628e-01	.955e+01	.387e-02	.955e+01	.155e-02	.235e-03	.954e-01	0.	.406e-03	.221e-03	.857e-06
323	58	.2866e-01	.894e+01	.386e-02	.894e+01	.181e-02	.250e-03	.103e+00	0.	.432e-03	.257e-03	.996e-06
324	57	.3125e-01	.837e+01	.385e-02	.837e+01	.211e-02	.266e-03	.112e+00	0.	.460e-03	.300e-03	.116e-05
325	56	.3408e-01	.784e+01	.385e-02	.785e+01	.246e-02	.284e-03	.121e+00	0.	.491e-03	.349e-03	.134e-05
326	55	.3716e-01	.735e+01	.384e-02	.735e+01	.287e-02	.302e-03	.131e+00	0.	.523e-03	.406e-03	.156e-05
327	54	.4053e-01	.689e+01	.384e-02	.689e+01	.334e-02	.322e-03	.142e+00	0.	.557e-03	.473e-03	.182e-05
328	53	.4419e-01	.646e+01	.384e-02	.647e+01	.389e-02	.343e-03	.153e+00	0.	.594e-03	.550e-03	.211e-05
329	52	.4819e-01	.607e+01	.384e-02	.607e+01	.453e-02	.365e-03	.165e+00	0.	.633e-03	.639e-03	.245e-05
330	51	.5256e-01	.570e+01	.384e-02	.570e+01	.527e-02	.389e-03	.178e+00	0.	.674e-03	.742e-03	.285e-05
331	50	.5731e-01	.536e+01	.385e-02	.536e+01	.613e-02	.415e-03	.192e+00	0.	.718e-03	.861e-03	.331e-05
332	49	.6250e-01	.504e+01	.386e-02	.505e+01	.713e-02	.442e-03	.206e+00	0.	.766e-03	.998e-03	.384e-05
333	48	.6816e-01	.475e+01	.387e-02	.475e+01	.828e-02	.471e-03	.222e+00	0.	.815e-03	.116e-02	.447e-05
334	47	.7433e-01	.447e+01	.388e-02	.448e+01	.962e-02	.501e-03	.238e+00	0.	.868e-03	.134e-02	.519e-05
335	46	.8105e-01	.422e+01	.390e-02	.423e+01	.112e-01	.534e-03	.255e+00	0.	.925e-03	.155e-02	.603e-05
336	45	.8839e-01	.399e+01	.393e-02	.399e+01	.130e-01	.569e-03	.273e+00	0.	.985e-03	.179e-02	.700e-05
337	44	.9639e-01	.377e+01	.396e-02	.378e+01	.150e-01	.606e-03	.292e+00	0.	.105e-02	.206e-02	.813e-05
338	43	.1051e+00	.357e+01	.399e-02	.358e+01	.174e-01	.646e-03	.312e+00	0.	.112e-02	.238e-02	.944e-05
339	42	.1146e+00	.339e+01	.403e-02	.339e+01	.201e-01	.688e-03	.333e+00	0.	.119e-02	.273e-02	.110e-04
340	41	.1250e+00	.322e+01	.407e-02	.322e+01	.833e-01	.732e-03	.354e+00	0.	.127e-02	.314e-02	.127e-04
341	40	.1363e+00	.306e+01	.412e-02	.306e+01	.269e-01	.780e-03	.377e+00	0.	.135e-02	.360e-02	.148e-04
342	39	.1487e+00	.291e+01	.418e-02	.292e+01	.310e-01	.830e-03	.400e+00	0.	.143e-02	.413e-02	.171e-04
343	38	.1621e+00	.278e+01	.425e-02	.279e+01	.367e-01	.884e-03	.424e+00	0.	.153e-02	.472e-02	.199e-04
344	37	.1768e+00	.266e+01	.432e-02	.266e+01	.411e-01	.941e-03	.448e+00	0.	.163e-02	.539e-02	.231e-04
345	36	.1928e+00	.255e+01	.441e-02	.255e+01	.473e-01	.100e-02	.473e+00	0.	.173e-02	.614e-02	.268e-04
346	35	.2102e+00	.244e+01	.451e-02	.245e+01	.542e-01	.107e-02	.498e+00	0.	.184e-02	.699e-02	.311e-04
347	34	.2293e+00	.235e+01	.462e-02	.235e+01	.622e-01	.114e-02	.523e+00	0.	.197e-02	.793e-02	.362e-04
348	33	.2500e+00	.226e+01	.474e-02	.227e+01	.712e-01	.121e-02	.549e+00	0.	.209e-02	.898e-02	.420e-04
349	32	.2726e+00	.219e+01	.488e-02	.219e+01	.813e-01	.129e-02	.575e+00	0.	.223e-02	.101e-01	.488e-04
350	31	.2973e+00	.212e+01	.506e-02	.212e+01	.927e-01	.137e-02	.600e+00	0.	.238e-02	.114e-01	.568e-04
351	30	.3242e+00	.206e+01	.523e-02	.206e+01	.106e+00	.146e-02	.626e+00	0.	.255e-02	.129e-01	.662e-04
352	29	.3536e+00	.200e+01	.543e-02	.200e+01	.120e+00	.166e-02	.651e+00	0.	.272e-02	.145e-01	.771e-04
353	28	.3856e+00	.194e+01	.566e-02	.195e+01	.136e+00	.166e-02	.675e+00	0.	.291e-02	.162e-01	.899e-04
354	27	.4204e+00	.190e+01	.592e-02	.191e+01	.154e+00	.177e-02	.699e+00	0.	.312e-02	.181e-01	.105e-03
355	26	.4585e+00	.186e+01	.622e-02	.186e+01	.175e+00	.189e-02	.722e+00	.868e-03	.336e-02	.202e-01	.123e-03
356	25	.5000e+00	.182e+01	.655e-02	.183e+01	.197e+00	.202e-02	.746e+00	.376e-02	.360e-02	.225e-01	.144e-03
357	24	.5453e+00	.179e+01	.692e-02	.179e+01	.222e+00	.217e-02	.766e+00	.678e-02	.388e-02	.250e-01	.168e-03
358	23	.5946e+00	.176e+01	.734e-02	.176e+01	.250e+00	.232e-02	.786e+00	.984e-02	.418e-02	.278e-01	.198e-03
359	22	.6484e+00	.173e+01	.781e-02	.174e+01	.281e+00	.249e-02	.806e+00	.132e-01	.452e-02	.308e-01	.233e-03
360	21	.7071e+00	.171e+01	.834e-02	.171e+01	.316e+00	.267e-02	.824e+00	.167e-01	.489e-02	.340e-01	.275e-03

361	20	.7711e+00	.169e+01	.894e-02	.170e+01	.352e+00	.287e-02	.841e+00	.203e-01	.530e-02	.375e-01	.324e-03
362	19	.8409e+00	.167e+01	.961e-02	.168e+01	.394e+00	.308e-02	.857e+00	.241e-01	.575e-02	.413e-01	.383e-03
363	18	.9170e+00	.166e+01	.104e-01	.167e+01	.439e+00	.332e-02	.872e+00	.281e-01	.625e-02	.455e-01	.454e-03
364	17	.1000e+01	.165e+01	.112e-01	.166e+01	.489e+00	.359e-02	.886e+00	.323e-01	.681e-02	.499e-01	.538e-03
365	16	.1091e+01	.164e+01	.122e-01	.165e+01	.544e+00	.387e-02	.898e+00	.367e-01	.742e-02	.547e-01	.639e-03
366	15	.1189e+01	.163e+01	.132e-01	.164e+01	.604e+00	.419e-02	.910e+00	.414e-01	.810e-02	.599e-01	.760e-03
367	14	.1297e+01	.163e+01	.144e-01	.164e+01	.669e+00	.454e-02	.920e+00	.462e-01	.886e-02	.655e-01	.905e-03
368	13	.1414e+01	.162e+01	.157e-01	.164e+01	.741e+00	.493e-02	.930e+00	.514e-01	.970e-02	.716e-01	.108e-02
369	12	.1542e+01	.162e+01	.172e-01	.164e+01	.819e+00	.535e-02	.938e+00	.567e-01	.106e-01	.781e-01	.129e-02
370	11	.1682e+01	.162e+01	.189e-01	.164e+01	.904e+00	.582e-02	.946e+00	.624e-01	.117e-01	.851e-01	.154e-02
371	10	.1834e+01	.162e+01	.208e-01	.165e+01	.996e+00	.634e-02	.953e+00	.683e-01	.128e-01	.926e-01	.184e-02
372	9	.2000e+01	.163e+01	.229e-01	.165e+01	.110e+01	.692e-02	.959e+00	.745e-01	.141e-01	.101e+00	.220e-02
373	8	.2181e+01	.163e+01	.252e-01	.166e+01	.121e+01	.755e-02	.964e+00	.810e-01	.155e-01	.110e+00	.263e-02
374	7	.2378e+01	.163e+01	.278e-01	.166e+01	.133e+01	.825e-02	.969e+00	.877e-01	.170e-01	.119e+00	.315e-02
375	6	.2594e+01	.164e+01	.307e-01	.167e+01	.145e+01	.902e-02	.973e+00	.948e-01	.187e-01	.129e+00	.378e-02
376	5	.2828e+01	.165e+01	.339e-01	.168e+01	.160e+01	.987e-02	.977e+00	.102e+00	.206e-01	.140e+00	.453e-02
377	4	.3084e+01	.165e+01	.375e-01	.169e+01	.175e+01	.108e-01	.980e+00	.110e+00	.227e-01	.152e+00	.543e-02
378	3	.3364e+01	.166e+01	.415e-01	.170e+01	.191e+01	.119e-01	.983e+00	.118e+00	.251e-01	.165e+00	.651e-02
379	2	.3668e+01	.166e+01	.460e-01	.171e+01	.209e+01	.130e-01	.985e+00	.126e+00	.276e-01	.179e+00	.781e-02
380	1	.4000e+01	.167e+01	.509e-01	.172e+01	.228e+01	.143e-01	.987e+00	.134e+00	.305e-01	.193e+00	.937e-02

APPENDIX B

Tabulated CYLTRAN Output for
1, 2, 3, and 4 MeV Monoenergetic
Electron Beams Into a Small
Aperture Faraday Cup

```
595 lines. (120a)
0october 14 ,1976 version
0 nset  matl
    1     3
0 nmat  ntab
    1     1
0mpair  mtax
   25    41
0gamma ray cross section data
0energies (mev)
 1000.000000  800.000000  600.000000  500.000000  400.000000  300.000000
  200.000000  150.000000  100.000000   80.000000   60.000000   50.000000
   40.000000   30.000000   20.000000   15.000000   10.000000    8.000000
    6.000000    5.000000    4.000000    3.000000    2.000000    1.500000
    1.000000     .800000     .600000     .500000     .400000     .300000
     .200000     .150000     .100000     .080000     .060000     .050000
     .040000     .030000     .020000     .015000     .010000
0total attenuation coefficients (cm2/g)
     .133015     .115792     .097314     .087552     .077436     .067025
     .056529     .051401     .046420     .044377     .042060     .040625
     .038802     .036353     .033322     .031958     .030918     .030686
     .030945     .031565     .032919     .035741     .041882     .047769
     .058536     .065369     .075103     .082004     .091659     .107638
     .146661     .205315     .421761     .705562    1.487422    2.456969
    4.613069   10.492178   33.180213   73.691769  215.150145
0ratio of scattering plus pair production to total attenuation coefficients
     .999999     .999998     .999997     .999996     .999995     .999992
     .999986     .999979     .999965     .999955     .999936     .999920
     .999895     .999849     .999747     .999641     .999422     .999249
     .998956     .998721     .998371     .997787     .996538     .995083
     .991319     .987487     .978709     .969185     .949887     .903104
     .762317     .594141     .321116     .201461     .100774     .062778
     .034460     .015642     .005116     .002345     .000818
0ratio of scattering to scattering plus pair production attenuation coefficients
     .001662     .002382     .003765     .005007     .007046     .010778
     .018909     .027362     .044314     .056913     .077841     .094684
     .120290     .163683     .248185     .323842     .453488     .536768
     .651019     .722340     .802503     .886979     .963836     .991964
    1.000000
0k shell ionization data
0binding energy (mev), photoeffect efficiency and fluorescent efficiency
     .008981     .871336     .392853
0k x-ray energies (mev)
     .008150     .008150     .008150     .008150
0k x-ray accumulated relative intensities
    1.000000    1.000000    1.000000    1.000000
0auger electron energies (mev)
     .008150     .008150     .008150
0auger electron accumulated relative intensities
    1.000000    1.000000    1.000000
0 nmat  ntab
    2     1
0mpair  mtax
   25    41
0gamma ray cross section data
[illegible]800.000000  600.000000  500.000000  400.000000  300.000000
  200.000000  150.000000  100.000000   80.000000   60.000000   50.000000
   40.000000   30.000000   20.000000   15.000000   10.000000    8.000000
    6.000000    5.000000    4.000000    3.000000    2.000000    1.500000
    1.000000     .800000     .600000     .500000     .400000     .300000
```

```
      .200000     .150000     .100000     .080000     .060000     .050000
      .040000     .030000     .020000     .015000     .010000
@total attenuation coefficients (cm2/g)
      .042664     .037443     .031861     .028924     .025899     .022819
      .010298     .018399     .018998     .019885     .020488     .026802
      .024515     .026632     .029693     .034451     .042729     .049688
      .061023     .067886     .077309     .083599     .091601     .102329
      .117953     .129244     .146076     .157139     .177347     .197927
      .240815     .359073     .869633    1.932250    6.538225
@ratio of scattering plus pair production to total attenuation coefficients
     1.000000    1.000000    1.000000    1.000000    1.000000    1.000000
     1.000000     .999999     .999999     .999999     .999998     .999998
      .999989     .999988     .999998     .999998     .999988     .999988
      .999908     .999868     .999775     .999673     .999458     .998892
      .996690     .992470     .974912     .951171     .888740     .819442
      .694128     .480603     .205262     .094029     .028300
@ratio of scattering to scattering plus pair production attenuation coefficients
      .005449     .007745     .012092     .015937     .022153     .033290
      .056784     .080393     .125794     .158022     .208788     .247184
      .301520     .383491     .513893     .607020     .731386     .793818
      .863227     .899113     .933997     .965506     .990010     .997897
     1.000000
@k shell ionization data
@binding energy (mev), photoeffect efficiency and fluorescent efficiency
      .000687     .831990     .003376
@k x-ray energies (mev)
      .000687     .000687     .000687     .000687
@k x-ray accumulated relative intensities
     1.000000    1.000000    1.000000    1.000000
@auger electron energies (mev)
      .000687     .000687     .000687
@auger electron accumulated relative intensities
     1.000000    1.000000    1.000000
@ nmat  ntab
     3     1
@mpair  mtax
    25    41
@gamma ray cross section data
@energies (mev)
  1000.000000  800.000000  600.000000  500.000000  400.000000  300.000000
   200.000000  150.000000  100.000000   80.000000   60.000000   50.000000
     6.000000    5.000000    4.000000    3.000000    2.000000    1.500000
     1.000000     .800000     .600000     .500000     .400000     .300000
      .200000     .150000     .100000     .080000     .060000     .050000
      .040000     .030000     .020000     .015000     .010000
@total attenuation coefficients (cm2/g)
      .047459     .040496     .033058     .029154     .025144     .021091
      .017198     .015493     .014218     .013934     .013862     .013935
      .014112     .014480     .015476     .016765     .019512     .021495
      .024631     .027011     .030385     .035532     .044349     .051688
      .063513     .070654     .080455     .086995     .095307     .106425
      .122475     .133783     .149253     .157712     .169540     .178754
      .194556     .232360     .387554     .719226    2.228837
@ratio of scattering plus pair production to total attenuation coefficients
     1.000000    1.000000    1.000000    1.000000    1.000000    1.000000
     1.000000    1.000000    1.000000    1.000000     .999999     .999999
      .999999     .999999     .999998     .999998     .999997     .999997
.
```

```
      .959996     .999906     .999908     .999989     .999890     .999980
      .999123     .997987     .993163     .986454     .967663     .944418
      .894285     .773048     .479415     .262940     .086410
0ratio of scattering to scattering plus pair production attenuation coefficients
      .005099     .007454     .012130     .016458     .021751     .037489
      .068025     .099356     .158345     .198381     .258494     .302099
      .361954     .449719     .584721     .675399     .786023     .838082
      .894243     .922718     .950047     .974365     .992814     .998465
     1.000000
0k shell ionization data
0binding energy (mev), photoeffect efficiency and fluorescent efficiency
      .000284     .958303     .000382
0k x-ray energies .000284     .000284     .000284
0k x-ray accumulated relative intensities
     1.000000    1.000000    1.000000    1.000000
0auger electron energies (mev)
      .000284     .000284     .000284
0auger electron accumulated relative intensities
     1.000000    1.000000    1.000000
1number of sets on datapac tape =   3
0input from datapac

   ##1 mev electron beam into bare fx-100 faraday cup##
0 nrun  itrm  izip  isgn  isub  inel  icyc  ncyc  nmax       emax           emin          rmax        lmat
     1     5     0     1     7     1     1     8    64  1.0000000e+00  3.9062500e-03  6.2492930e-01    1
 dataprep data for datapac set   1    64    33     7   121  6.249293e-01
0 nrun  itrm  izip  isgn  isub  inel  icyc  ncyc  nmax       emax           emin          rmax        lmat
     2     5     0     1     3     1     1     8    64  1.0000000e+00  3.9062500e-03  5.1516960e-01    2

 dataprep data for datapac set   2    64    33     3   121  5.151696e-01
0 nrun  itrm  izip  isgn  isub  inel  icyc  ncyc  nmax       emax           emin          rmax        lmat
     3     5     0     1     3     1     1     8    64  1.0000000e+00  3.9062500e-03  4.8893680e-01    1

 dataprep data for datapac set   3    64    33     3   121  4.889368e-01

 collision / total de/dx ratios for datapac set   3

 cumulative bremsstrahlung cross sections for datapac set   3

 cumulative bremsstrahlung angular distributions for datapac set   3

 langauss - equiprobable endpoints for interpolation

 k x-ray production for datapac set   3

 photoelectron angular distributions

 pair electron energy division distribution (lead)
1
0 nrun   inc istrg  inok  inel iphot  ibad  ides  ipun itape
    1     1     1     1     2     1     1     1     2     2
0 zone  material  left plane  right plane  inner cylinder  outer cylinder    ecut      ptcz
    1      1      0.           .25400e+01   0.               .14350e-01    .100e-01   0.
    2      2      0.           .25400e+01     .14350e-01     .94000e-01    .100e-01   0.
    3      1      0.           .25400e+01     .94000e-01     .11900e+00    .100e-01   0.
    4      3      0.           .25400e+01     .11900e+00     .75000e+00    .100e-01   0.
0incident electrons
```

```
0electron collision and radiation energy loss straggling
0knock-on electron production
0no coupled inelastic scattering deflections
0bremsstrahlung and characteristic x-ray quanta followed
0bremsstrahlung intrinsic angle of emission from tabulated distribution
0photon-produced particles followed
0 iunt  imax  itmk  jmax  ipmk jpmax  iamk  kmax  ibmk kpmax
     2     1     1    20     1    20     1     6     1     6
0 imax  nzon iflux  ncyc  inran
 30000     4     2   -1100000000000000000
0$$$$$$$$$$$$$$$$ the standard error estimates are based on    10 batches of  3000 histories $$$$$$$$$$$$$$$
0        tin        tcut       tpcut       cthin      sorcin
     1.00000      .01000      .01000     1.00000      .74900
0      tsave                             tmfac        rlan        qblk
      .01000                          10.00000      .50000     1.00000
0electron energy classifications (mev)
      .95000      .90000      .85000      .80000      .75000      .70000
      .65000      .60000      .55000      .50000      .45000      .40000
      .35000      .30000      .25000      .20000      .15000      .10000
      .05000      .01000
0photon energy classifications (mev)
      .95000      .90000      .85000      .80000      .75000      .70000
      .65000      .60000      .55000      .50000      .45000      .40000
      .35000      .30000      .25000      .20000      .15000      .10000
      .05000      .01000
0electron obliquity classifications (degrees)
    30.00000    60.00000    90.00000   120.00000   150.00000   180.00000
0electron azimuth classifications (degrees)
   180.00000
0photon obliquity classifications (degrees)
    30.00000    60.00000    90.00000   120.00000   150.00000   180.00000
0photon azimuth classifications (degrees)
   180.00000
0ntfst        rgmax     scale skale       tcut       tpcut       tfcut       tsave        dlim        bnum        xnum
     1   .62493e+00     1     1         .01000      .01000     0.00000      .01000     1.00000         0.0         0.0
0k x-ray quanta not followed in material     1
0ntfst        rgmax     scale skale       tcut       tpcut       tfcut       tsave        dlim        bnum        xnum
     1   .51517e+00     1     1         .01000      .01000     0.00000      .01000     1.00000         0.0         0.0
0k x-ray quanta not followed in material     2
0ntfst        rgmax     scale skale       tcut       tpcut       tfcut       tsave        dlim        bnum        xnum
     1   .48894e+00     1     1         .01000      .01000     0.00000      .01000     1.00000         0.0         0.0
0k x-ray quanta not followed in material     3
0annihilation quanta followed
1the problem is 100  per cent complete.  time to finish is      0.000 seconds. average time per batch is     103.122
0average source energy = 1.0000e+00 mev
0      inran           ira             irc
 0000000000000000 5405677252600465 1546362076272651
0     ---------------------------------- histories ------------------------------------      rej       --- steps ----
     prim       sec     knock      p e      pair      com     auger      brem      rad      xray      land      prim       sec
    30000    148524    148141      301         0       82         0      1408     4483         0      7007   1421941   1418193
0                           energy (mev)       ave energy (mev)       number/primary       number generated
  first knock (above tcut)   1.4620e-01          3.1105e-02          4.7003e+00           141009
  total knock (above tcut)   1.5037e-01          3.0451e-02          4.9380e+00           148141
  photo-electron             2.2994e-04          1.9766e-02          1.1633e-02              349
  pair                       0.                  0.                  0.                        0
  compton                    1.3276e-04          1.2848e-02          1.0333e-02              310
  auger                      0.                  0.                  0.                        0
  first bremsstrahlung       3.6363e-03          2.8730e-02          1.2657e-01             3797
  total bremsstrahlung       3.7052e-03          2.4845e-02          1.4913e-01             4474
  k x-ray                    0.                  0.                  0.                        0
```

```
 annihilation quanta        0.                 0.                 0.                       0
0unscattered primary photons number and energy
 0.        99 0.      99
0number coefficients - knock-ons, photon descendants
0                                                      transmission
 0.        99
 0.        99
0
                                                        reflection
  .34e-02 11
 0.        99
0
                                                     lateral escape
  .11e-02 19
 0.        99
0
                                                number and energy coefficients
0                                                      transmission
0               cylinder dimensions       ---------- electron ----------      ----------- photon -----------
               length(cm)  radius(cm)       number       energy      counts      number      energy       counts

                 .254e+01    .750e+00  0.        99 0.        99          0   .14e-02 10  .20e-03 15          124
0                                                      reflection
0               cylinder dimensions       ---------- electron ----------      ----------- photon -----------
               length(cm)  radius(cm)       number       energy      counts      number      energy       counts

                 .254e+01    .750e+00   .36e-01  6  .15e-01  7       1094   .75e-02  5  .40e-03  4          299
0                                                     lateral escape
0               cylinder dimensions       ---------- electron ----------      ----------- photon -----------
               length(cm)  radius(cm)       number       energy      counts      number      energy       counts

                 .254e+01    .750e+00   .10e+00  2  .59e-01  2       3096   .26e-01  4  .25e-02  5         1278
1                                                   energy deposition
                                           (normalized to one incident particle)
0                                                                                   energy deposition (mev)
          zone       material       mass(gm)   volume(cc)                                  prim         knock            g-sec            to
tal

             1           1          .1471e-01       .1643e-02                          .7493e-03 17  -.1012e-04 99   .2511e-05 43    .7
417e-03 17
             2           2          .1584e+00       .6886e-01                          .1185e-01  3  -.2764e-05 99   .8798e-05 37    .1
186e-01  3
             3           1          .3803e+00       .4249e-01                          .1437e-01  2  -.3922e-05 99   .1666e-03  8    .1
454e-01  2
             4           3          .8314e+01       .4376e+01                          .8967e+00  0  -.4589e-03 12   .2256e-03 10    .8
965e+00  0
0                                                                  total               .9237e+00  0  -.4757e-03 12   .4035e-03  7    .9
236e+00  0
0
                                                   charge distribution
                                           (normalized to one incident particle)
0                                                                                   electrons
          zone       material      zl          zr            ri           r0           prim        knock        g-sec          total

             1           1     0.          .254e+01   0.              .144e-01     .67e-03 21  .33e-04 99 0.         99   .70e-03 2
7
             2           2     0.          .254e+01    .144e-01       .940e-01     .10e-01  4 -.10e-03 99  .33e-04 99   .99e-02
6
             3           1     0.          .254e+01    .940e-01       .119e+00     .18e-01  4 -.67e-04 99 -.67e-04 67   .18e-01
4
             4           3     0.          .254e+01    .119e+00       .750e+00     .84e+00  0 -.46e-02  9  .33e-04 99   .83e+00
0
0                                         total                                    .86e+00  0 -.48e-02  9  .27e-18 67   .86e+00
0
.
```

```
                                                energy spectra of transmitted electrons
                                          (number/mev, normalized to one incident particle)
      e (mev)  length=       2.5400

   1.0000 -   .9500  0.        99
    .9500 -   .9000  0.        99
    .9000 -   .8500  0.        99
    .8500 -   .8000  0.        99
    .8000 -   .7500  0.        99
    .7500 -   .7000  0.        99
    .7000 -   .6500  0.        99
    .6500 -   .6000  0.        99
    .6000 -   .5500  0.        99
    .5500 -   .5000  0.        99
    .5000 -   .4500  0.        99
    .4500 -   .4000  0.        99
    .4000 -   .3500  0.        99
    .3500 -   .3000  0.        99
    .3000 -   .2500  0.        99
    .2500 -   .2000  0.        99
    .2000 -   .1500  0.        99
    .1500 -   .1000  0.        99
    .1000 -   .0500  0.        99
    .0500 -   .0100  0.        99
                                                energy spectra of reflected electrons
                                          (number/mev, normalized to one incident particle)
      e (mev)  length=       2.5400

   1.0000 -   .9500   .27e-02 41
    .9500 -   .9000   .67e-02 47
    .9000 -   .8500   .15e-01 18
    .8500 -   .8000   .13e-01 27
    .8000 -   .7500   .22e-01 11
    .7500 -   .7000   .25e-01 17
    .7000 -   .6500   .25e-01 18
    .6500 -   .6000   .31e-01  8
    .6000 -   .5500   .45e-01 20
    .5500 -   .5000   .46e-01 12
    .5000 -   .4500   .61e-01 14
    .4500 -   .4000   .62e-01 14
    .4000 -   .3500   .58e-01 11
    .3500 -   .3000   .60e-01 10
    .3000 -   .2500   .47e-01 11
    .2500 -   .2000   .48e-01 17
    .2000 -   .1500   .55e-01 12
    .1500 -   .1000   .37e-01 12
    .1000 -   .0500   .36e-01 12
    .0500 -   .0100   .42e-01 14

                                              energy spectra of laterally escaping electrons
                                          (number/mev, normalized to one incident particle)
      e (mev)  length=       2.5400

   1.0000 -   .9500   .22e-01 17
    .9500 -   .9000   .10e+00  8
    .9000 -   .8500   .11e+00 11
    .8500 -   .8000   .13e+00  8
    .8000 -   .7500   .17e+00  7
    .7500 -   .7000   .15e+00  9
    .7000 -   .6500   .17e+00  5
    .6500 -   .6000   .16e+00  6
```

```
     .6000 -   .5500   .15e+00  5
     .5500 -   .5000   .13e+00  7
     .5000 -   .4500   .14e+00 10
     .4500 -   .4000   .11e+00  6
     .4000 -   .3500   .12e+00  9
     .3500 -   .3000   .10e+00  9
     .3000 -   .2500   .84e-01 12
     .2500 -   .2000   .83e-01  9
     .2000 -   .1500   .61e-01 15
     .1500 -   .1000   .43e-01  8
     .1000 -   .0500   .28e-01 20
     .0500 -   .0100   .11e-01 34
                                     angular distributions of transmitted and reflected electrons
                                         (number/sr, normalized to one incident particle)
                phi(deg)=  0.000
     theta (deg)        180.000

    0.0000 - 30.0000  0.        99
   30.0000 - 60.0000  0.        99
   60.0000 - 90.0000  0.        99
   90.0000 -120.0000   .24e-02  6
  120.0000 -150.0000   .82e-02  7
  150.0000 -180.0000   .12e-01  8
                                       angular distributions of laterally escaping electrons
                                         (number/sr, normalized to one incident particle)
                phi(deg)=  0.000
     theta (deg)        180.000

    0.0000 - 30.0000   .13e-01  9
   30.0000 - 60.0000   .15e-01  3
   60.0000 - 90.0000   .10e-01  4
   90.0000 -120.0000   .60e-02  6
  120.0000 -150.0000   .27e-02  8
  150.0000 -180.0000   .67e-03 25
                              energy spectra and angular distributions of electrons transmitted and reflected
                                    azimuthal interval is   0.00000 to 180.00000 degrees
                                      (number/(mev$sr), normalized to one particle)
      e (mev)  theta=  0.000       30.000       60.000       90.000      120.000      150.000
                      30.000       60.000       90.000      120.000      150.000      180.000

    1.0000 -   .9500  0.        99 0.        99 0.        99 0.        99  .29e-03 99  .24e-02 51
     .9500 -   .9000  0.        99 0.        99 0.        99  .42e-03 99  .20e-02 43  .79e-03 99
     .9000 -   .8500  0.        99 0.        99 0.        99  .13e-02 37  .41e-02 24  .16e-02 67
     .8500 -   .8000  0.        99 0.        99 0.        99  .15e-02 30  .29e-02 33  .16e-02 67
     .8000 -   .7500  0.        99 0.        99 0.        99  .23e-02 16  .52e-02 14  .32e-02 41
     .7500 -   .7000  0.        99 0.        99 0.        99  .21e-02 37  .52e-02 23  .79e-02 26
     .7000 -   .6500  0.        99 0.        99 0.        99  .21e-02 39  .58e-02 20  .55e-02 43
     .6500 -   .6000  0.        99 0.        99 0.        99  .11e-02 33  .78e-02 14  .12e-01 20
     .6000 -   .5500  0.        99 0.        99 0.        99  .28e-02 26  .99e-02 25  .17e-01 24
     .5500 -   .5000  0.        99 0.        99 0.        99  .21e-02 30  .13e-01  8  .12e-01 25
     .5000 -   .4500  0.        99 0.        99 0.        99  .32e-02 23  .13e-01 20  .26e-01 18
     .4500 -   .4000  0.        99 0.        99 0.        99  .53e-02 18  .13e-01 18  .19e-01 26
     .4000 -   .3500  0.        99 0.        99 0.        99  .49e-02 26  .11e-01 18  .21e-01 21
     .3500 -   .3000  0.        99 0.        99 0.        99  .42e-02 24  .12e-01 18  .23e-01 20
     .3000 -   .2500  0.        99 0.        99 0.        99  .21e-02 33  .96e-02 16  .21e-01 19
     .2500 -   .2000  0.        99 0.        99 0.        99  .28e-02 38  .12e-01 23  .14e-01 14
     .2000 -   .1600  0.        99 0.        99 0.        99  .21e-02 21  .14e-01 15  .20e-01 12
     .1500 -   .1000  0.        99 0.        99 0.        99  .30e-02 27  .87e-02 19  .95e-02 27
     .1000 -   .0500  0.        99 0.        99 0.        99  .15e-02 37  .93e-02 16  .12e-01 25
     .0500 -   .0100  0.        99 0.        99 0.        99  .37e-02 24  .87e-02 21  .12e-01 21
```

energy spectra and angular distributions of electrons laterally escaping
azimuthal interval is 0.00000 to 180.00000 degrees
(number/(mev*sr), normalized to one particle)

e (mev)		theta= 0.000 30.000		30.000 60.000		60.000 90.000		90.000 120.000		120.000 150.000		150.000 180.000	
1.0000 -	.9500	.16e-01	17	.35e-02	27	0.	99	.21e-03	99	0.	99	0.	99
.9500 -	.9000	.57e-01	10	.18e-01	14	.34e-02	31	.21e-03	99	0.	99	0.	99
.9000 -	.8500	.32e-01	10	.29e-01	15	.57e-02	22	.13e-02	27	0.	99	0.	99
.8500 -	.8000	.32e-01	19	.27e-01	10	.98e-02	22	.19e-02	39	.58e-03	67	0.	99
.8000 -	.7500	.32e-01	21	.32e-01	12	.15e-01	11	.40e-02	24	.20e-02	30	0.	99
.7500 -	.7000	.17e-01	31	.29e-01	9	.16e-01	13	.49e-02	15	.17e-02	27	0.	99
.7000 -	.6500	.18e-01	21	.26e-01	9	.22e-01	9	.79e-02	15	.14e-02	45	.79e-03	99
.6500 -	.6000	.17e-01	36	.23e-01	6	.16e-01	18	.11e-01	20	.35e-02	35	.79e-03	99
.6000 -	.5500	.95e-02	27	.19e-01	14	.17e-01	9	.11e-01	15	.43e-02	18	.79e-03	99
.5500 -	.5000	.87e-02	21	.13e-01	15	.20e-01	12	.83e-02	15	.20e-02	37	.79e-03	99
.5000 -	.4500	.55e-02	37	.14e-01	12	.17e-01	15	.11e-01	19	.49e-02	20	.79e-03	99
.4500 -	.4000	.32e-02	55	.11e-01	14	.12e-01	11	.85e-02	14	.70e-02	21	.79e-03	99
.4000 -	.3500	.40e-02	45	.12e-01	19	.13e-01	15	.93e-02	13	.58e-02	25	.79e-03	99
.3500 -	.3000	.16e-02	67	.11e-01	19	.10e-01	14	.10e-01	17	.41e-02	27	.16e-02	67
.3000 -	.2500	.40e-02	45	.58e-02	24	.87e-02	22	.83e-02	23	.55e-02	18	.16e-02	67
.2500 -	.2000	.24e-02	51	.49e-02	22	.95e-02	11	.87e-02	15	.43e-02	35	.32e-02	41
.2000 -	.1500	.24e-02	71	.61e-02	31	.72e-02	13	.53e-02	25	.23e-02	41	.79e-03	99
.1500 -	.1000	.79e-03	99	.38e-02	26	.40e-02	28	.45e-02	32	.29e-02	21	.79e-03	99
.1000 -	.0500	.16e-02	67	.20e-02	48	.23e-02	29	.34e-02	27	.17e-02	44	0.	99
.0500 -	.0100	.99e-03	99	.72e-03	67	.19e-02	43	.27e-03	99	.72e-03	67	0.	99

energy spectra of transmitted photons
(number/mev, normalized to one incident particle)

e (mev)		length= 2.5400	
1.0000 -	.9500	0.	99
.9500 -	.9000	0.	99
.9000 -	.8500	0.	99
.8500 -	.8000	0.	99
.8000 -	.7500	.47e-03	99
.7500 -	.7000	0.	99
.7000 -	.6500	0.	99
.6500 -	.6000	0.	99
.6000 -	.5500	0.	99
.5500 -	.5000	0.	99
.5000 -	.4500	0.	99
.4500 -	.4000	.79e-03	67
.4000 -	.3500	.18e-02	57
.3500 -	.3000	.81e-03	67
.3000 -	.2500	.12e-02	51
.2500 -	.2000	.18e-02	33
.2000 -	.1500	.22e-02	49
.1500 -	.1000	.51e-02	30
.1000 -	.0500	.61e-02	23
.0500 -	.0100	.96e-02	10

energy spectra of reflected photons
(number/mev, normalized to one incident particle)

e (mev)		length= 2.5400	
1.0000 -	.9500	0.	99
.9500 -	.9000	0.	99
.9000 -	.8500	0.	99
.8500 -	.8000	0.	99
.8000 -	.7500	0.	99
.7500 -	.7000	0.	99

```
   .7000 -   .6500  0.        99
   .6500 -   .6000  0.        99
   .6000 -   .5500  0.        99
   .5500 -   .5000  0.        99
   .5000 -   .4500  0.        99
   .4500 -   .4000  0.        99
   .4000 -   .3500  0.        99
   .3500 -   .3000   .66e-03 99
   .3000 -   .2500   .61e-03 99
   .2500 -   .2000   .24e-02 41
   .2000 -   .1500   .32e-02 33
   .1500 -   .1000   .12e-01 22
   .1000 -   .0500   .37e-01 10
   .0500 -   .0100   .12e+00 10
                                         energy spectra of laterally escaping photons
                                      (number/mev, normalized to one incident particle)
0      e (mev)  length=      2.5400

  1.0000 -   .9500  0.        99
   .9500 -   .9000  0.        99
   .9000 -   .8500  0.        99
   .8500 -   .8000   .58e-03 99
   .8000 -   .7500  0.        99
   .7500 -   .7000   .48e-03 99
   .7000 -   .6500   .11e-02 99
   .6500 -   .6000   .58e-03 99
   .6000 -   .5500   .17e-02 51
   .5500 -   .5000   .55e-02 26
   .5000 -   .4500   .24e-02 41
   .4500 -   .4000   .27e-02 34
   .4000 -   .3500   .84e-02 30
   .3500 -   .3000   .85e-02 27
   .3000 -   .2500   .11e-01 34
   .2500 -   .2000   .20e-01 14
   .2000 -   .1500   .28e-01 20
   .1500 -   .1000   .70e-01  7
   .1000 -   .0500   .11e+00  6
   .0500 -   .0100   .30e+00  5
                                  angular distributions of transmitted and reflected photon intensity
                                         (mev/sr, normalized to one incident particle)
0               phi(deg)=  0.000
     theta (deg)         180.000

   0.0000 - 30.0000      .23e-03 15
  30.0000 - 60.0000      .53e-05 82
  60.0000 - 90.0000   0.         99
  90.0000 -120.0000      .52e-04 13
 120.0000 -150.0000      .77e-04 12
 150.0000 -180.0000      .68e-04 22
                                   angular distributions of laterally escaping photon intensity
                                         (mev/sr, normalized to one incident particle)
0               phi(deg)=  0.000
     theta (deg)         180.000

   0.0000 - 30.0000      .40e-03 13
  30.0000 - 60.0000      .49e-03 10
  60.0000 - 90.0000      .22e-03  9
  90.0000 -120.0000      .62e-04 17
 120.0000 -150.0000      .10e-04 37
 150.0000 -180.0000      .19e-04 63
```

```
                          energy spectra and angular distributions of photons transmitted and reflected
                                azimuthal interval is   0.00000 to 180.00000 degrees
                                (number/(mev*sr), normalized to one particle)
     e (mev)  theta=  0.000       30.000       60.000       90.000      120.000      150.000
                     30.000       60.000       90.000      120.000      150.000      180.000

  1.0000 -  .9500  0.        99 0.        99 0.        99 0.        99 0.        99 0.        99
   .9500 -  .9000  0.        99 0.        99 0.        99 0.        99 0.        99 0.        99
   .9000 -  .8500  0.        99 0.        99 0.        99 0.        99 0.        99 0.        99
   .8500 -  .8000  0.        99 0.        99 0.        99 0.        99 0.        99 0.        99
   .8000 -  .7500   .56e-03 99 0.        99 0.        99 0.        99 0.        99 0.        99
   .7500 -  .7000  0.        99 0.        99 0.        99 0.        99 0.        99 0.        99
   .7000 -  .6500  0.        99 0.        99 0.        99 0.        99 0.        99 0.        99
   .6500 -  .6000  0.        99 0.        99 0.        99 0.        99 0.        99 0.        99
   .6000 -  .5500  0.        99 0.        99 0.        99 0.        99 0.        99 0.        99
   .5500 -  .5000  0.        99 0.        99 0.        99 0.        99 0.        99 0.        99
   .5000 -  .4500  0.        99 0.        99 0.        99 0.        99 0.        99 0.        99
   .4500 -  .4000   .94e-03 67 0.        99 0.        99 0.        99 0.        99 0.        99
   .4000 -  .3500   .15e-02 51  .23e-03 99 0.        99 0.        99 0.        99 0.        99
   .3500 -  .3000   .96e-03 67 0.        99 0.        99 0.        99  .29e-03 99 0.        99
   .3000 -  .2500   .14e-02 51 0.        99 0.        99  .20e-03 99 0.        99 0.        99
   .2500 -  .2000   .21e-02 33 0.        99 0.        99  .57e-03 51  .29e-03 99 0.        99
   .2000 -  .1500   .27e-02 49 0.        99 0.        99  .38e-03 67  .56e-03 67  .78e-03 99
   .1500 -  .1000   .60e-02 30 0.        99 0.        99  .17e-02 25  .19e-02 38  .31e-02 55
   .1000 -  .0500   .65e-02 23  .28e-03 99 0.        99  .44e-02 15  .78e-02 17  .62e-02 24
   .0500 -  .0100   .11e-01 10 0.        99 0.        99  .14e-01 15  .25e-01 12  .21e-01 24
    integral (/sr)  .16e-02 10  .25e-04 67 0.        99  .91e-03 11  .15e-02  9  .14e-02 13
                            energy spectra and angular distributions of photons laterally escaping
                                azimuthal interval is   0.00000 to 180.00000 degrees
                                (number/(mev*sr), normalized to one particle)
     e (mev)  theta=  0.000       30.000       60.000       90.000      120.000      150.000
                     30.000       60.000       90.000      120.000      150.000      180.000

  1.0000 -  .9500  0.        99 0.        99 0.        99 0.        99 0.        99 0.        99
   .9500 -  .9000  0.        99 0.        99 0.        99 0.        99 0.        99 0.        99
   .9000 -  .8500  0.        99 0.        99 0.        99 0.        99 0.        99 0.        99
   .8000 -  .8000  0.        99 0.25e-03 99 0.        99 0.        99 0.        99 0.        99
   .7500 -  .7000   .58e-03 99 0.        99 0.        99 0.        99 0.        99 0.        99
   .7000 -  .6500  0.        99  .49e-03 99 0.        99 0.        99 0.        99 0.        99
   .6500 -  .6000  0.        99  .25e-03 99 0.        99 0.        99 0.        99 0.        99
   .6000 -  .5500   .62e-03 99  .25e-03 99  .18e-03 99 0.        99 0.        99 0.        99
   .5500 -  .5000   .71e-03 99  .19e-02 31  .20e-03 99 0.        99 0.        99 0.        99
   .5000 -  .4000   .55e-02 09 0.83e-03 99 0.56e-03 99 0.        99 0.        99 0.        99
   .4000 -  .3500   .34e-02 44  .97e-03 56  .10e-02 45 0.        99 0.        99 0.        99
   .3500 -  .3000   .17e-02 51  .23e-02 34  .58e-03 51 0.        99 0.        99 0.        99
   .3000 -  .2500   .13e-02 67  .25e-02 40  .98e-03 45 0.        99 0.        99  .78e-03 99
   .2500 -  .2000   .59e-02 42  .49e-02 17  .11e-02 46  .19e-03 99 0.        99 0.        99
   .2000 -  .1500   .45e-02 40  .51e-02 30  .27e-02 35  .12e-02 51 0.        99 0.        99
   .1500 -  .1000   .12e-01 20  .11e-01 11  .79e-02 15  .27e-02 29 0.        99  .64e-03 99
   .1000 -  .0500   .19e-01 12  .18e-01 11  .12e-01 11  .50e-02 19  .18e-02 37  .79e-04 99
   .0500 -  .0100   .40e-01 12  .47e-01  5  .33e-01 10  .15e-01 14  .28e-02 45  .35e-02 41
    integral (/sr)  .42e-02  7  .43e-02  5  .27e-02  6  .11e-02 12  .20e-03 37  .21e-03 44
 the number of mcs words used for statistics is        717
```

```
rix ac'o'output'tt,140'tt,60
01 lines. (120s)
 1 @o c t o b e r  1 4  , 1 9 7 6  v e r s i o n
 2 @ nset  matl
 3     2     3
 4 @ nmat  ntab
 5     1     1
 6 @mpair  mtax
 7    25    41
 8 @gamma ray cross section data
 9 @energies (mev)
10  1000.000000  800.000000  600.000000  500.000000  400.000000  300.000000
11   200.000000  150.000000  100.000000   80.000000   60.000000   50.000000
12    40.000000   30.000000   20.000000   15.000000   10.000000    8.000000
13     6.000000    5.000000    4.000000    3.000000    2.000000    1.500000
14     1.000000     .800000     .600000     .500000     .400000     .300000
15      .200000     .150000     .100000     .080000     .060000     .050000
16      .040000     .030000     .020000     .015000     .010000
17 @total attenuation coefficients (cm2/g)
18      .133015     .115792     .097314     .087552     .077436     .067025
19      .056529     .051401     .046420     .044377     .042060     .040625
20      .038802     .036353     .033322     .031958     .030918     .030686
21      .030945     .031565     .032919     .035741     .041882     .047769
22      .058536     .065369     .075103     .082004     .091659     .107638
23      .146661     .205315     .421761     .705562    1.487422    2.456969
24     4.613069   10.492178   33.180213   73.691769  215.150145
25 @ratio of scattering plus pair production to total attenuation coefficients
26      .999999     .999998     .999997     .999996     .999995     .999992
27      .999986     .999979     .999965     .999955     .999936     .999920
28      .999895     .999849     .999747     .999641     .999422     .999249
29      .998956     .998721     .998371     .997787     .996538     .995083
30      .991319     .987487     .978709     .969185     .949887     .903104
32      .002260     .090642     .005116     .002285     .000878     .062778
33 @ratio of scattering to scattering plus pair production attenuation coefficients
34      .001662     .002382     .003765     .005007     .007046     .010778
35      .018909     .027362     .044314     .056913     .077841     .094684
36      .120290     .163683     .248185     .323842     .453488     .536768
37      .651019     .722340     .802503     .886979     .963836     .991964
38     1.000000
39 @k shell ionization data
40 @binding energy (mev), photoeffect efficiency and fluorescent efficiency
41      .008981     .871336     .392853
42 @k x-ray energies (mev)
43      .008150     .008150     .008150     .008150
45 @k xir@0000umulat00000ative.000000ities1.000000
46 @auger electron energies (mev)
47      .008150     .008150     .008150
48 @auger electron accumulated relative intensities
49     1.000000    1.000000    1.000000
50 @ nmat  ntab
51     2     1
52 @mpair  mtax
53    25    41
54 @gamma ray cross section data
55 @energies (mev)
56  1000.000000  800.000000  600.000000  500.000000  400.000000  300.000000
57   200.000000  150.000000  100.000000   80.000000   60.000000   50.000000
58    40.000000   30.000000   20.000000   15.000000   10.000000    8.000000
59     6.000000    5.000000    4.000000    3.000000    2.000000    1.500000
60     1.000000     .800000     .600000     .500000     .400000     .300000
.t44,45
44 @k x-ray accumulated relative intensities
45     1.000000    1.000000    1.000000    1.000000
.
```

```
61       .200000      .150000      .100000      .080000      .060000      .050000
62       .040000      .030000      .020000      .015000      .010000
63 @total attenuation coefficients (cm2/g)
64       .042664      .037443      .031861      .028924      .025899      .022819
65       .013793      .018395      .017194      .016805      .016488      .016362
66       .016276      .016313      .016918      .017921      .020146      .021802
67       .024515      .026632      .029693      .034451      .042729      .049688
68       .061023      .067886      .077309      .083599      .091601      .102329
69       .117953      .129244      .146076      .157139      .177347      .197927
70       .240815      .359073      .869633     1.932250     6.538229
71 @ratio of scattering plus pair production to total attenuation coefficients
72      1.000000     1.000000     1.000000     1.000000     1.000000     1.000000
73      1.000000      .999999      .999999      .999999      .999998      .999998
74       .999997      .999996      .999994      .999993      .999990      .999988
75       .999985      .999983      .999979      .999974      .999962      .999947
76       .999908      .999868      .999775      .999673      .999458      .998892
78       .998688      .998688      .998862      .998029      .988300      .819442
79 @ratio of scattering to scattering plus pair production attenuation coefficients
80       .005449      .007745      .012092      .015937      .022153      .033290
81       .056784      .080393      .125794      .158022      .208788      .247184
82       .301520      .383491      .513893      .607020      .731386      .793818
83       .863227      .899113      .933997      .965506      .990010      .997897
84      1.000000
85 @k shell ionization data
86 @binding energy (mev), photoeffect efficiency and fluorescent efficiency
87       .000687      .831990      .003376
88 @k x-ray energies (mev)
89       .000687      .000687      .000687      .000687
90 @k x-ray accumulated relative intensities
91      1.000000     1.000000     1.000000     1.000000
92 @auger electron energies (mev)
93       .000687      .000687      .000687
94 @auger electron accumulated relative intensities
95      1.000000     1.000000     1.000000
96 @ nmat  ntab
97      3     1
98 @mpair  mtax
99     25    41
100 @gamma ray cross section data
101 @energies (mev)
102  1000.000000  800.000000  600.000000  500.000000  400.000000  300.000000
103   200.000000  150.000000  100.000000   88.000000   60.000000   50.000000
105     6.000000    5.000000    4.000000    3.000000    2.000000    1.500000
106     1.000000     .800000     .600000     .500000     .400000     .300000
107      .200000     .150000     .100000     .080000     .060000     .050000
108      .040000     .030000     .020000     .015000     .010000
109 @total attenuation coefficients (cm2/g)
110      .047459      .040496      .033058      .029154      .025144      .021091
111      .017198      .015493      .014218      .013934      .013862      .013935
112      .014112      .014480      .015476      .016765      .019512      .021495
113      .024631      .027011      .030385      .035532      .044349      .051688
114      .063513      .070654      .080455      .086995      .095307      .106425
115      .122475      .133783      .149253      .157712      .169540      .178754
116      .194556      .232360      .387554      .719226     2.228837
117 @ratio of scattering plus pair production to total attenuation coefficients
118     1.000000     1.000000     1.000000     1.000000     1.000000     1.000000
119     1.000000     1.000000     1.000000     1.000000      .999999      .999999
120      .999999      .999999      .999998      .999998      .999997      .999997
```

```
121      .999996      .999995      .999994      .999993      .999990      .999986
122      .999976      .999966      .999942      .999915      .999859      .999710
123      .999123      .997987      .993163      .986454      .967663      .944418
124      .894285      .773048      .479415      .262940      .086410
125 0ratio of scattering to scattering plus pair production attenuation coefficients
126      .005099      .007454      .012130      .016458      .023751      .037489
127      .068025      .099356      .158345      .198381      .258494      .302099
128      .361954      .449719      .584721      .675399      .786023      .838082
129      .894243      .922718      .950047      .974365      .992814      .998465
130     1.000000
131 0k shell ionization data
132 0binding energy (mev), photoeffect efficiency and fluorescent efficiency
133      .000284      .958303      .000382
134 0k x-ray energies (mev)
135      .000284      .000284      .000284      .000284
136 0k x-ray accumulated relative intensities
137     1.000000     1.000000     1.000000     1.000000
138 0auger electron energies (mev)
139      .000284      .000284      .000284
140 0auger electron accumulated relative intensities
141     1.000000     1.000000     1.000000
142 1number of sets on datapac tape =    3
143 0input from datapac
144
145   **2 mev electron beam into bare fx-100 faraday cup**
146 0 nrun  itrm  izip  isgn  isub  inel  icyc  ncyc  nmax        emax            emin            rmax        lmat
147     1     5     0     1    10     1     1     8    64  2.0000000e+00  7.8125000e-03  1.3637750e+00     1
148
149  dataprep data for datapac set   1    64    33    10   121  1.363775e+00
150 0 nrun  itrm  izip  isgn  isub  inel  icyc  ncyc  nmax        emax            emin            rmax        lmat
151     2     5     0     1     6     1     1     8    64  2.0000000e+00  7.8125000e-03  1.1525970e+00     2
152
153  dataprep data for datapac set   2    64    33     6   121  1.152597e+00
154 0 nrun  itrm  izip  isgn  isub  inel  icyc  ncyc  nmax        emax            emin            rmax        lmat
155     3     5     0     1     3     1     1     8    64  2.0000000e+00  7.8125000e-03  1.0971910e+00     1
156
157  dataprep data for datapac set   3    64    33     3   121  1.097191e+00
158  collision / total de/dx ratios for datapac set   3
160
161  cumulative bremsstrahlung cross sections for datapac set   3
162
163  cumulative bremsstrahlung angular distributions for datapac set   3
164
165  langauss - equiprobable endpoints for interpolation
166
167  k x-ray production for datapac set   3
168
169  photoelectron angular distributions
170
171  pair electron energy division distribution (lead)
172 1
173 0 nrun   inc istrg  inok  ine2 iphot  ibad  ides  ipun itape
175 0 zone  material  left plane  right plane  inner cylinder  outer cylinder    ecut        ptcz
176     1       1     0.          .25400e+01     0.               .14350e-01    .100e-01   0.
177     2       2     0.          .25400e+01     .14350e-01       .94000e-01    .100e-01   0.
178     3       1     0.          .25400e+01     .94000e-01       .11900e+00    .100e-01   0.
179     4       3     0.          .25400e+01     .11900e+00       .75000e+00    .100e-01   0.
180 0incident electrons
.t173,174
173 0 nrun   inc istrg  inok  ine2 iphot  ibad  ides  ipun itape
.t173,174
173 0 nrun   inc istrg  inok  inel iphot  ibad  ides  ipun itape
174     2     1     1     1     2     1     1     1     2     2
```

```
 81 @electron collision and radiation energy loss straggling
182 @knock-on electron production
183 @no coupled inelastic scattering deflections
184 @bremsstrahlung and characteristic x-ray quanta followed
185 @bremsstrahlung intrinsic angle of emission from tabulated distribution
186 @photon produced particles followed
187 @ iunt  lmax  ilmk  jmax  ipmk jpmax  lamk  kmax  ibmk kpmax
188      2     1     1    40     1    40     1     6     1     6
189 @ imax  nzon iflux  ncyc  inran
190  30000     4     2  -1100000000000000000
191 @zzzzzzzzzzzzzzzz the standard error estimates are based on    10 batches of  3000 histories zzzzzzzzzzzzzzz
19a @     2.00000      t00000      tp00000      ct10000      sor74000
194 @       tsave                                tmfac         rlan         qblk
195        .01000                             10.00000       .50000      1.00000
196 @electron energy classifications (mev)
197       1.95000     1.90000     1.85000     1.80000     1.75000     1.70000
198       1.65000     1.60000     1.55000     1.50000     1.45000     1.40000
199       1.35000     1.30000     1.25000     1.20000     1.15000     1.10000
200       1.05000     1.00000      .95000      .90000      .85000      .80000
201        .75000      .70000      .65000      .60000      .55000      .50000
202        .45000      .40000      .35000      .30000      .25000      .20000
203        .15000      .10000      .05000      .01000
204 @photon energy classifications (mev)
205       1.95000     1.90000     1.85000     1.80000     1.75000     1.70000
206       1.65000     1.60000     1.55000     1.50000     1.45000     1.40000
207       1.35000     1.30000     1.25000     1.20000     1.15000     1.10000
208       1.05000     1.00000      .05000      .00000      .85000      .80000
210        .45000      .40000      .35000      .30000      .25000      .20000
211        .15000      .10000      .05000      .01000
212 @electron obliquity classifications (degrees)
213     30.00000    60.00000    90.00000   120.00000   150.00000   180.00000
214 @electron azimuth classifications (degrees)
215    180.00000
216 @photon obliquity classifications (degrees)
217     30.00000    60.00000    90.00000   120.00000   150.00000   180.00000
218 @photon azimuth classifications (degrees)
219    180.00000
220 @ntfst        rgmax     scale skale      tcut        tpcut       tfcut        tsave        dlim        bnum       xnum
221      1     .13638e+01     1     1      .01000       .01000     0.00000       .01000     1.00000         0.0        0.0
222 @k x-ray quanta not followed in material     1
223 @ntfst        rgmax     scale skale      tcut        tpcut       tfcut        tsave        dlim        bnum       xnum
224      1     .11526e+01     1     1      .01000       .01000     0.00000       .01000     1.00000         0.0        0.0
225 @k x-ray quanta not followed in material     2
226 @ntfst        rgmax     scale skale      tcut        tpcut       tfcut        tsave        dlim        bnum       xnum
227      1     .10972e+01     1     1      .01000       .01000     0.00000       .01000     1.00000         0.0        0.0
228 @k x-ray quanta not followed in material     3
229 @annihilation quanta followed
230 1the problem is 100  per cent complete.  time to finish is       0.000 seconds. average time per batch is      171.432
231 @average source energy = 2.0000e+00 mev
232 @     inran           ira           irc
233  0000000000000000 2025166701752431 1241741267011501
234 @  ------------------------------------ histories ----------------------------------------      rej       --- steps ----
235      prim      sec     knock      p e      pair      com     auger      brem      rad      xray      land      prim      sec
236     30000   289173    288171      718        0       284        0      3406     8358        0     11607   1488973   2960171
237 @                                energy (mev)       ave energy (mev)      number/primary      number generated
238  first knock (above tcut)        3.3275e-01          3.7391e-02          8.8993e+00          266978
239  total knock (above tcut)        3.4670e-01          3.6093e-02          9.6057e+00          288171
240  photo-electron                  5.9255e-04          2.1264e-02          2.7867e-02             836
.t192,193
192 @      tin        tcut       tpcut       cthin       sorcin
193     2.00000      .01000      .01000     1.00000      .74900
.
```

```
pair                          0.              0.              0.              0
compton                       7.3042e-04      2.5871e-02      2.8233e-02      847
auger                         0.              0.              0.              0
first bremsstrahlung          1.4196e-02      6.3640e-02      2.2307e-01      6692
total bremsstrahlung          1.4458e-02      5.1963e-02      2.7823e-01      8347
k x-ray                       0.              0.              0.              0
annihilation quanta           0.              0.              0.              0
@unscattered primary photons number and energy
 0.        99 0.        99
@number coefficients - knock-ons, photon descendants
@                                               transmission
 0.        99
 0.        99
@                                               reflection
  .30e-02  8
 0.        99
@                                               lateral escape
  .42e-02  8
@ .33e-04 99
                                   number andrenomggscoefficients
@          cylinder dimensions     ---------- electron ----------      ----------- photon -----------
          length(cm)  radius(cm)     number     energy      counts      number     energy       counts

           .254e+01   .750e+00  0.        99 0.      99         0    .65e-02  4  .79e-03  8        488
@                                                reflection
@          cylinder dimensions     ---------- electron ----------      ----------- photon -----------
          length(cm)  radius(cm)     number     energy      counts      number     energy       counts

           .254e+01   .750e+00   .17e-01  4  .56e-02  5      516    .98e-02  6  .42e-03  8        436
@                                                lateral escape
@          cylinder dimensions     ---------- electron ----------      ----------- photon -----------
          length(cm)  radius(cm)     number     energy      counts      number     energy       counts

           .254e+01   .750e+00   .22e+00  1  .11e+00  1     6701    .70e-01  2  .51e-02  3       3284
1                                              energy deposition
                                       (normalized to one incident particle)
@
        zone      material     mass(gm)   volume(cc)                                energy deposition (mev)
tal                                                                 prim          knock              g-sec          to

           1          1        .1471e-01    .1643e-02
524e-02 10                                                   .1528e-02 11  -.1773e-04 99  .1433e-04 51   .1
           2          2        .1584e+00    .6886e-01
149e-01  3                                                   .2151e-01  2  -.4305e-04 99  .2433e-04 36   .2
           3          1        .3803e+00    .4249e-01
728e-01  2                                                   .3678e-01  2   .5798e-04 99  .4412e-03 12   .3
           4          3        .8314e+01    .4376e+01
690e+01  0                                                   .1691e+01  0  -.1518e-02 10  .9326e-03  9   .1
@
750e+01  0                                           total   .1750e+01  0  -.1521e-02 10  .1412e-02  7   .1
@
                                             charge distribution
                                       (normalized to one incident particle)
@                                                                     electrons
        zone      material    zl        zr          rl          r0          prim        knock        g-sec        total

           1          1       0.        .254e+01    0.          .144e-01    .80e-03 23 -.13e-03 99 0.        99  .67e-03 3
2
           2          2       0.        .254e+01    .144e-01    .940e-01    .89e-02  6 -.33e-04 99  .33e-04 99  .89e-02
8
```

```
        3           1      0.            .254e+01     .940e-01     .119e+00     .25e-01  2 -.20e-03 99 -.33e-04 99  .25e-0

        4           3      0.            .254e+01     .119e+00     .750e+00     .73e+00  0 -.71e-02  7 -.33e-04 99  .72e+00

                                                 total                          .77e+00  0 -.75e-02  6 -.33e-04 99  .76e+00

                                                   energy spectra of transmitted electrons
                                          (number/mev, normalized to one incident particle)
       e (mev)  length=       2.5400

  2.0000 -  1.9500  0.        99
  1.9500 -  1.9000  0.        99
  1.9000 -  1.8500  0.        99
  1.8500 -  1.8000  0.        99
  1.8000 -  1.7500  0.        99
  1.7500 -  1.7000  0.        99
  1.7000 -  1.6500  0.        99
  1.6500 -  1.6000  0.        99
  1.6000 -  1.5500  0.        99
  1.5500 -  1.5000  0.        99
  1.5000 -  1.4500  0.        99
  1.4500 -  1.4000  0.        99
  1.4000 -  1.3500  0.        99
  1.3500 -  1.3000  0.        99
  1.3000 -  1.2500  0.        99
  1.2500 -  1.2000  0.        99
  1.2000 -  1.1500  0.        99
  1.1500 -  1.1000  0.        99
  1.1000 -  1.0500  0.        99
  1.0500 -  1.0000  0.        99
  1.0000 -   .9500  0.        99
   .9500 -   .9000  0.        99
   .9000 -   .8500  0.        99
   .8500 -   .8000  0.        99
   .8000 -   .7500  0.        99
   .7500 -   .7000  0.        99
   .7000 -   .6500  0.        99
   .6500 -   .6000  0.        99
   .6000 -   .5500  0.        99
   .5500 -   .5000  0.        99
   .5000 -   .4500  0.        99
   .4500 -   .4000  0.        99
   .4000 -   .3500  0.        99
   .3500 -   .3000  0.        99
   .3000 -   .2000  0.        99
   .2000 -   .1500  0.        99
   .1500 -   .1000  0.        99
   .1000 -   .0500  0.        99
   .0500 -   .0100  0.        99

                                                   energy spectra of reflected electrons
                                          (number/mev, normalized to one incident particle)
       e (mev)  length=       2.5400

  2.0000 -  1.9500  0.        99
  1.9500 -  1.9000  0.        99
  1.9000 -  1.8500   .13e-02 67
  1.8500 -  1.8000   .67e-03 99
  1.8000 -  1.7500   .20e-02 71
  1.7500 -  1.7000   .47e-02 43
```

1.7000 - 1.6500	.67e-03	99
1.6500 - 1.6000	0.	99
1.6000 - 1.5500	.67e-02	30
1.5500 - 1.5000	.47e-02	30
1.5000 - 1.4500	.27e-02	55
1.4500 - 1.4000	.60e-02	26
1.4000 - 1.3500	.67e-02	26
1.3500 - 1.3000	.40e-02	37
1.3000 - 1.2500	.93e-02	22
1.2500 - 1.2000	.67e-02	26
1.2000 - 1.1500	.40e-02	37
1.1500 - 1.1000	.80e-02	24
1.1000 - 1.0500	.67e-02	39
1.0500 - 1.0000	.67e-02	37
1.0000 - .9500	.11e-01	17
.9500 - .9000	.67e-02	21
.9000 - .8500	.10e-01	25
.8500 - .8000	.15e-01	22
.8000 - .7500	.67e-02	45
.7500 - .7000	.11e-01	29
.7000 - .6500	.13e-01	23
.6500 - .6000	.11e-01	18
.6000 - .5500	.10e-01	18
.5500 - .5000	.14e-01	28
.5000 - .4500	.19e-01	16
.4500 - .4000	.15e-01	17
.4000 - .3500	.11e-01	15
.3500 - .3000	.17e-01	16
.3000 - .2500	.11e-01	14
.2500 - .2000	.11e-01	23
.2000 - .1500	.11e-01	23
.1500 - .1000	.14e-01	26
.1000 - .0500	.21e-01	18
.0500 - .0100	.29e-01	11

energy spectra of laterally escaping electrons
(number/mev, normalized to one incident particle)

e (mev) length= 2.5400

2.0000 - 1.9500	.13e-02	67
1.9500 - 1.9000	.34e-01	9
1.9000 - 1.8500	.74e-01	10
1.8500 - 1.8000	.85e-01	12
1.8000 - 1.7500	.83e-01	9
1.7500 - 1.7000	.11e+00	6
1.7000 - 1.6500	.11e+00	7
1.6500 - 1.6000	.12e+00	9
1.6000 - 1.5500	.11e+00	7
1.5500 - 1.5000	.12e+00	8
1.5000 - 1.4500	.13e+00	8
1.4500 - 1.4000	.12e+00	9
1.4000 - 1.3500	.13e+00	5
1.3500 - 1.3000	.13e+00	9
1.3000 - 1.2500	.14e+00	4
1.2500 - 1.2000	.13e+00	7
1.2000 - 1.1500	.15e+00	7
1.1500 - 1.1000	.15e+00	5
1.1000 - 1.0500	.16e+00	5
1.0500 - 1.0000	.15e+00	8
1.0000 - .9500	.14e+00	4
.9500 - .9000	.14e+00	4

```
    .9000 -   .8500   .15e+00  5
    .8500 -   .8000   .16e+00  7
    .8000 -   .7500   .13e+00  5
    .7500 -   .7000   .14e+00  7
    .7000 -   .6500   .16e+00  6
    .6500 -   .6000   .14e+00  6
    .6000 -   .5500   .14e+00  5
    .5500 -   .5000   .14e+00  6
    .5000 -   .4500   .13e+00  8
    .4500 -   .4000   .12e+00  5
    .4000 -   .3500   .99e-01  8
    .3500 -   .3000   .96e-01  8
    .3000 -   .2500   .77e-01  9
    .2500 -   .2000   .74e-01 11
    .2000 -   .1500   .72e-01 12
    .1500 -   .1000   .42e-01 12
    .1000 -   .0500   .36e-01 12
    .0500 -   .0100   .17e-01 20
                                     angular distributions of transmitted and reflected electrons
                                        (number/sr, normalized to one incident particle)
 0               phi(deg)=  0.000
       theta (deg)        180.000

     0.0000 - 30.0000  0.         99
    30.0000 - 60.0000  0.         99
    60.0000 - 90.0000  0.         99
    90.0000 -120.0000   .13e-02  10

 120.0000 -150.0000    .37e-02  6
  150.0000 -180.0000   .53e-02  9
                                       angular distributions of laterally escaping electrons
                                        (number/sr, normalized to one incident particle)
 0               phi(deg)=  0.000
       theta (deg)        180.000

     0.0000 - 30.0000   .43e-01  4
    30.0000 - 60.0000   .36e-01  2
    60.0000 - 90.0000   .21e-01  1
    90.0000 -120.0000   .95e-02  3
   120.0000 -150.0000   .37e-02  6
   150.0000 -180.0000   .99e-03 22
 0                              energy spectra and angular distributions of electrons transmitted and reflected
                                     azimuthal interval is   0.00000 to 180.00000 degrees
                                      (number/(mev*sr), normalized to one particle)
 0       e (mev)  theta=  0.000      30.000      60.000      90.000      120.000     150.000
                         30.000      60.000      90.000     120.000      150.000     180.000

     2.0000 -  1.9500  0.        99 0.        99 0.        99 0.        99 0.        99 0.        99
     1.9500 -  1.9000  0.        99 0.        99 0.        99 0.        99 0.        99 0.        99
     1.9000 -  1.8500  0.        99 0.        99 0.        99 0.        99  .58e-03 67 0.        99
     1.8500 -  1.8000  0.        99 0.        99 0.        99  .21e-03 99 0.        99 0.        99
     1.8000 -  1.7500  0.        99 0.        99 0.        99  .42e-03 99 0.        99  .79e-03 99
     1.7500 -  1.7000  0.        99 0.        99 0.        99  .64e-03 51  .58e-03 99  .16e-02 67
     1.7000 -  1.6500  0.        99 0.        99 0.        99  .21e-03 99 0.        99 0.        99
     1.6500 -  1.6000  0.        99 0.        99 0.        99 0.        99 0.        99 0.        99
     1.6000 -  1.5500  0.        99 0.        99 0.        99  .11e-02 33  .87e-03 51  .16e-02 67
     1.5500 -  1.5000  0.        99 0.        99 0.        99  .85e-03 41  .58e-03 67  .79e-03 99
     1.5000 -  1.4500  0.        99 0.        99 0.        99  .21e-03 99  .87e-03 51 0.        99
     1.4500 -  1.4000  0.        99 0.        99 0.        99  .64e-03 71  .87e-03 51  .24e-02 51
     1.4000 -  1.3500  0.        99 0.        99 0.        99  .11e-02 54  .87e-03 51  .16e-02 67
     1.3500 -  1.3000  0.        99 0.        99 0.        99  .42e-03 67  .12e-02 55 0.        99
```

```
1.3000 -  1.2500  0.        99 0.        99 0.        99  .15e-02 37  .12e-02 55  .24e-02 51
1.2500 -  1.2000  0.        99 0.        99 0.        99  .64e-03 51  .17e-02 27  .79e-03 99
1.2000 -  1.1500  0.        99 0.        99 0.        99 0.        99  .12e-02 55  .16e-02 67
1.1500 -  1.1000  0.        99 0.        99 0.        99  .64e-03 51  .17e-02 37  .24e-02 51
1.1000 -  1.0500  0.        99 0.        99 0.        99  .85e-03 76  .58e-03 67  .32e-02 41
1.0500 -  1.0000  0.        99 0.        99 0.        99  .21e-03 99  .14e-02 54  .32e-02 55
1.0000 -   .9500  0.        99 0.        99 0.        99  .13e-02 51  .20e-02 30  .24e-02 71
 .9500 -   .9000  0.        99 0.        99 0.        99  .42e-03 67  .14e-02 33  .24e-02 51
 .9000 -   .8500  0.        99 0.        99 0.        99  .64e-03 51  .17e-02 51  .48e-02 51
 .8500 -   .8000  0.        99 0.        99 0.        99  .42e-03 99  .43e-02 25  .48e-02 37
 .8000 -   .7500  0.        99 0.        99 0.        99  .64e-03 71  .20e-02 48 0.        99
 .7500 -   .7000  0.        99 0.        99 0.        99  .11e-02 33  .29e-02 42  .16e-02 67
 .7000 -   .6500  0.        99 0.        99 0.        99  .64e-03 51  .35e-02 32  .32e-02 41
 .6500 -   .6000  0.        99 0.        99 0.        99  .64e-03 51  .29e-02 30  .32e-02 55
 .6000 -   .5500  0.        99 0.        99 0.        99  .64e-03 51  .35e-02 27 0.        99
 .5500 -   .5000  0.        99 0.        99 0.        99  .64e-03 99  .35e-02 21  .48e-02 37
 .5000 -   .4500  0.        99 0.        99 0.        99  .85e-03 55  .55e-02 15  .48e-02 37
 .4500 -   .4000  0.        99 0.        99 0.        99  .64e-03 51  .20e-02 37  .10e-01 26
 .4000 -   .3500  0.        99 0.        99 0.        99  .11e-02 33  .23e-02 17  .32e-02 41
 .3500 -   .3000  0.        99 0.        99 0.        99  .15e-02 30  .35e-02 35  .55e-02 30
 .3000 -   .2500  0.        99 0.        99 0.        99  .85e-03 41  .26e-02 20  .24e-02 51
 .2500 -   .2000  0.        99 0.        99 0.        99  .64e-03 51  .23e-02 31  .48e-02 37
 .2000 -   .1500  0.        99 0.        99 0.        99 0.        99  .32e-02 37  .40e-02 45
 .1500 -   .1000  0.        99 0.        99 0.        99  .64e-03 51  .26e-02 35  .71e-02 31
 .1000 -   .0500  0.        99 0.        99 0.        99  .19e-02 39  .41e-02 16  .63e-02 36
 .0500 -   .0100  0.        99 0.        99 0.        99  .29e-02 21  .43e-02 24  .12e-01 24
                   energy spectra and angular distributions of electrons laterally escaping
                          azimuthal interval is   0.00000 to 180.00000 degrees
                            (number/(mev*sr), normalized to one particle)
     e (mev)  theta=  0.000       30.000      60.000      90.000     120.000     150.000
                     30.000       60.000      90.000     120.000     150.000     180.000

2.0000 -  1.9500  .16e-02 67 0.        99 0.        99 0.        99 0.        99 0.        99
1.9500 -  1.9000  .34e-01 12  .17e-02 27  .21e-03 99  .21e-03 99 0.        99 0.        99
1.9000 -  1.8500  .70e-01 10  .55e-02 23  .85e-03 41 0.        99 0.        99 0.        99
1.8500 -  1.8000  .68e-01  8  .11e-01 23  .85e-03 55 0.        99 0.        99 0.        99
1.8000 -  1.7500  .50e-01 12  .15e-01 12  .15e-02 30  .21e-03 99 0.        99 0.        99
1.7500 -  1.7000  .64e-01 11  .20e-01 10  .23e-02 29  .42e-03 67  .29e-03 99 0.        99
1.7000 -  1.6500  .55e-01 10  .23e-01 17  .30e-02 30  .42e-03 67 0.        99 0.        99
1.6500 -  1.6000  .51e-01 11  .29e-01 11  .40e-02 24 0.        99  .29e-03 99 0.        99
1.6000 -  1.5500  .45e-01 13  .23e-01  9  .62e-02 26  .85e-03 41  .58e-03 67 0.        99
1.5500 -  1.5000  .42e-01 14  .28e-01  9  .64e-02 19  .11e-02 33 0.        99 0.        99
1.5000 -  1.4500  .29e-01 22  .36e-01  8  .74e-02 21  .85e-03 41  .58e-03 67 0.        99
1.4500 -  1.4000  .29e-01 19  .26e-01 16  .11e-01 14  .11e-02 45  .29e-03 99 0.        99
1.4000 -  1.3500  .29e-01 20  .27e-01 10  .12e-01 10  .28e-02 26  .29e-03 99 0.        99
1.3500 -  1.3000  .20e-01 30  .30e-01 12  .89e-02 16  .28e-02 20  .14e-02 45 0.        99
1.3000 -  1.2500  .30e-01 31  .28e-01  9  .12e-01 12  .42e-02 18  .58e-03 67 0.        99
1.2500 -  1.2000  .18e-01 21  .30e-01  8  .14e-01 12  .19e-02 35  .29e-03 99 0.        99
1.2000 -  1.1500  .21e-01 17  .33e-01  9  .15e-01 13  .34e-02 17  .29e-03 99 0.        99
1.1500 -  1.1000  .18e-01 18  .30e-01  8  .18e-01 10  .40e-02 30  .29e-03 99 0.        99
1.1000 -  1.0500  .13e-01 20  .30e-01 11  .19e-01  9  .59e-02 17  .14e-02 61  .79e-03 99
1.0500 -  1.0000  .21e-01 23  .24e-01  9  .19e-01 10  .53e-02 15  .87e-03 71 0.        99
1.0000 -   .9500  .21e-01 14  .23e-01 13  .17e-01  7  .59e-02 22  .12e-02 55 0.        99
 .9500 -   .9000  .12e-01 20  .23e-01 10  .18e-01  7  .66e-02 13  .12e-02 55 0.        99
 .9000 -   .8500  .13e-01 21  .21e-01 12  .19e-01 10  .68e-02 15  .14e-02 45  .24e-02 51
 .8500 -   .8000  .10e-01 26  .20e-01 15  .21e-01 12  .10e-01 11  .35e-02 24  .79e-03 99
 .8000 -   .7500  .10e-01 26  .18e-01 12  .15e-01  6  .91e-02 13  .26e-02 26 0.        99
 .7500 -   .7000  .12e-01 20  .18e-01 13  .17e-01  9  .70e-02 18  .29e-02 33  .24e-02 71
 .7000 -   .6500  .79e-02 30  .20e-01 12  .18e-01 12  .12e-01  8  .43e-02 29 0.        99
 .6500 -   .6000  .55e-02 48  .20e-01 10  .17e-01 10  .85e-02 10  .32e-02 29  .16e-02 67
```

```
 .6000 -  .5500  .95e-02 24  .18e-01 11  .16e-01  9  .79e-02 15  .49e-02 20 0.         99
 .5500 -  .5000  .11e-01 24  .15e-01 14  .16e-01 12  .93e-02 16  .46e-02 33  .24e-02 51
 .5000 -  .4500  .40e-02 33  .14e 01 15  .17e-01 15  .10e-01 12  .41e-02 40  .16e-02 67
 .4500 -  .4000  .40e-02 45  .10e-01 12  .13e-01 10  .11e-01 13  .70e-02 19  .24e-02 51
 .4000 -  .3500  .24e-02 71  .84e 02 16  .12e-01 10  .98e-02 10  .43e-02 33  .79e-03 99
 .3500 -  .3000  .32e-02 55  .10e-01 11  .91e-02 16  .93e-02 13  .46e-02 25  .79e-03 99
 .3000 -  .2500  .48e-02 51  .49e-02 30  .10e-01 13  .66e-02 23  .38e-02 20  .79e-03 99
 .2500 -  .2000  .71e-02 26  .52e-02 25  .85e-02 14  .81e-02 13  .17e-02 37 0.         99
 .2000 -  .1500  .32e-02 41  .43e-02 27  .81e-02 12  .76e-02 26  .41e-02 30  .79e-03 99
 .1500 -  .1000  .79e-03 99  .32e-02 29  .40e-02 17  .38e-02 14  .32e-02 25  .24e-02 51
 .1000 -  .0500 0.        99  .41e-02 30  .38e-02 16  .30e-02 32  .23e-02 31 0.         99
 .0500 -  .0100 0.        99  .72e-03 99  .11e-02 55  .21e-02 25  .22e-02 44 0.         99
                                   energy spectra of transmitted photons
                           (number/mev, normalized to one incident particle)
      e (mev)  length=    2.5400

2.0000 - 1.9500 0.        99
1.9500 - 1.9000 0.        99
1.9000 - 1.8500 0.        99
1.8500 - 1.8000 0.        99
1.8000 - 1.7500 0.        99
1.7500 - 1.7000 0.        99
1.6500 - 1.6000 0.        99
1.6000 - 1.5500 0.        99
1.5500 - 1.5000  .52e-03 99
1.5000 - 1.4500 0.        99
1.4500 - 1.4000 0.        99
1.4000 - 1.3500  .10e-02 67
1.3500 - 1.3000 0.        99
1.3000 - 1.2500 0.        99
1.2500 - 1.2000  .47e-03 99
1.2000 - 1.1500  .50e-03 99
1.1500 - 1.1000 0.        99
1.1000 - 1.0500  .54e-03 99
1.0500 - 1.0000  .15e-02 51
1.0000 -  .9500  .99e-03 67
 .9500 -  .9000  .15e-02 51
 .9000 -  .8500  .48e-03 99
 .8500 -  .8000  .13e-02 52
 .8000 -  .7500  .90e-03 67
 .7500 -  .7000  .24e-02 33
 .7000 -  .6500  .88e-03 67
 .6500 -  .6000  .23e-02 45
 .6000 -  .5500  .90e-03 67
 .5500 -  .5000  .15e-02 74
 .5000 -  .4500  .33e-02 45
 .4500 -  .4000  .27e-02 28
 .4000 -  .3500  .45e-02 46
 .3500 -  .3000  .37e-02 26
 .3000 -  .2500  .62e-02 26
 .2500 -  .2000  .87e-02 28
 .2000 -  .1500  .17e-01 17
 .1500 -  .1000  .15e-01 13
 .1000 -  .0500  .22e-01 16
 .0600 -  .0100  .35e-01  9
                                   energy spectra of reflected photons
                           (number/mev, normalized to one incident particle)
      e (mev)  length=    2.5400
```

```
 2.0000 -  1.3500  0.         99
 1.9500 -  1.3000  0.         99
 1.9000 -  1.8500  0.         99
 1.8500 -  1.8000  0.         99
 1.8000 -  1.7500  0.         99
 1.7500 -  1.7000  0.         99
 1.7000 -  1.6500  0.         99
 1.6500 -  1.6000  0.         99
 1.6000 -  1.5500  0.         99
 1.5500 -  1.5000  0.         99
 1.5000 -  1.4500  0.         99
 1.4500 -  1.4000  0.         99
 1.4000 -  1.3500  0.         99
 1.3500 -  1.3000  0.         99
 1.3000 -  1.2500  0.         99
 1.2500 -  1.2000  0.         99
 1.2000 -  1.1500  0.         99
 1.1500 -  1.1000  0.         99
 1.1000 -  1.0500  0.         99
 1.0500 -  1.0000  0.         99
 1.0000 -   .9500  0.         99
  .9500 -   .9000  0.         99
  .9000 -   .8500  0.         99
  .8500 -   .8000  0.         99
  .8000 -   .7500  0.         99
  .7500 -   .7000  0.         99
  .7000 -   .6500  0.         99
  .6500 -   .6000   .64e-03   99
  .6000 -   .5500  0.         99
  .5500 -   .5000   .12e-02   67
  .5000 -   .4500   .13e-02   67
  .4500 -   .4000   .65e-03   99
  .4000 -   .3500   .18e-02   51
  .3500 -   .3000   .19e-02   51
  .3000 -   .2500   .36e-02   37
  .2500 -   .2000   .75e-02   31
  .2000 -   .1500   .12e-01   19
  .1500 -   .1000   .24e-01   21
  .1000 -   .0500   .52e-01   10
  .0500 -   .0100   .11e+00    5
                                              energy spectra of laterally escaping photons
                                          (number/mev, normalized to one incident particle)
0      e (mev)  length=      2.5400

 2.0000 -  1.9500  0.         99
 1.9500 -  1.9000  0.         99
 1.9000 -  1.8500  0.         99
 1.8500 -  1.8000  0.         99
 1.8000 -  1.7500   .56e-03   99
 1.7500 -  1.7000  0.         99
 1.7000 -  1.6500  0.         99
 1.6500 -  1.6000  0.         99
 1.6000 -  1.5500  0.         99
 1.5500 -  1.5000  0.         99
 1.5000 -  1.4500  0.         99
 1.4500 -  1.4000  0.         99
 1.4000 -  1.3500   .64e-03   99
 1.3500 -  1.3000   .56e-03   99
 1.3000 -  1.2500   .17e-02   51
 1.2500 -  1.2000   .17e-02   51
```

```
  1.2000 -  1.1500  0.        99
  1.1500 -  1.1000   .16e-02 51
  1.1000 -  1.0500   .23e-02 55
  1.0500 -  1.0000   .27e-02 54
  1.0000 -   .9500   .44e-02 25
   .9500 -   .9000   .37e-02 67
   .9000 -   .8500   .57e-02 30
   .8500 -   .8000   .76e-02 36
   .8000 -   .7500   .72e-02 22
   .7500 -   .7000   .70e-02 29
   .7000 -   .6500   .77e-02 31
   .6500 -   .6000   .70e-02 40
   .6000 -   .5500   .15e-01 19
   .5500 -   .5000   .15e-01 20
   .5000 -   .4500   .15e-01 11
   .4500 -   .4000   .19e-01 15
   .4000 -   .3500   .25e-01 16
   .3500 -   .3000   .30e-01 15
   .3000 -   .2500   .46e-01 12
   .2500 -   .2000   .66e-01  9
   .2000 -   .1500   .95e-01  6
   .1500 -   .1000   .16e+00  8
   .1000 -   .0500   .29e+00  5
   .0500 -   .0100   .71e+00  3
                                 angular distributions of transmitted and reflected photon intensity
                                              (mev/sr, normalized to one incident particle)
                  phi(deg)=  0.000
     theta (deg)          180.000

   0.0000 - 30.0000      .18e-02  8
  30.0000 - 60.0000      .24e-04 39
  60.0000 - 90.0000      .76e-06 89
  90.0000 -120.0000      .90e-04  9
 120.0000 -150.0000      .19e-03 13
 150.0000 -180.0000      .16e-03 14
                                  angular distributions of laterally escaping photon intensity
                                              (mev/sr, normalized to one incident particle)
                  phi(deg)=  0.000
     theta (deg)          180.000

   0.0000 - 30.0000      .32e-02  9
  30.0000 - 60.0000      .18e-02  5
  60.0000 - 90.0000      .72e-03  4
  90.0000 -120.0000      .29e-03 12
 120.0000 -150.0000      .99e-04 24
 150.0000 -180.0000      .37e-04 40
                               energy spectra and angular distributions of photons transmitted and reflected
                                     azimuthal interval is   0.00000 to 180.00000 degrees
                                      (number/(mev*sr), normalized to one particle)
      e (mev)  theta= 30.000      60.000      90.000      180.000     180.000     180.000

  2.0000 -  1.9500  0.        99 0.        99 0.        99 0.        99 0.        99 0.        99
  1.9500 -  1.9000  0.        99 0.        99 0.        99 0.        99 0.        99 0.        99
  1.9000 -  1.8500  0.        99 0.        99 0.        99 0.        99 0.        99 0.        99
  1.8500 -  1.8000  0.        99 0.        99 0.        99 0.        99 0.        99 0.        99
  1.8000 -  1.7500  0.        99 0.        99 0.        99 0.        99 0.        99 0.        99
  1.7500 -  1.7000  0.        99 0.        99 0.        99 0.        99 0.        99 0.        99
  1.7000 -  1.6500  0.        99 0.        99 0.        99 0.        99 0.        99 0.        99
  1.6500 -  1.6000  0.        99 0.        99 0.        99 0.        99 0.        99 0.        99
```

```
 1.6000 -  1.5500  0.         99 0.         99 0.         99 0.         99 0.         99 0.         99
 1.5500 -  1.5000   .62e-03 99 0.         99 0.         99 0.         99 0.         99 0.         99
 1.5000 -  1.4500  0.         99 0.         99 0.         99 0.         99 0.         99 0.         99
 1.4500 -  1.4000  0.         99 0.         99 0.         99 0.         99 0.         99 0.         99
 1.4000 -  1.3500   .12e-02 67 0.         99 0.         99 0.         99 0.         99 0.         99
 1.3500 -  1.3000  0.         99 0.         99 0.         99 0.         99 0.         99 0.         99
 1.3000 -  1.2500  0.         99 0.         99 0.         99 0.         99 0.         99 0.         99
 1.2500 -  1.2000   .56e-03 99 0.         99 0.         99 0.         99 0.         99 0.         99
 1.2000 -  1.1500   .60e-03 99 0.         99 0.         99 0.         99 0.         99 0.         99
 1.1500 -  1.1000  0.         99 0.         99 0.         99 0.         99 0.         99 0.         99
 1.1000 -  1.0500   .64e-03 99 0.         99 0.         99 0.         99 0.         99 0.         99
 1.0000 -  1.0000   .12e-02 67 0.         99 0.         99 0.         99 0.         99 0.         99
  .9500 -   .9000   .17e-02 51 0.         99 0.         99 0.         99 0.         99 0.         99
  .9000 -   .8500   .58e-03 99 0.         99 0.         99 0.         99 0.         99 0.         99
  .8500 -   .8000   .15e-02 52 0.         99 0.         99 0.         99 0.         99 0.         99
  .8000 -   .7500   .11e-02 67 0.         99 0.         99 0.         99 0.         99 0.         99
  .7500 -   .7000   .28e-02 33 0.         99 0.         99 0.         99 0.         99 0.         99
  .7000 -   .6500   .10e-02 67 0.         99 0.         99 0.         99 0.         99 0.         99
  .6500 -   .6000   .27e-02 45 0.         99 0.         99  .20e-03 99 0.         99 0.         99
  .6000 -   .5500   .11e-02 67 0.         99 0.         99 0.         99 0.         99 0.         99
  .5000 -   .5000   .40e-02 89 0.28e-03 99 0.         99 0.19e-03 99  .88e-03 89 0.         99
  .4500 -   .4000   .25e-02 33  .24e-03 99 0.         99 0.         99  .28e-03 99 0.         99
  .4000 -   .3500   .54e-02 46 0.         99 0.         99  .57e-03 51 0.         99 0.         99
  .3500 -   .3000   .44e-02 26 0.         99 0.         99 0.         99  .81e-03 51 0.         99
  .3000 -   .2500   .73e-02 26 0.         99 0.         99  .59e-03 51  .78e-03 51 0.         99
  .2500 -   .2000   .10e-01 28 0.         99 0.         99  .96e-03 62  .15e-02 37  .13e-02 67
  .2000 -   .1500   .19e-01 16  .46e-03 68 0.         99  .89e-03 34  .32e-02 32  .22e-02 51
  .1500 -   .1000   .18e-01 13 0.         99 0.         99  .23e-02 36  .50e-02 26  .57e-02 35
  .1000 -   .0500   .22e-01 15  .14e-02 41  .21e-03 99  .50e-02 24  .11e-01 11  .14e-01 19
  .0500 -   .0100   .37e-01  9  .15e-02 29  .47e-04 99  .85e-02 13  .25e-01  8  .34e-01 11
    integral (/sr)  .71e-02  4  .18e-03 24  .12e-04 84  .88e-03 10  .21e-02  8  .25e-02  8
                     energy spectra and angular distributions of photons laterally escaping
                            azimuthal interval is   0.00000 to 180.00000 degrees
                            (number/(mev*sr), normalized to one particle)
     e (mev)  theta=  0.000       30.000      60.000      90.000      120.000     150.000
                     30.000       60.000      90.000     120.000      150.000     180.000

 2.0000 -  1.9500  0.         99 0.         99 0.         99 0.         99 0.         99 0.         99
 1.9500 -  1.9000  0.         99 0.         99 0.         99 0.         99 0.         99 0.         99
 1.9000 -  1.8500  0.         99 0.         99 0.         99 0.         99 0.         99 0.         99
 1.8500 -  1.8000  0.         99 0.         99 0.         99 0.         99 0.         99 0.         99
 1.8000 -  1.7500   .66e-03 99 0.         99 0.         99 0.         99 0.         99 0.         99
 1.7500 -  1.7000  0.         99 0.         99 0.         99 0.         99 0.         99 0.         99
 1.7000 -  1.6500  0.         99 0.         99 0.         99 0.         99 0.         99 0.         99
 1.6500 -  1.6000  0.         99 0.         99 0.         99 0.         99 0.         99 0.         99
 1.6000 -  1.5500  0.         99 0.         99 0.         99 0.         99 0.         99 0.         99
 1.5500 -  1.5000  0.         99 0.         99 0.         99 0.         99 0.         99 0.         99
 1.5000 -  1.4500  0.         99 0.         99 0.         99 0.         99 0.         99 0.         99
 1.4500 -  1.4000  0.         99 0.         99 0.         99 0.         99 0.         99 0.         99
 1.4000 -  1.3500  0.         99 0.         99  .21e-03 99 0.         99 0.         99 0.         99
 1.3500 -  1.3000   .67e-03 99 0.         99 0.         99 0.         99 0.         99 0.         99
 1.3000 -  1.2500   .61e-03 99  .49e-03 67 0.         99 0.         99 0.         99 0.         99
 1.2500 -  1.2000   .13e-02 67  .26e-03 99 0.         99 0.         99 0.         99 0.         99
 1.2000 -  1.1500  0.         99 0.         99 0.         99 0.         99 0.         99 0.         99
 1.1500 -  1.1000   .65e-03 99  .46e-03 67 0.         99 0.         99 0.         99 0.         99
 1.1000 -  1.0500   .72e-03 99  .73e-03 51 0.         99 0.         99 0.         99 0.         99
 1.0500 -  1.0000   .19e-02 51  .48e-03 67 0.         99 0.         99 0.         99 0.         99
 1.0000 -   .9500   .32e-02 45  .50e-03 67  .17e-03 99 0.         99 0.         99 0.         99
```

81	.9500 -	.9000	.21e-02	51	.53e-03	99	.21e-03	99	0.	99	0.	99	0. 99
82	.9000 -	.8500	.14e-02	67	.15e-02	36	.34e-03	67	0.	99	0.	99	0. 99
83	.8500 -	.8000	.24e-02	56	.13e-02	45	.41e-03	67	.38e-03	99	0.	99	0. 99
84	.8000 -	.7500	.20e-02	51	.13e-02	34	.58e-03	51	.21e-03	99	0.	99	0. 99
785	.7500 -	.7000	.41e-02	37	.10e-02	54	.36e-03	67	0.	99	0.	99	0. 99
786	.7000 -	.6500	.36e-02	46	.99e-03	56	.75e-03	41	0.	99	0.	99	0. 99
787	.6500 -	.6000	.12e-02	67	.15e-02	37	.61e-03	71	.19e-03	99	0.	99	0. 99
788	.6000 -	.5500	.46e-02	37	.31e-02	20	.11e-02	36	0.	99	.29e-03	99	0. 99
789	.5500 -	.5000	.66e-02	35	.26e-02	30	.93e-03	33	.17e-03	99	0.	99	0. 99
790	.5000 -	.4500	.25e-02	42	.47e-02	17	.77e-03	55	0.	99	0.	99	0. 99
791	.4500 -	.4000	.86e-02	32	.37e-02	18	.99e-03	44	.21e-03	99	0.	99	0. 99
792	.4000 -	.3500	.87e-02	17	.34e-02	25	.26e-02	31	.55e-03	71	0.	99	0. 99
793	.3500 -	.3000	.10e-01	25	.66e-02	19	.12e-02	43	.60e-03	51	.28e-03	99	0. 99
794	.3000 -	.2500	.84e-02	21	.71e-02	19	.40e-02	22	.21e-02	30	.11e-02	75	.78e-03 99
795	.2500 -	.2000	.20e-01	20	.96e-02	14	.49e-02	23	.34e-02	19	.73e-03	51	0. 99
796	.2000 -	.1500	.25e-01	12	.17e-01	10	.74e-02	10	.35e-02	25	.83e-03	71	0. 99
797	.1500 -	.1000	.35e-01	15	.24e-01	8	.14e-01	12	.72e-02	19	.16e-02	41	.70e-03 99
798	.1000 -	.0500	.62e-01	8	.44e-01	4	.23e-01	5	.14e-01	19	.76e-02	27	.38e-02 36
799	.0500 -	.0100	.14e+00	9	.11e+00	5	.62e-01	4	.36e-01	6	.16e-01	16	.46e-02 45
800	integral (/sr)		.16e-01	4	.11e-01	3	.57e-02	2	.31e-02	6	.13e-02	13	.45e-03 35
801	the number of ecs words used for statistics is						1317						

```
output!t!.60
39 lines. (120a)
0october 14 ,1976 version
0 nset  matl
    3     3
0 nmat  ntab
    1     1
0mpair  mtax
   25    41
0gamma ray cross section data
0energies (mev)
  1000.000000  800.000000  600.000000  500.000000  400.000000  300.000000
   200.000000  150.000000  100.000000   80.000000   60.000000   50.000000
    40.000000   30.000000   20.000000   15.000000   10.000000    8.000000
     6.000000    5.000000    4.000000    3.000000    2.000000    1.500000
     1.000000     .800000     .600000     .500000     .400000     .300000
      .200000     .150000     .100000     .080000     .060000     .050000
      .040000     .030000     .020000     .015000     .010000
0total attenuation coefficients (cm2/g)
      .133015     .115792     .097314     .087552     .077436     .067025
      .056529     .051401     .046420     .044377     .042060     .040625
      .038802     .036353     .033322     .031958     .030918     .030686
      .030945     .031565     .032919     .035741     .041882     .047769
      .058536     .065369     .075103     .082004     .091659     .107638
      .146661     .205315     .421761     .705562    1.487422    2.456969
     4.613069   10.492178   33.180213   73.691769  215.150145
0ratio of scattering plus pair production to total attenuation coefficients
      .999999     .999998     .999997     .999996     .999995     .999992
      .999986     .999979     .999965     .999955     .999936     .999920
      .999895     .999849     .999747     .999641     .999422     .999249
      .998956     .998721     .998371     .997787     .996538     .995083
      .991319     .987487     .978709     .969185     .949887     .903104
      .762317     .594141     .321116     .201461     .100774     .062778
      .034460     .015642     .005116     .002345     .000818
0ratio of scattering to scattering plus pair production attenuation coefficients
      .001662     .002382     .003765     .005007     .007046     .010778
      .018909     .027362     .044314     .056913     .077841     .094684
      .120290     .163683     .248185     .323842     .453488     .536768
      .651019     .722340     .802503     .886979     .963836     .991964
     1.000000
0k shell ionization data
0binding energy (mev), photoeffect efficiency and fluorescent efficiency
      .008981     .871336     .392853
0k x-ray energies (mev)
      .008150     .008150     .008150     .008150
0k x-ray accumulated relative intensities
     1.000000    1.000000    1.000000    1.000000
0auger electron energies (mev)
      .008150     .008150     .008150
0auger electron accumulated relative intensities
     1.000000    1.000000    1.000000
0 nmat  ntab
    2     1
0mpair  mtax
   25    41
0gamma ray cross section data
0energies (mev)
  1000.000000  800.000000  600.000000  500.000000  400.000000  300.000000
   200.000000  150.000000  100.000000   80.000000   60.000000   50.000000
    40.000000   30.000000   20.000000   15.000000   10.000000    8.000000
     6.000000    5.000000    4.000000    3.000000    2.000000    1.500000
     1.000000     .800000     .600000     .500000     .400000     .300000
```

```
      .200000     .150000     .100000     .080000     .060000     .050000
      .040000     .030000     .020000     .015000     .010000
@total attenuation coefficients (cm2/g)
      .042664     .037443     .031861     .028924     .025899     .022819
      .019793     .018395     .017194     .016805     .016488     .016362
      .020876     .026838     .028898     .037881     .040720     .049808
      .061023     .067886     .077309     .083599     .091601     .102329
      .117953     .129244     .146076     .157139     .177347     .197927
      .240815     .359073     .869633    1.932250    6.538229
@ratio of scattering plus pair production to total attenuation coefficients
     1.000000    1.000000    1.000000    1.000000    1.000000    1.000000
     1.000000     .999999     .999999     .999999     .999998     .999998
      .999997     .999996     .999994     .999993     .999990     .999988
      .999985     .999983     .999979     .999974     .999962     .999947
      .999908     .999868     .999775     .999673     .999458     .998892
      .996690     .992470     .974912     .951171     .888740     .819442
      .694128     .480603     .205262     .094029     .028300
@ratio of scattering to scattering plus pair production attenuation coefficients
      .005449     .007745     .012092     .015937     .022153     .033290
      .056784     .080393     .125794     .158022     .208788     .247184
      .301520     .383491     .513893     .607020     .731386     .793818
      .863227     .899113     .933997     .965506     .990010     .997897
     1.000000
@k shell ionization data
@binding energy (mev), photoeffect efficiency and fluorescent efficiency
      .000687     .831990     .003376
@k x-ray energies (mev)
      .000687     .000687     .000687     .000687
@k x-ray accumulated relative intensities
     1.000000    1.000000    1.000000    1.000000
@auger electron energies (mev)
      .000687     .000687     .000687
@auger electron accumulated relative intensities
     1.000000    1.000000    1.000000
@ nmat  ntab
     3     1
@npair  mtax
    25    41
@gamma ray cross section data
@energies (mev)
  1000.000000  800.000000  600.000000  500.000000  400.000000  300.000000
   200.000000  150.000000  100.000000   80.000000   60.000000   50.000000
    40.000000   30.000000   20.000000   15.000000   10.000000    8.000000
     6.000000    5.000000    4.000000    3.000000    2.000000    1.500000
     1.000000     .800000     .600000     .500000
 .400000     .300000
      .200000     .150000     .100000     .080000     .060000     .050000
      .040000     .030000     .020000     .015000     .010000
@total attenuation coefficients (cm2/g)
      .047459     .040496     .033058     .029154     .025144     .021091
      .017198     .015493     .014218     .013934     .013862     .013935
      .014112     .014480     .015476     .016765     .019512     .021495
      .024631     .027011     .030385     .035532     .044349     .051688
      .063513     .070654     .080456     .086995     .095307     .106425
      .122475     .133783     .149253     .157712     .169540     .178754
      .194556     .232360     .387554     .719226    2.228837
@ratio of scattering plus pair production to total attenuation coefficients
     1.000000    1.000000    1.000000    1.000000    1.000000    1.000000
     1.000000    1.000000    1.000000    1.000000     .999999     .999999
      .999999     .999999     .999998     .999998     .999997     .999997
..
```

```
       .999996     .999995     .999994     .999993     .999990     .999986
       .999976     .999966     .999942     .999915     .999859     .999710
       .999123     .997987     .993163     .986454     .967663     .944418
       .894285     .773048     .479415     .262940     .086410
0ratio of scattering to scattering plus pair production attenuation coefficients
       .005099     .007454     .012130     .016458     .023751     .037489
       .068025     .099356     .158345     .198381     .258494     .302099
       .361954     .449719     .584721     .675399     .786023     .838082
       .894243     .922718     .950047     .974365     .992814     .998465
      1.000000
0k shell ionization data
0binding energy (mev), photoeffect efficiency and fluorescent efficiency
       .000284     .958303     .000382
0k x-ray energies (mev)
       .000284     .000284     .000284     .000284
0k x-ray accumulated relative intensities
      1.000000    1.000000    1.000000    1.000000
0auger electron energies (mev)
       .000284     .000284     .000284
0auger electron accumulated relative intensities
      1.000000    1.000000    1.000000
1number of sets on datapac tape =    3
0input from datapac

   ##3 mev electron beam into bare fx-100 faraday cup##
0 nrun  itrm  izip  isgn  isub  inel  icyc  ncyc  nmax       emax            emin            rmax        imat
     1     5     0     1    14     1     1     8    64  3.0000000e+00  1.1718750e-02  2.0655130e+00     1

  dataprep data for datapac set   1    64    33    14   121  2.065513e+00
0 nrun  itrm  izip  isgn  isub  inel  icyc  ncyc  nmax       emax            emin            rmax        imat
     2     5     0     1     9     1     1     8    64  3.0000000e+00  1.1718750e-02  1.7789810e+00     2

  dataprep data for datapac set   2    64    33     9   121  1.778981e+00
0 nrun  itrm  izip  isgn  isub  inel  icyc  ncyc  nmax       emax            emin            rmax        imat
     3     5     0     1     3     1     1     8    64  3.0000000e+00  1.1718750e-02  1.6970910e+00     1

  dataprep data for datapac set   3    64    33     3   121  1.697091e+00
   collision / total de/dx ratios for datapac set   3

  cumulative bremsstrahlung cross sections for datapac set   3

  cumulative bremsstrahlung angular distributions for datapac set   3

  langausa - equiprobable endpoints for interpolation

  k x-ray production for datapac set   3

  photoelectron angular distributions

  pair electron energy division distribution (lead)
1
0 nrun   inc  istrg  inok  inel iphot  ibad  ides  ipun  itape
     3     1     1     1     2     1     1     1     2     2
0 zone  material  left plane  right plane  inner cylinder  outer cylinder    ecut       ptcs
     1      1      0.          .25400e+01   0.                .14350e-01   .100e-01   0.
     2      2      0.          .25400e+01     .14350e-01      .94000e-01   .100e-01   0.
     3      1      0.          .25400e+01     .94000e-01      .11900e+00   .100e-01   0.
     4      3      0.          .25400e+01     .11900e+00      .75000e+00   .100e-01   0.
0incident electrons
```

```
@electron collision and radiation energy loss straggling
@knock-on electron production
@no coupled inelastic scattering deflections
@bremsstrahlung and characteristic x-ray quanta followed
@bremsstrahlung intrinsic angle of emission from tabulated distribution
@photon-produced electron... (overprinted)          lamk   kmax   ibek kpmax
      2      1      1     30      1     30      1      6      1      6
@ imax  nzon  iflux  ncyc  inran
  30000     4     2   -1100000000000000000
@############### the standard error estimates are based on     10 batches of   3000 histories ###############
@        tin          tcut          tpcut         cthin        sorcin
       3.00000       .01000        .01000       1.00000        .74900
@##############electron cut-off energy below electron energy list. cut-off energy has been changed to em(nmax)##########
####
@       tsave                                    tmfac          rlan          qblk
        .01225                                 10.00000        .50000       1.00000
@electron energy classifications (mev)
       2.90000       2.80000       2.70000       2.60000       2.50000       2.40000
       2.30000       2.20000       2.10000       2.00000       1.90000       1.80000
       1.70000       1.60000       1.50000       1.40000       1.30000       1.20000
       1.10000       1.00000        .90000        .80000        .70000        .60000
        .50000        .40000        .30000        .20000        .10000        .01225
@photon energy classifications (mev)
       2.90000       2.80000       2.70000       2.60000       2.50000       2.40000
       2.30000       2.20000       2.10000       2.00000       1.90000       1.80000
       1.70000       1.60000       1.50000       1.40000       1.30000       1.20000
       1.10000       1.00000        .90000        .80000        .70000        .60000
@electr50000bliquity40000sificat30000(degree20000        .10000        .01000
      30.00000      60.00000      90.00000     120.00000     150.00000     180.00000
@electron azimuth classifications (degrees)
     180.00000
@photon obliquity classifications (degrees)
      30.00000      60.00000      90.00000     120.00000     150.00000     180.00000
@photon azimuth classifications (degrees)
     180.00000
@ntfst        rgmax      scale skale       tcut        tpcut        tfcut        tsave        dlim        bnum       xnum
@k x-ray quan80666e+00llowed in material.01225        .01000      0.00000      .01225      1.00000       0.0        0.0
@ntfst        rgmax      scale skale       tcut        tpcut        tfcut        tsave        dlim        bnum       xnum
      1      .17790e+01     1     1       .01225       .01000      0.00000      .01225      1.00000       0.0        0.0
@k x-ray quanta not followed in material      2
@ntfst        rgmax      scale skale       tcut        tpcut        tfcut        tsave        dlim        bnum       xnum
      1      .16971e+01     1     1       .01225       .01000      0.00000      .01225      1.00000       0.0        0.0
@k x-ray quanta not followed in material      3
@annihilation quanta followed
1the problem is 100  per cent complete.  time to finish is       0.000 seconds. average time per batch is      204.419
@average source energy = 3.0000e+00 mev
@     inran           ira           irc
  0000000000000000 1361516456613215 3061637164470405
@ ----------------------------------- histories ------------------------------------      rej       --- steps ----
      prim     sec    knock      p e      pair      com     auger      brem      rad      xray      land      prim      sec
     30000  333877   332549      841       0        487       0        5733     11950      0       11924   1392170   3492808
@                                energy (mev)      ave energy (mev)      number/primary      number generated
 first knock (above tcut)      4.9701e-01         4.8828e-02           1.0179e+01           305368
 total knock (above tcut)      5.1993e-01         4.6904e-02           1.1085e+01           332549
 photo-electron                8.8340e-04         2.0138e-02           4.3867e-02             1316
 pair                          0.                 0.                   0.                        0
 compton                       2.0222e-03         4.2159e-02           4.7967e-02             1439
```

```
241.300
41   auger                          0.                   0.                   0.                      0
242  first bremsstrahlung           3.2168e-02           1.0258e-01           3.1360e-01           9408
243  total bremsstrahlung           3.2644e-02           8.2062e-02           3.9780e-01          11934
244  k x-ray                        0.                   0.                   0.                      0
245  annihilation quanta            0.                   0.                   0.                      0
246 @unscattered primary photons number and energy
247  0.         99 0.      99
248 @number coefficients - knock-ons, photon descendants
249 @
250  0.         99                                  transmission
252 @0.         99
253   .34e-02  15                                   reflection
254  0.         99
255 @
256   .93e-02   4                                  lateral escape
257   .17e-03  33
258 @
259 @                                    number and energy coefficients
260 @                                               transmission
261            cylinder dimensions      ---------- electron ----------      ----------- photon -----------
262          length(cm)  radius(cm)      number      energy      counts      number      energy      counts
263
264 @          .254e+01    .750e+00  0.        99 0.       99           0   .15e-01  3  .18e-02  6      1054
265 @                                                reflection
266            cylinder dimensions      ---------- electron ----------      ----------- photon -----------
267          length(cm)  radius(cm)      number      energy      counts      number      energy      counts
268
269 @          .254e+01    .750e+00   .12e-01  8  .33e-02  8       357    .10e-01  5  .37e-03 15       487
270 @                                               lateral escape
271            cylinder dimensions      ---------- electron ----------      ----------- photon -----------
272          length(cm)  radius(cm)      number      energy      counts      number      energy      counts
273
274 1          .254e+01    .750e+00   .34e+00  1  .16e+00  1     10109    .12e+00  1  .76e-02  3      5557
275                                              energy deposition
276 @                                   (normalized to one incident particle)
277           zone       material     mass(gm)    volume(cc)                          energy deposition (mev)
278 tal                                                                   prim          knock         g-sec         to
279
280             1
281 072e-02     6         1        .1471e-01     .1643e-02               .2085e-02  6  -.3671e-04 99  .2415e-04 52   .2
282             2
283 507e-01     2         2        .1584e+00     .6886e-01               .3522e-01  2  -.2080e-03 63  .6222e-04 34   .3
284             3
285 024e-01     2         1        .3803e+00     .4249e-01               .5941e-01  2   .1751e-03 94  .6613e-03  5   .6
286             4
287 386e+01     0         3        .8314e+01     .4376e+01               .2387e+01  0  -.3417e-02  8  .2250e-02  8   .2
288 @
289 484e+01     0                                              total     .2484e+01  0  -.3486e-02  5  .2998e-02  7   .2
290 @
291                                               charge distribution
292 @                                   (normalized to one incident particle)
293           zone       material    zl          zr          ri          r0         electrons
294                                                                                    prim        knock       g-sec        total
295             1         1       0.          .254e+01    0.          .144e-01
296 3                                                                             .97e-03 17   .33e-04 99 0.          99  .10e-02 2
297             2         2       0.          .254e+01    .144e-01    .940e-01
298 7                                                                             .12e-01  5  -.53e-03 58  .10e-03 51   .11e-01
299             3         1       0.          .254e+01    .940e-01    .119e+00
300 3                                                                             .28e-01  3   .17e-03 99 -.13e-03 55   .28e-01
```

```
        4          3     0.          .254e+01    .119e+00    .750e+00    .62e+00  1 -.13e-01  4 -.13e-03 41  .61e+00
 1
 0                                                  total                .66e+00  1 -.13e-01  3 -.17e-03 33  .65e+00
 1
 0                                                   energy spectra of transmitted electrons
                                                 (number/mev, normalized to one incident particle)
 0       e (mev)  length=       2.5400

      3.0000 -  2.9000  0.        99
      2.9000 -  2.8000  0.        99
      2.8000 -  2.7000  0.        99
      2.7000 -  2.6000  0.        99
      2.6000 -  2.5000  0.        99
      2.5000 -  2.4000  0.        99
      2.4000 -  2.3000  0.        99
      2.3000 -  2.2000  0.        99
      2.2000 -  2.1000  0.        99
      2.1000 -  2.0000  0.        99
      2.0000 -  1.9000  0.        99
      1.9000 -  1.8000  0.        99
      1.8000 -  1.7000  0.        99
      1.7000 -  1.6000  0.        99
      1.6000 -  1.5000  0.        99
      1.5000 -  1.4000  0.        99
      1.4000 -  1.3000  0.        99
      1.3000 -  1.2000  0.        99
      1.2000 -  1.1000  0.        99
      1.1000 -  1.0000  0.        99
      1.0000 -   .9000  0.        99
       .9000 -   .8000  0.        99
       .8000 -   .7000  0.        99
       .7000 -   .6000  0.        99
       .6000 -   .5000  0.        99
       .5000 -   .4000  0.        99
       .4000 -   .3000  0.        99
       .3000 -   .2000  0.        99
       .2000 -   .1000  0.        99
       .1000 -   .0122  0.        99
 0                                                    energy spectra of reflected electrons
                                                 (number/mev, normalized to one incident particle)
 0       e (mev)  length=       2.5400

      3.0000 -  2.9000   .33e-03 99
      2.9000 -  2.8000   .67e-03 67
      2.8000 -  2.7000   .10e-02 71
      2.7000 -  2.6000   .33e-03 99
      2.6000 -  2.5000   .33e-03 99
      2.5000 -  2.4000   .20e-02 51
      2.4000 -  2.3000   .17e-02 45
      2.3000 -  2.2000   .33e-03 99
      2.2000 -  2.1000   .17e-02 45
      2.1000 -  2.0000   .67e-03 67
      2.0000 -  1.9000   .17e-02 45
      1.9000 -  1.8000   .23e-02 48
      1.8000 -  1.7000   .20e-02 37
      1.7000 -  1.6000   .47e-02 29
      1.6000 -  1.5000   .30e-02 39
      1.5000 -  1.4000   .37e-02 29
      1.4000 -  1.3000   .33e-02 30
      1.3000 -  1.2000   .37e-02 32
```

```
   1.2000 -  1.1000   .47e-02 22
   1.1000 -  1.0000   .43e-02 30
   1.0000 -   .9000   .47e-02 22
    .9000 -   .8000   .50e-02 15
    .8000 -   .7000   .50e-02 32
    .7000 -   .6000   .53e-02 23
    .6000 -   .5000   .67e-02 15
    .5000 -   .4000   .67e-02 31
    .4000 -   .3000   .53e-02 17
    .3000 -   .2000   .70e-02 18
    .2000 -   .1000   .93e-02 19
    .1000 -   .0122   .25e-01 18
                                      energy spectra of laterally escaping electrons
                                    (number/mev, normalized to one incident particle)
0      e (mev)  length=      2.5400

   3.0000 -  2.9000   .37e-02 25
   2.9000 -  2.8000   .46e-01 10
   2.8000 -  2.7000   .60e-01  5
   2.7000 -  2.6000   .78e-01  6
   2.6000 -  2.5000   .87e-01  5
   2.5000 -  2.4000   .99e-01  7
   2.4000 -  2.3000   .98e-01  4
   2.3000 -  2.2000   .11e+00  5
   2.2000 -  2.1000   .11e+00  5
   2.1000 -  2.0000   .13e+00  5
   2.0000 -  1.9000   .13e+00  6
   1.9000 -  1.8000   .14e+00  6
   1.8000 -  1.7000   .14e+00  6
   1.7000 -  1.6000   .16e+00  5
   1.6000 -  1.5000   .15e+00  4
   1.5000 -  1.4000   .15e+00  5
   1.4000 -  1.3000   .15e+00  5
   1.3000 -  1.2000   .15e+00  5
   1.2000 -  1.1000   .16e+00  3
   1.1000 -  1.0000   .15e+00  5
   1.0000 -   .9000   .16e+00  3
    .9000 -   .8000   .14e+00  4
    .8000 -   .7000   .14e+00  3
    .7000 -   .6000   .13e+00  6
    .6000 -   .5000   .12e+00  5
    .5000 -   .4000   .11e+00  6
    .4000 -   .3000   .10e+00  5
    .3000 -   .2000   .88e-01  4
    .2000 -   .1000   .66e-01  9
    .1000 -   .0122   .40e-01 10
                                   angular distributions of transmitted and reflected electrons
                                       (number/sr, normalized to one incident particle)
0              phi(deg)=  0.000
         theta (deg)      180.000

    0.0000 - 30.0000  0.         99
   30.0000 - 60.0000  0.         99
   60.0000 - 90.0000  0.         99
   90.0000 -120.0000   .90e-03 12
  120.0000 -150.0000   .27e-02  9
  150.0000 -180.0000   .35e-02 13
                                     angular distributions of laterally escaping electrons
                                       (number/sr, normalized to one incident particle)
0              phi(deg)=  0.000
```

```
     theta (deg)       180.000

   0.0000 - 30.0000    .77e-01  2
  30.0000 - 60.0000    .56e-01  2
  60.0000 - 90.0000    .29e-01  2
  90.0000 -120.0000    .13e-01  2
 120.0000 -150.0000    .46e-02  7
0                                energy spectra and angular distributions of electrons transmitted and reflected
                                          azimuthal interval is   0.00000 to 180.00000 degrees
                                          (number/(mev$sr), normalized to one particle)
0       e (mev)  theta=  0.000       30.000       60.000       90.000       120.000       150.000
                        30.000       60.000       90.000      120.000       150.000       180.000

    3.0000 -   2.9000  0.         99 0.         99 0.         99 0.         99  .14e-03 99 0.         99
    2.9000 -   2.8000  0.         99 0.         99 0.         99 0.         99  .29e-03 67 0.         99
    2.8000 -   2.7000  0.         99 0.         99 0.         99  .21e-03 67 0.         99  .40e-03 99
    2.7000 -   2.6000  0.         99 0.         99 0.         99  .11e-03 99 0.         99 0.         99
    2.6000 -   2.5000  0.         99 0.         99 0.         99 0.         99  .14e-03 99 0.         99
    2.5000 -   2.4000  0.         99 0.         99 0.         99  .42e-03 41  .29e-03 99 0.         99
    2.4000 -   2.3000  0.         99 0.         99 0.         99  .32e-03 51  .29e-03 67 0.         99
    2.3000 -   2.2000  0.         99 0.         99 0.         99  .11e-03 99 0.         99 0.         99
    2.2000 -   2.1000  0.         99 0.         99 0.         99  .11e-03 99  .43e-03 51  .40e-03 99
    2.1000 -   2.0000  0.         99 0.         99 0.         99  .11e-03 99 0.         99  .40e-03 99
    2.0000 -   1.9000  0.         99 0.         99 0.         99 0.         99  .58e-03 55  .40e-03 99
    1.9000 -   1.8000  0.         99 0.         99 0.         99  .21e-03 99  .58e-03 41  .40e-03 99
    1.8000 -   1.7000  0.         99 0.         99 0.         99  .21e-03 99  .58e-03 41 0.         99
    1.7000 -   1.6000  0.         99 0.         99 0.         99  .53e-03 33  .72e-03 45  .16e-02 55
    1.6000 -   1.5000  0.         99 0.         99 0.         99  .11e-03 99  .10e-02 48  .40e-03 99
    1.5000 -   1.4000  0.         99 0.         99 0.         99  .64e-03 37  .58e-03 41  .40e-03 99
    1.4000 -   1.3000  0.         99 0.         99 0.         99  .53e-03 45  .58e-03 55  .40e-03 99
    1.3000 -   1.2000  0.         99 0.         99 0.         99  .32e-03 51  .58e-03 41  .16e-02 41
    1.2000 -   1.1000  0.         99 0.         99 0.         99  .42e-03 41  .43e-03 51  .28e-02 30
    1.1000 -   1.0000  0.         99 0.         99 0.         99  .11e-03 99  .13e-02 35  .12e-02 51
    1.0000 -    .9000  0.         99 0.         99 0.         99  .42e-03 55  .10e-02 30  .12e-02 51
     .9000 -    .8000  0.         99 0.         99 0.         99  .21e-03 67  .12e-02 25  .20e-02 33
     .8000 -    .7000  0.         99 0.         99 0.         99  .32e-03 51  .13e-02 39  .12e-02 51
     .7000 -    .6000  0.         99 0.         99 0.         99  .11e-03 99  .12e-02 25  .28e-02 43
     .6000 -    .5000  0.         99 0.         99 0.         99  .53e-03 33  .12e-02 17  .28e-02 52
     .5000 -    .4000  0.         99 0.         99 0.         99  .53e-03 45  .14e-02 33  .20e-02 33
     .4000 -    .3000  0.         99 0.         99 0.         99  .21e-03 67  .16e-02 25  .12e-02 51
     .3000 -    .2000  0.         99 0.         99 0.         99  .42e-03 55  .16e-02 37  .24e-02 37
     .2000 -    .1000  0.         99 0.         99 0.         99  .64e-03 37  .26e-02 25  .16e-02 41
     .1000 -    .0122  0.         99 0.         99 0.         99  .13e-02 34  .58e-02 26  .86e-02 18
0                                  energy spectra and angular distributions of electrons laterally escaping
                                          azimuthal interval is   0.00000 to 180.00000 degrees
                                          (number/(mev$sr), normalized to one particle)
0       e (mev)  theta=  0.000       30.000       60.000       90.000       120.000       150.000
                        30.000       60.000       90.000      120.000       150.000       180.000

    3.0000 -   2.9000   .40e-02 26  .14e-03 99 0.         99 0.         99 0.         99 0.         99
    2.9000 -   2.8000   .50e-01 10  .13e-02 39  .32e-03 71 0.         99 0.         99 0.         99
    2.8000 -   2.7000   .57e-01  7  .48e-02 23  .53e-03 33 0.         99 0.         99 0.         99
    2.7000 -   2.6000   .64e-01  7  .96e-02 13  .64e-03 37 0.         99 0.         99 0.         99
    2.6000 -   2.5000   .61e-01  8  .14e-01  9  .85e-03 41  .32e-03 51 0.         99 0.         99
    2.5000 -   2.4000   .63e-01  6  .18e-01 13  .14e-02 30  .42e-03 41 0.         99 0.         99
    2.4000 -   2.3000   .53e-01  7  .20e-01 10  .21e-02 22  .21e-03 67  .29e-03 67 0.         99
    2.3000 -   2.2000   .42e-01  9  .26e-01  7  .41e-02 15  .32e-03 51 0.         99 0.         99
    2.2000 -   2.1000   .38e-01  9  .28e-01  5  .49e-02  8  .42e-03 55  .29e-03 67 0.         99
    2.1000 -   2.0000   .47e-01 11  .30e-01  6  .66e-02 12  .74e-03 57  .14e-03 99 0.         99
```

```
 2.0000 -  1.9000   .41e-01  9   .18e-01  7   .68e-02 13   .18e-02 23   .14e-03 99 0.        99
 1.9000 -  1.8000   .32e-01 11   .33e-01  8   .86e-02 13   .16e-02 20   .29e-03 67 0.        99
 1.8000 -  1.7000   .31e-01 10   .31e-01 12   .11e-01  8   .17e-02 21 0.
9 0.      99
 1.7000 -  1.6000   .30e-01  8   .34e-01  6   .14e-01  9   .22e-02 21 0.          99 0.        99
 1.6000 -  1.5000   .22e-01 13   .31e-01  8   .16e-01  9   .24e-02 23   .10e-02 37   .40e-03 99
 1.5000 -  1.4000   .21e-01 12   .30e-01  7   .17e-01  8   .32e-02 22   .58e-03 41 0.        99
 1.4000 -  1.3000   .17e-01 12   .29e-01  6   .16e-01 10   .56e-02 12   .10e-02 48 0.        99
 1.3000 -  1.2000   .18e-01 21   .25e-01  8   .16e-01  7   .71e-02 13   .12e-02 25 0.        99
 1.2000 -  1.1000   .15e-01 17   .28e-01  6   .20e-01  6   .64e-02 12   .14e-02 26 0.        99
 1.1000 -  1.0000   .12e-01 16   .23e-01  5   .17e-01  7   .85e-02 13   .16e-02 29 0.        99
 1.0000 -   .9000   .12e-01 23   .21e-01  5   .20e-01  6   .98e-02  9   .36e-02 16 0.        99
  .9000 -   .8000   .11e-01 17   .17e-01 10   .16e-01  7   .99e-02 11   .26e-02 25   .40e-03 99
  .8000 -   .7000   .83e-02 18   .14e-01  8   .16e-01  8   .11e-01 12   .43e-02 19   .79e-03 67
  .7000 -   .6000   .75e-02 25   .12e-01 14   .16e-01  5   .10e-01 14   .39e-02 12   .12e-02 51
  .6000 -   .5000   .44e-02 37   .13e-01  9   .13e-01  9   .90e-02 13   .48e-02 13   .79e-03 67
  .5000 -   .4000   .44e-02 34   .13e-01 11   .13e-01 10   .84e-02 11   .39e-02 15   .79e-03 67
  .4000 -   .3000   .55e-02 29   .10e-01 12   .12e-01 11   .64e-02 14   .62e-02 17   .40e-03 99
  .3000 -   .2000   .16e-02 55   .67e-02 15   .92e-02 10   .94e-02  6   .45e-02  9   .28e-02 48
  .2000 -   .1000   .24e-02 37   .67e-02 25   .71e-02 14   .58e-02 14   .29e-02 28   .12e-02 51
  .1000 -   .0122   .90e-03 67   .20e-02 44   .48e-02 15   .48e-02 13   .17e-02 33   .90e-03 67
0                                        energy spectra of transmitted photons
                                 (number/mev, normalized to one incident particle)
0      e (mev)  length=      2.5400

 3.0000 -  2.9000  0.          99
 2.9000 -  2.8000  0.          99
 2.8000 -  2.7000  0.          99
 2.7000 -  2.6000   .28e-03 99
 2.6000 -  2.5000  0.          99
 2.5000 -  2.4000  0.          99
 2.4000 -  2.3000   .27e-03 99
 2.3000 -  2.2000   .28e-03 99
 2.2000 -  2.1000  0.          99
 2.1000 -  2.0000   .27e-03 99
 2.0000 -  1.9000   .54e-03 67
 1.9000 -  1.8000   .80e-03 51
 1.8000 -  1.7000   .27e-03 99
 1.7000 -  1.6000   .11e-02 55
 1.6000 -  1.5000   .18e-02 48
 1.5000 -  1.4000   .78e-03 51
 1.4000 -  1.3000   .10e-02 41
 1.3000 -  1.2000   .76e-03 51
 1.2000 -  1.1000   .21e-02 31
 1.1000 -  1.0000   .29e-02 25
 1.0000 -   .9000   .32e-02 24
  .9000 -   .8000   .36e-02 37
  .8000 -   .7000   .34e-02 48
  .7000 -   .6000   .44e-02 22
  .6000 -   .5000   .62e-02 14
  .5000 -   .4000   .82e-02 18
  .4000 -   .3000   .12e-01 15
  .3000 -   .2000   .18e-01  8
  .2000 -   .1000   .29e-01  8
  .1000 -   .0100   .58e-01  5
0                                          energy spectra of reflected photons
                                 (number/mev, normalized to one incident particle)
0      e (mev)  length=      2.5400

 3.0000 -  2.9000  0.          99
 2.9000 -  2.8000  0.          99
```

```
 2.8000 -  2.7000  0.         99
 2.7000 -  2.6000  0.         99
 2.6000 -  2.5000  0.         99
 2.5000 -  2.4000  0.         99
 2.4000 -  2.3000  0.         99
 2.3000 -  2.2000  0.         99
 2.2000 -  2.1000  0.         99
 2.1000 -  2.0000  0.         99
 2.0000 -  1.9000  0.         99
 1.9000 -  1.8000  0.         99
 1.8000 -  1.7000  0.         99
 1.7000 -  1.6000  0.         99
 1.6000 -  1.5000  0.         99
 1.5000 -  1.4000  0.         99
 1.4000 -  1.3000  0.         99
 1.3000 -  1.2000  0.         99
 1.2000 -  1.1000   .30e-03 99
 1.1000 -  1.0000   .63e-03 67
 1.0000 -   .9000   .31e-03 99
  .9000 -   .8000   .32e-03 99
  .8000 -   .7000   .93e-03 72
  .7000 -   .6000   .29e-03 99
  .6000 -   .5000   .29e-03 99
  .5000 -   .4000   .18e-02 36
  .4000 -   .3000   .23e-02 37
  .3000 -   .2000   .55e-02 33
  .2000 -   .1000   .19e-01  9
  .1000 -   .0100   .75e-01  7
                                       energy spectra of laterally escaping photons
                                      (number/mev, normalized to one incident particle)
0       e (mev)  length=      2.5400

 3.0000 -  2.9000  0.         99
 2.9000 -  2.8000  0.         99
 2.8000 -  2.7000  0.         99
 2.7000 -  2.6000  0.         99
 2.6000 -  2.5000   .31e-03 99
 2.5000 -  2.4000  0.         99
 2.4000 -  2.3000  0.         99
 2.3000 -  2.2000   .12e-02 77
 2.2000 -  2.1000   .93e-03 51
 2.1000 -  2.0000   .33e-03 99
 2.0000 -  1.9000   .12e-02 57
 1.9000 -  1.8000   .93e-03 51
 1.8000 -  1.7000   .63e-03 67
 1.7000 -  1.6000   .20e-02 37
 1.6000 -  1.5000   .29e-02 21
 1.5000 -  1.4000   .11e-02 41
 1.4000 -  1.3000   .66e-02 15
 1.3000 -  1.2000   .35e-02 40
 1.2000 -  1.1000   .76e-02 19
 1.1000 -  1.0000   .81e-02 19
 1.0000 -   .9000   .75e-02 22
  .9000 -   .8000   .11e-01 16
  .8000 -   .7000   .17e-01 17
  .7000 -   .6000   .20e-01  9
  .6000 -   .5000   .25e-01 13
  .5000 -   .4000   .38e-01  9
  .4000 -   .3000   .59e-01 10
  .3000 -   .2000   .96e-01  5
```

.2000 -	1000	.21e+00	3
.1000 -	0100	.77e+00	1

angular distributions of transmitted and reflected photon intensity
(mev/sr, normalized to one incident particle)

theta (deg)	phi(deg)= 0.000 180.000	
0.0000 - 30.0000	.60e-02	6
30.0000 - 60.0000	.12e-03	32
60.0000 - 90.0000	.69e-05	49
90.0000 -120.0000	.10e-03	32
120.0000 -150.0000	.23e-03	13
150.0000 -180.0000	.30e-03	12

angular distributions of laterally escaping photon intensity
(mev/sr, normalised to one incident particle)

theta (deg)	phi(deg)= 0.000 180.000	
0.0000 - 30.0000	.89e-02	6
30.0000 - 60.0000	.38e-02	4
60.0000 - 90.0000	.14e-02	7
90.0000 -120.0000	.53e-03	6
120.0000 -150.0000	.19e-03	11
150.0000 -180.0000	.32e-04	23

energy spectra and angular distributions of photons transmitted and reflected
azimuthal interval is 0.00000 to 180.00000 degrees
(number/(mev*sr), normalized to one particle)

e (mev) theta=	0.000 30.000		30.000 60.000		60.000 90.000		90.000 120.000		120.000 150.000		150.000 180.000	
3.0000 - 2.9000	0.	99	0.	99	0.	99	0.	99	0.	99	0.	99
2.9000 - 2.8000	0.	99	0.	99	0.	99	0.	99	0.	99	0.	99
2.8000 - 2.7000	0.	99	0.	99	0.	99	0.	99	0.	99	0.	99
2.7000 - 2.6000	.33e-03	99	0.	99	0.	99	0.	99	0.	99	0.	99
2.6000 - 2.5000	0.	99	0.	99	0.	99	0.	99	0.	99	0.	99
2.5000 - 2.4000	0.	99	0.	99	0.	99	0.	99	0.	99	0.	99
2.4000 - 2.3000	.33e-03	99	0.	99	0.	99	0.	99	0.	99	0.	99
2.3000 - 2.2000	.33e-03	99	0.	99	0.	99	0.	99	0.	99	0.	99
2.2000 - 2.1000	0.	99	0.	99	0.	99	0.	99	0.	99	0.	99
2.1000 - 2.0000	.32e-03	99	0.	99	0.	99	0.	99	0.	99	0.	99
2.0000 - 1.9000	.64e-03	67	0.	99	0.	99	0.	99	0.	99	0.	99
1.9000 - 1.8000	.95e-03	51	0.	99	0.	99	0.	99	0.	99	0.	99
1.8000 - 1.7000	.32e-03	99	0.	99	0.	99	0.	99	0.	99	0.	99
1.7000 - 1.6000	.13e-02	55	0.	99	0.	99	0.	99	0.	99	0.	99
1.6000 - 1.5000	.22e-02	48	0.	99	0.	99	0.	99	0.	99	0.	99
1.5000 - 1.4000	.92e-03	51	0.	99	0.	99	0.	99	0.	99	0.	99
1.4000 - 1.3000	.12e-02	41	0.	99	0.	99	0.	99	0.	99	0.	99
1.3000 - 1.2000	.91e-03	51	0.	99	0.	99	0.	99	0.	99	0.	99
1.2000 - 1.1000	.21e-02	37	.13e-03	99	0.	99	0.	99	.13e-03	99	0.	99
1.1000 - 1.0000	.35e-02	25	0.	99	0.	99	0.	99	.27e-03	67	0.	99
1.0000 - .9000	.35e-02	25	.11e-03	99	0.	99	.97e-04	99	0.	99	0.	99
.9000 - .8000	.40e-02	37	.12e-03	99	0.	99	.10e-03	99	0.	99	0.	99
.8000 - .7000	.33e-02	42	.26e-03	99	0.	99	.30e-03	72	0.	99	0.	99
.7000 - .6000	.52e-02	22	0.	99	0.	99	.92e-04	99	0.	99	0.	99
.6000 - .5000	.74e-02	14	0.	99	0.	99	.93e-04	99	0.	99	0.	99
.5000 - .4000	.91e-02	15	.22e-03	69	0.	99	.95e-04	99	.40e-03	51	.64e-03	67
.4000 - .3000	.13e-01	16	.44e-03	56	0.	99	.37e-03	56	.37e-03	51	.36e-03	99
.3000 - .2000	.19e-01	9	.74e-03	37	.93e-04	99	.53e-03	56	.13e-02	29	.97e-03	52
.2000 - .1000	.31e-01	6	.81e-03	40	.17e-03	68	.81e-03	29	.40e-02	9	.91e-02	19
.1000 - .0100	.63e-01	5	.14e-02	26	.42e-03	41	.33e-02	14	.17e-01	9	.29e-01	9

```
     integral (/sr)   .17e-01  4  .41e-03 19  .64e-04 36  .55e-03 17  .22e-02  9  .37e-02  5
                              energy spectra and angular distributions of photons laterally escaping
                                        azimuthal interval is    0.00000 to 180.00000 degrees
                                          (number/(mev*sr), normalized to one particle)
       e (mev)  theta=  0.000        30.000       60.000       90.000      120.000      150.000
                       30.000        60.000       90.000      120.000      150.000      180.000

   3.0000 -  2.9000  0.          99 0.          99 0.          99 0.          99 0.          99 0.          99
   2.9000 -  2.8000  0.          99 0.          99 0.          99 0.          99 0.          99 0.          99
   2.8000 -  2.7000  0.          99 0.          99 0.          99 0.          99 0.          99 0.          99
   2.7000 -  2.6000  0.          99 0.          99 0.          99 0.          99 0.          99 0.          99
   2.6000 -  2.5000   .37e-03 99 0.          99 0.          99 0.          99 0.          99 0.          99
   2.5000 -  2.4000  0.          99 0.          99 0.          99 0.          99 0.          99 0.          99
   2.4000 -  2.3000  0.          99 0.          99 0.          99 0.          99 0.          99 0.          99
   2.3000 -  2.2000   .10e-02 71  .13e-03 99 0.          99 0.          99 0.          99 0.          99
   2.2000 -  2.1000   .11e-02 51 0.          99 0.          99 0.          99 0.          99 0.          99
   2.1000 -  2.0000  0.          99  .14e-03 99 0.          99 0.          99 0.          99 0.          99
   2.0000 -  1.9000   .32e-03 99  .26e-03 67  .10e-03 99 0.          99 0.          99 0.          99
   1.9000 -  1.8000   .75e-03 67  .13e-03 99 0.          99 0.          99 0.          99 0.          99
   1.8000 -  1.7000   .36e-03 99 0.          99 0.          99  .11e-03 99 0.          99 0.          99
   1.7000 -  1.6000   .14e-02 41  .25e-03 67  .92e-04 99 0.          99 0.          99 0.          99
   1.6000 -  1.5000   .31e-02 26  .13e-03 99 0.          99 0.          99 0.          99 0.          99
   1.5000 -  1.4000  0.          99  .49e-03 41 0.          99 0.          99 0.          99 0.          99
   1.4000 -  1.3000   .25e-02 22  .17e-02 23  .20e-03 67 0.          99 0.          99 0.          99
   1.3000 -  1.2000   .20e-02 50  .41e-03 70  .29e-03 51 0.          99 0.          99 0.          99
   1.2000 -  1.1000   .53e-02 29  .13e-02 25  .10e-03 99 0.          99 0.          99 0.          99
   1.1000 -  1.0000   .24e-02 22  .17e-02 23  .58e-03 45  .99e-04 99 0.          99 0.          99
   1.0000 -   .9000   .29e-02 46  .18e-02 16  .19e-03 67  .10e-03 99 0.          99 0.          99
    .9000 -   .8000   .56e-02 30  .14e-02 21  .86e-03 25  .94e-04 99 0.          99 0.          99
    .8000 -   .7000   .85e-02 20  .31e-02 26  .49e-03 33  .19e-03 67  .14e-03 99 0.          99
    .7000 -   .6000   .79e-02 17  .41e-02  9  .12e-02 33  .18e-03 67 0.          99 0.          99
    .6000 -   .5000   .10e-01 14  .38e-02 19  .21e-02 24  .30e-03 51  .14e-03 99 0.          99
    .8000 -   .3000   .25e-01 19  .00e-02 10  .33e-02 15  .80e-03 24  .40e-03 99 0.          99
    .3000 -   .2000   .23e-01 10  .16e-01  7  .76e-02 10  .35e-02 13  .15e-02 21 0.          99
    .2000 -   .0000   .59e+00  8  .33e+00  4  .65e-01  8  .80e-02 18  .37e-02 18  .88e-03 88
     integral (/sr)   .32e-01  3  .19e-01  2  .91e-02  3  .50e-02  5  .22e-02  7  .59e-03 18
 the number of eca words used for statistics is        1017
4dd//
end

 all done
```

```
'ou.put'ti, i1 1.0
.03 lines. (.20s)
 1 0o c t o b e r  1 4  , 1 9 7 6  v e r s i o n
 2 0 nset  matl
 3      4      3
 4 0 nmat  ntab
 5      1      1
 6 0mpair  mtax
 7     25     41
 8 0gamma ray cross section data
 9 0energies (mev)
10  1000.000000  800.000000  600.000000  500.000000  400.000000  300.000000
11   200.000000  150.000000  100.000000   80.000000   60.000000   50.000000
12    40.000000   30.000000   20.000000   15.000000   10.000000    8.000000
13     6.000000    5.000000    4.000000    3.000000    2.000000    1.500000
14     1.000000     .800000     .600000     .500000     .400000     .300000
15      .200000     .150000     .100000     .080000     .060000     .050000
16      .040000     .030000     .020000     .015000     .010000
17 0total attenuation coefficients (cm2/g)
18      .133015     .115792     .097314     .087552     .077436     .067025
19      .056529     .051401     .046420     .044377     .042060     .040625
20      .038802     .036353     .033322     .031958     .030918     .030686
21      .030945     .031565     .032919     .035741     .041882     .047769
22      .058536     .065369     .075103     .082004     .091659     .107638
23     4.600069   10.000378   33.080263   73.005968  215.000128    2.456969
25 0ratio of scattering plus pair production to total attenuation coefficients
26      .999999     .999998     .999997     .999996     .999995     .999992
27      .999986     .999979     .999965     .999955     .999936     .999920
28      .999895     .999849     .999747     .999641     .999422     .999249
30      .988950     .988787     .988300     .089785     .900000     .008000
32      .034460     .015642     .005116     .002345     .000818
33 0ratio of scattering to scattering plus pair production attenuation coefficients
34      .001662     .002382     .003765     .005007     .007046     .010778
35      .018909     .027362     .044314     .056913     .077841     .094684
36      .120290     .163683     .248185     .323842     .453488     .536768
37      .651019     .722340     .802503     .886979     .963836     .991964
38     1.000000
39 0k shell ionization data
40 0binding energy (mev), photoeffect efficiency and fluorescent efficiency
41      .008981     .871336     .392853
42 0k x-ray energies (mev)
43      .008150     .008150     .008150     .008150
44 0k x-ray accumulated relative intensities
45     1.000000    1.000000    1.000000    1.000000
46 0auger electron energies (mev)
47      .008150     .008150     .008150
48 0auger electron accumulated relative intensities
49     1.000000    1.000000    1.000000
50 0 nmat  ntab
51      2      1
52 0mpair  mtax
53     25     41
54 0gamma ray cross section data
55 0energies (mev)
56  1000.000000  800.000000  600.000000  500.000000  400.000000  300.000000
57   200.000000  150.000000  100.000000   80.000000   60.000000   50.000000
58    40.000000   30.000000   20.000000   15.000000   10.000000    8.000000
59     6.000000    5.000000    4.000000    3.000000    2.000000    1.500000
60     1.000000     .800000     .600000     .500000     .400000     .300000
.t23,24
23      .146661     .205315     .421761     .705562    1.487422    2.456969
24     4.613069   10.492178   33.180213   73.691769  215.150145
.t61,121
```

```
     .0200000   .0300000   .0200000   .0080000   .0000000    .050000
@total attenuation coefficients (cm2/g)
     .042664    .037443    .031861    .028924    .025899    .022819
     .019793    .018395    .017194    .016805    .016488    .016362
     .016276    .016313    .016918    .017921    .020146    .021802
     .024515    .026632    .029693    .034451    .042729    .049688
     .061023    .067886    .077309    .083599    .091601    .102329
     .117953    .129244    .146076    .157139    .177347    .197927
     .240815    .359073    .869633   1.932250   6.538229
@ratio of scattering plus pair production to total attenuation coefficients
    1.000000   1.000000   1.000000   1.000000   1.000000   1.000000
    1.000000    .999999    .999999    .999999    .999998    .999998
     .999997    .999996    .999994    .999993    .999990    .999988
     .999985    .999983    .999979    .999974    .999962    .999947
     .999908    .999868    .999775    .999673    .999458    .998892
     .996690    .992470    .974912    .951171    .888740    .819442
     .694128    .480603    .205262    .094029    .028300
@ratio of scattering to scattering plus pair production attenuation coefficients
     .005449    .007745    .012092    .015937    .022153    .033290
     .056784    .080393    .125794    .158022    .208788    .247184
     .301520    .383491    .513893    .607020    .731386    .793818
     .863227    .899113    .933997    .965506    .990010    .997897
    1.000000
@k shell ionization data
@binding energy (mev), photoeffect efficiency and fluorescent efficiency
     .000687    .831990    .003376
@k x-ray energies (mev)
     .000687    .000687    .000687    .000687
@k x-ray accumulated relative intensities
    1.000000   1.000000   1.000000   1.000000
@auger electron energies (mev)
     .000687    .000687    .000687
@auger electron accumulated relative intensities
    1.000000   1.000000   1.000000
@ nmat  ntab
     3     1
@mpair  mtax
    25    41
@gamma ray cross section data
@energies (mev)
 1000.000000  800.000000  600.000000  500.000000  400.000000  300.000000
  200.000000  150.000000  100.000000   80.000000   60.000000   50.000000
   40.000000   30.000000   20.000000   15.000000   10.000000    8.000000
                                                                    105     6.000000    5.000000    4.000000    3.000000    2
.000000    1.500000
    1.000000    .800000    .600000    .500000    .400000    .300000
     .200000    .150000    .100000    .080000    .060000    .050000
     .040000    .030000    .020000    .015000    .010000
@total attenuation coefficients (cm2/g)
     .047459    .040496    .033058    .029154    .025144    .021091
     .017198    .015493    .014218    .013934    .013862    .013935
     .024632    .027080    .030386    .036988    .048948    .081088
     .063513    .070654    .080455    .086995    .095307    .106425
     .182696    .232780    .389852    .759228   2.280880    .178754
@ratio of scattering plus pair production to total attenuation coefficients
    1.000000   1.000000   1.000000   1.000000   1.000000   1.000000
    1.000000   1.000000   1.000000   1.000000    .999999    .999999
     .999999    .999999    .999998    .999998    .999997    .999997
     .999996    .999995    .999994    .999993    .999990    .999986
```

```
      .999996     .999995     .999994     .999993     .999990     .999986
      .999976     .999966     .999942     .999915     .999859     .999710
      .999123     .997987     .993163     .986454     .967663     .944418
      .894285     .773048     .479415     .262940     .086410
0ratio of scattering to scattering plus pair production attenuation coefficients
      .005099     .007454     .012130     .016458     .023751     .037489
      .068025     .099356     .158345     .198381     .258494     .302099
      .361954     .449719     .584721     .675399     .786023     .838082
      .894243     .922718     .950047     .974365     .992814     .998465
     1.000000
0k shell ionization data
0binding energy (mev), photoeffect efficiency and fluorescent efficiency
      .000284     .958303     .000382
0k x-ray energies (mev)
      .000284     .000284     .000284     .000284
0k x-ray accumulated relative intensities
     1.000000    1.000000    1.000000    1.000000
0auger electron energies (mev)
      .000284     .000284     .000284
0auger electron accumulated relative intensities
     1.000000    1.000000    1.000000
1number of sets on datapac tape =   3
0input from datapac

  ##4 mev electron beam into bare fx-100 faraday cup##
0 nrun  itre  izip  isgn  isub  inel  icyc  ncyc  nmax       emax            emin            rmax        lmat
     1     5     0     1    17     1     1     8    64  4.0000000e+00  1.5625000e-02  2.7291480e+00     1

 dataprep data for datapac set   1    64    33    17   121  2.729148e+00
0 nrun  itre  izip  isgn  isub  inel  icyc  ncyc  nmax       emax            emin            rmax        lmat
     2     5     0     1    11     1     1     8    64  4.0000000e+00  1.5625000e-02  2.3896380e+00     2

 dataprep data for datapac set   2    64    33    11   121  2.389638e+00
0 nrun  itre  izip  isgn  isub  inel  icyc  ncyc  nmax       emax            emin            rmax        lmat
     3     5     0     1     3     1     1     8    64  4.0000000e+00  1.5625000e-02  2.2837680e+00     1

 dataprep data for datapac set   3    64    33     3   121  2.283768e+00

 collision / total de/dx ratios for datapac set   3

 cumulative bremsstrahlung cross sections for datapac set   3

 cumulative bremsstrahlung angular distributions for datapac set   3

 lengauss - equiprobable endpoints for interpolation

 k x-ray production for datapac set   3

 photoelectron angular distributions

 pair electron energy division distribution (lead)
0 nrun   inc  iatrg  inok  inel  iphot  ibad  idas  ipun  itape
      4     1     1     1     2     1     1     1     2     2
0 zone  material  left plane  right plane  inner cylinder  outer cylinder    ecut       ptcz
     1      1     0.          .25400e+01    0.               .14350e-01   .100e-01   0.
     2      2     0.          .25400e+01     .14350e-01      .94000e-01   .100e-01   0.
     3      1     0.          .25400e+01     .94000e-01      .11900e+00   .100e-01   0.
     4      3     0.          .25400e+01     .11900e+00      .75000e+00   .100e-01   0.
0incident electrons
```

```
181 @electron collision and radiation energy loss straggling
182 @knock-on electron production
183 @no coupled inelastic scattering deflections
188 @bremsstrahlung [illegible] distribution
186 @photon-produced particles followed
187 @ iunt  imax  itmk  jmax  ipmk jpmax  iamk  kmax  ibmk kpmax
188      2     1     1    40     1    40     1     6     1     6
189 @ imax  nzon iflux  ncyc  inran
190  30000     4     2   -1100000000000000000
191 @$$$$$$$$$$$$$$$ the standard error estimates are based on    10 batches of  3000 histories $$$$$$$$$$$$$$$
192 @     4.00000     [illegible]
194 @$$$$$$$$$$$$$$electron cut-off energy below electron energy list. cut-off energy has been changed to em(nmax)$$$$$$$$$$
195 $$$$
196 @       tsave                                   tmfac        rlan        qblk
197        .01633                                10.00000      .50000     1.00000
198 @electron energy classifications (mev)
199       3.90000     3.80000     3.70000     3.60000     3.50000     3.40000
200       3.30000     3.20000     3.10000     3.00000     2.90000     2.80000
201       2.70000     2.60000     2.50000     2.40000     2.30000     2.20000
202       2.10000     2.00000     1.90000     1.80000     1.70000     1.60000
203       1.50000     1.40000     1.30000     1.20000     1.10000     1.00000
204        .90000      .80000      .70000      .60000      .50000      .40000
205        .30000      .20000      .10000      .01633
206 @photon energy classifications (mev)
207       3.90000     3.80000     3.70000     3.60000     3.50000     3.40000
208       3.30000     3.20000     3.10000     3.00000     2.90000     2.80000
209       2.70000     2.60000     2.50000     2.40000     2.30000     2.20000
210       2.10000     2.00000     1.90000     1.80000     1.70000     1.60000
211       1.50000     1.40000     1.30000     1.20000     1.10000     1.00000
212        .90000      .80000      .70000      .60000      .50000      .40000
213        .30000      .20000      .10000      .01000
214 @electron obliquity classifications (degrees)
215      30.00000    60.00000    90.00000   120.00000   150.00000   180.00000
216 @electron azimuth classifications (degrees)
217     180.00000
218 @photon obliquity classifications (degrees)
219      30.00000    60.00000    90.00000   120.00000   150.00000   180.00000
220 @photon azimuth classifications (degrees)
221     180.00000
222 @ntfst        rgmax     scale skale       tcut        tpcut        tfcut         tsave        dlim        bnum       xnum
223      1     .27291e+01     1     1      .01633       .01000      0.00000        .01633     1.00000         0.0        0.0
224 @k x-ray quanta not followed in material     1
225 @ntfst        rgmax     scale skale       tcut        tpcut        tfcut         tsave        dlim        bnum       xnum
226      1     .23896e+01     1     1      .01633       .01000      0.00000        .01633     1.00000         0.0        0.0
227 @k x-ray quanta not followed in material     2
228 @ntfst        rgmax     scale skale       tcut        tpcut        tfcut         tsave        dlim        bnum       xnum
229      1     .22838e+01     1     1      .01633       .01000      0.00000        .01633     1.00000         0.0        0.0
230 @k x-ray quanta not followed in material     3
231 @annihilation quanta followed
232 1the problem is 100  per cent complete.  time to finish is       0.000 seconds. average time per batch is      208.338
233 @average source energy = 4.0000e+00 mev
234 @     inran          irn           irc
235  @@@@@@@@@@@@@@@@ 5264073242715201 6415355352001645
236 @  ---------------------------------- histories ------------------------------------         rej        --- steps ----
237       prim      sec     knock       p e      pair      com     auger      brem      rad      xray      land      prim       sec
238      30000   313094    311758       716         0      620         0      7925    14570         0      9747   1258552   3304719
239 @                              energy (mev)       ave energy (mev)      number/primary      number generated
240  first knock (above tcut)      6.3309e-01         6.6399e-02          9.5346e+00            286039
.t192,193
192 @       tin        tcut       tpcut       cthin       sorcin
193     4.00000      .01000      .01000     1.00000       .74900
.
```

```
total knock (above tcut)     6.6193e-01          6.3697e-02          1.0392e+01          311758
photo-electron               1.2560e-03          2.1085e-02          5.9567e-02            1787
pair                         0.                  0.                  0.                       0
compton                      3.5322e-03          5.3410e-02          6.6133e-02            1984
auger                        0.                  0.                  0.                       0
first bremsstrahlung         5.6152e-02          1.4605e-01          3.8447e-01           11534
total bremsstrahlung         5.6837e-02          1.1716e-01          4.8513e-01           14554
k x-ray                      0.                  0.                  0.                       0
annihilation quanta          0.                  0.                  0.                       0
0unscattered primary photons number and energy
 0.        99 0.      99
0number coefficients - knock-ons, photon descendants
0                                                         transmission
  .33e-04 99
  .13e-03 41
0                                                          reflection
  .27e-02 12
 0.        99
0                                                        lateral escape
  .16e-01  4
  .33e-03 30
0                                                number and energy coefficients
0                                                         transmission
0           cylinder dimensions       ---------- electron ----------      ----------- photon -----------
          length(cm)  radius(cm)       number      energy       counts      number      energy       counts

            .254e+01    .750e+00   .17e-03 45  .29e-04 58           5   .27e-01  2  .28e-02  6       1786
0                                                          reflection
0           cylinder dimensions       ---------- electron ----------      ----------- photon -----------
          length(cm)  radius(cm)       number      energy       counts      number      energy       counts

            .254e+01    .750e+00   .77e-02  6  .19e-02  6         232   .90e-02  6  .29e-03 14        456
0                                                        lateral escape
0           cylinder dimensions       ---------- electron ----------      ----------- photon -----------
          length(cm)  radius(cm)       number      energy       counts      number      energy       counts

            .254e+01    .750e+00   .44e+00  1  .20e+00  0       13159   .17e+00  2  .96e-02  3       7545
1                                                       energy deposition
                                                (normalized to one incident particle)
0                                                                                   energy deposition (mev)
        zone       material      mass(gm)    volume(cc)                          prim        knock           g-sec            to
tal

           1           1          .1471e-01      .1643e-02                    .2863e-02  8  -.4870e-04 99   .3659e-04 31    .2
851e-02  9
           2           2          .1584e+00      .6886e-01                    .4473e-01  3  -.2799e-03 66   .9692e-04 29    .4
455e-01  3
           3           1          .3803e+00      .4249e-01                    .7962e-01  2   .2633e-03 99   .1080e-02  7    .8
097e-01  2
           4           3          .8314e+01      .4376e+01                    .3023e+01  0  -.7369e-02  5   .3490e-02  7    .3
019e+01  0
0                                                            total            .3150e+01  0  -.7435e-02  4   .4703e-02  6    .3
148e+01  0
0                                                      charge distribution
                                                (normalized to one incident particle)
0                                                                            electrons
        zone       material      zl          zr          ri          r0          prim        knock         g-sec         total

           1           1       0.          .254e+01    0.          .144e-01    .10e-02 23 -.10e-03 99  .33e-04 99  .97e-03 3
7
.
```

```
   8    2   0.      .254e+01   .144e-01   .940e-01   .13e-01  6 -.53e-03 99 -.31e-04 99  .12e-01
   9
   3    1   0.      .254e+01   .940e-01   .119e+00   .27e-01  5 -.33e-03 99 -.23e-03 48  .26e-01
   4
   4    3   0.      .254e+01   .119e+00   .750e+00   .53e+00  0 -.19e-01  5 -.23e-03 57  .51e+00
 0
 0                        total                      .57e+00  0 -.20e-01  4 -.47e-03 19  .55e+00
 0
 0                                energy spectra of transmitted electrons
                        (number/mev, normalized to one incident particle)
 0      e (mev)  length=      2.5400

     4.0000 -  3.9000  0.       99
     3.9000 -  3.8000  0.       99
     3.8000 -  3.7000  0.       99
     3.7000 -  3.6000  0.       99
  18 3.800000 -3.9000000.0.     9999
     3.4000 -  3.3000  0.       99
     3.3000 -  3.2000  0.       99
     3.2000 -  3.1000  0.       99
     3.1000 -  3.0000  0.       99
     3.0000 -  2.9000  0.       99
     2.9000 -  2.8000  0.       99
     2.8000 -  2.7000  0.       99
     2.7000 -  2.6000  0.       99
     2.6000 -  2.5000  0.       99
     2.5000 -  2.4000  0.       99
     2.4000 -  2.3000  0.       99
     2.3000 -  2.2000  0.       99
     2.2000 -  2.1000  0.       99
     2.1000 -  2.0000  0.       99
     2.0000 -  1.9000  0.       99
     1.9000 -  1.8000   .33e-03 99
     1.8000 -  1.7000  0.       99
     1.7000 -  1.6000  0.       99
     1.6000 -  1.5000  0.       99
     1.5000 -  1.4000  0.       99
     1.4000 -  1.3000  0.       99
     1.3000 -  1.2000  0.       99
     1.2000 -  1.1000  0.       99
     1.1000 -  1.0000  0.       99
     1.0000 -   .9000   .33e-03 99
      .9000 -   .8000  0.       99
      .8000 -   .7000  0.       99
      .7000 -   .6000  0.       99
      .6000 -   .5000  0.       99
      .5000 -   .4000   .33e-03 99
      .4000 -   .3000  0.       99
      .3000 -   .2000   .33e-03 99
      .2000 -   .1000   .33e-03 99
      .1000 -   .0163  0.       99
 0                                energy spectra of reflected electrons
                        (number/mev, normalized to one incident particle)
 0      e (mev)  length=      2.5400

     4.0000 -  3.9000  0.       99
     3.9000 -  3.8000  0.       99
     3.8000 -  3.7000  0.       99
     3.7000 -  3.6000   .33e-03 99
```

```
361    3.6000 -   3.5000    .67e-03 39
362    3.5000 -   3.4000    .33e-03 99
363    3.4000 -   3.3000   0.        99
364    3.3000 -   3.2000   0.        99
365    3.2000 -   3.1000    .67e-03 67
366    3.1000 -   3.0000    .67e-03 67
367    3.0000 -   2.9000    .33e-03 99
368    2.9000 -   2.8000    .10e-02 71
369    2.8000 -   2.7000    .67e-03 67
370    2.7000 -   2.6000    .33e-03 99
371    2.6000 -   2.5000    .13e-02 55
372    2.5000 -   2.4000    .13e-02 41
373    2.4000 -   2.3000    .67e-03 67
374    2.3000 -   2.2000    .10e-02 51
375    2.2000 -   2.1000    .67e-03 67
376    2.1000 -   2.0000    .13e-02 41
377    2.0000 -   1.9000    .10e-02 71
378    1.9000 -   1.8000    .13e-02 41
379    1.8000 -   1.7000    .23e-02 43
380    1.7000 -   1.6000    .30e-02 35
381    1.6000 -   1.5000    .17e-02 45
382    1.5000 -   1.4000    .20e-02 37
383    1.4000 -   1.3000    .33e-02 21
384    1.3000 -   1.2000    .17e-02 45
385    1.2000 -   1.1000    .20e-02 27
386    1.1000 -   1.0000    .33e-02 33
388    1.0000 -    .8000    .37e-02 39
389     .8000 -    .7000    .10e-02 51
390     .7000 -    .6000    .33e-02 30
391     .6000 -    .5000    .23e-02 37
392     .5000 -    .4000    .47e-02 32
393     .4000 -    .3000    .23e-02 30
394     .3000 -    .2000    .47e-02 27
395     .2000 -    .1000    .67e-02 22
396     .1000 -    .0163    .17e-01  8
398                                        (nmbogdmopochosmofitaiebolàgoiaupdagtopuctroie)
399 0      e (mev)  length=      2.5400
400
401    4.0000 -   3.9000    .33e-03 99
402    3.9000 -   3.8000    .23e-01 11
403    3.8000 -   3.8000    .59e-01 10
405    3.6000 -   3.5000    .61e-01  5
406    3.5000 -   3.4000    .63e-01  8
407    3.4000 -   3.3000    .79e-01  9
408    3.3000 -   3.2000    .95e-01  3
409    3.2000 -   3.1000    .96e-01  5
410    3.1000 -   3.0000    .97e-01  4
411    3.0000 -   2.9000    .11e+00  6
412    2.9000 -   2.8000    .11e+00  6
413    2.8000 -   2.7000    .12e+00  5
414    2.7000 -   2.6000    .12e+00  4
415    2.6000 -   2.5000    .12e+00  4
416    2.5000 -   2.4000    .12e+00  4
417    2.4000 -   2.3000    .13e+00  4
418    2.3000 -   2.2000    .14e+00  6
419    2.2000 -   2.1000    .13e+00  6
420    2.1000 -   2.0000    .14e+00  4
.t397,398
397                                          energy spectra of laterally escaping electrons
398                                        (number/mev, normalized to one incident particle)
.
```

```
  2.1000 -  1.9000   .15e+00  3
  1.9000 -  1.8000   .15e+00  5
  1.8000 -  1.7000   .14e+00  5
  1.7000 -  1.6000   .14e+00  7
  1.6000 -  1.5000   .14e+00  4
  1.5000 -  1.4000   .16e+00  4
  1.4000 -  1.3000   .15e+00  4
  1.3000 -  1.2000   .15e+00  6
  1.2000 -  1.1000   .15e+00  3
  1.1000 -  1.0000   .15e+00  3
  1.0000 -   .9000   .15e+00  5
   .9000 -   .8000   .14e+00  5
   .8000 -   .7000   .14e+00  7
   .7000 -   .6000   .12e+00  9
   .6000 -   .5000   .12e+00  5
   .5000 -   .4000   .11e+00  6
   .4000 -   .3000   .10e+00  5
   .3000 -   .2000   .80e-01  5
   .2000 -   .1000   .64e-01  6
   .1000 -   .0163   .43e-01  6
                                  angular distributions of transmitted and reflected electrons
                                       (number/sr, normalized to one incident particle)
            phi(deg)=  0.000
     theta (deg)     180.000

  0.0000 - 30.0000   .12e-03 51
 30.0000 - 60.0000   .29e-04 67
 60.0000 - 90.0000  0.        99
 90.0000 -120.0000   .56e-03 13
120.0000 -150.0000   .18e-02  9
150.0000 -180.0000   .21e-02 15
                                    angular distributions of laterally escaping electrons
                                       (number/sr, normalized to one incident particle)
            phi(deg)=  0.000
     theta (deg)     180.000

  0.0000 - 30.0000   .11e+00  2
 30.0000 - 60.0000   .74e-01  1
 60.0000 - 90.0000   .35e-01  1
 90.0000 -120.0000   .16e-01  3
120.0000 -150.0000   .62e-02  3
150.0000 -180.0000   .11e-02 17
                             energy spectra and angular distributions of electrons transmitted and reflected
                                   azimuthal interval is   0.00000 to 180.00000 degrees
                                     (number/(mev*sr), normalized to one particle)
      e (mev)  theta=  0.000      30.000      60.000      90.000     120.000     150.000
                      30.000      60.000      90.000     120.000     150.000     180.000

  4.0000 -  3.9000  0.        99 0.        99 0.        99 0.        99 0.        99 0.        99
  3.9000 -  3.8000  0.        99 0.        99 0.        99 0.        99 0.        99 0.        99
  3.8000 -  3.7000  0.        99 0.        99 0.        99 0.        99 0.        99 0.        99
  3.7000 -  3.6000  0.        99 0.        99 0.        99 0.        99 0.        99  .40e-03 99
  3.6000 -  3.5000  0.        99 0.        99 0.        99 0.        99  .14e-03 99  .40e-03 99
  3.5000 -  3.4000  0.        99 0.        99 0.        99  .11e-03 99 0.        99 0.        99
  3.4000 -  3.3000  0.        99 0.        99 0.        99 0.        99 0.        99 0.        99
  3.3000 -  3.2000  0.        99 0.        99 0.        99 0.        99 0.        99 0.        99
  3.2000 -  3.1000  0.        99 0.        99 0.        99  .11e-03 99  .14e-03 99 0.        99
  3.1000 -  3.0000  0.        99 0.        99 0.        99  .11e-03 99  .14e-03 99 0.        99
  3.0000 -  2.9000  0.        99 0.        99 0.        99 0.        99  .14e-03 99 0.        99
  2.9000 -  2.8000  0.        99 0.        99 0.        99 0.        99  .14e-03 99  .79e-03 99
```

```
2.8000 - 2.7000  0.        99 0.        99 0.        99 0.        99  .14e-03 99  .40e-03 99
2.7000 - 2.6000  0.        99 0.        99 0.        99  .11e-03 99 0.        99 0.        99
2.6000 - 2.5000  0.        99 0.        99 0.        99  .32e 03 51 0.        99  .40e-03 99
2.5000 - 2.4000  0.        99 0.        99 0.        99  .21e-03 67  .29e-03 67 0.        99
2.4000 - 2.3000  0.        99 0.        99 0.        99  .11e-03 99  .14e-03 99 0.        99
2.3000 - 2.2000  0.        99 0.        99 0.        99 0.        99  .29e-03 67  .40e-03 99
2.2000 - 2.1000  0.        99 0.        99 0.        99  .11e-03 99 0.        99  .40e-03 99
2.1000 - 2.0000  0.        99 0.        99 0.        99  .11e-03 99  .43e-03 51 0.        99
2.0000 - 1.9000  0.        99 0.        99 0.        99  .21e-03 67 0.        99  .40e-03 99
1.9000 - 1.8000   .40e-03 99 0.        99 0.        99  .11e-03 99  .14e-03 99  .79e-03 67
1.8000 - 1.7000  0.        99 0.        99 0.        99  .11e-03 99  .72e-03 54  .40e-03 99
1.7000 - 1.6000  0.        99 0.        99 0.        99  .21e-03 67  .87e-03 37  .40e-03 99
1.6000 - 1.5000  0.        99 0.        99 0.        99 0.        99  .58e-03 55  .40e-03 99
1.5000 - 1.4000  0.        99 0.        99 0.        99  .11e-03 99  .43e-03 51  .79e-03 67
1.4000 - 1.3000  0.        99 0.        99 0.        99  .32e-03 51  .72e-03 33  .79e-03 67
1.3000 - 1.2000  0.        99 0.        99 0.        99  .21e-03 67  .29e-03 99  .40e-03 99
1.2000 - 1.1000  0.        99 0.        99 0.        99  .11e-03 99  .29e-03 67  .12e-02 51
1.1000 - 1.0000  0.        99 0.        99 0.        99  .21e-03 67  .10e-02 48  .40e-03 99
1.0000 -  .9000  0.        99  .14e-03 99 0.        99 0.        99  .43e-03 51  .79e-03 67
 .9000 -  .8000  0.        99 0.        99 0.        99  .32e-03 51  .87e-03 27  .79e-03 99
 .8000 -  .7000  0.        99 0.        99 0.        99  .11e-03 99  .29e-03 67 0.        99
 .7000 -  .6000  0.        99 0.        99 0.        99 0.21e-03 99  .83e-03 74  .70e-03 67
 .5000 -  .4000   .40e-03 99 0.        99 0.        99  .21e-03 67  .12e-02 45  .16e-02 41
 .4000 -  .3000  0.        99 0.        99 0.        99  .21e-03 67  .72e-03 33 0.        99
 .3000 -  .2000   .40e-03 99 0.        99 0.        99  .42e-03 41  .10e-02 30  .12e-02 71
 .2000 -  .1000  0.        99  .14e-03 99 0.        99  .64e-03 44  .14e-02 26  .16e-02 55
 .1000 -  .0163  0.        99 0.        99 0.        99  .76e-03 44  .45e-02 16  .47e-02 30
                     energy spectra and angular distributions of electrons laterally escaping
                          azimuthal interval is   0.00000 to 180.00000 degrees
                           (number/(mev*sr), normalized to one particle)
     e (mev)  theta=  0.000      30.000      60.000      90.000     120.000     150.000
                     30.000      60.000      90.000     120.000     150.000     180.000

4.0000 - 3.9000   .40e-03 99 0.        99 0.        99 0.        99 0.        99 0.        99
3.9000 - 3.8000   .26e-01 11  .43e-03 71  .11e-03 99 0.        99 0.        99 0.        99
3.8000 - 3.7000   .41e-01  9  .72e-03 61  .11e-03 99 0.        99 0.        99 0.        99
3.7000 - 3.6000   .60e-01  6  .29e-02 20  .32e-03 51 0.        99  .14e-03 99 0.        99
3.6000 - 3.5000   .56e-01  6  .57e-02 14  .32e-03 71  .11e-03 99 0.        99 0.        99
3.5000 - 3.4000   .53e-01 11  .71e-02 12  .64e-03 37  .11e-03 99 0.        99 0.        99
3.4000 - 3.3000   .62e-01 12  .11e-01 13  .53e-03 45  .11e-03 99 0.        99 0.        99
3.3000 - 3.2000   .69e-01  5  .15e-01  7  .74e-03 37  .11e-03 99 0.        99 0.        99
3.2000 - 3.1000   .62e-01 10  .17e-01  5  .16e-02 23  .21e-03 67 0.        99 0.        99
3.1000 - 3.0000   .59e-01  9  .18e-01  7  .12e-02 42  .32e-03 71  .14e-03 99 0.        99
3.0000 - 2.9000   .56e-01  8  .22e-01  7  .28e-02 21  .11e-03 99  .14e-03 99 0.        99
2.9000 - 2.8000   .53e-01 13  .25e-01 10  .33e-02 18  .42e-03 55  .14e-03 99 0.        99
2.8000 - 2.7000   .46e-01 14  .29e-01  8  .32e-02 19  .64e-03 37  .14e-03 99 0.        99
2.7000 - 2.6000   .40e-01 11  .27e-01  7  .62e-02 12  .53e-03 45  .14e-03 99 0.        99
2.6000 - 2.5000   .42e-01  9  .30e-01  6  .55e-02 14  .53e-03 45 0.        99 0.        99
2.5000 - 2.4000   .40e-01  8  .28e-01  6  .63e-02  9  .74e-03 37  .14e-03 99 0.        99
2.4000 - 2.3000   .30e-01 14  .33e-01  6  .66e-02 10  .15e-02 27  .14e-03 99 0.        99
2.3000 - 2.2000   .32e-01 12  .32e-01  8  .91e-02 11  .17e-02 23 0.        99 0.        99
2.2000 - 2.1000   .29e-01 11  .30e-01  6  .88e-02 11  .17e-02 42 0.        99 0.        99
2.1000 - 2.0000   .28e-01 10  .33e-01  9  .11e-01 10  .24e-02 26  .29e-03 67 0.        99
2.0000 - 1.9000   .22e-01  9  .34e-01  8  .14e-01 11  .36e-02 22  .29e-03 99 0.        99
1.9000 - 1.8000   .22e-01 13  .30e-01  5  .15e-01 10  .30e-02 13  .58e-03 55 0.        99
1.8000 - 1.7000   .16e-01 24  .27e-01 10  .15e-01  7  .49e-02 16  .58e-03 55  .40e-03 99
1.7000 - 1.6000   .17e-01 22  .27e-01  9  .14e-01 12  .47e-02 10  .10e-02 30 0.        99
1.6000 - 1.5000   .17e-01 15  .25e-01  7  .16e-01  6  .47e-02 13  .13e-02 39 0.        99
1.5000 - 1.4000   .17e-01 19  .28e-01  8  .16e-01  7  .83e-02 11  .19e-02 16  .40e-03 99
```

1.4000	-	1.3000	.15e-01	13	.23e-01	16	.19e-01	7	.68e-02	11	.12e-02	45	0.		99
1.3000	-	1.2000	.15e-01	13	.22e-01	9	.19e-01	8	.75e-02	9	.32e-02	13	0.		99
1.2000	-	1.1000	.11e-01	17	.22e-01	4	.17e-01	8	.91e-02	14	.26e-02	20	.79e-03		67
1.1000	-	1.0000	.12e-01	14	.21e-01	6	.16e-01	8	.94e-02	11	.46e-02	18	.79e-03		99
1.0000	-	.9000	.13e-01	19	.21e-01	8	.17e-01	7	.94e-02	6	.38e-02	22	0.		99
.9000	-	.8000	.91e-02	26	.18e-01	9	.18e-01	8	.80e-02	13	.38e-02	25	.12e-02		71
.8000	-	.7000	.48e-02	43	.16e-01	13	.16e-01	6	.11e-01	11	.46e-02	15	.12e-02		51
.7000	-	.6000	.44e-02	29	.13e-01	12	.15e-01	9	.10e-01	12	.45e-02	20	0.		99
.6000	-	.5000	.71e-02	27	.11e-01	11	.13e-01	11	.11e-01	12	.68e-02	13	.12e-02		51
.5000	-	.4000	.32e-02	36	.11e-01	11	.12e-01	8	.10e-01	9	.46e-02	15	.32e-02		41
.4000	-	.3000	.12e-02	51	.91e-02	14	.11e-01	9	.11e-01	11	.41e-02	20	.79e-03		67
.3000	-	.2000	.40e-02	26	.70e-02	15	.82e-02	9	.75e-02	13	.46e-02	12	.40e-03		99
.2000	-	.1000	.16e-02	55	.48e-02	14	.79e-02	12	.59e-02	7	.35e-02	23	.40e-03		99
.1000	-	.0163	.19e-02	67	.31e-02	28	.53e-02	17	.30e-02	21	.35e-02	17	.47e-03		99

energy spectra of transmitted photons
(number/mev, normalized to one incident particle)

e (mev) length= 2.5400

4.0000	-	3.9000	0.	99
3.9000	-	3.8000	0.	99
3.8000	-	3.7000	0.	99
3.7000	-	3.6000	0.	99
3.6000	-	3.5000	0.	99
3.5000	-	3.4000	.29e-03	99
3.4000	-	3.3000	.28e-03	99
3.3000	-	3.2000	0.	99
3.2000	-	3.1000	.28e-03	99
3.1000	-	3.0000	.56e-03	99
3.0000	-	2.9000	.55e-03	67
2.9000	-	2.8000	.11e-02	41
2.8000	-	2.7000	.84e-03	71
2.7000	-	2.6000	.56e-03	67
2.6000	-	2.5000	.84e-03	71
2.5000	-	2.4000	.60e-03	67
2.4000	-	2.3000	.69e-03	54
2.3000	-	2.2000	0.	99
2.2000	-	2.1000	.83e-03	51
2.1000	-	2.0000	.16e-02	37
2.0000	-	1.9000	.21e-02	26
1.9000	-	1.8000	.80e-03	51
1.8000	-	1.7000	.27e-02	26
1.7000	-	1.6000	.22e-02	30
1.6000	-	1.5000	.78e-03	71
1.5000	-	1.4000	.31e-02	21
1.4000	-	1.3000	.23e-02	38
1.3000	-	1.2000	.28e-02	31
1.2000	-	1.1000	.24e-02	28
1.1000	-	1.0000	.33e-02	21
1.0000	-	.9000	.48e-02	23
.9000	-	.8000	.31e-02	33
.8000	-	.7000	.60e-02	22
.7000	-	.6000	.10e-01	18
.6000	-	.5000	.11e-01	15
.5000	-	.4000	.15e-01	15
.4000	-	.3000	.21e-01	15
.3000	-	.2000	.31e-01	9
.2000	-	.1000	.46e-01	5
.1000	-	.0100	.10e+00	5

energy spectra of reflected photons
(number/mev, normalized to one incident particle)

```
        e (mev)  length=       2.5400

  4.0000 -  3.9000  0.          99
  3.9000 -  3.8000  0.          99
  3.8000 -  3.7000  0.          99
  3.7000 -  3.6000  0.          99
  3.6000 -  3.5000  0.          99
  3.5000 -  3.4000  0.          99
  3.4000 -  3.3000  0.          99
  3.3000 -  3.2000  0.          99
  3.2000 -  3.1000  0.          99
  3.1000 -  3.0000  0.          99
  3.0000 -  2.9000  0.          99
  2.9000 -  2.8000  0.          99
  2.8000 -  2.7000  0.          99
  2.7000 -  2.6000  0.          99
  2.6000 -  2.5000  0.          99
  2.5000 -  2.4000  0.          99
  2.4000 -  2.3000  0.          99
  2.3000 -  2.2000  0.          99
  2.2000 -  2.1000  0.          99
  2.1000 -  2.0000  0.          99
  2.0000 -  1.9000  0.          99
  1.9000 -  1.8000  0.          99
  1.8000 -  1.7000   .31e-03 99
  1.7000 -  1.6000  0.          99
  1.6000 -  1.5000  0.          99
  1.5000 -  1.4000  0.          99
  1.4000 -  1.3000  0.          99
  1.3000 -  1.2000   .59e-03 67
  1.2000 -  1.1000   .33e-03 99
  1.1000 -  1.0000  0.          99
  1.0000 -   .9000   .61e-03 99
   .9000 -   .8000   .63e-03 67
   .8000 -   .7000   .62e-03 67
   .7000 -   .6000   .30e-03 99
   .6000 -   .5000   .58e-03 67
   .5000 -   .4000   .62e-03 67
   .4000 -   .3000   .29e-02 15
   .3000 -   .2000   .59e-02 21
   .2000 -   .1000   .19e-01 13
   .1000 -   .0100   .63e-01  7
                                        energy spectra of laterally escaping photons
                                      (number/mev, normalized to one incident particle)
        e (mev)  length=       2.5400

  4.0000 -  3.9000  0.          99
  3.9000 -  3.8000  0.          99
  3.8000 -  3.7000  0.          99
  3.7000 -  3.6000  0.          99
  3.6000 -  3.5000  0.          99
  3.5000 -  3.4000   .30e-03 99
  3.4000 -  3.3000   .60e-03 67
  3.3000 -  3.2000   .61e-03 67
  3.2000 -  3.1000   .94e-03 51
  3.1000 -  3.0000   .32e-03 99
  3.0000 -  2.9000   .94e-03 51
  2.9000 -  2.8000   .28e-03 99
  2.8000 -  2.7000   .28e-03 99
  2.7000 -  2.6000   .13e-02 41
```

```
 2.6000 -  2.5000   .90e-03 76
 2.5000 -  2.4000   .31e-03 99
 2.4000 -  2.3000   .86e-03 99
 2.3000 -  2.2000   .15e-02 54
 2.2000 -  2.1000   .19e-02 27
 2.1000 -  2.0000   .24e-02 40
 2.0000 -  1.9000   .22e-02 47
 1.9000 -  1.8000   .24e-02 25
 1.8000 -  1.7000   .53e-02 28
 1.7000 -  1.6000   .54e-02 22
 1.6000 -  1.5000   .38e-02 29
 1.5000 -  1.4000   .57e-02 23
 1.4000 -  1.3000   .12e-01 16
 1.3000 -  1.2000   .73e-02 17
 1.2000 -  1.1000   .93e-02 13
 1.1000 -  1.0000   .84e-02 18
 1.0000 -   .9000   .15e-01 12
  .9000 -   .8000   .21e-01 11
  .8000 -   .7000   .21e-01 10
  .7000 -   .6000   .35e-01 10
  .6000 -   .5000   .39e-01  8
  .5000 -   .4000   .49e-01  5
  .4000 -   .3000   .91e-01  4
  .3000 -   .2000   .15e+00  4
  .2000 -   .1000   .29e+00  4
  .1000 -   .0100   .98e+00  3
                              angular distributions of transmitted and reflected photon intensity
                                         (mev/sr, normalized to one incident particle)
                  phi(deg)=  0.000
      theta (deg)          180.000

   0.0000 - 30.0000   .13e-01  6
  30.0000 - 60.0000   .14e-03 23
  60.0000 - 90.0000   .95e-05 39
  90.0000 -120.0000   .58e-04 33
 120.0000 -150.0000   .32e-03 18
 150.0000 -180.0000   .27e-03 21
                                angular distributions of laterally escaping photon intensity
                                         (mev/sr, normalized to one incident particle)
                  phi(deg)=  0.000
      theta (deg)          180.000

   0.0000 - 30.0000   .17e-01  5
  30.0000 - 60.0000   .63e-02  3
  60.0000 - 90.0000   .19e-02  4
  90.0000 -120.0000   .89e-03  6
 120.0000 -150.0000   .33e-03  9
 150.0000 -180.0000   .84e-04 17
                            energy spectra and angular distributions of photons transmitted and reflected
                                   azimuthal interval is   0.00000 to 180.00000 degrees
                                    (number/(mev*sr), normalized to one particle)
        e (mev)  theta=  0.000       30.000       60.000       90.000      120.000      150.000
                        30.000       60.000       90.000      120.000      150.000      180.000

 4.0000 -  3.9000  0.        99 0.        99 0.        99 0.        99 0.        99 0.        99
 3.9000 -  3.8000  0.        99 0.        99 0.        99 0.        99 0.        99 0.        99
 3.8000 -  3.7000  0.        99 0.        99 0.        99 0.        99 0.        99 0.        99
 3.7000 -  3.6000  0.        99 0.        99 0.        99 0.        99 0.        99 0.        99
 3.6000 -  3.5000  0.        99 0.        99 0.        99 0.        99 0.        99 0.        99
 3.5000 -  3.4000   .34e-03 99 0.        99 0.        99 0.        99 0.        99 0.        99
```

```
  1   3.4000 -  3.3000   .34e-03 99 0.        99 0.        99 0.        99 0.        99 0.        99
  2   3.3000 -  3.2000  0.        99 0.        99 0.        99 0.        99 0.        99 0.        99
 23   3.2000 -  3.1000   .33e-03 99 0.        99 0.        99 0.        99 0.        99 0.        99
 24   3.1000 -  3.0000   .67e-03 99 0.        99 0.        99 0.        99 0.        99 0.        99
 25   3.0000 -  2.9000   .65e-03 67 0.        99 0.        99 0.        99 0.        99 0.        99
726   2.9000 -  2.8000   .13e-02 41 0.        99 0.        99 0.        99 0.        99 0.        99
727   2.8000 -  2.7000   .10e-02 71 0.        99 0.        99 0.        99 0.        99 0.        99
728   2.7000 -  2.6000   .66e-03 67 0.        99 0.        99 0.        99 0.        99 0.        99
729   2.6000 -  2.5000   .99e-03 71 0.        99 0.        99 0.        99 0.        99 0.        99
730   2.5000 -  2.4000   .71e-03 67 0.        99 0.        99 0.        99 0.        99 0.        99
731   2.4000 -  2.3000   .82e-03 54 0.        99 0.        99 0.        99 0.        99 0.        99
732   2.3000 -  2.2000  0.        99 0.        99 0.        99 0.        99 0.        99 0.        99
733   2.2000 -  2.1000   .98e-03 51 0.        99 0.        99 0.        99 0.        99 0.        99
734   2.1000 -  2.0000   .20e-02 37 0.        99 0.        99 0.        99 0.        99 0.        99
735   2.0000 -  1.9000   .25e-02 26 0.        99 0.        99 0.        99 0.        99 0.        99
736   1.9000 -  1.8000   .95e-03 51 0.        99 0.        99 0.        99 0.        99 0.        99
737   1.8000 -  1.7000   .32e-02 26 0.        99 0.        99 0.        99  .13e-03 99 0.        99
738   1.7000 -  1.6000   .22e-02 37  .14e-03 99 0.        99 0.        99 0.        99 0.        99
739   1.6000 -  1.5000   .93e-03 71 0.        99 0.        99 0.        99 0.        99 0.        99
740   1.5000 -  1.4000   .36e-02 21 0.        99 0.        99 0.        99 0.        99 0.        99
741   1.4000 -  1.3000   .27e-02 38 0.        99 0.        99 0.        99 0.        99 0.        99
742   1.3000 -  1.2000   .31e-02 30  .11e-03 99 0.        99 0.        99  .26e-03 67 0.        99
743   1.2000 -  1.1000   .28e-02 28 0.        99 0.        99 0.        99  .14e-03 99 0.        99
744   1.1000 -  1.0000   .39e-02 21 0.        99 0.        99 0.        99 0.        99 0.        99
745   1.0000 -   .9000   .57e-02 23 0.        99 0.        99 0.        99  .27e-03 99 0.        99
746    .9000 -   .8000   .37e-02 33 0.        99 0.        99  .10e-03 99  .13e-03 99 0.        99
747    .8000 -   .7000   .71e-02 22 0.        99 0.        99 0.        99  .13e-03 99  .38e-03 99
748    .7000 -   .6000   .11e-01 15  .25e-03 67 0.        99  .96e-04 99 0.        99 0.        99
749    .6000 -   .5000   .13e-01 15  .13e-03 99 0.        99 0.        99  .25e-03 67 0.        99
750    .5000 -   .4000   .17e-01 15  .31e-03 52 0.        99  .10e-03 99  .13e-03 99 0.        99
751    .4000 -   .3000   .24e-01 15  .27e-03 67 0.        99  .28e-03 71  .88e-03 22 0.        99
752    .3000 -   .2000   .33e-01  9  .10e-02 24  .19e-03 67  .18e-03 67  .17e-02 19  .16e-02 53
753    .2000 -   .1000   .51e-01  6  .13e-02 40  .18e-03 68  .11e-02 27  .41e-02 16  .77e-02 22
754    .1000 -   .0100   .11e+00  4  .30e-02 17  .61e-03 57  .31e-02 17  .14e-01 12  .27e-01 12
755 0   integral (/sr)   .30e-01  3  .62e-03 15  .92e-04 44  .46e-03 12  .20e-02  9  .34e-02 12
756 0                            energy spectra and angular distributions of photons laterally escaping
757                                   azimuthal interval is   0.00000 to 180.00000 degrees
758                                      (number/(mev&sr), normalized to one particle)
759 0     e (mev)  theta-  0.000        30.000       60.000       90.000      120.000      150.000
760                       30.000        60.000       90.000      120.000      150.000      180.000
761
762   4.0000 -  3.9000  0.        99 0.        99 0.        99 0.        99 0.        99 0.        99
763   3.9000 -  3.8000  0.        99 0.        99 0.        99 0.        99 0.        99 0.        99
764   3.8000 -  3.7000  0.        99 0.        99 0.        99 0.        99 0.        99 0.        99
765   3.7000 -  3.6000  0.        99 0.        99 0.        99 0.        99 0.        99 0.        99
766   3.6000 -  3.5000  0.        99 0.        99 0.        99 0.        99 0.        99 0.        99
767   3.5000 -  3.4000   .36e-03 99 0.        99 0.        99 0.        99 0.        99 0.        99
768   3.4000 -  3.3000   .34e-03 99  .14e-03 99 0.        99 0.        99 0.        99 0.        99
769   3.3000 -  3.2000  0.        99  .27e-03 67 0.        99 0.        99 0.        99 0.        99
770   3.2000 -  3.1000   .73e-03 67  .14e-03 99 0.        99 0.        99 0.        99 0.        99
771   3.1000 -  3.0000   .38e-03 99 0.        99 0.        99 0.        99 0.        99 0.        99
772   3.0000 -  2.9000   .11e-02 51 0.        99 0.        99 0.        99 0.        99 0.        99
773   2.9000 -  2.8000   .33e-03 99 0.        99 0.        99 0.        99 0.        99 0.        99
774   2.8000 -  2.7000   .34e-03 99 0.        99 0.        99 0.        99 0.        99 0.        99
775   2.7000 -  2.6000   .11e-02 51 0.        99 0.        99  .11e-03 99 0.        99 0.        99
776   2.6000 -  2.5000   .11e-02 70 0.        99 0.        99 0.        99 0.        99 0.        99
777   2.5000 -  2.4000   .37e-03 99 0.        99 0.        99 0.        99 0.        99 0.        99
778   2.4000 -  2.3000   .10e-02 99 0.        99 0.        99 0.        99 0.        99 0.        99
780   2.3000 -  2.2000   .69e-03 67  .41e-03 90 0.        99 0.        99 0.        99 0.        99
```

```
 31    2.1000 -  2.0000   .14e-02 55  .53e-03 55 0.         99 0.         99 0.         99 ).         99
 32    2.0000 -  1.9000   .15e-02 41  .40e-03 71 0.         99 0.         99 0.         99 0.         99
 83    1.9000 -  1.8000   .21e-02 37  .26e-03 67 0.         99 0.         99 0.         99 0.         99
784    1.8000 -  1.7000   .26e-02 44  .95e-03 30  .28e-03 51 0.         99 0.         99 0.         99
785    1.7000 -  1.6000   .35e-02 33  .66e-03 54  .29e-03 51 0.         99 0.         99 0.         99
786    1.6000 -  1.5000   .10e-02 51  .76e-03 51  .29e-03 70  .95e-04 99 0.         99 0.         99
787    1.5000 -  1.4000   .28e-02 31  .15e-02 25 0.         99 0.         99 0.         99 0.         99
788    1.4000 -  1.3000   .69e-02 23  .17e-02 39  .59e-03 37  .20e-03 67 0.         99 0.         99
789    1.3000 -  1.2000   .54e-02 17  .92e-03 22  .19e-03 67 0.         99 0.         99 0.         99
790    1.2000 -  1.1000   .46e-02 35  .13e-02 15  .30e-03 51  .49e-03 33 0.         99 0.         99
791    1.1000 -  1.0000   .49e-02 31  .12e-02 31  .49e-03 33 0.         99 0.         99 0.         99
792    1.0000 -   .9000   .67e-02 23  .29e-02 17  .69e-03 31  .99e-04 99  .14e-03 99 0.         99
793     .9000 -   .8000   .10e-01 17  .35e-02 11  .13e-02 29  .94e-04 99 0.         99 0.         99
794     .8000 -   .7000   .11e-01 22  .35e-02 12  .85e-03 26  .39e-03 41  .13e-03 99 0.         99
796     .8000 -   .6000   .18e-01 13  .79e-02 13  .84e-02 38  .70e-03 80  .26e-03 67 0.         99
797     .5000 -   .4000   .21e-01 10  .92e-02 13  .23e-02  9  .86e-03 26  .27e-03 67 0.         99
798     .4000 -   .3000   .34e-01  9  .13e-01  7  .61e-02  7  .34e-02 16  .69e-03 61 0.         99
799     .3000 -   .2000   .49e-01  7  .23e-01  7  .10e-01 10  .58e-02  9  .17e-02 36  .11e-02 51
800     .2000 -   .1000   .80e-01  5  .49e-01  6  .18e-01  7  .13e-01  7  .66e-02 10  .12e-02 53
801     .1000 -   .0100   .24e+00  5  .15e+00  4  .73e-01  3  .44e-01  4  .25e-01  6  .12e-01 23
802 0the subbgraf(deg)word50es00 for s86bt0tic3 isl1e-01 1317.65e-02  3  .33e-02  6  .13e-02 19
.t802,1
802 0    integral (/sr)   .50e-01  4  .26e-01  3  .11e-01  3  .65e-02  3  .33e-02  6  .13e-02 19
803  the number of ecs words used for statistics is      1317
.end

 all done
%bp 0014.2046
```

APPENDIX F

MONTE CARLO ELECTRON BEAM TRANSPORT IN AIR

SECURITY CLASSIFICATION OF THIS PAGE (When Data Entered)

REPORT DOCUMENTATION PAGE

READ INSTRUCTIONS BEFORE COMPLETING FORM

1. REPORT NUMBER	2. GOVT ACCESSION NO.	3. RECIPIENT'S CATALOG NUMBER
4. TITLE (and Subtitle) Monte Carlo Electron Beam Transport in Air		5. TYPE OF REPORT & PERIOD COVERED Interim Report
		6. PERFORMING ORG. REPORT NUMBER AMRC-N-186
7. AUTHOR(s) D. J. Sullivan C. A. Ekdahl		8. CONTRACT OR GRANT NUMBER(s) F49620-81-C-0016
9. PERFORMING ORGANIZATION NAME AND ADDRESS Mission Research Corporation 1400 San Mateo Boulevard, S.E., Suite A Albuquerque, New Mexico 87108		10. PROGRAM ELEMENT, PROJECT, TASK AREA & WORK UNIT NUMBERS
11. CONTROLLING OFFICE NAME AND ADDRESS Air Force Office of Scientific Research Bolling Air Force Base Washington, DC 20332		12. REPORT DATE January 1982
		13. NUMBER OF PAGES 24
14. MONITORING AGENCY NAME & ADDRESS (if different from Controlling Office)		15. SECURITY CLASS (of this report) Unclassified
		15a. DECLASSIFICATION DOWNGRADING SCHEDULE

16. DISTRIBUTION STATEMENT (of this Report)

17. DISTRIBUTION STATEMENT (of the abstract entered in Block 20, if different from Report)

Approved for Public Release; Distribution Unlimited

18. SUPPLEMENTARY NOTES

19. KEY WORDS (Continue on reverse side if necessary and identify by block number)

Electron Beam Transport
Monte Carlo Transport Calculations
Delta Rays

20. ABSTRACT (Continue on reverse side if necessary and identify by block number)

The Monte Carlo transport of a 1.5 MeV electron beam in low density and full atmosphere air is studied. At a pressure of 0.5 Torr virtually none of the beam is deflected in 10 meters due to classical scattering or bremsstrahlung. At 760 Torr the beam is scattered in less than 2 meters. The main purpose of this research was to determine the angular dependence of secondary electrons (delta rays) leaving the beam-air interaction region on their energy. At low pressure, excellent agreement is observed between code results and an analytical formula for the scattering angle as a function of delta ray energy

DD FORM 1 JAN 73 1473 EDITION OF 1 NOV 65 IS OBSOLETE

SECURITY CLASSIFICATION OF THIS PAGE (When Data Entered)

down to energies of a few tens of keV.

ABSTRACT

The Monte Carlo transport of a 1.5 MeV electron beam in low density and full atmosphere air is studied. At a pressure of 0.5 Torr virtually none of the beam is deflected in 10 meters due to classical scattering or bremsstrahlung. At 760 Torr the beam is scattered in less than 2 meters. The main purpose of this research was to determine the angular dependence of secondary electrons (delta rays) leaving the beam-air interaction region on their energy. At low pressure, excellent agreement is observed between code results and an analytical formula for the scattering angle as a function of delta ray energy down to energies of a few tens of keV.

PROBLEM CONFIGURATION

A monoenergetic 1.5 MeV electron beam of radius 3.8 cm is injected into a cylindrical column of air 10 cm in radius and 10 meters deep. The air is composed of 79% Nitrogen, 20 % oxygen and 1% Argon. The low pressure simulation at 0.5 Torr is sectioned into 80 zones in an attempt to determine where the beam energy is deposited. The high pressure run at 760 Torr is divided into 2 zones from 0 to 2, and 2 to 10 meters. The primary purpose of this was to reduce computer running time, because we were mainly interested in the angular distribution of delta rays (secondary electrons) as a function of their energy. At high pressure, however, the angular dependence was unobtainable.

RESULTS

The Monte Carlo transport code CYLTRAN was used in this study. It is particuarly suitable, because it can calculate both electron and photon transport in cylindrical geometry. The problem may involve up to five materials each consisting of a maximum of ten elements without code modification. The problem cylinder may be zoned axially and radially into 100 compartments, if necessary. CYLTRAN is detailed in Reference 1.

Data on air at 0.5 Torr pertaining to beam stopping power, range and radiation yield up to a maximum beam energy of 1.5 MeV is compiled in Appendix A. It is generated based on material density, composition, and tabulated cross sections for the various elements. Transport data for the electron beam in 0.5 Torr air is also given in Appendix A. It shows that all of the electron beam is transmitted. Only those zones within the beam path have any energy from primary electrons deposited in them. Total energy deposition from primary and secondary electrons is .10%. No charge deposition due to primaries is recorded. Charge loss from secondaries leaving the beam volume is .7%. The 500,000 incident beam electrons generate only 3440 secondary electrons - all knockons. This results in rather poor statistics for delta ray production and angular dependence on energy. Nevertheless, those points which can be plotted show excellent agreement with an already existing, well-known formula for the angular dependence of delta rays. The equation which was derived from momentum and energy conservation, is

$$\cos\theta = \frac{w}{E}\left(\frac{E + 2\,mc^2}{w + 2mc^2}\right)^{1/2} \tag{1}$$

where E is the primary electron energy and w and θ are the delta ray energy and scattering angle. Equation (1) and the points derived from the CYLTRAN program are given in Figure 1.

A second run at full atmospheric pressure was made. CYLTRAN results at this higher pressure are given in Appendix B. In contrast with the prior results, all beam electrons are scattered with virtually all escaping the air cylinder laterally in less than 2 meters. A small percentage (< .2%) are reflected, but none are stopped in the cylinder volume. On average each primary deposits 9.1% of its energy to create .7 knockons/primary. Note, however, that delta rays which are created with energy of less than 10 keV are ignored, so that this number is an underestimate. Because the vast majority of the beam electrons are escaping laterally along with those deltas with sufficient energy to escape the cylinder, it is impossible to determine delta ray angular dependence on energy. Each 10° angular bin has electrons of all possible energies (1.5 MeV to 10 keV) in it. A code update which provides separate data on escaping primary and secondary electrons will be necessary to resolve this problem.

ACKNOWLEDGEMENT

The author is pleased to acknowledge helpful discussions with J. Mack of Los Alamos National Laboratory and J. A. Halbleib of Sandia National Laboratory on the use of the CYLTRAN code.

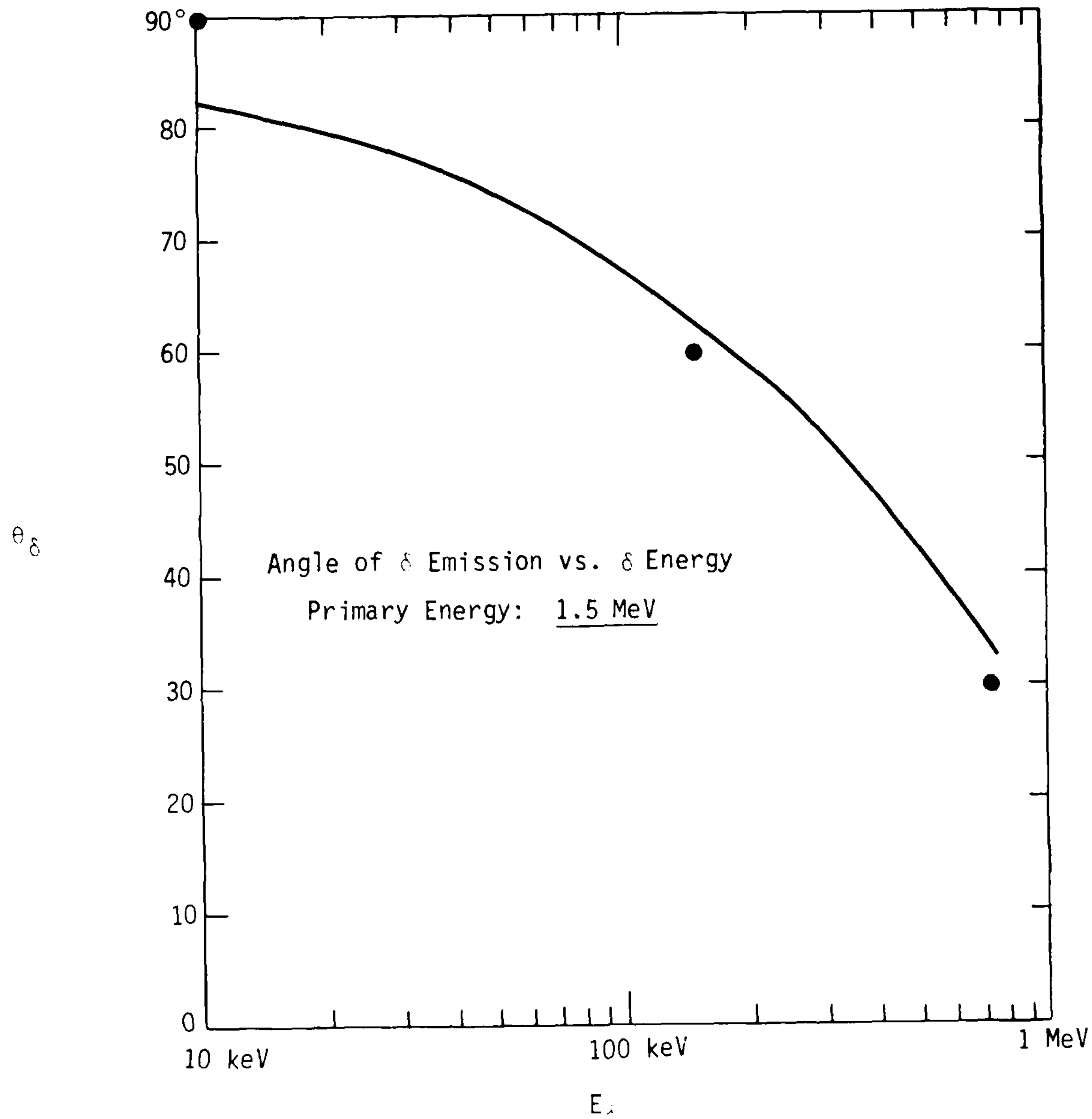

Figure 1. Angular dependence of delta rays on their energy for a 1.5 MeV beam. The solid line results from Equation (1). The points are based on CYLTRAN for air at 0.5 Torr.

REFERENCES

1. J. A. Halbleib Sr. and W. H. Vandevender, CYLTRAN: A Cylindrical-Geometry Multimaterial Electron/Photon Monte Carlo Transport Code, SAND 74-0030, Sandia National Laboratories, (1975), unpublished.

APPENDIX A

AIR PROPERTIES AND 1.5 MeV ELECTRON BEAM TRANSPORT AT 0.5 TORR

J 1

1.5 MEV FX100 BEAM INTO .5 TORR AIR

```
0
0 NSET  ITRM  IZIP  ISON  ISUB  INEL  ICYC  NCYC  NMAX        EMAX
   1     5     0     1     3     1     1     8     64      .15000E+01
0INPUT DATA TAPE IDENTIFICATION
 DATATAPE-2 (RESTER-AIGINGER PH-RAD CORR), 84 STERNHEIMER SETS, 30 JAN 8
0DETOUR         DENSITY
  .83500E+00    .84815E-06
0
ORANGE TABLE
0     EMAX        NCYC       EFAC        NMAX    TINMAX+1)    NCAL      TINCAL)
   .15000E+01      8     .81700E+00      64     .8850E-02      88     .84803E-03
0 JMAX  LMAX
   3     1
0        Z            A            W
     7.00000      14.00670      .76500
     8.00000      15.99938      .22120
    18.00000      39.94700      .01380
0        PI           PID
     86.84160     86.84160
0 ---------------------PARAMETERS FOR DENSITY EFFECT--------------------
        PI          C            B          DM          XI          X0

     86.84160   -17.88264     .21283     3.00000     9.58092     3.38092
     86.84160   -17.88264     .21263     3.00000     9.58092     3.38092
   .1500E+00   -.1667E+02    .7866E-01
1                                              ELECTRON RESULTS
0     EFFECTIVE Z/A = .49914    EFFECTIVE MEAN IONIZATION POTENTIAL = 86.84 EV    CRITICAL ENERGY = 0.000 MEV
```

N	ENERGY MEV	STOPPING POWER COLLISION MEV CM2/G	RADIATION MEV CM2/G	TOTAL MEV CM2/G	RANGE G/CM2	RADIATION YIELD	BETA**2	DENSITY CORR MEV CM2/G	RAD/COL	DRANGE G/CM2	DYIELD
86	.9490E-03	.105E+03	.548E-02	.105E+03	.451E-05	0.	.371E-02	0.	.519E-04	0.	0.
85	.1036E-02	.990E+02	.546E-02	.990E+02	.535E-05	.442E-05	.404E-02	0.	.547E-04	.839E-06	.494E-08
84	.1130E-02	.945E+02	.545E-02	.946E+02	.632E-05	.872E-05	.441E-02	0.	.577E-04	[illegible]	[illegible]
83	.1232E-02	.895E+02	.544E-02	.895E+02	.743E-05	.129E-04	.480E-02	0.	[illegible]	[illegible]	[illegible]
82	.1343E-02	.846E+02	.544E-02	.846E+02	.871E-05	.170E-04	.524E-02	0	[illegible]	[illegible]	[illegible]
81	.1465E-02	.799E+02	.543E-02	.800E+02	.102E-04	.211E-04	.571E-02	0.	[illegible]	[illegible]	[illegible]
80	.1597E-02	.755E+02	.542E-02	.755E+02	.119E-04	[illegible]	[illegible]	0.	[illegible]	[illegible]	[illegible]
79	.1742E-02	.712E+02	.541E-02	.712E+02	.139E-04	[illegible]	[illegible]	0.	[illegible]	[illegible]	[illegible]
78	.1900E-02	.671E+02	.539E-02	.671E+02	.162E-04	.333E-04	.739E-02	0.	[illegible]	[illegible]	[illegible]
77	.2072E-02	.632E+02	.538E-02	.632E+02	.188E-04	.374E-04	[illegible]	0.	[illegible]	[illegible]	[illegible]
76	.2259E-02	.595E+02	.537E-02	.594E+02	.219E-04	.415E-04	[illegible]	0.	[illegible]	[illegible]	[illegible]
75	.2464E-02	.560E+02	.535E-02	.560E+02	.254E-04	[illegible]	.957E-02	0.	[illegible]	[illegible]	[illegible]
74	.2687E-02	.526E+02	.533E-02	.526E+02	.295E-04	.502E-04	.104E-01	0.	[illegible]	.411E-05	[illegible]
73	.2930E-02	.495E+02	.532E-02	.495E+02	.343E-04	.547E-04	.114E-01	0.	[illegible]	.477E-05	[illegible]
72	.3195E-02	.465E+02	.530E-02	.465E+02	.398E-04	.593E-04	.124E-01	0.	[illegible]	[illegible]	[illegible]
71	.3484E-02	.436E+02	.528E-02	.436E+02	.462E-04	.641E-04	[illegible]	0.	[illegible]	[illegible]	[illegible]
70	.3799E-02	.409E+02	.526E-02	.409E+02	.537E-04	.692E-04	.147E-01	0.	[illegible]	[illegible]	[illegible]
69	.4143E-02	.384E+02	.523E-02	.384E+02	.624E-04	.744E-04	.160E-01	0.	[illegible]	[illegible]	[illegible]
68	.4518E-02	.360E+02	.521E-02	.360E+02	.725E-04	.798E-04	.175E-01	0.	.145E-03	[illegible]	[illegible]
67	.4927E-02	.336E+02	.519E-02	.336E+02	.842E-04	.857E-04	.190E-01	0.	.154E-03	.117E-04	[illegible]
66	.5373E-02	.316E+02	.516E-02	.316E+02	.979E-04	.917E-04	.207E-01	0.	.163E-03	.137E-04	[illegible]
65	.5859E-02	.296E+02	.514E-02	.296E+02	.114E-03	.981E-04	.225E-01	0.	.173E-03	.159E-04	[illegible]
64	.6390E-02	.277E+02	.511E-02	.278E+02	.132E-03	.105E-03	.245E-01	0.	.184E-03	[illegible]	[illegible]
63	.6968E-02	.260E+02	.509E-02	.260E+02	.154E-03	.112E-03	.267E-01	0.	[illegible]	[illegible]	[illegible]
62	.7599E-02	.243E+02	.506E-02	.243E+02	.179E-03	.119E-03	.291E-01	0.	[illegible]	[illegible]	[illegible]
61	.8287E-02	.228E+02	.504E-02	.228E+02	.208E-03	.127E-03	.317E-01	0.	[illegible]	[illegible]	[illegible]
60	.9036E-02	.213E+02	.501E-02	.213E+02	.242E-03	.136E-03	.345E-01	0.	[illegible]	[illegible]	[illegible]
59	.9854E-02	.199E+02	.498E-02	.199E+02	.282E-03	.144E-03	.375E-01	0.	[illegible]	[illegible]	[illegible]
58	.1075E-01	.186E+02	.496E-02	.186E+02	.328E-03	.154E-03	.408E-01	0.	[illegible]	[illegible]	[illegible]
57	.1172E-01	.174E+02	.493E-02	.174E+02	.382E-03	.164E-03	.443E-01	0.	.283E-03	[illegible]	.267E-06
56	.1278E-01	.163E+02	.491E-02	.163E+02	.445E-03	.175E-03	.482E-01	0.	[illegible]	[illegible]	[illegible]
55	.1394E-01	.153E+02	.488E-02	.153E+02	.518E-03	.186E-03	.524E-01	0.	.320E-03	.734E-04	[illegible]

J 1

K 1

N	ENERGY MEV	COLLISION	RADIATION	TOTAL	RANGE	RADIATION YIELD	BETA**2	DENSITY CORR	RAD/COL	DRANGE	DYIELD
54	.1520E-01	.143E+02	.486E-02	.143E+02	.604E-03	.198E-03	.569E-01	0.	.341E-03	[illegible]	.417E-06
53	.1657E-01	.133E+02	.484E-02	.133E+02	.704E-03	.211E-03	.618E-01	0.	[illegible]	[illegible]	[illegible]
52	.1807E-01	.125E+02	.481E-02	.125E+02	.820E-03	.224E-03	.672E-01	0.	[illegible]	.116E-03	[illegible]
51	.1971E-01	.117E+02	.479E-02	.117E+02	.956E-03	.239E-03	.729E-01	0.	.410E-03	[illegible]	[illegible]
50	.2149E-01	.109E+02	.477E-02	.109E+02	.111E-02	[illegible]	.791E-01	0.	[illegible]	[illegible]	[illegible]
49	.2344E-01	.102E+02	.476E-02	.102E+02	.130E-02	.270E-03	.858E-01	0.	[illegible]	[illegible]	[illegible]
48	.2556E-01	[illegible]	.474E-02	[illegible]	[illegible]	.286E-03	.930E-01	0.	[illegible]	.214E-03	[illegible]
47	.2787E-01	.896E+01	.472E-02	.896E+01	.176E-02	.306E-03	.101E+00	0.	[illegible]	[illegible]	.110E-05
46	.3039E-01	[illegible]	.471E-02	[illegible]	[illegible]	.326E-03	.109E+00	0.	[illegible]	[illegible]	[illegible]
45	[illegible]	.786E+01	.470E-02	.787E+01	[illegible]	[illegible]	.118E+00	0.	[illegible]	[illegible]	[illegible]
44	[illegible]	.737E+01	.469E-02	.737E+01	[illegible]	[illegible]	.128E+00	0.	[illegible]	[illegible]	[illegible]
43	.3942E-01	[illegible]	.468E-02	[illegible]	.324E-02	.393E-03	.136E+00	0.	[illegible]	[illegible]	[illegible]
42	.4298E-01	.648E+01	.467E-02	.649E+01	.378E-02	.418E-03	.149E+00	0.	.721E-03	[illegible]	[illegible]
41	.4687E-01	[illegible]	.467E-02	[illegible]	[illegible]	.445E-03	.161E+00	0.	[illegible]	[illegible]	[illegible]
40	[illegible]	.572E+01	.467E-02	.572E+01	.512E-02	[illegible]	.174E+00	0.	[illegible]	[illegible]	[illegible]
39	.5574E-01	.537E+01	.467E-02	.538E+01	.595E-02	[illegible]	.187E+00	0.	[illegible]	[illegible]	[illegible]
38	[illegible]	.505E+01	.468E-02	.506E+01	.692E-02	.537E-03	.201E+00	0.	[illegible]	[illegible]	[illegible]
37	.6629E-01	.476E+01	.469E-02	.476E+01	.804E-02	.572E-03	.216E+00	0.	[illegible]	.112E-02	[illegible]
36	.7229E-01	.449E+01	.471E-02	.449E+01	.934E-02	.609E-03	.233E+00	0.	[illegible]	[illegible]	[illegible]
35	.7883E-01	.423E+01	.472E-02	.424E+01	.108E-01	.648E-03	.249E+00	0.	[illegible]	[illegible]	[illegible]
34	.8597E-01	.400E+01	.475E-02	.400E+01	.126E-01	.690E-03	.267E+00	0.	.119E-02	[illegible]	[illegible]
33	.9375E-01	.378E+01	.478E-02	.378E+01	.146E-01	.734E-03	.285E+00	0.	.126E-02	[illegible]	[illegible]
32	.1022E+00	.358E+01	.481E-02	.358E+01	.169E-01	.781E-03	.306E+00	0.	.134E-02	[illegible]	.111E-04
31	.1115E+00	.339E+01	.485E-02	.340E+01	.195E-01	.832E-03	.326E+00	0.	.143E-02	[illegible]	[illegible]
30	.1216E+00	.322E+01	.490E-02	.322E+01	.226E-01	[illegible]	.347E+00	0	[illegible]	[illegible]	[illegible]
29	.1326E+00	.306E+01	.495E-02	.307E+01	[illegible]	[illegible]	.370E+00	0.	[illegible]	[illegible]	.172E-04
28	.1446E+00	[illegible]	.502E-02	.292E+01	[illegible]	.100E-02	.392E+00	0	[illegible]	[illegible]	[illegible]
27	.1577E+00	.278E+01	.509E-02	.279E+01	.347E-01	.107E-02	.416E+00	0	[illegible]	[illegible]	[illegible]
26	.1719E+00	[illegible]	.518E-02	.266E+01	[illegible]	.113E-02	[illegible]	0.	[illegible]	[illegible]	[illegible]
25	.1875E+00	.254E+01	.527E-02	.255E+01	[illegible]	[illegible]	[illegible]	0	.207E-02	[illegible]	[illegible]
24	.2045E+00	.244E+01	.538E-02	.245E+01	.527E-01	.128E-02	[illegible]	0	[illegible]	[illegible]	[illegible]
23	.2231E+00	.235E+01	[illegible]	.235E+01	[illegible]	.137E-02	[illegible]	0	[illegible]	[illegible]	[illegible]
22	.2432E+00	.226E+01	.565E-02	.226E+01	.692E-01	.146E-02	[illegible]	0	[illegible]	[illegible]	[illegible]
21	[illegible]	[illegible]	[illegible]	[illegible]	[illegible]	.155E-02	.567E+00	0	[illegible]	[illegible]	[illegible]
20	[illegible]	.211E+01	[illegible]	[illegible]	[illegible]	.165E-02	[illegible]	0	[illegible]	[illegible]	[illegible]
19	.3153E+00	.204E+01	.627E-02	.205E+01	.103E+00	.175E-02	[illegible]	0	[illegible]	.126E-01	[illegible]
18	.3439E+00	.199E+01	.643E-02	.199E+01	.117E+00	.187E-02	.643E+00	0	.324E-02	.141E-01	[illegible]
17	.3750E+00	.193E+01	[illegible]	.194E+01	.133E+00	.199E-02	[illegible]	0	[illegible]	[illegible]	.104E-03
16	.4089E+00	.189E+01	[illegible]	.189E+01	.150E+00	[illegible]	[illegible]	0	[illegible]	[illegible]	.121E-03
15	.4461E+00	.185E+01	.732E-02	.185E+01	.170E+00	.226E-02	[illegible]	0	[illegible]	[illegible]	.141E-03
14	.4863E+00	[illegible]	.770E-02	.182E+01	.192E+00	[illegible]	.737E+00	0.	[illegible]	[illegible]	[illegible]
13	.5303E+00	.178E+01	[illegible]	.179E+01	.217E+00	.250E-02	[illegible]	0.	[illegible]	[illegible]	[illegible]
12	.5783E+00	.175E+01	[illegible]	.176E+01	.244E+00	[illegible]	[illegible]	0	[illegible]	[illegible]	[illegible]
11	.6307E+00	.173E+01	[illegible]	.174E+01	.274E+00	.290E-02	[illegible]	0.	[illegible]	[illegible]	[illegible]
10	.6878E+00	[illegible]	.975E-02	.172E+01	.307E+00	[illegible]	[illegible]	0	[illegible]	[illegible]	[illegible]
9	.7500E+00	.169E+01	.104E-01	.170E+01	.343E+00	.330E-02	[illegible]	0	[illegible]	[illegible]	[illegible]
8	[illegible]	.164E+01	.112E-01	.169E+01	.383E+00	.363E-02	.852E+00	0	[illegible]	[illegible]	[illegible]
7	[illegible]	.167E+01	.121E-01	.168E+01	.427E+00	[illegible]	[illegible]	0	[illegible]	[illegible]	[illegible]
6	.9726E+00	.166E+01	.130E-01	.167E+01	.475E+00	[illegible]	[illegible]	0	[illegible]	[illegible]	[illegible]
5	[illegible]	.166E+01	[illegible]	.167E+01	.528E+00	[illegible]	.894E+00	0	[illegible]	[illegible]	[illegible]
4	[illegible]	.165E+01	.153E-01	.167E+01	[illegible]	.480E-02	[illegible]	0	[illegible]	[illegible]	[illegible]
3	[illegible]	.165E+01	[illegible]	.167E+01	.648E+00	.527E-02	[illegible]	0	[illegible]	[illegible]	[illegible]
2	.1376E+01	[illegible]	[illegible]	.167E+01	.716E+00	.570E-02	[illegible]	0	[illegible]	[illegible]	[illegible]
1	.1500E+01	.166E+01	.199E-01	.168E+01	.791E+00	[illegible]	.935E+00	0	[illegible]	[illegible]	[illegible]

```
0O C T O B E R  1 4 , 1 9 7 8  V E R S I O N
0 NSET  MATL
    1      1
0 NMAT  NTAB
    1      1
0NPAIR  NTAX
   25     41
0GAMMA RAY CROSS SECTION DATA
0ENERGIES (MEV)
 1000.000000  800.000000  600.000000  500.000000  400.000000  300.000000
  200.000000  150.000000  100.000000   80.000000   60.000000   50.000000
   40.000000   30.000000   20.000000   15.000000   10.000000    8.000000
    6.000000    5.000000    4.000000    3.000000    2.000000    1.500000
    1.000000     .800000     .600000     .500000     .400000     .300000
     .200000     .150000     .100000     .080000     .060000     .050000
     .040000     .030000     .020000     .015000     .010000
0TOTAL ATTENUATION COEFFICIENTS (CM2/G)
     .034183     .030724     .026988     .024888     .022822     .020782
     .018555     .017473     .016471     .016124     .015848     .015760
     .015757     .015964     .016848     .017888     .020378     .022163
     .025095     .027374     .030651     .035698     .044400     .051665
     .063465     .070602     .080400     .086939     .095257     .106398
     .122574     .134163     .150941     .161339     .178978     .195848
     .229594     .319830     .701217    1.488718    4.800483
0RATIO OF SCATTERING PLUS PAIR PRODUCTION TO TOTAL ATTENUATION COEFFICIENTS
    1.000000    1.000000    1.000000    1.000000    1.000000    1.000000
    1.000000     .999999     .999999     .999999     .999998     .999998
     .999998     .999997     .999995     .999994     .999992     .999991
     .999988     .999987     .999984     .999980     .999971     .999960
     .999331     .999932     .999833     .999757     .999598     .999173
     .997523     .994368     .981279     .963511     .915911     .861312
     .757208     .561182     .264757     .126930     .039270
0RATIO OF SCATTERING TO SCATTERING PLUS PAIR PRODUCTION ATTENUATION COEFFICIENTS
     .007074     .009816     .014847     .019178     .026033     .038052
     .063000     .088027     .136576     .171296     .225945     .266902
     .323921     .407569     .536746     .628994     .75[illegible]46     .812171
     .877038     .909746     .941060     .969055     .980895     .988138
    1.000000
0K SHELL IONIZATION DATA
0BINDING ENERGY (MEV), PHOTOEFFECT EFFICIENCY AND FLUORESCENT EFFICIENCY
     .003203     .111213     .079438
0K X-RAY ENERGIES (MEV)
     .003203     .003203     .003203     .003203
0K X-RAY ACCUMULATED RELATIVE INTENSITIES
    1.000000    1.000000    1.000000    1.000000
0AUGER ELECTRON ENERGIES (MEV)
     .003203     .003203     .003203
0AUGER ELECTRON ACCUMULATED RELATIVE INTENSITIES
    1.000000    1.000000    1.000000
1NUMBER OF SETS ON DATAPAC TAPE =    1
0INPUT FROM DATAPAC

  **1.5 MEV FX100 BEAM INTO .5 TORR AIR**
0 NRUN  ITRM  IZIP  ISGN  ISUB  INAL  ICYC  NCYC  NMAX       EMAX            EMIN            RMAX        LMAT
     1     5     0     1     3     1     1     8    64  1.5000000E+00  5.0593750E-03  7.8075230E-01     3

 DATAPREP DATA FOR DATAPAC SET    1    64    33     3   121  7.807523E-01

 COLLISION / TOTAL DE/DX RATIOS FOR DATAPAC SET    1

 CUMULATIVE BREMSSTRAHLUNG CROSS SECTIONS FOR DATAPAC SET    1

 CUMULATIVE BREMSSTRAHLUNG ANGULAR DISTRIBUTIONS FOR DATAPAC SET    1
```

D 2

E 2

```
 LANGAUSS - EQUIPROBABLE ENDPOINTS FOR INTERPOLATION

 K X-RAY PRODUCTION FOR DATAPAC SET    1

 PHOTOELECTRON ANGULAR DISTRIBUTIONS

 PAIR ELECTRON ENERGY DIVISION DISTRIBUTION (LEAD)
1
0 NRUN    INC ISTRG   INOK   INEL  IPHOT   IBAD   IDES   IPUN ITAPE
     1      1     1      1      2      1      1      1      2     2
```

0 ZONE	MATERIAL	LEFT PLANE	RIGHT PLANE	INNER CYLINDER	OUTER CYLINDER	ECUT	PTCZ
1	1	0.	.25000E+02	0.	.20000E+01	.100E-01	0.
2	1	.25000E+02	.50000E+02	0.	.20000E+01	.100E-01	0.
3	1	.50000E+02	.75000E+02	0.	.20000E+01	.100E-01	0.
4	1	.75000E+02	.10000E+03	0	.20000E+01	.100E-01	0.
5	1	.10000E+03	.12500E+03	0.	.20000E+01	.100E-01	0.
6	1	.12500E+03	.15000E+03	0.	.20000E+01	.100E-01	0.
7	1	.15000E+03	.17500E+03	0	.20000E+01	.100E-01	0.
8	1	.17500E+03	.20000E+03	0.	.20000E+01	.100E-01	0.
9	1	0.	.25000E+02	.20000E+01	.40000E+01	.100E-01	0.
10	1	.25000E+02	.50000E+02	.20000E+01	.40000E+01	.100E-01	0
11	1	.50000E+02	.75000E+02	.20000E+01	.40000E+01	.100E-01	0.
12	1	.75000E+02	.10000E+03	.20000E+01	.40000E+01	.100E-01	0
13	1	.10000E+03	.12500E+03	.20000E+01	.40000E+01	.100E-01	0
14	1	.12500E+03	.15000E+03	.20000E+01	.40000E+01	.100E-01	0.
15	1	.15000E+03	.17500E+03	.20000E+01	.40000E+01	.100E-01	0.
16	1	.17500E+03	.20000E+03	.20000E+01	.40000E+01	.100E-01	0
17	1	0	.25000E+02	.40000E+01	.60000E+01	.100E-01	0.
18	1	.25000E+02	.50000E+02	.40000E+01	.60000E+01	.100E-01	0.
19	1	.50000E+02	.75000E+02	.40000E+01	.60000E+01	.100E-01	0.
20	1	.75000E+02	.10000E+03	.40000E+01	.60000E+01	.100E-01	0.
21	1	.10000E+03	.12500E+03	.40000E+01	.60000E+01	.100E-01	0
22	1	.12500E+03	.15000E+03	.40000E+01	.60000E+01	.100E-01	0.
23	1	.15000E+03	.17500E+03	.40000E+01	.60000E+01	.100E-01	0.
24	1	.17500E+03	.20000E+03	.40000E+01	.60000E+01	.100E-01	0.
25	1	0	.25000E+02	.60000E+01	.80000E+01	.100E-01	0
26	1	.25000E+02	.50000E+02	.60000E+01	.80000E+01	.100E-01	0
27	1	.50000E+02	.75000E+02	.60000E+01	.80000E+01	.100E-01	0
28	1	.75000E+02	.10000E+03	.60000E+01	.80000E+01	.100E-01	0
29	1	.10000E+03	.12500E+03	.60000E+01	.80000E+01	.100E-01	0
30	1	.12500E+03	.15000E+03	.60000E+01	.80000E+01	.100E-01	0
31	1	.15000E+03	.17500E+03	.60000E+01	.80000E+01	.100E-01	0
32	1	.17500E+03	.20000E+03	.60000E+01	.80000E+01	.100E-01	0
33	1	0	.25000E+02	.80000E+01	.10000E+02	.100E-01	0
34	1	.25000E+02	.50000E+02	.80000E+01	.10000E+02	.100E-01	0
35	1	.50000E+02	.75000E+02	.80000E+01	.10000E+02	.100E-01	0
36	1	.75000E+02	.10000E+03	.80000E+01	.10000E+02	.100E-01	0
37	1	.10000E+03	.12500E+03	.80000E+01	.10000E+02	.100E-01	0
38	1	.12500E+03	.15000E+03	.80000E+01	.10000E+02	.100E-01	0
39	1	.15000E+03	.17500E+03	.80000E+01	.10000E+02	.100E-01	0
40	1	.17500E+03	.20000E+03	.80000E+01	.10000E+02	.100E-01	0
41	1	.20000E+03	.30000E+03	0	.20000E+01	.100E-01	0
42	1	.30000E+03	.40000E+03	0	.20000E+01	.100E-01	0
43	1	.40000E+03	.50000E+03	0	.20000E+01	.100E-01	0
44	1	.50000E+03	.60000E+03	0	.20000E+01	.100E-01	0
45	1	.60000E+03	.70000E+03	0	.20000E+01	.100E-01	0
46	1	.70000E+03	.80000E+03	0	.20000E+01	.100E-01	0
47	1	.80000E+03	.90000E+03	0	.20000E+01	.100E-01	0
48	1	.90000E+03	.10000E+04	0	.20000E+01	.100E-01	0
49	1	.20000E+03	.30000E+03	.20000E+01	.40000E+01	.100E-01	0
50	1	.30000E+03	.40000E+03	.20000E+01	.40000E+01	[illegible]	0
51	1	.40000E+03	[illegible]	.20000E+01	[illegible]	[illegible]	0
52	[illegible]	[illegible]	[illegible]	[illegible]	[illegible]	[illegible]	[illegible]

AD-A170 204 BEAM PROPAGATION EXPERIMENTAL STUDY(U) MISSION RESEARCH 4/4
CORP ALBUQUERQUE NM C A EKDAHL MAR 82 AMRC-R-352
AFOSR-TR-86-0503 F49620-81-C-0016

UNCLASSIFIED F/G 20/7 NL

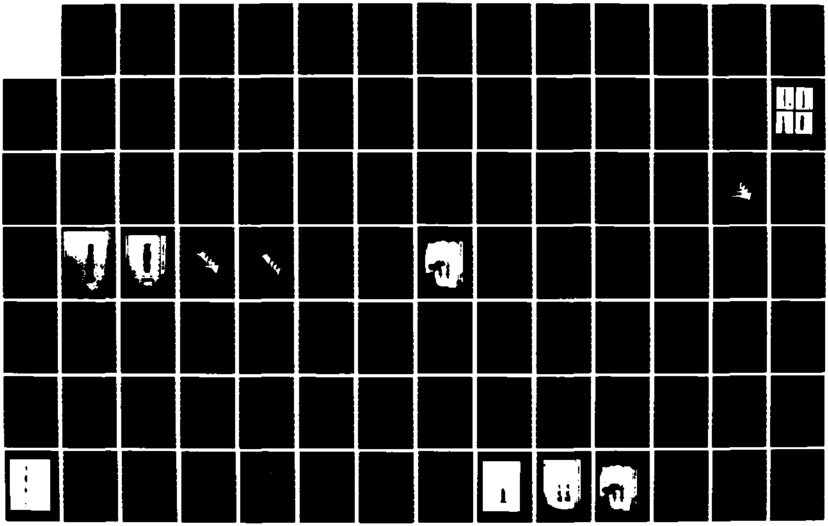

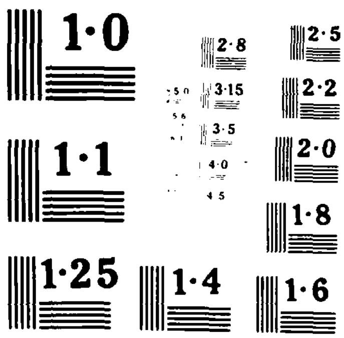

1·0
2·8
2·5
3·15
2·2
3·5
1·1
4·0
2·0
1·8
1·25
1·4
1·6

54	1	.70[illegible]E+03	.8[illegible]E+03	.2[illegible]E+01	.4[illegible]E+01	.1[illegible]E-01	0.
55	1	.80000E+03	.90000E+03	.20000E+01	.40000E+01	.100E-01	0.
56	1	.90000E+03	.10000E+04	.20000E+01	.40000E+01	.100E-01	0.
57	1	.20000E+03	.30000E+03	.40000E+01	.60000E+01	.100E-01	0.
58	1	.30000E+03	.40000E+03	.40000E+01	.60000E+01	.100E-01	0.
59	1	.40000E+03	.50000E+03	.40000E+01	.60000E+01	.100E-01	0.
60	1	.50000E+03	.60000E+03	.40000E+01	.60000E+01	.100E-01	0.
61	1	.60000E+03	.70000E+03	.40000E+01	.60000E+01	.100E-01	0.
62	1	.70000E+03	.80000E+03	.40000E+01	.60000E+01	.100E-01	0.
63	1	.80000E+03	.90000E+03	.40000E+01	.60000E+01	.100E-01	0.
64	1	.90000E+03	.10000E+04	.40000E+01	.60000E+01	.100E-01	0.
65	1	.20000E+03	.30000E+03	.60000E+01	.80000E+01	.100E-01	0.
66	1	.30000E+03	.40000E+03	.60000E+01	.80000E+01	.100E-01	0.
67	1	.40000E+03	.50000E+03	.60000E+01	.80000E+01	.100E-01	0.
68	1	.50000E+03	.60000E+03	.60000E+01	.80000E+01	.100E-01	0.
69	1	.60000E+03	.70000E+03	.60000E+01	.80000E+01	.100E-01	0.
70	1	.70000E+03	.80000E+03	.60000E+01	.80000E+01	.100E-01	0.
71	1	.80000E+03	.90000E+03	.60000E+01	.80000E+01	.100E-01	0.
72	1	.90000E+03	.10000E+04	.60000E+01	.80000E+01	.100E-01	0.
73	1	.20000E+03	.30000E+03	.80000E+01	.10000E+02	.100E-01	0.
74	1	.30000E+03	.40000E+03	.80000E+01	.10000E+02	.100E-01	0.
75	1	.40000E+03	.50000E+03	.80000E+01	.10000E+02	.100E-01	0.
76	1	.50000E+03	.60000E+03	.80000E+01	.10000E+02	.100E-01	0.
77	1	.60000E+03	.70000E+03	.80000E+01	.10000E+02	.100E-01	0.
78	1	.70000E+03	.80000E+03	.80000E+01	.10000E+02	.100E-01	0.
79	1	.80000E+03	.90000E+03	.80000E+01	.10000E+02	.100E-01	0.
80	1	.90000E+03	.10000E+04	.80000E+01	.10000E+02	.100E-01	0.

```
0INCIDENT ELECTRONS
0ELECTRON COLLISION AND RADIATION ENERGY LOSS STRAGGLING
0KNOCK-ON ELECTRON PRODUCTION
0NO COUPLED INELASTIC SCATTERING DEFLECTIONS
0BREMSSTRAHLUNG AND CHARACTERISTIC X-RAY QUANTA FOLLOWED
0BREMSSTRAHLUNG INTRINSIC ANGLE OF EMISSION FROM TABULATED DISTRIBUTION
0PHOTON-PRODUCED PARTICLES FOLLOWED
0 IUNT  LMAX  ITMX  JMAX  IPMX JPMAX  IAMX  KMAX  IBMX KPMAX
     2     1     1    30     1    30     1     8     1     8
0 IMAX  NZON IFLUX  NCYC  INRAN
500000    80     2    -11000000000000000000
0*************** THE STANDARD ERROR ESTIMATES ARE BASED ON    10 BATCHES OF 50000 HISTORIES ***************
0       TIN          TCUT         TPCUT        CTHIN        SORCIN
    1.50000       .01000       .01000      1.00000      3.01000
0     TSAVE                                  THFAC         RLAN         QBLK
     .01000                                10.00000       .50000      1.00000
0ELECTRON ENERGY CLASSIFICATIONS (MEV)
    1.45000      1.40000      1.35000      1.30000      1.25000      1.20000
    1.15000      1.10000      1.05000      1.00000       .95000       .90000
     .85000       .80000       .75000       .70000       .65000       .60000
     .55000       .50000       .45000       .40000       .35000       .30000
     .25000       .20000       .15000       .10000       .05000       .01000
0PHOTON ENERGY CLASSIFICATIONS (MEV)
    1.45000      1.40000      1.35000      1.30000      1.25000      1.20000
    1.15000      1.10000      1.05000      1.00000       .95000       .90000
     .85000       .80000       75000       .70000       .65000       .60000
     .55000       .50000       .45000       .40000       .35000       .30000
     25000        .20000       .15000       .10000       .05000       .01000
0ELECTRON OBLIQUITY CLASSIFICATIONS (DEGREES)
   30 00000     60 00000     90 00000    120 00000    150.00000    180.00000
0ELECTRON AZIMUTH CLASSIFICATIONS (DEGREES)
   180 00000
0PHOTON OBLIQUITY CLASSIFICATIONS (DEGREES)
   30 00000     60 00000     90 00000    120 00000    150.00000    180.00000
0PHOTON AZIMUTH CLASSIFICATIONS (DEGREES)
   180 00000
0NTFST        RGMAX      SCALE SKALE       TCUT        TPCUT        TFCUT        TSAVE        BLIN        EMUM        EMUM
```

F 2

0 2

```
     1       79075E+00      1      1      .01000      .01000      0.00000      .01000      1.00000      0.0      0.0
0K X-RAY QUANTA NOT FOLLOWED IN MATERIAL      1
0ANNIHILATION QUANTA FOLLOWED
1THE PROBLEM IS 100  PER CENT COMPLETE   TIME TO FINISH IS       0 000 SECONDS. AVERAGE TIME PER BATCH IS       32.000
0AVERAGE SOURCE ENERGY = 1 5000E+00 MEV
0      INRAN                IRA                 IRC
 0000000000000000 6121501151342561 3444553113232105
0    ---------------------------------------- HISTORIES ----------------------------------------    REJ      --- STEPS ----
    PRIM       SEC      KNOCK        P E      PAIR       COM      AUGER       BREM       RAD      XRAY     LAND      PRIM        SEC
  500000      3440      3440          0          0         0          0         50        90         0        15    500000       3440
0                                 ENERGY (MEV)        AVE ENERGY (MEV)        NUMBER PRIMARY        NUMBER GENERATED
 FIRST KNOCK (ABOVE TCUT)         3 0369E-04           4 4142E-02              6 8800E-03            3440
 TOTAL KNOCK (ABOVE TCUT)         3 0369E-04           4 4142E-02              6 8800E C3            3440
 PHOTO-ELECTRON                   0                    0                       0                        0
 PAIR                             0.                   0                       0.                       0
 COMPTON                          0.                   0                       0.                       0
 AUGER                            0.                   0                       0                        0
 FIRST BREMSSTRAHLUNG             1 5035E-05           8 7072E-02              1 8000E-04              90
 TOTAL BREMSSTRAHLUNG             1 5035E-05           8 7072E-02              1 8000E-04              90
 K X-RAY                          0.                   0                       0                        0
 ANNIHILATION QUANTA              0                    0                       0.                       0
0UNSCATTERED PRIMARY PHOTONS NUMBER AND ENERGY
 0         99 0          99
0NUMBER COEFFICIENTS - KNOCK-ONS, PHOTON DESCENDANTS
0                                                      TRANSMISSION
   28E-04  32
 0         99
0                                                       REFLECTION
 0         99
 0         99
C                                                     LATERAL ESCAPE
  .67E-02   2
 0         99
0                                          NUMBER AND ENERGY COEFFICIENTS
0                                                     TRANSMISSION
0          CYLINDER DIMENSIONS         ---------- ELECTRON ----------      ----------- PHOTON -----------
        LENGTH(CM)   RADIUS(CM)         NUMBER       ENERGY       COUNTS       NUMBER       ENERGY       COUNTS

          .100E+04     .100E+02     .10E+01   0   .10E+01   0    500014    .10E-04 33   .38E-08 54            5
0                                                      REFLECTION
C          CYLINDER DIMENSIONS         ---------- ELECTRON ----------      ----------- PHOTON -----------
        LENGTH(CM)   RADIUS(CM)         NUMBER       ENERGY       COUNTS       NUMBER       ENERGY       COUNTS

           100E+04     .100E+02   0          99 0         99           0   0          99 0         99            0
0                                                    LATERAL ESCAPE
0          CYLINDER DIMENSIONS         ---------- ELECTRON ----------      ----------- PHOTON -----------
        LENGTH(CM)   RADIUS(CM)         NUMBER       ENERGY       COUNTS       NUMBER       ENERGY       COUNTS

          .100E+04      100E+02     .67E-02   2    20E-03   3      3368    .11E-03 12   .10E-04 22           53
1                                                  ENERGY DEPOSITION
                                          (NORMALIZED TO ONE INCIDENT PARTICLE)
C                                                                                        ENERGY DEPOSITION (MEV)
      ZONE        MATERIAL        MASS(GM)     VOLUME(CC)                       PRIM            KNOCK          G-SEC              TOTAL
```

ZONE	MATERIAL	MASS(GM)	VOLUME(CC)	PRIM		KNOCK		G-SEC		TOTAL
1	1	2668E-03	3142E+03	8641E-05	2	-.3290E-05 29	0		99	6744E-05 16
2	1	2668E 03	3142E+03	4377E 05	2	-.2306E-05 43	0		99	7000E 05 15
3	1	2668E C3	3142E+03	9326E 05	2	-.3885E 05 35	0		99	54[illegible] 05 20
4	1	26[illegible] C3	3142E+03	9422E 05	2	-.5 64[illegible] 05 23	0		99	[illegible] 05 30
5	1	26[illegible] C3	3 42E+03	9369E 05	2	-.[illegible] 05 22	0		99	8[illegible] 05 4
6	1	2668E C3	3 42E+03	9[illegible]8E C5	2	-.9468E 06 30	0		99	8[illegible] 05 4
7	1	2668E C3	3 42E+03	93[illegible] C4	2	-.1350E 05 20	0		99	7[illegible] 05 7
8	1	2668E C3	3 42E+03	829[illegible] C4	1	-.22[illegible] C4 29	0		99	708[illegible] 05 8
9	1	8 [illegible] C3	9425E+03	2482E 04	2	-.4835E C4 26	0		99	1994E 04 7
10	1	8 [illegible]	9425E+03	244[illegible] C4		-.58[illegible] C4 2[illegible]	C		99	8[illegible] C4 8

11	1	.8003E-03	.9425E+03	.2404E-04	1	-.47[illegible]E-05	24	0.	99	.2[illegible]E-04	6
12	1	.8003E-03	.9425E+03	.2481E-04	1	-.4057E-05	10	0.	99	.19[illegible]E-04	6
13	1	.8003E-03	.9425E+03	.2500E-04	1	-.7103E-05	33	0.	99	.17[illegible]E-04	13
14	1	.8003E-03	.9425E+03	.2427E-04	1	-.2[illegible]E-05	20	0.	99	.213[illegible]E-04	8
15	1	.8003E-03	.9425E+03	.2443E-04	1	-.45[illegible]E-05	27	0.	99	.19[illegible]E-04	7
16	1	.8003E-03	.9425E+03	.2408E-04	1	-.05[illegible]E-05	29	0.	99	.18[illegible]E-04	8
17	1	.1334E-02	.1571E+04	0.	99	.3572E-08	40	0.	99	.3[illegible]E-08	40
18	1	.1334E-02	.1571E+04	0.	99	.6254E-08	30	0.	99	.62[illegible]E-08	30
19	1	.1334E-02	.1571E+04	0.	99	.30[illegible]E-08	21	0.	99	.3[illegible]E-08	21
20	1	.1334E-02	.1571E+04	0.	99	.4015E-08	23	0.	99	.4[illegible]E-08	23
21	1	.1334E-02	.1571E+04	0.	99	.83[illegible]E-08	26	0.	99	.83[illegible]E-08	26
22	1	.1334E-02	.1571E+04	0.	99	.3[illegible]E-08	29	0.	99	.3[illegible]E-08	29
23	1	.1334E-02	.1571E+04	0.	99	.34[illegible]E-08	20	0.	99	.3[illegible]E-08	20
24	1	.1334E-02	.1571E+04	0.	99	.4578E-08	21	0.	99	.457[illegible]E-08	21
25	1	.1067E-02	.2199E+04	0.	99	.3341E-08	32	0.	99	.33[illegible]E-08	32
26	1	.1067E-02	.2199E+04	0.	99	.738[illegible]E-08	26	0.	99	.73[illegible]E-08	26
27	1	.1067E-02	.2199E+04	0.	99	.24[illegible]E-08	47	0.	99	.24[illegible]E-08	47
28	1	.1067E-02	.2199E+04	0.	99	.366[illegible]E-08	27	0.	99	.3[illegible]E-08	27
29	1	.1067E-02	.2199E+04	0.	99	.28[illegible]E-08	30	0.	99	.2[illegible]E-08	30
30	1	.1067E-02	.2199E+04	0.	99	.16[illegible]E-08	30	0.	99	.16[illegible]E-08	30
31	1	.1067E-02	.2199E+04	0.	99	.34[illegible]E-08	34	0.	99	.34[illegible]E-08	34
32	1	.1067E-02	.2199E+04	0.	99	.413[illegible]E-08	20	0.	99	.413[illegible]E-08	20
33	1	.2401E-02	.2827E+04	0.	99	.427[illegible]E-08	37	0.	99	.427[illegible]	37
34	1	.2401E-02	.2827E+04	0.	99	.62[illegible]E-08	24	0.	99	.6[illegible]E-08	24
35	1	.2401E-02	.2827E+04	0.	99	.62[illegible]E-08	23	0.	99	.6[illegible]E-08	23
36	1	.2401E-02	.2827E+04	0.	99	.377[illegible]E-08	26	0.	99	.377[illegible]E-08	26
37	1	.2401E-02	.2827E+04	0.	99	.3124E-08	32	0.	99	.312[illegible]	32
38	1	.2401E-02	.2827E+04	0.	9K	.2753E-08	37	0.	99	.275[illegible]E-08	37
39	1	.2401E-02	.2827E+04	0.	99	.28[illegible]E-08	35	0.	99	.28[illegible]E-08	35
40	1	.2401E-02	.2827E+04	0.	99	.34[illegible]E-08	33	0.	99	.3[illegible]E-08	33
41	1	.1067E-02	.1257E+04	.3800E-04	1	-.67[illegible]E-05	21	0.	99	.3[illegible]E-04	4
42	1	.1067E-02	.1257E+04	.3753E-04	1	-.7767E-05	18	0.	99	.2[illegible]E-04	9
43	1	.1067E-02	.1257E+04	.3748E-04	1	-.7649E-05	16	0.	99	.29[illegible]E-04	4
44	1	.1067E-02	.1257E+04	.3773E-04	1	-.80[illegible]E-05	20	0.	99	.311[illegible]E-04	4
45	1	.1067E-02	.1257E+04	.3730E-04	1	-.8[illegible]E-05	20	0.	99	.2[illegible]E-04	6
46	1	.1067E-02	.1257E+04	.3769E-04	1	-.1[illegible]E-04	22	0.	99	.2[illegible]E-04	8
47	1	.1067E-02	.1257E+04	.373[illegible]E-04	1	-.9[illegible]E-05	26	0.	99	.2[illegible]E-04	8
48	1	.1067E-02	.1257E+04	.373[illegible]E-04	0	-.7[illegible]E-05	27	0.	99	.2[illegible]E-04	7
49	1	.3201E-02	.3770E+04	.8826E-04	1	-.2[illegible]E-04	17	0.	99	.74[illegible]E-04	6
50	1	.3201E-02	.3770E+04	.8807E-04	0	-.23[illegible]E-04	10	0.	99	.7407E-04	3

1

ENERGY DEPOSITION
(NORMALIZED TO ONE INCIDENT PARTICLE)

0

ZONE	MATERIAL	MASS(GM)	VOLUME(CC)	ENERGY DEPOSITION (MEV) PRIM		KNOCK		D-SEC		TOTAL	
51	1	.3201E-02	.3770E+04	.8043E-04	1	-.1003E-04	11	0.	99	.7861E-04	3
52	1	.3201E-02	.3770E+04	.8039E-04	1	-.1950E-04	8	0.	99	.707[illegible]E-04	2
53	1	.3201E-02	.3770E+04	.8034E-04	0	-.2337E-04	14	0.	99	.74[illegible]E-04	4
54	1	.3201E-02	.3770E+04	.80[illegible]E-04	0	-.22[illegible]E-04	12	0.	99	.78[illegible]E-04	3
55	1	.3201E-02	.3770E+04	.87[illegible]E-04	0	-.23[illegible]E-04	13	0.	99	.7[illegible]E-04	4
56	1	.3201E-02	.3770E+04	.8064E-04	1	-.2[illegible]E-04	8	0.	99	.7[illegible]E-04	3
57	1	.5335E-02	.6283E+04	0.	99	.15[illegible]E-07	12	0.	99	.15[illegible]E-07	12
58	1	.5335E-02	.6283E+04	0.	99	.1721E-07	26	0.	99	.172[illegible]E-07	26
59	1	.5335E-02	.6283E+04	0.	99	.15[illegible]E-07	18	0.	99	.15[illegible]E-07	18
60	1	.5335E-02	.6283E+04	0.	99	.1547E-07	17	0.	99	.154[illegible]E-07	17
61	1	.5335E-02	.6283E+04	0.	99	.1709E-07	15	0.	99	.17[illegible]E-07	15
62	1	.5335E-02	.6283E+04	0.	99	.1707E-07	6	0.	99	.17[illegible]E-07	6
63	1	.5335E-02	.6283E+04	0.	99	.1412E-07	13	0.	99	.14[illegible]E-07	13
64	1	.5335E-02	.6283E+04	0.	99	.1561E-07	18	0.	99	.156[illegible]E-07	18
65	1	.7470E-02	.8796E+04	0.	99	.1777E-07	17	0.	99	.177[illegible]E-07	17
66	1	.7470E-02	.8796E+04	0.	99	.1092E-07	25	0.	99	.10[illegible]E-07	25
67	1	.7470E-02	.8796E+04	0.	99	.1529E-07	18	0.	99	.15[illegible]E-07	18
68	1	.7470E-02	.8796E+04	0.	99	.1145E-07	18	0.	99	.1145E-07	18
69	1	.7470E-02	.8796E+04	0.	99	.1778E-07	17	0.	99	.1778E-07	17

H 2 H 2

I 2 I 2

70	1	.7470E-02	.8796E+04	0.	99	.1565E-07	13	0.	99	.1565E-07	13
71	1	.7470E-02	.8796E+04	0.	99	.1572E-07	10	0.	99	.1572E-07	10
72	1	.7470E-02	.8796E+04	0.	99	.1544E-07	10	0.	99	.1544E-07	10
73	1	.9604E-02	.1131E+05	0	99	.2024E-07	21	0.	99	.20[illegible]E-07	21
74	1	.9604E-02	.1131E+05	0	99	.1226E-07	18	0.	99	.122[illegible]E-07	18
75	1	.9604E-02	.1131E+05	0.	99	.1340E-07	17	0.	99	.134[illegible]E-07	17
76	1	.9604E-02	.1131E+05	0.	99	.1512E-07	15	0.	99	.15[illegible]E-07	15
77	1	.9604E-02	.1131E+05	0.	99	.1639E-07	18	0.	99	.163[illegible]E-07	18
78	1	.9604E-02	.1131E+05	0.	99	.1440E-07	10	0.	99	.144[illegible]E-07	10
79	1	.9604E-02	.1131E+05	0.	99	.8425E-08	14	0.	99	.84[illegible]E-08	14
80	1	.9604E-02	.1131E+05	0.	99	.1509E-07	10	0.	99	.1509E-07	10
0 TOTAL				.1358E-02	0	-.3030E-03	3	0.	99	.1055E-02	1

0

CHARGE DISTRIBUTION
(NORMALIZED TO ONE INCIDENT PARTICLE)

0

ZONE	MATERIAL	ZL	ZR	RI	RO	ELECTRONS PRIM		KNOCK		D-SEC		TOTAL	
1	1	0	.2500E+02	0	.2000E+01	0.	99	-.56E-04	18	0.	99	-.56E-04	18
2	1	.2500E+02	.5000E+02	0.	.2000E+01	0.	99	-.44E-04	25	0.	99	-.44E-04	25
3	1	.5000E+02	.7500E+02	0.	.2000E+01	0.	99	-.64E-04	15	0.	99	-.64E-04	15
4	1	.7500E+02	.1000E+03	0	.2000E+01	0.	99	-.76E-04	9	0.	99	-.76E-04	9
5	1	.1000E+03	.1250E+03	0.	.2000E+01	0.	99	-.40E-04	18	0.	99	-.40E-04	18
6	1	.1250E+03	.1500E+03	0	.2000E+01	0.	99	-.38E-04	18	0.	99	-.38E-04	18
7	1	.1500E+03	.1750E+03	0.	.2000E+01	0.	99	-.44E-04	26	0.	99	-.44E-04	26
8	1	.1750E+03	.2000E+03	0.	.2000E+01	0.	99	-.46E-04	15	0.	99	-.46E-04	15
9	1	0	.2500E+02	.2000E+01	.4000E+01	0.	99	-.11E-03	13	0.	99	-.11E-03	13
10	1	.2500E+02	.5000E+02	.2000E+01	.4000E+01	0.	99	-.14E-03	13	0.	99	-.14E-03	13
11	1	.5000E+02	.7500E+02	.2000E+01	.4000E+01	0	99	-.12E-03	18	0	99	-.12E-03	18
12	1	.7500E+02	.1000E+03	.2000E+01	.4000E+01	0.	99	-.14E-03	10	0	99	-.14E-03	10
13	1	.1000E+03	.1250E+03	.2000E+01	.4000E+01	0.	99	-.12E-03	18	0.	99	-.12E-03	18
14	1	.1250E+03	.1500E+03	.2000E+01	.4000E+01	0	99	-.92E-04	13	0.	99	-.92E-04	13
15	1	.1500E+03	.1750E+03	.2000E+01	.4000E+01	0	99	-.11E-03	13	0.	99	-.11E-03	13
16	1	.1750E+03	.2000E+03	.2000E+01	.4000E+01	0.	99	-.18E-03	10	0.	99	-.18E-03	10
17	1	0	.2500E+02	.4000E+01	.6000E+01	0	99	0	99	0.	99	0.	99
18	1	.2500E+02	.5000E+02	.4000E+01	.6000E+01	0.	99	0	99	0.	99	0.	99
19	1	.5000E+02	.7500E+02	.4000E+01	.6000E+01	0.	99	0	99	0	99	0.	99
20	1	.7500E+02	.1000E+03	.4000E+01	.6000E+01	0	99	0	99	0	99	0.	99
21	1	.1000E+03	.1250E+03	.4000E+01	.6000E+01	0	99	0	99	0	99	0	99
22	1	.1250E+03	.1500E+03	.4000E+01	.6000E+01	0	99	0	99	0	99	0.	99
23	1	.1500E+03	.1750E+03	.4000E+01	.6000E+01	0	99	0	99	0	99	0	99
24	1	.1750E+03	.2000E+03	.4000E+01	.6000E+01	0	99	0	99	0	99	0	99
25	1	0	.2500E+02	.6000E+01	.8000E+01	0	99	0	99	0	99	0	99
26	1	.2500E+02	.5000E+02	.6000E+01	.8000E+01	0	99	0	99	0	99	0.	99
27	1	.5000E+02	.7500E+02	.6000E+01	.8000E+01	0	99	0	99	0	99	0.	99
28	1	.7500E+02	.1000E+03	.6000E+01	.8000E+01	0	99	0	99	0	99	0.	99
29	1	.1000E+03	.1250E+03	.6000E+01	.8000E+01	0	99	0	99	0	99	0	99
30	1	.1250E+03	.1500E+03	.6000E+01	.8000E+01	0	99	0	99	0	99	0.	99
31	1	.1500E+03	.1750E+03	.6000E+01	.8000E+01	0	99	0	99	0	99	0	99
32	1	.1750E+03	.2000E+03	.6000E+01	.8000E+01	0	99	0	99	0	99	0	99
33	1	0	.2500E+02	.8000E+01	.1000E+02	0	99	0	99	0.	99	0	99
34	1	.2500E+02	.5000E+02	.8000E+01	.1000E+02	0	99	0	99	0	99	0	99
35	1	.5000E+02	.7500E+02	.8000E+01	.1000E+02	0	99	0	99	0	99	0	99
36	1	.7500E+02	.1000E+03	.8000E+01	.1000E+02	0	99	0	99	0	99	0	99
37	1	.1000E+03	.1250E+03	.8000E+01	.1000E+02	0	99	0	99	0	99	0	99
38	1	.1250E+03	.1500E+03	.8000E+01	.1000E+02	0	99	0	99	0	99	0	99
39	1	.1500E+03	.1750E+03	.8000E+01	.1000E+02	0	99	0	99	0	99	0	99
40	1	.1750E+03	.2000E+03	.8000E+01	.1000E+02	0	99	0	99	0	99	0	99
41	1	.2000E+03	.3000E+03	0	.2000E+01	0	99	-.20E-03	10	0	99	-.20E-03	10
42	1	.3000E+03	.4000E+03	0	.2000E+01	0	99	-.17E-03	9	0	99	-.17E-03	9
43	1	.4000E+03	.5[illegible]E+03	0	.2000E+01	0	99	-.18E-03	9	0	99	-.18E-03	9
44	1	.5000E+03	.600[illegible]E+03	0	.2000E+01	0	99	-.18E-03	12	0	99	-.18E-03	12
45	1	.6000E+03	.7000E+03	0	.2000E+01	0	99	-.2[illegible]E-03	7	0	99	-.2[illegible]E-03	7
46	1	.7000E+03	[illegible]	0	.2000E+01	0	99	-.23E-03	13	0	99	-.23E-03	13
47	[illegible]	[illegible]	[illegible]	[illegible]	[illegible]	0	99	-.8[illegible]	[illegible]	[illegible]	99	-.8[illegible]	[illegible]

ZONE	MATERIAL	ZL	ZR	RI	RO	PRIM		KNOCK		D-SEC		TOTAL	
48	1	.800E+03	.100E+04	0.	.200E+01	0.	99	[illegible]	6	0.	99	[illegible]	8
49	1	.200E+03	.300E+03	.200E+01	.400E+01	0.	99	-.50E-03	8	0.	99	-.50E-03	8
50	1	.300E+03	.400E+03	.200E+01	.400E+01	0.	99	-.61E-03	7	0.	99	-.61E-03	7

0

CHARGE DISTRIBUTION
(NORMALIZED TO ONE INCIDENT PARTICLE)

0

ZONE	MATERIAL	ZL	ZR	RI	RO	ELECTRONS PRIM		KNOCK		D-SEC		TOTAL	
51	1	.400E+03	.500E+03	.200E+01	.400E+01	0.	99	-.40E-03	6	0.	99	-.40E-03	6
52	1	.500E+03	.600E+03	.200E+01	.400E+01	0.	99	-.40E-03	6	0.	99	-.40E-03	6
53	1	.600E+03	.700E+03	.200E+01	.400E+01	0.	99	-.81E-03	7	0.	99	-.81E-03	7
54	1	.700E+03	.800E+03	.200E+01	.400E+01	0.	99	-.40E-03	7	0.	99	-.40E-03	7
55	1	.800E+03	.900E+03	.200E+01	.400E+01	0.	99	-.40E-03	7	0.	99	-.40E-03	7
56	1	.900E+03	.100E+04	.200E+01	.400E+01	0.	99	-.47E-03	7	0.	99	-.47E-03	7
57	1	.200E+03	.300E+03	.400E+01	.600E+01	0.	99	0.	99	0.	99	0.	99
58	1	.300E+03	.400E+03	.400E+01	.600E+01	0.	99	0.	99	0.	99	0.	99
59	1	.400E+03	.500E+03	.400E+01	.600E+01	0.	99	0.	99	0.	99	0.	99
60	1	.500E+03	.600E+03	.400E+01	.600E+01	0.	99	0.	99	0.	99	0.	99
61	1	.600E+03	.700E+03	.400E+01	.600E+01	0.	99	0.	99	0.	99	0.	99
62	1	.700E+03	.800E+03	.400E+01	.600E+01	0.	99	0.	99	0.	99	0.	99
63	1	.800E+03	.900E+03	.400E+01	.600E+01	0.	99	0.	99	0.	99	0.	99
64	1	.900E+03	.100E+04	.400E+01	.600E+01	0.	99	0.	99	0.	99	0.	99
65	1	.200E+03	.300E+03	.600E+01	.800E+01	0.	99	0.	99	0.	99	0.	99
66	1	.300E+03	.400E+03	.600E+01	.800E+01	0.	99	0.	99	0.	99	0.	99
67	1	.400E+03	.500E+03	.600E+01	.800E+01	0.	99	0.	99	0.	99	0.	99
68	1	.500E+03	.600E+03	.600E+01	.800E+01	0.	99	0.	99	0.	99	0.	99
69	1	.600E+03	.700E+03	.600E+01	.800E+01	0.	99	0.	99	0.	99	0.	99
70	1	.700E+03	.800E+03	.600E+01	.800E+01	0.	99	0.	99	0.	99	0.	99
71	1	.800E+03	.900E+03	.600E+01	.800E+01	0.	99	0.	99	0.	99	0.	99
72	1	.900E+03	.100E+04	.600E+01	.800E+01	0.	99	0.	99	0.	99	0.	99
73	1	.200E+03	.300E+03	.800E+01	.100E+02	0.	99	0.	99	0.	99	0.	99
74	1	.300E+03	.400E+03	.800E+01	.100E+02	0.	99	0.	99	0.	99	0.	99
75	1	.400E+03	.500E+03	.800E+01	.100E+02	0.	99	0.	99	0.	99	0.	99
76	1	.500E+03	.600E+03	.800E+01	.100E+02	0.	99	0.	99	0.	99	0.	99
77	1	.600E+03	.700E+03	.800E+01	.100E+02	0.	99	0.	99	0.	99	0.	99
78	1	.700E+03	.800E+03	.800E+01	.100E+02	0.	99	0.	99	0.	99	0.	99
79	1	.800E+03	.900E+03	.800E+01	.100E+02	0.	99	0.	99	0.	99	0.	99
80	1	.900E+03	.100E+04	.800E+01	.100E+02	0.	99	0.	99	0.	99	0.	99
			TOTAL			0.	99	-.60E-02	2	0.	99	-.60E-02	2

0

0

ENERGY SPECTRA OF TRANSMITTED ELECTRONS
(NUMBER/MEV, NORMALIZED TO ONE INCIDENT PARTICLE)

0 E (MEV) LENGTH= 1000.0000

1.5000	-	1.4500	.20E+02	0
1.4500	-	1.4000	.60E-03	23
1.4000	-	1.3500	.80E-04	67
1.3500	-	1.3000	.20E-03	33
1.3000	-	1.2500	.12E-03	51
1.2500	-	1.2000	.40E-04	99
1.2000	-	1.1500	.80E-04	67
1.1500	-	1.1000	.40E-04	99
1.1000	-	1.0500	.40E-04	99
1.0500	-	1.0000	.80E-04	67
1.0000	-	.9500	.40E-04	99
.9500	-	.9000	.80E-04	67
.9000	-	.8500	0.	99
.8500	-	.8000	0.	99
.8000	-	.7500	0.	99
.7500	-	.7000	0.	99
.7000	-	.6500	.40E-04	99
.6500	-	.6000	.40E-04	99
.6000	-	.5500	0.	99
.5500	-	.5000	.40E-04	99
.5000	-	.4500	0.	99
.4500	-	.4000	0.	99
.4000	-	.3500	0.	99
.3500	-	.3000	0.	99
.3000	-	.2500	0.	99
.2500	-	.2000	0.	99
.2000	-	.1500	0.	99
.1500	-	.1000	.12E-03	71
.1000	-	.0500	.40E-04	99
.0500	-	.0100	.35E-03	22

J 2

K 2

0

ENERGY SPECTRA OF REFLECTED ELECTRONS
(NUMBER MEV, NORMALIZED TO ONE INCIDENT PARTICLE)

0 E (MEV) LENGTH= 1000 0000

1.5000	-	1.4500	0	99
1.4500	-	1.4000	0	99
1.4000	-	1.3500	0	99
1.3500	-	1.3000	0.	99
1.3000	-	1.2500	0.	99
1.2500	-	1.2000	0.	99
1.2000	-	1.1500	0	99
1.1500	-	1.1000	0	99
1.1000	-	1.0500	0.	99
1.0500	-	1.0000	0.	99
1.0000	-	.9500	0	99
.9500	-	.9000	0	99
.9000	-	.8500	0	99
.8500	-	.8000	0	99
.8000	-	.7500	0	99
.7500	-	.7000	0	99
.7000	-	.6500	0	99
.6500	-	.6000	0	99
.6000	-	.5500	0	99
.5500	-	.5000	0	99
.5000	-	.4500	0	99
.4500	-	.4000	0.	99
.4000	-	.3500	0	99
.3500	-	.3000	0	99
.3000	-	.2500	0	99
.2500	-	.2000	0	99
.2000	-	.1500	0	99
.1500	-	.1000	0	99
.1000	-	.0500	0	99
.0500	-	.0100	0	99

ENERGY SPECTRA OF LATERALLY ESCAPING ELECTRONS
(NUMBER MEV, NORMALIZED TO ONE INCIDENT PARTICLE)

0 E (MEV) LENGTH= 1000 0000

1.5000	-	1.4500	0	99
1.4500	-	1.4000	0	99
1.4000	-	1.3500	0	99
1.3500	-	1.3000	0.	99
1.3000	-	1.2500	0	99
1.2500	-	1.2000	0	99
1.2000	-	1.1500	0	99
1.1500	-	1.1000	0	99
1.1000	-	1.0500	0	99
1.0500	-	1.0000	0	99
1.0000	-	.9500	0	99
.9500	-	.9000	0	99
.9000	-	.8500	0	99
.8500	-	.8000	0	99
.8000	-	.7500	0	99
.7500	-	.7000	.6E-03	[illegible]
[illegible]	-	.6500	[illegible]	[illegible]

E (MEV)		
.6500 - .6000	.12E-03	51
.6000 - .5500	.12E-03	71
.5500 - .5000	.20E-03	40
.5000 - .4500	.40E-03	21
.4500 - .4000	.44E-03	32
.4000 - .3500	.20E-03	37
.3500 - .3000	.60E-03	32
.3000 - .2500	.82E-03	24
.2500 - .2000	.14E-02	29
.2000 - .1500	.20E-02	9
.1500 - .1000	.44E-02	12
.1000 - .0500	.14E-01	5
.0500 - .0100	.14E+00	2

ANGULAR DISTRIBUTIONS OF TRANSMITTED AND REFLECTED ELECTRONS
(NUMBER/SR, NORMALIZED TO ONE INCIDENT PARTICLE)

THETA (DEG)	PHI(DEG)= 0.000 180.000	
0.0000 - 30.0000	.12E+01	0
30.0000 - 60.0000	.26E-05	71
60.0000 - 90.0000	.70E-05	29
90.0000 -120.0000	0.	99
120.0000 -150.0000	0.	99
150.0000 -180.0000	0.	99

ANGULAR DISTRIBUTIONS OF LATERALLY ESCAPING ELECTRONS
(NUMBER/SR, NORMALIZED TO ONE INCIDENT PARTICLE)

THETA (DEG)	PHI(DEG)= 0.000 180.000	
0.0000 - 30.0000	0.	99
30.0000 - 60.0000	.14E-03	5
60.0000 - 90.0000	.18E-02	2
90.0000 -120.0000	.17E-03	4
120.0000 -150.0000	0.	99
150.0000 -180.0000	0.	99

ENERGY SPECTRA AND ANGULAR DISTRIBUTIONS OF ELECTRONS TRANSMITTED AND REFLECTED
AZIMUTHAL INTERVAL IS 0.00000 TO 180.00000 DEGREES
(NUMBER/(MEV*SR), NORMALIZED TO ONE PARTICLE)

E (MEV) THETA=	0.000 30.000		30.000 60.000		60.000 90.000		90.000 120.000		120.000 150.000		150.000 180.000	
1.5000 - 1.4500	.24E+02	0	0.	99	0.	99	0.	99	0.	99	0.	99
1.4500 - 1.4000	.71E-03	23	0.	99	0.	99	0.	99	0.	99	0.	99
1.4000 - 1.3500	.95E-04	67	0.	99	0.	99	0.	99	0.	99	0.	99
1.3500 - 1.3000	.24E-03	33	0.	99	0.	99	0.	99	0.	99	0.	99
1.3000 - 1.2500	.14E-03	51	0.	99	0.	99	0.	99	0.	99	0.	99
1.2500 - 1.2000	.48E-04	99	0.	99	0.	99	0.	99	0.	99	0.	99
1.2000 - 1.1500	.95E-04	67	0.	99	0.	99	0.	99	0.	99	0.	99
1.1500 - 1.1000	.48E-04	99	0.	99	0.	99	0.	99	0.	99	0.	99
1.1000 - 1.0500	.48E-04	99	0.	99	0.	99	0.	99	0.	99	0.	99
1.0500 - 1.0000	.95E-04	67	0.	99	0.	99	0.	99	0.	99	0.	99
1.0000 - .9500	.48E-04	99	0.	99	0.	99	0.	99	0.	99	0.	99
.9500 - .9000	.95E-04	67	0.	99	0.	99	0.	99	0.	99	0.	99
.9000 - .8500	0.	99	0.	99	0.	99	0.	99	0.	99	0.	99
.8500 - .8000	0.	99	0.	99	0.	99	0.	99	0.	99	0.	99
.8000 - .7500	0.	99	0.	99	0.	99	0.	99	0.	99	0.	99
.7500 - .7000	0.	99	0.	99	0.	99	0.	99	0.	99	0.	99
.7000 - .6500	0.	99	.17E-04	99	0.	99	0.	99	0.	99	0.	99
.6500 - .6000	0.	99	.17E-04	99	0.	99	0.	99	0.	99	0.	99
.6000 - .5500	0.	99	0.	99	0.	99	0.	99	0.	99	0.	99
.5500 - .5000	0.	99	.17E-04	99	0.	99	0.	99	0.	99	0.	99
.5000 - .4500	0.	99	0.	99	0.	99	0.	99	0.	99	0.	99
.4500 - .4000	0.	99	0.	99	0.	99	0.	99	0.	99	0.	99
.4000 - .3500	0.	99	0.	99	0.	99	0.	99	0.	99	0.	99

L 2 L 2

M 2 M 2

E (MEV) THETA=	0.000 30.000		30.000 60.000		60.000 90.000		90.000 120.000		120.000 150.000		150.000 180.000	
.3500 - .3000	0.	99	0.	99	0.	99	0.	99	0.	99	0.	99
.3000 - .2500	0.	99	0.	99	0.	99	0.	99	0.	99	0.	99
.2500 - .2000	0.	99	0.	99	0.	99	0.	99	0.	99	0.	99
.2000 - .1500	0.	99	0.	99	0.	99	0.	99	0.	99	0.	99
.1500 - .1000	0.	99	0.	99	.38E-04	71	0.	99	0.	99	0.	99
.1000 - .0500	0.	99	0.	99	.13E-04	99	0.	99	0.	99	0.	99
.0500 - .0100	0.	99	0.	99	.11E-03	22	0.	99	0.	99	0.	99

ENERGY SPECTRA AND ANGULAR DISTRIBUTIONS OF ELECTRONS LATERALLY ESCAPING
AZIMUTHAL INTERVAL IS 0.00000 TO 180.00000 DEGREES
(NUMBER/(MEV*SR), NORMALIZED TO ONE PARTICLE)

E (MEV) THETA=	0.000 30.000		30.000 60.000		60.000 90.000		90.000 120.000		120.000 150.000		150.000 180.000	
1.5000 - 1.4500	0.	99	0.	99	0.	99	0.	99	0.	99	0.	99
1.4500 - 1.4000	0.	99	0.	99	0.	99	0.	99	0.	99	0.	99
1.4000 - 1.3500	0.	99	0.	99	0.	99	0.	99	0.	99	0.	99
1.3500 - 1.3000	0.	99	0.	99	0.	99	0.	99	0.	99	0.	99
1.3000 - 1.2500	0.	99	0.	99	0.	99	0.	99	0.	99	0.	99
1.2500 - 1.2000	0.	99	0.	99	0.	99	0.	99	0.	99	0.	99
1.2000 - 1.1500	0.	99	0.	99	0.	99	0.	99	0.	99	0.	99
1.1500 - 1.1000	0.	99	0.	99	0.	99	0.	99	0.	99	0.	99
1.1000 - 1.0500	0.	99	0.	99	0.	99	0.	99	0.	99	0.	99
1.0500 - 1.0000	0.	99	0.	99	0.	99	0.	99	0.	99	0.	99
1.0000 - .9500	0.	99	0.	99	0.	99	0.	99	0.	99	0.	99
.9500 - .9000	0.	99	0.	99	0.	99	0.	99	0.	99	0.	99
.9000 - .8500	0.	99	0.	99	0.	99	0.	99	0.	99	0.	99
.8500 - .8000	0.	99	0.	99	0.	99	0.	99	0.	99	0.	99
.8000 - .7500	0.	99	0.	99	0.	99	0.	99	0.	99	0.	99
.7500 - .7000	0.	99	.70E-04	41	0.	99	0.	99	0.	99	0.	99
.7000 - .6500	0.	99	.79E-04	41	0.	99	0.	99	0.	99	0.	99
.6500 - .6000	0.	99	.52E-04	51	0.	99	0.	99	0.	99	0.	99
.6000 - .5500	0.	99	.52E-04	71	0.	99	0.	99	0.	99	0.	99
.5500 - .5000	0.	99	.12E-03	40	0.	99	0.	99	0.	99	0.	99
.5000 - .4500	0.	99	.17E-03	21	0.	99	0.	99	0.	99	0.	99
.4500 - .4000	0.	99	.19E-03	32	0.	99	0.	99	0.	99	0.	99
.4000 - .3500	0.	99	.12E-03	37	0.	99	0.	99	0.	99	0.	99
.3500 - .3000	0.	99	.30E-03	32	0.	99	0.	99	0.	99	0.	99
.3000 - .2500	0.	99	.40E-03	24	0.	99	0.	99	0.	99	0.	99
.2500 - .2000	0.	99	.63E-03	29	0.	99	0.	99	0.	99	0.	99
.2000 - .1500	0.	99	.54E-03	18	.52E-03	15	0.	99	0.	99	0.	99
.1500 - .1000	0.	99	0.	99	.14E-02	12	0.	99	0.	99	0.	99
.1000 - .0500	0.	99	0.	99	.43E-02	5	0.	99	0.	99	0.	99
.0500 - .0100	0.	99	.20E-03	35	.39E-02	2	.42E-02	4	0.	99	0.	99

ENERGY SPECTRA OF TRANSMITTED PHOTONS
(NUMBER/MEV, NORMALIZED TO ONE INCIDENT PARTICLE)

E (MEV) LENGTH=	1000.0000	
1.5000 - 1.4500	0.	99
1.4500 - 1.4000	0.	99
1.4000 - 1.3500	0.	99
1.3500 - 1.3000	0.	99
1.3000 - 1.2500	0.	99
1.2500 - 1.2000	0.	99
1.2000 - 1.1500	0.	99
1.1500 - 1.1000	0.	99
1.1000 - 1.0500	0.	99
1.0500 - 1.0000	0.	99
1.0000 - .9500	0.	99
.9500 - .9000	0.	99
.9000 - .8500	0.	99
.8500 - .8000	0.	99
.8000 - .7500	0.	99
.7500 - .7000	0.	99
.7000 - .6500	0.	99

```
      .9500 -    .9000  0.          99 0          99 0          99 0.         99 0          99 0.         99
      .9000 -    .8500  0.          99 0          99 0          99 0          99 0.         99 0.         99
      .8500 -    .8000  0.          99 0          99 0          99 0          99 0.         99 0.         99
      .8000 -    .7500  0.          99 0          99 0          99 0          99 0          99 0.         99
      .7500 -    .7000  0.          99 0          99 0          99 0          99 0.         99 0.         99
      .7000 -    .6500  0.          99 0          99 0          99 0.         99 0.         99 0.         99
      .6500 -    .6000  0           99 0          99 0          99 0          99 0.         99 0.         99
      .6000 -    .5500  0           99 0          99 0          99 0.         99 0          99 0.         99
      .5500 -    .5000     .48E-04  99 0          99 0.         99 0          99 0          99 0.         99
      .5000 -    .4500  0           99    .17E-04 99 0          99 0.         99 0.         99 0.         99
      .4500 -    .4000     .18E-03  51 0          99 0          99 0.         99 0.         99 0.         99
0     INTEGRAL (/SR)      .95E-05  41   .87E-06  99 0          99 0          99 0          99 0          99
0                              ENERGY SPECTRA AND ANGULAR DISTRIBUTIONS OF PHOTONS LATERALLY ESCAPING
                                        AZIMUTHAL INTERVAL IS   0.00000 TO 180.00000 DEGREES
                                         (NUMBER (MEV*SR) , NORMALIZED TO ONE PARTICLE)
0      E (MEV)   THETA=  0.000        30.000        60.000        90.000       120.000       150.000
                        30.000        60.000        90.000       120.000       150.000       180.000

    1.5000 -  1.4500  0           99 0          99 0          99 0          99 0.         99 0          99
    1.4500 -  1.4000  0           99 0          99 0          99 0          99 0          99 0.         99
    1.4000 -  1.3500  0.          99 0          99 0          99 0.         99 0          99 0.         99
    1.3500 -  1.3000  0           99 0          99 0          99 0          99 0          99 0.         99
    1.3000 -  1.2500  0.          99 0          99 0          99 0.         99 0.         99 0.         99
    1.2500 -  1.2000  0           99 0          99 0          99 0          99 0          99 0.         99
    1.2000 -  1.1500  0           99 0          99 0          99 0          99 0          99 0.         99
    1.1500 -  1.1000  0           99 0          99 0.         99 0          99 0          99 0          99
    1.1000 -  1.0500  0           99 0          99 0.         99 0          99 0          99 0          99
    1.0500 -  1.0000  0.          99 0          99 0          99 0          99 0          99 0.         99
    1.0000 -   .9500  0           99 0          99 0          99 0          99 0          99 0.         99
     .9500 -   .9000  0           99 0          99 0          99 0          99 0          99 0.         99
     .9000 -   .8500  0           99 0          99 0          99 0          99 0          99 0          99
     .8500 -   .8000  0           99 0          99 0          99 0          99 0          99 0          99
     .8000 -   .7500  0           99 0          99 0          99 0          99 0          99 0          99
     .7500 -   .7000  0           99 0          99 0          99 0          99 0          99 0          99
     .7000 -   .6500  0           99 0          99 0          99 0          99 0          99 0          99
     .6500 -   .6000  0           99 0          99 0          99 0          99 0          99 0          99
     .6000 -   .5500     .95E-04  67 0          99 0          99 0          99 0          99 0          99
     .5500 -   .5000     .48E-04  99 0          99 0          99 0          99 0          99 0          99
     .5000 -   .4500     .95E-04  67 0          99 0          99 0          99 0          99 0          99
     .4500 -   .4000     .48E-04  99 0          99 0          99 0          99 0          99 0          99
     .4000 -   .3500     .48E-04  99 0          99 0          99 0          99 C          99 0          99
     .3500 -   .3000     .95E-04  67 0          99 0          99 0          99 0          99 0          99
     .3000 -   .2500     .48E-04  99 C          99 0          99 0          99 0          99 0          99
     .2500 -   .2000     .14E-03  51 0          99 0          99 0          99 0.         99 0          99
     .2000 -   .1500     .19E-03  41 0          99    .13E-04 99 0          99 0          99 0          99
     .1500 -   .1000     .48E-04  99 0          99 0          99 0          99 0          99 0          99
     .1000 -   .0500     .38E-03  36   .87E-04  33 0          99 0          99 0          99 0          99
     .0500 -   .0100     .95E-03  25   .11E-03  33 0          99 0          99 0          99 0          99
0     INTEGRAL (/SR)      .10E-03  16   .87E-05  28   .64E-06  99 0          99 0          99 0          99
 THE NUMBER OF ECS WORDS USED FOR STATISTICS IS       1929
```

APPENDIX B

AIR PROPERTIES AND 1.5 MeV ELECTRON BEAM TRANSPORT AT 760 TORR

I I

J I

1.5 MEV FX100 BEAM INTO 760 TORR AIR

0

0 NSET	ITRN	IZIP	ISGN	ISUB	INEL	ICYC	NCYC	NMAX	EMAX
1	8	0	1	80	1	1	8	84	.15000E+01

0INPUT DATA TAPE IDENTIFICATION

DATATAPE-2 (RESTER-AIGINGER PH-RAD CORR), 84 STERNHEIMER SETS. 30 JAN 8

0DETOUR	DENSITY
.83500E+00	.12907E-02

0

0RANGE TABLE

0 EMAX	NCYC	EFAC	NMAX	T(NMAX+1)	NCAL	T(NCAL)
.15000E+01	8	.91700E+00	84	.8858[illegible]E-02	86	.9[illegible]E-03

0 JMAX	LMAX
3	1

0 Z	A	W
7.00000	14.00670	.78500
8.00000	15.99939	.22120
18.00000	39.94780	.01300

0 PI	PIO
86.84168	86.84168

0 ----------------------PARAMETERS FOR DENSITY EFFECT--------------------

PI	C	B	DM	X1	X0
86.84168	-10.55486	.21283	3.00000	4.00000	1.80000
86.84168	-10.55486	.21283	3.00000	4.00000	1.80000
.1500E+00	-.1867E+02	.7888E-01			

ELECTRON RESULTS

0 EFFECTIVE Z/A = .49914 EFFECTIVE MEAN IONIZATION POTENTIAL = 86.84 EV CRITICAL ENERGY = 0.000 MEV

N	ENERGY MEV	STOPPING POWER COLLISION MEV CM2/G	STOPPING POWER RADIATION MEV CM2/G	STOPPING POWER TOTAL MEV CM2/G	RANGE G/CM2	RADIATION YIELD	BETA**2	DENSITY CORR MEV CM2/G	RAD/COL	DRANGE G/CM2	DYIELD
86	.9498E-03	.105E+03	.546E-02	.105E+03	.451E-05	0.	.371E-02	0.	.518E-04	0.	0.
85	.1036E-02	.990E+02	.546E-02	.990E+02	.535E-05	.442E-05	.404E-02	0.	.547E-04	.839E-06	.498E-08
84	.1130E-02	.945E+02	.545E-02	.946E+02	.632E-05	.872E-05	.441E-02	0.	.577E-04	.865E-06	.527E-08
83	.1232E-02	.895E+02	.544E-02	.895E+02	.743E-05	.128E-04	.480E-02	0.	.608E-04	.111E-05	.606E-08
82	.1343E-02	.846E+02	.544E-02	.846E+02	.871E-05	.170E-04	.524E-02	0.	.642E-04	.128E-05	.697E-08
81	.1465E-02	.799E+02	.543E-02	.800E+02	.102E-04	.211E-04	.571E-02	0.	.679E-04	.148E-05	[illegible]E-08
80	.1597E-02	.755E+02	.542E-02	.755E+02	.118E-04	.251E-04	.622E-02	0.	.718E-04	.171E-05	[illegible]E-08
79	.1742E-02	.712E+02	.541E-02	.712E+02	.139E-04	.292E-04	.678E-02	0.	.759E-04	.197E-05	.107E-07
78	.1900E-02	.671E+02	.539E-02	.671E+02	.162E-04	.333E-04	.739E-02	0.	.804E-04	.228E-05	.123E-07
77	.2072E-02	.632E+02	.538E-02	.632E+02	.188E-04	.374E-04	.806E-02	0.	.851E-04	.264E-05	.142E-07
76	.2259E-02	.595E+02	.537E-02	.595E+02	.219E-04	.415E-04	.878E-02	0.	.902E-04	.306E-05	.164E-07
75	.2464E-02	.560E+02	.535E-02	.560E+02	.254E-04	.458E-04	.957E-02	0.	.956E-04	.354E-05	.190E-07
74	.2687E-02	.526E+02	.533E-02	.526E+02	.295E-04	.502E-04	.104E-01	0.	.101E-03	.411E-05	.220E-07
73	.2930E-02	.495E+02	.532E-02	.495E+02	.343E-04	.547E-04	.114E-01	0.	.107E-03	.477E-05	.254E-07
72	.3195E-02	.465E+02	.530E-02	.465E+02	.398E-04	.593E-04	.124E-01	0.	.114E-03	.553E-05	.294E-07
71	.3484E-02	.436E+02	.528E-02	.436E+02	.462E-04	.641E-04	.135E-01	0.	.1[illegible]E-03	.643E-05	.340E-07
70	.3799E-02	.409E+02	.526E-02	.409E+02	.537E-04	.692E-04	.147E-01	0.	.12[illegible]E-03	.747E-05	.393E-07
69	.4143E-02	.384E+02	.523E-02	.384E+02	.624E-04	.744E-04	.160E-01	0.	.136E-03	.868E-05	.455E-07
68	.4518E-02	.360E+02	.521E-02	.361E+02	.725E-04	.799E-04	.175E-01	0.	.145E-03	.101E-04	.527E-07
67	.4927E-02	.338E+02	.519E-02	.338E+02	.842E-04	.857E-04	.190E-01	0.	.154E-03	.117E-04	.612E-07
66	.5373E-02	.316E+02	.516E-02	.316E+02	.979E-04	.917E-04	.207E-01	0.	.163E-03	.137E-04	.707E-07
65	.5859E-02	.296E+02	.514E-02	.296E+02	.114E-03	.981E-04	.225E-01	0.	.173E-03	.159E-04	.819E-07
64	.6390E-02	.277E+02	.511E-02	.278E+02	.132E-03	.105E-03	.245E-01	0.	.184E-03	.185E-04	.948E-07
63	.6968E-02	.260E+02	.509E-02	.260E+02	.154E-03	.112E-03	.267E-01	0.	.196E-03	.215E-04	.110E-06
62	.7593E-02	.243E+02	.506E-02	.243E+02	.179E-03	.119E-03	.291E-01	0.	.208E-03	.25[illegible]E-04	.127E-06
61	.8286E-02	.228E+02	.504E-02	.228E+02	.208E-03	.127E-03	.317E-01	0.	.22[illegible]E-03	.292E-04	.148E-06
60	.9036E-02	.213E+02	.501E-02	.213E+02	.242E-03	.136E-03	.345E-01	0.	.235E-03	.341E-04	.171E-06
59	.9854E-02	.199E+02	.498E-02	.199E+02	.282E-03	.144E-03	.375E-01	0.	.25[illegible]E-03	.397E-04	.198E-06
58	.1075E-01	.186E+02	.496E-02	.186E+02	.328E-03	.154E-03	.408E-01	0.	.266E-03	.463E-04	.230E-06
57	.1172E-01	.174E+02	.493E-02	.174E+02	.382E-03	.164E-03	.443E-01	0.	.283E-03	.540E-04	.267E-06
56	.1278E-01	.163E+02	.491E-02	.163E+02	.445E-03	.175E-03	.482E-01	0.	.301E-03	.629E-04	.310E-06
55	.1394E-01	.153E+02	.488E-02	.153E+02	.518E-03	.186E-03	.524E-01	0.	.320E-03	.734E-04	.359E-06

J I

K I

N	ENERGY MEV	COLLISION	RADIATION	TOTAL	RANGE	RADIATION YIELD	BETA**2	DENSITY CORR	RAD/COL	DRANGE	DYIELD
54	.1520E-01	.143E+02	.486E-02	.143E+02	.604E-03	.198E-03	.569E-01	0.	.341E-03	.855E-04	.417E-06
53	.1657E-01	.133E+02	.484E-02	.133E+02	.704E-03	.211E-03	.618E-01	0.	.362E-03	.997E-04	.483E-06
52	.1807E-01	.125E+02	.481E-02	.125E+02	.820E-03	.224E-03	.672E-01	0.	.386E-03	.116E-03	.561E-06
51	.1971E-01	.117E+02	.479E-02	.117E+02	.956E-03	.239E-03	.729E-01	0.	.410E-03	.136E-03	.651E-06
50	.2149E-01	.109E+02	.477E-02	.109E+02	.111E-02	.254E-03	.791E-01	0.	.437E-03	.158E-03	.754E-06
49	.2344E-01	.102E+02	.476E-02	.102E+02	.130E-02	.270E-03	.858E-01	0.	.465E-03	.184E-03	.877E-06
48	.2556E-01	.957E+01	.474E-02	.957E+01	.151E-02	.286E-03	.930E-01	0.	.49[illegible]E-03	.214E-03	.102E-05
47	.2787E-01	.894E+01	.472E-02	.894E+01	.176E-02	.306E-03	.101E+00	0.	.527E-03	.25[illegible]E-03	.118E-05
46	.3039E-01	.83[illegible]E+01	.47[illegible]E-02	.840E+01	.205E-02	.326E-03	.109E+00	0.	.561E-03	.29[illegible]E-03	.137E-05
45	.33[illegible]E-01	.786E+01	.470E-02	.7[illegible]E+01	.239E-02	.347E-03	.118E+00	0.	.597E-03	.33[illegible]E-03	.159E-05
44	.36[illegible]E-01	.737E+01	.46[illegible]E-02	.737E+01	.279E-02	.369E-03	.128E+00	0.	.63[illegible]E-03	.39[illegible]E-03	.18[illegible]E-05
43	.39[illegible]E-01	.69[illegible]E+01	.468E-02	.69[illegible]E+01	.324E-02	.393E-03	.138E+00	0.	.67[illegible]E-03	.45[illegible]E-03	.215E-05
42	.4298E-01	.648E+01	.467E-02	.6[illegible]E+01	.378E-02	.418E-03	.149E+00	0.	.721E-03	.53[illegible]E-03	.24[illegible]E-05
41	.4687E-01	.608E+01	.467E-02	.6[illegible]E+01	.440E-02	.445E-03	.161E+00	0	.764E-03	.6[illegible]E-03	.2[illegible]E-05
40	.5[illegible]E-01	.572E+01	.467E-02	.572E+01	.512E-02	.474E-03	.174E+00	0.	.81[illegible]E-03	.7[illegible]E-03	.33[illegible]E-05
39	.5574E-01	.537E+01	.467E-02	.538E+01	.59[illegible]E-02	.505E-03	.187E+00	0.	.87[illegible]E-03	.83[illegible]E-03	.39[illegible]E-05
38	.6079E-01	.505E+01	.468E-02	.506E+01	.692E-02	.537E-03	.201E+00	0.	.92[illegible]E-03	.96[illegible]E-03	.45[illegible]E-05
37	.6629E-01	.476E+01	.469E-02	.476E+01	.80[illegible]E-02	.572E-03	.216E+00	0.	.98[illegible]E-03	.112E-02	.52[illegible]E-05
36	.7229E-01	.449E+01	.471E-02	.449E+01	.934E-02	.609E-03	.233E+00	0.	.105E-02	.13[illegible]E-02	.61[illegible]E-05
35	.7883E-01	.423E+01	.472E-02	.424E+01	.108E-01	.648E-03	.249E+00	0.	.112E-02	.15[illegible]E-02	.708E-05
34	.8597E-01	.400E+01	.475E-02	.400E+01	.126E-01	.690E-03	.267E+00	0.	.118E-02	.173E-02	.821E-05
33	.9375E-01	.378E+01	.478E-02	.378E+01	.148E-01	.734E-03	.286E+00	0.	.126E-02	.200E-02	.953E-05
32	.1022E+00	.358E+01	.481E-02	.358E+01	.169E-01	.781E-03	.306E+00	0	.134E-02	.231E-02	.111E-04
31	.1115E+00	.339E+01	.485E-02	.34[illegible]E+01	.195E-01	.832E-03	.326E+00	0	.143E-02	.26[illegible]E-02	.128E-04
30	.12[illegible]	.322E+01	.490E-02	.322E+01	.226E-01	.885E-03	.347E+00	0	.152E-02	.30[illegible]E-02	.149E-04
29	.1326[illegible]	.306E+01	.495E-02	.307E+01	.261E-01	.942E-03	.370E+00	0	.162E-02	.3[illegible]E-02	.172E-04
28	.1446[illegible]	.291E+01	.512E-02	.292E+01	.301E-01	.100E-02	.392E+00	0	.172E-02	.401E-02	.200E-04
27	.1577[illegible]	.278E+01	.503E-02	.279E+01	.347E-01	.107E-02	.418E+00	[illegible]	.183E-02	.453E-02	.232E-04
26	.1719[illegible]	.266E+01	.518E-02	.266E+01	.399E-01	.113E-02	.440E+00	0	.195E-02	.505E-02	.269E-04
25	.1875[illegible]	.254E+01	.527E-02	.255E+01	.459E-01	.121E-02	.465E+00	0	.207E-02	.5[illegible]E-02	.312E-04
24	.2045[illegible]	.244E+01	.538E-02	.245E+01	.527E-01	.128E-02	.491E+00	0	.22[illegible]E-02	.6[illegible]E-02	.36[illegible]E-04
23	.2230[illegible]	.235E+01	.55[illegible]E-02	.235E+01	.604E-01	.137E-02	.5[illegible]E+00	0.	.235E-02	.7[illegible]E-02	.420E-04
22	.2432E+00	.226E+01	.565E-02	.226E+01	.692E-01	.145E-02	.54[illegible]E+00	0.	.25[illegible]E-02	.875E-02	.486E-04
21	.2652E+00	.218E+01	.58[illegible]E-02	.219E+01	.79[illegible]E-01	.155E-02	.567E+00	0.	.26[illegible]E-02	.9[illegible]E-02	.567E-04
20	.2892E+00	.21[illegible]E+01	.599E-02	.2[illegible]E+01	.902E-01	.165E-02	.592E+00	0	.28[illegible]E-02	.112E-01	.65[illegible]E-04
19	.3153E+00	.204E+01	.62[illegible]E-02	.205E+01	.103E+00	.175E-02	.6[illegible]E+00	0	.3[illegible]E-02	.126E-01	.76[illegible]E-04
18	.3439E+00	.199E+01	.6[illegible]E-02	.199E+01	.117E+00	.187E-02	.6[illegible]E+00	0	.32[illegible]E-02	.14[illegible]E-01	.89[illegible]E-04
17	.375[illegible]	.193E+01	.66[illegible]E-02	.194E+01	.133E+00	.193E-02	.66[illegible]E+00	0	.34[illegible]E-02	.158E-01	.104E-03
16	.40[illegible]	.18[illegible]E+01	.69[illegible]E-02	.189E+01	.150E+00	.2[illegible]E-02	.69[illegible]E+00	0	.37[illegible]E-02	.17[illegible]E-01	.121E-03
15	.44[illegible]	.185E+01	.73[illegible]E-02	.185E+01	.170E+00	.226E-02	.7[illegible]E+00	0	.39[illegible]E-02	.198E-01	.14[illegible]E-03
14	.48[illegible]	.18[illegible]E+01	.7[illegible]E-02	.182E+01	.192E+00	.24[illegible]E-02	.73[illegible]E+00	0	.42[illegible]E-02	.22[illegible]E-01	.165E-03
13	.53[illegible]E+00	.178E+01	.82[illegible]E-02	.179E+01	.21[illegible]E+00	.258E-02	.759E+00	0	.457E-02	.24[illegible]E-01	.193E-03
12	.578[illegible]E+00	.17[illegible]E+01	.86[illegible]E-02	.176E+01	.244E+00	.275E-02	.78[illegible]E+00	0	.49[illegible]E-02	.27[illegible]E-01	.226E-03
11	.63[illegible]	.173E+01	.91[illegible]E-02	.174E+01	.274E+00	.295E-02	.8[illegible]E+00	0	.529E-02	.30[illegible]E-01	.26[illegible]E-03
10	.68[illegible]	.17[illegible]	.975E-02	.172E+01	.307E+00	.3[illegible]E-02	.8[illegible]E+00	0	.57[illegible]E-02	.33[illegible]E-01	.3[illegible]E-03
9	.7[illegible]	.16[illegible]	.104E-01	.17[illegible]	.343E+00	.33[illegible]E-02	.83[illegible]E+00	0	.6[illegible]E-02	.36[illegible]E-01	.36[illegible]E-03
8	.8[illegible]	.16[illegible]	.1[illegible]E-01	.169E+01	.38[illegible]E+00	.36[illegible]E-02	.85[illegible]E+00	0	.66[illegible]E-02	[illegible]	.433E-03
7	.89[illegible]	.16[illegible]	.1[illegible]E-01	.168E+01	.42[illegible]E+00	.39[illegible]E-02	.86[illegible]E+00	0	.72[illegible]E-02	[illegible]	.5[illegible]E-03
6	.97[illegible]	.16[illegible]	.1[illegible]E-01	.16[illegible]	.4[illegible]E+00	.42[illegible]E-02	.88[illegible]E+00	0	.78[illegible]E-02	[illegible]	.6[illegible]E-03
5	[illegible]	[illegible]	[illegible]	.16[illegible]	.5[illegible]E+00	.45[illegible]E-02	.89[illegible]E+00	0	.8[illegible]E-02	.5[illegible]E-01	.7[illegible]E-03
4	[illegible]	[illegible]	[illegible]	.16[illegible]	.5[illegible]E+00	.48[illegible]E-02	.9[illegible]E+00	0	.9[illegible]E-02	[illegible]	.8[illegible]E-03
3	[illegible]	[illegible]	[illegible]	.16[illegible]	.6[illegible]E+00	.5[illegible]E-02	.9[illegible]E+00	0	.10[illegible]E-01	.6[illegible]E-01	.10[illegible]E-02
2	[illegible]	[illegible]	.16[illegible]	.16[illegible]	.7[illegible]E+00	.5[illegible]E-02	.9[illegible]E+00	0	.1[illegible]E-01	.6[illegible]E-01	.1[illegible]E-02
1	.150[illegible]	.166E+01	.199[illegible]	.168E+01	.79[illegible]E+00	.617E-02	.935E+00	0	.120E-01	.74[illegible]	.14[illegible]E-02

```
0                              ENERGY (MEV)        AVE ENERGY (MEV)      NUMBER PRIMARY      NUMBER GENERATED
 FIRST KNOCK (ABOVE TCUT)      2.9020E-02          4.1992E-02            8.8108E-01              34554
 TOTAL KNOCK (ABOVE TCUT)      2.9603E-02          4.0894E-02            7.2390E-01              38180
 PHOTO-ELECTRON                3.2275E-08          1.4670E-02            2.2000E-04                 11
 PAIR                          0.                  0.                    0.                          0
 COMPTON                       8.1300E-07          2.0347E-02            4.0000E-05                  2
 AUGER                         0.                  0.                    0.                          0
 FIRST BREMSSTRAHLUNG          1.8357E-03          8.8228E-02            1.8840E-02                827
 TOTAL BREMSSTRAHLUNG          1.8433E-03          7.4198E-02            2.2160E-02               1100
 K X-RAY                       0.                  0.                    0.                          0
 ANNIHILATION QUANTA           0.                  0.                    0.                          0
0UNSCATTERED PRIMARY PHOTONS NUMBER AND ENERGY
 0.          99 0.          99
0NUMBER COEFFICIENTS - KNOCK-ONS, PHOTON DESCENDANTS
0                                                           TRANSMISSION
 0.          99
 0.          99
0                                                           REFLECTION
  .10E-02 15
 0.          99
0                                                           LATERAL ESCAPE
  .40E-01  1
 0.          99
0                                                  NUMBER AND ENERGY COEFFICIENTS
0                                                           TRANSMISSION
0              CYLINDER DIMENSIONS       -------- ELECTRON ------       ----------- PHOTON -----------
          LENGTH(CM)  RADIUS(CM)         NUMBER      ENERGY      COUNTS      NUMBER      ENERGY       COUNTS

            .100E+04     .100E+02  0.        99 0.        99           0  .17E-04 99  .28E-05 99          1
0                                                           REFLECTION
0              CYLINDER DIMENSIONS       ---------- ELECTRON ----------    ----------- PHOTON -----------
          LENGTH(CM)  RADIUS(CM)         NUMBER      ENERGY      COUNTS      NUMBER      ENERGY       COUNTS

            .100E+04     .100E+02  .10E-02 14  .13E-03 34          82  .37E-04 87  .41E-08 73          2
0                                                           LATERAL ESCAPE
0              CYLINDER DIMENSIONS       ---------- ELECTRON ----------    ----------- PHOTON -----------
          LENGTH(CM)  RADIUS(CM)         NUMBER      ENERGY      COUNTS      NUMBER      ENERGY       COUNTS

            .100E+04     .100E+02  .10E+01  0  .81E+00  0       52288  .11E-01  5  .11E-02  8        988
1                                                           ENERGY DEPOSITION
                                                  (NORMALIZED TO ONE INCIDENT PARTICLE)
0                                                                                        ENERGY DEPOSITION (MEV)
      ZONE       MATERIAL       MASS(GM)     VOLUME(CC)                        PRIM           KNOCK            G-SEC              TOTAL

        1            1          .8110E+02     .6283E+05                   .1384E+00  0  -.8827E-02  2   .3881E-05 28    .1279E+00  8
        2            1          .3244E+03     .2513E+06                   .1560E-03 15  -.8599E-05 97   .2729E-06 99    .1497E-03 14
0                                                       TOTAL             .1386E+00  8  -.8934E-02  2   .4234E-05 27    .1276E+00  8
0                                                  CHARGE DISTRIBUTION
                                                  (NORMALIZED TO ONE INCIDENT PARTICLE)
C                                                                            ELECTRONS
      ZONE       MATERIAL       ZL           ZR           RI           RO           PRIM        KNOCK          G-SEC        TOTAL

        1            1       0.            .200E+03   0.           .100E+02   0.          99 -.40E-01  2 0.          99 -.40E-01  2
        2            1        .200E+03     .100E+04   0.           .100E+02   0.          99 -.60E-04 51 0.          99 -.60E-04 51
0                                           TOTAL                              0           99 -.40E-01  2 0.          99 -.40E-01  2
0                                                  ENERGY SPECTRA OF TRANSMITTED ELECTRONS
                                              (NUMBER MEV, NORMALIZED TO ONE INCIDENT PARTICLE)
0        E (MEV)   LENGTH=    1000.0000

   1.5000 -   1.4500  0.          99
   1.4500 -   1.4000  0.          99
   1.4000 -   1.3500  0.          99
   1.3500 -   1.3000  0.          99
   1.3000 -   1.2500  0           99

F 2                                                                                                                     F 2       F 3

0 2                                                                                                                     0 2       0 3

   1.2500 -   1.2000  0           99
   1.2000 -   1.1500  0.          99
   1.1500 -   1.1000  0.          99
   1.1000 -   1.0500  0.          99
   1.0500 -   1.0000  0.          99
   1.0000 -    .9500  0.          99
    .9500 -    .9000  0.          99
    .9000 -    .8500  0.          99
    .8500 -    .8000  0.          99
    .8000 -    .7500  0.          99
    .7500 -    .7000  0.          99
    .7000 -    .6500  0           99
    .6500 -    .6000  0           99
    .6000 -    .5500  0           99
    .5500 -    .5000  0           99
    .5000 -    .4500  0.          99
    .4500 -    .4000  0.          99
    .4000 -    .3500  0           99
    .3500 -    .3000  0           99
    .3000 -    .2500  0           99
    .2500 -    .2000  0           99
    .2000 -    .1500  0.          99
    .1500 -    .1000  0.          99
    .1000 -    .0500  0.          99
    .0500 -    .0100  0.          99
0                                                  ENERGY SPECTRA OF REFLECTED ELECTRONS
                                              (NUMBER MEV, NORMALIZED TO ONE INCIDENT PARTICLE)
0        E (MEV)   LENGTH=    1000.0000

   1.5000 -   1.4500    .12E-02 71
   1.4500 -   1.4000    .40E-03 99
   1.4000 -   1.3500  0           99
   1.3500 -   1.3000  0.          99
   1.3000 -   1.2500  0.          99
   1.2500 -   1.2000  0.          99
   1.2000 -   1.1500  0           99
   1.1500 -   1.1000  0           99
   1.1000 -   1.0500  0.          99
   1.0500 -   1.0000  0           99
   1.0000 -    .9500  0.          99
    .9500 -    .9000  0           99
    .9000 -    .8500  0           99
    .8500 -    .8000  0           99
    .8000 -    .7500  0           99
    .7500 -    .7000  0           99
    .7000 -    .6500  0           99
    .6500 -    .6000  0           99
    .6000 -    .5500  0           99
    .5500 -    .5000  0           99
    .5000 -    .4500  0           99
    .4500 -    .4000  0           99
    .4000 -    .3500  0           99
    .3500 -    .3000  0           99
    .3000 -    .2500  0           99
    .2500 -    .2000  0           99
    .2000 -    .1500  0           99
    .1500 -    .1000    .24E-02 37
    .1000 -    .0500    .64E-02 2[illegible]
    .0500 -    .0100    .28E-0[illegible] 14
                                                  ENERGY SPECTRA OF LATERALLY ESCAPING ELECTRONS
                                              (NUMBER MEV, NORMALIZED TO ONE INCIDENT PARTICLE)
 0       E (MEV)   LENGTH=    1000.0000
```

```
0 NSET  MATL
    1     1
0 NMAT  NTAB
    1     1
0NPAIR  NTAX
   20    41
0GAMMA RAY CROSS SECTION DATA
0ENERGIES (MEV)
 1000.000000  800.000000  600.000000  500.000000  400.000000  300.000000
  200.000000  150.000000  100.000000   80.000000   60.000000   50.000000
   40.000000   30.000000   20.000000   15.000000   10.000000    8.000000
    6.000000    5.000000    4.000000    3.000000    2.000000    1.500000
    1.000000     .800000     .600000     .500000     .400000     .300000
     .200000     .150000     .100000     .080000     .060000     .050000
     .040000     .030000     .020000     .015000     .010000
0TOTAL ATTENUATION COEFFICIENTS (CM2/G)
     .034103     .030724     .026900     .024990     .022922     .020782
     .018558     .017473     .016471     .016124     .015846     .015760
     .015757     .015904     .016646     .017900     .020378     .022183
     .025099     .027374     .030651     .035699     .044400     .051065
     .063469     .070602     .080400     .086939     .095257     .106390
     .122574     .134163     .150941     .161339     .170970     .195046
     .229594     .318830     .701217    1.408718    4.900403
0RATIO OF SCATTERING PLUS PAIR PRODUCTION TO TOTAL ATTENUATION COEFFICIENTS
    1.000000    1.000000    1.000000    1.000000    1.000000    1.000000
    1.000000     .999990     .999999     .999999     .999998     .999998
     .999998     .999997     .999995     .999994     .999992     .999991
     .999988     .999987     .999984     .999980     .993971     .999960
     .999931     .999902     .999833     .999757     .999596     .999173
     .997523     .994360     .981279     .983511     .915911     .861312
     .787200     .561182     .284757     .126930     .038270
0RATIO OF SCATTERING TO SCATTERING PLUS PAIR PRODUCTION ATTENUATION COEFFICIENTS
     .007074     .009818     .014847     .019178     .026033     .038052
     .063000     .080027     .138578     .171288     .225945     .266902
     .323921     .407568     .536746     .628994     .752048     .812171
     .877038     .909746     .941060     .969056     .990896     .998138
    1.000000
0K SHELL IONIZATION DATA
0BINDING ENERGY (MEV), PHOTOEFFECT EFFICIENCY AND FLUORESCENT EFFICIENCY
     .003203     .111213     .079438
0K X-RAY ENERGIES (MEV)
     .003203     .003203     .003203     .003203
0K X-RAY ACCUMULATED RELATIVE INTENSITIES
    1.000000    1.000000    1.000000    1.000000
0AUGER ELECTRON ENERGIES (MEV)
     .003203     .003203     .003203
0AUGER ELECTRON ACCUMULATED RELATIVE INTENSITIES
    1.000000    1.000000    1.000000
1NUMBER OF SETS ON DATAPAC TAPE =    1
0INPUT FROM DATAPAC

  **1.5 MEV FX100 BEAM INTO 760 TORR AIR**
0 NRUN  ITRH  IZIP  ISON  ISUB  INAL  ICYC  NCYC  NMAX         EMAX            EMIN            RMAX        LMAT
    1     5     0     1    50     1     1     8    84  1.5000000E+00  5.0593750E-03  7.9075230E-01     3

 DATAPREP DATA FOR DATAPAC SET   1    84    33    50   121  7.907523E-01

 COLLISION / TOTAL DE/DX RATIOS FOR DATAPAC SET   1

 CUMULATIVE BREMSSTRAHLUNG CROSS SECTIONS FOR DATAPAC SET   1

 CUMULATIVE BREMSSTRAHLUNG ANGULAR DISTRIBUTIONS FOR DATAPAC SET   1
```

D 2 D 2

E 2 E 2

```
 LANDAUSS - EQUIPROBABLE ENDPOINTS FOR INTERPOLATION

 K X-RAY PRODUCTION FOR DATAPAC SET   1

 PHOTOELECTRON ANGULAR DISTRIBUTIONS

 PAIR ELECTRON ENERGY DIVISION DISTRIBUTION (LEAD)
1
0 NRUN   INC ISTRO  INOK  INEL IPHOT  IBAD  IDES  IPUN ITAPE
    1     1     1     1     2     1     1     1     2     2
0 ZONE  MATERIAL  LEFT PLANE  RIGHT PLANE  INNER CYLINDER  OUTER CYLINDER    ECUT       PTCZ
    1      1     0.           .20000E+03    0.                .10000E+02    .100E-01   0.
    2      1     .20000E+03   .10000E+04    0.                .10000E+02    .100E-01   0.
0INCIDENT ELECTRONS
0ELECTRON COLLISION AND RADIATION ENERGY LOSS STRAGGLING
0KNOCK ON ELECTRON PRODUCTION
0NOT COUPLED INELASTIC SCATTERING DEFLECTIONS
0BREMSSTRAHLUNG AND CHARACTERISTIC X-RAY QUANTA FOLLOWED
0BREMSSTRAHLUNG INTRINSIC ANGLE OF EMISSION FROM TABULATED DISTRIBUTION
0PHOTON-PRODUCED PARTICLES FOLLOWED
0 IUNT  LMAX  ITRK  JMAX  IPRK JPMAX  IARK  KMAX  IBRK KPMAX
    2     1     1    30     1    30     1    18     1    18
0 IMAX  NZON IFLUX  NCYC   INRAN
 50000     2     2   -11000000000000000000
0*************** THE STANDARD ERROR ESTIMATES ARE BASED ON    10 BATCHES OF  5000 HISTORIES **************
0        TIN         TCUT        TPCUT        CTHIN       SORCIN
     1.50000      .01000       .01000      1.00000      3.01000
0       TSAVE                                 THFAC        RLAN        QBLK
      .01000                               10.00000      .50000     1.00000
0ELECTRON ENERGY CLASSIFICATIONS (MEV)
     1.45000     1.40000     1.35000      1.30000     1.25000     1.20000
     1.15000     1.10000     1.05000      1.00000      .95000      .90000
      .85000      .80000      .75000       .70000      .65000      .60000
      .55000      .50000      .45000       .40000      .35000      .30000
      .25000      .20000      .15000       .10000      .05000      .01000
0PHOTON ENERGY CLASSIFICATIONS (MEV)
     1.45000     1.40000     1.35000      1.30000     1.25000     1.20000
     1.15000     1.10000     1.05000      1.00000      .95000      .90000
      .85000      .80000      .75000       .70000      .65000      .60000
      .55000      .50000      .45000       .40000      .35000      .30000
      .25000      .20000      .15000       .10000      .05000      .01000
0ELECTRON OBLIQUITY CLASSIFICATIONS (DEGREES)
    10.00000    20.00000    30.00000     40.00000    50.00000    60.00000
    70.00000    80.00000    90.00000    100.00000   110.00000   120.00000
   130.00000   140.00000   150.00000    160.00000   170.00000   180.00000
0ELECTRON AZIMUTH CLASSIFICATIONS (DEGREES)
   180.00000
0PHOTON OBLIQUITY CLASSIFICATIONS (DEGREES)
    10.00000    20.00000    30.00000     40.00000    50.00000    60.00000
    70.00000    80.00000    90.00000    100.00000   110.00000   120.00000
   130.00000   140.00000   150.00000    160.00000   170.00000   180.00000
0PHOTON AZIMUTH CLASSIFICATIONS (DEGREES)
   180.00000
0NTEST        RGMAX      SCALE SKALE       TCUT        TPCUT        TECUT         TSAVE        DLIM         BNUM        XNUM
    1        790754E+00     1     1       .01000       .01000      0.00000       .01000      1.00000       0.0         0.0
0K X RAY QUANTA NOT FOLLOWED IN MATERIAL       1
0ANNIHILATION QUANTA FOLLOWED
1THE PROBLEM IS 100 PER CENT COMPLETE    TIME TO FINISH IS       0.000 SECONDS  AVERAGE TIME PER BATCH IS      196.767
0AVERAGE SOURCE ENERGY = 1.5000E+00 MEV
0      INRAN                IRA               IRC
 0000000000000000 5340.0154114506 5710:14434132621:
1C  ------------------------------ HISTORIES ------------------------------------------   REL           STEPS
      PRIM        SEC      KNOCK        P.E      PAIR       COM     AUGER      BREM       RAD      XRAY     LAND      PRIM       S.
      [illegible] 36[illegible]  44.94      8        [illegible]  1      [illegible]  54[illegible]  [illegible]8   C    [illegible]   8[illegible]   [illegible]
```

```
0                                ENERGY (MEV)        AVE ENERGY (MEV)     NUMBER PRIMARY      NUMBER GENERATED
  FIRST KNOCK (ABOVE TCUT)      2.8020E-02          4.1982E-02           8.8108E-01                  34554
  TOTAL KNOCK (ABOVE TCUT)      2.8603E-02          4.0094E-02           7.2393E-01                  36185
  PHOTO-ELECTRON                3.2279E-06          1.4670E-02           2.2000E-04                     11
  PAIR                          0.                  0.                   0.                              0
  COMPTON                       8.1380E-07          2.0347E-02           4.0000E-05                      2
  AUGER                         0.                  0.                   0.                              0
  FIRST BREMSSTRAHLUNG          1.8357E-03          8.8228E-02           1.8940E-02                    827
  TOTAL BREMSSTRAHLUNG          1.8433E-03          7.4196E-02           2.2180E-02                   1100
  K X-RAY                       0.                  0.                   0.                              0
  ANNIHILATION QUANTA           0.                  0.                   0.                              0
0UNSCATTERED PRIMARY PHOTONS NUMBER AND ENERGY
  0.        99 0.         99
0NUMBER COEFFICIENTS - KNOCK-ONS, PHOTON DESCENDANTS
0                                                           TRANSMISSION
 0.         99
 0.         99
0                                                            REFLECTION
  .18E-02 19
 0.         99
0                                                          LATERAL ESCAPE
  .40E-01  1
 0.         99
0                                                  NUMBER AND ENERGY COEFFICIENTS
0                                                           TRANSMISSION
0              CYLINDER DIMENSIONS        --------- ELECTRON ------         ----------- PHOTON -----------
            LENGTH(CM)  RADIUS(CM)         NUMBER      ENERGY      COUNTS      NUMBER      ENERGY       COUNTS

             .100E+04     .100E+02  0.         99 0.         99          0   .17E-04 99  .20E-05 99          1
0                                                            REFLECTION
0              CYLINDER DIMENSIONS        ---------- ELECTRON ----------     ----------- PHOTON -----------
            LENGTH(CM)  RADIUS(CM)         NUMBER      ENERGY      COUNTS      NUMBER      ENERGY       COUNTS

             .100E+04     .100E+02   .18E-02 14  .13E-03 34         82   .37E-04 67  .41E-06 73          2
0                                                          LATERAL ESCAPE
0              CYLINDER DIMENSIONS        ---------- ELECTRON ----------     ----------- PHOTON -----------
            LENGTH(CM)  RADIUS(CM)         NUMBER      ENERGY      COUNTS      NUMBER      ENERGY       COUNTS

             .100E+04     .100E+02   .10E+01  0  .81E+00  0      52200   .11E-01  9  .11E-02  0        900
1                                                        ENERGY DEPOSITION
                                                (NORMALIZED TO ONE INCIDENT PARTICLE)
0                                                                                      ENERGY DEPOSITION (MEV)
        ZONE        MATERIAL       MASS(GM)    VOLUME(CC)                       PRIM          KNOCK          D-SEC              TOTAL

          1            1          .8110E+02     .6283E+05                   .1384E+00  0  -.8827E-02  2   .3861E-05 26   .1275E+00  0
          2            1          .3244E+03     .2513E+06                   .1560E-03 15  -.6599E-05 97   .2725E-06 99   .1497E-03 14
0                                                           TOTAL           .1386E+00  0  -.8834E-02  2   .4234E-05 27   .1276E+00  0
0                                                      CHARGE DISTRIBUTION
                                                (NORMALIZED TO ONE INCIDENT PARTICLE)
0                                                                         ELECTRONS
        ZONE        MATERIAL       ZL            ZR           RI            RO          PRIM          KNOCK          D-SEC        TOTAL

          1            1       0.             .200E+03   0.           .100E+02   0.          99 -.40E-01  2 0.          99 -.40E-01  2
          2            1        .200E+03      .100E+04   0.           .100E+02   0.          99 -.60E-04 51 0.          99 -.60E-04 51
0                                                TOTAL                           0           99 -.40E-01  2 0.          99 -.40E-01  2
0                                          ENERGY SPECTRA OF TRANSMITTED ELECTRONS
                                         (NUMBER MEV, NORMALIZED TO ONE INCIDENT PARTICLE)
0       E (MEV)  LENGTH=   1000.0000

   1.5000 -   1.4500  0.          99
   1.4500 -   1.4000  0.          99
   1.4000 -   1.3500  0.          99
   1.3500 -   1.3000  0.          99
   1.3000 -   1.2500  0.          99
```

F 2

0 2

```
   1.2500 -   1.2000  0.          99
   1.2000 -   1.1500  0.          99
   1.1500 -   1.1000  0.          99
   1.1000 -   1.0500  0.          99
   1.0500 -   1.0000  0.          99
   1.0000 -    .9500  0.          99
    .9500 -    .9000  0.          99
    .9000 -    .8500  0           99
    .8500 -    .8000  0.          99
    .8000 -    .7500  0.          99
    .7500 -    .7000  0.          99
    .7000 -    .6500  0.          99
    .6500 -    .6000  0           99
    .6000 -    .5500  0.          99
    .5500 -    .5000  0.          99
    .5000 -    .4500  0.          99
    .4500 -    .4000  0.          99
    .4000 -    .3500  0           99
    .3500 -    .3000  0.          99
    .3000 -    .2500  0.          99
    .2500 -    .2000  0           99
    .2000 -    .1500  0.          99
    .1500 -    .1000  0.          99
    .1000 -    .0500  0.          99
    .0500 -    .0100  0.          99
0                                          ENERGY SPECTRA OF REFLECTED ELECTRONS
                                         (NUMBER MEV, NORMALIZED TO ONE INCIDENT PARTICLE)
0       E (MEV)  LENGTH=   1000.0000

   1.5000 -   1.4500   .12E-02 71
   1.4500 -   1.4000   .40E-03 99
   1.4000 -   1.3500  0.          99
   1.3500 -   1.3000  0.          99
   1.3000 -   1.2500  0.          99
   1.2500 -   1.2000  0.          99
   1.2000 -   1.1500  0           99
   1.1500 -   1.1000  0           99
   1.1000 -   1.0500  0.          99
   1.0500 -   1.0000  0           99
   1.0000 -    .9500  0           99
    .9500 -    .9000  0           99
    .9000 -    .8500  0.          99
    .8500 -    .8000  0.          99
    .8000 -    .7500  0           99
    .7500 -    .7000  0           99
    .7000 -    .6500  0           99
    .6500 -    .6000  0           99
    .6000 -    .5500  0           99
    .5500 -    .5000  0           99
    .5000 -    .4500  0           99
    .4500 -    .4000  0           99
    .4000 -    .3500  0           99
    .3500 -    .3000  0           99
    .3000 -    .2500  0           99
    .2500 -    .2000  0           99
    .2000 -    .1500  0           99
    .1500 -    .1000    .24E-02 37
    .1000 -    .0500    .64E-02 21
    .0500 -    .0100    .20E-01 14
                                          ENERGY SPECTRA OF LATERALLY ESCAPING ELECTRONS
                                         (NUMBER MEV, NORMALIZED TO ONE INCIDENT PARTICLE)
0       E (MEV)  LENGTH=   1000.0000
```

1.4000 -	1.3500	.61E+01	1
1.3500 -	1.3000	.28E+01	1
1.3000 -	1.2500	.14E+01	1
1.2500 -	1.2000	.74E+00	2
1.2000 -	1.1500	.41E+00	5
1.1500 -	1.1000	.22E+00	4
1.1000 -	1.0500	.13E+00	5
1.0500 -	1.0000	.67E-01	8
1.0000 -	.9500	.40E-01	13
.9500 -	.9000	.30E-01	15
.9000 -	.8500	.18E-01	14
.8500 -	.8000	.13E-01	16
.8000 -	.7500	.10E-01	9
.7500 -	.7000	.82E-02	13
.7000 -	.6500	.13E-01	14
.6500 -	.6000	.12E-01	17
.6000 -	.5500	.18E-01	16
.5500 -	.5000	.21E-01	11
.5000 -	.4500	.27E-01	8
.4500 -	.4000	.28E-01	8
.4000 -	.3500	.35E-01	12
.3500 -	.3000	.43E-01	8
.3000 -	.2500	.60E-01	4
.2500	.2000	.85E-01	5
.2000 -	.1500	.12E+00	7
.1500 -	.1000	.18E+00	3
.1000 -	.0500	.20E+00	5
.0500 -	.0100	.14E+00	5

ANGULAR DISTRIBUTIONS OF TRANSMITTED AND REFLECTED ELECTRONS
(NUMBER/SR, NORMALIZED TO ONE INCIDENT PARTICLE)

0 PHI(DEG)= 0.000

THETA (DEG)	180.000	
0.0000 - 10.0000	0.	99
10.0000 - 20.0000	0.	99
20.0000 - 30.0000	0.	99
30.0000 - 40.0000	0.	99
40.0000 - 50.0000	0.	99
50.0000 - 60.0000	0.	99
60.0000 - 70.0000	0.	99
70.0000 - 80.0000	0.	99
80.0000 - 90.0000	0.	99
90.0000 - 100.0000	0.	99
100.0000 - 110.0000	.15E-03	36
110.0000 - 120.0000	.24E-03	27
120.0000 - 130.0000	.38E-03	25
130.0000 - 140.0000	.49E-03	21
140.0000 - 150.0000	.29E-03	31
150.0000 - 160.0000	.43E-03	47
160.0000 - 170.0000	.42E-03	51
170.0000 - 180.0000	.42E-03	67

ANGULAR DISTRIBUTIONS OF LATERALLY ESCAPING ELECTRONS
(NUMBER/SR, NORMALIZED TO ONE INCIDENT PARTICLE)

0 PHI(DEG)= 0.000

THETA (DEG)	180.000	
0.0000 - 10.0000	.58E+00	2
10.0000 - 20.0000	.14E+01	1
20.0000 - 30.0000	.84E+00	1
30.0000 - 40.0000	.20E+00	2
40.0000 - 50.0000	.44E-01	3
50.0000 - 60.0000	.18E-01	3
60.0000 - 70.0000	.11E-01	4

H 2 H 2

I 2 I 2

70.0000 - 80.0000	.70E-02	5
80.0000 - 90.0000	.56E-02	7
90.0000 - 100.0000	.45E-02	6
100.0000 - 110.0000	.3 E-02	9
110.0000 - 120.0000	.22E-02	5
120.0000 - 130.0000	.17E-02	12
130.0000 - 140.0000	.16E-02	12
140.0000 - 150.0000	.96E-03	13
150.0000 - 160.0000	.35E-03	31
160.0000 - 170.0000	.14E-03	99
17[illegible] - 180.0000	.42E-03	67

0 ENERGY SPECTRA AND ANGULAR DISTRIBUTIONS OF ELECTRONS TRANSMITTED AND REFLECTED
AZIMUTHAL INTERVAL IS 0.00000 TO 180.00000 DEGREES
(NUMBER/(MEV*SR), NORMALIZED TO ONE PARTICLE)

E (MEV) \ THETA=	0.000 - 10.000	10.000 - 20.000	20.000 - 30.000	30.000 - 40.000	40.000 - 50.000	50.000 - 60.000	60.000 - 70.000	70.000 - 80.000	80.000 - 90.000
1.5000 - 1.4500	0 99	0 99	0 99	0 99	0. 99	0. 99	0. 99	0 99	0. 99
1.4500 - 1.4000	0 99	0. 99	0 99	0 99	0 99	0 99	0 99	0 99	0 99
1.4000 - 1.3500	0 99	0 99	0 99	0 99	0 99	0 99	0 99	0 99	0. 99
1.3500 - 1.3000	0 99	0 99	0 99	0 99	0 99	0 99	0 99	0. 99	0. 99
1.3000 - 1.2500	0 99	0 99	0. 99	0 99	0 99	0 99	0 99	0. 99	0. 99
1.2500 - 1.2000	0 99	0 99	0 99	0 99	0. 99	0 99	0 99	0. 99	0. 99
1.2000 - 1.1500	0 99	0. 99	0 99	0. 99	0 99	0 99	0 99	0. 99	0. 99
1.1500 - 1.1000	0 99	0 99	0 99	0 99	0 99	0 99	0 99	0 99	0 99
1.1000 - 1.0500	0 99	0 99	0 99	0 99	0 99	0 99	0 99	0. 99	0. 99
1.0500 - 1.0000	0 99	0 99	0 99	0 99	0 99	0 99	0 99	0 99	0 99
1.0000 - .9500	0 99	0 99	0 99	0 99	0 99	0 99	0 99	0. 99	0. 99
.9500 - .9000	0 99	0 99	0 99	0 99	0 99	0 99	0 99	0 99	0 99
.9000 - .8500	0 99	0 99	0 99	0 99	0 99	0 99	0 99	0 99	0 99
.8500 - .8000	0 99	0 99	0 99	0 99	0 99	0 99	0 99	0 99	0 99
.8000 - .7500	0 99	0 99	0 99	0 99	0 99	0 99	0 99	0 99	0 99
.7500 - .7000	0 99	0 99	0 99	0 99	0 99	0 99	0 99	0 99	0 99
.7000 - .6500	0 99	0 99	0 99	0 99	0 99	0 99	0 99	0 99	0 99
.6500 - .6000	0 99	0 99	0 99	0 99	0 99	0 99	0 99	0 99	0 99
.6000 - .5500	0 99	0 99	0 99	0 99	0 99	0 99	0 99	0 99	0. 99
.5500 - .5000	0 99	0 99	0 99	0 99	0 99	0 99	0 99	0 99	0 99
.5000 - .4500	0 99	0 99	0 99	0 99	0 99	0 99	0 99	0 99	0 99
.4500 - .4000	0 99	0 99	0 99	0 99	0 99	0 99	0 99	0 99	0 99
.4000 - .3500	0 99	0 99	0 99	0 99	0 99	0 99	0 99	0 99	0 99
.3500 - .3000	0 99	0 99	0 99	0 99	0 99	0 99	0 99	0 99	0 99
.3000 - .2500	0 99	0 99	0 99	0 99	0 99	0 99	0 99	0 99	0 99
.2500 - .2000	0 99	0 99	0 99	0 99	0 99	0 99	0 99	0 99	0 99
.2000 - .1500	0 99	0 99	0 99	0 99	0 99	0 99	0 99	0 99	0 99
.1500 - .1000	0 97	0 99	0 99	0 95	0 99	0 99	0 99	0 99	0 99
.1000 - .0500	0 99	0 99	0 99	0 99	0 99	0 99	0 99	0 99	0 99
.0500 - .0100	0 99	0 99	0 99	0 99	0 99	0 99	0 99	0 99	0 99

1 0 ENERGY SPECTRA AND ANGULAR DISTRIBUTIONS OF ELECTRONS TRANSMITTED AND REFLECTED
AZIMUTHAL INTERVAL IS 0.00000 TO 180.00000 DEGREES
(NUMBER/(MEV*SR), NORMALIZED TO ONE PARTICLE)

E (MEV) \ THETA=	90.000 - 100.000	100.000 - 110.000	110.000 - 120.000	120.000 - 130.000	130.000 - 140.000	140.000 - 150.000	150.000 - 160.000	160.000 - 170.000	170.000 - 180.000
1.5000 - 1.4500	0 99	0 99	0 99	0 99	.10E-02 67	.84E-03 99	0 99	0 99	0 99
1.4500 - 1.4000	0 99	0 99	0 99	.45E-03 99	0 99	0 99	0 99	0 99	0 99
1.4000 - 1.3500	0 99	0 99	0 99	0 99	0 99	0 99	0 99	0 99	0 99
1.3500 - 1.3000	0 99	0 99	0 99	0 99	0 99	0 99	0 99	0 99	0 99
1.3000 - 1.2500	0 99	0 99	0 99	0 99	0 99	0 99	0 99	0 99	0 99
1.2500 - 1.2000	0 99	0 99	0 99	0 99	0 99	0 99	0 99	0 99	0 99
1.2000 - 1.1500	0 99	0 99	0 99	0 99	0 99	0 99	0 99	0 99	0 99
1.1500 - 1.1000	0 99	0 99	0 99	0 99	0 99	0 99	0 99	0 99	0 99
1.1000 - 1.0500	0 99	0 99	0 99	0 99	0 99	[illegible]	[illegible]	[illegible]	[illegible]
[illegible]	[illegible]	[illegible]	[illegible]	[illegible]	[illegible]	[illegible]	[illegible]	[illegible]	[illegible]

.9500 - .9000	0. 99	0. 99	0. 99	0. 99	0. 99	0. 99	0. 99	0. 99	0. 99
.9000 - .8500	0. 99	0. 99	0. 99	0. 99	0. 99	0. 99	0. 99	0. 99	0. 99
.8500 - .8000	0. 99	0. 99	0. 99	0. 99	0. 99	0. 99	0. 99	0. 99	0. 99
.8000 - .7500	0. 99	0. 99	0. 99	0. 99	0. 99	0. 99	0. 99	0. 99	0. 99
.7500 - .7000	0. 99	0. 99	0. 99	0. 99	0. 99	0. 99	0. 99	0. 99	0. 99
.7000 - .6500	0. 99	0. 99	0. 99	0. 99	0. 99	0. 99	0. 99	0. 99	0. 99
.6500 - .6000	0. 99	0. 99	0. 99	0. 99	0. 99	0. 99	0. 99	0. 99	0. 99
.6000 - .5500	0. 99	0. 99	0. 99	0. 99	0. 99	0. 99	0. 99	0. 99	0. 99
.5500 - .5000	0. 99	0. 99	0. 99	0. 99	0. 99	0. 99	0. 99	0. 99	0. 99
.5000 - .4500	0. 99	0. 99	0. 99	0. 99	0. 99	0. 99	0. 99	0. 99	0. 99
.4500 - .4000	0. 99	0. 99	0. 99	0. 99	0. 99	0. 99	0. 99	0. 99	0. 99
.4000 - .3500	0. 99	0. 99	0. 99	0. 99	0. 99	0. 99	0. 99	0. 99	0. 99
.3500 - .3000	0. 99	0. 99	0. 99	0. 99	0. 99	0. 99	0. 99	0. 99	0. 99
.3000 - .2500	0. 99	0. 99	0. 99	0. 99	0. 99	0. 99	0. 99	0. 99	0. 99
.2500 - .2000	0. 99	0. 99	0. 99	0. 99	0. 99	0. 99	0. 99	0. 99	0. 99
.2000 - .1500	0. 99	0. 99	0. 99	0. 99	0. 99	0. 99	0. 99	0. 99	0. 99
.1500 - .1000	0. 99	0. 99	.40E-03 99	.45E-03 99	.15E-02 71	.64E-03 99	0. 99	0. 99	0. 99
.1000 - .0500	0. 99	.38E-03 99	.81E-03 99	.22E-02 45	.15E-02 71	.13E-02 67	.86E-03 99	.28E-02 67	0. 99
.0500 - .0100	0. 99	.33E-02 37	.45E-02 39	.50E-02 31	.71E-02 18	.40E-02 45	.87E-02 45	.71E-02 56	.18E-01 67

ENERGY SPECTRA AND ANGULAR DISTRIBUTIONS OF ELECTRONS LATERALLY ESCAPING
AZIMUTHAL INTERVAL IS 0.00000 TO 180.00000 DEGREES
(NUMBER/(MEV*SR), NORMALIZED TO ONE PARTICLE)

E (MEV) THETA=	0.000 10.000	10.000 20.000	20.000 30.000	30.000 40.000	40.000 50.000	50.000 60.000	60.000 70.000	70.000 80.000	80.000 90.000
1.5000 - 1.4500	.84E-02 67	.28E+00 10	.55E+00 6	.28E+00 5	.93E-01 6	.40E-01 15	.17E-01 18	.10E-01 15	.51E-02 37
1.4500 - 1.4000	.24E+01 6	.88E+01 1	.88E+01 1	.15E+01 2	.27E+00 7	.79E-01 8	.35E-01 15	.11E-01 13	.11E-01 16
1.4000 - 1.3500	.44E+01 4	.83E+01 2	.48E+01 2	.85E+00 2	.18E+00 6	.46E-01 10	.20E-01 12	.95E-02 28	.40E-02 20
1.3500 - 1.3000	.24E+01 4	.44E+01 2	.22E+01 2	.47E+00 4	.91E-01 10	.21E-01 12	.87E-02 22	.42E-02 28	.33E-02 38
1.3000 - 1.2500	.12E+01 6	.21E+01 2	.11E+01 3	.25E+00 5	.45E-01 9	.11E-01 21	.89E-02 32	.19E-02 33	.22E-02 51
1.2500 - 1.2000	.55E+00 8	.11E+01 3	.55E+00 4	.15E+00 5	.24E-01 15	.45E-02 33	.24E-02 37	.11E-02 71	0. 99
1.2000 - 1.1500	.27E+00 10	.53E+00 5	.34E+00 8	.80E-01 6	.10E-01 14	.71E-02 27	.16E-02 41	.23E-02 27	0. 99
1.1500 - 1.1000	.17E+00 14	.27E+00 8	.18E+00 7	.46E-01 11	.83E-02 27	.45E-02 39	.18E-02 67	0. 99	.37E-03 99
1.1000 - 1.0500	.80E-01 18	.16E+00 7	.10E+00 8	.29E-01 18	.83E-02 23	0. 99	.81E-03 67	.38E-03 99	0. 99
1.0500 - 1.0000	.17E-01 55	.83E-01 12	.48E-01 17	.26E-01 8	.26E-02 45	.88E-03 67	0. 99	0. 99	0. 99
1.0000 - .9500	.21E-01 61	.45E-01 24	.35E-01 16	.12E-01 30	.21E-02 55	.45E-03 99	0. 99	0. 99	0. 99
.9500 - .9000	.17E-01 41	.25E-01 30	.26E-01 25	.89E-02 29	.21E-02 55	.13E-02 51	0. 99	.38E-03 99	0. 99
.9000 - .8500	.42E-02 99	.17E-01 27	.14E-01 23	.84E-02 33	0. 99	0. 99	0. 99	0. 99	.37E-03 99
.8500 - .8000	0 99	.14E-01 30	.86E-02 26	.57E-02 31	.10E-02 99	0. 99	.40E-03 99	.38E-03 99	0. 99
.8000 - .7500	.84E-02 67	.42E-02 51	.95E-02 16	.25E-02 41	.26E-02 45	0. 99	0. 99	0. 99	0. 99
.7500 - .7000	.42E-02 99	.28E-02 87	.43E-02 33	.38E-02 37	.46E-02 20	0. 99	0. 99	0. 99	0. 99
.7000 - .6500	0. 99	.56E-02 55	.35E-02 41	.57E-02 38	.46E-02 26	.13E-02 51	.18E-02 41	0. 99	0. 99
.6500 - .6000	0. 99	.28E-02 87	.35E-02 41	.45E-02 30	.36E-02 37	.31E-02 30	.40E-03 99	.38E-03 99	0. 99
.6000 - .5500	.42E-02 99	0. 99	.26E-02 51	.76E-02 32	.57E-02 25	.22E-02 33	.20E-02 54	.76E-03 67	.37E-03 99
.5500 - .5000	0. 99	.85E-02 37	.69E-02 31	.57E-02 26	.57E-02 25	.36E-02 36	.28E-02 37	.38E-03 99	.73E-03 67
.5000 - .4500	0. 99	.28E-02 87	.43E-02 45	.11E-01 22	.93E-02 22	.49E-02 34	.44E-02 29	.38E-03 99	.37E-03 99
.4500 - .4000	0. 99	.28E-02 87	.52E-02 44	.76E-02 17	.57E-02 29	.85E-02 23	.36E-02 39	.11E-02 51	.15E-02 41
.4000 - .3500	0. 99	.42E-02 51	.43E-02 33	.76E-02 17	.83E-02 19	.76E-02 18	.89E-02 23	.19E-02 45	.29E-02 45
.3500 - .3000	0. 99	.56E-02 41	.60E [illegible]	[illegible] 30	.98E-02 18	.85E-02 21	.10E-01 16	.53E-02 27	.18E-02 33
.3000 - .2500	0. 99	.56E-02 41	.35E-02 41	.17E-01 20	.12E-01 20	.15E-01 19	.10E-01 22	.64E-02 23	.37E-02 33
.2500 - .2000	.84E-02 67	.14E-02 99	.10E-01 32	.12E-01 17	.72E-02 32	.18E-01 13	.14E-01 21	.11E-01 13	.88E-02 26
.2000 - .1500	.42E-02 99	.42E-02 51	.69E-02 25	.12E-01 20	.13E-01 19	.20E-01 11	.17E-01 15	.17E-01 16	.12E-01 13
.1500 - .1000	0 99	.28E-02 87	.69E-02 45	.13E-01 28	.15E-01 22	.21E-01 13	.18E-01 12	.19E-01 15	.22E-01 13
.1000 - .0500	.42E-02 99	.85E-02 37	.43E-02 45	.13E-01 20	.20E-01 20	.20E-01 11	.27E-01 15	.24E-01 15	.19E-01 14
.0500 - .0100	0. 99	.18E-02 99	.11E-02 99	.80E-02 26	.10E-01 30	.13E-01 27	.15E-01 20	.18E-01 23	.13E-01 20

ENERGY SPECTRA AND ANGULAR DISTRIBUTIONS OF ELECTRONS LATERALLY ESCAPING
AZIMUTHAL INTERVAL IS 0.00000 TO 180.00000 DEGREES
(NUMBER/(MEV*SR), NORMALIZED TO ONE PARTICLE)

E (MEV) THETA=	90.000 100.000	100.000 110.000	110.000 120.000	120.000 130.000	130.000 140.000	140.000 150.000	150.000 160.000	160.000 170.000	170.000 180.000
1.5000 - 1.4500	.22E-02 37	.19E-02 33	.16E-02 55	0. 99	0. 99	0. 99	.86E-03 99	0. 99	0. 99
1.4500 - 1.4000	.81E-02 20	.38E-02 49	.81E-03 67	.89E-03 67	.52E-03 99	.64E-03 99	0. 99	0. 99	0. 99
1.4000 - 1.3500	.22E-02 44	.19E-02 45	.40E-03 99	.45E-03 99	.52E-03 99	0. 99	0. 99	0. 99	0. 99

J 2 J 2

K 2 K 2

1.3500 - 1.3000	.26E-02 43	.38E-03 99	.40E-03 99	0. 99	0 99	.64E-03 99	0. 99	0. 99	0. 99
1.3000 - 1.2500	.11E-02 71	.38E-03 99	.81E-03 67	0. 99	0 99	0 99	0. 99	0. 99	0. 99
1.2500 - 1.2000	.15E-02 55	0 99	.40E-03 99	.45E-03 99	0. 99	0 99	0. 99	0. 99	0. 99
1.2000 - 1.1500	.37E-03 99	0 99	0 99	.45E-03 99	0 99	0 99	0. 99	0. 99	0. 99
1.1500 - 1.1000	0 99	.76E-03 67	0 99	0 99	0 99	0 99	0. 99	0. 99	0. 99
1.1000 - 1.0500	.37E-03 99	0 99	0 99	0 99	0 99	0 99	0. 99	0. 99	0. 99
1.0500 - 1.0000	0. 99	0 99	0 99	0 99	0 99	0 99	0. 99	0. 99	0. 99
1.0000 - .9500	0. 99	0 99	0 99	0 99	0 99	0 99	0. 99	0. 99	0. 99
.9500 - .9000	0. 99	0 99	0 99	0 99	0 99	0 99	0. 99	0. 99	0. 99
.9000 - .8500	0 99	0 99	0 99	0 99	0 99	0 99	0. 99	0. 99	0. 99
.8500 - .8000	0 99	0 99	0 99	0 99	0 99	0 99	0. 99	0. 99	0. 99
.8000 - .7500	0 99	.38E-03 99	0 99	0 99	0 99	0 99	0. 99	0. 99	0. 99
.7500 - .7000	0. 99	0 99	0 99	0 99	0 99	0 99	0. 99	0. 99	0. 99
.7000 - .6500	0. 99	0 99	0 99	0 99	0 99	0 99	0. 99	0. 99	0. 99
.6500 - .6000	0 99	0 99	0 99	0 99	0 99	0 99	0. 99	0. 99	0. 99
.6000 - .5500	0 99	0 99	0 99	0 99	0 99	0 99	0. 99	0. 99	0. 99
.5500 - .5000	0 99	0 99	0 99	0 99	0 99	0 99	0. 99	0. 99	0. 99
.5000 - .4500	0 99	.38E-03 99	0 99	0 99	0 99	0 99	0. 99	0. 99	0. 99
.4500 - .4000	.11E-02 71	.38E-03 99	0 99	0 99	.52E-03 99	0 99	0. 99	0. 99	0. 99
.4000 - .3500	0 99	.38E-03 99	.81E-03 99	0 99	.52E-03 99	0 99	0. 99	0. 99	0. 99
.3500 - .3000	.18E-02 33	.76E-03 67	.40E-03 99	0 99	0 99	0 99	0 99	0. 99	0. 99
.3000 - .2500	.11E-02 51	.76E-03 67	.40E-03 99	.45E-03 99	0 99	0 99	0 99	0. 99	0. 99
.2500 - .2000	.62E-02 30	.42E-02 21	.20E-02 33	.89E-03 99	.52E-03 99	0 99	0. 99	0 99	.42E-02 99
.2000 - .1500	.99E-02 15	.60E-02 27	.56E-02 27	.40E-02 31	.31E-02 44	0 99	.86E-03 99	0 99	0 99
.1500 - .1000	.18E-01 10	.12E-01 14	.97E-02 14	.71E-02 25	.41E-02 3	.57E-02 20	.26E-02 51	.14E-02 99	.42E-02 99
.1000 - .0500	.23E-01 10	.17E-01 18	.12E-01 15	.12E-01 9	.10E-01 20	.78E-02 24	.26E-02 51	.14E-02 99	0 99
.0500 - .0100	.14E-01 9	.14E-01 19	.12E-01 23	.89E-02 17	.14E-01 20	.56E-02 30	0 99	0. 99	0. 99

ENERGY SPECTRA OF TRANSMITTED PHOTONS
(NUMBER/MEV, NORMALIZED TO ONE INCIDENT PARTICLE)

E (MEV) LENGTH=	1000.0000
1.5000 - 1.4500	0 99
1.4500 - 1.4000	0 99
1.4000 - 1.3500	0 99
1.3500 - 1.3000	0 99
1.3000 - 1.2500	0 99
1.2500 - 1.2000	0 99
1.2000 - 1.1500	0 99
1.1500 - 1.1000	0 99
1.1000 - 1.0500	0 99
1.0500 - 1.0000	0 99
1.0000 - .9500	0 99
.9500 - .9000	0 99
.9000 - .8500	0 99
.8500 - .8000	0 99
.8000 - .7500	0 99
.7500 - .7000	0 99
.7000 - .6500	0 99
.6500 - .6000	0 99
.6000 - .5500	0 99
.5500 - .5000	0 99
.5000 - .4500	0 99
.4500 - .4000	0 99
.4000 - .3500	0 99
.3500 - .3000	0 99
.3000 - .2500	0 99
.2500 - .2000	.35E-03 99
.2000 - .1500	0 99
.1500 - .1000	0 99
.1000 - .0500	0 99
.0500 - .0100	0 99

ENERGY SPECTRA OF REFLECTED PHOTONS
(NUMBER/MEV, NORMALIZED TO ONE INCIDENT PARTICLE)

1.5000 -	1.4500	0.	99
1.4500 -	1.4000	0.	99
1.4000 -	1.3500	0.	99
1.3500 -	1.3000	0.	99
1.3000 -	1.2500	0.	99
1.2500 -	1.2000	0.	99
1.2000 -	1.1500	0.	99
1.1500 -	1.1000	0.	99
1.1000 -	1.0500	0.	99
1.0500 -	1.0000	0.	99
1.0000 -	.9500	0.	99
.9500 -	.9000	0.	99
.9000 -	.8500	0.	99
.8500 -	.8000	0.	99
.8000 -	.7500	0.	99
.7500 -	.7000	0.	99
.7000 -	.6500	0.	99
.6500 -	.6000	0.	99
.6000 -	.5500	0.	99
.5500 -	.5000	0.	99
.5000 -	.4500	0.	99
.4500 -	.4000	0.	99
.4000 -	.3500	0.	99
.3500 -	.3000	0.	99
.3000 -	.2500	0.	99
.2500 -	.2000	0.	99
.2000 -	.1500	0.	99
.1500 -	.1000	0.	99
.1000 -	.0500	0.	99
.0500 -	.0100	.93E-03	67

ENERGY SPECTRA OF LATERALLY ESCAPING PHOTONS
(NUMBER/MEV, NORMALIZED TO ONE INCIDENT PARTICLE)

E (MEV)	LENGTH=	1000.0000	
1.5000 -	1.4500	0.	99
1.4500 -	1.4000	0.	99
1.4000 -	1.3500	0.	99
1.3500 -	1.3000	.40E-03	99
1.3000 -	1.2500	0.	99
1.2500 -	1.2000	.40E-03	99
1.2000 -	1.1500	.40E-03	99
1.1500 -	1.1000	.40E-03	99
1.1000 -	1.0500	.40E-03	99
1.0500 -	1.0000	.40E-03	99
1.0000 -	.9500	.40E-03	99
.9500 -	.9000	0.	99
.9000 -	.8500	.12E-02	51
.8500 -	.8000	0.	99
.8000 -	.7500	.80E-03	99
.7500 -	.7000	.16E-02	41
.7000 -	.6500	.12E-02	51
.6500 -	.6000	.28E-02	31
.6000 -	.5500	.24E-02	45
.5500 -	.5000	.12E-02	51
.5000 -	.4500	.48E-02	17
.4500 -	.4000	.40E-02	37
.4000 -	.3500	.55E-02	22
.3500 -	.3000	.56E-02	28
.3000 -	.2500	.80E-02	25
.2500 -	.2000	.86E-02	18
.2000 -	.1500	.10E-01	19
.1500 -	.1000	.15E-01	13
.1000 -	.0500	.44E-01	8

L 2 L 2

M 2 M 2

.0500 -	.0100	.13E+00	7

ANGULAR DISTRIBUTIONS OF TRANSMITTED AND REFLECTED PHOTON INTENSITY
(MEV/SR, NORMALIZED TO ONE INCIDENT PARTICLE)

0 PHI(DEG)= 0.000

THETA (DEG)	180.000	
0.0000 - 10.0000	.44E-04	99
10.0000 - 20.0000	0.	99
20.0000 - 30.0000	0.	99
30.0000 - 40.0000	0.	99
40.0000 - 50.0000	0.	99
50.0000 - 60.0000	0.	99
60.0000 - 70.0000	0.	99
70.0000 - 80.0000	0.	99
80.0000 - 90.0000	0.	99
90.0000 -100.0000	0.	99
100.0000 -110.0000	0.	99
110.0000 -120.0000	0.	99
120.0000 -130.0000	0.	99
130.0000 -140.0000	0.	99
140.0000 -150.0000	0.	99
150.0000 -160.0000	0.	99
160.0000 -170.0000	0.	99
170.0000 -180.0000	.85E-05	73

ANGULAR DISTRIBUTIONS OF LATERALLY ESCAPING PHOTON INTENSITY
(MEV/SR, NORMALIZED TO ONE INCIDENT PARTICLE)

0 PHI(DEG)= 0.000

THETA (DEG)	180.000	
0.0000 - 10.0000	.32E-02	17
10.0000 - 20.0000	.18E-02	12
20.0000 - 30.0000	.92E-03	17
30.0000 - 40.0000	.24E-03	25
40.0000 - 50.0000	.13E-03	24
50.0000 - 60.0000	.49E-04	30
60.0000 - 70.0000	.42E-04	63
70.0000 - 80.0000	.18E-04	60
80.0000 - 90.0000	.56E-05	92
90.0000 -100.0000	.24E-04	81
100.0000 -110.0000	.82E-05	70
110.0000 -120.0000	.23E-06	99
120.0000 -130.0000	.17E-05	84
130.0000 -140.0000	.29E-05	85
140.0000 -150.0000	.48E-06	99
150.0000 -160.0000	0.	99
160.0000 -170.0000	0.	99
170.0000 -180.0000	0.	99

0

ENERGY SPECTRA AND ANGULAR DISTRIBUTIONS OF PHOTONS TRANSMITTED AND REFLECTED
AZIMUTHAL INTERVAL IS 0.00000 TO 180.00000 DEGREES
(NUMBER (MEV*SR), NORMALIZED TO ONE PARTICLE)

0 E (MEV)	THETA=	0.000 10.000	10.000 20.000	20.000 30.000	30.000 40.000	40.000 50.000	50.000 60.000	60.000 70.000	70.000 80.000	80.000 90.000
1.5000 -	1.4500	0. 99	0. 99	0. 99	0. 99	0. 99	0. 99	0. 99	0. 99	0. 99
1.4500 -	1.4000	0. 99	0. 99	0. 99	0. 99	0. 99	0. 99	0. 99	0. 99	0. 99
1.4000 -	1.3500	0. 99	0. 99	0. 99	0. 99	0. 99	0. 99	0. 99	0. 99	0. 99
1.3500 -	1.3000	0. 99	0. 99	0. 99	0. 99	0. 99	0. 99	0. 99	0. 99	0. 99
1.3000 -	1.2500	0. 99	0. 99	0. 99	0. 99	0. 99	0. 99	0. 99	0. 99	0. 99
1.2500 -	1.2000	0. 99	0. 99	0. 99	0. 99	0. 99	0. 99	0. 99	0. 99	0. 99
1.2000 -	1.1500	0. 99	0. 99	0. 99	0. 99	0. 99	0. 99	0. 99	0. 99	0. 99
1.1500 -	1.1000	0. 99	0. 99	0. 99	0. 99	0. 99	0. 99	0. 99	0. 99	0. 99
1.1000 -	1.0500	0. 99	0. 99	0. 99	0. 99	0. 99	0. 99	0. 99	0. 99	0. 99
1.0500 -	1.0000	0. 99	0. 99	0. 99	0. 99	0. 99	0. 99	0. 99	0. 99	0. 99
[illegible]	[illegible]	[illegible]	[illegible]	[illegible]	[illegible]	[illegible]	[illegible]	[illegible]	[illegible]	[illegible]

.6500 -	.6000	0.	99
.6000 -	.5500	0.	99
.5500 -	.5000	0.	99
.5000 -	.4500	0.	99
.4500 -	.4000	0.	99
.4000 -	.3500	0.	99
.3500 -	.3000	0.	99
.3000 -	.2500	0.	99
.2500 -	.2000	0.	99
.2000 -	.1500	0.	99
.1500 -	.1000	.40E-04	99
.1000 -	.0500	.40E-04	99
.0500 -	.0100	.19E-03	51

0

ENERGY SPECTRA OF REFLECTED PHOTONS
(NUMBER/MEV, NORMALIZED TO ONE INCIDENT PARTICLE)

0 E (MEV) LENGTH= 1000.0000

E (MEV)		LENGTH= 1000.0000	
1.5000 -	1.4500	0.	99
1.4500 -	1.4000	0.	99
1.4000 -	1.3500	0.	99
1.3500 -	1.3000	0.	99
1.3000 -	1.2500	0.	99
1.2500 -	1.2000	0.	99
1.2000 -	1.1500	0.	99
1.1500 -	1.1000	0.	99
1.1000 -	1.0500	0.	99
1.0500 -	1.0000	0.	99
1.0000 -	.9500	0.	99
.9500 -	.9000	0.	99
.9000 -	.8500	0.	99
.8500 -	.8000	0.	99
.8000 -	.7500	0.	99
.7500 -	.7000	0.	99
.7000 -	.6500	0.	99
.6500 -	.6000	0.	99
.6000 -	.5500	0.	99
.5500 -	.5000	0.	99
.5000 -	.4500	0.	99
.4500 -	.4000	0.	99
.4000 -	.3500	0.	99
.3500 -	.3000	0.	99
.3000 -	.2500	0.	99
.2500 -	.2000	0.	99
.2000 -	.1500	0.	99
.1500 -	.1000	0.	99
.1000 -	.0500	0.	99
.0500 -	.0100	0.	99

ENERGY SPECTRA OF LATERALLY ESCAPING PHOTONS
(NUMBER/MEV, NORMALIZED TO ONE INCIDENT PARTICLE)

0 E (MEV) LENGTH= 1000.0000

E (MEV)		LENGTH= 1000.0000	
1.5000 -	1.4500	0.	99
1.4500 -	1.4000	0.	99
1.4000 -	1.3500	0.	99
1.3500 -	1.3000	0.	99
1.3000 -	1.2500	0.	99
1.2500 -	1.2000	0.	99
1.2000 -	1.1500	0.	99
1.1500 -	1.1000	0.	99
1.1000 -	1.0500	0.	99
1.0500 -	1.0000	0.	99
1.0000 -	.9500	0.	99
.9500 -	.9000	0.	99
.9000 -	.8500	0.	99

N 2 N 2

O 2 O 2

.8500 -	.8000	0.	99
.8000 -	.7500	0.	99
.7500 -	.7000	0.	99
.7000 -	.6500	0.	99
.6500 -	.6000	0.	99
.6000 -	.5500	.80E-04	67
.5500 -	.5000	.40E-04	99
.5000 -	.4500	.80E-04	67
.4500 -	.4000	.40E-04	99
.4000 -	.3500	.40E-04	99
.3500 -	.3000	.80E-04	67
.3000 -	.2500	.40E-04	99
.2500 -	.2000	.12E-03	51
.2000 -	.1500	.20E-03	33
.1500 -	.1000	.40E-04	99
.1000 -	.0500	.52E-03	28
.0500 -	.0100	.10E-02	22

ANGULAR DISTRIBUTIONS OF TRANSMITTED AND REFLECTED PHOTON INTENSITY
(MEV/SR, NORMALIZED TO ONE INCIDENT PARTICLE)

THETA (DEG)	PHI(DEG)= 0.000 - 180.000	
0.0000 - 30.0000	.47E-06	72
30.0000 - 60.0000	.75E-07	99
60.0000 - 90.0000	0.	99
90.0000 - 120.0000	0.	99
120.0000 - 150.0000	0.	99
150.0000 - 180.0000	0.	99

ANGULAR DISTRIBUTIONS OF LATERALLY ESCAPING PHOTON INTENSITY
(MEV/SR, NORMALIZED TO ONE INCIDENT PARTICLE)

THETA (DEG)	PHI(DEG)= 0.000 - 180.000	
0.0000 - 30.0000	.18E-04	28
30.0000 - 60.0000	.50E-06	28
60.0000 - 90.0000	.10E-06	99
90.0000 - 120.0000	0	99
120.0000 - 150.0000	0	99
150.0000 - 180.0000	0	99

ENERGY SPECTRA AND ANGULAR DISTRIBUTIONS OF PHOTONS TRANSMITTED AND REFLECTED
AZIMUTHAL INTERVAL IS 0.00000 TO 180.00000 DEGREES
(NUMBER/MEV/SR, NORMALIZED TO ONE PARTICLE)

E (MEV)	THETA= 0.000 - 30.000		30.000 - 60.000		60.000 - 90.000		90.000 - 120.000		120.000 - 150.000		150.000 - 180.000	
1.5000 - 1.4500	0	99	0	99	0	99	0	99	0	99	0	99
1.4500 - 1.4000	0	99	0	99	0	99	0	99	0	99	0	99
1.4000 - 1.3500	0	99	0	99	0	99	0	99	0	99	0	99
1.3500 - 1.3000	0	99	0	99	0	99	0	99	0	99	0	99
1.3000 - 1.2500	0	99	0	99	0	99	0	99	0	99	0	99
1.2500 - 1.2000	0	99	0	99	0	99	0	99	0	[illegible]	0	99
1.2000 - 1.1500	0	99	0	99	0	99	0	99	0	[illegible]	0	99
1.1500 - 1.1000	0	99	0	99	0	99	0	99	0	99	0	99
1.1000 - 1.0500	0	99	0	99	0	99	0	99	0	99	0	99
1.0500 - 1.0000	0	99	0	99	0	99	0	99	0	99	0	99
1.0000 - .9500	0	99	0	99	0	99	0	99	0	99	0	99
.9500 - .9000	0	99	0	99	0	99	0	99	0	99	0	99
.9000 - .8500	0	99	0	99	0	99	0	99	0	99	0	99
.8500 - .8000	0	99	0	99	0	99	0	99	0	99	0	99
.8000 - .7500	0	99	0	99	0	99	0	99	0	99	0	99
.7500 - .7000	0	99	0	99	0	99	0	99	0	99	0	99
.7000 - .6500	0	99	0	99	0	99	0	99	0	99	0	99
.6500 - .6000	0	99	0	99	0	99	0	99	0	99	0	99
.6000 - .5500	0	99	0	99	0	99	0	99	0	99	0	99

.1000 - .0500	0.	99	.75E-03	99	0.	99	0.	99	.52E-03	99	0.	99	0.	99	0.	99	0.	99
.0500 - .0100	.14E-02	71	.45E-03	99	.48E-03	99	.22E-02	77	.64E-03	96	.76E-03	99	0.	99	0.	99	0.	99
INTEGRAL (SR)	.91E-04	44	.75E-04	55	.19E-04	99	.87E-04	77	.51E-04	67	.31E-04	99	0.	99	0.	99	0.	99

NUMBER OF ECS WORDS USED FOR STATISTICS IS 2505

APPENDIX G

PARTICLE SIMULATION OF FX-100 BEAM PROPAGATION AND COMPARISON WITH EXPERIMENT

SECURITY CLASSIFICATION OF THIS PAGE (When Data Entered)

REPORT DOCUMENTATION PAGE

READ INSTRUCTIONS BEFORE COMPLETING FORM

1. REPORT NUMBER	2. GOVT ACCESSION NO.	3. RECIPIENT'S CATALOG NUMBER
4. TITLE (and Subtitle) Particle Simulations of FX-100 Beam Propagation and Comparison with Experiment		5. TYPE OF REPORT & PERIOD COVERED Interim Report
		6. PERFORMING ORG. REPORT NUMBER AMRC-R-187
7. AUTHOR(s) Thomas Hughes Carl Ekdahl Brendan Godfrey		8. CONTRACT OR GRANT NUMBER(s) F49620-81-C-0016
9. PERFORMING ORGANIZATION NAME AND ADDRESS Mission Research Corporation 1400 San Mateo Boulevard, S.E., Suite A Albuquerque, New Mexico 87108		10. PROGRAM ELEMENT PROJECT, TASK AREA & WORK UNIT NUMBERS
11. CONTROLLING OFFICE NAME AND ADDRESS Air Force Office of Scientific Research Bolling Air Force Base Washington, D.C. 20332		12. REPORT DATE January 1982
		13. NUMBER OF PAGES 14
14. MONITORING AGENCY NAME & ADDRESS (if different from Controlling Office)		15. SECURITY CLASS (of this report) Unclassified
		15a. DECLASSIFICATION DOWNGRADING SCHEDULE

16. DISTRIBUTION STATEMENT (of this Report)

17. DISTRIBUTION STATEMENT (of the abstract entered in Block 20, if different from Report)

18. SUPPLEMENTARY NOTES

19. KEY WORDS (Continue on reverse side if necessary and identify by block number)

Electron beam propagation
Particle simulations

20. ABSTRACT (Continue on reverse side if necessary and identify by block number)

The propagation code CPROP and the linear theory code KMRAD are used to simulate the FX-100 beam propagating in air. When avalanching is significant, return current tends to concentrate on axis and defocuses the beam head. A strong filamentation instability accompanies large return current fractions. We attempt to correlate these results with the experimental data.

DD FORM 1 JAN 73 1473 EDITION OF 1 NOV 65 IS OBSOLETE

SECURITY CLASSIFICATION OF THIS PAGE (When Data Entered)

CONTENTS

LIST OF ILLUSTRATIONS

I. INTRODUCTION

Theoretical investigations in support of the FX-100 experiments have relied on two existing MRC computer codes: CPROP, which is a propagation code, and KMRAD, a linear theory code. The usefulness of these codes is hampered by lack of an air conductivity model whose known range of validity encompasses the 0.1 - 2.0 Torr regime. At present, CPROP uses a conductivity model developed for use at pressures in the range 10^2 - 10^3 Torr.[1] The validity of this model at pressures in the neighborhood of 1 Torr is certainly questionable, but its degree of inaccuracy is unknown. We shall interpret our numerical results in this light and seek to extract information which will guide future efforts.

The CPROP model for the beam is straightforward. The beam is initialized with current and voltage ramps close to those measured experimentally, and is given a Bennett profile in radius (Fig. 1). Due to computing expense and computer core limitations only the first 15 ns of the pulse were simulated. At each location in z (direction of propagation) the beam particles were assigned an emittance based on an approximate formula for the scattering produced by the titanium anode foil.[2] The initialization of the code is completed by computing the self-consistent fields, conductivity, and return current in the frozen field approximation[3] (the initialization is the only stage at which this approximation is used by CPROP).

The code KMRAD requires the input of a beam equilibrium and conductivity profile. It provides linear growth rates and is much cheaper to run than CPROP. It simulates only the body of the pulse and cannot deal with the head of the beam.

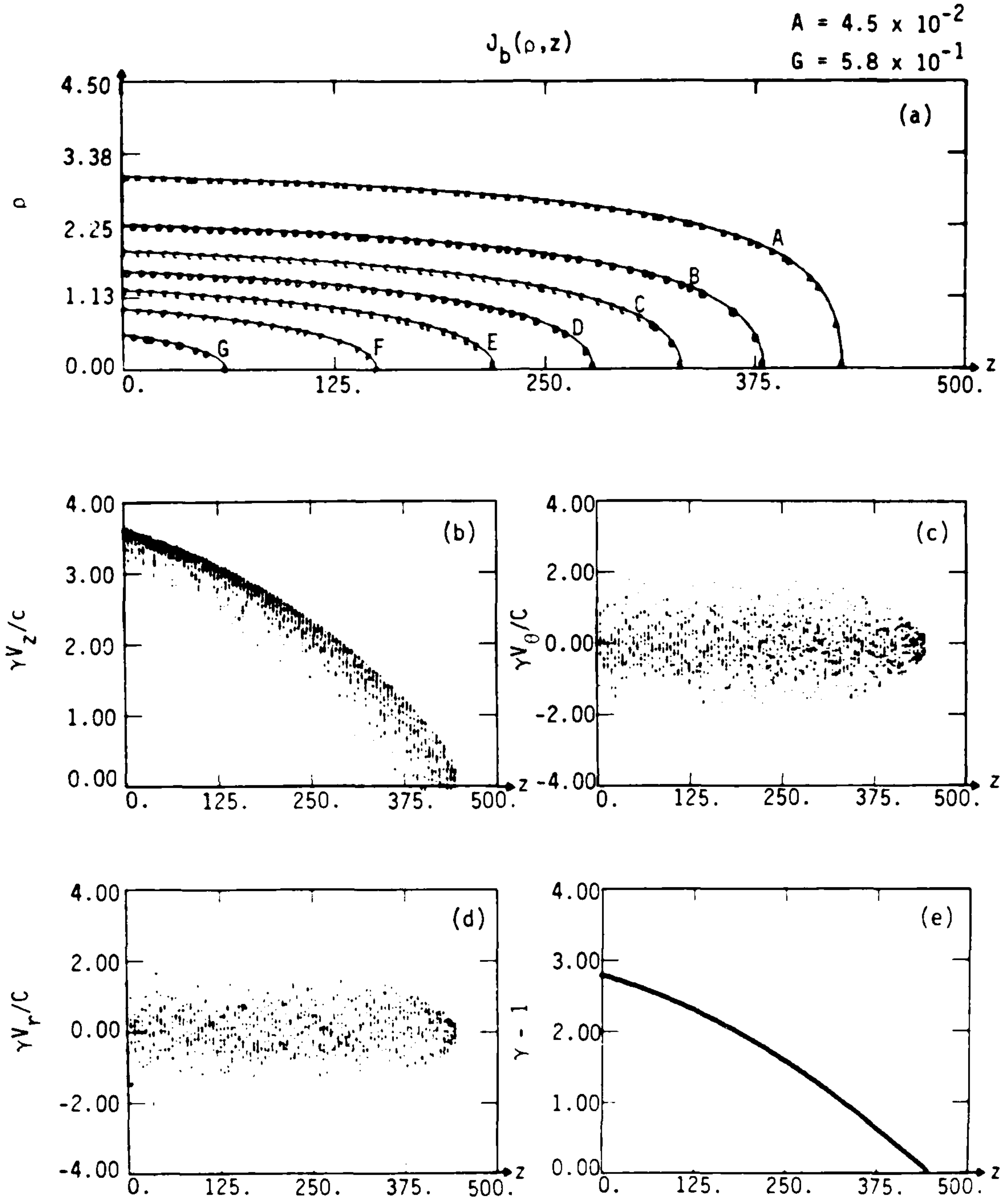

Figure 1. Initialization of CPROP at 0.4 Torr. Part (a) shows contours of the beam current density $J_b(\rho,z)$ in units of 17 kA/cm^2. The values of the contours, labeled by A, B, C, D, E, F, G, are linearly spaced. The z coordinate is in cm. The radial coordinate ρ is related to the physical coordinate r by $\rho = a\ln(1 + r/a)$ where a is the Bennett radius in cm. The Bennett radius is at $\rho = 2.2$. In (b), (c), (d), (e) phase plots of the beam are depicted. The current and voltage ramps in (a) and (e), respectively, are approximately those of the experiment.

II. NUMERICAL RESULTS

The result of initializing CPROP at a pressure of 0.4 Torr, which is in the experimental propagation window, is shown in Fig. 2. This figure shows the presence of both an electrostatic radial and an inductive longitudinal electric field at the head of the beam where the conductivity is lowest. Comparing Fig. 2 with Fig. 3, we see that the avalanching these fields produce have a large effect on the magnitude and profile of the return current. In Fig. 2, the return current fraction obtained is f ≈ 80% and the return current is more peaked on axis than the beam current so that the B_θ field peaks near the wall instead of at the Bennett radius. When the particles are "let go," the beam expands out radially and loses almost one third of the particles to the wall before contracting. Most of these lost particles come from the nose of the beam. The beam continues to bounce but few particles are subsequently lost. It has been suggested[4] that at low pressures, avalanching will not occur on a significant scale because of the long mean free path of secondary electrons. With avalanching turned off in CPROP, we obtain f ≈ 35% and the return current has approximately the same radial profile as the beam. If propagated, this beam will start to pinch inward. The experimental evidence tends to favor the inclusion of avalanching in the conductivity model. At pressures near 0.35 Torr, return current fractions of 80 - 95% are observed near the diode. Furthermore, several open shutter photographs taken near the diode (Fig. 4a) show some of the beam blowing off radially.

The large conductivity produced by avalanching leads to a long magnetic decay time for the monopole return current, $\tau \sim 900$ ns (the pulse length is about 120 ns). This means that the resistive instabilities most likely to develop are those with short transverse wavelength $\lambda_\perp$, i.e. filamentary instabilities, since the magnetic decay time is proportional to $\lambda_\perp^2$. The linearized simulation code KMRAD was used to look for such instabilities. The open shutter photographs seem to indicate that the fine structure in the beam is azimuthally symmetric so we set m=0

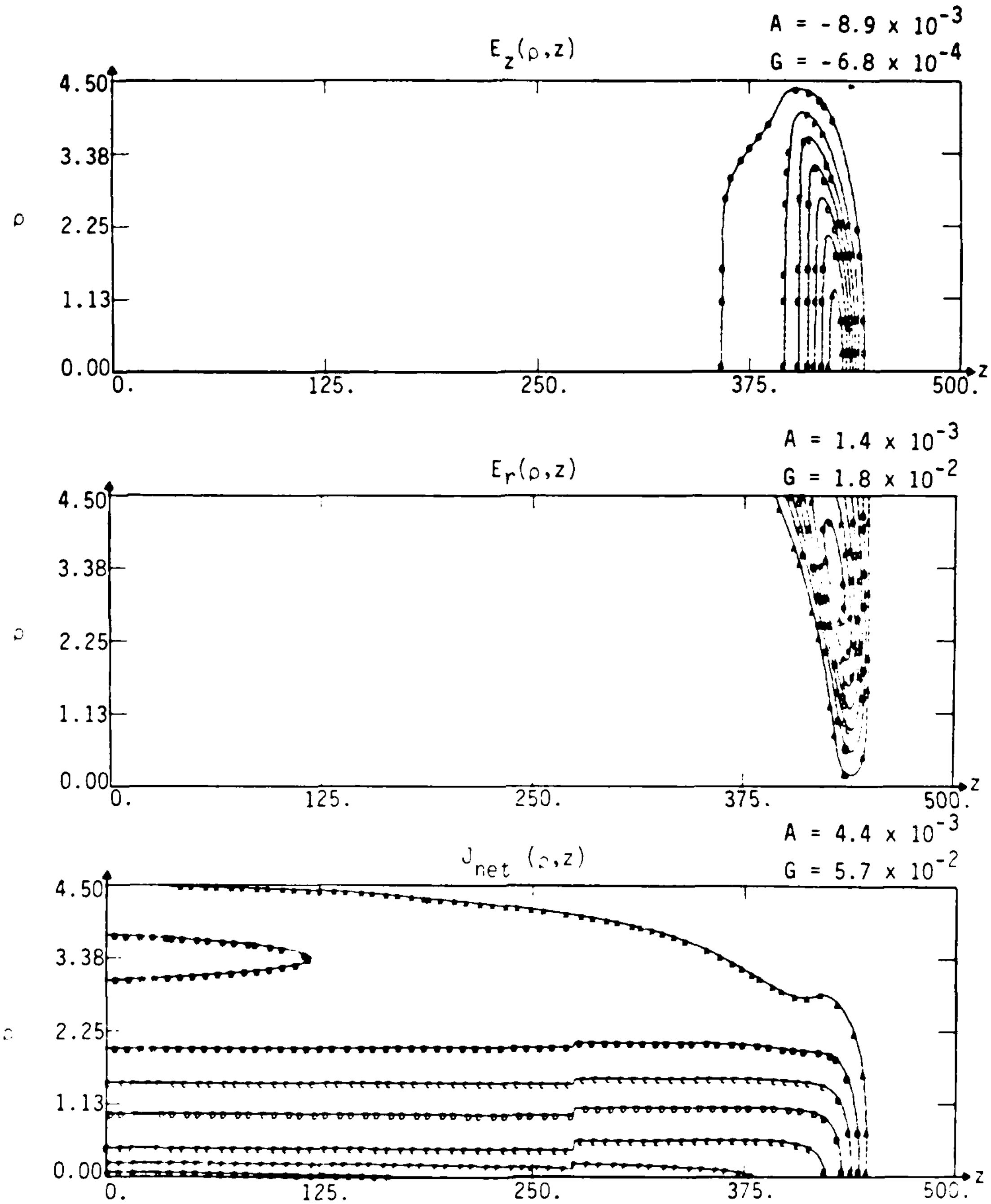

Figure 2. Contour plots of the fields E_z, E_r, in units of 0.51 MV/cm, the B_θ field in units of $0.51 \times 10^4/3$ gauss, the z component of the net current density J_{net}, and the conductivity σ in units of $3 \times 10^{10}/4\pi$ sec^{-1}, at an air pressure of 0.4 Torr. Avalanching is included in the conductivity model.

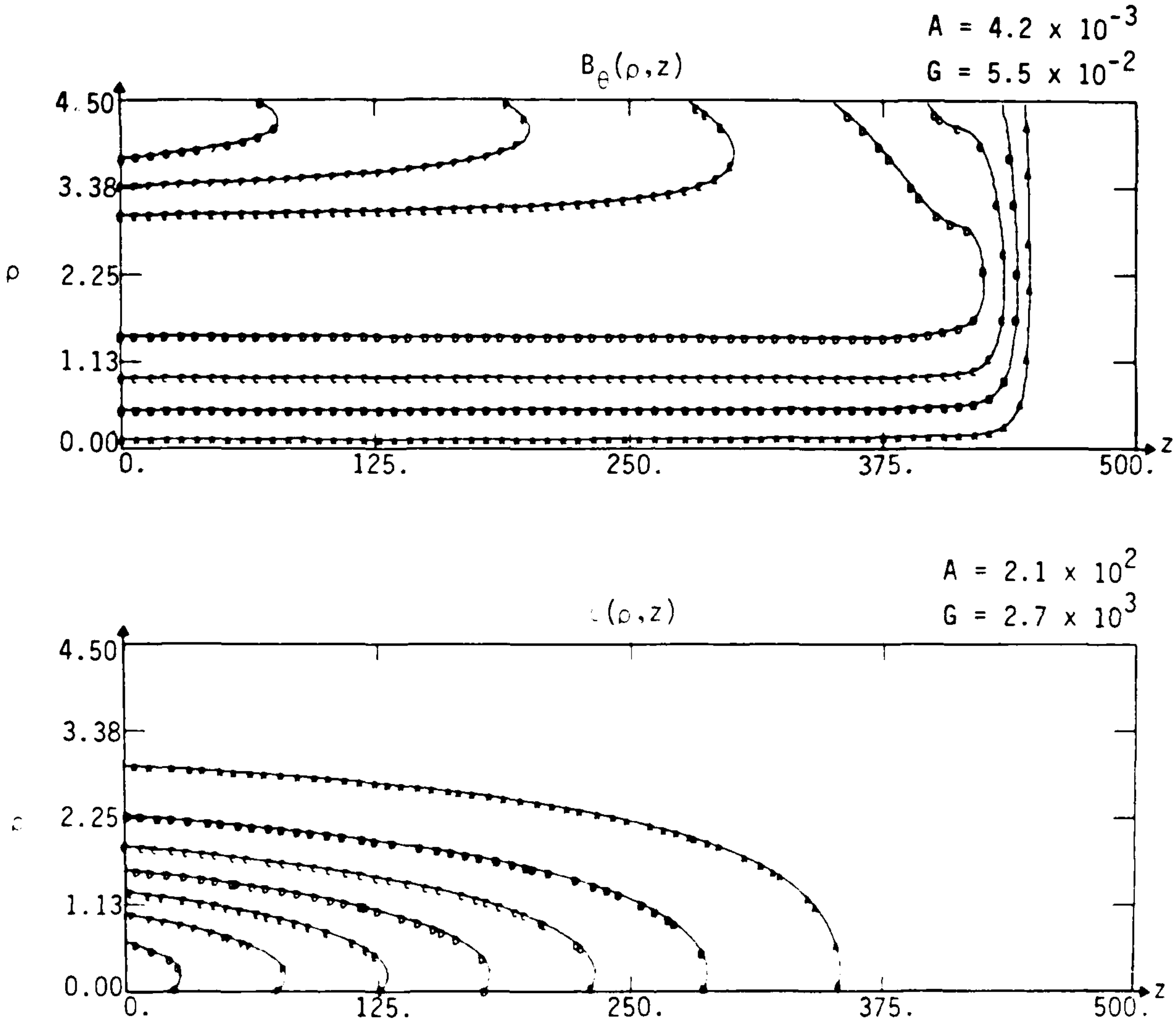

Figure 2 (continued).

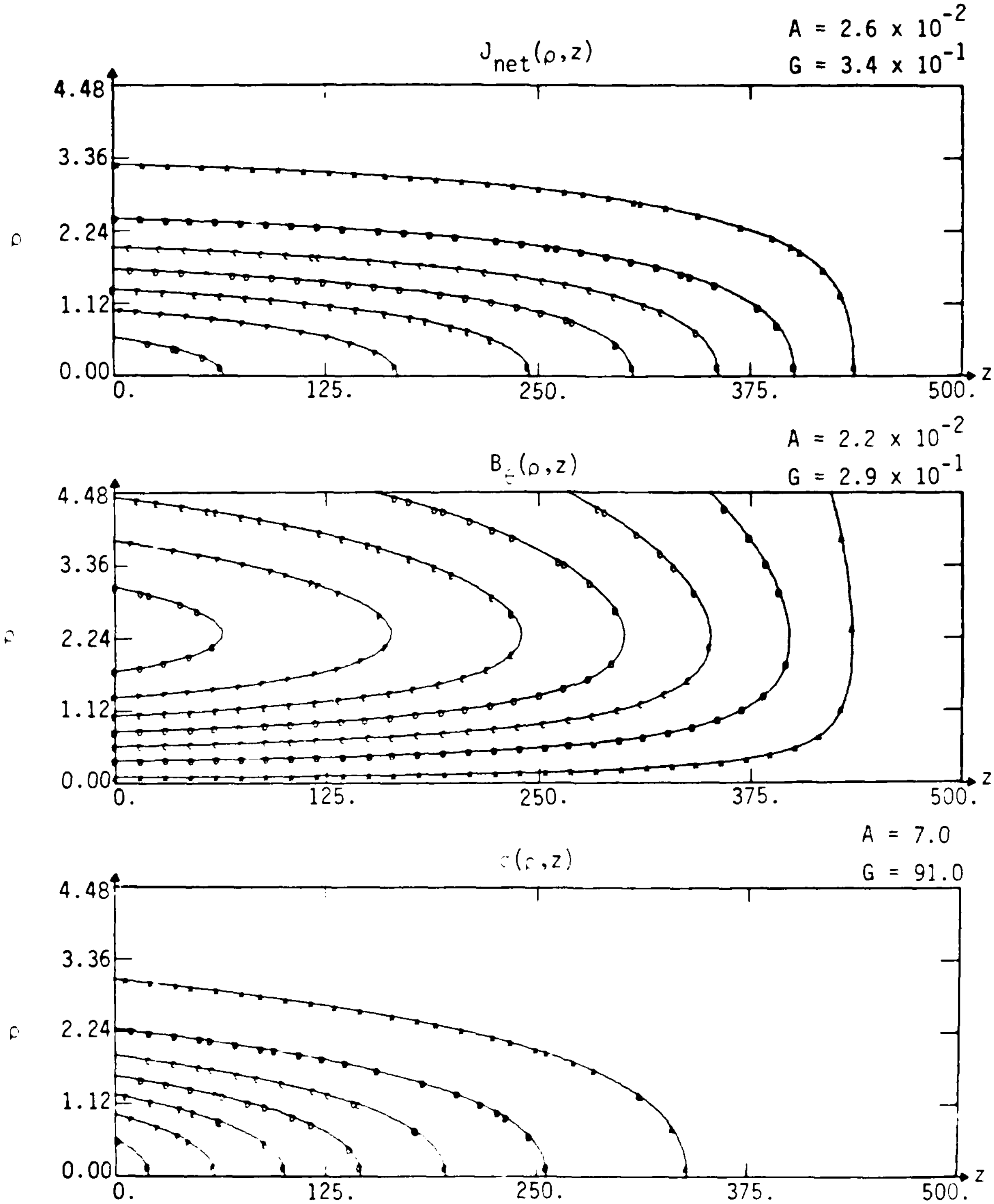

Figure 3. Contour plots of J_{net}, B_θ, and σ with the same normalization as in Fig. 2, also at 0.4 Torr. The avalanching term in the conductivity model has been removed.

(a) p = 0.4 Torr

(c) p = 0.1 Torr

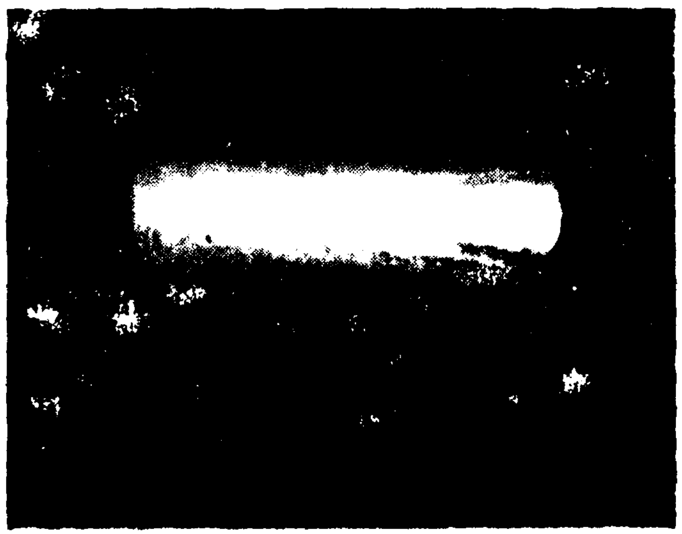

(b) p = 0.1 Torr

(d) p = 0.2 Torr

Figure 4. Open shutter photographs of the FX-100 beam at various air pressures (p). The beam is propagating from left to right. In (a), (c) and (d), the camera is positioned 13 cm downstream from the diode. In (b), it is 4.4 m downstream.

in the simulations. We chose a return current fraction of 95% and the return current and conductivity profiles were assumed to follow the beam profile. The magnitude of the conductivity was taken from CPROP. We found growth rates on the order of 2×10^8 sec^{-1}, with a transverse wavelength of 0.8 - 1 cm (The beam Bennett radius is 3 cm). The growth rates are largest for $k_z << k_\perp$ which corresponds to low real frequencies, and low group velocities. The latter implies that the number of e-foldings which the instability can undergo is roughly $N_\gamma \approx \gamma\tau_p$, where γ is the growth-rate and τ_p is the pulse length. Assuming that our estimate of the growth rate is reasonable, then $N_\gamma \approx 20$ can be attained, which would allow the instability to develop strongly. However, while these calculations are suggestive, the experimental data is not detailed enough to allow us to rule out other explanations for the fine structure seen both in the open shutter (Figs. 4b, 4d) and streak photographs.

At lower pressures, in the neighborhood of 0.1 Torr, CPROP predicts return current fractions of about 70%, and a return current profile close to that of the beam current (Fig. 5). When propagated, the beam collapses to a smaller radius than its initial one of 3 cm. This behavior is qualitatively similar to that observed experimentally. The measured return current fraction is about 45% and the open shutter photographs (Fig. 4c) show a pinched beam with a radius of about 2 cm.

No significant nose erosion is seen experimentally. CPROP predicts that at p = 0.4 Torr, the beam loses about 1 meter in propagating the first 2 meters, as we see by comparing Figs. 1 and 6. This erosion is at the limit of the experimental precision. The steepening of the longitudinal beam current profile in Fig. 6 gives rise to an increase in the amplitude of E_z at the beam head by a factor of six over its value at t = 0 (Fig. 2). This does not lead to a dramatic increase in the erosion rate however since the beam energy γ also increases as one moves back from the head.

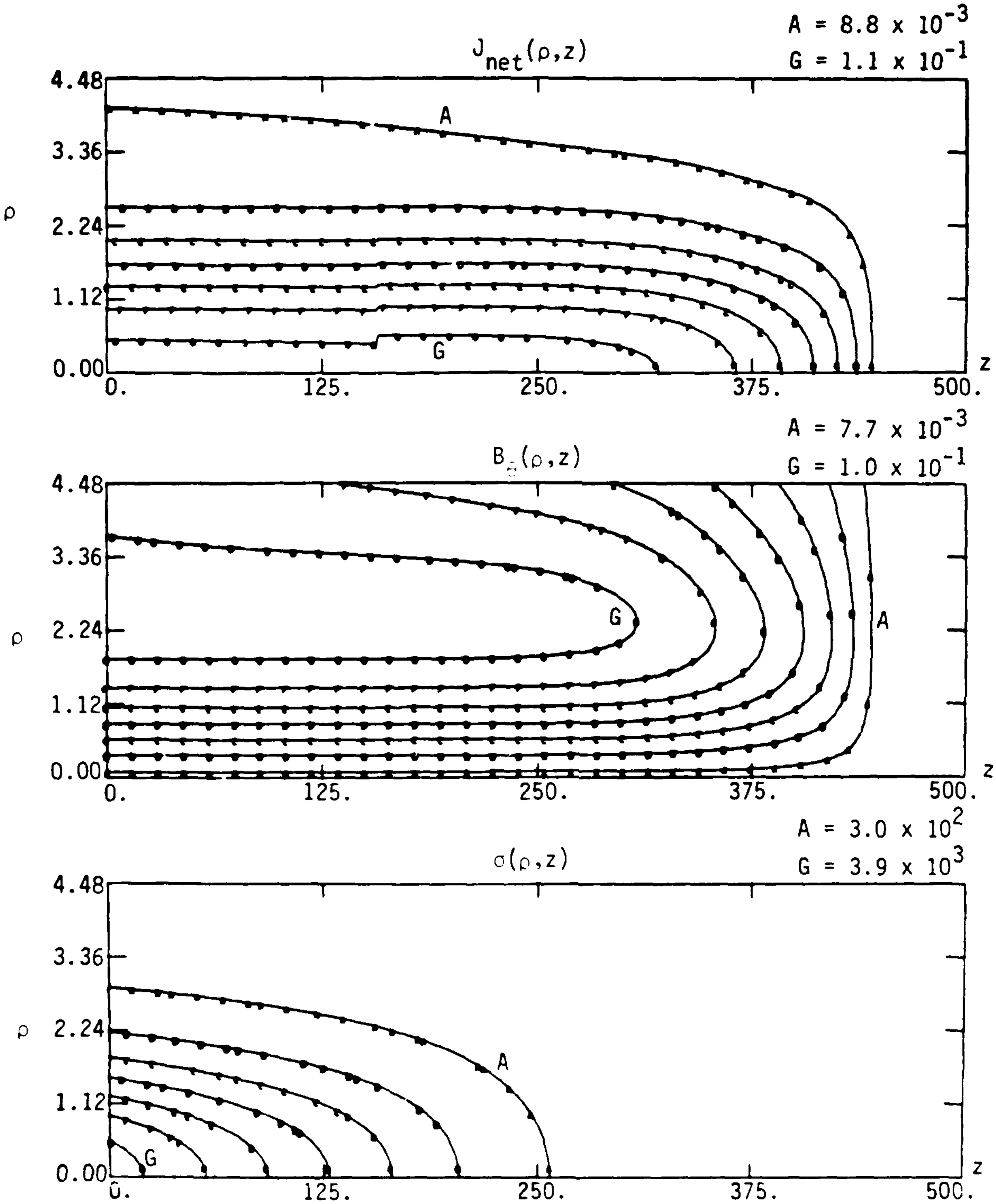

Figure 5. Contour plots of J_{net}, B_θ and σ at 0.125 Torr. Avalanching is included.

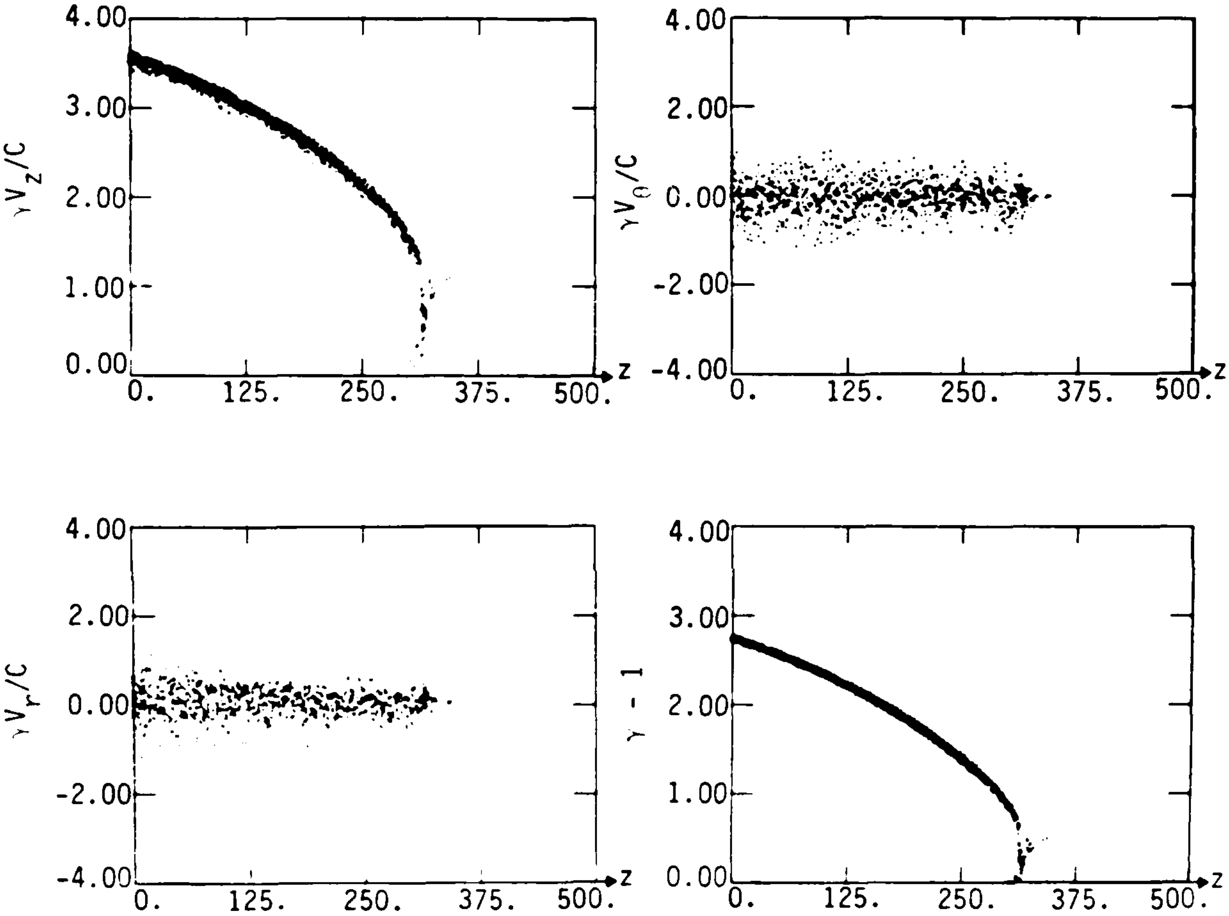

Figure 6. Phase plots of beam after traveling two meters through air at 0.4 Torr, showing nose erosion. Cf. Fig. 1.

III. SUMMARY

We have used the simulation codes CPROP and KMRAD to attempt to explain some of the phenomena seen in the FX-100 experiments. Since we have doubts about the appropriateness of the conductivity model employed, our conclusions are tentative. The simulations show that:

(1) The large return current fractions measured experimentally near 0.4 Torr and above are consistent with the presence of avalanching.

(2) At 0.4 Torr and above, avalanching causes the return current to concentrate on axis, and this may be responsible for the radial blowing-off of some of the beam seen in open shutter photographs.

(3) Resistive filamentation instabilities driven by the large return current fraction may be the source of the fine structure seen in open shutter and streak photographs at 0.2 - 0.4 Torr.

(4) Near 0.1 Torr the return current profile tends to follow the beam current profile.

To put the above conclusions on a more secure footing, an improved conductivity model is essential. In addition, more carefully controlled experimental conditions would benefit future work. In the present series of experiments, the beam exhibited diverse behavior on different shots under apparently identical conditions.

ACKNOWLEDGMENT

We would like to thank Dr. Winston Bostick and Mr. Ray Lemke for useful conversations.

REFERENCES

1. F. W. Chambers, UCID-18302, Lawrence Livermore National Laboratory (1979).

2. L. E. Thode, private communication.

3. E. P. Lee, UCID-17826, Lawrence Livermore National Laboratory (1976).

4. R. J. Briggs, UCID-19187, Lawrence Livermore National Laboratory (1981).

APPENDIX H

FX-100 PROPAGATION EXPERIMENTS--RADLAC REVIEW MEETING

SECURITY CLASSIFICATION OF THIS PAGE (When Data Entered)

REPORT DOCUMENTATION PAGE

READ INSTRUCTIONS BEFORE COMPLETING FORM

1. REPORT NUMBER

2. GOVT ACCESSION NO.

3. RECIPIENT'S CATALOG NUMBER

4. TITLE (and Subtitle)

FX-100 PROPAGATION EXPERIMENTS - RADLAC REVIEW MEETING

5. TYPE OF REPORT & PERIOD COVERED

INTERIM REPORT

6. PERFORMING ORG. REPORT NUMBER

AMRC-R-189

7. AUTHOR(s)

C. A. Ekdahl, W. Bostick,
L. A. Wright and T. P. Hughes

8. CONTRACT OR GRANT NUMBER(s)

F49620-81-C-0016

9. PERFORMING ORGANIZATION NAME AND ADDRESS

Mission Research Corporation
1400 San Mateo Boulevard, S. E., Suite A
Albuquerque, New Mexico 87108

10. PROGRAM ELEMENT, PROJECT, TASK AREA & WORK UNIT NUMBERS

11. CONTROLLING OFFICE NAME AND ADDRESS

Air Force Office of Scientific Research
Bolling Air Force Base
Washington, D. C. 20332

12. REPORT DATE

January 1982

13. NUMBER OF PAGES

22

14. MONITORING AGENCY NAME & ADDRESS (if different from Controlling Office)

15. SECURITY CLASS. (of this report)

Unclassified

15a. DECLASSIFICATION DOWNGRADING SCHEDULE

16. DISTRIBUTION STATEMENT (of this Report)

Approved for public release; distribution unlimited.

17. DISTRIBUTION STATEMENT (of the abstract entered in Block 20, if different from Report)

18. SUPPLEMENTARY NOTES

19. KEY WORDS (Continue on reverse side if necessary and identify by block number)

Intense Relativistic Electron Beam Propagation
Intense Relativistic Electron Beam Diagnostics

20. ABSTRACT (Continue on reverse side if necessary and identify by block number)

A hollowing instability of the FX-100 electron beam was observed in air propagation experiments at pressures in the range of the energy transport pressure window. This instability, observed with both time-integrated and time-resolved diagnostics, occurred late in time and may have been triggered by a diode mismatch as well as a peak of conductivity on axis.

DD FORM 1 JAN 73 1473 EDITION OF 1 NOV 65 IS OBSOLETE

SECURITY CLASSIFICATION OF THIS PAGE (When Data Entered)

PARTICIPATION IN 1981 FX-100
PROPAGATION EXPERIMENTS

CARL EKDAHL, MRC

WINSTON BOSTICK, AFWL

LARRY WRIGHT, MRC

TOM HUGHES, MRC

THIS RESEARCH WAS JOINTLY SUPPORTED BY THE AIR FORCE WEAPONS LABORATORY AND THE AIR FORCE OFFICE OF SCIENTIFIC RESEARCH (AFSC) UNDER CONTRACTS F49620-81-C-0016 AND IPA-905-79-01016C.

THE FOLLOWING MEMBERS OF THE DYNAMIC TESTING DIVISION AT LANL PROVIDED TIME RESOLVED PHOTOGRAPHY OF THE FX-100 EXPERIMENTS: BOB BENJAMIN (M-6), STEVE SCHMIDT (M-6), TOM STARKE (M-2), DAVE MOIR (M-2), AND LEE BUILTA (M-2).

PAST AFWL/AFOSR/MRC EXPERIMENTS

FX-25 (1.5 MEV, 23 KA, 20 NS)

- STABLE PROPAGATION WINDOW ($P < P_A$)
  - EROSION; HOSE LIMITED
  - CHEMISTRY IN WINDOW (VISIBLE EMISSION)
- STABILIZATION OF HOSE WITH LOW PRESSURE DRIFT CELL ($>10\lambda_\beta$?)

FX-100 (1.5 MEV, 40 KA, 120 NS)

- STABLE PROPAGATION WINDOW ($P < P_A$)
  - EROSION; HOSE LIMITED
  - "HALO" MODE OBSERVATIONS
  - CHEMISTRY IN WINDOW
    EMISSION SPECTROSCOPY
    TIME RESOLVED (LANL)
  - ENERGY RESOLUTION

<u>AFOSR/AFWL/MRC</u>

FX-100 EXPERIMENT DIAGNOSTICS

I. <u>BEAM CURRENT - DENSITY DISTRIBUTION</u>

A. PROBE ARRAY #1 (1 MIL KAPTON; 5 MIL Ti)

Z = 1.3 CM (VAC)

= 0.25; 0.5; 1; 3; 5 (M) @

P = 0.13; <u>0.35</u>; <u>0.5</u>; 0.7; 1; 1.5; 2; 3; 10 (TORR)

B. SIMULTANEOUS C CALORIMETRY WITH (A)

C. V_{DIODE}; I_{DIODE}; FAST I_{NET} (AT VARIOUS Z)

D. OPEN SHUTTER PHOTOGRAPHY

E. RADIOCHROMIC FOILS

F. TLD ARRAY

(D–F: TIME INTEGRATED MEASUREMENTS)

II. <u>TOTAL BEAM AND NET CURRENT</u>

A. FAST I_{NET}

B. I_{BEAM} (5_{MIL} Ti - VACUUM; C-CALORIMETER; ROGOWSKI)

Z = 0.5; 1; 3; 5 (M)

P = 0.13; 0.35; 0.5; 0.7; 1; 1.5 (TORR)

III. OPTICAL EMISSION DIAGNOSTICS

A. OPEN SHUTTER CAMERA Z = 0.2; 4 M

B. FAST, TIME-RESOLVED PHOTOGRAPHY (WITH M-6 & M-2)
IMACON & QUESTAR @ Z = 4 M

C. TIME INTEGRATED SPECTROSCOPY
JACO @ Z = 4 M

P = 0.13; 0.2; 0.35; 0.5; 0.7; 1; 1.5; 3; 10
(TORR)

IV. BEAM ENERGY DISTRIBUTION

A. P-1 β-SPECTROMETER

~700 SHOTS IN 4.5 MO

SHUT DOWN 19 AUG 81

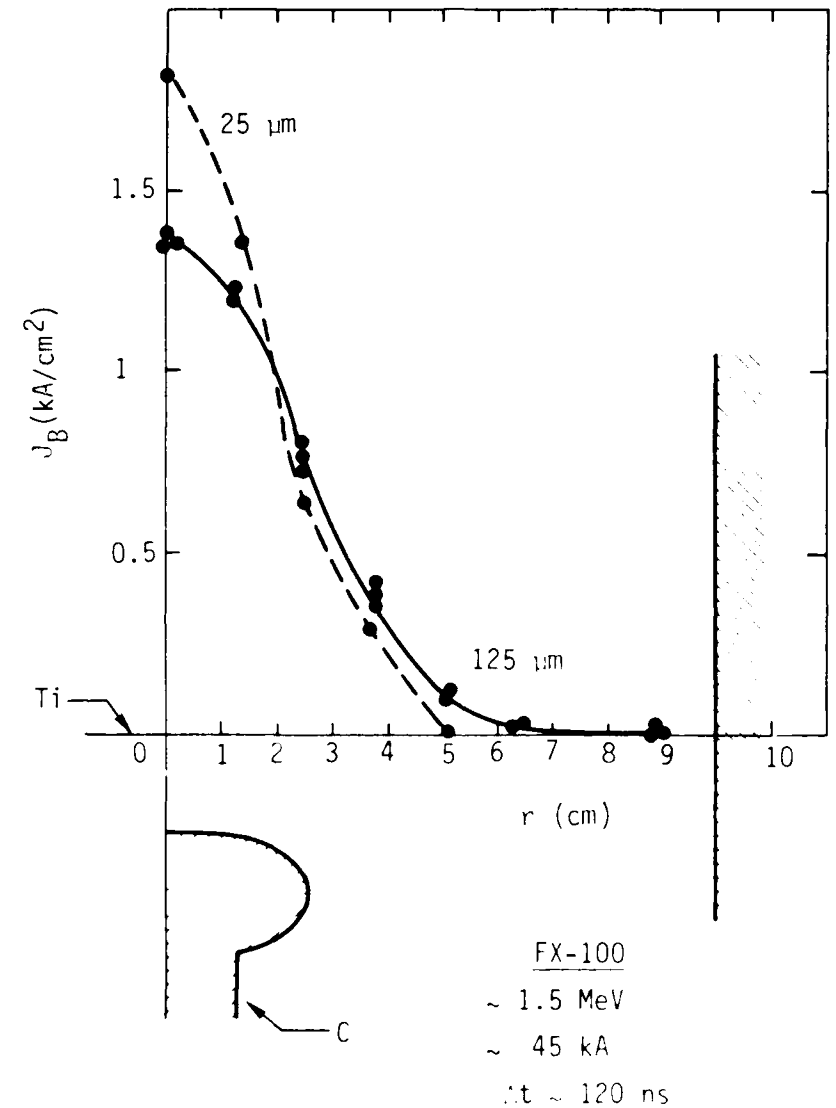

Figure 1. Multiple Faraday collector array measurements of FX-100 beam current density distribution in vacuum 1.[illegible] cm from the anode foil. Distribution for two different foil thicknesses are shown. However, all propagation experiments were performed using 25-μm Ti foil anodes.

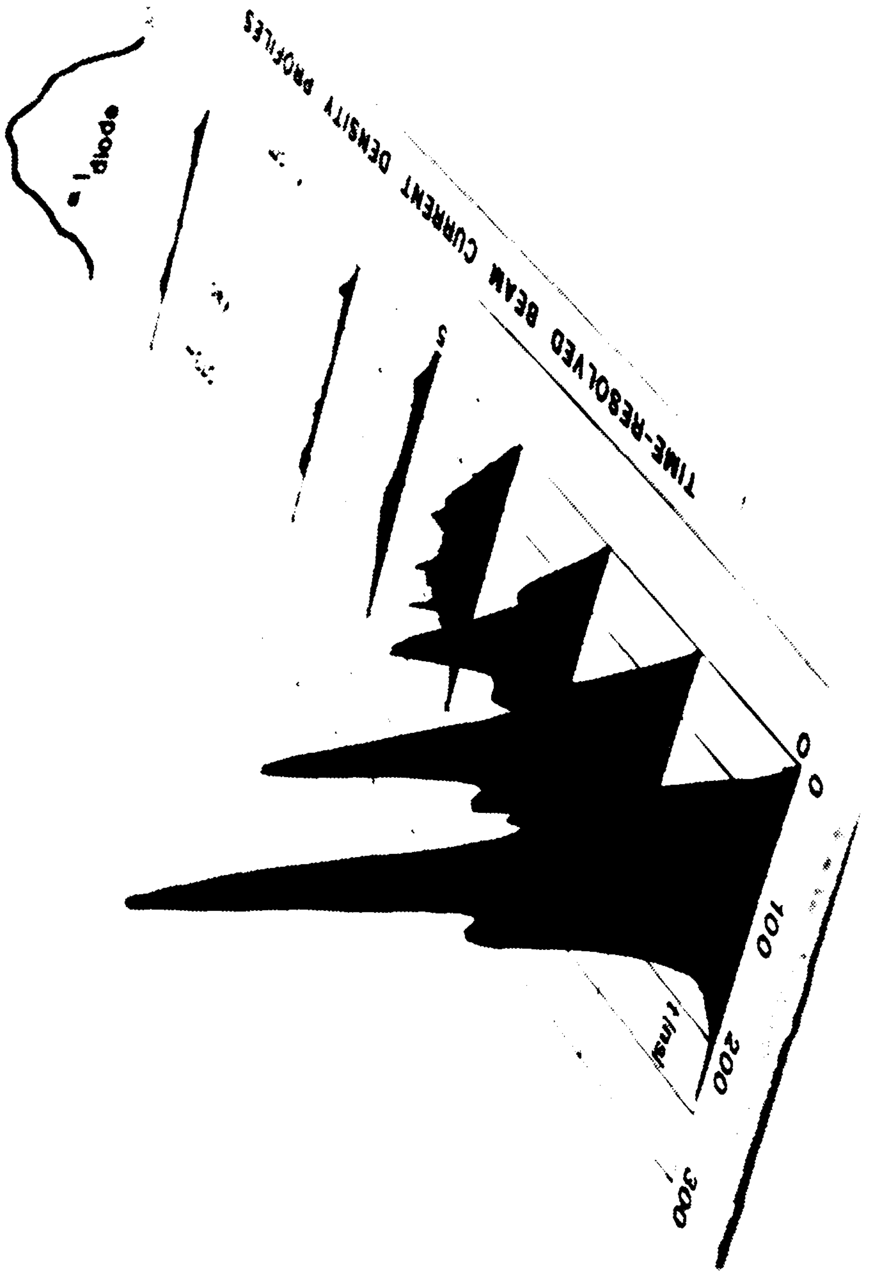

Figure 2. Time-resolved beam current density, profile measured 1.3 cm from 25-μm Ti anode foil in vacuum.

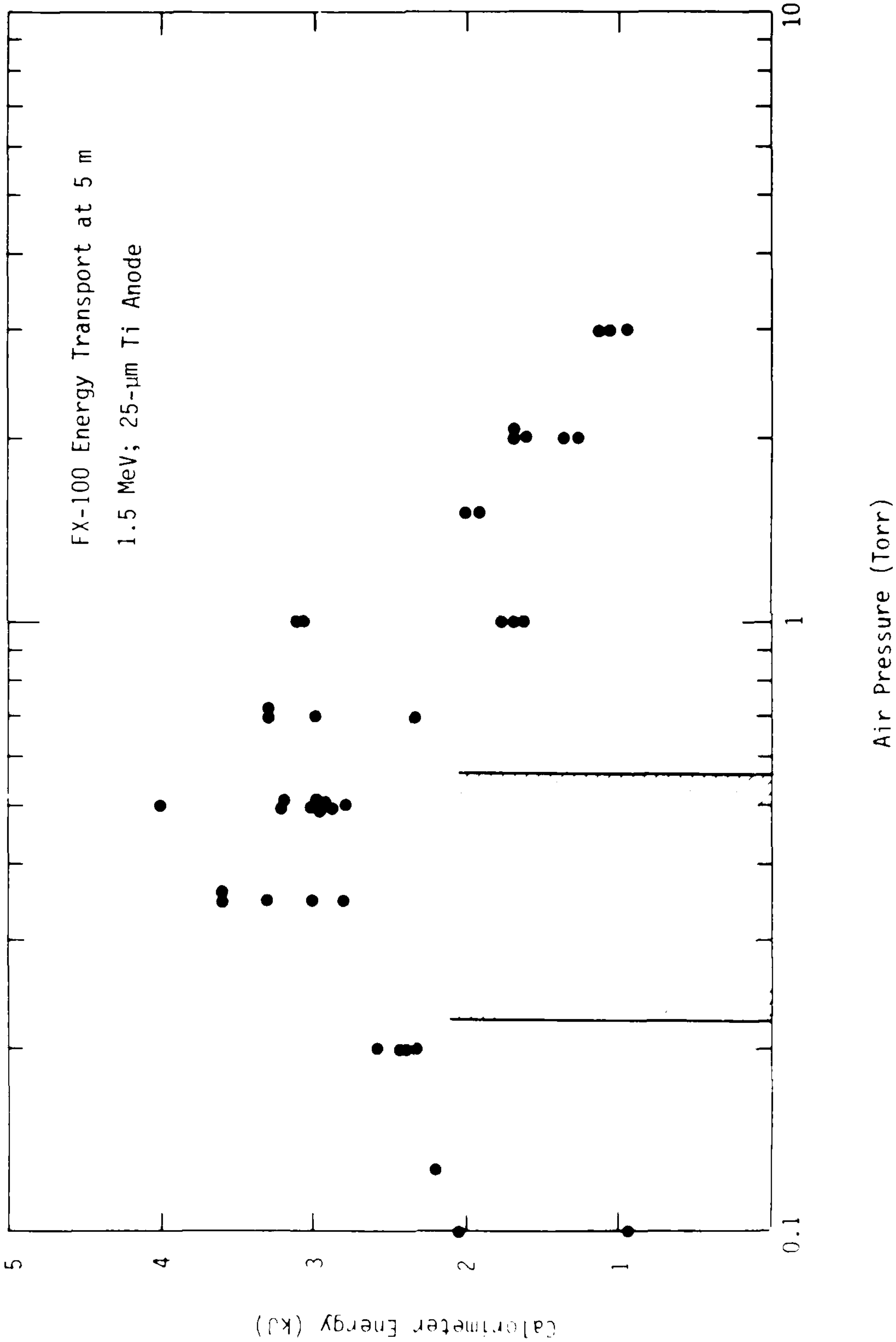

Figure 3. FX-100 beam energy deposition in C calorimeter at end of 5-m drift tube filled with air at pressure shown.

ANNULAR "HALO" PROPAGATION

- OBSERVED WITH:

    1 - Ti-FOIL SHIELDED RADIOCHROMIC FOILS

    2 - OPEN SHUTTER PHOTOGRAPHY

    3 - STREAK PHOTOGRAPHY

    4 - TIME-RESOLVED FARADAY CUP ARRAY

- CHARACTERISTICS:

    - RADIUS $\sim$ 2 x 1/e RADIUS

    - ELECTRON ENERGY $\gtrsim$ 150 keV (5 mil Ti on (1) & (4))

    - DEVELOPS "LATE" IN TIME ($\gtrsim$ 20 - 30 ns)

    - NOT RESULT OF DIODE SHANK EMISSION (C COLLIMATOR)

    - PRESSURE REGIME CORRESPONDS TO MAX ENERGY TRANSPORT (0.3 - 0.7 TORR)

    - MAY CARRY AS MUCH AS $\sim$ 90% I_B

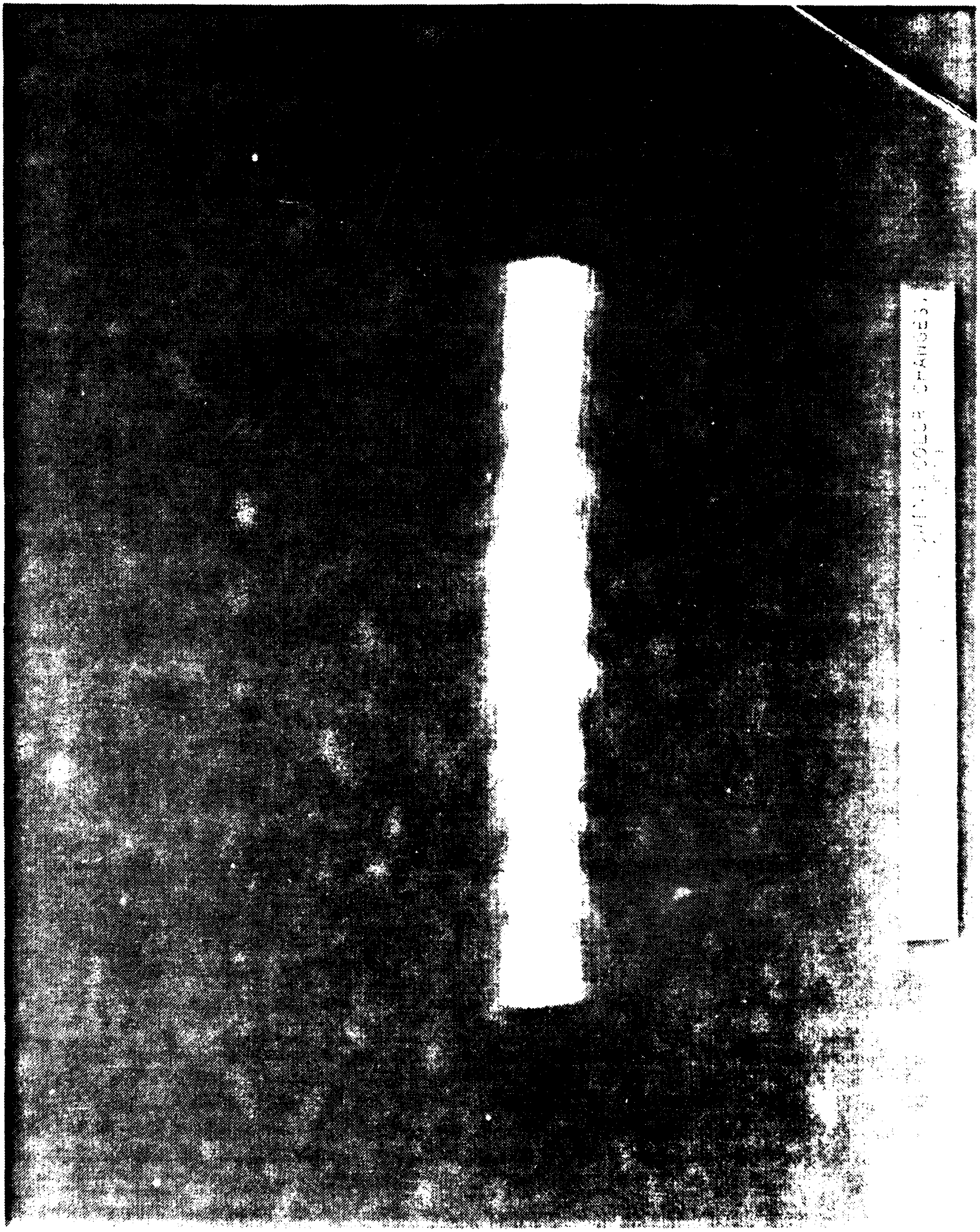

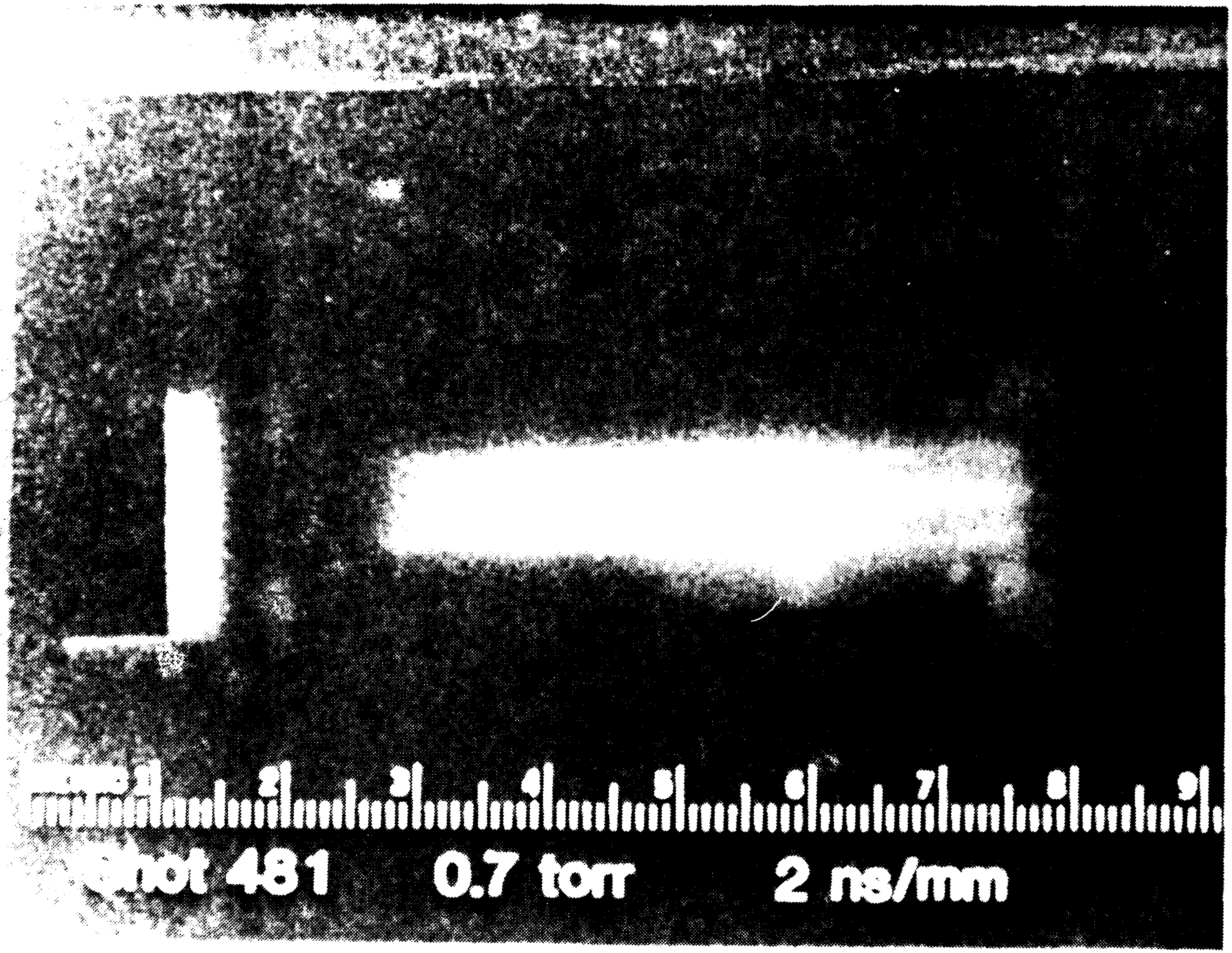

Figure 5. Imacon streak camera picture taken through a vertical slit at 4.5 m showing development of annular halo emission.

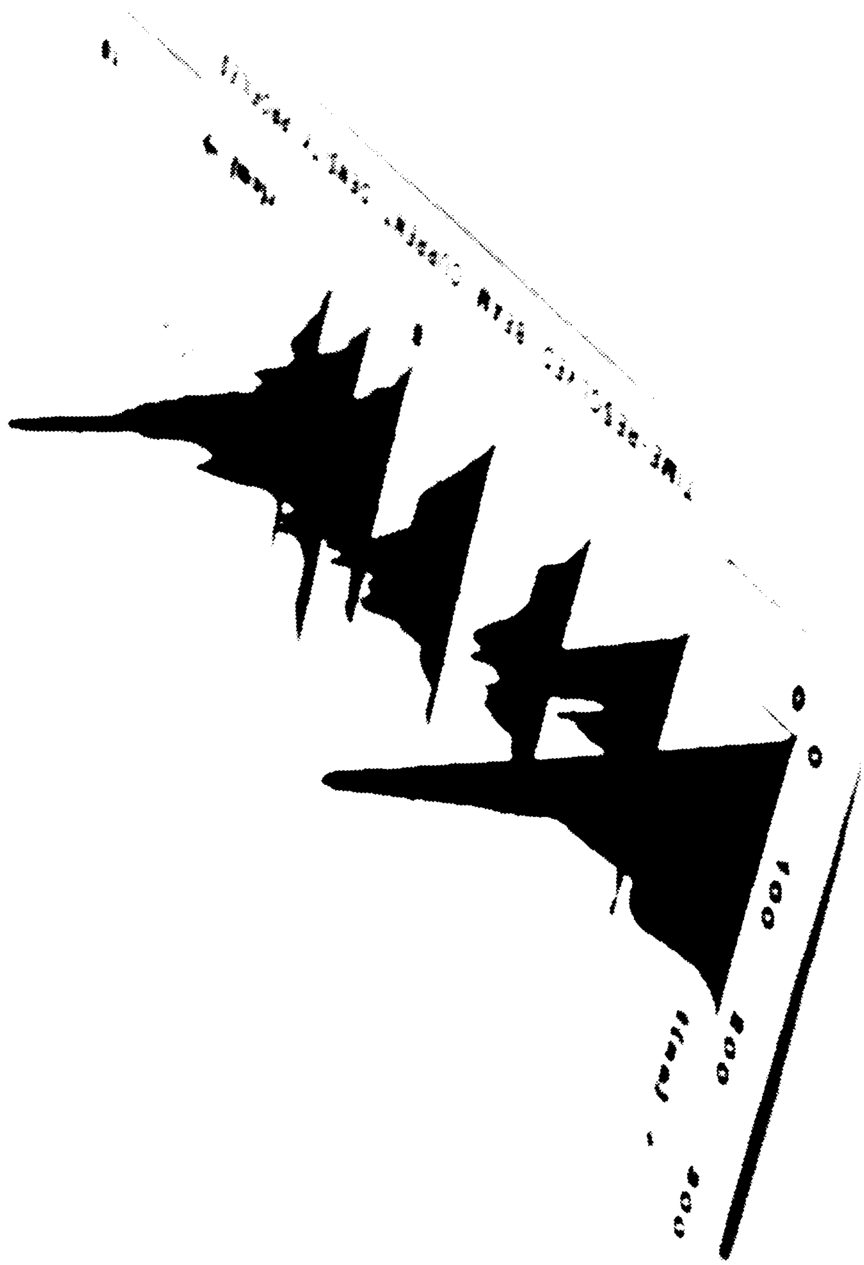

Figure 6. Time-resolved beam current density profile at Z = 0.81 m. p_0 = 0.35 Torr. Note development of "halo" current of high energy (150 keV) electrons.

Figure 7. Time-resolved beam current density profile at Z = 0.29-m. p_0 = 0.7 Torr.

CPROP SIMULATIONS SUGGEST SEVERAL TENTATIVE BUT IMPORTANT CONCLUSIONS.

- HOLLOWING INSTABILITY SENSITIVE TO RADIAL CONDUCTIVITY PROFILE
- PROFILE BROADENED BY LITTLE MORE THAN 20% MAY ASSURE $m = 0$ STABILITY TO 100 kA
- SOME RADIAL FILAMENTATION, CONVECTIVE DAMPING SUGGESTED BY HIGH CURRENT SIMULATIONS
- SIMULATION OF LONGITUDINAL PARTICLE DYNAMICS IMPORTANT FOR LOW ENERGY EXPERIMENT (ETA, IBEX, ETC.) INTERPRETATION
- LOW PRESSURE PROPAGATION NOT SO WELL UNDERSTOOD AS SOMETIMES SUPPOSED

LIMITED AGREEMENT BETWEEN CPROP SIMULATIONS, FX-100 EXPERIMENTS.

- CPROP PREDICTS 40-80% RETURN CURRENT; EXPERIMENT GIVES 70-90%
- CPROP SHOWS 1 M BEAM FRONT LOSS IN FIRST 2 M PROPAGATION, SLOWER EROSION THEREAFTER; NOT INCONSISTENT WITH EXPERIMENT
- NO INSTABILITIES EARLY IN BEAM PULSE
- APPARENT HOLLOWING OF EXPERIMENTAL BEAM LATE INTO PULSE PERHAPS DUE TO STRONG CONDUCTIVITY PEAK ON AXIS IN SIMULATIONS FOR $p > 0.5$ TORR
- INADEQUATE LOW PRESSURE CHEMISTRY MODEL, INCORRECT INITIAL CONDITIONS MAKE DETAILED COMPARISON DUBIOUS

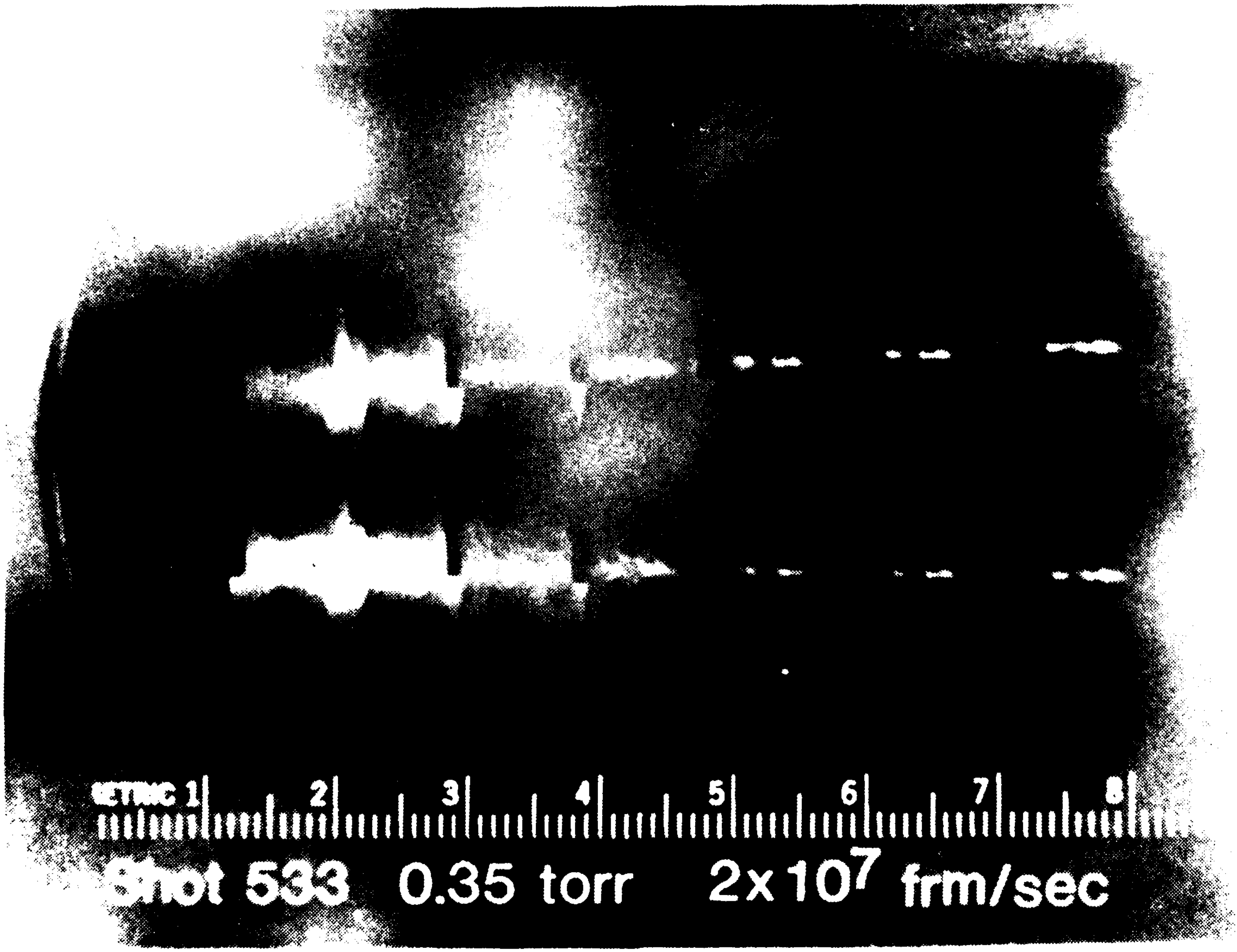

Figure 8. Fast framing photograph (with M-2 and M-6 LANL).
(Beam motion right to left).

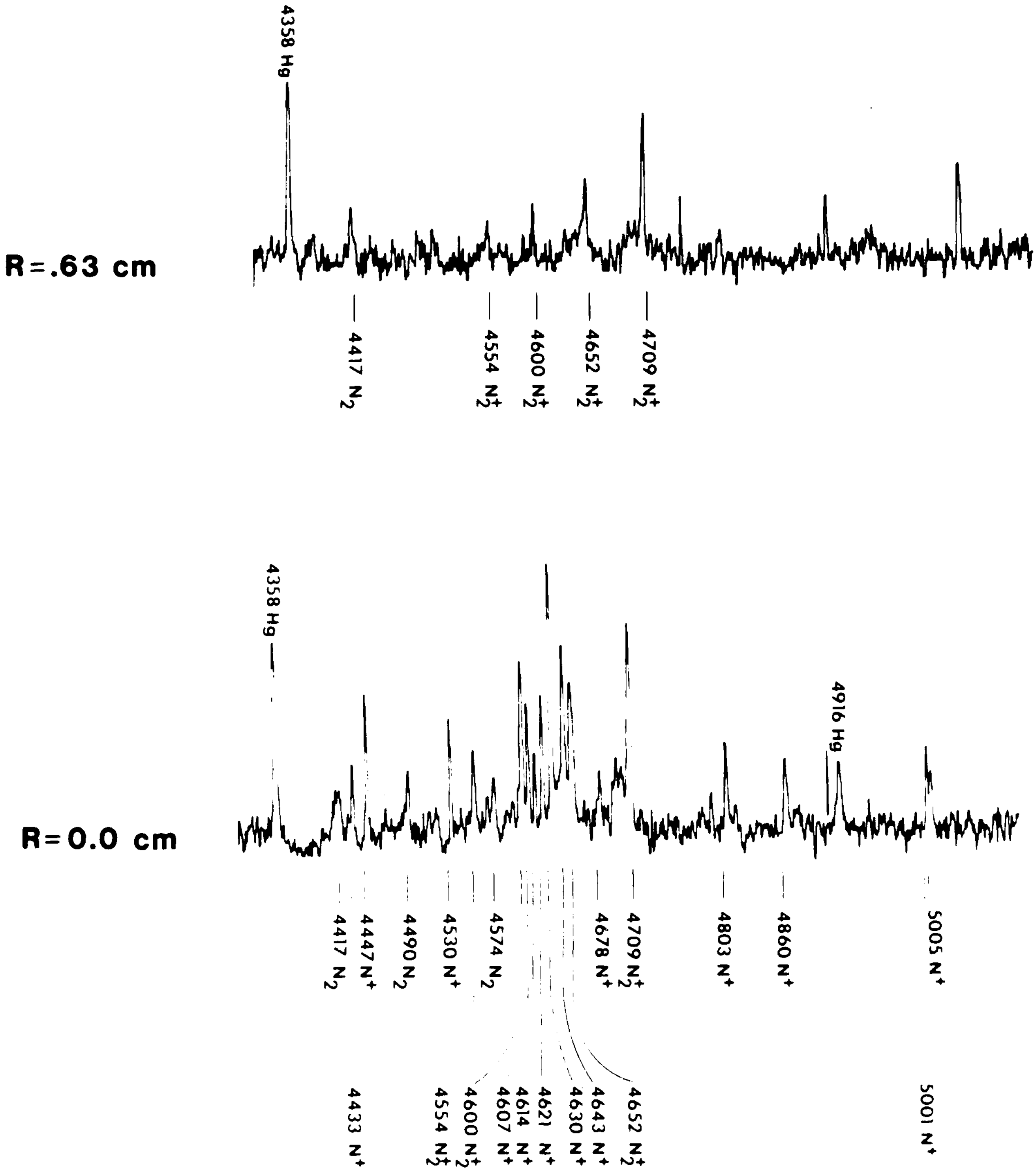

Figure 9. Atomic and molecular lines have different spatial de[illegible]

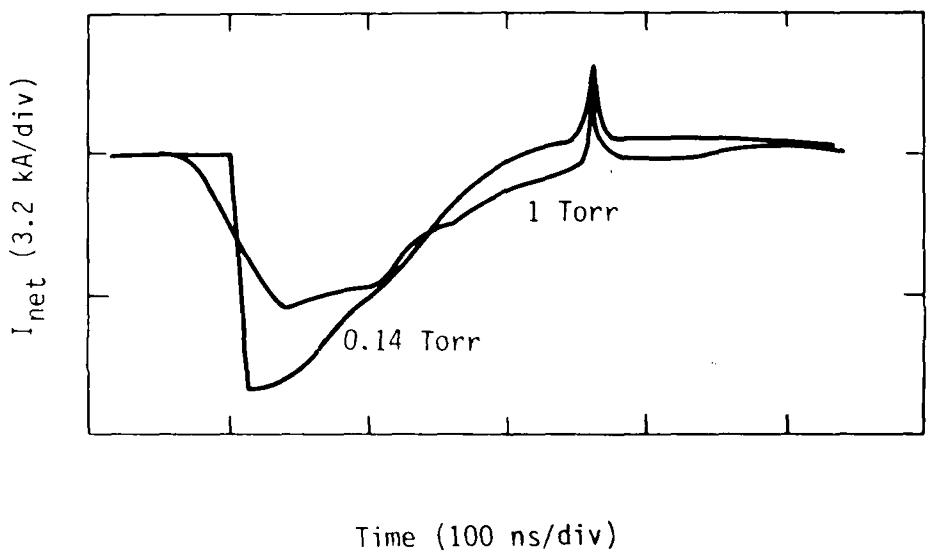

Figure 10. Net current measured in FX-100 propagation experiments at high and low air pressures in the propagation window. The pulse sharpening seen at pressures lower than that for maximum energy transport (0.5 Torr) is thought to result from rapid loss of the beam front and subsequent slow erosion.

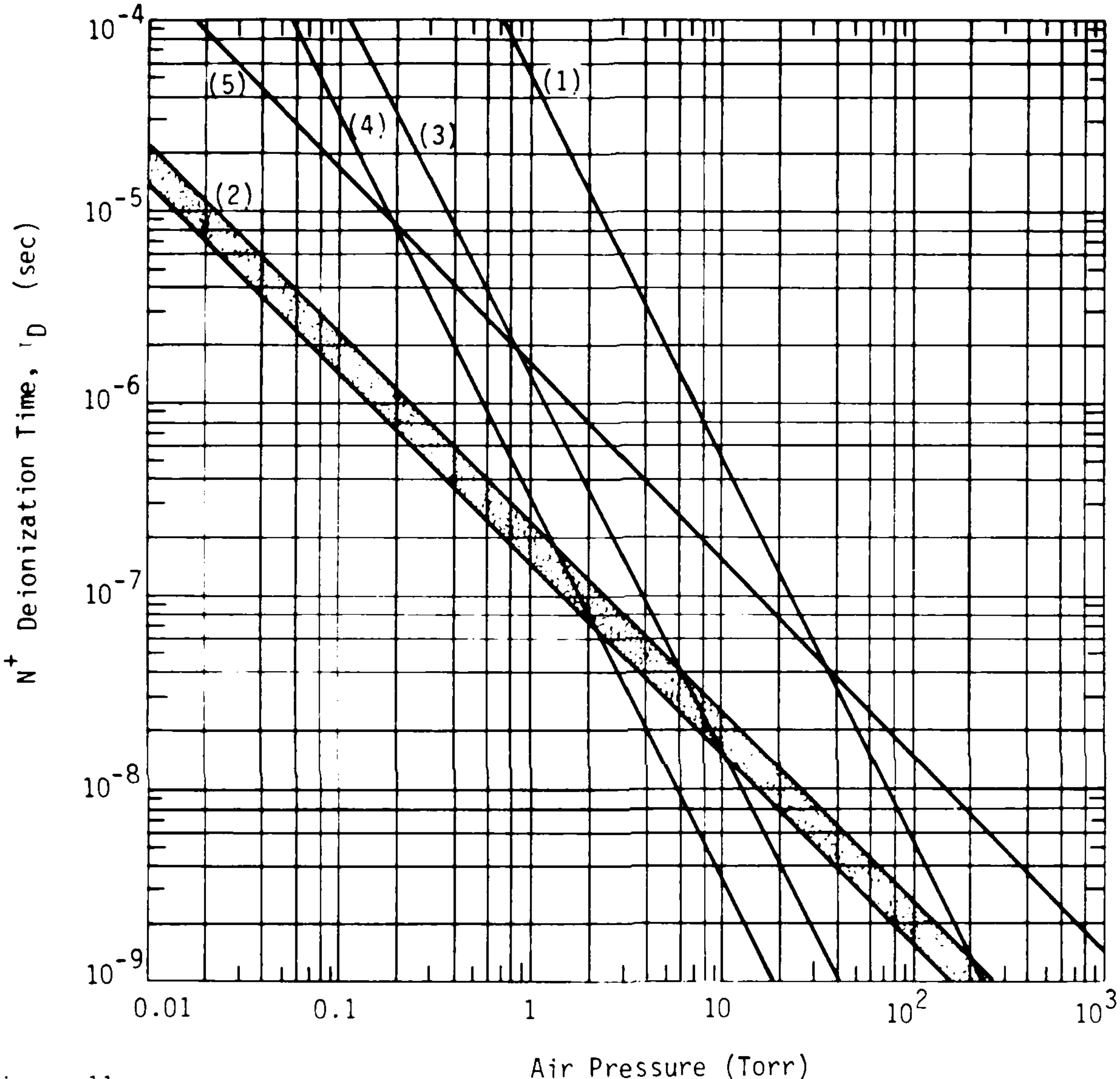

Figure 11.
Persistance of N^+ ions in air resulting from the following deionization reactions:

(1) $N^+ + 2N_2 \rightarrow N_3^+ + N_2$ ($T_g = 0.025$ eV; $\tau_D \propto n_a^{-2} T_g$)

(2) $N^+ + O_2 \rightarrow O_2^+ + N$; $\rightarrow NO^+ + O$; $\rightarrow NO + O^+$ ($0.025 \text{ eV} < T_g < 1.0 \text{ eV}$; $\tau_D \propto n_a^{-1} T_g^{0.57}$)

(3) $e + M + N^+ \rightarrow M + N$ ($T_e = 0.025$; $n_e = 0.1\, n_a$; $\tau_D \propto n_e^{-1} n_a^{-1} T_e^{2.5}$)

(4) $e + e + N^+ \rightarrow e + N$ ($T_e = 0.025$; $n_e = 0.1\, n_a$; $\tau_D \propto n_e^{-2} T_e^{4.5}$)

(5) $e + N^+ \rightarrow N + h$ ($T_e = 0.025$; $n_e = 0.1\, n_a$; $\tau_D \propto n_e^{-1} T_e^{0.5}$)

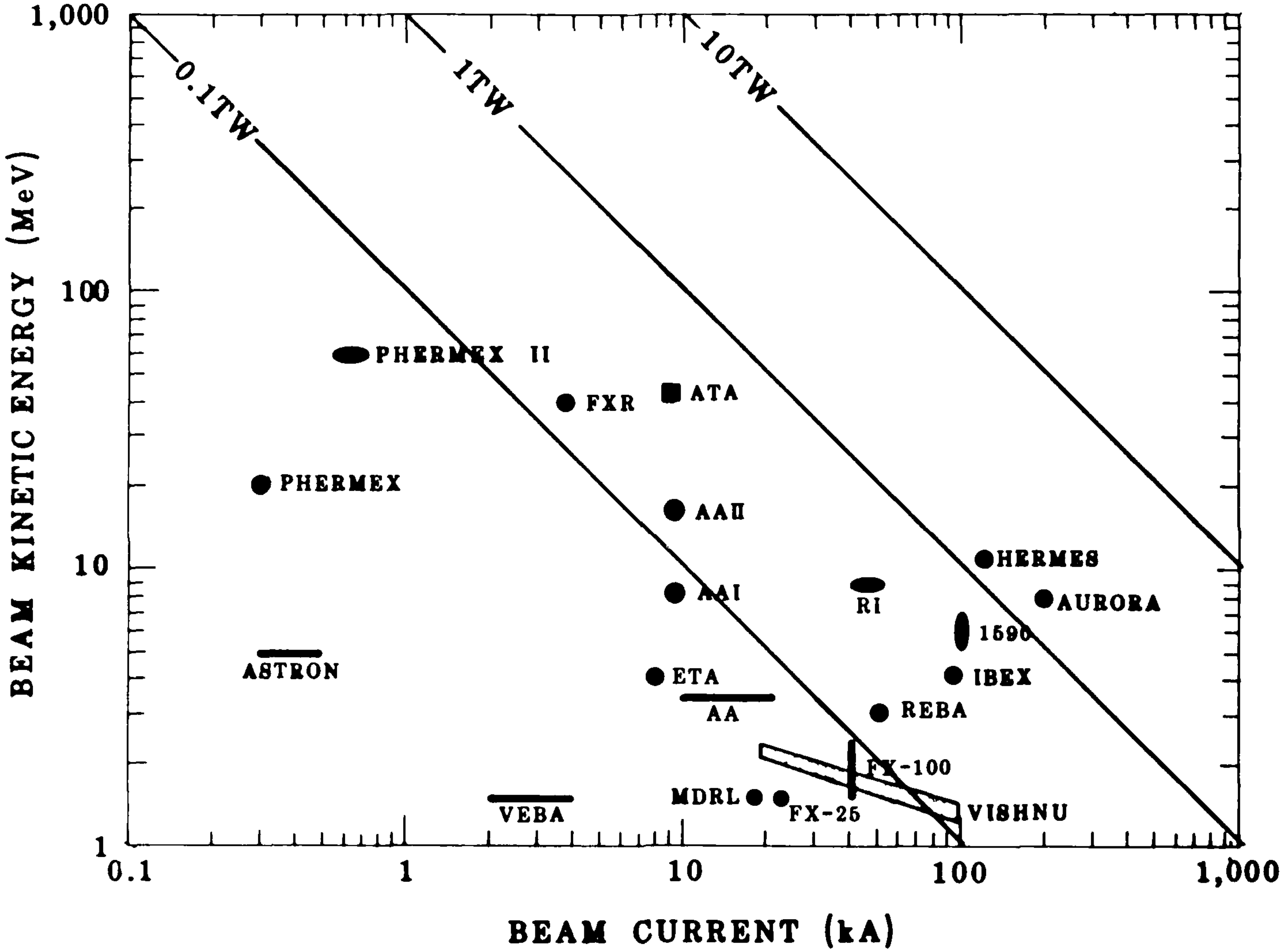

Figure 12. Intense electron beam accelerators presently available for propagation experiments. Also shown are several upgrades and accelerators under development. The entire available range of current and voltage of the AFWL VISHNU accelerator is shown because a final decision as the exact operating point has not been made.

DIAGNOSTIC DEVELOPMENT

I. FOURIER ANALYZING TRANSFORMERS

(FAST "SIN-COS" COILS)

- I_{NET}; M = 1; ω(K) VS ρ
- I_{BEAM}; M = 1; (HOSE SHORTED BY FOIL)

II. EMITTANCE PROBE ARRAY

(COLLIMATED FARADAY CUPS & "PEPPER POT")

- HOSE STABILITY AS EMITTANCE VARIES

III. β - SPECTROMETER

- BEAM ENERGY DISTRIBUTION AT NOSE
- δ-RAY DISTRIBUTION

IV. TIME RESOLVED OPTICAL DIAGNOSTICS

- SPECTROSCOPY
- FILTERED STREAKS & FRAMES

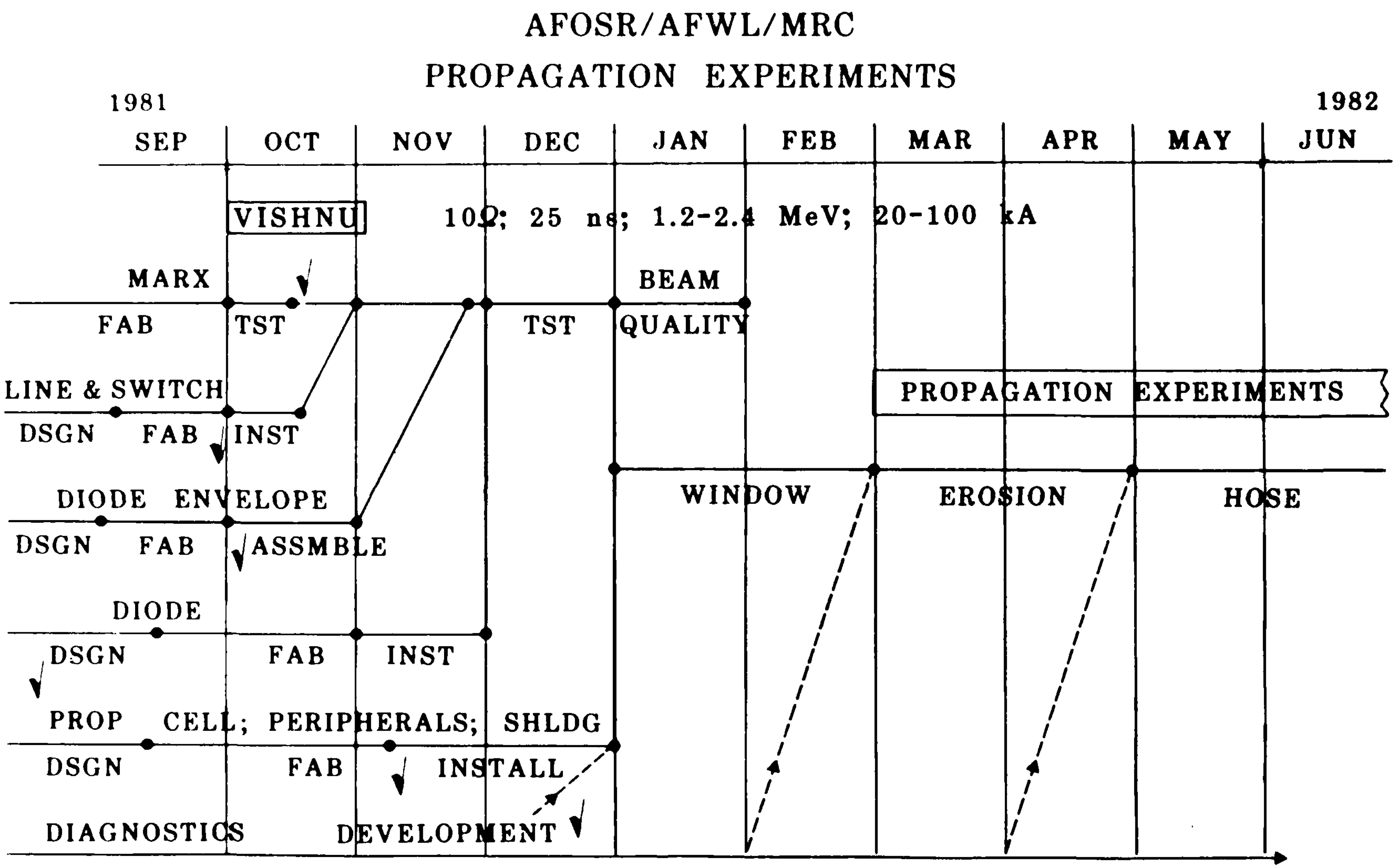

Figure 13. Planned schedule for completion of the AFWL VISHNU intense electron beam accelerator and AFOSR supported low pressure propagation experiments.

APPENDIX I

OPTICAL EMISSION FROM INTENSE RELATIVISTIC ELECTRON BEAM EXCITED AIR

UNCLASSIFIED

SECURITY CLASSIFICATION OF THIS PAGE (When Data Entered)

REPORT DOCUMENTATION PAGE

READ INSTRUCTIONS BEFORE COMPLETING FORM

1. REPORT NUMBER

2. GOVT ACCESSION NO.

3. RECIPIENT'S CATALOG NUMBER

4. TITLE (and Subtitle)
Optical Emissions from Intense Relativistic Electron Beam Excited Air

5. TYPE OF REPORT & PERIOD COVERED
Topical Report

6. PERFORMING ORG. REPORT NUMBER
AMRC-R-326

7. AUTHOR(s)

L. A. Wright, C. A. Ekdahl, R. F. Benjamin and T. P. Starke

8. CONTRACT OR GRANT NUMBER(s)
F49620-81-C-0016

9. PERFORMING ORGANIZATION NAME AND ADDRESS

MISSION RESEARCH CORPORATION
1400 San Mateo Blvd., S.E. Suite A
Albuquerque, New Mexico 87108

10. PROGRAM ELEMENT PROJECT, TASK AREA & WORK UNIT NUMBERS

11. CONTROLLING OFFICE NAME AND ADDRESS
Air Force Office of Scientific Research
Bolling Air Force Base
Washington, DC 20332

12. REPORT DATE
November 1981

13. NUMBER OF PAGES
41

14. MONITORING AGENCY NAME & ADDRESS (if different from Controlling Office)

15. SECURITY CLASS (of this report)
Unclassified

15a. DECLASSIFICATION DOWNGRADING SCHEDULE

16. DISTRIBUTION STATEMENT (of this Report)

Approved for Public Release; Distribution Unlimited.

17. DISTRIBUTION STATEMENT (of the abstract entered in Block 20, if different from Report)

18. SUPPLEMENTARY NOTES

19. KEY WORDS (Continue on reverse side if necessary and identify by block number)

Relativistic electron beam diagnostics
Molecular Spectra
Atomic Spectra

20. ABSTRACT (Continue on reverse side if necessary and identify by block number)

During recent low-pressure air propagation experiments with the FX-100 electron beam ($E \sim 1.5$ MeV, $I \sim 40$ kA, $\Delta t \sim 120$ ns, $p \approx 0.1 - 20$ Torr) several diagnostics that used visible light emission were employed. These included time-integrated (open-shutter) photography, time-resolved (streak and framing) photography, and time-integrated spectroscopy. In this report we develop a theoretical framework for interpretation of these diagnostics and discuss the results of the measurements.

(Continued)

DD FORM 1 JAN 73 1473 EDITION OF 1 NOV 65 IS OBSOLETE

UNCLASSIFIED

SECURITY CLASSIFICATION OF THIS PAGE (When Data Entered)

ABSTRACT

During the low-pressure air propagation experiments with the FX-100 electron beam ($E \sim 1.5$ MeV, $I \sim 40$ kA, $\Delta t \sim 120$ ns, $p \sim 0.1 - 20$ Torr) several diagnostics that used visible light emission were employed. These included time-integrated (open shutter) photography, time-resolved (streak and framing) photography, and time-integrated spectroscopy. In this report we develop a theoretical framework for interpretation of these diagnostics and discuss the results of the measurements.

We find that for propagation experiments in general there may be large contributions to the observed emission from both delta rays and the ionized-channel electrons. The plasma electron contribution is sensitive to temperature and to distortion of the tail of the distribution through high E/p effects. The emitted light can be used to observe the beam current in regions not dominated by high E/p because of the proportionality of the descendent electron density to the beam electron density. However, radial resolution of the current density profile may be blurred by the contribution of delta rays ejected at large angles. The temporal response of the emitted light can be expected to faithfully reproduce the beam current history only when the pressure is higher than a minimum, which depends on the highest frequency of interest in the beam current.

From the spectral measurements we have identified observed red emission to be atomic oxygen at 6157Å, we have identified a large number of N_2, N_2^+ and N^+ emissions, and we have shown the atomic line radiation to emanate from a region of limited radial extent. In the streak photographs we have seen some results of the magnetic field collapse at the end of the beam. We have observed that the molecular emissions temporally track the beam and that the atomic emission persists at late times, after the beam has passed. The framing photos also show the collapse of the field and radiating volume, and the long history of the atomic emissions.

CONTENTS

I. INTRODUCTION

Observation of visible light emission is a commonly used diagnostic technique in high-intensity relativistic electron-beam propagation experiments. Photography is an obvious and useful way of observing the behavior of self-luminous experiments, and much information has been obtained from both high-speed and time-integrated photography. For example, estimates of the hose-instability growth length, betatron wavelength, and beam radius have been obtained from photographic records.[1-3] Visible light emitted in beam experiments has also been observed by other methods such as wavelength-filtered fast photodetectors measuring the total light emitted from a region of limited axial extent.[4] For some beam and air pressure parameter regimes, these measurements were found to be correlated with the total beam current, which suggests that this technique could be employed as a nonperturbing beam-current monitor ("optical Faraday-cup").[5-6] Furthermore, if the excitation of air fluorescence by primary beam electrons is indeed the dominant source of light, then the analysis of high-speed streak or framing camera photographs would be a convenient method for obtaining time-resolved details of the beam current density distribution.

As indicated, there is a wealth of information to be gained from the proper interpretation of optical emissions. The purpose of this report is two-fold: to develop a rough theoretical basis for such an interpretation, and to present the results of optical measurements from recent FX-100 experiments. In Section II the underlying assumptions about optical emissions are reviewed, excitation mechanisms other than by the primary beam identified and the importance of these mechanisms estimated.

We will show that for propagation experiments in general there may be significant contributions to the emitted light resulting from delta rays (knock on electrons) and ionized-channel electrons. The contribution from the channel-plasma electrons is sensitive to the temperature and can be enhanced by distortions of the high-energy tail of the distribution by large electric fields. We will develop the necessary conditions on the air pressure that must be met in order to reproduce the beam current temporal history with high fidelity. We will conclude that because of the proportionality of the descendent-electron distribution to the beam electron distribution, reproduction of the beam current is possible within these constraints, although delta rays can lead to a blurring of the radial current profile. In Section III experimental results are presented and discussed. These results include spectra, streak photographs and framing photographs. Observed red emission from the low-pressure FX-100 experiments was spectrally identified as an atomic oxygen line. Additionally, we identified a large number of singly ionized nitrogen lines confined in a region much smaller than the beam radius, as well as the typical beam-excited molecular nitrogen bands seen over the entire radial extent of the beam. The atomic emissions were seen to persist for times much longer than the passage of the beam, leading to an "over-exposure" of persistent stationary structure in the time-integrated open-shutter photographs.

II. THEORY OF VISIBLE EMISSION FROM ELECTRON BEAMS PROPAGATING IN AIR

In high-density air propagation experiments with p_0 greater than a few Torr the emission is dominated by the molecular nitrogen purple-blue light emissions.[7] Of these, the N_2^+ first negative (1^-) band emission at 3914 Å and the N_2 second positive (2^+) band emission at 3371 Å are transitions that have been suggested as useful for beam diagnostics. The excited states of these transitions are rapidly quenched and it is assumed that the time history of these transitions accurately reflects the time history of the electron density that excites the molecules. With this assumption and if the emission results from only the beam primaries, the light emitted from an axially limited region measures the beam current and accurately maps the radial distribution of the high-energy beam.

Possible sources of error in these interpretations can result if there is significant excitation of the molecular states by the secondary (delta-ray) electron population or by the weakly-ionized channel electrons. The cross sections for excitation generally have thresholds of about 5- 20 eV, have maxima near 70-90 eV, and fall off as $\ell nE/E$ in the high energy limit.[8] Figure 1 presents the excitation cross section for the N_2^+ first negative band. The delta-ray distribution, which extends outside of the beam radius, will provide a significant contribution to the excitation because of the large proportion of delta-rays with energies near the excitation cross-section maximum. This is evident from inspection of the delta-ray distribution[9] presented in Figure 2. Furthermore, light emitted from a particular axial location is to some degree dependent on delta rays created at a different axial position. Thus, the spatial dependence of the emission intensity is highly dependent on the spatial distribution of delta-ray secondaries, which tends to mask the correlation with primary beam excitation. Finally, the weakly-ionized channel electrons can contribute strongly to the observed light; as a result of high E/p (electric-field to pressure ratio) distortion of the channel-plasma electron distribution, there may be a significant number of electrons with energies greater than the threshold or near the peak of the excitation cross section. As seen in Figure 3, without the high E/p effects the overlap of the plasma electron distribution and the excitation cross-section is inconsequential for temperatures less than 1 eV. These secondary electrons can produce a light intensity competitive with that produced by primary beam excitation and correct interpretation of visible observations thus depends on an understanding of these effects.

Thus, the problems of interpreting measurements of visible light emission are somewhat analogous to the problems that arise in attempts to interpret measurements of currents using Rogowski belts or B-dot probes. These inductive current diagnostics are sensitive only to the net current (sum of primary beam and secondary return currents)and additional diagnostics must be employed to resolve each component . The light emission diagnostics are, in turn, also sensitive to a weighted net current (sum of primary beam and secondary currents weighted by effective excitation factors).

There are two steps in unfolding beam parameters from the observed emission. The first is to determine the position dependent excited state population density from the given visible intensity. The intensity of visible radiation emitted by an optically-thin line radiator with thickness z is

$$I = \frac{h\nu}{4\pi} A \int_0^z N_{ex} dZ \quad , \tag{1}$$

where $h\nu$ is the photon energy, $A(s^{-1})$ is the spontaneous emission transition probability, and N_{ex} (cm^{-3}) is the position dependent excited state population density. The spatial variation of N_{ex} can be obtained by tomographic inversion techniques (eg. Abel inversion for cylindrically symmetric systems such as beams). Photography can thus provide an accurate measurement of the time-integrated spatial distribution of excited states if an optical filter at wavelength $\lambda = c/\nu$ is used. Time resolution can be obtained with a streak or framing camera. The remaining question is that of establishing beam parameters through a knowledge of N_{ex}.

For the optically thin radiator, radiative excitation can be neglected, and the excitation to the upper state by collisions occurs at a rate given by $\langle \sigma n_e v \rangle$, where σ is the (velocity dependent) excitation cross section. The average is taken over the electron distribution in velocity space, n_e. The total density distribution is composed of n_b (primary-beam electrons), n_δ (delta-ray secondary electrons) and n_p (ionized-channel plasma electrons); each has a very different velocity distribution. The upper state of the transition can be de-excited collisionally (in addition to radiating) and the rate for this process is $q_0 N_0$, where N_0 is the density of air molecules, and q_0 is the quenching coefficient in air.

Including these processes and neglecting other means of populating the upper level (such as recombination) one gets the rate equation for the excited state population,

$$\dot{N}_{ex} = \langle \sigma n_e v \rangle N_o - AN_{ex} - qN_{ex}N_o \quad . \tag{2}$$

Equation (2) can be rewritten as

$$\dot{N}_{ex} + N_{ex}/\tau = \langle \sigma n v \rangle N_o \quad , \tag{3}$$

which has the solution

$$N_{ex} = \exp[-t/\tau] \int^{t} \exp[t'/\tau] \langle \sigma n_e v \rangle N_o dt' + C \exp[-t/\tau], \tag{4}$$

The time constant, τ, in equations (3) and (4) is

$$\tau = [A + qN_o]^{-1} \tag{5}$$

Several features of Equations (2)-(5) that relate to the applicability of optical emission diagnostics are worth pointing out. The lower pressure for practical use of this radiation diagnostic is the pressure at which quenching first dominates τ. For pressure greater than this minimum and time variations of the electron density much larger than τ, the density of excited states is independent of air pressure and is given by

$$N_{ex} \sim \langle \sigma n_e v \rangle / q \qquad (6)$$

As an example, we will use the first negative emission of N_2(3914 Å); for this transition the spontaneous emission coefficient is $A = 1.24 \times 10^7$ s^{-1} and the quenching coefficient in air is $q = 5.1 \times 10^{-10}$ cm^3 s^{-1} (Ref. 10). Therefore, quenching dominates τ for air densities $N_0 > A/q$ = 2.4×10^{16} cm^{-3} (p_0 > .74 Torr at 20°C). For full atmospheric pressure, τ = 78 ps, which is much faster than the time variations in present experiments. For comparison the second positive emission of N_2(3371 Å) ($A = 1.1 \times 10^7$ s^{-1} and $q = 6.6 \times 10^{-11}$ cm^3 s^{-1})[11] has a minimum useful pressure of ~5.1 Torr (τ ~ .60 ns for 3371 Å emission in full density air).

Equation (5) can be solved for N_0, the minimum neutral number density required to assure a required response time t_r.

$$N_o = \frac{1}{qt_r} - \frac{A}{q}$$

For $N_2^+(1-)$ and $N_2(2^+)$ this becomes, respectively,

$$p = \frac{59.4}{t_r(ns)} - .74 \text{ Torr} \qquad (7a)$$

$$p = \frac{459.}{t_r(ns)} - 5.05 \text{ Torr} \qquad (7b)$$

Equations (7) are plotted in Figure 4. This figure is useful for the determination of the minimum pressure for which the emission intensity can be expected to faithfully follow an experimental density variation.

Furthermore, this figure indicates the expected delay time between the onset of a rapid electron density increase at low pressures (where the density rise time is much less than t_r given by Eq. (7)) and the appearance of the optical emission. For example, at pressures less than 1 Torr, the emission from density increases occurring in less than ~ 10 ns would have a rise time of ~ 20 - 30 ns. This lack of temporal fidelity is a further limitation on the pressure range for use of emission diagnostics.

To summarize, to be assured that the emission intensity faithfully reproduces the electron density variation, one is restricted to pressures greater than given in Fig. 4 for any expected time variation of the electron density, and to insure independence of the emission from the neutral gas density the pressure must be greater than 0.74 Torr (for 3914 Å light) or 5.1 Torr (for 3371 Å).

Assuming that the density variations in the experiment satisfy the foregoing restrictions, then the observed emission intensity will be proportional to $\langle \sigma n_e v \rangle$ (Equation (1) and Equation (6)). However, n_e is composed of n_b, n_δ and n_p; the beam, secondary and plasma electron distributions; each with its own widely differing energy distribution. The observed fluorescence is a combination (both temporaly and spatially) of these, and any information about n_b (or $j_b = \langle n_b v \rangle$) must be further unfolded.

To unfold the observed fluorescence first consider the plasma electrons. At the higher pressures a significant fraction of the plasma electrons result from direct ionization and, therefore, have a density proportional to the beam density. These electrons cannot distort the optical measurements unless there exists a mechanism for locally distorting the light intensity resulting from their excitation of the molecular levels. Such a mechanism is found in high E/p effects. For high electric field-to-pressure ratios (E/p) a large number of particles go into the high energy tail of the distribution raising the effective temperature of the electrons.[12] For E/p = 10 V cm^{-1} $Torr^{-1}$ in air, $T_e^{eff}/T_{gas} \sim 50$ (Ref. 13). Because of high effective temperature electrons with more than the threshold for excitation (~11eV for $N_2(2^+)$) will be present. The large number of plasma electrons relative to the beam electrons (~10^3) could contribute greatly to the observed emission. Because of the time dependent fields and skewed distribution, a simple but accurate estimate of these effects cannot be made here.

However, a rough estimate of $\langle n\sigma v\rangle$ can be made for both the plasma and the beam. The ratio of these gives the relative amount of excitation due to both sources. The average for the plasma electrons can be done by using a Maxwellian distribution and a linear fit for the excitation cross section near its threshold, if the Maxwellian temperature is much less than the threshold energy. Then,

$$\begin{aligned} \sigma &= aE + b \qquad & E > E_0 \\ &= 0 \qquad & E \leq E_0 \quad . \end{aligned} \tag{8}$$

For $N_2^+(1-)$, $E_0 \sim 18.8$ eV and $a = 10^{-18}$ cm^2 eV^{-1} and $b = 1.88\times10^{-17}$ cm^2. The average for beam electrons was calculated from a monoenergetic distribution. The result is

$$\frac{\langle n\sigma v\rangle_p}{\langle n\sigma v\rangle_b} \sim \left(\frac{n_p}{n_b}\right)\left(\frac{8kT}{\pi mc^2}\right)^{1/2} \frac{a(E_0 + 2kT)}{\sigma(E_b)}\, e^{-E_0/kT} \quad , \tag{9}$$

where the subscripts p or b refer to plasma or beam electrons, n is the particle density, kT the plasma temperature, E_b the beam electron energy, mc^2 the electron rest mass, $\sigma(E_b)$ the excitation cross section at the beam energy, E_0 the threshold energy for excitation, and b is the slope of the cross section at threshold. For the $N_2^+(1-)$ band, assuming that $n_p/n_b = 10^3$ and 1.5 MeV beam electrons,

$$\frac{\langle n\sigma v\rangle_p}{\langle n\sigma v\rangle_b} \sim 37.2(kT)^{1/2}\,(18.8 + 2kT)\,e^{-18.8/kT} \quad . \tag{10}$$

For 20 MeV beams

$$\frac{\langle n\sigma v\rangle_p}{\langle n\sigma v\rangle_b} \sim 27.9(kT)^{1/2}\,(18.8 + 2kT)\,e^{-18.8/kT} \; . \tag{11}$$

The 1.5 MeV result is plotted on Figure 5. For plasma temperatures greater than 2.6 eV, the excitation from plasma electrons is greater than from beam electrons. The curve is very steep between 1 and 3 eV and probably quite sensitive to the model. The curve is, therefore, intended only as a rough guideline and an indication of the magnitude of possible plasma electron effects. What is clearly evident is that the light resulting from the plasma electron distribution can equal that resulting from beam primaries if the effective plasma temperature is only slightly increased by high E/p effects. That is, the emission resulting from plasma electrons is greatly and non-linearly enhanced in regions of high E/p. A 20 MeV curve could be similar to the 1.5 MeV curve only scaled in magnitude by .75. On the scale of Figure 5 the two would be almost indistinguishable.

Next we examine the delta-ray (knock-on) secondary electrons. Bombarding N_2 with 1.5 MeV electrons and monitoring the $N_2^+(1-)$ emissions, Hirsch, et al., found that roughly 1/3 of the emission was due to primaries and 2/3 due to secondaries. A theoretical estimate of $\langle n\sigma v\rangle_\delta / \langle n\sigma v\rangle_b$ can be made to compare to the experimental results. Again $\langle n\sigma v\rangle_b$ is calculated by characterizing the distribution as monoenergetic and using the cross section evaluated at the beam energy. The number of particles, n, is left unspecified,

$$\langle n\sigma v\rangle_b \sim 1.8\times10^{-19} n_b \quad . \tag{12}$$

For every n_b that forms N_2^+, there are n_b delta electrons formed and a total of secondaries, tertiaries, etc. of $\sim 3\ n_b$. By integrating over the electron distribution and cross section

$$\langle n\sigma v\rangle_\delta \sim 3.9\times10^{-19} n_b \quad . \tag{13}$$

This gives 32% of the emission due to primaries and 68% due to secondaries, in very close agreement with experimental results. At 20 Mev these fractions are 38% and 62%, respectively.

Considering the case of a 20 MeV beam of .1 cm radius in full density air, neglecting the fields gives half the energy of the secondaries deposited within a radius of .1 cm (in the beam) and half outside of the beam. Considering only primaries and secondaries, 1/3 of the $N_2^+(1^-)$ emission is due to primaries, 1/3 due to secondaries in the beam and 1/3 due to secondaries outside the beam. The effect of the delta-ray secondaries is, therefore, to blur the radial spatial resolution. The time history of the total light from a region of limited axial extent will, however, not be significantly different than the time history of the beam current as a result of delta ray effects because of the proportionality of

n_b and n_δ. Thus, an optical Faraday cup based on this principle should not be affected by delta-ray electrons. Indeed, the additional signal resulting from delta ray secondaries helps to enhance the wanted signal (proportional to n_b) compared with the "noise" (proportional to n_p, for example).

In summary, there are large contributions to the observed emission from both delta rays and the plasma electrons. The contribution from the plasma is very sensitive to the temperature and high energy tail of the distribution and the delta ray contribution differs spatially from the beam contribution. Although much information must be decoupled to obtain beam parameters from optical emissions, the emissions do appear to be good monitors of total energy deposition. In regions not dominated by high E/p effects, the total (radially integrated) light from a region of limited axial extent can probably be used as an "optical Faraday cup" to measure $I_b(t)$ because of the proportionality of the descendent electron density to n_b. The temporal response of such a diagnostic can be expected to follow I_b only at pressures higher than a minimum determined by the most rapid fluctuations of I_b.

III. EXPERIMENTAL RESULTS AND DISCUSSION

To this point the discussion has centered on the interpretation of observed emissions, primarily $N_2(2^+)$ and $N_2^+(1^-)$. Also important, and of future diagnostic use, is the understanding of the gross features of open shutter and high-speed photographs. In this section we will attempt to understand some of these features by examining optical measurements made during the course of propagation experiments using the AFWL FX-100 accelerator. The parameters of these experiments appear in Table 1.

Two striking features on some open-shutter photographs are color changes (red and/or green-blue) and feathering (see Figure 6 for this effect). Time integrated spectra were obtained to identify the source of this emission. Streak and framing photographs give both a temporal history of the emissions and an indication of feathering.

Spectral measurements were taken at 0.35 Torr (near the 0.5 Torr air pressure for maximum energy transport; i.e., "middle" of the propagation window). Because of time constraints spectra at other pressures could not be taken. The spectra were taken after propagating 4.5 m. They were integrated over 10 shots. The dispersing instrument used for these data was a Jarell-Ash 1/2-meter Fastie-Ebert spectrometer with a 1200 groove/mm (5500 Å blaze wavelength) grating. The recording medium was Polaroid type 47 film.

Figures 7-11 display densitometer scans of the photographs of the spectral lines, and Table 2 lists the identified lines and bands and their designations. There are three major wavelength regions where emission are observed: 3750-4450Å, 4600-4710Å, and 6157Å. Lower wavelengths were not recorded because the acrylic windows used have a sharp cutoff at

~ 3500Å. The lowest wavelength region is the characteristic purple-blue emissions and is dominated by N_2 and N_2^+. The band emission intensity in these regions was probably sufficient to saturate the film response. The wavelength region 4600-4710Å is dominated by singly ionized atomic nitrogen (N^+). Emission in the red wavelength range is dominated by a line at 6157Å.

The red (6157 Å) emission appears only in a narrow range of pressures. In the FX-100 experiments the red emission is observed between ~ 0.1 → 0.8 Torr, and is not observed at any pressure in pure N_2 experiments. At higher and lower air pressures the emission is the characteristic purple-blue from N_2 and N_2^+.

The 6157Å emission line is from atomic oxygen, and was the only neutral atomic emission observed. The oxygen transition is $4d^5D$ - $3p^5P$ while the ground state is $2p^3P$. Although forbidden transitions such as $^3P \rightarrow {}^5D$ frequently occur through scattering, it seems unlikely that for the most intense oxygen transition the upper state would be populated in this manner. Probably, the beam produces O^+, which recombines with electrons to form oxygen in the ^5D state. This interpretation is also consistent with no emission being observed at higher pressures. O^+ would be lost through charge exchange to O_2 which is exoergic, so there would be no recombination to form $O(^5D)$. Similarly, at very low pressures, recombination would not be as likely because of the reduced collision frequency. Figure 12 is a more detailed densitometer scan for this oxygen line, actually 3 lines at 6156.0, 6156.8 and 6158.2Å corresponding to J = 1, 2 and 3.

Figure 13 shows two densitometer scans over the same portion of the spectra. The bottom one was taken along the axis of the beam as were all the earlier scans. The upper scan corresponds to a radial position 0.63 cm off axis. At this radial position the atomic nitrogen (N^+) lines were no longer apparent. This was a general characteristic of the spectra. The spatial extent of the atomic lines was much smaller than for the molecular lines. The molecular emission had a radius of ~ 30 mm, the atomic emission ~ 2.4 mm, and the radius of the beam was ~ 30 mm. This is indicative of a very high electron-distribution average energy near the axis, because the electron energy needed to dissociate and ionize the N_2 molecules is ~ 24.3 eV.

An Imacon 790 image-converter camera was used to obtain streak and framing pictures of the emission. These observations were made through the same window used for the spectrometer but were not simultaneous with spectral measurements. The image-converter camera had a rather long delay after triggering, and in order to record the head of the beam it was necessary to delay the emission light by folding the optical path through 2.2 m and locating the camera next to the FX-100 output switch. The camera trigger was derived directly from the light emitted by the FX-100 output switch. This physical arrangement provided the required delay of the beam emission signal through the beam vacuum-diode delay, beam-propagation delay, and optical-path delay. A 1200-mm Questar collection lens used at the camera provided adequate magnification and light intensity without the use of intermediate field or relay lenses.

Figure 14 is a streak photograph taken at 0.35 Torr. The abrupt decrease in the diameter of the emission is at ~ 120 ns, the length of the beam pulse. It is clear from this photograph that the intense emission near the axis persists in stationary patterns for long times after the beam has passed through the region. The radial contraction is probably due to the collapse of the magnetic field set up by the beam. Because the spectra had shown the spatial depedence of the atomic and molecular emissions to be different, streak photographs were made with wavelength filters with passbands at typical molecular and atomic emission wavelengths. One filter had a passband centered at the N^+ band at 4278A and these photographs showed that the molecular emission turned off at 120 ns (at the same time that the beam turned off). This light was observed to originate over the larger radial extent previously observed in the time-integrated spectral measurements. The other filter allowed for the transmission of the atomic nitrogen lines between 4607Å and 4643Å. In agreement with the spectra, the atomic emissions were of limited radial extent. Unfortunately, the intensity of the atomic emissions was low and the starting time for these could not be accurately determined. They appear to start ~ 100 ns after the beam head and continue for more than 800 ns after the beam passage.

Although plasma currents continue to flow in the gas long after the beam passage, the L/R decay of these currents is too rapid (100 - 200 ns) to explain the observed afterglow emission from excited atomic states, which persists for more than 800 ns. Another possible mechanism for the continued excitation of these states is the collisional transfer of energy initially stored as molecular vibrational energy (T_v) by beam or delta-ray electron excitation. However, the most likely explanation for the persistance of atomic states such as N^+ after their initial formation is simply the extremely slow deionization rate at the low air pressures of these experiments. To show this, the deionization times for the various collisional reactions[14] as well as radiative recombination [15] are graphed for a wide range of dry air pressures in Fig. 17. Also given is the scaling of this time with neutral gas and electron density and temperature.

For calculation of the N^+ deionization times that are graphed in Figure 17 the gas temperatures (T_g), electron temperature (T_e) and electron density, n_e, were chosen to give the fastest rates for realistic values of these parameters. That is, it is unreasonable to assume that the N^+ concentrate could be depleted more rapidly than indicated by the graph. It is clear from this figure that the observed afterglow from N^+ states for > 500 ns in 0.35 Torr air is not surprising. Note that, although deionization of high pressure and weakly ionized air is controlled by neutral association, deionization at pressures higher than ~ 2 Torr can be dominated by three-body recombination if the fractional ionization ($f = n_e/n_a$) is great enough. However, at the pressures relevant to the FX-100 experiments reported here the rate determining reactions for N^+ deionization are $N^+ + O_2$ reactions. All deionization times increase with temperature and even with an air temperature as cold as 1/40 eV, deionization by these reactions in 0.35 Torr air is slow enough that N^+ ions would persist in the afterglow for several hundred ns, in agreement with the observations.

Framing photographs are shown in Figures 15 and 16. Each frame is integrated over 10 ns and the interval between frames is 40 ns. The sequence in which the frames were taken alternates between the lower and upper rows, left to right (in the N shaped sequence characteristic of the Imacon camera). These photographs clearly show the formation of the feather patterns seen earlier in the open shutter photographs (Fig. 6). The feathering appears to occur at the end of the beam (Frames 3 and 4), possibly as the fields (and thus E/p) are rapidly changing. However, the feathering may be present at all times and masked by other intense emissions. As the region of emission collapses at the end of the beam, the vertices of the feathers remain in the same location and continue to radiate for long times (the last frame is ~ 600 ns in Fig. 16, and ~ 700 ns in Fig. 17). The integration of the radiation from these vertices is responsible for the intense exposure previously seen near the axis of the open shutter pictures. Thus, the "hot spots" previously seen in open shutter photographs do not result from extremely intense emission for a short duration, but rather are the result of long time exposure compared with the remainder of the emission.

In summary, from the spectral measurements we have identified the observed red emission to be atomic oxygen at 6157Å, we have identified a large number of N_2, N_2^+ and N^+ emissions, and we have shown the atomic line radiation to emanate from a region of limited radial extent. In the streak photographs we have seen some results of the magnetic field collapse at the end of the beam. We have observed that the molecular emissions temporally track the beam and that the atomic emission persists at late times, after the beam has passed. The framing photos give the first hint of the feathering process, show the collapse of the field and radiating volume, and the long time history of the atomic emissions. Further development of these techniques (i.e., time-resolved spectroscopy) holds great promise for providing much information on beam-air chemistry (and hence conductivity) and on basic beam parameters.

This research was sponsored by the Air Force Office of Scientific Research (AFSC) under contract F49620-81-C-0016. The authors wish to acknowledge the assistance of Winston Bostick in performing these experiments. Professor Bostick was a senior research physicist in the University Residency Program sponsored by the Air Force Office of Scientific Research under IPA-905-79-01016C. Finally, the authors are deeply indebted to the following members of the Dynamic Testing Division (M Division) at Los Alamos National Laboratory for the time-resolved photography of the FX-100 propagation experiments: Lee Builta, Dave Moir, and Steve Schmidt.
Starke.

TABLE 1. FX-100 BEAM PROPAGATION EXPERIMENT PARAMETERS

Maximum Beam Energy,	E_b = 1.5 - 2.0 MeV
Maximum Beam Current,	I_b = 35 - 40 kA
Beam Pulse Duration,	Δt = 120 ns
Beam 1/e-radius at injection,	r_{bo} = 3 cm
Propagation Chamber Radius,	R_w = 10 cm
Observation Port Position,	z_o = 4.5 m
Air Pressure,	p_o = 0.1 - 20 Torr

TABLE 2. IDENTIFICATION OF OBSERVED LINES AND BANDS.

WAVELENGTH Å	ATOM/MOLECULE	TRANSITION (band)	(v', v")
3755	N_2	(2+)	(1,3)
3805	N_2	(2+)	(0,2)
3858	N_2	(2+)	(4,7)
3884	N_2+	(1-)	(1,1)
3914	N_2+	(1-)	(0,0)
3943	N_2	(2+)	(2,5)
3998	N_2	(2+)	(1,4)
4059	N_2	(2+)	(0,3)
4095	N_2	(2+)	(4,8)
4142	N_2	(2+)	(3,7)
4167	N_2+	(1-)	(3,4)
4200	N_2	(2+)	(2,6)
4236	N_2+	(1-)	(1,2)
4270	N_2	(2+)	(1,5)
4278	N_2+	(1-)	(0,1)
4344	N_2	(2+)	(0,4)
4417	N_2	(2+)	(3,8)
4433	N+	3d $^3P^o$-4f D(5/2)	
4447	N+	3p ^3D - 3d $^3D^o$	
4490	N_2	(2+)	(2,7)
4530	N+	3d ^1F - 4f G(9/2)	
4554	N_2+	(1-)	(3,5)
4574	N_2	(2+)	(1,6)
4600	N_2+	(1-)	(2,4)
4607	N+	3s $^3P^o$ - 3p ^3P	
4614	N+	3s $^3P^o$ - 3p ^3P	
4621	N+	3s $^3P^o$ - 3p ^3P	
4630	N+	3s $^3P^o$ - 3p ^3P	
4643	N+	3s $^3P^o$ - 3p ^3P	
4652	N_2+	(1-)	(1,3)
4678	N+	3d $^1P^o$ - 4f D(3/2)	
4709	N_2+	(1-)	(0,2)
4803	N+	3p ^3D - 3d $^3D^o$	
4860	N+	3p ^3D - 3d $^3D^o$	
5001	N+	3p ^3D - 3d $^3F^o$	
5005	N+	3s ^5P - 3p $^5P^o$ 3p ^3D - 3d $^3F^o$	
5667	N+	3s ^3P - 3p ^3D	
5680	N+	3s ^3P - 3p ^3D	
5686	N+	3s ^3P - 3p ^3D	
5711	N+	3s ^3P - 3p ^3D	
6157	O	3p ^5P - 4d $^5D^o$	

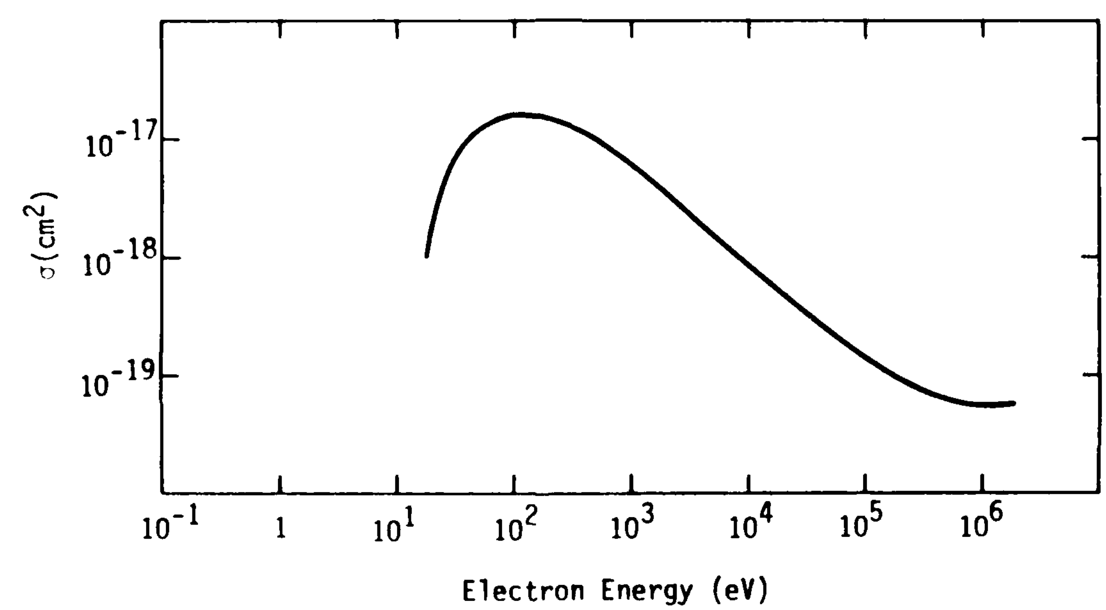

Figure 1. Excitation cross section for $N_2^+(1-)$. (Data from Ref. 8)

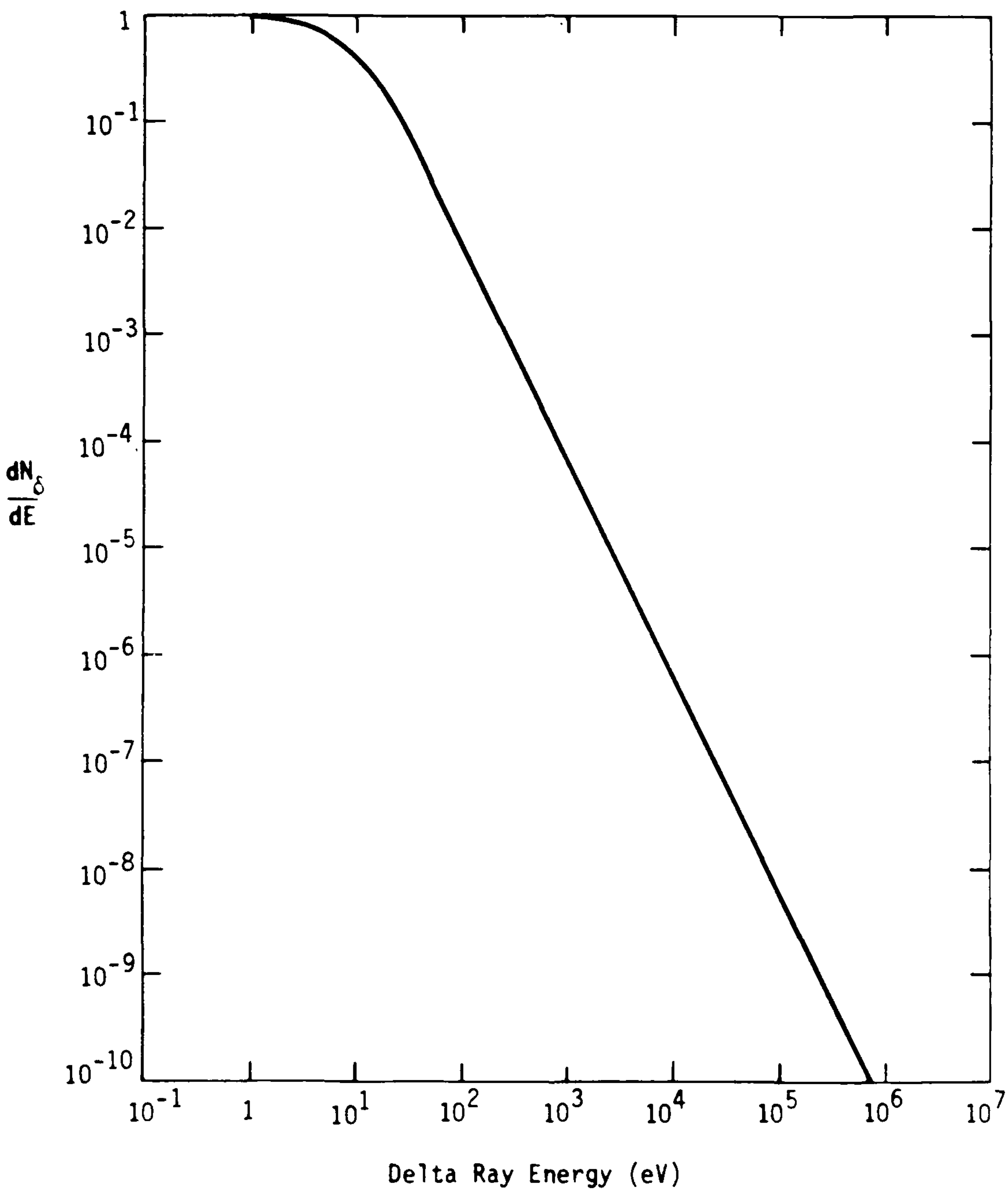

Figure 2. Distribution of delta rays with energy.
(Calculated for $\gamma \gtrsim 4$)

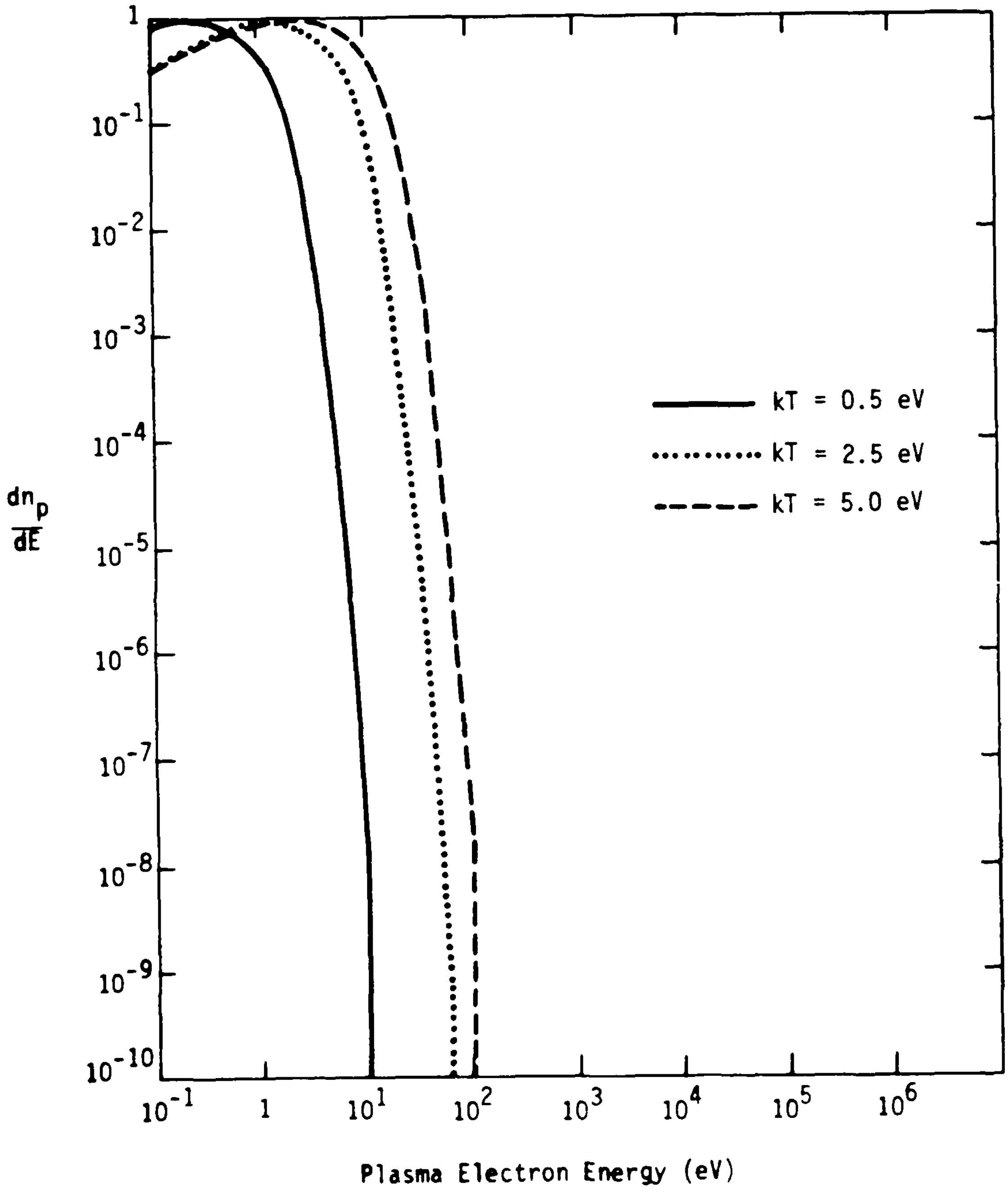

Figure 3. Distribution of plasma electrons with energy for three Maxwellian temperature distributions.

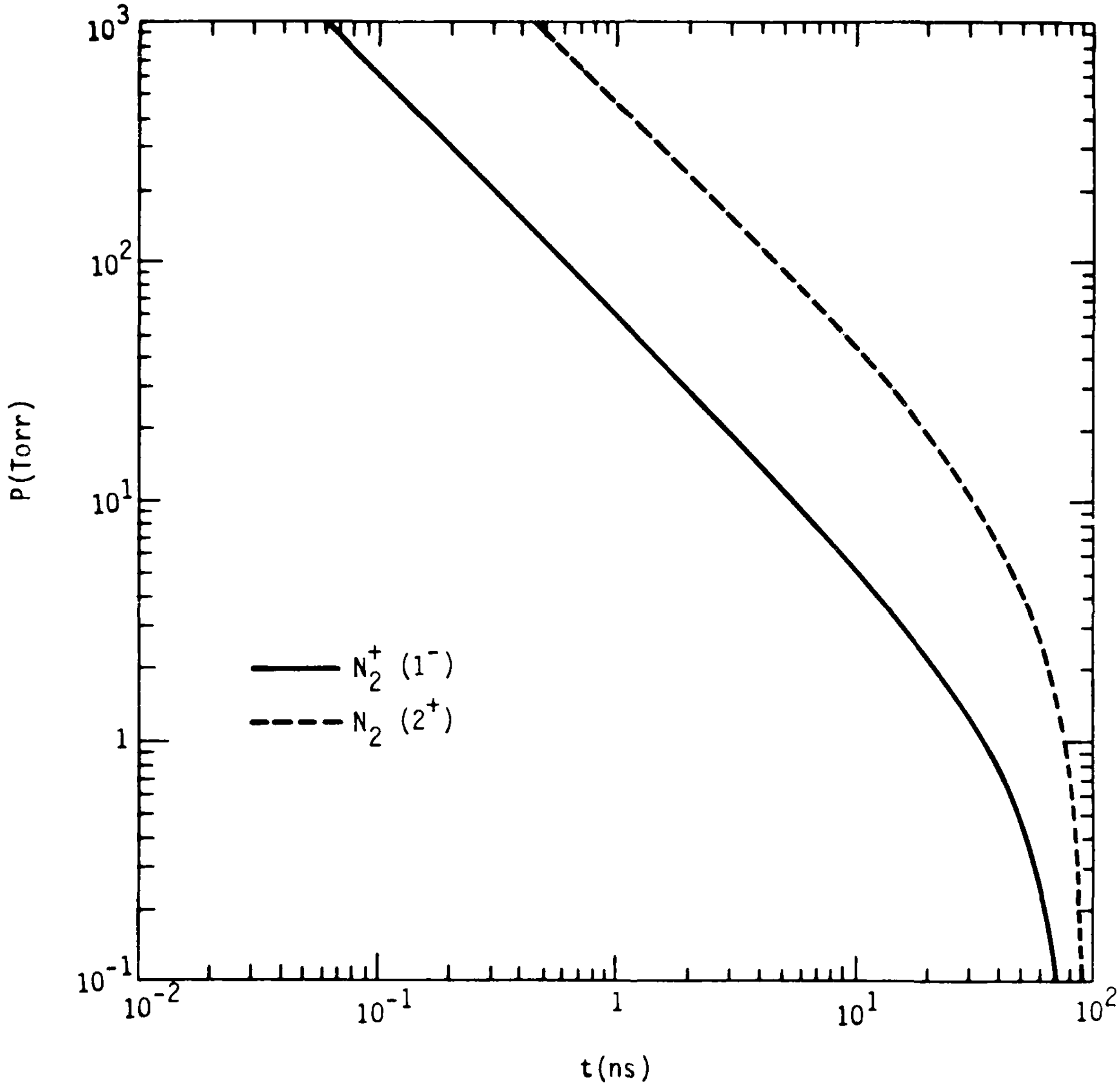

Figure 4. Pressure required for a given response time for two nitrogen bands.

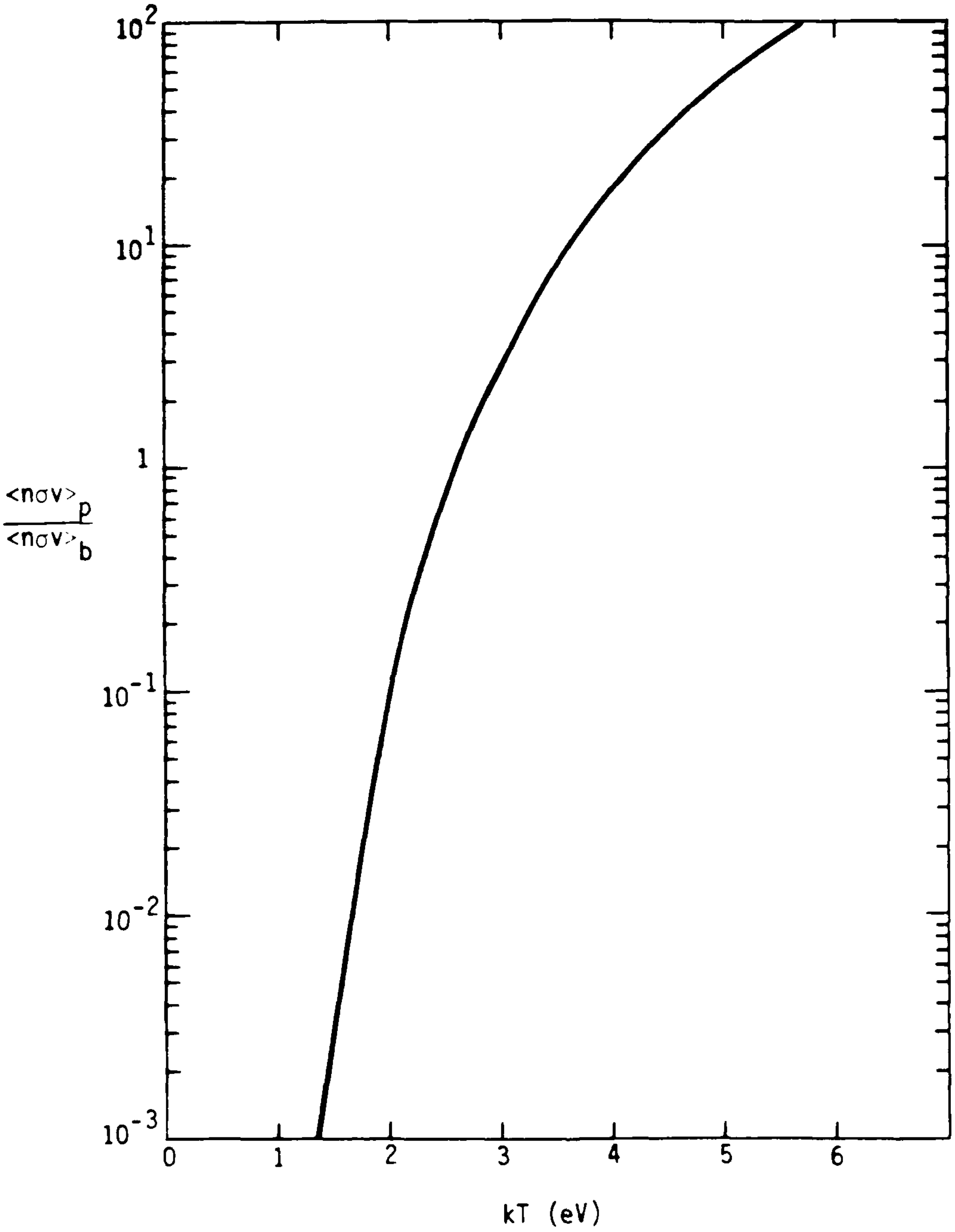

Figure 5. Ratio of $N_2^+(1^-)$ excitation caused by plasma electrons to beam electrons as a function of plasma temperature, assuming $n_p/n_b = 10^3$ and $E_b = 1.5$ MeV.

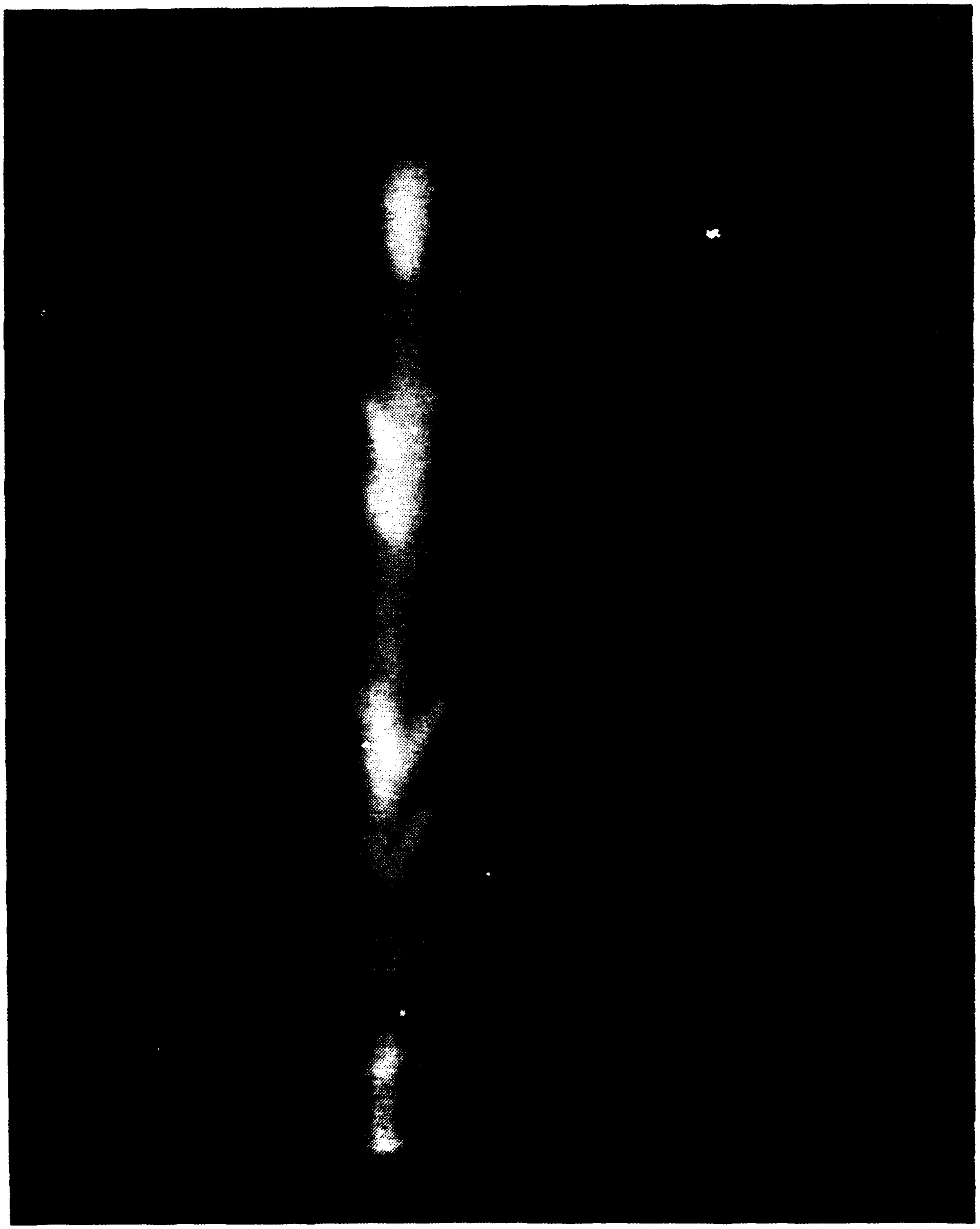

Figure 6. Open shutter photograph of FX-100 beam showing feathering.

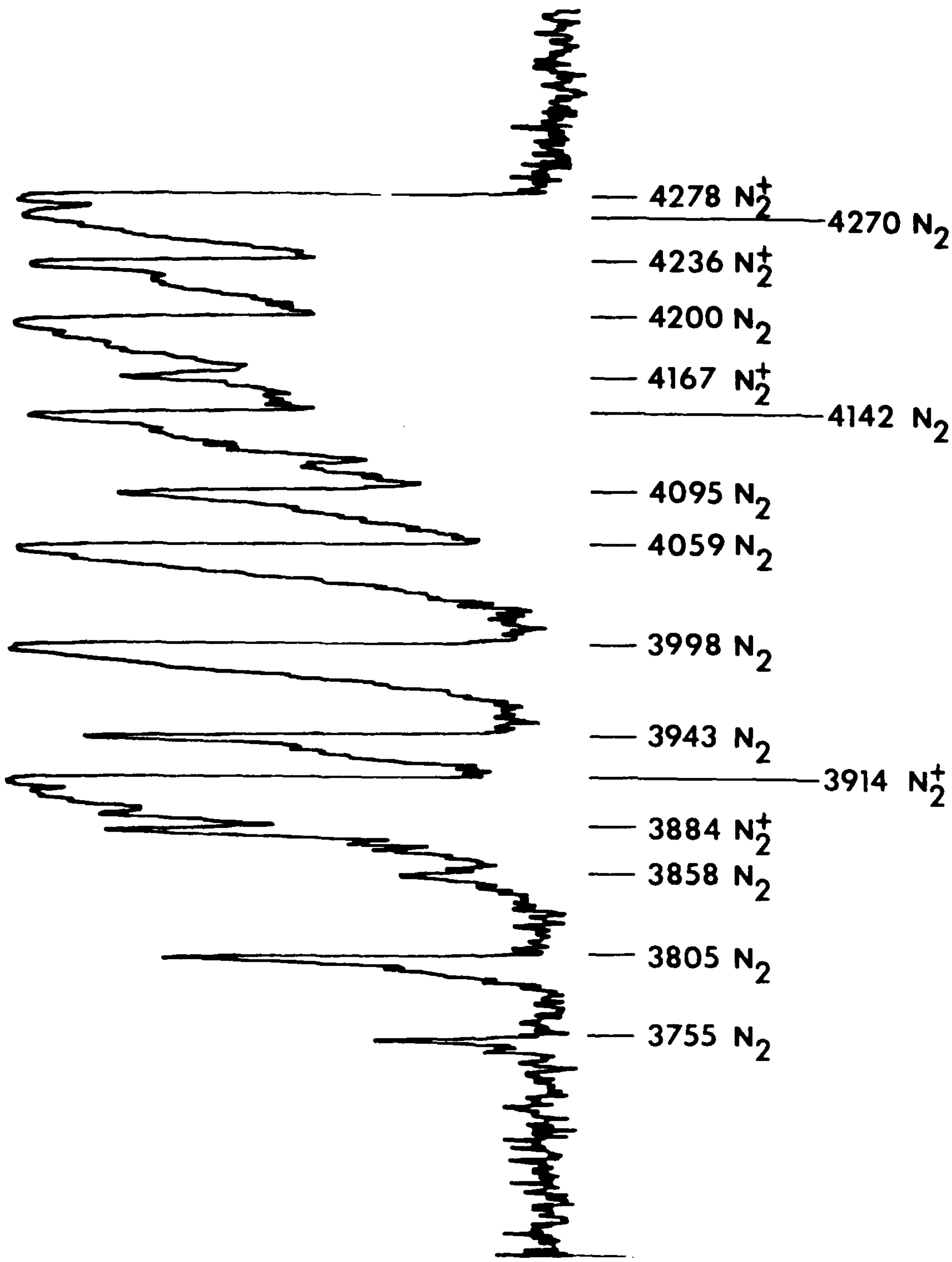

Figure 7. Densitometer scan of FX-100 spectra.

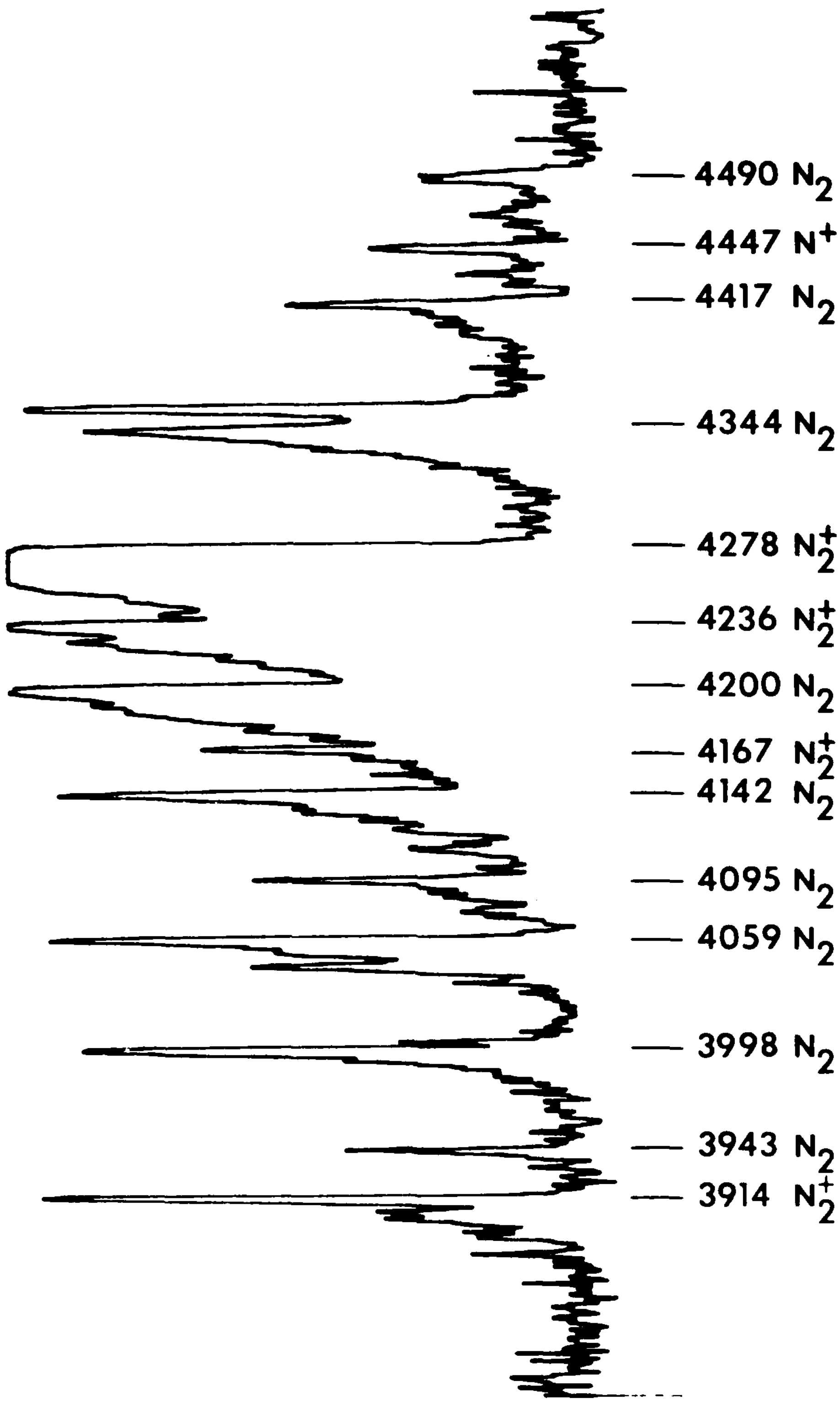

Figure 8. Densitometer scan of FX-100 spectra.

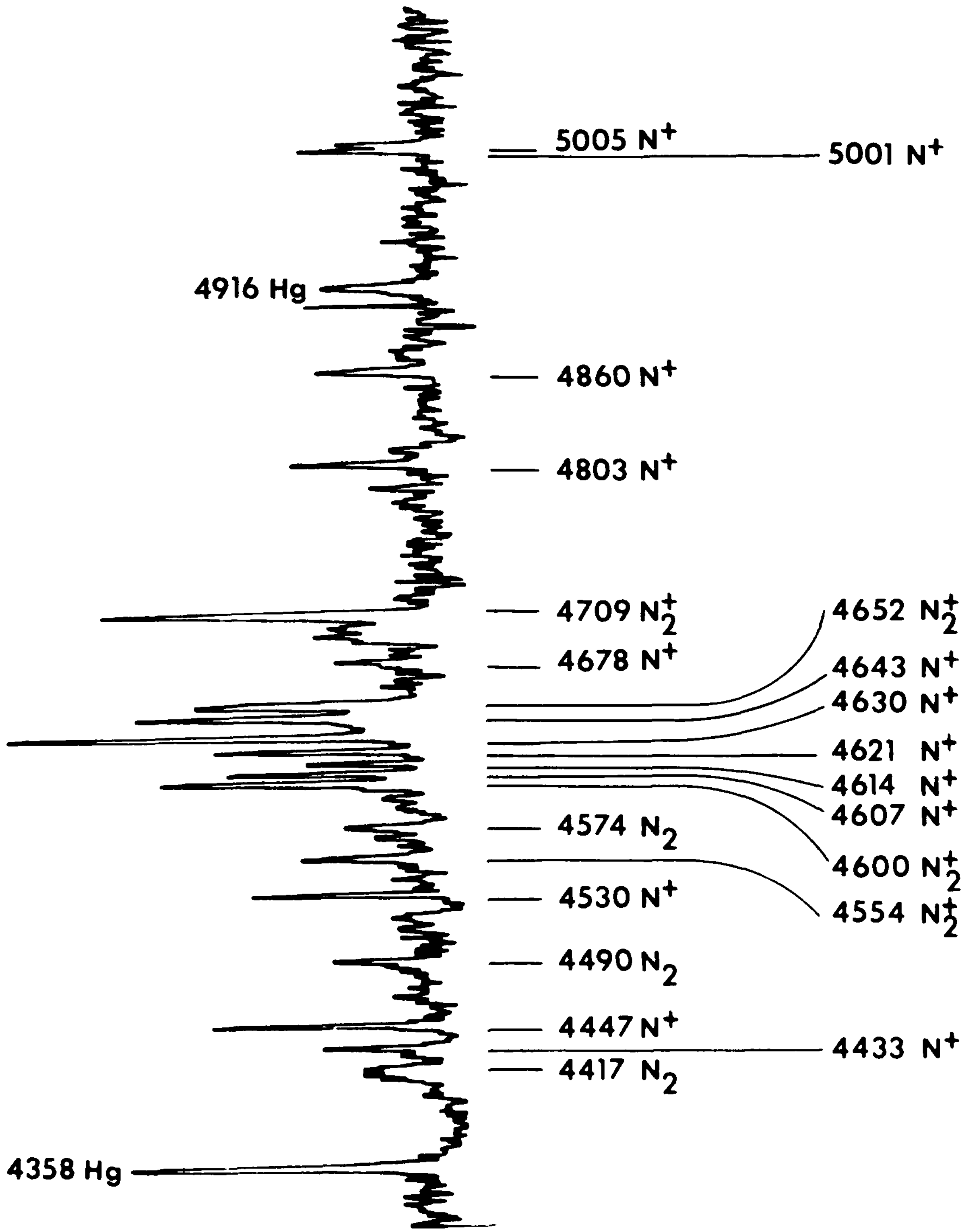

Figure 9. Densitometer scan of FX-100 spectra.

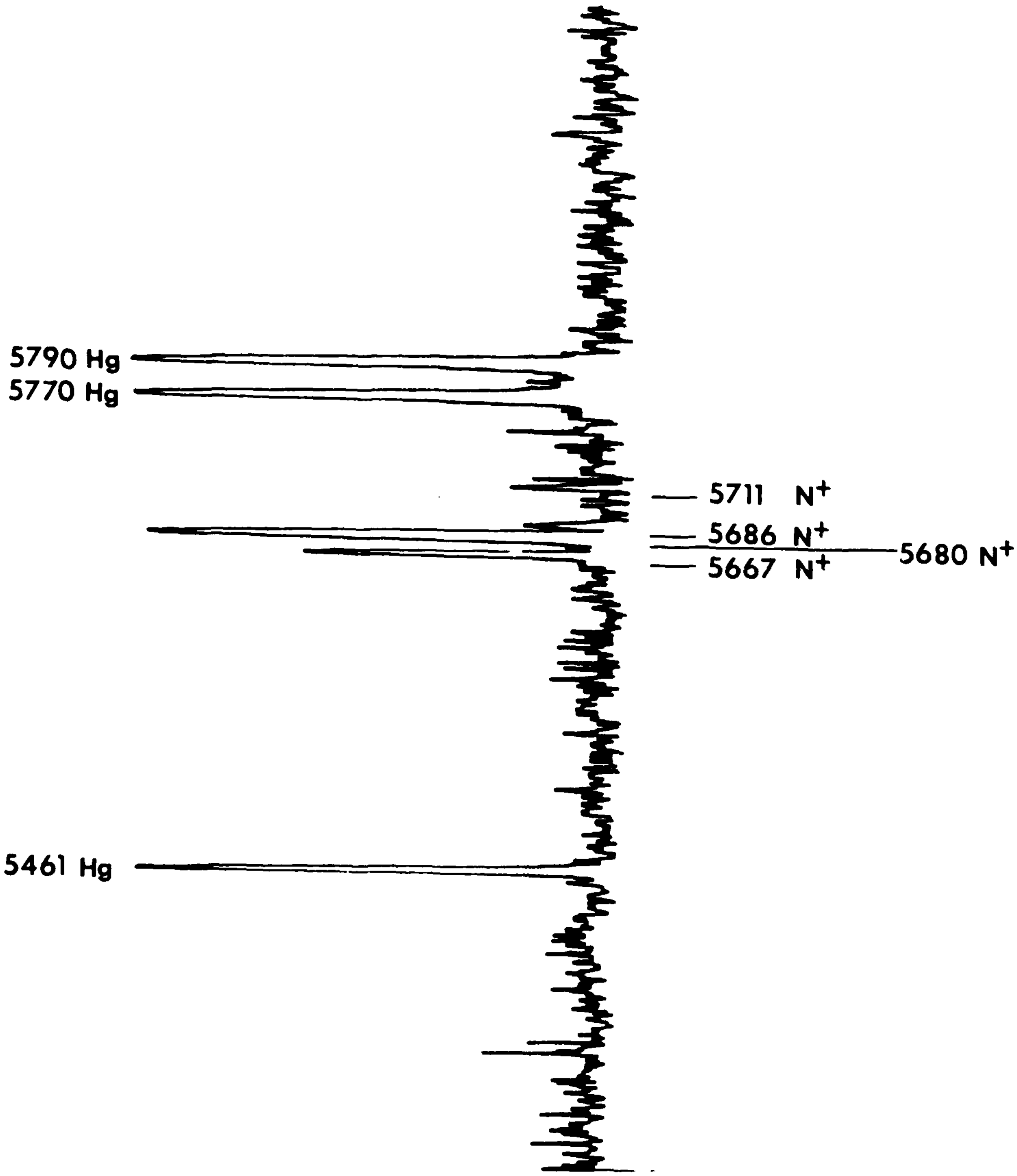

Figure 10. Densitometer scan of FX-100 spectra.

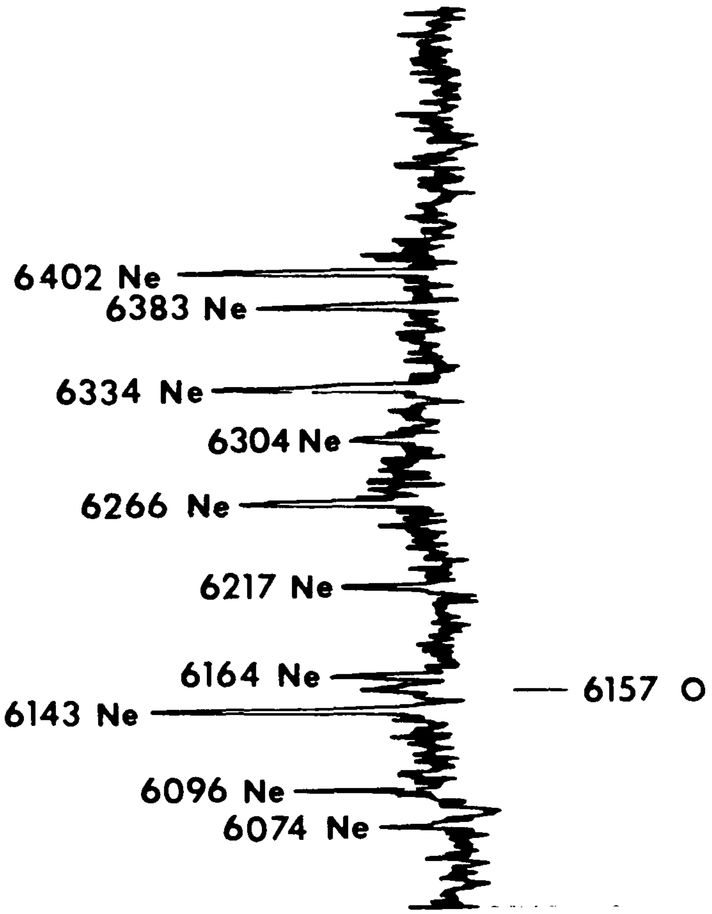

Figure 11. Densitometer scan of FX-100 spectra.

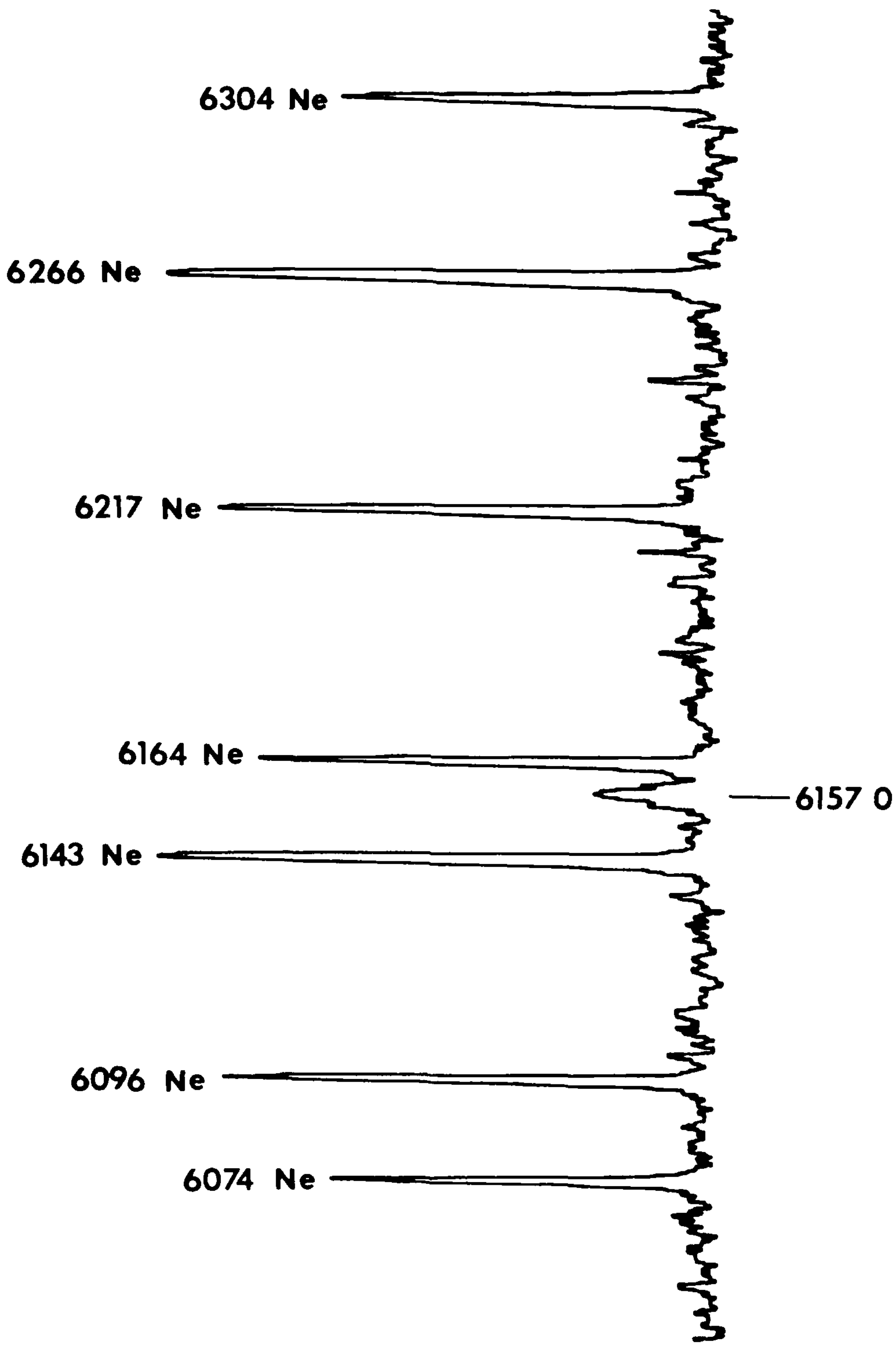

Figure 12. Detailed densitometer scan of oxygen line.

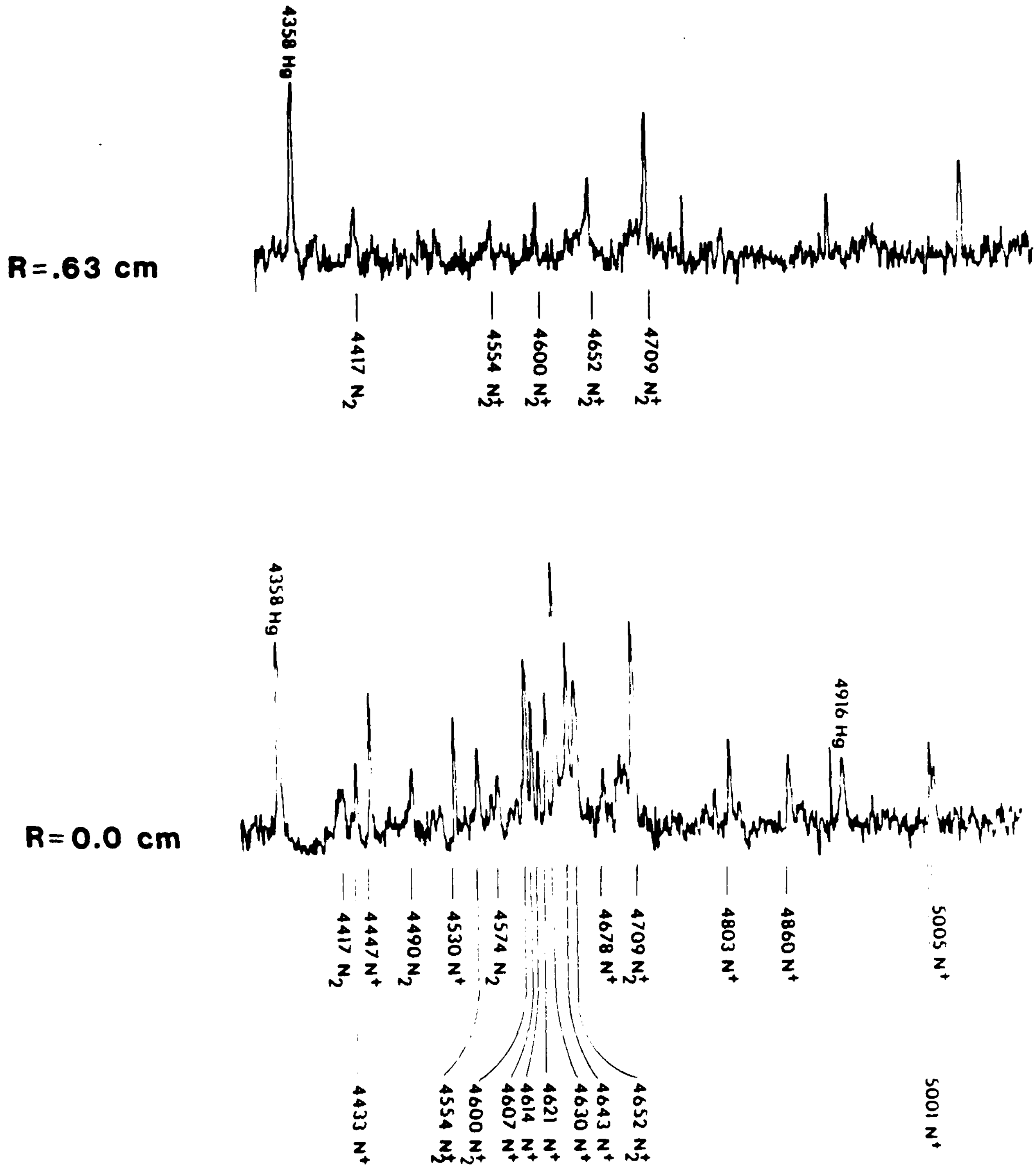

Figure 13. Densitometer scan of FX-100 spectra off axis and on axis.

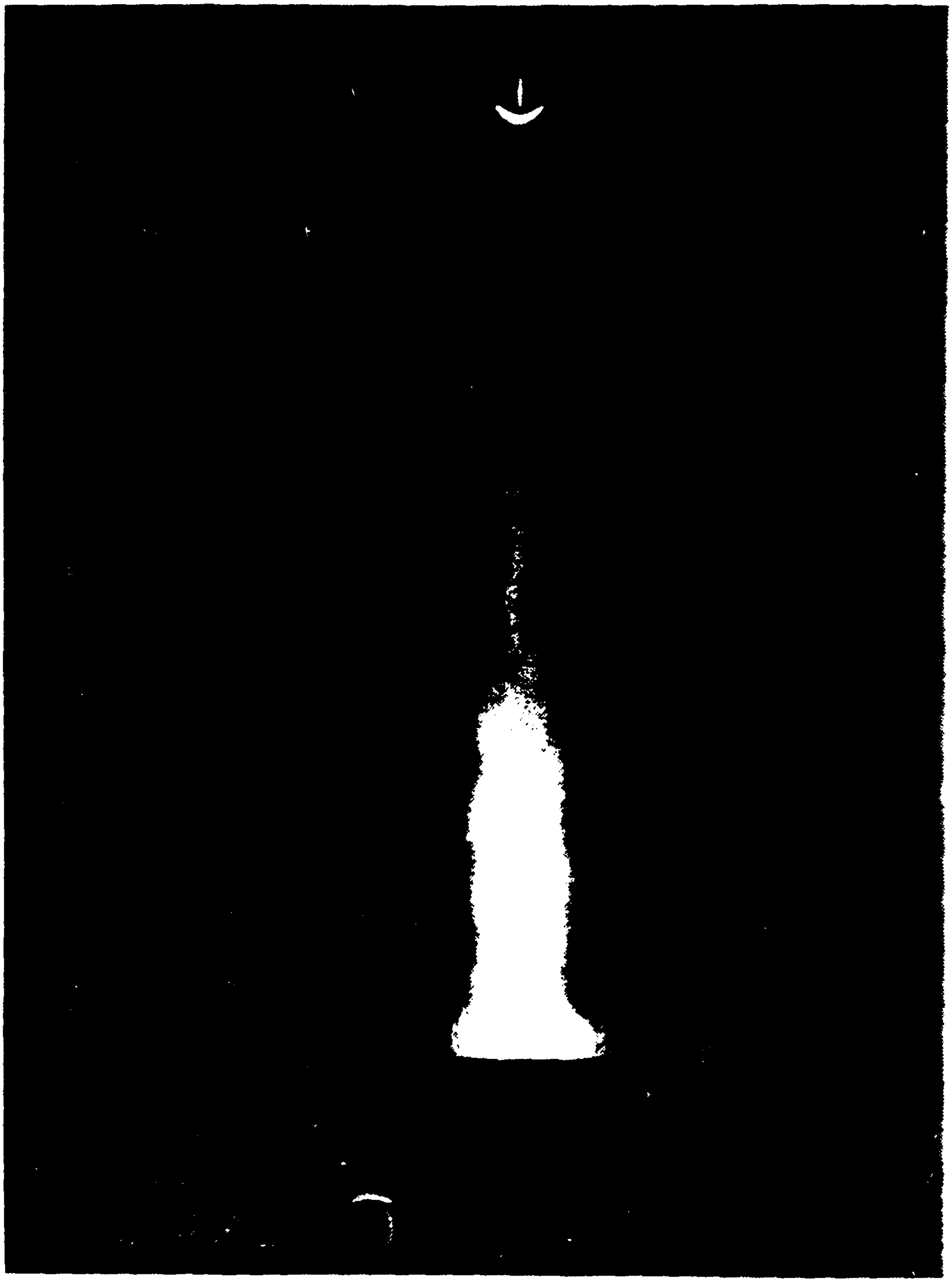

Figure 14. Streak photograph of beam at .35 Torr.

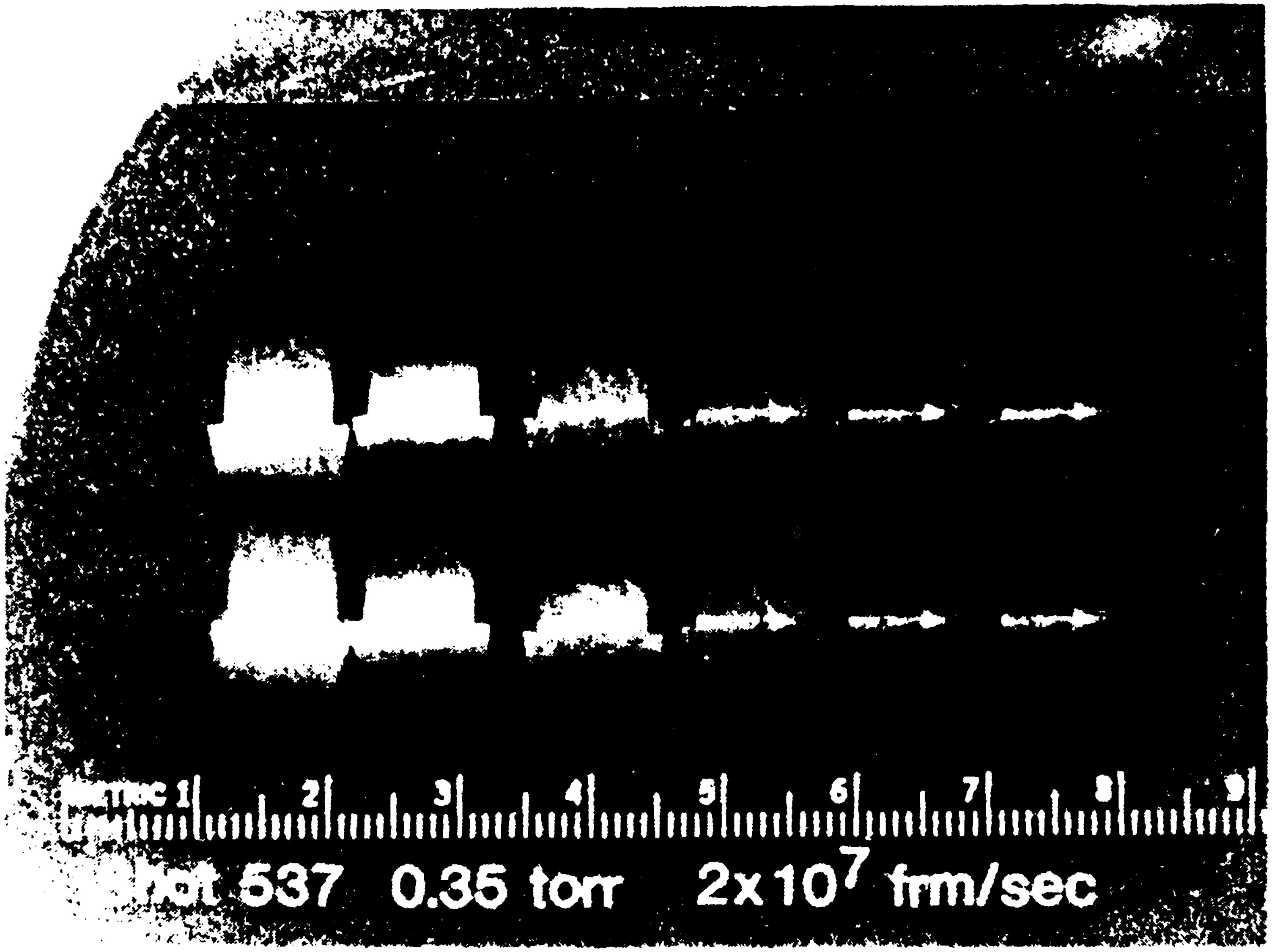

Figure 15. Framing photograph of FX-100 beam at .35 Torr.

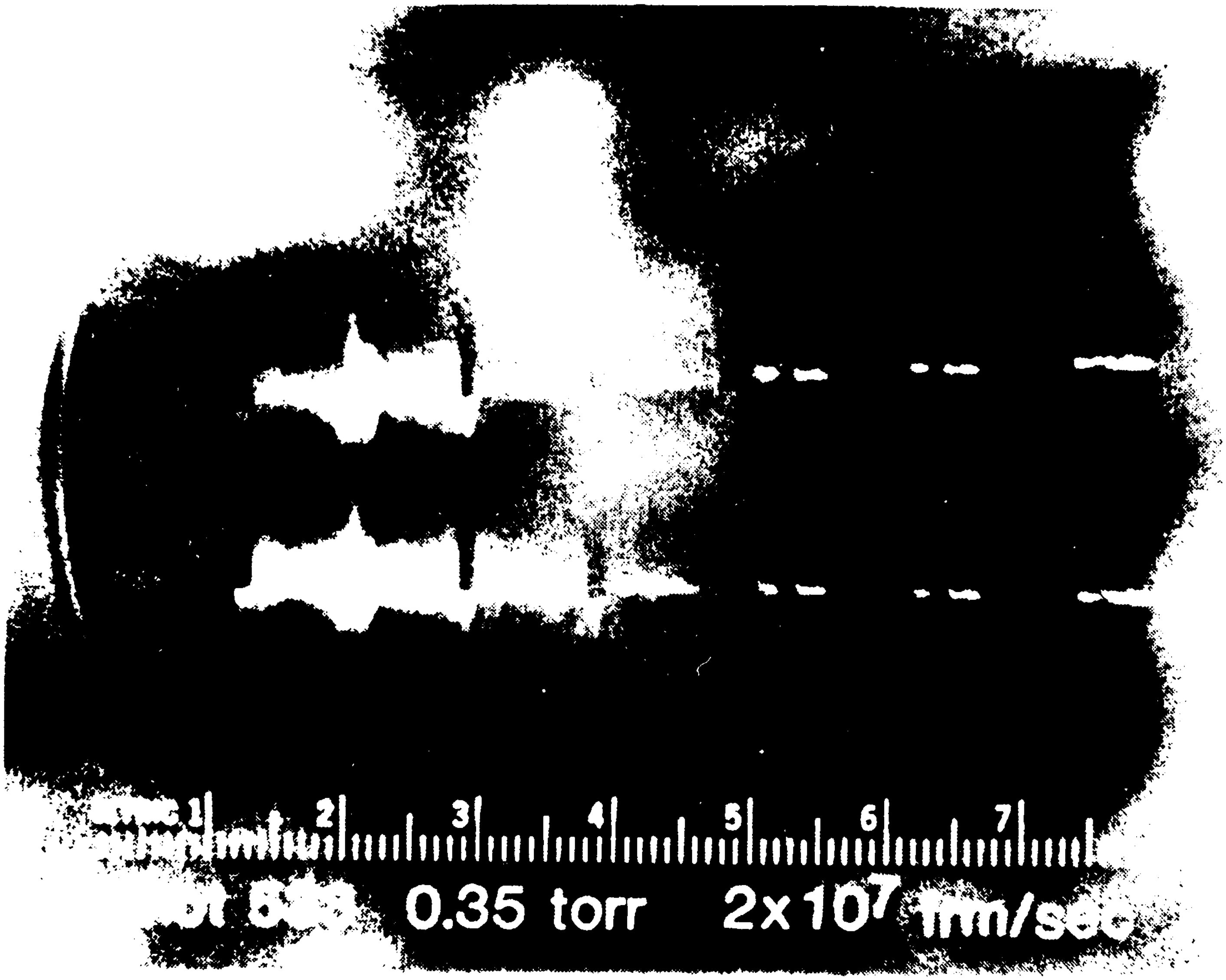

Figure 16. Framing photograph of FX-100 beam at .35 Torr.

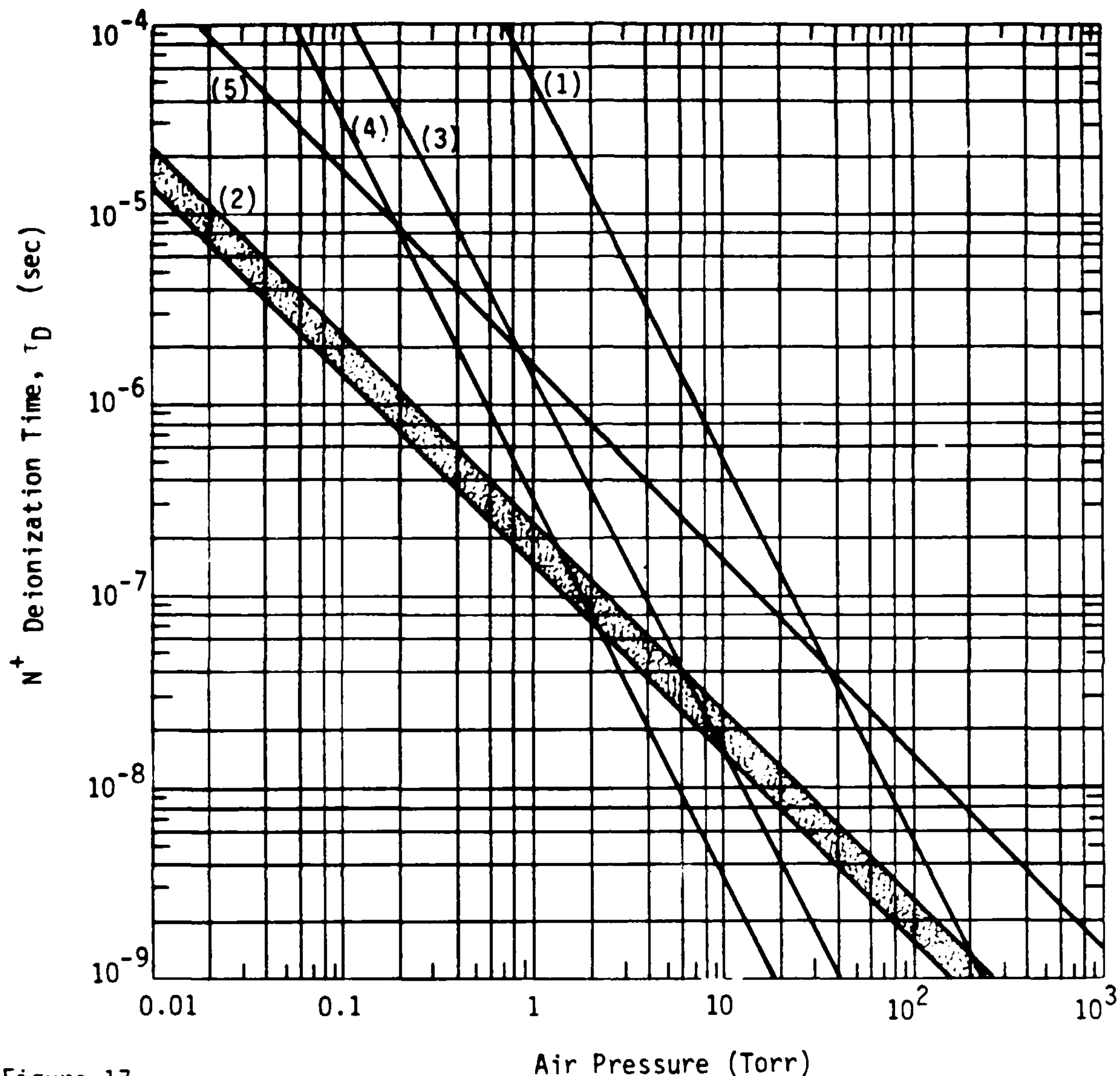

Figure 17.

Persistance of N^+ ions in air resulting from the following deionization reactions:

(1) $N^+ + 2N_2 \rightarrow N_3^+ + N_2$ ($T_g = 0.025$ eV; $\tau_D \propto n_a^{-2}T_g$)

(2) $N^+ + O_2 \rightarrow O_2^+ + N$ / $NO^+ + O$ / $NO + O^+$ ($0.025 \text{ eV} < T_g < 1.0$ eV; $\tau_D \propto n_a^{-1}T_g^{0.57}$)

(3) $e + M + N^+ \rightarrow M + N$ ($T_e = 0.025$; $n_e = 0.1\ n_a$; $\tau_D \propto n_e^{-1}n_a^{-1}T_e^{2.5}$)

(4) $e + e + N^+ \rightarrow e + N$ ($T_e = 0.025$; $n_e = 0.1\ n_a$; $\tau_D \propto n_e^{-2}T_e^{4.5}$)

(5) $e + N^+ \rightarrow N + h\nu$ ($T_e = 0.025$; $n_e = 0.1\ n_a$; $\tau_D \propto n_e^{-1}T_e^{0.5}$)

REFERENCES

1. T. J. Fessenden, R. J. Briggs, J. C. Clark, E. J. Lauer, and D. O. Trimble, Lawrence Livermore National Laboratory Report UCID-17840 (1978).

2. R. B. Miller, Sandia National Laboratory Report SAND-79-2129 (1979).

3. R. B. Fiorito, E. W. Fordham, J. R. Greig, R. E. Pechacek, J. D. Sethian, R. Fernsler, and J. Halle, Naval Research Laboratory Memorandum Report 4557, (1981).

4. R. M. Hill, K. Y. Tang, B. E. Perry, D. J. Eckstrom, and D. L. Huestis, SRI International Report MP80-41 (1980).

5. A. M. Frank, S. S. Yu, and J. M. Masmitsu, Lawrence Livermore National Laboratory Report (1982).

6. T. J. Fessenden, W. L. Atkinson, W. A. Barletta, J. F. Campbell, J. C. Clark, L. D. Clendenen, R. B. Fiorito, A. M. Frank, F. D. Lee, H. A. Koehler, and K. W. Struve, Lawrence Livermore National Laboratory Report UCID-19245 (1981).

7. G. Davidson and R. O'Niel, J. Chem. Phys. 41, 3946 (1964).

8. M. N. Hirsch, E. Poss, and P. N. Eisner, Phys. Rev. A1, 1615 (1970).

9. H. A. Bethe and J. Ashkin, in Experimental Nuclear Physics, Vol. I, ed. by E. Segre, (1953).

10. P. Millet, Y. Salamero, H. Brunet, J. Galy, D. Blane, and J. L. Teyssier, J. Chem. Phys. 58, 5893 (1973).

11. G. A. Baraff and S. J. Buchsbaum, Phys. Rev. 130, 1007 (1963).

12. G. W. Sutter and A. Sherman, Engineering Magnetohydrodynamics, (McGraw-Hill, N.Y., 1965), pp. 125-210.

13. S. Brown, Basic Data of Plasma Physics, (Wiley, N.Y. 1959).

14. A. W. Ali, Naval Research Laboratory Memorandum Report 4619, (1981) and references therein.

15. R. W. P. McWhirter, in Plasma Diagnostic Techniques, ed. by R. H. Huddlestone and S. L. Leonard, (Academic Press, N.Y., 1965), pp. 208-214 and references therein.

END
DTIC
8-86